GeoFocus volume 3

Philip BASSANT

The high-resolution stratigraphic architecture and evolution of the Burdigalian carbonate-siliciclastic sedimentary systems of the Mut Basin, Turkey

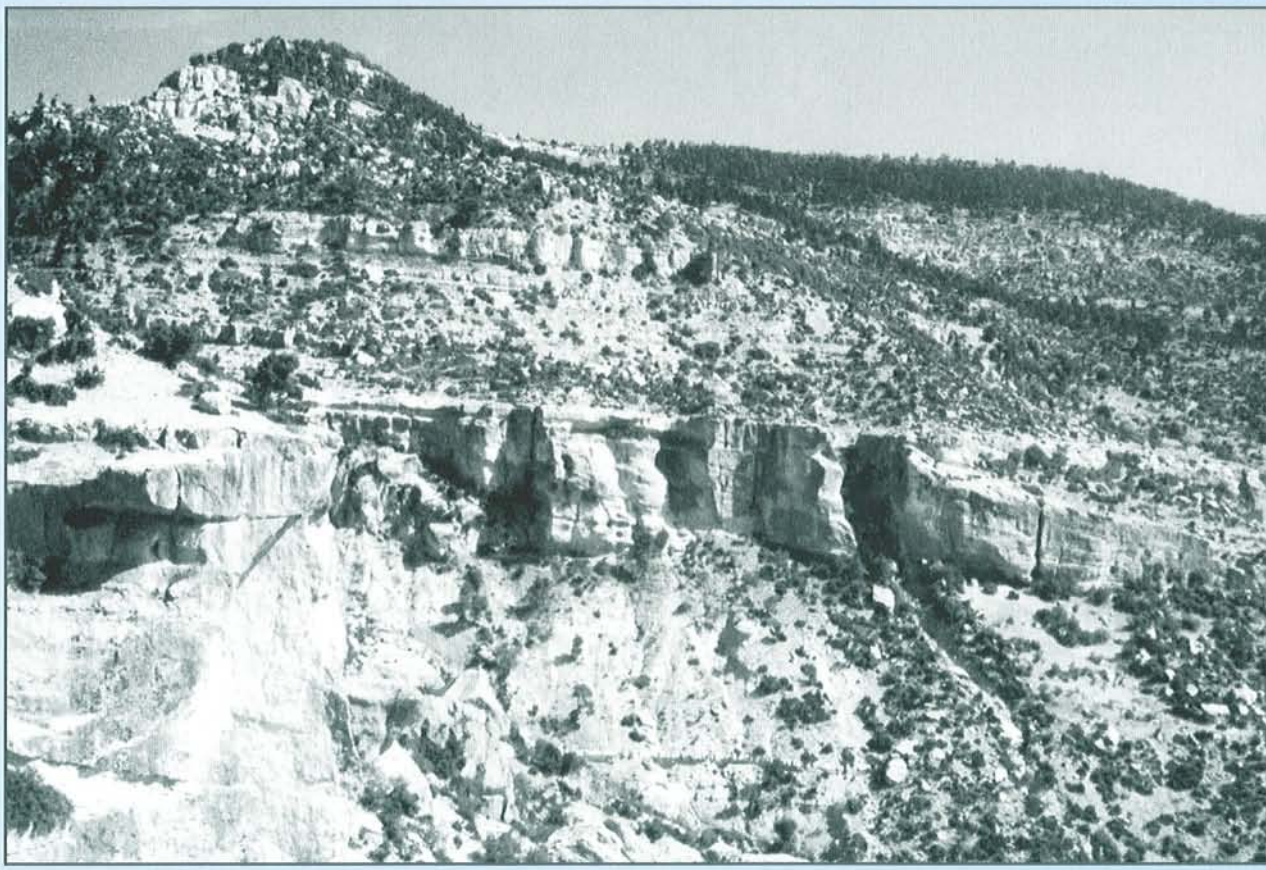

Institut de Géologie et Paléontologie de l'Université de Fribourg (Suisse)

INSTITUT DE GEOLOGIE DE L'UNIVERSITE DE FRIBOURG (SUISSE)

The high-resolution stratigraphic architecture and evolution of the Burdigalian carbonate-siliciclastic sedimentary systems of the Mut Basin, Turkey

THESE

présentée à la Faculté des Sciences de l'Université de Fribourg (Suisse)
pour l'obtention du grade de *Doctor rerum naturalium*

Philip BASSANT

de King's Lynn, Angleterre

Thèse N^{o} 1256

Multiprint SA, Fribourg, 1999

Acceptée par la Faculté des Sciences de l'Université de Fribourg (Suisse)

---

sur la proposition de:

Prof. André STRASSER, Université de Fribourg (Suisse)

Prof. Luis POMAR, Université de Palma de Mallorca (Espagne)

Dr. Frans S.P. van Buchem, Institut Français du Pétrole, Paris (France)

Fribourg, le 16 juin 1999

Le Doyen: Prof. Béat Hirsbrunner

Directeur de thèse: Prof. André Strasser

ABSTRACT

The factors influencing the production and deposition of carbonate sediments are known. These are namely accommodation variations (eustasy and tectonics), siliciclastic sediment input, environmental changes (temperature, salinity, trophic level), nature of the producing ecologies, and the hydrodynamic regime. However, the manner in which these factors integrate through time to produce the diversity of stratigraphic architectures that we see is not well understood. This study addresses this question by describing the organisation of shallow marine carbonate-mixed platforms in three environmentally distinct contemporaneous settings across a basin. Chronostratigraphic correlations are made between the different sites, and this permits the comparison of coeval depositional facies and geometries, and the understanding of the factors that create the different stratigraphic architectures observed.

The study interval is the Lower Miocene (Burdigalian) of the Mut Basin in Southern Turkey. This area is chosen because it presents extraordinary large-scale 3D outcrops showing depositional geometries, and such outcrops are found throughout the basin.

The Mut Basin opened during the Oligocene and was partially filled by syn-extensional continental sediments. Post-extensional basin-wide thermal subsidence then occurred during the Lower Miocene, and at the same time rapid marine transgression flooded a complex relict topography, depositing shallow platform carbonates in a variety of settings, accompanied by some localised siliciclastic input.

The Miocene stratigraphy of two areas was mapped out in the field. This allowed three Burdigalian margin transects to be chosen for detailed study (Dibekli, Pirinç and Alahan). Observations of the stratal geometries and the facies were combined into a high resolution sequence stratigraphic framework of retrograding/prograding sedimentary cycles in order to construct stratigraphic cross-sections of each transect. 3346m of section were logged, 400 thin sections were studied, and 145 biostratigraphic samples were analysed for nannoplankton dates (C.Müller). 10 samples were dated for planktonic foraminifers (R.Wernli). The three transects were then correlated: large-scale correlations were made by using the biostratigraphic dating, then high-resolution sequence stratigraphy and the construction of the relative sea-level curve for each site permitted correlation beyond the resolution of the biostratigraphy.

The first transect (Dibekli, Silifke region) has a steep asymmetric basement graben topography, forming a narrow strait, linking the Mut Basin to the Mediterranean, where strong tidal currents are generated. Siliciclastic input is low and localised. 80m of cross-bedded bioclastic sands are deposited in a tidal regime at the base. Subsequently carbonate platforms backstep against the shallow-dipping northern flank, while platforms only develop on the steep southern flank when a firm, wide shallow-marine area is provided by a fan-delta or the shallow-dipping top shoulder of the foot-wall. The energy of the environment decreases with increased flooding of the strait area.

The second transect (Pirinç, Mut region) is the open northern basin margin, and shows a complete platform-to-basin transition. An isolated platform complex develops during the initial flooding, which is drowned during a time of environmental stress, possibly associated with increased nutrient levels. The platform margin then retrogrades forming large-scale clinoform geometries, and progrades, before a major sea-level fall provokes slumping collapse, followed by rebuilding of the platform margin as sea-level rises again.

The third stratigraphic cross-section (Alahan, Mut area) is also on the northern basin margin. Here the siliciclastic input is high due to the presence of the palaeo-Goksu River bringing in dominantly fine grained sediment from an ophiolitic hinterland. The siliciclastic depocentre migrates landwards during transgressions, creating an ecological window allowing carbonates to develop in the distal part of the delta. Carbonate production shuts down during the progradation when siliciclastics return. Environmental pressure on carbonate growth is here coupled to the relative sea-level cycles that drive the transgressions and regressions. This motif is repeated at three different scales, and possesses a distinct hierarchical organisation.

The stratigraphic architecture can be broken down into four scales of cycle, each with a characteristic amplitude and period. The very large-scale cycle, (period >3.4Ma, possibly non-periodic, amplitude of 200m) is attributed to a combination of glacio-eustasy and basinwide subsidence. Large-scale cycles (average period of <570Ka, amplitudes of 100-150m),

and medium scale cycles (average period <100ka, amplitudes of 18-30m) are attributed to glacio-eustatic variations, possibly driven by astronomical eccentricity cycles. The small-scale cycles (average period 10-20ka, amplitudes 3-6m) are likely to be caused by other climatic changes, or autocyclic processes.

The tidal deposits in Silifke and the isolated platforms in Mut are shown to have developed contemporaneously: the dramatic difference in architectural style is due principally to the very different hydrodynamic regime, brought about by the basin topography.

The chronostratigraphic framework permits the recognition of condensation and omission surfaces in the basinal and platform settings, to identify basinwide variations in sedimentation patterns, and to evaluate the relative influence of tectonism, eustatism and the environment. The exceptional quality of the outcrops with its variety of environments, and its location at the Tethys margin make this a good candidate for a reference model for Burdigalian reef and platform architectures.

CONTENTS

1 – INTRODUCTION

The study of facies and sediments allows us to reconstruct with considerable accuracy the depositional environments and diagenetic history of rocks that we observe. It tells us about the processes involved in the deposition of a given body of sediment, and it tells us what the world was like when this sediment was deposited. The tool of sequence stratigraphy places time in the sediment in a qualitative fashion, allowing us to reconstruct the lateral shifting of facies belts and the vertical oscillations of sea-level through geological history. It provides a conceptual framework in which to place, organise and better understand the observations we make of the rock record. Cyclostratigraphy tells us about the driving forces that create these changes, and gives us a potentially quantitative control on the distribution of time within the sediment, above and beyond the resolution provided by biostratigraphy.

With these tools we are well-equiped to measure and describe the rock record, and to explain how the landscaped evolved through time, and what processes were active. Ultimately we should also develop predictive hypotheses about the response of a sedimentary system to a given signal. However, sedimentary systems are very complex, involving feedback, damping and resonance, and it is often difficult to distinguish between the external forces that act on the system and the internal characteristics of the system.

AIMS

The aim of this project is to describe and explain the stratigraphic architecture and facies distributions from within a single time interval in three different depositional settings across a basin, and to determine the driving forces that create the architectures observed in each setting. This will then permit the comparison of contemporaneous intervals which share a common external signal (eustatic sea-level variations and climate on a basin scale) but have a different systems response.

The Mut Basin in Southern Turkey has been chosen for this study since it provides large, often 3-dimensional outcrops of Lower Miocene carbonates and siliciclastics across the basin in which the bedding geometries are exceptionally clear and the facies are accessible. Study of the rocks is possible from the bedding scale to the seismic scale (300m), and continuous platform-to-basin transects are available. High-resolution sequence stratigraphy is applied in a field-based study to construct stratigraphic cross-sections of chosen study sites from bedding geometries and facies observations.

ORGANISATION OF CHAPTERS

This work is organised into three distinct parts: the first part, comprising of chapters 1-5, introduces the study area. Chapter 2 describes the current state of knowledge in this region. Chapter 3 sets out the working methodology applied here. Chapter 4 defines two general study areas within the Mut Basin, one to the south (Silifke area) and one to the north (Mut area), and describes the geological mapping work performed during this study in these areas. The general stratigraphy observed is described here, and this places into a larger context the more detailed studies that form the main bulk of this thesis. Chapter 5 describes the sedimentology of the transects studied, illustrating facies and faunal content.

The second part of this thesis (chapters 6-10) describes the stratigraphic architectures which form the focus for this work. Three key transects are described, two in the Mut area to the north (Pirinç – chapter 6, and Alahan-chapter 7), and one in the Silifke area to the south (Dibekli-chapter 8). These three transects are the central elements to the correlations and comparisons made .Each transect has very specific characteristics: the Pirinç transect (north-east corner of the Mut Basin) shows a complete platform to basin transition in a carbonate dominated environment, and here the large-scale features are emphasised. The Alahan transect is a mixed system, situated in a proximal position on the platform, near to a major river system. The Dibekli transect is located on the flanks of a steep-sided graben-structure. Two additional smaller transects are also described, that focus on a particular stratigraphic interval, describing

two contemporaneous stratigraphic objects from this interval. They are Zincir Kaya (chapter 9) and Kizil Kaya (chapter 10), both situated in the Mut area.

The third part of this thesis (chapters 11-13) presents the synthesis, discussions and conclusions.

2 - GENERAL CONTEXT

2.1 STRUCTURAL HISTORY

First the general tectonic evolution of the Eastern Mediterranean will be presented, then within this context the basin forming processes of the Mut Basin and the surrounding basins will be discussed.

General tectonic history

The tectonic history of Southern Turkey, as concerns this study, can be summarised into three major periods (see figure 2.1):

1/ Late Palaeozoic to Middle Eocene: formation of the Tethyan orogenic collage.

2/ Middle Eocene to Middle Miocene: Tauride Orogeny and migration of deformation front south of Turkey.

3/ Late Miocene to Recent: collision of Eurasia with the Arabic Plate (Late Miocene) and start of the Neotectonic Regime.

1/ During the first period (Late Palaeozoic-Middle Eocene), the Tethyan orogenic collage that now forms most of modern Turkey was created by complex north-south convergence. During this time, Tethyan units rifted from Gondwana in the south, sailed north across the Tethys, and were progressively accreted to Eurasia. The precise kinematic reconstruction is under debate: Robertson et al. (1996) summarise three alternative models, as proposed by Robertson and Dixon (1984), Dercourt et al. (1986,1993) and Sengör et al. (1984), though in this study the details that distinguish these three alternatives do not concern us. Essentially, each of the three models describes progressive Tethyan closure from the late Cretaceous to the Early Tertiary. In the latest Palaeocene (?)-Early Eocene (Sengör et al. 1985) collision started to occur along a northern branch of the Tethys, the Inner Tauride Ocean of Görür et al. (1984), and final closure happened in the Late Eocene (Sengör et al. 1985) along the Pontide-Anatolide Suture (see figure 2.1).

2/ During the second period as defined here, from the Middle Eocene to the Middle Miocene (Serravalian), continuing north-south convergence and general tightening of the orogenic belt characterised much of Southern Turkey, with the emplacement of the Lycian Nappes in the west continuing until the Early Miocene. In the east, in the Adana Basin, thrusting may have continued until the Middle Miocene (Williams et al. 1995). Northward subduction of remnant ocean crust to the south of Cyprus seems to have started in the Early Miocene (Eaton and Robertson, 1993). The Arabian Peninsula in the East continued its northward movement, eventually colliding with Eurasia, along the Bitlis Suture Zone, in the Serravalian (Dewey et al. 1986).

Middle Eocene (Lutetian) platform carbonates are the last marine sediments to be found in Southern Turkey before the Lower Miocene. From Middle Eocene to Early Miocene the whole area undergoes uplift of 2-5km (Sengör et al. 1985). During this time episodes of fluvial and lacustrine sedimentation occur in intramontane settings across most of the region (Yetis et al. 1995). A diachronous marine transgression floods the southern part of Turkey, starting from the south, in the Late Oligocene in Cyprus, but not arriving in the Mut, Antalya and Adana regions until the Lower Miocene (see figure 2.2 and 2.3).

3/ The third phase in the tectonic history starts with the Eurasia-Arabia collision in the east in the Serravalian: it is this convergence that results in the westward expulsion of Turkey, along the North Anatolian and East Anatolian Faults, and is the start of the present Neotectonic regime (Sengör et al. 1985). Southern Turkey is at this time uplifted by epeirogenic processes to its present elevation of 1-2km above sea-level. This induces a marine regression across the southern Turkey areas (Antalya, Adana, Mut and Cyprus) from the Late Serravalian onwards, with deposition of Tortonian evaporites in the west and the south (Yetis et al. 1995).

Basin formation

In the Late Oligocene to Early Miocene the Mut, Adana, Antalya and Cyprus basins opened up in the south of Turkey. These areas share a common stratigraphic heritage (Kelling et al. 1995a), and hence they are here considered together. Figure 2.3 illustrates the stratigraphies for different southern Turkish basins, and figure 2.5 presents the geological map of the area. The precise basin dynamics are currently the subject of discussion in the literature.

In the Mut Basin, Kelling et al. (1995b) suggest an Early Oligocene phase of crustal extension, probably associated with orogenic collapse, leading to "trap

door" subsidence. An alternative hypothesis is that the basin opened during the Late Oligocene to Early Miocene due to back-arc extension associated with the northward subduction of oceanic crust occurring in Cyprus around this time. This is consistent with the tectonic reconstruction proposed by Robertson (1998). During the Oligocene basin opening phase, continental sediments are deposited, and it is only from the Early Miocene that marine sediments, dominantly carbonates, appear. These are associated with the regional marine transgression, and fill a mountainous pre-existing topography, as post-extensional infill (see figure 2.5, 2.6, 2.7 and 2.8).

In the Adana Basin, Sengör et al. (1985) describe how the basin extension results from an "incompatibility problem arising from the buoyancy of the continental lithosphere (which) may generate complex basin types at strike-slip fault intersections," while Williams et al. (1995), propose that the Adana Basin formed in the Early Miocene as a foreland basin, due to the southward overthrusting of Tauride nappes to the north of the basin area. During the Late Miocene sinistral strike-slip faulting was initiated by the collision in the east of Arabia with Eurasia and the resultant westward expulsion of Anatolia.

In the Antalya region there are a number of sub-basins to be considered: Flecker et al. (1995) and Flecker (1995), propose that the Köprü and Manavgat Basins are foreland basins, formed during the Early Miocene. The south-eastward advance of the Lycian Nappes caused flexural loading and may have induced block-faulting along inherited Mesozoic structures in the foreland, though the area was not over-ridden by the nappes. This is a very similar story to that proposed for the Adana Basin.

In the south of Cyprus, the Pakhna Basin (Eaton and Robertson, 1993) was formed by an Early Miocene thrusting event with the basin in a local foreland setting. This thrusting event was interpreted by Eaton and Robertson (1993) as related to the initiation of subduction to the south of Cyprus.

2.2 PALAEOCLIMATOLOGY

Firstly the local Mediterranean climatic conditions will be discussed. Then the global climatic variations will be presented, including discussion of the creation of the Antarctic ice cap, since this plays a fundamental role in global climate change and eustatic sea level variations.

Miocene climatic and faunal evolution of the Mediterranean Tethyan region

Throughout the Miocene, Tethyan ocean circulation patterns were controlled by the steady closing of the eastern end of the Mediterranean Tethys: the link between the modern Eastern Mediterranean and the Persian Gulf. As the Arabian Plate converged on, and finally collided with the Eurasian Plate along the Bitlis Suture Zone, this passage was episodically shut off, being restricted in the Burdigalian, fully open in the Langhian, and closing finally in the Late Miocene (Steininger and Rögl, 1984).

Fluctuations between different faunal assemblages at the scale of the Mediterranean Basin have been observed in the Miocene. These faunal assemblages are considered to be characteristic of climatic conditions. Foramol assemblages are associated with a temperate climate, rhodalgal assemblages with a sub-tropical climate, and coralgal facies with a sub-tropical to tropical climate. Observation of their variations in time at the scale of the Miocene Basin has allowed the reconstruction of Miocene climate change in this area. It is in this context that Esteban (1996) describes the Mediterranean Neogene climatic evolution as follows: a Middle Oligocene temperate climate in the Mediterranean Tethys was replaced by a tropical to sub-tropical climate during the Late Oligocene, as indicated by the invasion of large benthic foraminifera that reached as far as the North Sea. Wide and deep sea-ways existed from the Indo-Pacific, via the Mediterranean to the Atlantic, and extensive coralgal-rhodalgal carbonates were deposited from Mesopotamia to the Mediterranean throughout the Aquitanian. The highest coral diversity of the Mediterranean Miocene occurred at this time. At the Aquitanian-Burdigalian boundary the eastern end of the Mediterranean was closed off from the Persian Gulf and the Mediterranean Tethys carbonates were limited to temperate rhodalgal-foramol types. This corresponds to a time of climatic deterioration and sea-level lowstand as proposed by Barron and Keller (1982). The climate warmed in the Late Burdigalian-Langhian to tropical or sub-tropical conditions, once again permitting coralgal-rhodalgal carbonates to develop, with moderate coral diversity (Esteban, 1996). Environmental conditions deteriorated in the Serravalian, due to apparent climatic cooling, and only impoverished sub-tropical to temperate carbonates are found in the western and middle parts of the Mediterranean region. The Late Serravalian saw a major global sea-level fall, and uplift of the Turkish and Arabian Plates. The connection to the Persian Gulf was finally closed. Corals survived in the Mediterranean from the Latest Serravalian to the Messinian. Then, during the Messinian, repeated major evaporitic draw-down

interbedded thick evaporite deposits with fully marine deposits across much of the Mediterranean (Hsü et al. 1973).

According to Cavelier et al. (1993) the Late Burdigalian (Early Miocene) was the warmest time of the Neogene, and it was considerably warmer than the current climate. As evidence they cite the high northerly limits of tropical molluscan fauna and tropical carbonate shelf deposits, as well as the distribution of terrestrial fauna and flora. They evoke a seasonal climate with contrasting semi-arid and humid periods, the climate being too humid to deposit evaporites in the present desert areas such as the Sahara and the Arabian Peninsula. During this time, Southern Turkey was at roughly 35 degrees of latitude, not far from its present position (Savostin et al. 1986; Yilmaz and Ozer, 1994; Westphal et al. 1986; Lauer, 1984). Making a direct comparison with the distribution of modern reefal fauna, such a high latitude would place the Mut Basin at the very limits of the coral growth area, and beyond that of Halimeda algae, in the zone of rare reef growth (Schlanger, 1981). Continuing the modern comparison, the Mut Basin is considered a temperate zone, dominated by a foramol assemblage (foraminifera and molluscs), and absence of non-skeletal carbonate grains (Lees, 1975).

Oxygen isotopes: global temperature and ice-volume

When considering the oxygen isotope signal two key elements are thought to be important: global ice volumes, and water temperature. In hothouse climatic conditions, when there is no significant storage of water as ice, variations in the O-18 abundance are thought to be the result of temperature changes in ocean waters. But when significant amounts of ice are stored, from about the Middle Miocene onwards, O-18 variations are considered to be the result of preferential light isotope storage as well as temperature changes. The creation of ice-caps will induce eustatic sea-level changes, and will also affect patterns of oceanic circulation, and therefore global temperatures.

Global temperature changes

Global climatic changes for the Oligocene to Recent have been described by Fulthorpe and Schlanger (1989) based on smoothed oxygen isotope curves for planktonic and benthic foraminifera: the Late Oligocene to the Early Miocene interval is considered as a time of general global climatic warming, contrary to the general Cenozoic cooling trend. A pronounced cooling then occurs in the Middle Miocene, followed by a significant warming then cooling again in the Late Miocene. In the Pliocene there is a sharp cooling and it is at this time that the current rapid glacial-interglacial cycles begin (Frakes, 1979).

Antarctic ice-cap development

Consideration of the development of the Antarctic ice-cap helps in understanding these changes. At the Eocene-Oligocene boundary precipitous cooling to temperatures in the glacial range occurs for the first time since the Palaeozoic (Frakes, 1979), and glaciers grow in the Antarctic, though no ice-cap forms. This shift is observed in both the surface and bottom water O-18 signal: which indicates a different global thermal state to that of the present.

In the Middle Miocene a general cooling is accompanied by an increase in the polar-equatorial temperature gradient. At the same time an antithetic trend in the surface and bottom water O-18 signal indicates a cooling of the bottom waters and warming of surface waters: Savin et al. (1975) interpreted this as signifying a change in the manner of heat distribution across the Earth's surface and related it to the opening of the Drake's Passage and the initiation of the Circum-Antarctic Current. This also corresponds to the first significant formation of ice-cap in Antarctica. Van Andel et al. (1975) tell us that the initiation of a stratified ocean in the equatorial Pacific also occurred at this time, in the Middle Miocene.

Unsmoothed oxygen isotope data published by Abreu and Anderson (1998) show high frequency and relatively high amplitude fluctuations in the isotope signal in the study interval (Burdigalian) (figure 2.4). This is compared with the global eustatic curve of Haq et al. (1987) which shows a gradual sea-level rise throughout the Burdigalian with smaller fluctuations superimposed, then two major sea-level drops and rises of over 100m at the base and the top of the Langhian. The Burdigalian/Langhian represents the highstand of a second order cycle.

2.3 PREVIOUS STUDIES OF THE MUT AREA

Surprisingly little work has previously been done in this area, considering the quality of the outcrop, and the relatively large volume of work performed in the Adana Basin to the east, and the Antalya Basins to the west. The chronostratigraphy of the Adana Basin of Schmidt (1961) is presented in figure 2.6 to illustrate how continued transgression invaded a relict topography during the Early Miocene. This is a factor common to all three areas of Adana, Mut and Antalya

(Yetis et al. 1989). The geological map of the Mut area is shown in figure 2.5 (Blumenthal, 1963). Sezer (1970) in his thesis described the Miocene stratigraphy, performed planktonic foraminifera dating, catalogued the Miocene macrofauna, and made a geological map of the area to the north of Mut. Gökten (1976) mapped out the Silifke area in the south-east of the basin, defining all the Phanerozoic units found. He placed major unconformities in the Carboniferous (Breton orogenic phase), in the Triassic (Palatin orogenic phase), astride the Jurassic-Cretaceous boundary (Ostervald orogenic phase), between the Cretaceous and the Eocene (Laramian orogenic phase), and between the Eocene and the Burdigalian (Helvetic orogenic phase). He defined five planktonic foraminiferal biozones in the Miocene limestones and marls, three of which are Burdigalian, the other two Helvetian to Tortonian.

Gedik et al. (1979) mapped out the whole Mut Basin and revised the Phanerozoic stratigraphy: this stratigraphy is presented in figure 2.7. He also made a present-day isobath map of the basement (Pre-Miocene) topography, which is presented in figure 2.8. Bizon et al. (1974) observed a Neogene transgression (Burdigalian to Langhian, dated with planktonic foraminifera) in the Antalya, Mut and Adana Basins (as part of the CNEXO project in the early 1970's, in which the IFP collaborated). Korkmaz and Gedik (1990) studied the source-rock potential of the Phanerozoic stratigraphy. Tanar and Gökçen (1990) provided a summary of the biostratigraphy of the Mut Basin, which is shown here in figure 2.9. Kelling et al. (1995a,b) in two abstracts briefly describe the stratigraphy and tectonic setting of the Mut Basin, and Gürbüz and Uçar (1995) describe the existence of biohermal and biostromal reef bodies in the Mut Formation limestones of the Mut Basin.

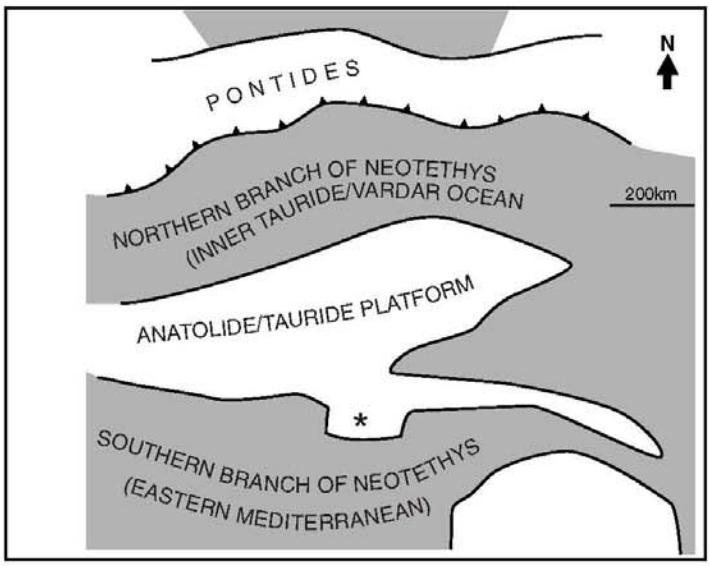

1/ Palaeotectonic map of the Late Cretaceous - Palaeocene
(modified after Sengor and Yilmaz, 1981)

* approximate location of the Mut Basin

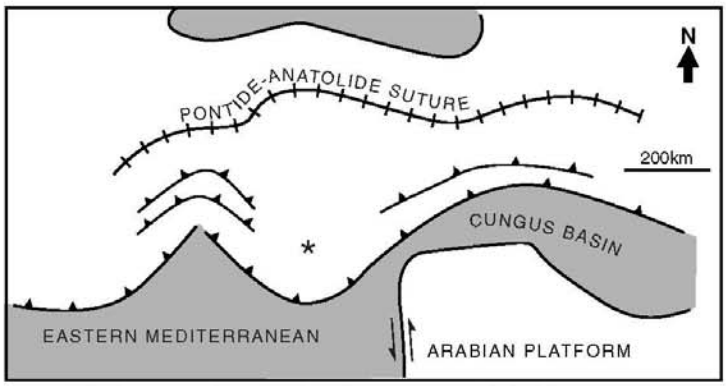

2/ Palaeotectonic map of the Late Eocene -Early Miocene
(modified after Sengor and Yilmaz, 1981)

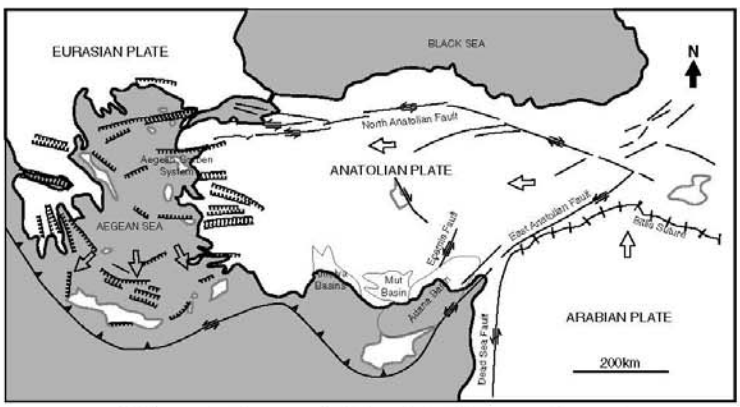

3/ Neotectonic map of Turkey, Late Miocene - Recent
(modified from Gorur, 1992)

Figure 2.1 The tectonic evolution of Turkey

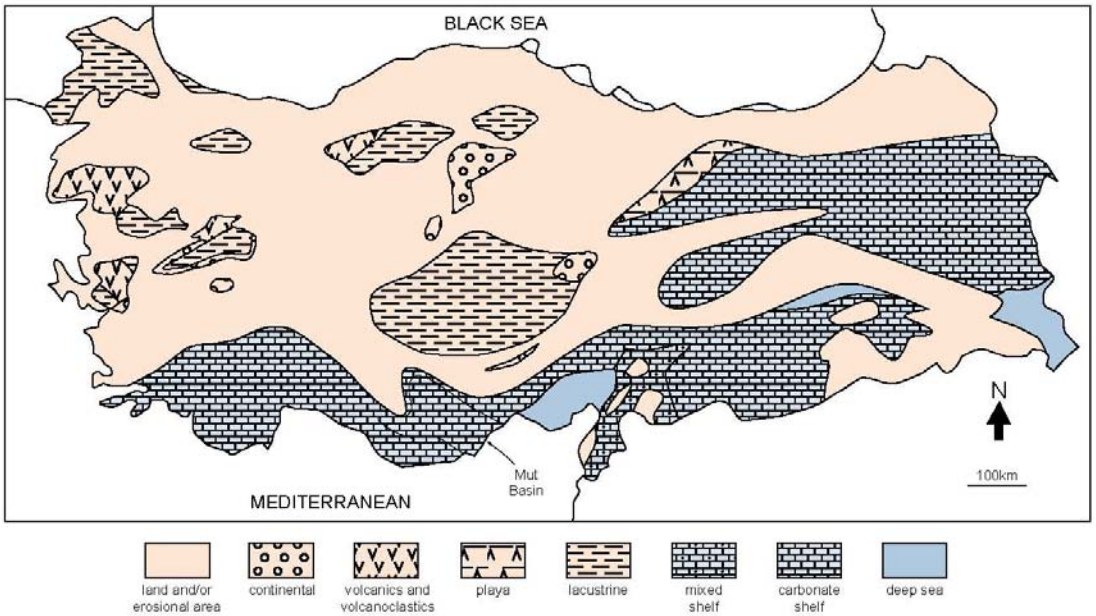

Figure 2.2 Early Miocene palaeogeography of Turkey (*modified from Gorur et al., 1995*)
This figure shows how the southern part of Turkey is flooded by the Mediterranean during the Lower Miocene, before the collision of the Arabic plate and the associated regional uplift begins.

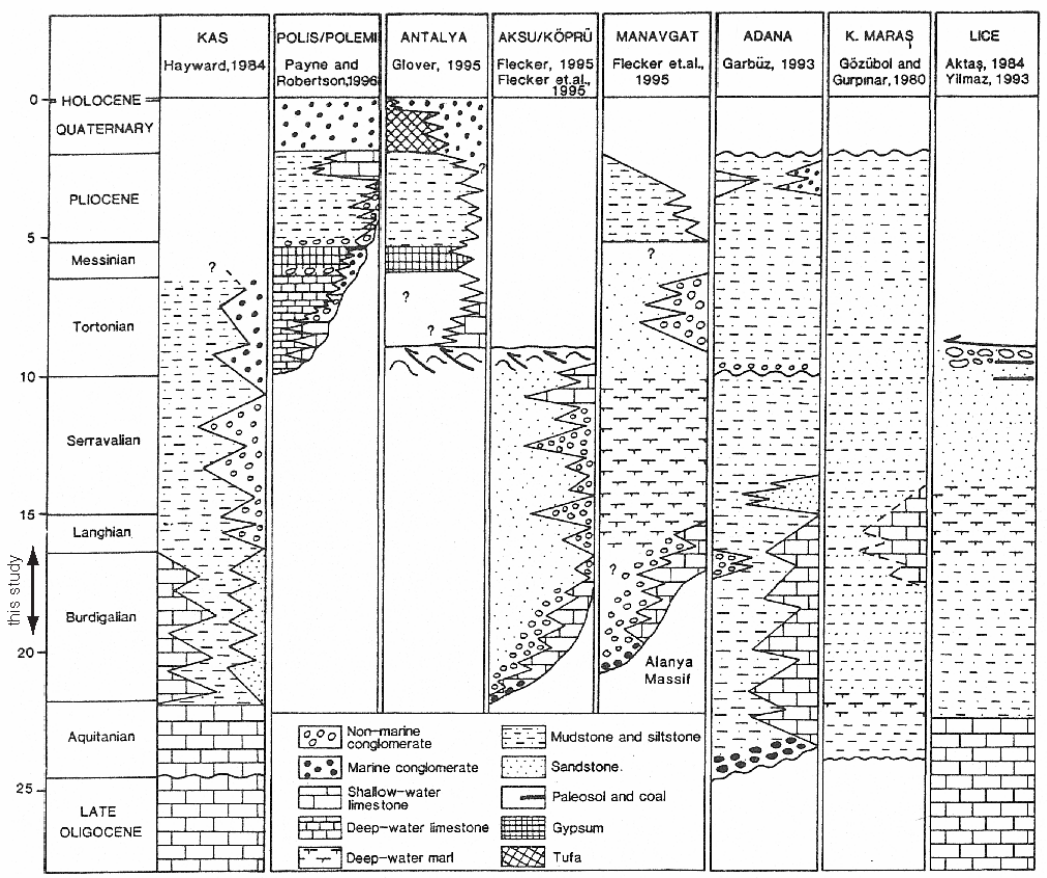

Figure 2.3 Comparative Miocene stratigraphy of Southern Turkey (Robertson, 1998)
This diagram illustrate the Miocene stratigraphies of the Southern Turkish and Cyprus areas, illustrating how marine onlap of a previously exposed relict topography is a common feature in this area.

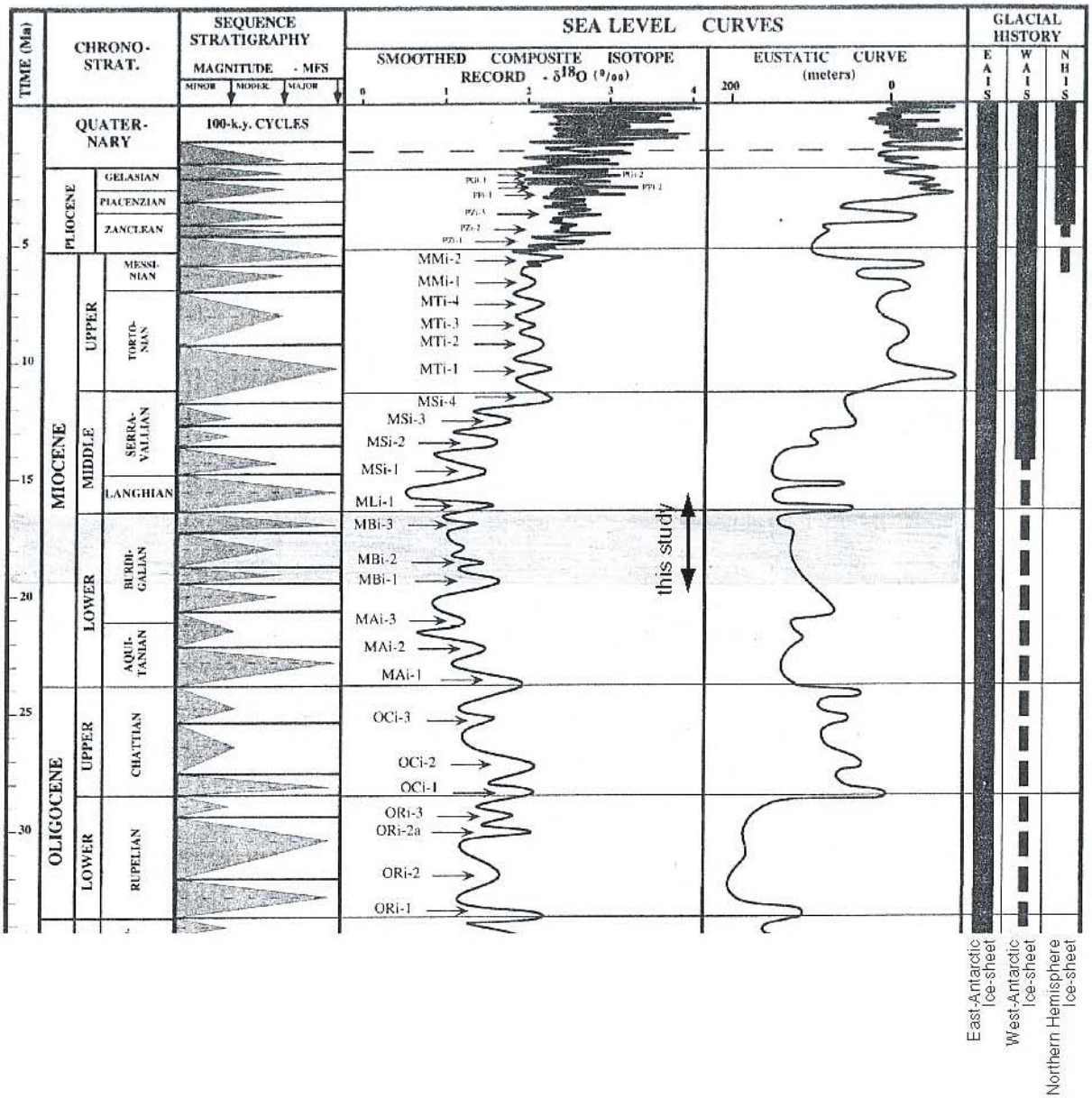

Figure 2.4 Tertiary oxygen isotopes, ice-caps and eustasy (Abreu and Anderson, 1998)

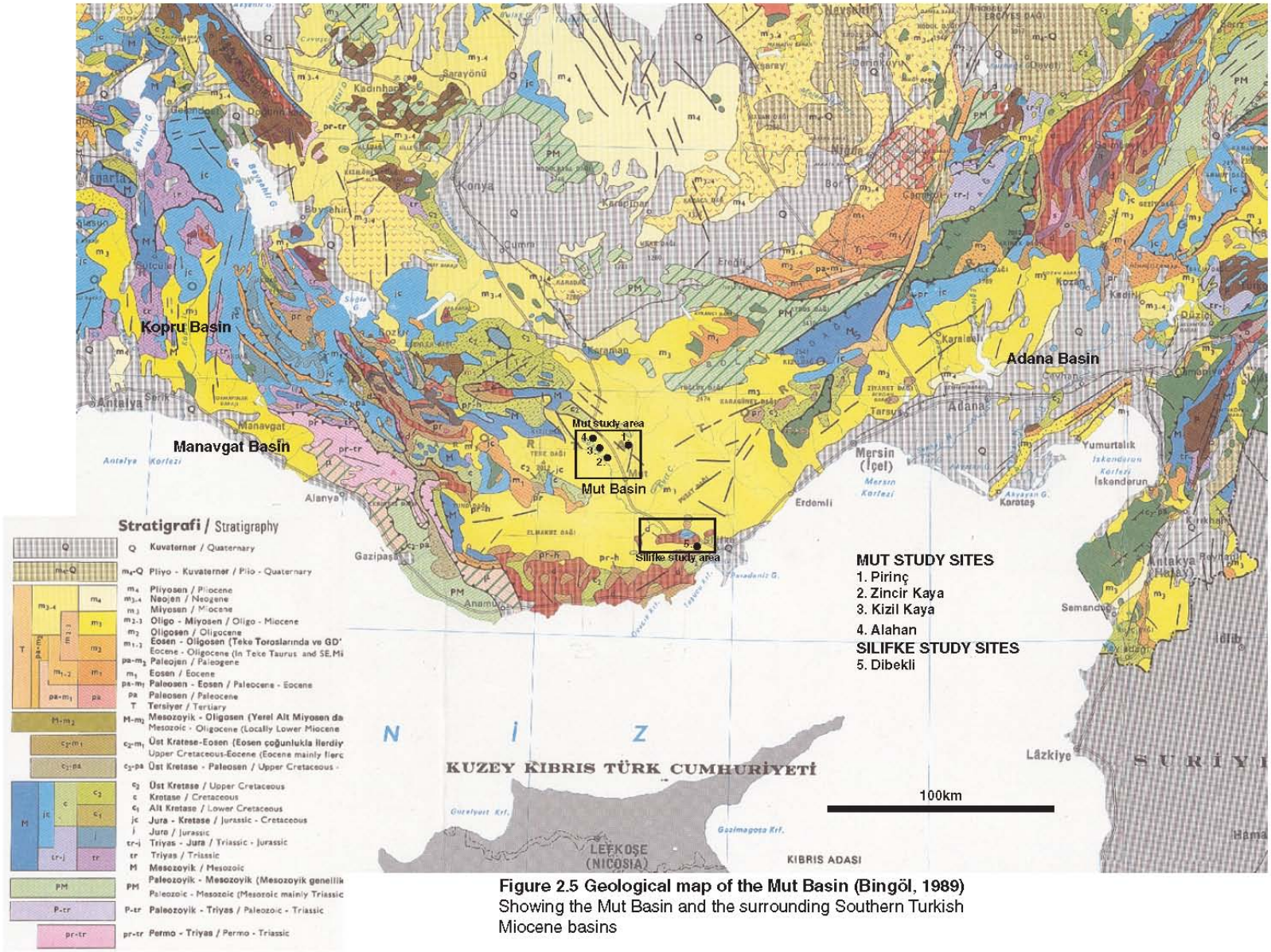

Figure 2.5 Geological map of the Mut Basin (Bingöl, 1989)
Showing the Mut Basin and the surrounding Southern Turkish Miocene basins

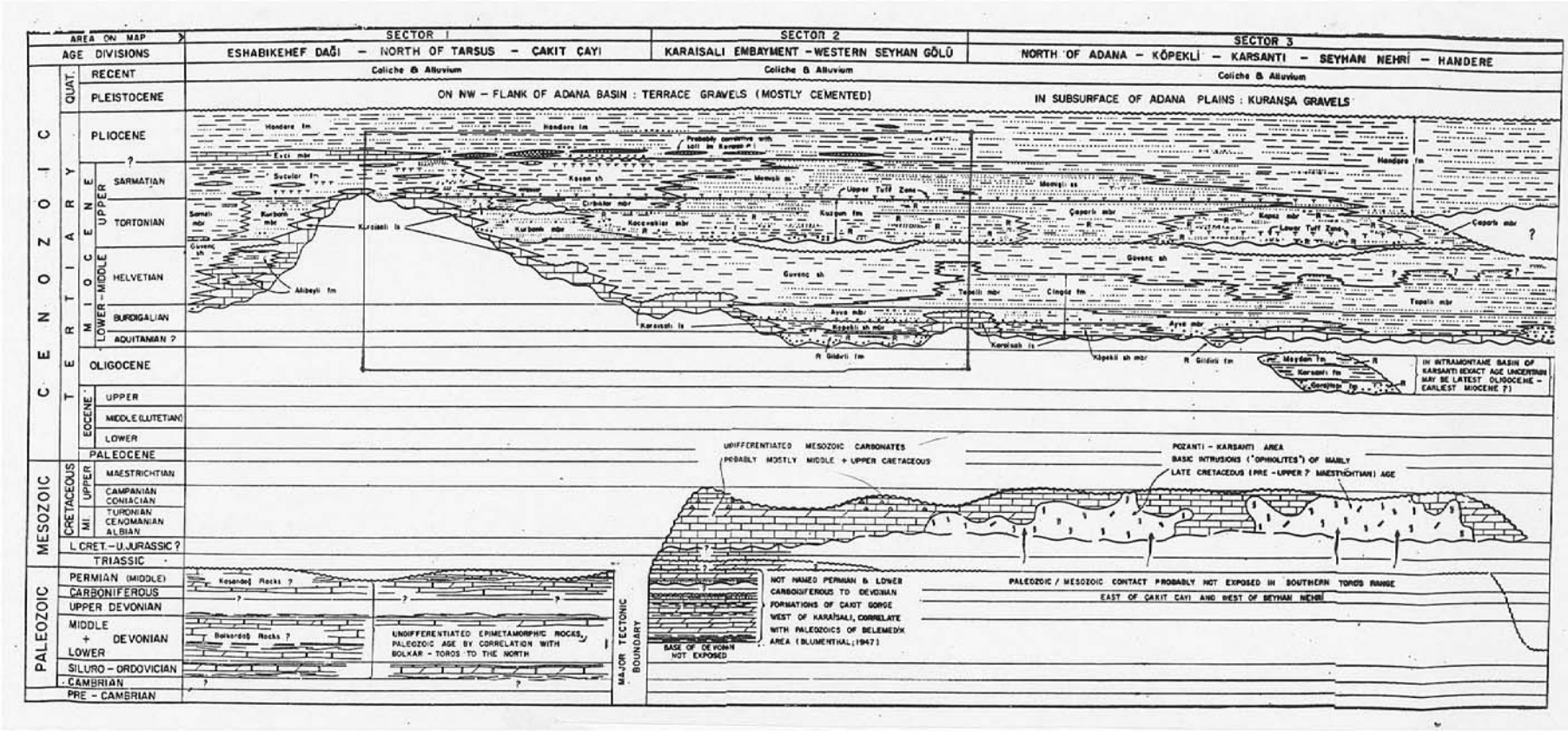

Figure 2.6 Chronostratigraphy of the Adana Basin (Schmidt, 1961)
This illustrates how the Early Miocene limestones onlap a relict topography formed during the Early Tertiary.

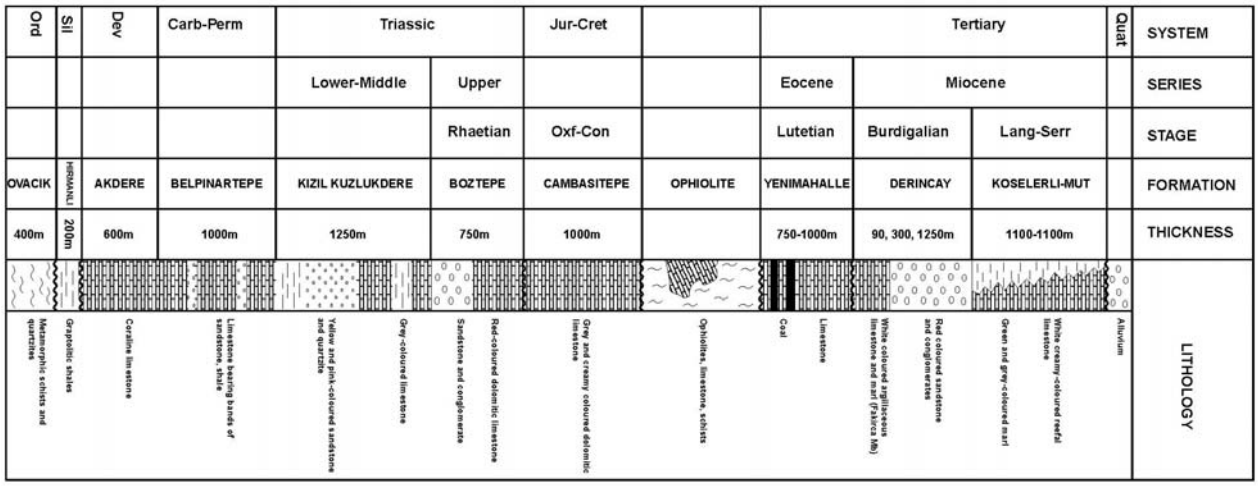

Figure 2.7 Synthetic stratigraphic column for the Mut Basin (redrawn and simplified from Gedik et al. 1979)

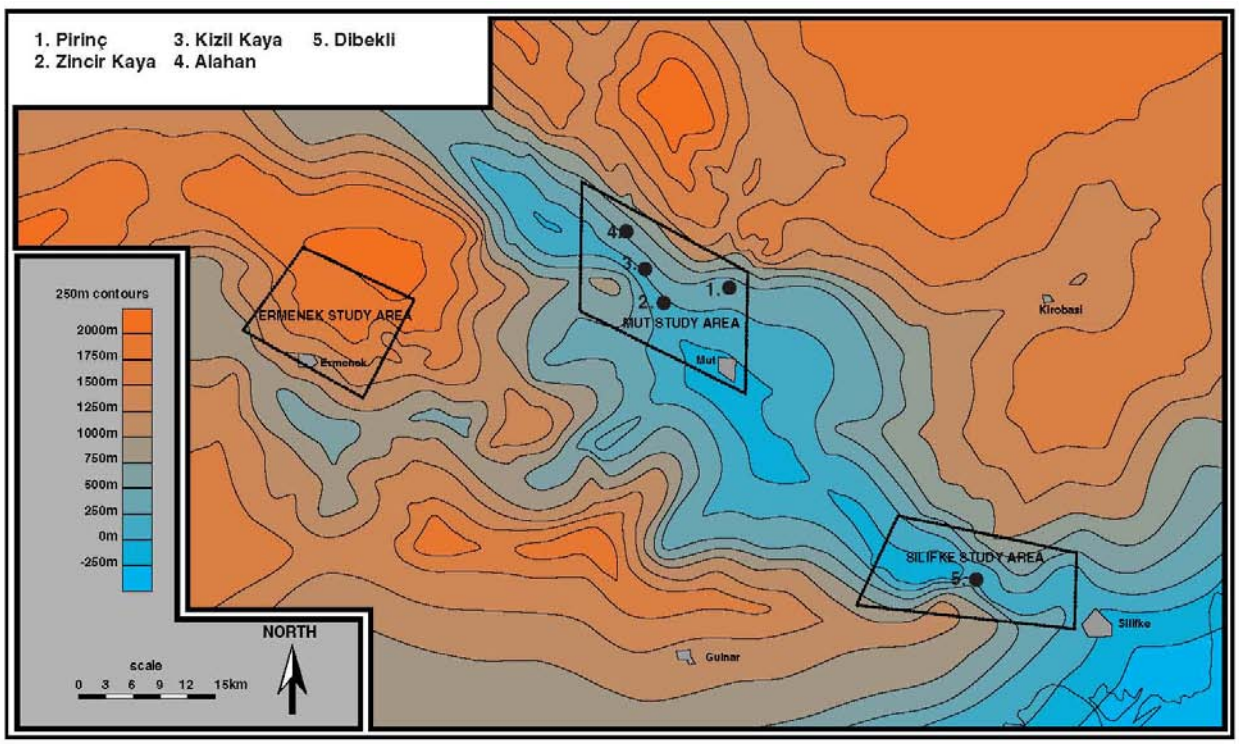

Figure 2.8 Basement topography of the Mut Basin (Gedik et al. 1979)
This map shows the present-day relief of the Pre-Miocene (Pre-Extensional) in the Mut Basin reconstructed from the geological map. The Miocene topography is considered to be similar to this, though the relief has been accentuated since the Miocene by tectonic sagging of the basin area.

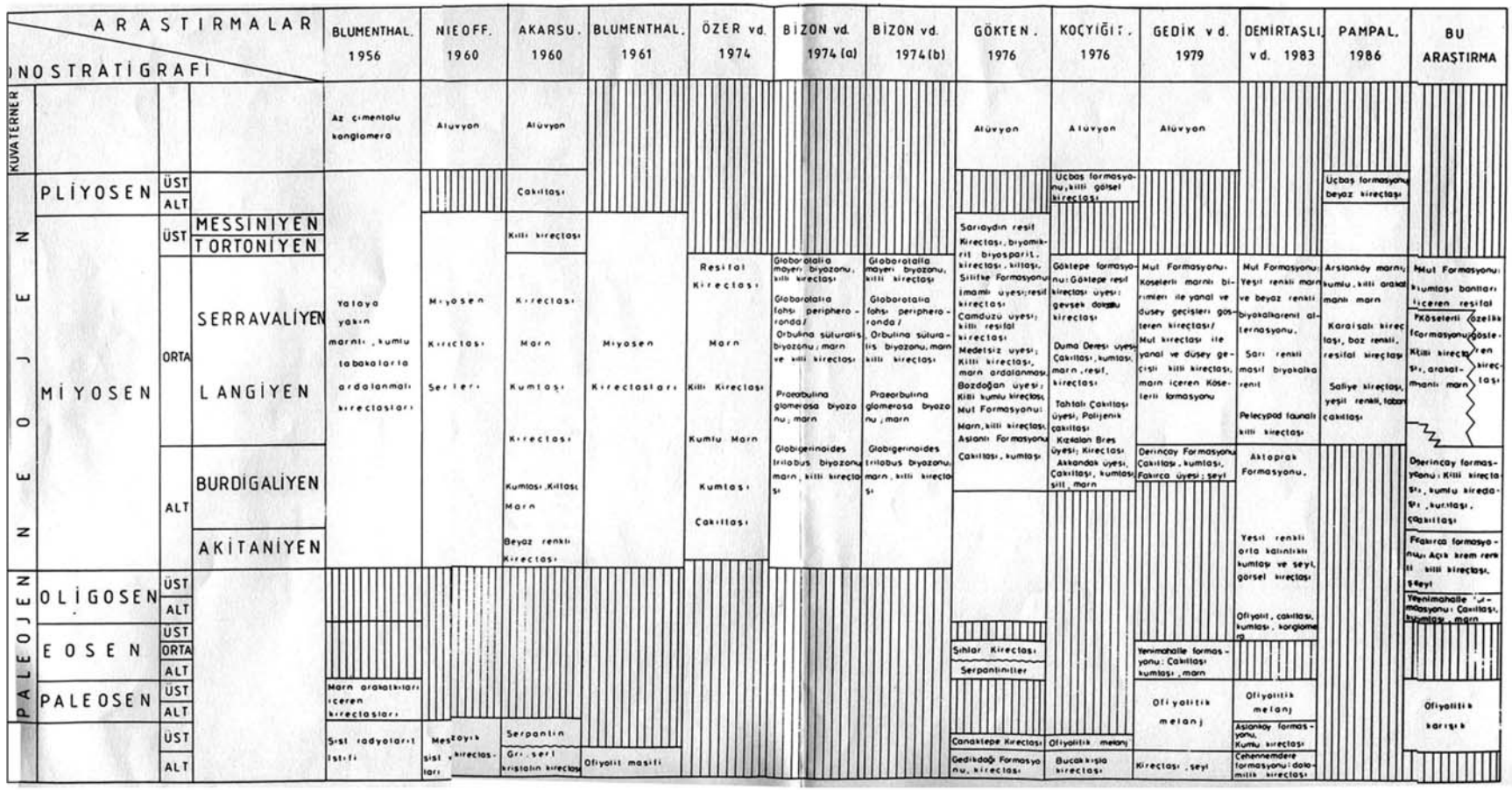

Figure 2.9. *Biostratigraphy of the Mut Basin (Tanar and Gokcen, 1989)*

3 – METHODOLOGY

The approach to describing the general stratigraphy in order to correlate between different parts of the basin is twofold: biostratigraphy defines the major timelines for the broad basin correlations. Sequence stratigraphy then permits the correlation at a resolution greater than that of the biostratigraphy.

3.1 BIOSTRATIGRAPHY

Nannoplankton were principally used to date the sections: the dating was performed by Carla Müller (IFP, Paris) on 145 samples (see figure 4.2). Ages were defined using the nannoplankton stratigraphy of Martini and Müller (1986). The fauna used to define the biozones is illustrated in figure 4.3. This stratigraphy attributes 1.7Ma to the NN4 nannoplankton zone: being the interval of interest in this study. Basinal marls were ideal for this dating, and many slope deposits such as fine packstones also contained sufficient nannoplankton to determine an age. For each data point a relative abundance of nannoplankton is given in order to qualify the validity of the information.

Also, planktonic foraminifera were dated by Roland Wernli (University of Geneva, Switzerland) on 10 samples (see figure 4.2). Ages were determined using the foraminifera stratigraphy in Bolli et al. (1985). The fauna used to define the biozones is specified in figure 4.4. Biozones N7 and N8 are observed in these samples.

Observations were made by the Institute of Palaeontology in Vienna (O.Mandic, pers.com.) concerning the molluscan biostratigraphy of two of the study areas (Pirinç and Alahan, see later), corroborating the other dating methods.

3.2 SEQUENCE STRATIGAPHIC ANALYSIS

This section seeks to define and illustrate the sequence stratigraphic principles that have been applied as a working methodology in this study, and to explain why they have been chosen. It is not intended either to provide a summary of the history and development of sequence stratigraphy, or to enter into arguments of the pros and cons of different models: such discussions can be found elsewhere. The development of sequence stratigraphy can be traced through a number of major publications: Vail et al. (1977), Van Wagoner et al. (1988), Posamentier and Vail (1988), Posamentier et al. (1988), and Van Wagoner et al. (1990) describe the "Exxon School" of sequence stratigraphy, while Sarg (1988) and Handford and Loucks (1993) describe how these concepts can be applied specifically to carbonates. Schlager (1992), Posamentier and James (1993), Emery and Myers (1996), and Miall (1997) provide enlightening syntheses and discussions, while useful concepts for the application of sequence stratigraphy on the outcrop scale are provided by Homewood et al. (1992), and in the congress volume of Eschard and Doligez (1993).

3.3 CYCLOSTRATIGRAPHY

It is important to recognise that astronomical cycles with distinct frequencies can at times be preserved in the stratigraphic record (Gilbert, 1895; Berger, 1988), so that when such cyclicity occurs it can be identified. Orbital forcing, especially in the Milankovitch wavebands (Milankovitch, 1941), has been shown to influence global climate and ocean circulation patterns (de Boer and Smith, 1994). The climatic variations can have a direct expression in the sedimentary record (Bradley, 1929; Fischer, 1964; Van Buchem and McCave, 1989), and may also drive glacio-eustatic cycles during ice-house times by influencing the growth and melting of polar ice-caps (Hays et al. 1976; Imbrie et al. 1984). It is known that an ice-cap existed in the Antarctic (Abreu and Anderson, 1998) during the Burdigalian interval examined in this study, so both a climatic signal, and an astronomically driven glacio-eustatic signal may potentially be preserved here.

However, when considering the interpretation of sedimentary cycles as the result of astronomical forcing, care must be taken, since Algeo and Wilkinson (1988) warn us that: "For many cyclic

sequences, calculation of a Milankovitch-range period may be a virtual certainty, regardless of the actual generic mechanism of cycle formation". So other information needs to be considered to support or reject such an interpretation: for instance, does the hierarchical organisation of the cycles (the scale-ratio) correspond to that expected from astronomical cycles, and can more than one period of cycle corresponding to Milankovitch-periods be observed?

3.4 METHODOLOGY ADAPTED TO OUTCROPS

A working methodology of stratigraphic analysis has been adapted to suit the outcrop quality and the aims of the project. Within this context a tool is required that can combine the facies and geometries information coherently, without forcing the result into a pre-conceived model. Any a priori about the relative importance of climate, eustasy and tectonics must be absent from the methodology chosen.

It is observed that the sedimentary record is often organised into cycles of advancing and retreating facies belts. An advancing (normally seaward-stepping) facies belt has prograding bedding geometries, and a shallowing-up vertical facies evolution. A retreating (normally landward-stepping) facies belt has retrograding geometries and a deepening-up vertical facies evolution. These correspond to retrograding/prograding cycles, and can be recognised from either the facies evolution or the depositional geometries. They serve as the principle starting point from which to develop the methodology. Definitions of the terms used are found in figure 3.2.

Schlager (1993) considers the net balance between the rate of creation of accommodation space (a'), the rate of sedimentation (s'), and the resulting geometries, along a given depositional profile (figure 3.3). If accommodation space is created (a'>0) a number of sedimentary geometries are possible: if a' is greater than s', the geometries will retrograde, or backstep; if a' and s' are equal, the geometries will aggrade; if a' is less than s' the geometries will prograde, with some aggradational component. If accommodation space is neither created nor destroyed (a'=0) the geometries will simply prograde. If accommodation space is destroyed (a'<0) a downward shift will occur and the platform top may be exposed.

Let us now consider the facies evolution on a vertical facies profile. If Walther's Law (Walther, 1894) applies, a sedimentary log in a prograding succession will have a shallowing-up (or proximal trending) facies evolution. A sedimentary log in a retrograding succession will have a deepening-up (or distal trending) facies evolution. If Walther's Law does not apply, and the nature of the facies distributed along a depositional profile changes through time, it may be more difficult to evaluate whether a given vertical facies evolution is deepening or shallowing. The bedding pattern geometries may resolve this problem. Also very different facies can be compared by determining the general depositional environment, and deciding which environment is most distal: this is similar to the facies substitution procedure of Homewood et al. (1992).

Thus cycles of retrogradation and progradation can be defined from either the depositional geometries or the vertical facies evolution, but preferably from both. This allows the construction of cycles from an heterogenous data set, and from partial information, when either the facies or the bedding geometries information is absent. Ideally both informations are available. So to summarise:

Retrogradation corresponds to:

a'>s'

retrogradational depositional geometries,

deepening-up vertical facies evolution.

Progradation corresponds to:

a'<s'

progradational depositional geometries,

shallowing-up vertical facies evolution.

Definition of retrograding/prograding cycles of a carbonate system

Major differences exist between carbonate and siliciclastic systems that need to be considered when defining progradation/retrogradation cycles. In marine siliciclastic systems sediment is normally supplied from outside the study area, by rivers and longshore processes. This means that s' can be defined for the area. However, for carbonate systems sediment is produced locally by organisms, and their production rates are controlled by complex processes involving feedback with the surrounding environment. The s' for a given time period can vary dramatically along a depositional profile, and the stratigraphic response can be very different: retrogradation in one area may be contemporaneous with progradation in another area because of the difference in s'. This has great significance for both the methodology and the interpretations: the definition of retrograding/prograding cycles is not a generality for the whole area, but is an observation of the

stratigraphic organisation in a precise location or outcrop.

Volume and surfaces

Sediment is not deposited simultaneously everywhere: for a given period of time a depositional locus exists that is thick in one area and thins laterally to nothing. Beyond the limits of the depositional locus the time corresponding to the packet of sediment is represented by a surface. This is a temporal hiatus. Such surfaces develop beyond the proximal extremity of the depositional locus because the environment is too shallow and there is no longer any space in which to deposit and preserve sediment. A proximal temporal hiatus is here termed a cycle boundary (CB). A temporal hiatus may also develop in a position that is beyond the distal extremity of the depositional locus, because the environment is too deep, or too far from the source, to receive a significant amount of sediment. Such an hiatus is here termed a maximum flooding surface (MFS). These terms are illustrated in figure 3.5. The cycle boundary normally has a prograding sedimentary packet below and a retrograding sedimentary packet above: the depositional locus must shift in a distal direction (seaward) before a cycle boundary is created in a given area, then to preserve the cycle boundary in the rock record it must be covered by sediment, so the depositional locus must shift back in a proximal direction (landward). The sediment between one cycle boundary and the next one above defines one cycle of retrogradation and progradation. The maximum flooding surface defines the boundary between the retrograding packet below and the prograding packet above.

The lateral time-equivalent of a cycle boundary surface is a packet of sediment that separates a prograding packet below from a retrograding packet above. In this case the exact turn-around from progradation to retrogradation may not be expressed by a surface, but by an interval of sediment. This interval is termed a cycle boundary zone (CBZ) and is illustrated in figure 3.5 (lower diagram showing the chronostratigraphy). This lateral shifting of the depositional locus is similar to the volumetric partitioning described by Sonnenfeld and Cross (1993).

The term cycle boundary is used to distinguish it from the sequence boundary, since they do not always correspond to the same thing. The cycle boundary is placed at the turn around from progradation to retrogradation, which occurs within, or at the top of a lowstand systems tract, whereas the sequence boundary is placed at the base of the lowstand.

Scales of cycle

The concepts presented so far are independent of scale. Sedimentary cycles or sequences are known to occur on a wide range of frequencies ranging from hundreds of millions of years to a few hours. The upper limit on the frequencies potentially observed in the rock record is controlled by the frequency of the blurring function that convolutes the signal (bioturbation, current reworking, diagenesis, etc.). The lower limit is the size of the field of observation, the age of the Earth! The distribution in the time domain of driving forces that act on the stratigraphic record are illustrated in figure 3.4.

The frequency of the cycle that we observe will depend on where the observation is made: figure 3.5 shows how if we inspect log 1 we will see a single large-scale cycle boundary, whereas if we inspect log 2 we will see two distinct smaller-scale cycle boundaries. Remark that the temporal resolution with which we can define a cycle boundary increases proportionally with the period of the cycle we are trying to define. This has implications for the spatial resolution: if we want to define the large-scale cycle boundary in log site 1 there is no problem, since there is only one surface. However, if we want to define the same cycle boundary in log 2 we are confronted with two possible candidates, both smaller-scale cycle boundaries. Two possible choices exist:

1/ if one surface seems more important than the others it may be chosen as the cycle boundary

2/ stacking pattern analysis (Goldhammer et al. 1990) may allow the definition of a larger-scale cycle from the evolution of smaller-scale cycles, by the identification of the convergence of an aspect of the cycle to a specific horizon. Otherwise we must accept that we are unable to choose between them, and a cycle boundary zone (CBZ) is defined that encompasses all the potential candidates (Strasser et al. in press; Pittet, 1996, Hillgärtner, 1999). This concept is illustrated in figure 3.5. The definition of a cycle boundary zone is often the most honest choice, since it expresses the margin of uncertainty within which we work.

3.5 PRACTICAL APPLICATION

The methodology applied in this study as described here is also illustrated as a flow diagram in figure 3.6:

1/ geological mapping: an initial reconnaissance trip defines areas of the basin of potential interest, and possible detailed study sites. The field geological mapping builds on previous maps made of the area (Sezer, 1970; Gökten, 1976; Gedik, 1979) by adding information about the Miocene stratigraphic organisation, including the biostratigraphy. It places areas chosen for detailed study within a more general stratigraphic context.

2/ bedding geometries descriptions: the bedding patterns of areas chosen for detailed study are examined and sedimentary packets are defined. These

packets are bound by surfaces, and possess a characteristic internal bedding geometry. This is done in the field from sketches and photographs, and in the office from photographs. It is important to return to the field to re-assess the geometries described as the understanding of the outcrop progresses. Field measurements of length, height and angle are also made across the outcrop. From this information cycles of progradation and retrogradation can be defined.

3/ facies descriptions: measured sedimentary logs are made at key areas on the outcrop. It is important to measure the thicknesses carefully in order to accurately reconstruct the outcrop. Facies are identified and classified. To help in this facies analysis samples are studied in thin section. A semi-quantitative approach is opted for, in which the relative abundances of the important faunal elements are given a value from 1-5, 5 being the most abundant, and 1 being simply present. The microfacies have been sometimes documented by making a scanned image (in positive transmitted light) of the complete thin section: this has the advantage of illustrating the centimetre-scale sedimentary textures found. The nature and importance of different types of surfaces are recognised. Shallowing and deepening trends are identified in the logs, and this defines shallowing/deepening cycles of different scales.

4/ construction of stratigraphic cross-section: the geometrical and facies information are then combined to define cycles of retrogradation and progradation on different scales, and a stratigraphic cross-section is constructed of the outcrop showing the facies distribution, the bedding patterns and the positions of the cycle boundaries.

5/ feedback: the construction of the stratigraphic cross-section involves the assessment and comparison of large amounts of data, and an iterative convergent process is implicitly applied to arrive at the best-fit solution for the definition of cycles and the integration of the different data sets into a coherent story. This often involves a re-examination of the data and the outcrop.

Diagenesis: examination of the diagenetic environments of these sediments was not included in this study. However, spot observations of cement types and dissolution fabrics have been made during the microfacies analysis of the thin-section samples, and these have been described in the text where relevant. It must be stressed that a full diagenetic study would be necessary to make valid conclusions.

Figure 3.1: legend

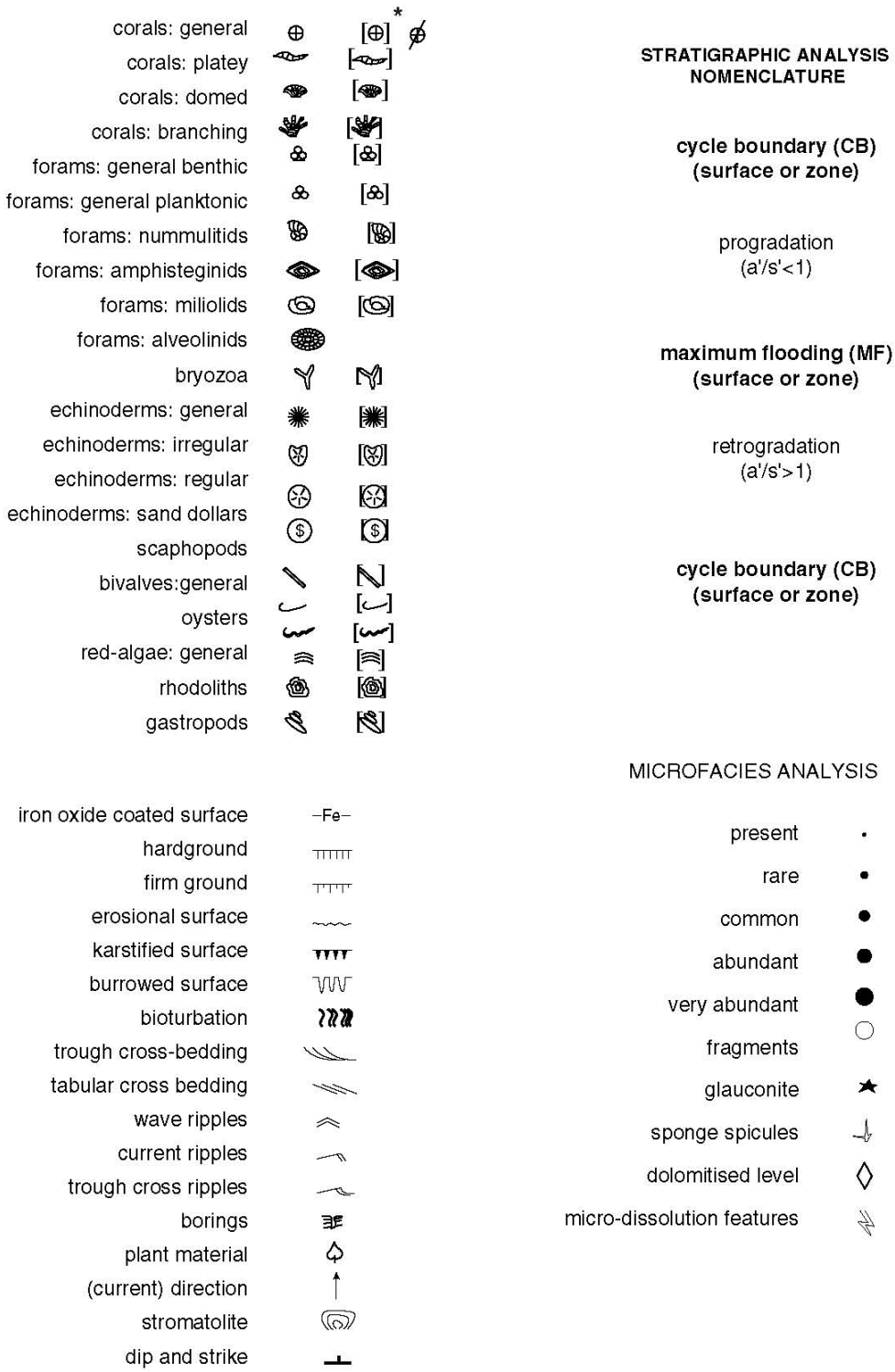

*Brackets or slash indicate fragments

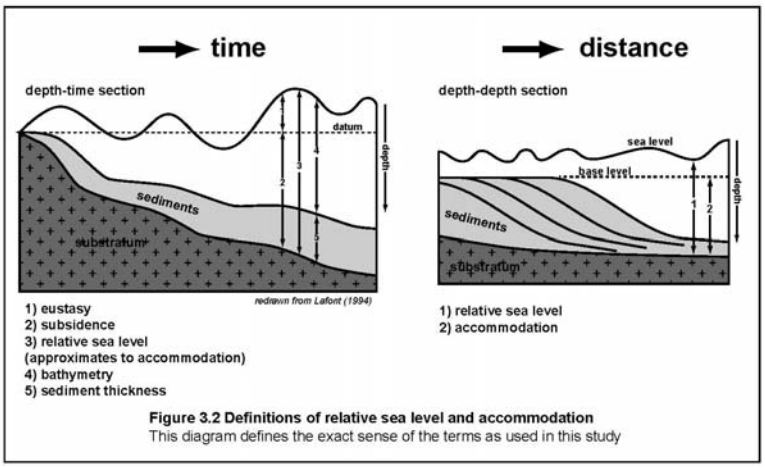

Figure 3.2 Definitions of relative sea level and accommodation
This diagram defines the exact sense of the terms as used in this study

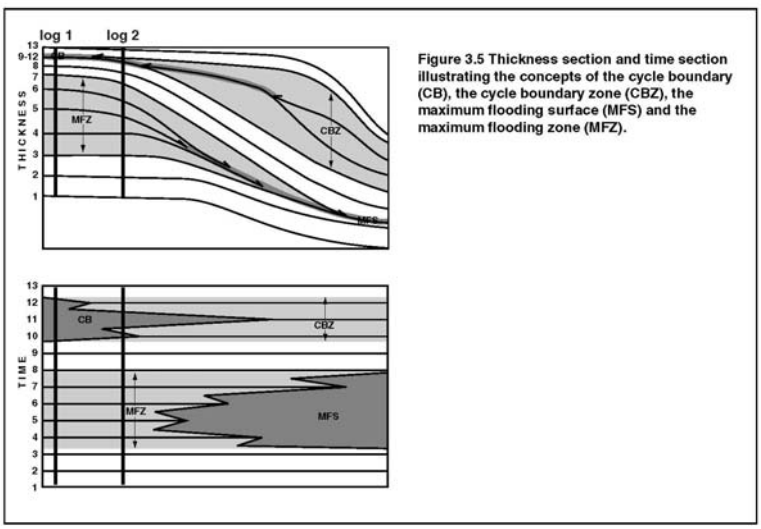

Figure 3.5 Thickness section and time section illustrating the concepts of the cycle boundary (CB), the cycle boundary zone (CBZ), the maximum flooding surface (MFS) and the maximum flooding zone (MFZ).

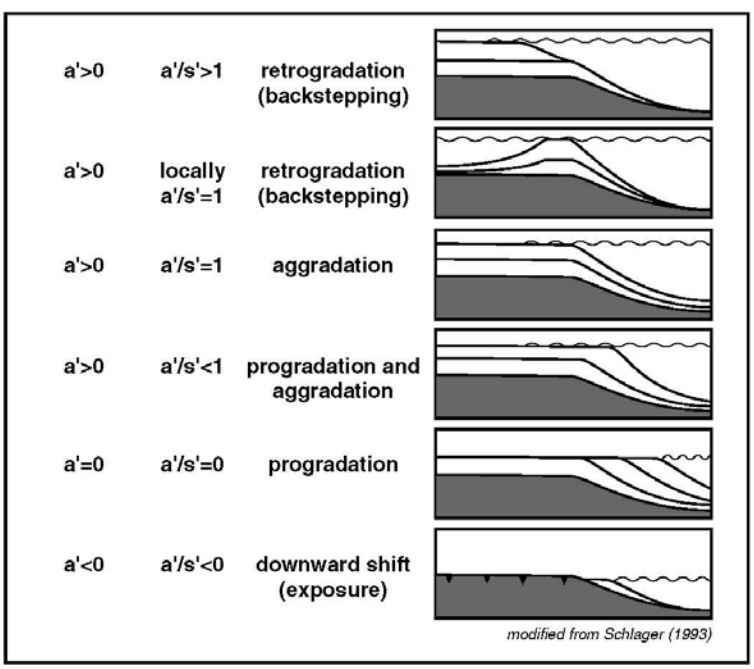

Figure 3.3 Sedimentary geometries from the accommodation/sedimentation rate ratio

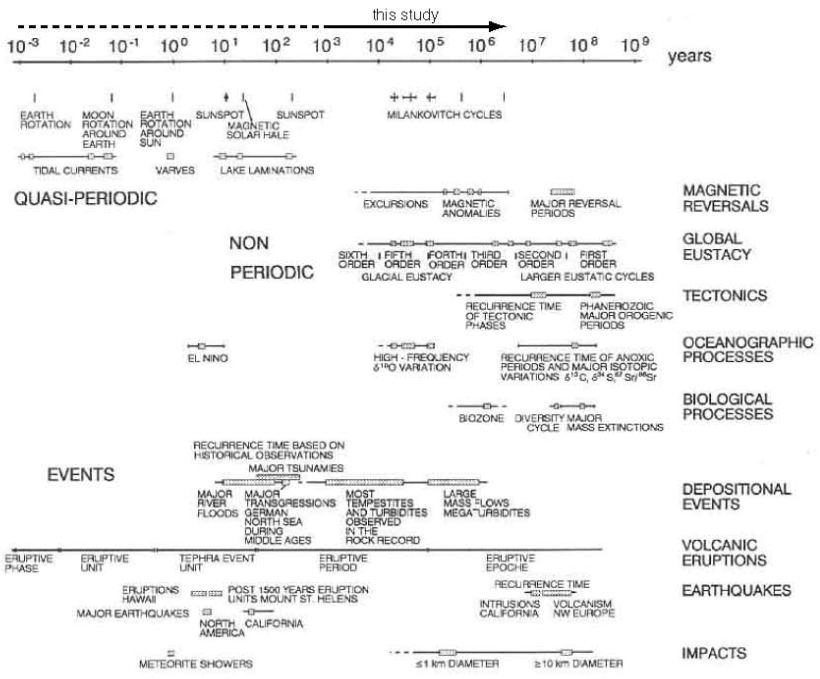

Figure 3.4 Process distributions in the time domain (from Einsele et al. 1991)
This diagram shows how the factors influencing the stratigraphic record can be alloted characteristic bandwidths in the time domain

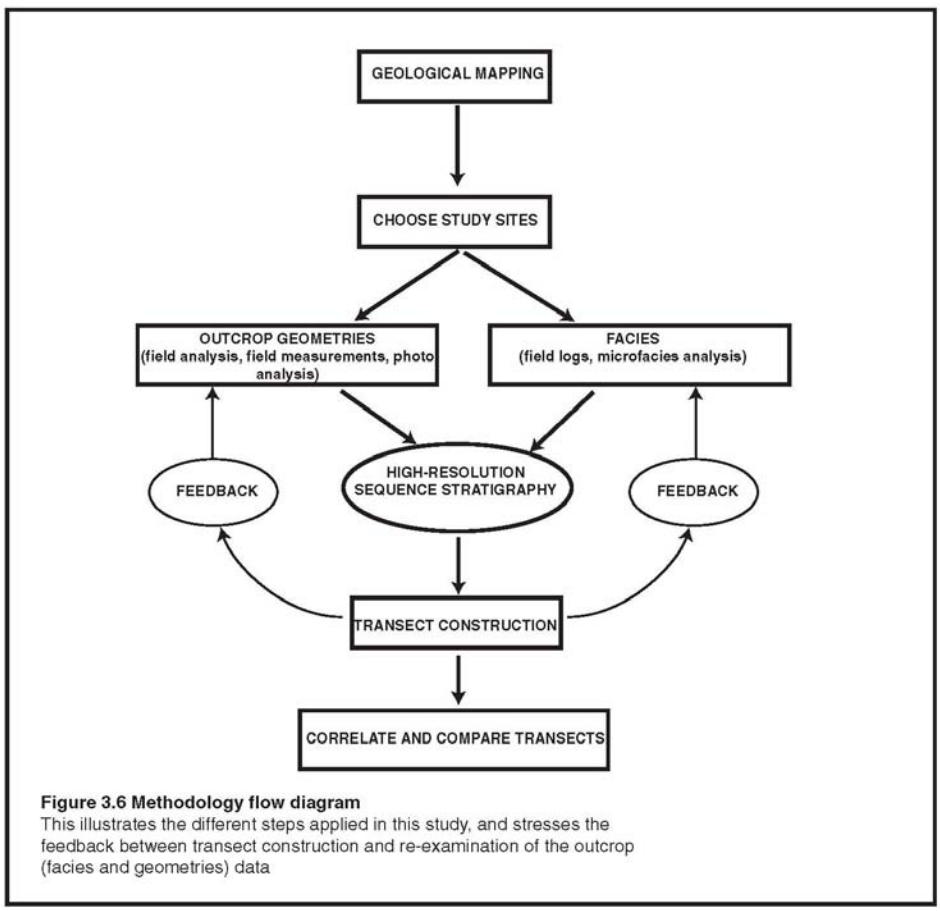

Figure 3.6 Methodology flow diagram
This illustrates the different steps applied in this study, and stresses the feedback between transect construction and re-examination of the outcrop (facies and geometries) data

4 - MAPPED AREAS

4.1 INTRODUCTION

Presentation of data set

During this study a total of 3280m of measured sedimentary log was described in 46 sections ranging from 5m to 512m in length (figure 4.1). 722 hand samples were taken, of which 400 were studied in thin section. 145 samples were analysed for the nannoplankton biostratigraphy (figure 4.2), and 800 sq.km of the basin were geologically mapped.

LOCATION	LOG NO.	THICKNESS (m)	NO. OF SAMPLES
SILIFKE			
Dibekli	3	250	60
Goksu Bridge	2	112	46
xbedding-m	4	41	6
xbedding-e	9	83	20
xbedding-m	10	43	12
xbedding-w	11	62	10
Barbarossa cafe	12	25	10
x-bedding-e	50	43	1
x-bedding-w	52	66	10
MUT			
Alahan	7	512	141
Kizil Kaya	24	102	9
	25	16	11
	26	16	3
	28	54	16
	29	24	10
	30	6	5
	31	11	4
	32	7	3
	33	9	0
	34	30	18
	35	31	27
	36	9	1
	37	17	0
	38	45	0
	54		25
Pirinc Suyu	14	190	8
	15	102	6
	16	120	31
	17	87	14
	18	11	5
	19	5	4
	20	97	10
	21	32	5
	22	70	14
	23	165	14
	45	17	0
Zincir Kaya	39	29	2
	40	39	23
	41	17	9
	42	16	3
	43	23	0
	44	20	0
	55		27
ERMENEK			
	1	262	52
	5	230	31
	6	200	26
TOTAL		3346m	732

Figure 4.1. *Log data list.*

1/ During the first year a general reconnaisance was made of three areas: Silifke, Mut and Ermenek. Figure 4.5 and figure 2.8 show the locations of the study sites. Long sedimentary logs were described in the field to define the general stratigraphy. The initial marine flooding in each area occurs in the Upper Burdigalian (NN4 nannoplankton biozone). In the Silifke area the stratigraphy is described up to the Langhian (nannoplankton zone NN5, see log 2). In the Mut area the stratigraphy possibly goes up to the Serravalian (nannoplankton zones NN6/7, but poor samples since they are in a shallow marine facies, see log 7), and definitely as young as the Langhian (NN5). In the Ermenek area the timing of the initial marine flooding is indicated by a single poor (NN4) Upper Burdigalian sample (see log 6), though Demirel and Koksoy (1992) tell us that the Lower Miocene is lacustrine and the marine flooding started in the Middle Miocene (Langhian). This difference in dating might be resolved by considering that the very top of

the NN4 biozone is situated in the Langhian. Most of the stratigraphy described in the Ermenek area is Langhian (NN5, log 5), though some poor samples indicating the Serravalian are found (NN6, log 6). Spot sampling across the basin identified the highest (youngest?) marls discovered (on the Gülnar plateau, on the southern flank of the basin) as being of Serravalian/Tortonian age (NN9).

2/ It was decided at the end of the first year that three areas were beyond the scope of this study, so Mut and Silifke were chosen in which to continue the work. The Ermenek area is not presented here. The Ermenek Langhian platform stratigraphy was chosen for study by a team of geologists from the IFP, TOTAL, and Elf (the "ARTEP" project), and this is currently in progress. A second study in this same area is now the subject of an ongoing PhD study by Xavier Janson, under the supervision of Gregor Eberli. Geological maps were made of the areas of Mut and Silifke: these are presented in figures 4.6 and 4.8.

3/ In the Mut area two major cross-sections were described (Pirinç Suyu and Alahan, see figure 4.6 for the location) while in the Silifke area one major cross section was described (Dibekli, see figure 4.8 for the location). These three sections were chosen because they:

a/ demonstrably covered the same interval of time, and

b/ contained very different settings, in terms of hydrodynamic regime, palaeotopography and clastic input.

4/ Two additional sites were then chosen for more detailed examination in the Mut area. A distinction can be made between the sites situated on the edges of the basin (Alahan and Pirinç), and two sites situated on a marginal shelf in the basin, where small isolated platforms develop (Zincir Kaya and Kizil Kaya). It is these platforms that form the object of a detailed study. They are located on figure 4.6.

LOG	SAMPLE	BIO-ZONE	ABUNDANCE	FORAMS	COMMENTS	LOCATION
SILIFKE						
log 2	2.5b(II)	nn5	poor			Sil: Goksu bridge
	2.23b	nn5	rich		sponge spicules	"
log 3	3.11b	nn4	rich			Sil: Dibekli
	3.15b	?	v.rare	N7		"
	3.20b	?	v.rare			"
	3.21b	nn4	rich	N7	diatoms	"
	3.36b	?	v.rare			"
	3.37b	nn4	rich	N7-N8		"
	3x1	nn4	poor		diatoms/sponge spics,	new samples taken during Oct 97
	3x2	nn4/5	poor		cold water, upwelling	"
	3x3	nn5	rich	N8	"	"
	3x4	nn5	rich	N8	"	"
	3x5	nn5	poor		"	"
log 8	8.15b	nn5	v.poor			Sililfke: Erenteri outcrop
log 9	9.4b	nn4	poor		sponge spicules	Silifke: east end of valley, north of river
	9.5b	nn4	poor		sponge spicules	"
	9.7b	nn4	poor		sponge spicules	"
	9.9b	nn4	poor		sponge spicules	"
	9.20b	nn5	v.poor			"
log 10	10.1b	n/a	barren			Silifke
	10.11b	n/a	barren			"
	10.12b	nn4	poor?			"
log 11	11.1b	(nn6?)	v.poor			Silifke
	11.3b	?	v.poor			"
	11.10b	?	v.poor			"
log 12	12.6b	nn4	poor			Silifke
	12.10b	nn4	poor			"

LOG	SAMPLE	BIO-ZONE	ABUNDANCE	FORAMS	COMMENTS	LOCATION
log 52	52.1b	nn4	v.rich			Sil: midway
	52.2b	nn4?	v.rich			"
	52.3b	nn4	rich-average			"
	52.11b	nn5	"			"
	52.12b	nn5	"			"
	52.13b	nn5	"			"
	52.14b	nn5	"			"
	52.15b	nn5	"			"
	52.16b	nn5	"			"
log 60	60.1b	nn4	v.rich			Silifke: w.end, see map
	60.2b	nn4	v.rich			"
Seyhler	S1	n/a	barren			Sil: Seyhler cliff
	S2	n/a	barren			"
	S3	nn5	v.poor			"
	S4	nn5	v.poor			"
	S5	nn5	v.poor			"
	S6	nn5	v.poor			"
	S7	nn5	v.poor			"
	S8	nn5	v.poor			"
	S9	nn5	v.poor			"
	S10	nn5	v.poor			"
MUT						
log 7	7.1b	nn4	v.poor			Mut: Alahan section
	7.3b	nn4	v.poor			"
	7.4b	nn4	v.poor			"
	7.6b	nn4	v.poor			"
	7.58b	nn4	v.poor			"
	7.59b	nn4 (?)	v.poor			"
	7.75b	nn4 (?)	v.poor			"
	7xb	n/a	barren			"
	7xa	nn4	poor			"
	7xc	n/a	barren			"
	7.80b	nn5	v.poor			"
	7.101b	nn5	v.poor			"
	7.108b	n/a	barren			"
	7.109	n/a	barren			"
	7.118b	n/a	barren			"
	7.119b	nn5	v.poor			"
	7.120b	?	v.poor			"
	7.122b	n/a	barren			"
	7.127b	nn6	v.poor			"
	7.133b	n/a	barren			"
	7.137b	nn6/7	v.poor			"
	7.139b	n/a	barren			"
	7.141b	n/a	barren			"
	7.201b	nn4?	v.poor		reworked	"
log 61	61.1b	nn4	rich		rich in 2° dolomite	Mut: road above Pirinç outcrop: 780m
	61.2b	nn4	rich		"	": 825m
	61.3b	nn5	rich			": 890m
	61.4b	nn5?	poor			": 960m
	61.5b	n/a	poor			": 1030m

LOG	SAMPLE	BIO-ZONE	ABUNDANCE	FORAMS	COMMENTS	LOCATION
	61.6b	n/a	poor			": 1060m
	61.7b	nn5	rich			": 1220m
log 62	62.1b	n/a	barren			Mut: delta front-Derincay Fm. (looking for nn3)
	62.2b	n/a	barren			"
	62.3b	nn4	average			"
	62.4b	n/a	barren			"
	63.5b	n/a	barren			"
	62.6b	n/a	v.poor			"
	62.7b	n/a	v.poor			"
Pirinç	P1	nn5	v.poor			Mut: Pirinç Suyu: looking for nn4/nn5
	P2	nn4	rich			"
	P3	nn4	rich			"
log 16	16.1b	nn4	rare	N7	small nannos, shallow	Pirinç Suyu: southern log
	16.14b	nn4	v.rare	N7	strong diagenesis	"
	16.20b	nn4	rare	N7		"
	16.23b	nn4	rich	N7	increasing water depth	"
	16.29b	nn4	v.rich	N7		"
log 24	24.3b	nn4	v.rare		small nannos, shallow	Kizil Kaya: west end
	24.7b	nn4	average		slightly deeper	"
	24.8b	nn4	rare			"
	24.11b	nn4	rare			"
ERMENEK						
log 5	5.1b	nn5	poor			Ermenek: valley 1, basinal section
	5.13b	nn5	rich			"
	5.14b	nn5	rich			"
	5.15b	?				"
	5.16b	?				"
	5.18b	nn5	rich			"
	5.19b	?				"
	5.20b	?				"
	5.21b	nn5	rich			"
	5.23b	?				"
	5.24b	nn5	poor			"
log 6	6.3b	nn4	poor			Ermenek: hill north-east of Ermenek
	6.17b	nn5?	v.poor			"
	6.18b	?	poor			"
	6.20b	nn6?	poor			"
	6.21b	n/a	barren			"
	6.22b	?	v.poor			"
	6.23b	?	v.poor			"
DIVERSE						
spot samples	bio 1	n/a	barren			Erm: bridge at bottom of basin
	bio 2	nn9	rich		nn3/4 reworked	Gulnar: high plateau
	bio 3	n/a	barren			Sil: road to Mut, N of Gulnar turnoff
	bio 4	nn5	rich			SII: road to Mut, below top slump
	bio 5	nn5	rich			SII: road to Mut, below lower slump
	bio 6	nn4	rich			Sil: road to Mut, Barbarossa site
	bio 7	nn4	poor			Sil: road to Mut, Barbarossa café

LOG	SAMPLE	BIO-ZONE	ABUNDANCE	FORAMS	COMMENTS	LOCATION
	bio 8	nn4	poor			Sil: Karakacili just above first cliff
	bio 9	nn5	v.rich			Sil: Karakacili just above slump
	bio 10	nn5	poor			Sil: Karakacili 1km up, after bend
	bio 11	nn5	poor			Erm: road to Bijou valley between hills
	bio 12	nn5	v.poor			Erm: road to Bijou valley, marl fields
	bio 13	(nn4)	v.poor		reworked?	Erm: bottom of basin, brown clastics
	bio 14	n/a	barren		reworked	"
	bio 15	nn5	v.rich			Erm-Gulnar: collapsed valley, top west side
	bio 16	nn5	v.rich			"
	bio 17	nn5	v.rich			"
	bio 18	nn6	rich			"
	bio 20	nn4	rare			Sil-Mut road, on top of faulted gorge
	bio 21		barren			Sil: Seyhlar, highest marls
	bio 22	nn4	rare			Mut: base of 7.1 below delta in shallow marls
	bio 25	nn4	rich			Mut-Karaman, first marls out of town
	bio 26	nn4	rich			Mut-Kirobasi: quarry in Mut below reefs
	bio 27	nn3	poor			Mut town, sandy marls beneath castle
	Kale_1	n/a	barren			Mut town, sandy marls just below castle
	bio 28	nn4	rich			Mut-Karaman: marls above basin reefs
	bio 29	(nn3)?			reworked	Erm: above Bijou valley
Limonlu	130m	nn4	poor			Limonlu (Adana-Silifke): 130m altitude
	1330m	nn5	average			": 1330m altitude

***Figure 4.2**. Biostratigraphic data.*

4.2 MUT AREA

The Mut geological map is presented in figure 4.6. Certain definitions of stratigraphic units are originally by Sezer (1970) or Akarsu (1963), but reference is made back to the more recent synthesis of Gedik et al. (1979). The following units have been used for the purposes of this study:

Basement Unit (Bu): all the units dating from before the Oligocene opening of the Mut Basin are grouped together under this title (see also Gokten, 1976). They include the Yenimahalle Formation (Eocene limestone), Ophiolitic Melange (Cretaceous-Eocene?), the Cambasitepe Formation (Jurassic dolomitic limestone), the Belpinar Formation (Permian-Carboniferous limestone), the Akdere Formation (Devonian limestone), the Hirmanli Formation (Silurian black shales) and the Ovacik Formation (Ordovician metamorphic schists) (Korkmaz and Gedik, 1990; Gedik et al. 1979). In the Mut region they outcrop principally in the Pirinç Suyu valley area and around Mahras Dagi. The isobath map of the top of this basement is shown in figure 4.6. It has a maximum altitude of 1100m within the Mut region mapped, but rises up to 2000m elsewhere on the flanks of the Mut Basin (Gedik et al. 1979). The lowest altitude in the Mut area mapped is less than100m (lowest point in the region is in the Goksu river bed that cuts down to this altitude, see the geological map figure 4.6).

Continental deposits

Derinçay Formation (D): this formation consists of red continental muds and sands. They have a maximum thickness of over 250m. The fluvial environment dominates, with channel sand and gravel deposits up to 5m thick interbedded with large amounts of red floodplain clays. The clay/sand ration is very high. A variety of fluvial settings was observed, but no detailed work has been done on this formation in this study. Other environments have also been observed, namely coarse grained alluvial fan systems, and the lacustrine deposits of the Fakirca Member (see lithostratigraphic diagram in figure 2.7). The siliciclastics are heterolithic and come from the erosion of the Basement Unit in the hinterland. The Derinçay Formation, has been dated with ostracods as Late Oligocene-Burdigalian in age by Tanar and Gökçen (1990). They consider the Fakirca Member as a separate formation distinct from the Derinçay Formation, but for the purposes of this study, Gedik et al.'s (1979) definition of the Fakirca as a member of the Derinçay Formation is used.

The top of the Derinçay Formation is contoured out in the figure 4.7. The top surface undulates and slopes south-southwest, with a maximum altitude of 700m in the north, disappearing into sub-crop to the south below 150m (see also cross-sections on the geological map, figure 4.6). An isopach map has been generated in figure 4.7 by deducting the Basement Unit isobaths from the Derinçay isobaths. This shows a maximum thickness of greater than 250m, filling a southeast trending elongate cuvette which opens out to the southeast.

Derinçay Formation, Fakirca Member (Df): defined by Gedik et al. (1979), this is considered by him to be a member of the Derinçay Formation. It consists of grey to white finely laminated marls with plant material and is void of marine fauna. It contains freshwater ostracods and is considered to be a lacustrine deposit (G. Kelling, pers. com.). An homogenous red clay found near 305620 (see figure 4.6: to the northeast of Terebelen) is also included in this Member. Tanar and Gökçen (1990) date this as Late Oligocene-Early Miocene (Aquitanian) and place it as older than the fluvial deposits of the Derinçay Formation. This is in agreement with the stratigraphic position as observed in the field. The maximum thickness of this member is estimated from the cross sections to be at least 100m.

Marine deposits

Mut Formation (M): it corresponds to the definition of Gedik et al. (1979). These have a maximum thickness of 1100m (Gedik et al. 1997). Shallow marine limestones are dominated by coralline red algae, Porites corals, large benthic foraminifera and molluscs. The textures are very variable, from diverse boundstones, rudstones, floatstones and grain-, pack-, and wackestones. A shelly mud-dominated facies is also included in this formation at the base (see Transitional Member below). This Mut Formation has been dated with nannoplankton as ranging from NN4-NN6/7 (Burdigalian-Serravalian) in the Mut region, and dates as young as NN9 have been found elsewhere, in the region of Gulnar to the south (sample: bio2). Dating is done either from the Mut Formation itself, or from marls of the Koserlerli Formation (see later) that can be followed physically into the Mut Formation limestones.

Mut Formation, Transitional Member (Mt): this is a new member, defined in this study. It contains a variety of lithologies: white, grey, and brown clays, marls and fine sands often interbedding with red fluvial sands and clays as well as with gravels and thin coral beds. It has an average thickness of 40m (see log 24 in Kizil Kaya outcrop), and thickens to the south-east of the Mut area. Diagnostic characteristics of this member are the high clay content and the presence of molluscs typical of a shallow marine littoral to sub-littoral environment (Schlaf et al. 1997). This unit shows a general deepening up trend, and represents the transition from a continental to a fully marine, carbonate dominated environment. It can be up to 40m in thickness (see log 24). Rare nannoplankton can be found in some levels, and these give a NN4 age (Upper Burdigalian). This is a previously undefined unit, and is here considered as being a member of the Mut Formation, due to its dominantly marine nature.

Mut Formation, Isolated Platforms Member (Mi): this is a member of the Mut Formation, and it shares the same lithology. It has a maximum thickness of 100m. It is a specific level (age NN4) of small isolated platforms that develop and are overlain by deep marine marls of the Koserlerli Formation (see below). This is a previously undefined member. Its creation is of practical use to the Miocene stratigraphy in this study.

Alahan Formation (A): this formation is defined in this study, and was previously considered part of the Mut Formation by Gedik et al. (1979). They are marine siliciclastic deposits which interbed with the shallow-platform limestones of the Mut Formation in the northwest corner of the mapped Mut region. They consist of diverse facies, including lower shoreface/offshore sandy muds, upper shoreface/foreshore sands, and coarse-grained gravels and conglomerates rich in shallow marine molluscs (mainly oysters) and echinoids (mainly Clypeaster), interpreted as being shallow-marine fan delta deposits.

Koserlerli Formation (K): this formation has previously been described by Gedik et al. (1979). Grey to white marls rich in planktonic foraminifera, nannoplankton and Pteropod gastropods, as well as other small molluscs, and concentrations of small infaunal echinoids (Schizaster, among others). These are considered to be deep water deposits. They share the same ages as the Mut Formation previously described.

Koserlerli Formation: Slump Member (Ks): this is a previously undefined unit. Different lithologies can be found within the slump deposits, but they are mainly formed of Mut Formation limestone and Koserlerli Formation marls. The diagnostic feature is the mechanical disruption evident within these deposits, caused by diverse processes of slumping, sliding and collapse. This can take the form of plastic or rigid deformation within the beds. A good outcrop may often be required to categorically say that an interval is slumped, since the overall form and limits of the deposit need to be visible: sometimes a slump is recognized simply by a small amount of deformation below a slipped basal contact, while the crumpled nature of the deformation may be clearly expressed laterally. The slump deposits are often to be found encased above and below in marls. Thicknesses can reach up to 50m. They are found to belong to the NN4 and NN5 nannoplankton zones (Upper Burdigalian and Langhian).

Summary of Mut area

The mapping study has shown:

1/ The pre-Miocene basement topography has a dramatic relief rising from below 100m altitude to over 1100m in the mapping area at the present day (and 2000m elsewhere on the basin flanks, Gedik et al. 1979).

2/ The Derinçay Formation partly fills this relief with over 250m of syn-extensional continental sediments of a diverse nature. The top of this formation rises from 300m to 700m, indicating a possible post-depositional tectonic deformation. These continental deposits form a wide delta-top area in the north-west corner of the basin. The delta-top edge is approximately defined by the increase in thickness of marine sediments of the Transitional Member of the Mut Formation to the south-east. It is this morphology that provides a shallow marine shelf on which the isolated platforms of the Mut Formation (Mi) develop during the initial marine flooding in the Burdigalian.

3/ Two sites of interest are observed in the Mut limestones. A carbonate dominated area along the northern margin, and a mixed siliciclastic/carbonate area in the north-west of the mapping region. The presence of a major river system is indicated by the continual arrival of siliciclastic sediments throughout the Burdigalian marine flooding.

4/ The presence of significant slump deposits near the margins to the north.

5/ A post-Burdigalian tectonic tilting or sagging of the Isolated Platforms Member has been observed, creating a drop of over 400m in the space of 4km in the north of the mapped area. No faulting has been observed associated with this sagging. This accentuates the original basement topography.

4.3 SILIFKE AREA

The same Formation names as in the Mut area are used in the Silifke region. However, there are some differences: neither the Fakirca Member (Derinçay Formation), or the Isolated Platform Member (Mut Formation) are found in this area, and a new unit, the Cross-bedded Member of the Mut Formation, is defined. The stratigraphic units found are as follows (figure 4.8).

Basement Unit (Bu): the different formations comprising this unit have not been distinguished in this study. They have been described by Gökten (1976) and Gedik et al. (1979). The present-day basement topography is contoured in figure 4.9.

Derinçay Formation (D): this Formation is dominated by alluvial fan conglomerates in this region. The isobath map of the top of this unit, and the isopach map are shown in figure 4.9. These indicate a maximum thickness of 300m.

Mut Formation (M): this is the same as defined above. However, it contains a new member, undefined in the Mut area (the Cross-bedded Member, Mx).

Mut Formation, Transitional Member (Mt): this unit is very thin to absent in this area. Where it does occur, it consists of a few metres of siliciclastic sands or conglomerates containing marine fauna, often including large amounts of in-situ oysters. It is found between the top of the Derinçay Formation and the base of the Mut Formation Cross-Bedded Member. This unit has not been mapped because it is too thin. Important outcrops occur at grid references 690303 (base of Dibekli outcrop, see later) and at 786305 in the eastern end of the area.

Mut Formation, Cross-bedded Member (Mx): this member is previously undefined in the literature. Bi-directionally cross-bedded, well sorted coarse grainstones to rudstones form a tabular 80m thick deposit across much of the Silifke region mapped. These carbonate sands are composed of the debris of red algae, bryozoans, large benthic foraminifera and molluscs. Some thin beds of algal bindstone also occur. Cross bedding varies dramatically in scale from 15m high bedsets to metre scale and smaller tabular and trough cross bedding. Marls directly overlying are dated as NN4 age (Upper Burdigalian).

Alahan Formation (A): very small outcrops of this formation occur locally as coarse-grained fan-delta deposits near the basement contact with the Mut limestone. They are normally too small to be indicated on the map (see grid reference 685303).

Koserlerli Formation (K): this is as previously defined. Here it is dated from NN4-NN5 (Upper Burdigalian to Langhian).

Koserlerli Formation: Slump Member (Ks): as previously defined in the Mut area. Three slump horizons have been identified. The lowest horizon marks the boundary between the NN4 and NN5 biozones. The other slumps are found within marls of NN5 (Langhian) age.

Summary of Silifke area

The mapping study has shown:

1/ that the basement topography forms an east-west graben structure connecting the Mediterranean Basin in the east to the Mut Basin in the west, and that this topography is asymmetric, with a steeper southern flank (see figure 4.9). The present-day basement relief rises dramatically from below 100m to 900m altitude.

2/ the Derinçay Formation represents the syn-extensional infill of the graben structure, partly filling the relief with up to 300m of dominantly coarse-grained alluvial-fan sediments. The depositional locus of these deposits indicates that they are sourced up-dip from the up-lifted footwall blocks of the graben system.

3/ The Burdigalian marine deposits of the Mut Formation fill in this graben topography. During the initial flooding coarse-grained bioclastic sands of the Mut Formation Cross-Bedded Member fill up the base of the strait, overlying the continental syn-sedimentary graben infill of the Derinçay Formation. The Transitional Member is very thin to absent, and consists of coarse-grained siliciclastics (sands-conglomerates) where it occurs. This is because there is no major source of siliciclastic input active during the time of marine flooding, as compared to the Mut region. As the strait area is progressively flooded, carbonate platforms develop against the margins of the graben structure, while basinal marls and slump deposits of the Koserlerli Formation are deposited in the centre.

4/ a small amount of tectonic activity occurs during the Burdigalian, with the largest fault observed having a throw of less than 20m (grid reference 766287). This fault is contemporaneous with the Mut Formation Cross-Bedded Member, and is sealed by slump unit 1 (see later in figure 8.15).

5/ Post-Burdigalian tectonic deformation occurs creating sagging in the eastern end of the mapped area, with a deformation of 300m to 400m altitude over 5-10km.

6/ Post-Burdigalian east-west extension occurs along a series of north-south striking normal faults. The maximum throw observed is of the order of 50-80m (grid reference 575335).

4.4 SUMMARY

The mapping of these two areas has identified certain elements on which the detailed sedimentological studies in chapters 5 to 10 are based:

1/ Three environmentally different sites have been identified in the same time interval, for detailed study (two in the Mut area and one in the Silifke area). The first is the Alahan site in the north-west corner of the Mut area, characterised by a mixed carbonate-siliciclastic system. The second is the Pirinç site in the north-east of the Mut area, characterised by being a purely carbonate system, and the third is the Dibekli outcrop on the southern flank of the Silifke graben, which develops against a steep-sided basement relief in a strait topography.

2/ The base of the studied interval in each case is defined as the top of the Transitional Member, the first Miocene marine sediments in this area. The top of the study interval is the NN4/NN5 nannoplankton biozone limit, which corresponds approximately to the Burdigalian/Langhian boundary.

3/ The Burdigalian sediments underwent very little syn-sedimentary tectonic deformation, and post-sedimentary deformation is limited to basinward sagging that enhances the basement topography.

AGE		STANDARD ZONATION (MARTINI 1971)	
Quaternary	NN 21	Emiliania huxleyi	E. huxleyi *
	NN 20	Gephyrocapsa oceanica	P. lacunosa +
	NN 19	Pseudoemiliania lacunosa a b	C. macintyrei + D. brouweri +
Late Pliocene	NN 18	Discoaster brouweri	D. pentaradiatus +
	NN 17	Discoaster pentaradiatus	D. surculus +
	NN 16	Discoaster surculus	R. pseudoumbilica +
Early Pliocene	NN 15	Reticulofenestra pseudoumbilica	A. tricorniculatus +
	NN 14	Discoaster asymmetricus	D. asymmetricus *
	NN 13	Ceratolithus rugosus	C. rugosus *
	NN 12	Amaurolithus tricorniculatus	D. quinqueramus +
Late Miocene	NN 11	Discoaster quinqueramus a b	A. delicatus * D. quinqueramus *
	NN 10	Discoaster calcaris	D. hamatus +
Middle Miocene	NN 9	Discoaster hamatus	D. hamatus *
	NN 8	Catinaster coalitus	C. coalitus *
	NN 7	Discoaster kugleri	D. kugleri *
	NN 6	Discoaster exilis	S. heteromorphus +
	NN 5	Sphenolithus heteromorphus	H. ampliaperta +
Early Miocene	NN 4	Helicosphaera ampliaperta	S. belemnos +
	NN 3	Sphenolithus belemnos	T. carinatus +
	NN 2	Discoaster druggii	D. druggii *
	NN 1	Triquetrorhabdulus carinatus	

this study

Figure 4.3 Nannoplankton biostratigraphy (from Martini and Muller, 1986)
This shows the fauna used by C. Muller to determine the nannoplankton biozones

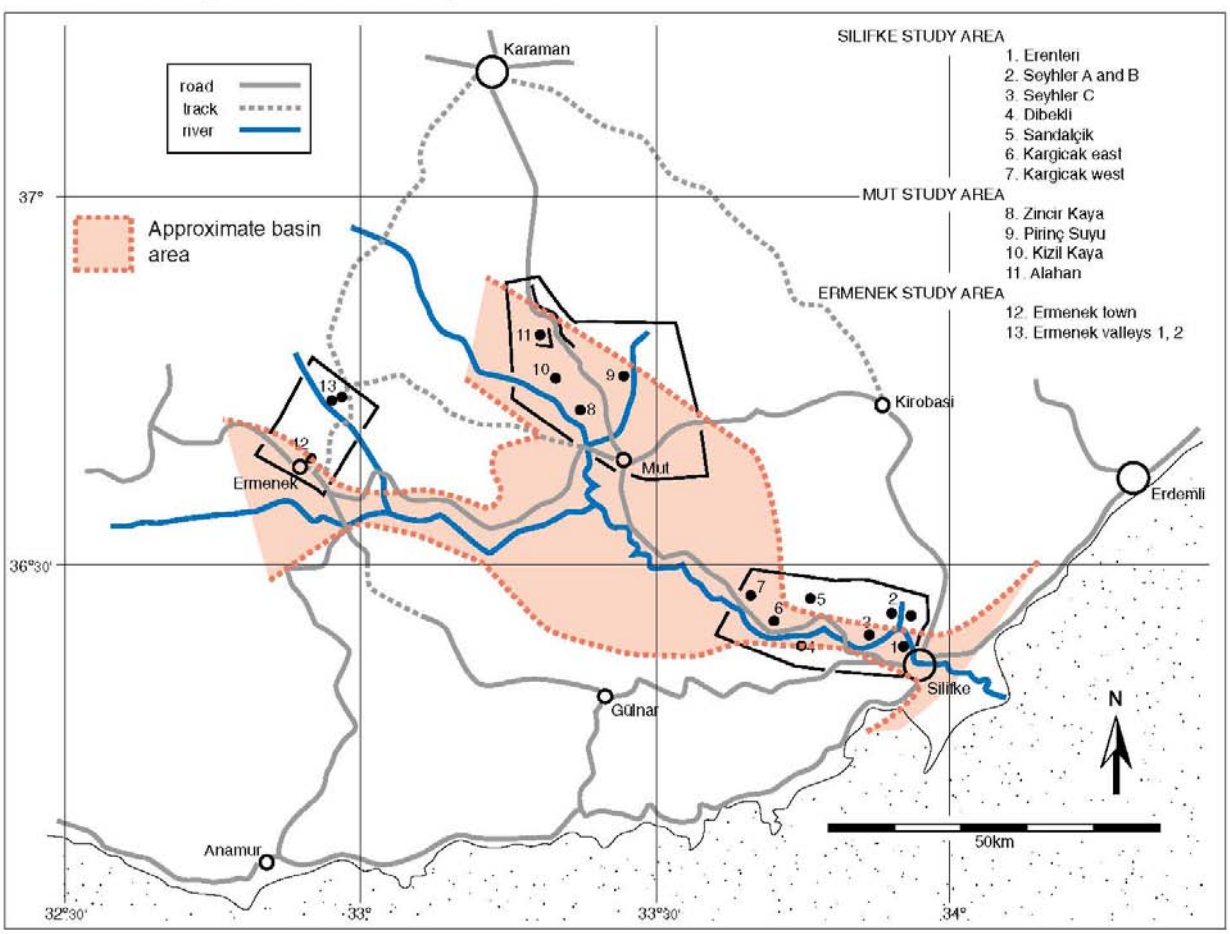

Figure 4.5 Location map showing the position of all the study sites across the Mut Basin

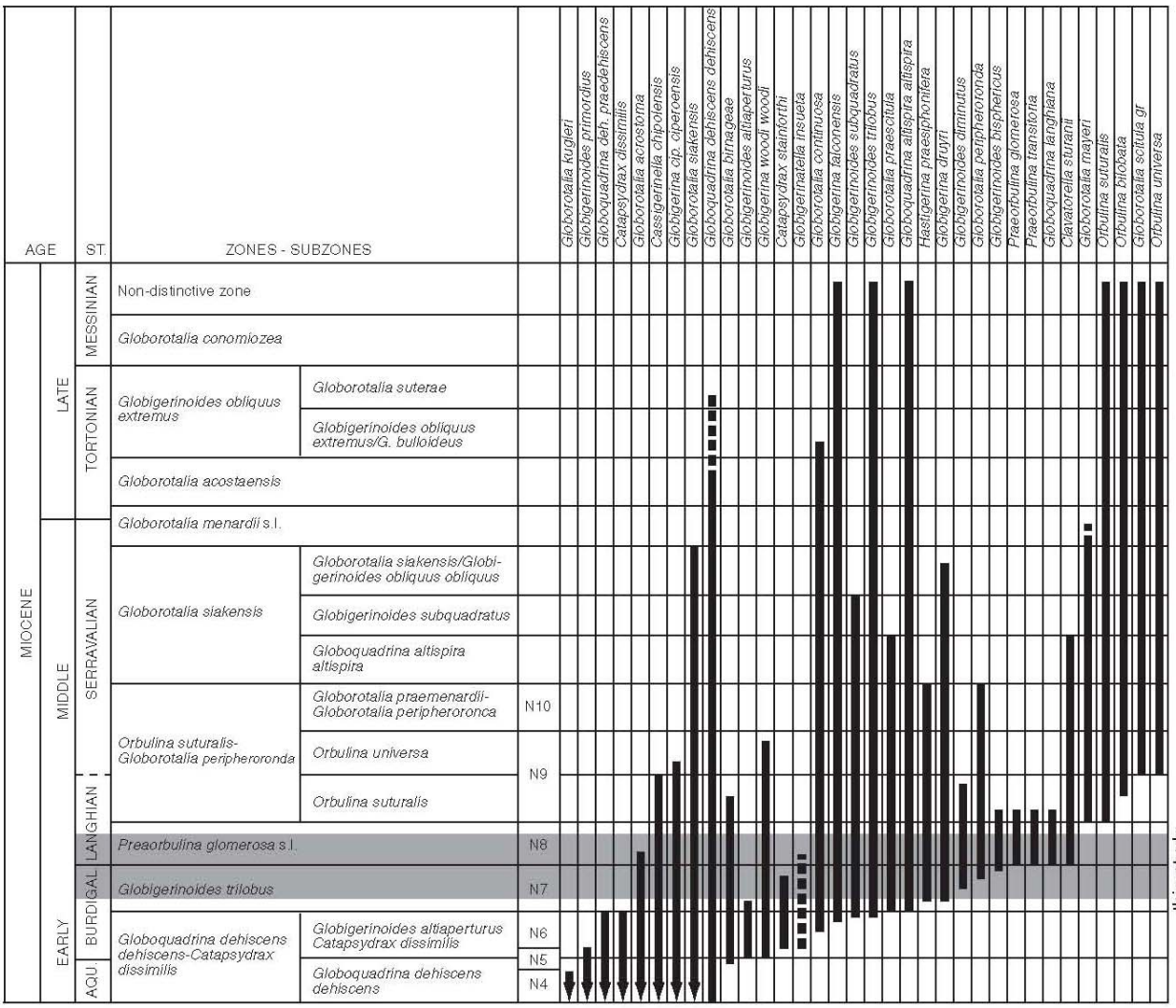

Figure 4.4 Planktonic foraminifera biostratigraphy (from Bolli *et al.* 1986)
This shows the fauna used by R.Wernli to determine the planktonic foraminifera biozones

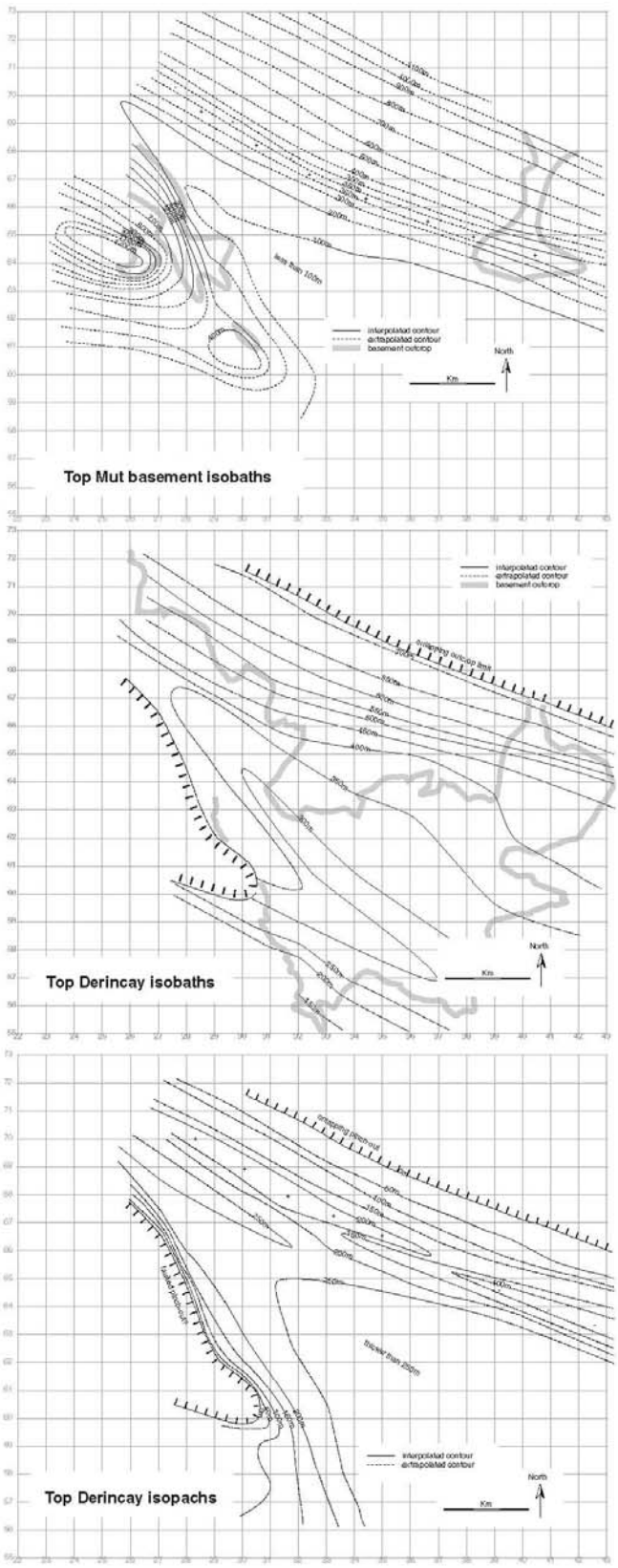

Figure 4.7 Mut basement and Derincay isobaths and isopach These contour maps are reconstructed from the geological map of the Mut region produced in this study. The contours are interpolated and extrapolated from the outcropping contact

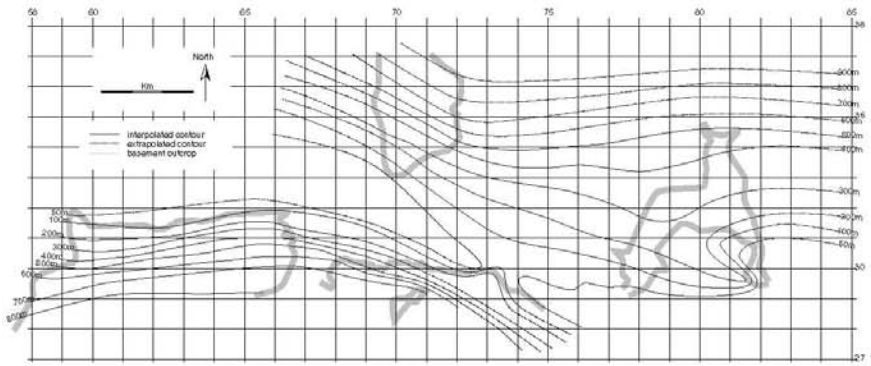

Silifke basement isobaths

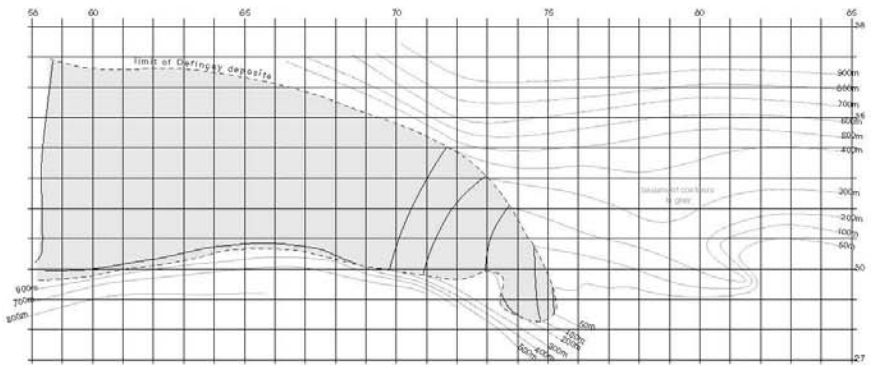

Derincay Formation isobaths

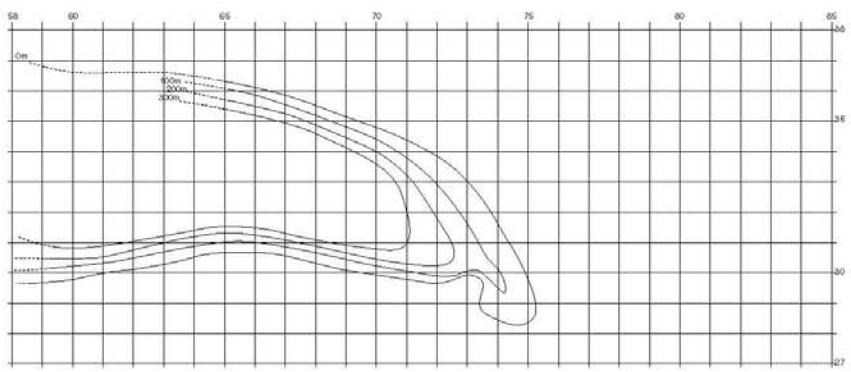

Derincay Formation isopachs

Figure 4.9 Silifke basement and Derincay Formation isobaths and isopachs
These contour maps are reconstructed from the Geological map of the Silifke region made in this study. The contours are interpolated and extrapolated from the outcropping contact.

5 - SEDIMENTOLOGY

This chapter illustrates the important faunal elements and describes their environmental significance. It describes the facies classification developed in this study, and explains the environmental settings of each facies, then it briefly describes the nature of the important surfaces observed.

5.1 FAUNAL ELEMENTS

The most common faunal elements identified from thin-section are described here and illustrated in figure 5.3. Figure 5.2 shows the distribution along a synthetic depositional profile of those organisms used in reconstructing the palaeoenvironments. This distribution is determined partly from the literature (see below), and partly from observations made during this study. The excellent outcrop quality allowed the bathymetry and geomorphogical environment (platform top, slope, basin...) to be determined from the bedding patterns, and so the faunal distribution was calibrated from field observations. The palaeoenvironments are of use in this study to establish the bathymetric trends of deepening or shallowing-up in a sedimentary sequence.

Foraminifera: it is the foraminifera that are the most useful for determining the depositional environments for practical reasons, since they are often abundant, and small enough to find significant amounts within a thin section. Additionally, most larger foraminifera were also found to be readily recognizable in the field with a hand lens. The most important foraminifera are illustrated in figure 5.3.

The distribution of foraminifera along a platform-to-basin profile is illustrated in figure 5.2. It was developed from Hallock and Glenn (1986), Murray (1991), Wagner (1964), and Brasier (1980), and was observed to agree very well with the field observations of the foraminifera distribution. The term Miliolids is here used to describe the roughly equant forms, such as Triloculinids and Quinqueloculinids, as distinct from the Soritids and Alveolinids. Soritids, Alveolinids and Miliolids are all characteristic of relatively quiet shallow water settings. The Soritids are the most proximal, and the Miliolids are the most distal within this setting. The Miliolids and Alveolinids are often reworked into grainstones by the action of currents on the platform, and are readily washed into a more distal, or more proximal setting than that in which they prosper. Such foraminifera can be found reworked into slope deposits.

Amphisteginids and Nummulitids are here typically found in slope or open platform settings. Different genera of foraminifera are grouped under the title of Nummulitids: these include Operculinids, Heterosteginids and Planosteginids. This grouping is necessary because it was not possible to systematically distinguish the individual members in thin section.

Planktonic foraminifera, mainly Globeriginids, are typical of the basin or slope settings. They may also be found on the platform, but rarely in great quantity.

Other foraminifera are also of use in determining the depositional environment. Bulminid foraminifera are commonly infaunal mud dwellers, while Cibicidids are considered to be epiphytal encrusters, and when found in quantity might infer the presence of sea-grass meadows. A variety of encrusting foraminifera are found in close association with coralline red algae and corals: Acervulinids are the most common and frequently compete with red algae in the formation of rhodoliths or macroids. Planorbulinid foraminifera also commonly form crusts in association with red algae, while Homotrematid encrusters are rare and normally solitary. A wide variety of agglutinating foraminifera (Textularinids) are very common and found in a variety of settings from platform to the toe-of-slope. Here only encrusting and non-encrusting Textularinids are distinguished in the microfacies analysis.

Coralline red algae: coralline red algae are among the main producers of biogenic carbonate sediment in this study area. They are a major constituent of most of the boundstones, are reworked into sand-grade sediment and redeposited, and are also found as rhodoliths -concentrically growing nodules of red algae. It is problematic to systematically identify the red algae species in thin-section (Braga and Aguirre, 1995; Braga et al. 1993), though certain possess diagnostic features, such as Lithoporella, and Sporolithon. These are illustrated in figure 5.3. Only the size of the red-algal fragments was noted when examining the microtextures, as less than, or greater than 2mm.

The growth of red algae is restricted to within the photic zone, and this can vary dramatically due to the

water turbidity, from 150m in clear waters, to 50m or less in turbid waters (Perrin et al. 1995). The growth forms can tell us something about the palaeoenvironments: delicate branching frameworks infer moderate energies, while robust fused frameworks infer high energies (Bosence, 1991).

Rhodoliths are of particular interest to this study since they are abundant, yet often restricted to specific horizons. The morphology and composition can tell us much about the environment: the bathymetry, the energy and the frequency of overturning events of the rhodoliths (Bosence, 1983; Hottinger, 1983; Braga and Martin, 1988, Rasser and Piller, 1997).

A wide variety of growth forms, sizes and settings exist, but some generalities can be made: large rhodoliths need a significant amount of time to form, they need to be overturned regularly and must not be smothered by sediment. Hottinger (1983) describes the ideal environment for rhodolith formation as being within a certain energy window, whereby the current or wave energy is not sufficient to wash the rhodoliths out of the production area, but is great enough to episodically overturn the rhodolith, and to winnow away any smothering sediment. Rhodoliths may also accumulate outside of their production area, for instance in fields of sea-grass, or at the base of a reef-slope (Piller and Rasser, 1996).

Corals: coral communities in the study area often form a volumetrically important component of the rock, though the diversity is very limited: Porites dominate, though Montastrea, Tarbellastrea and Faviid corals are also occasionally found (this study, and Sezer, 1970). The predominance of Porites indicates a very poor environment for coral growth, and times of high coral diversity are exceptional and episodic. For the purposes of this study the coral morphology is most frequently described (platey, domed, or branching), and the presence of other corals, apart from the common Porites, is noted, though the corals are not systematically identified.

Arthropods: arthropod fragments have been identified in thin-section and in hand specimen. Balanid (barnacle) fragments are common. These require a hard surface on which to grow, though they may form macroids.

Bryozoans: a large variety of bryozoan morphologies have been seen in thin-section, though their environmental significance is unclear. Bryozoans do not generally have photosymbionts, and do not give a good control on bathymetry. However, their morphologies may tell us something about the energy of the environment (Nelson et al. 1988). The diversity of growth forms is illustrated in figure 5.3.

Molluscs: little work was done on the molluscan fauna in this study by the author. Oysters, other bivalves, scaphopods, pteropods and other gastropods were distinguished. The scaphopods were often associated with muddier environments, most commonly in a slope setting, but were found from the platform to the toe-of-slope. The pteropods - planktonic gastropods- provide a useful indicator of palaeobathymetry, being found most commonly in a fully marine setting in more than 80-100m of water.

Echinoderms: two broad groups of echinoid were found in the rocks studied: small asymmetric infaunal Schizaster are found throughout the depositional profile, but are observed to be most abundant in finer sediment at the toe-of-slope. At times they exist in such abundance, burrowing through and churning up the sediment, that they are found in exclusion to most other fauna, except some small bivalves. The second group of echinoid commonly found is the Clypeaster. These are commonly observed here associated with reefal facies or coarse siliciclastics.

Serpulids: serpulid worm tubes are found in low concentrations throughout the rock, in a wide variety of settings. They have no exceptional distribution and are of limited value in this study in reconstructing the palaeoenvironments.

5.2 FACIES DESCRIPTIONS

The facies described in the field from the logging of measured sections, and from facies mapping of outcrops, have been classified into 21 facies types (Tucker and Wright, 1990; Flügel, 1982; Wilson, 1975). This classification is based on sedimentary textures, sedimentary structures and faunal content observed in the outcrop and from the microfacies analysis. The facies classification developed and applied in this study is functional, since the study of the facies per se is not the primary goal here. Facies descriptions use the nomenclature defined by Dunham (1962), as modified by Embry and Klovan (1971) for describing constructed reefal facies. Figure 5.1 summarises the facies, including diagnostic features, and interpretations. Figure 5.2 shows their distribution along a synthetic depositional profile. This profile is divided into platform (restricted, internal and open), slope (upper, middle and lower), and basin environments. Note that the basinal area is here very shallow, and can be in less than 150m of water-depth. This depositional profile is not a snapshot of the facies distribution at a given time, but simply shows where a particular facies is likely to be found on the profile. An environment may be characterised by a variety of different facies, and other factors control precisely which facies is deposited at which time. The carbonate facies defined here, and their distribution along the depositional profile, resemble those described by Görür (1994) in the Karaisali Formation (Early Miocene) of the Adana Basin.

facies	description	fauna and flora	diagnostic features	processes	energy of environment	interpretn. of depositl environ.
1	coralgal framestones	diverse coral, encrusting red-algae	in-situ corals and red-algae	constructed	medium	clay-free platform-slope
2	muddy coralgal framestones	diverse coral, encrusting red-algae	in-situ corals and red-algae in clays	constructed	medium-episodically low	platform-slope
3	coralgal floatstones		coralgal debris in finer matrix	pseudo-autochthonous debris		platform-slope
4	muddy coralgal floatstones		coralgal debris in finer clay-rich matrix	pseudo-autochthonous debris		platform-slope
5	rhodolithic float-bindstone	red-algae as rhodoliths	dominance of rhodoliths	autochthonous growth or allochthonous accumulation (currents or gravity)	medium-episodically high	sediment starved platform -slope
6	muddy rhodolithic float-bindstone	red-algae as rhodoliths	dominance of rhodoliths in clay-rich matrix	autochthonous growth or allochthonous accumulation	medium-episodically high	sediment starved platform -slope
7	microbial coralgal boundstones	small corals, encrusting red-algae, encrusting forams, sponges, oysters, barnacles	presence of encrusting foraminifera, sponges, microbial micrites with fenestrae	autochthonous growth	high	platform top
8	Miliolid grainstones-packstones	Miliolids, (Nummulitids, Amphisteginids, Soritids), red-algae, molluscs, echinoids	Miliolids common	1) transport and sorting by traction currents, 2) slope gravity flow	medium	shallow platform
9	Nummulitid grain-packstones	Nummulitids, Amphisteginids (Miliolids, planktonic forams), red-algae, molluscs, echinoids	Nummulitids and Amphisteginids common	1) transport and sorting by traction currents, 2) slope gravity flow 3) pseudo-autochthonous accumulations	medium	platform-slope
10	planktonic foram micro-packstones/marls	planktonic forams (Nummulitids) infaunal echinoids	planktonic forams and infaunal echinoids abundant	planktonic accumulation	low	slope-basin
11	slump deposits		extensive rigid and plastic deformation	allochthonous gravity flows		slope-basin
12	oyster rud-boundstones	oysters, red algae, Serpulids, barnacles	dominance of oysters	1) constructed 2) pseudo-autochthonous debris		restricted platform-slope
13	coralgal rudstones	corals red-algae, Amphisteginids, Nummulitids	sorted coralgal debris	pseudo-autochthonous-allochthonous debris		platform
14	marine conglomerates	large echinoids (Clypeaster), oysters, other molluscs	heterolithic basement conglomerates with marine fauna and cement	allochthonous		foreshore-upper shoreface
15	marine sands-calcarenites	diverse molluscs	heterolithic basement sands with marine fauna	allochthonous		upper-lower shoreface

16	marine silts-muds	planktonic forams and pteropods	silts-muds with pteropods and planktonic forams	allochthonous		lower shoreface-offshore
facies	**description**	**fauna and flora**	**diagnostic features**	**processes**	**energy of environment**	**interpretn. of depositl environ.**
17	coquina rudstone	diverse thick shelled molluscs	diverse molluscan debris with heterolithic basement gravels	pseudo-autochthonous-allochthonous	medium-high	foreshore-upper shoreface
18	continental gravels- muds	(stromatolites)	red colour, absence of marine fauna	allochthonous		fluvial-lacustrine
19	littoral-shallow sub-littoral muds-silts	diverse molluscs	presence of shallow marine molluscs in clays and silts	allochthonous	low	littoral-sub-littoral
20	bryozoan grain-rudstones	bryozoans, red-algae, molluscs, Amphisteginids	well sorted, dominance of bryozoan debris	allochthonous detrital carbonates	high	inter-subtidal
21	Soritid grain-packstones-wackestones	Soritids, red-algae, diverse molluscs, echinoids	Soritids common	allochthonous-pseudo-autochthonous detrital carbonates	low	very shallow-restricted platform

Figure 5.1. *Facies classification summary table.*

Constructed autochthonous and para-autochthonous carbonate facies

Clean coralgal framestones (facies 1): in outcrop this facies is beige to cream coloured, with well-defined decimetric to massive undefined bedding. Figure 5.4 (top photo) illustrates well bedded framestones separated by thin (5cm) wackestone intervals. Corals and red algae form a framestone texture. The corals vary in size, type and morphology. Size may vary from 10-80cm across. The dominant coral is Porites, though other corals such as Montastrea and Tarbellastrea (Sezer, 1970) are also found. Morphologies are dominantly platey or domed, while branching forms are rare, and always small (10-20cm). The corals are often extensively bored by diverse organisms, including Lithophaga bivalves. Red-algal encrustations are abundant, and almost always associated with encrusting Acervulinid foraminifera. Other encrusting organisms are also common, such as bryozoa and serpulid worm tubes. Figure 5.5 (top photo) shows encrusting layers of red algae (2) and Acervulinid foraminifera (1), with some serpulid worm tubes (3) and boring of the encrusters (4). In the same figure the lower photo shows a sliced hand-specimen of this facies, and illustrates a coral (1) highly bored by Lithophaga bivalves (2), and encrusted with red algae (3). The matrix of this facies is clay-free, distinguishing it from facies 2 (muddy coralgal framestones), and hence the name "clean" is added to the facies name. The matrix can be grainstones, packstones, floatstones or rudstones, and may contain Miliolid or Nummulitid foraminifera.

This is a broad facies category, encompassing constructed platform and slope sediments deposited within the photic zone, and formed principally by a coral framework, with accessory encrusters. It includes all framestones from lower reef-front to back-reef constructions (James, 1984; Pomar et al. 1985) deposited in a siliciclastic-free environment. The framestones dominated by platey Porites are described as being deposited in a lower reef-front setting, though the geomorphic position on the depositional profile may be quite different. Such platey Porites corals are found on slope and platform top settings, and indicate a low energy setting with low sedimentation rates. The dome morphologies are described as being in an upper reef-front setting which would imply moderate to high wave energy.

Muddy coralgal framestones (facies 2): this facies is distinguished from facies 1 by the presence of clay-rich sediment between the corals. This matrix is a green coloured, clay-rich marl, often containing Nummulitid foraminifera. In other respects it is very similar to facies 1. Red-algal crusts are less well developed on the surface of the corals, and Miliolid foraminifera are rarely found in the matrix around the corals. Both platey and dome coral morphologies are common. Figure 5.5 (middle photo) illustrates a sliced hand-specimen of a Porites plate growing in a clay-rich matrix. Figure 5.4 (lower photo) illustrates 20-30cm Porites domes growing surrounded by a clay-rich matrix.

This facies is found on the platform and in slope settings. Where it is found on the slope the bedding is often well defined, with 10-30cm marl beds separating 30-50cm coral beds. Such bedding is here referred to as coral carpets (Hottinger, 1977; Reiss and Hottinger, 1984; Piller and Pervesler, 1989), and is used to

distinguish low relief topographies of reefal facies, from higher relief reefal constructions (Riegl and Piller, 1997). Such bedding patterns are also found in the clean coralgal framestones (facies 1), such as those illustrated in figure 5.4 (top). The coeval growth of corals, and the deposition of fine siliciclastic sediments is at odds with the classic model of coral growth being limited to mud-poor environments. This may be explained by a relatively slow input of fine siliciclastic sediment, which is not great enough to smother the coral growth. An alternative is that the arrival of these muds is seasonal, and that the muds collect between the corals without smothering them. Whatever the reason, the mud input seems to inhibit to some degree the coral growth and diversity: coral morphologies are restricted to platey and domed forms, and coral species diversity is low, and dominated by Porites.

Microbial coralgal boundstones (facies 7): in outcrop this is a beige to cream coloured hard rock. Bedding is variable, from 10-30cm uneven lenticular bedding, to massive highly cemented beds 1-2m thick. Small knobby Porites corals are distributed throughout the sediment, though they rarely coalesce and do not form framestone textures. They form small (less than 10cm) flattened domes, or grow as stubby fingers from an original thin encrusting morphology. Only Porites corals have been found in this facies. Thin crusts of red algae coat the sediment and the surfaces of the corals. Small 5-10mm encrusting sponges, bryozoans, barnacles, arthropods and oysters are common at certain intervals in the sediment. Benthic epifaunal and infaunal foraminifera (Miliolids, Nummulitids, Amphisteginids) are rarely found. The surrounding sediment is a biodetrital wackestone to packstone. Abundant fenestral structures occur, as well as agglutinating encrusting foraminifera, and sponge spicules. The matrix of the packstone is micritic. Figure 5.9 and 5.10 illustrate this facies. The top photo of figure 5.10 shows the microtextures: in the centre (1) is seen an encrusting sponge (G. Camoin, pers. com.). The irregular grey veins (2) cross-cut the sediment, and are most concentrated around remanent coral textures, which have been almost completely altered to microsparitic textures (3). (4) indicates a typical matrix packstone texture. On closer examination many of the "clasts" of this packstone are observed to be sparite-filled chambers with micritic walls. These chambers are organised into evolute clusters encrusting the sediment surface. These are unidentified microencrusting organisms (probably foraminifera or sponges) that form a boundstone texture. No siliciclastic component is found.

This is interpreted as a bindstone, with corals, red algae, sponges and bryozoa poorly developed as macro-encrusters. These seem to float in the sediment and are never sufficiently common to create a framework. Micro-encrusters are abundant in the matrix: these include encrusting foraminifera, and sponges (inferred from the spicules). The presence of unidentified microbial encrusters and binders is inferred from the abundant fenestral structures in the sediment. Also some of the micritic matrix surrounding the wackestones is suspected to be of microbial origin. A medium to high energy environment is interpreted from the encrusting mode of life of the faunal elements. The poor development of corals and red algae, and the abundance of micro-encrusting foraminifera suggest a non-ideal environment for coralgal growth, possibly due to nutrient-rich waters, or cool temperatures.

Clean coralgal floatstones (facies 3): a beige coloured rock with well defined irregular decimetric bedding. Coral fragments 1-4cm are distributed throughout the sediment, and it is these that form the floatstone texture. Red algae often coat the coral fragments. This is illustrated in figure 5.6 (top photo). Porites coral fragments are indicated (1), and some of this debris is encrusted by red algae and Acervulinid foraminifera (2). These form incipient rhodoliths, though the red-algal element is not important enough for these to be classed as rhodolithic float-boundstones (see later, facies 5 and 6). The matrix is composed of bioclastic sands forming pack and grainstone textures, and may contain Miliolid, Alveolinid, Nummulitid and Amphisteginid foraminifera, as well as larger mollusc and arthropod debris. Small corals and rhodoliths may also be found growing in the sediment, though these are volumetrically unimportant in this facies. The matrix contains no siliciclastic component.

This facies is often found grading laterally into clean coralgal framestones (facies 1) and Miliolid and Nummulitid pack-grainstones (facies 8 and 9) over the space of a few metres. It is interpreted as autochthonous or pseudo-autochthonous reefal debris, sometimes surrounding a constructed reef area, and may be found on the platform or on the slope. A medium energy environment is inferred from the pack-grainstone matrix.

Muddy coralgal floatstones (facies 4): this is similar to the previous facies, except for the presence of siliciclastic muds in the matrix. These are green-coloured clay-rich marls and wackestones containing Nummulitid and also locally planktonic foraminifera. This facies is illustrated in figure 5.6 (lower photo).

The interpretation is similar to that of facies 3: they are autochthonous to pseudo-autochthonous reefal debris belonging to the platform or the slope area. Here the presence of mud-grade sediment indicates a low energy environment.

Clean rhodolithic float-bindstones (facies 5): a white to cream-coloured, often decimetrically bedded, hard, well cemented rock. Its principle constituent is rhodolithic forms of red algae. They may form a floatstone texture, or may be actively binding the matrix. Diverse rhodolith morphologies and sizes are

grouped together in this facies. Lamina, branching and columnar morphologies (Bosence, 1983) are not distinguished by the facies classification, and the rhodoliths may vary from 1-20cm in diameter. The matrix is normally a bioclastic grain-packstone, containing diverse foraminifera, including Miliolids, Alveolinids, Nummulitids and Amphisteginids. The rhodoliths may be formed from monospecific red algae, or may contain a variety of species. Acervulinid foraminifera are normally associated with the red-algal crusts, and encrusting Planorbulinid foraminifera, bryozoans, and Serpulid worm tubes are also commonly found. This facies is illustrated in figure 5.7.

The accumulation of concentrations of rhodoliths implies a quite specific environment of deposition (see discussion in the description of the faunal elements). Sufficiently high energy conditions are required to overturn (at least periodically) the size of rhodolith found, without being so high as to wash them out of the accumulation area (if the accumulation is autochthonous). Time is required for the formation of rhodoliths, and they must not be smothered by incoming sediment, so the rate of deposition of allochthonous sediments must be low. This may be due to a low sediment flux, or to the punctual winnowing of the sediment that may be deposited. A mobile substrate is also required, else the red algae will preferentially form binding and encrusting textures on the hard surface provided, and rhodoliths would be rare. So autochthonous accumulations of rhodoliths need slow sedimentation rates and medium energy levels, within the photic zone. Hence rhodolith deposits are often associated with maximum flooding intervals, where the allochthonous sediment input is low, or at flooding surfaces, where the red algae is a pioneering organism. Allochthonous rhodolith deposits can accumulate at the toe-of-slopes, within sea-grass meadows, or in depressions on the platform.

Muddy rhodolithic float-bindstones (facies 6): a soft green coloured rock with bedding rarely well preserved. Rhodoliths form a floatstone, to locally bindstone texture in a matrix of clay-rich green micrites, or clays. This facies is very similar to facies 5. It is distinguished by the presence of clays in the matrix. Two examples of this facies are illustrated in figure 5.8.

Oyster bound-rudstones (facies 12): a massive poorly bedded lithology made up dominantly of oysters. The oysters encrust one another, and may be preserved intact or as debris. Other organisms, including serpulid worms, bryozoans, red algae and barnacles may encrust the surface of the oysters. The matrix varies, and may contain siliciclastic sands and silts.

This is an autochthonous constructed facies. Oysters can be found from the restricted platform to the lower slope environment, and are common constituents in many other facies. Such monospecific accumulations of oysters may alternatively indicate abnormal salinity conditions of hypo- or hyper-salinity.

Bioclastic carbonates

Coralgal rudstones (facies 13): these are metre-thick grey, hard, well cemented beds. Certain occurrences of this facies display metre-scale cross-bedding, while others are organised into sloping coarsening-up metre-thick packets. Coral and red-algal debris forms a sorted rudstone texture. Coral fragments may be coated with thin crusts of red algae: the incipient stages of rhodolith formation.

A number of interpretations exist for this facies. The sloping coarsening-up beds are interpreted as allochthonous slope deposits, layed-down by shedding and down-slope exportation processes from the platform margin. The cross-bedded packets are deposited under the action of traction currents, and have been interpreted as platform channel-fill or shoal deposits.

Gravelly coquina beds (facies 17): a yellow to brown-coloured rock showing metre-scale bedding. Heterolithic unsorted gravels (up to centimetre-size pebbles), sands and silts are abundant. Thick-shelled, roughly equant, deeply ribbed diverse molluscan fauna, both complete and as debris, is abundant, and forms the bulk of the sediment. Bivalves are the most common, but gastropods are also abundant. The complete specimens are chaotically arranged. This facies is illustrated by figure 5.16. Locally echinoderms and oysters can form an important part of the sediment.

This has been interpreted as a shallow platform, medium-high energy setting.

Bryozoan grain-rudstones (facies 20): a grey to beige coloured, hard well-cemented rock with decimetric bedding. Oblique bedding in the form of metre-scale planar, and trough cross-bedding is typical for this facies. Cross-bedding bedset heights have been observed to be as great as 15m. Rhodoliths, oysters, and surfaces encrusted by red algae are common in this facies. Rounded bioclasts form a sorted to well-sorted rudstone texture. The bioclasts are formed by abundant bryozoan, red-algal, molluscan, Nummulitid foraminifera and echinoderm debris. Amphisteginid foraminifera are often preserved undamaged. Coral fragments are rare. Basement lithoclasts are rare to common. At times a micrite matrix is preserved, partially filling the void-space. This facies is illustrated in figure 5.17. The top photo illustrates the typical outcrop aspect, while the bottom photo shows the microfacies texture.

The depositional environment has been interpreted as being high energy, with the action of strong currents forming cross-bedding. Bi-directional cross-bedding is found in certain outcrops, and indicates that these currents may be of tidal origin. The exact

bathymetry of deposition is difficult to estimate from the facies alone, since these sediments are almost entirely transported. However, the presence of some in-situ red-algal crusts, and rhodoliths growing on the sediment surface, indicates that this is within the photic zone. A minimum water depth is given by the height of the cross-bedded bedsets. The sediment fills up to distinct horizontal surfaces traceable across a number of kilometres, and these surfaces represent base-level. This would imply that these sediments are deposited in a few tens of metres of water at most.

Soritid pack-wackestones (facies 21): a dark grey to cream-coloured rock, irregularly bedded on a decimetric scale. Siliciclastic sands are rare to common, while pebbles are occasionally found concentrated along specific bedding planes. This is a fine bioclastic pack-wackestone. Red-algal, molluscan, and echinoderm debris make up the bioclasts. Larger oyster and arthropod fragments are sometimes found in the sediment. Soritid foraminifera are common, and Miliolid foraminifera may also be found.

The depositional environment of this facies is determined as being the restricted to internal platform by the presence of Soritid foraminifera.

Miliolid grain-packstones (facies 8): this is a decimetre bedded beige-coloured, often hard, well cemented rock. It is a sorted fine-medium bioclastic grain-packstone formed by red-algal, echinoderm and molluscan debris, and characterised by the presence of Miliolid foraminifera. This facies is illustrated in figure 5.11.

The presence of Miliolids identifies this sediment as having a shallow platform origin. The exact environmental interpretation is based on the geomorphological position in which the deposits are found, on the degree of sorting of the sediment, and whether it is a grainstone or a packstone. Well sorted grainstone textures on the platform top indicate allochthonous to pseudo-autochthonous shoal or channel fill deposits, while similar textures found on the slopes, accompanied by a coasening-up bedding organisation, indicate exportation from the platform and deposition by gravitational processes in prograding packets. Poorly sorted packstone textures on the platform are interpreted as autochthonous or pseudo-autochthonous deposits.

Nummulitid grain-packstones (facies 9): a variety of rocks types are included in this definition, ranging from decimetre bedded hard beige-coloured lithologies, to irregularly bedded green-coloured soft rocks. It is a fine-coarse bioclastic grain-packstone formed by red-algal, echinoderm and molluscan debris, and characterised by the presence of Nummulitids. Amphisteginids are very common, and Miliolids or planktonic foraminifera can also be found in this facies. The green-coloured lithologies contain clays in the matrix, and may locally form wackestone textures. Figure 5.12 illustrates this facies at the microscopic scale and at the hand specimen scale.

The presence of Nummulitids identifies this sediment as belonging typically to the slope-external platform environment. Grainstones and sorted packstones found on the slope setting are para-autochthonous or allochthonous sediments deposited under the influence of down-slope transportation processes. This is determined principally from their good sorting, and their organisation into coarsening-up packets separated by flooding surfaces. Such grain-packstones in a platform setting are shoal or channel fill deposits. Packstone-wackestone textures are autochthonous to para-autochthonous deposits, and can be found on the platform in lagoonal areas, or on the slope. When the geomorphological setting cannot be observed from the outcrop geometries, it can be inferred by the associated accessory foraminifera: the presence of planktonic foraminifera indicating a slope to basin setting, and Miliolids and Alveolinids indicating a platform setting.

Marls (facies 10): a white to grey-coloured decimetrically to metrically bedded rock, with harder beds separated by softer, more friable, intervals. Small thin-shelled flat bivalves and small, irregular Schizaster echinoids are common. Certain intervals contain echinoids to the exclusion of all other organisms. Other fauna found include scaphopods and arthropod debris. In thin-section planktonic foraminifera are abundant. Often a very fine packstone texture is formed by the allochems, visible only when viewed with the microscope: when this is observed, the rock is referred to as a micro-packstone, though the facies classification remains unchanged. This facies is illustrated in figure 5.14: the top photo shows the outcrop bedding patterns, while the bottom photo shows the texture in thin section.

Other carbonates

Slump deposits (facies 11): this is not a classically defined facies, in the sense that the definition is based on large-scale bedding patterns, and on the demonstrably allochthonous, transported nature of the slumped units, not on the lithology of the sediment. It corresponds to the Slump Member of the Koserlerli Formation. These slumps form one of the categories into which the rocks are classified for the purposes of constructing the transects, and hence they are grouped here with the other facies.

They consists of plastically or rigidly deformed beds and sedimentary packets, including folded, contorted bedding, olistoliths and slid blocks, that are demonstrably allochthonous. These sediments are lithified or partially lithified, and then transported by down-slope gravitational processes. Allochthonality is demonstrated by the relationship of the slumped unit with the sediment around. A basal erosional surface is found, and this is the glide plane along which the

slump deposits travel. Deformation of the underlying sediment may also occur, with rucking and scouring of the rock beneath the glide plane, though this sediment remains un-transported. Slumped lithologies are mostly shallow platform carbonates. During the transport process other more distal sediments may be caught up in the slump, creating a heterogeneous melange.

These slumps are often found associated with an exposure surface on the platform top. The erosion and weakening of the lithified platform margin due to exposure, coupled with the steep topography often found at the front of the platform, are interpreted as direct causes for slumping.

Siliciclastic facies

Continental siliciclastics (facies 18): these are red to reddish-grey mudstones, siltstones and sandstones. Faunal debris is absent. Oncoids and stromatolites develop on specific horizons within the sands and silts, and can form up to 50cm oblate balls. Plant material is commonly found in the mudstone and siltstone horizons. Diverse forms of planar, oblique planar and trough cross-bedding and lamination occur throughout the sediment. Figure 5.16 illustrates this facies, showing the mudstones overlain by cross-bedded sands.

This broad facies category groups together all the lithologies which have been interpreted as being deposited in the continental environment. It includes fluvial floodplain and channel environments, as well as lacustrine deposits. It corresponds to the Derinçay Formation. Such a broad facies definition is justified, since this study is principly focused on the shallow marine carbonate systems, and detailed analysis of the continental clastic system is not required.

Littoral muds-silts (facies 19): these are bioturbated grey to greenish grey muds and silts with poorly defined bedding. Some intervals may contain heterolithic siliciclastic sands and gravels. They correspond to the Transitional Member of the Mut Formation. Diverse fine-shelled molluscan debris, and in-situ molluscs are abundant, and plant debris is rare to common. Planktonic foraminifera, and Pteropod gastropods are rare to absent. This facies is illustrated in figure 5.15.

This facies has been interpreted as being deposited in the shallow marine environment (see figure 5.2). The analysis of the molluscan assemblages by Schlaf et al. (1997) supports this interpretation, and recognises the depositional environment as shallow sub-littoral.

Marine conglomerates (facies 14): this is a poorly sorted, rounded, sub-spherical to angular, heterolithic clast supported conglomerate. Clast size ranges from silts (in the matrix) to 8cm pebbles. Diverse marine fauna are found in these conglomerates: large (up to 18cm wide) Clypeaster echinoderms, both complete, in life position, overturned, and as debris; large (up to 15cm wide) oysters; red-algal debris and barnacles encrusting the conglomerate surfaces. Figure 5.14 illustrates this facies: the top photo shows the outcrop aspect, while the lower photo shows an outcrop detail, with a barnacle (centre) and molluscan debris (centre, bottom). The pebbles may also be bored by bivalves and other marine organisms. Note also the poorly sorted, heterolithic nature of the conglomerates. The clasts are made up of a variety of different basement lithologies. The matrix is a poorly sorted mixture of siliciclastic silts and sands with a carbonate cement, and sometimes contains fine red-algal debris.

This facies has been interpreted as very shallow marine deposits, with siliciclastic material brought in by (small) rivers and rapidly dumped in a marine environment, with very few sorting processes occurring. The sedimentary bodies formed by these facies have erosional bases. They are normally one to a few metres thick, and extend laterally by a few hundred metres, pinching out, with the base remaining relatively flat. These have been interpreted as fan delta deposits. They are situated in the restricted to internal platform settings in the figure 5.2.

Marine sands (facies 15): a grey to light-brown coloured, decimetric to metric-scale bedded rock. This is a fine to medium unsorted-sorted heterolithic sandstone. Roundness of the sand grains is variable, ranging from angular to well-rounded. The clasts comprising the sand are of varied origin, all sourced from the basement. Diverse molluscan debris is common to abundant, as is echinoderm debris and rarer scaphopods. The microtexture of this facies is illustrated in figure 5.15.

This has been interpreted as marine upper to lower shoreface sands. The distinction between upper and lower shoreface is made case by case from the sedimentary structures found in the sands, by the microfauna (whether the sands contain Miliolids, Nummulitids, or planktonic foraminifera), and by the percentage of shales interbedded with the sands.

Offshore muds-silts (facies 16): a grey to light-brown coloured decimetric bedded rock. Laminations are sometimes preserved. The texture varies from claystone to sandy siltstone. Molluscan debris is rare to common. Pteropod gastropods are rare to abundant. In thin section glauconite and planktonic foraminifera are rare to common.

This facies has been interpreted as being deposited in the offshore domain.

5.3 SURFACES

A diversity of different types of surface have been recognised in this study. The most important are briefly described here:

exposure surface: these surfaces are indicated by the macroscopic features such as autobrecciation, infilled with a ferruginous matrix, fine laminated sediment or siliciclastic sands (see figures 6.24 and 7.17). Cavity development by karstic dissolution and resulting cavity-fill by breccias and spar cements has also been observed (see figure 8.9). Microscopic indicators of exposure include the formation of microcodium, seen in one location in sample 3.40 (see figure 8.4). Possible pendant cements have been observed (see figure 5.17), indicating the development of a meteoric vadose diagenetic environment. Extensive dissolution and infilling by microspar cements has also been observed (see log 40 samples in Zincir Kaya, illustrated by figure 5.10-top).

erosional surfaces: many erosional truncation surfaces occur in this area in the Miocene sediment. Slight erosional bevelling observed on platform edges varies up- and down-dip to a conformable contact: this is observed in many places (figures 6.21 top, 10.4, 10.6). More important erosional surfaces occur on platform margin edges and are associated with margin collapse (figures 6.4, 6.5 and 6.19).

hardground surfaces: bored and encrusted surfaces often with ferruginous coatings. Small corals are often seen to be the last fauna that encrusts these surfaces, and these are often overlain by basinal marls (see surfaces labelled 3.2 and 3.3 in figure 6.1). When such a distal facies shift is seen, this is also a flooding surface (see below).

maximum flooding surfaces: highly bioturbated centimetre-thick intervals of deeper water sediment (normally marls of facies type 10) surrounded above and below by shallower water sediment. Such a surface is a distal hiatus (see log 44 in figure 9.5).

Flooding surfaces: this is a surface across which an abrupt deepening occurs, as defined by a distal-shift in the facies. These are often associated with hardgrounds here (see log 28 from 49-54m in figure 10.13).

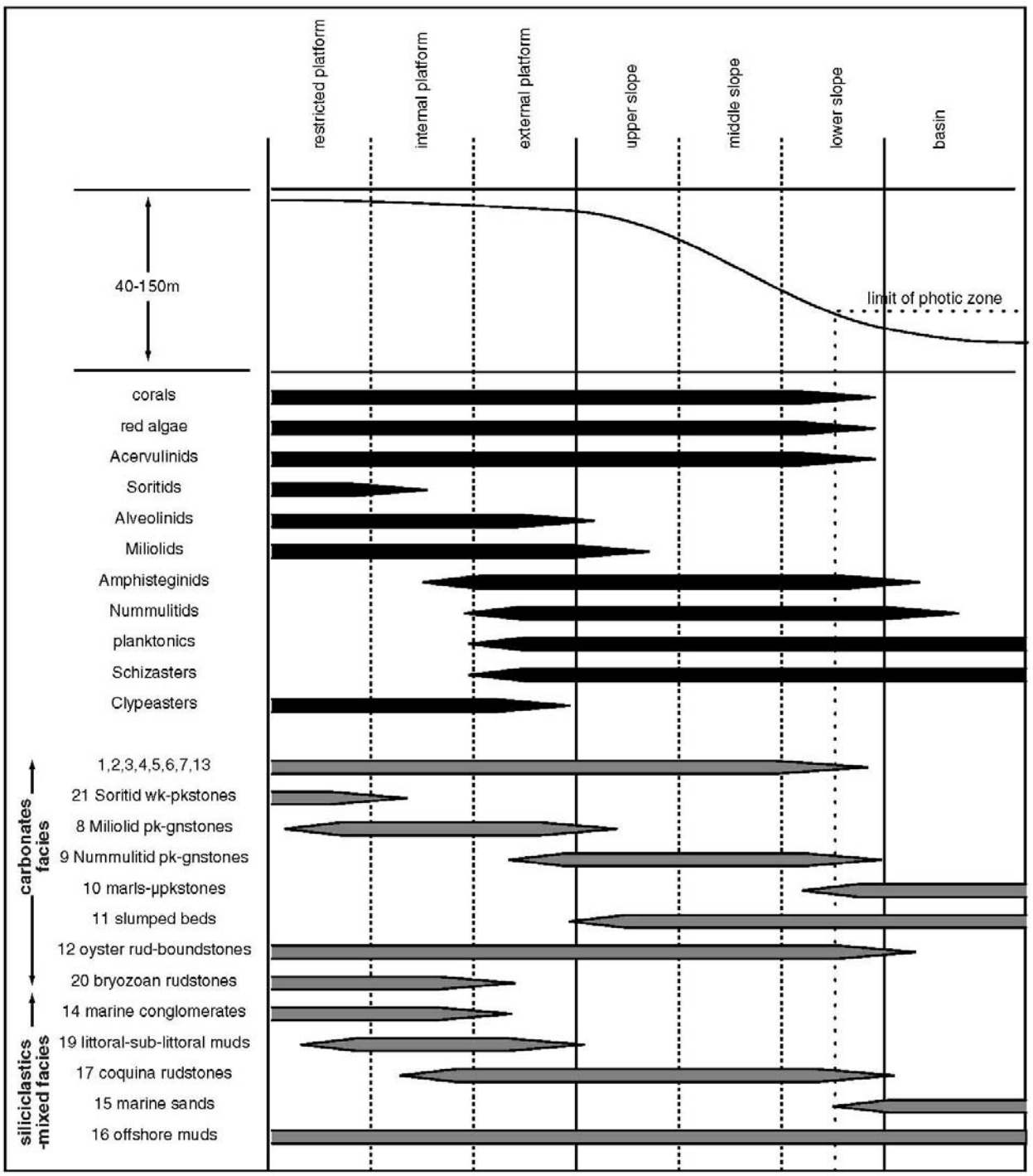

Figure 5.2 Fauna and facies distributions along a synthetic depositional profile

FIGURE 5.3a microfauna photo index

FIGURE 5.3b

Photo 1	Miliolids (sample 28.3)
Photo 2	Orbitolinid foraminifer (sample 3.13)
Photo 3	Alveolinid foraminifer (sample 28.5)
Photo 4	Alveolinid foraminifer (sample 29.2)
Photo 5	Soritid foraminifer (sample 29.2)
Photo 6	Soritid foraminifer (sample 41.5)
Photo 7	Peneroplid foraminifer (sample 41.5)
Photo 8	Cibidid foraminifer (sample 25.9)
Photo 9	Cibicidid foraminifer (sample 28.4)
Photo 10	Bulminid foraminifer (sample 25.6)
Photo 11	Nummulitid foraminifer (sample 35.4)
Photo 12	Amphisteginid foraminifer (sample 29.3)
Photo 13	Rotalid foraminifer (sample 30.3)
Photo 14	Homotrematid foraminifer (sample 30.5)
Photo 15	Homotrematid foraminifer (sample 35.15)
Photo 16	Acervulinid foraminifer (sample 28.6)
Photo 17	Planorbulinid encrusting hyaline foraminifer (sample 28.8)
Photo 18	Planobulinid encrusting hyaline foraminifer (sample 28.11)

FIGURE 5.3c

Photo 19	Textularinid foraminifer (sample 28.20)
Photo 20	Textularinid foraminifer (sample 41.5)
Photo 21	Encrusting textularinid foraminifer (sample 28.7)
Photo 22	Encrusting textularinid foraminifer (sample 30.2)
Photo 23	Planktonic foraminifer (sample 25.5)
Photo 24	Arthropod fragment (sample 29.3)
Photo 25	Arthropod fragment (sample 3.7)
Photo 26	Bryozoa (sample 28.10)
Photo 27	Bryozoa (sample 25.8)
Photo 28	Eschariform bryozoa (sample 28.11)
Photo 29	Bryozoa (sample 28.4)
Photo 30	Bryozoa (sample 29.3)
Photo 31	Bryozoa (sample 41.7)
Photo 32	Adeoniform bryozoa (sample 3.8)
Photo 33	Adeoniform bryozoa (sample 3.5)
Photo 34	Sporolithon coralline red-algae (sample 28.7)
Photo 35	Detail of sporolithon coralline red-algae (sample 25.7)
Photo 36	Lithoporella coralline red-algae (sample 29.4)

FIGURE 5.3d

Photo 37	Coralline red-algae (sample 1.51)
Photo 38	Porites coral with boring (sample 1.36)
Photo 39	Coral (sample 25.6)
Photo 40	Pelecypod with boring (sample 40.9)
Photo 41	Scaphopod mollusc (sample 28.21)
Photo 42	Encrusting foraminifer (?: Bacinella-type?) (sample 25.7)
Photo 43	Serpulid worm tubes (sample 29.5)
Photo 44	Echinoid spine (sample 1.47)
Photo 45	Unknown (green algae/sponge?) (sample 3.8)

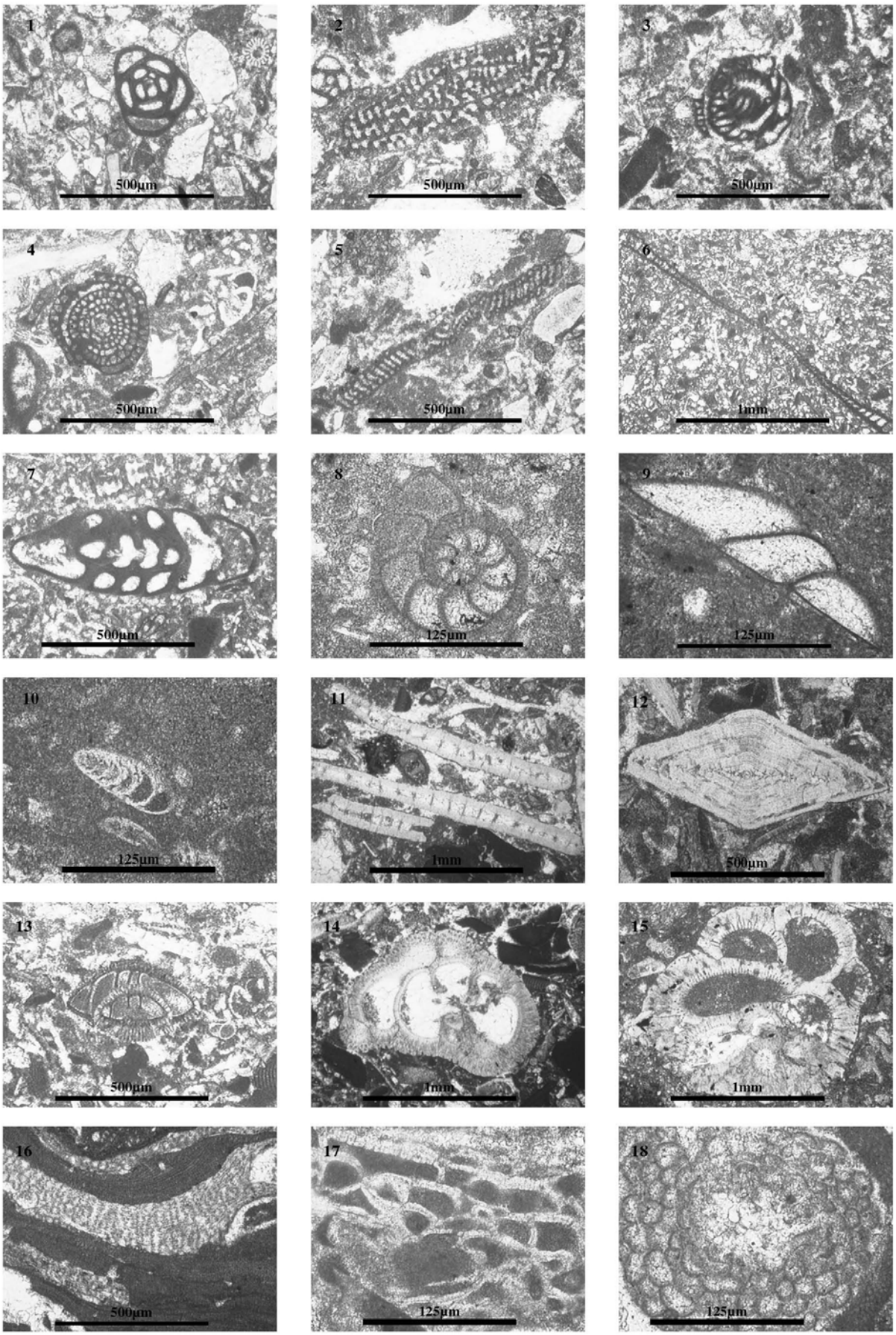

Figure 5.3b Microfauna photos

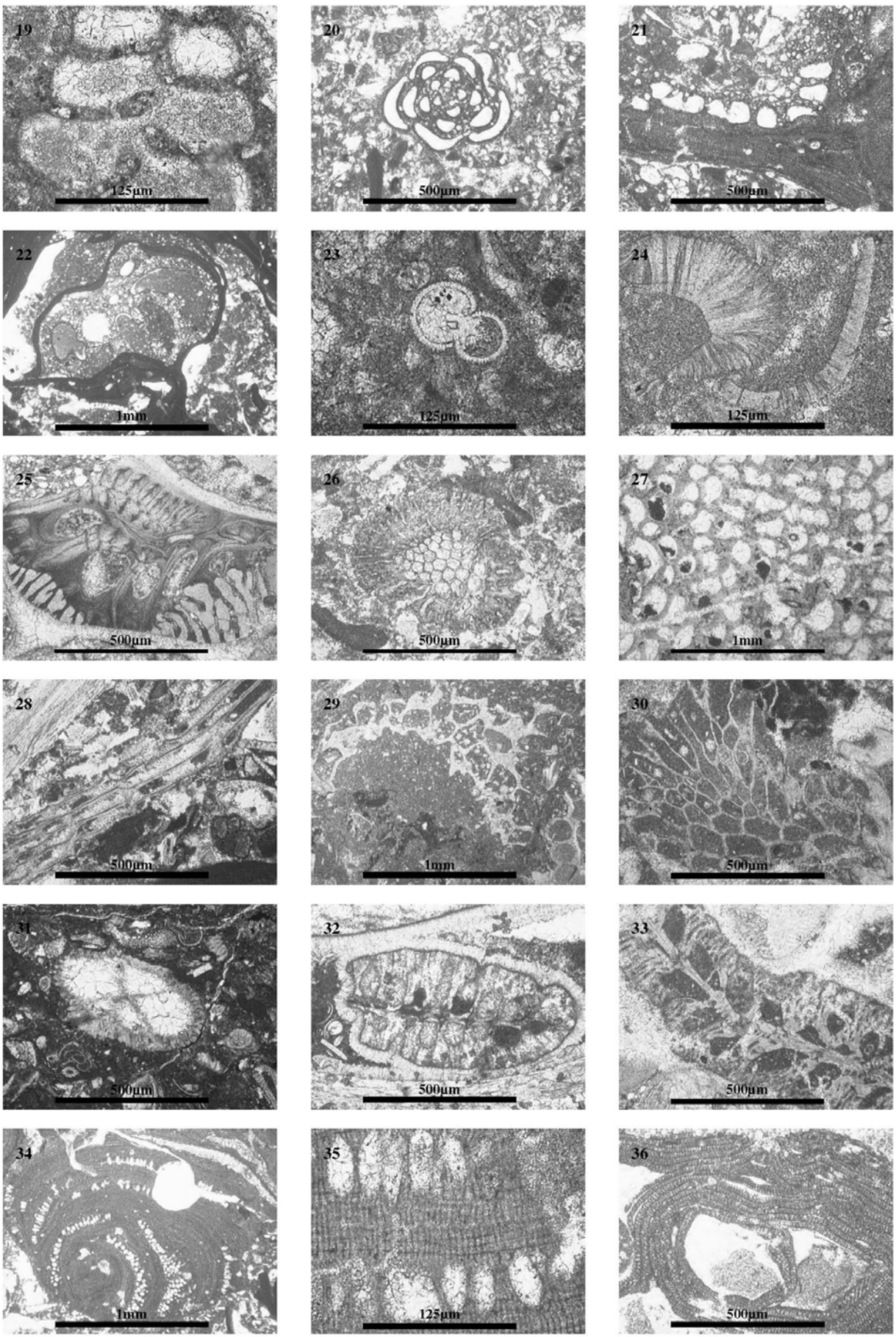

Figure 5.3c Microfauna photos

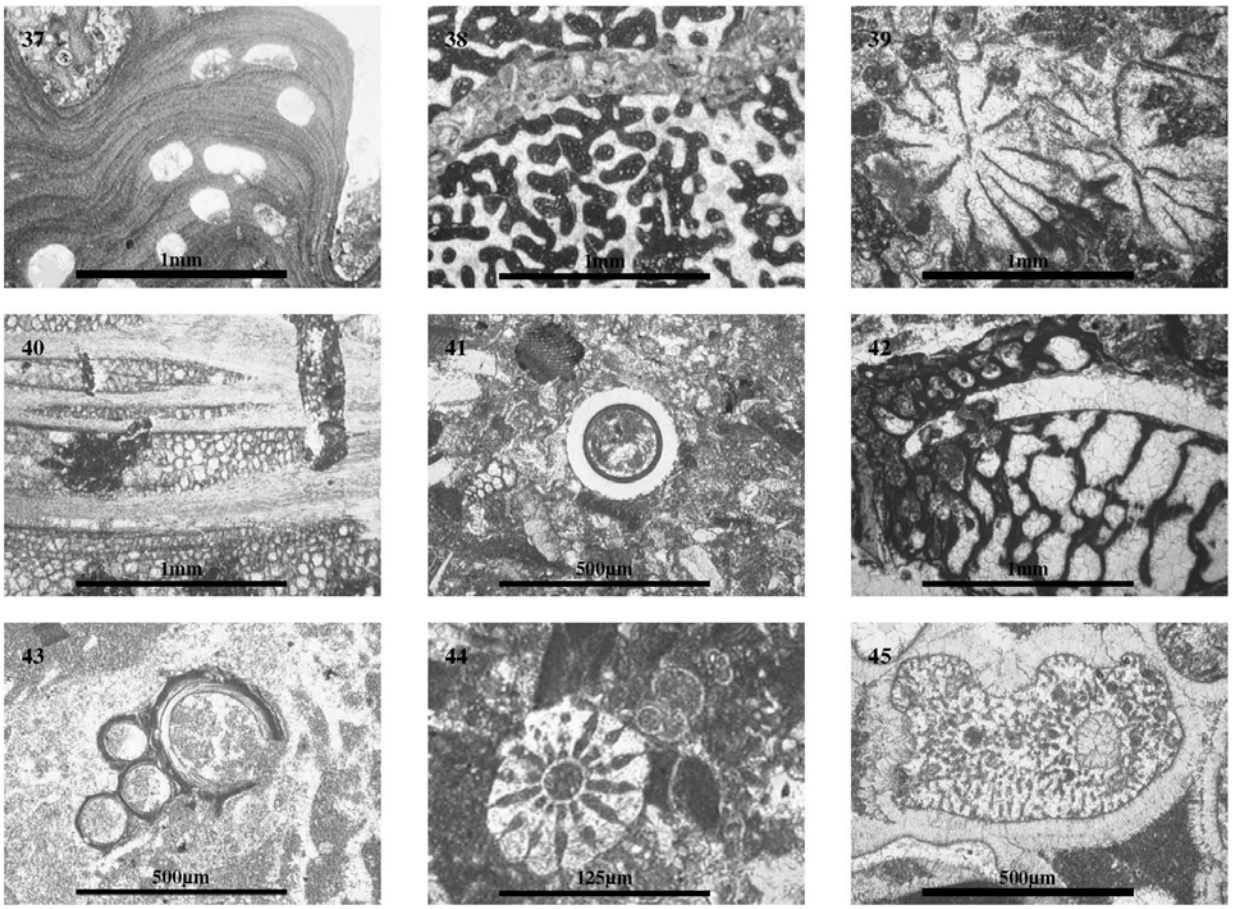

Figure 5.3d Microfauna photos

Figure 5.4 Coralgal framestone facies (1 and 2) outcrop textures
The top photo illustrates very well bedded coralgal framestone carpets (facies 1) from the Pirinc outcrop, while the bottom photo shows dome corals surrounded by clays (facies 2) at the base of the Zincir Kaya outcrop

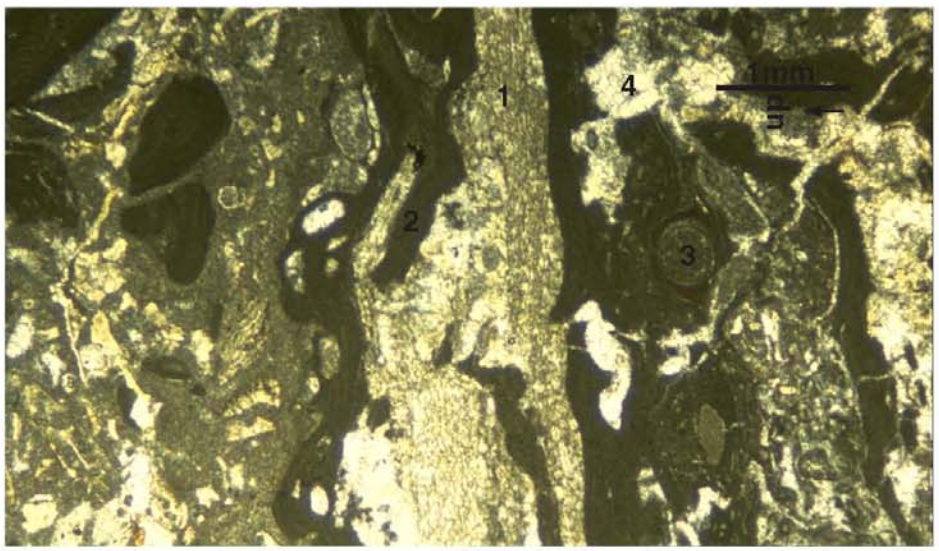

1. Acervulinids
2. Red algae
3. Serpulid tubes
4. Bioerosion

sample 30.4 (Kizil Kaya)

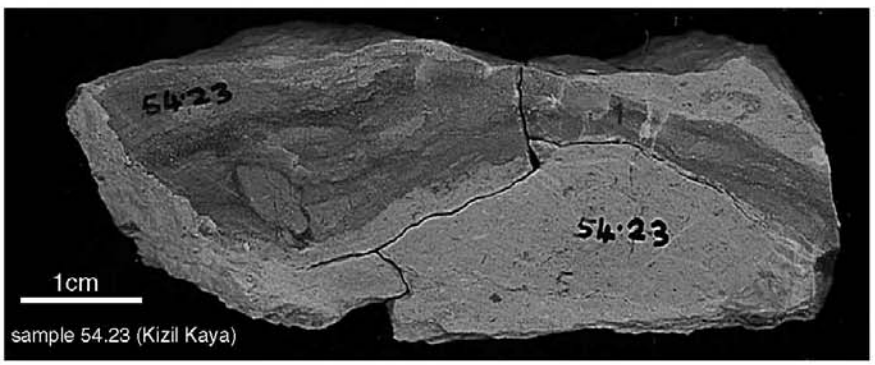

1. Platey *Porites* with borings

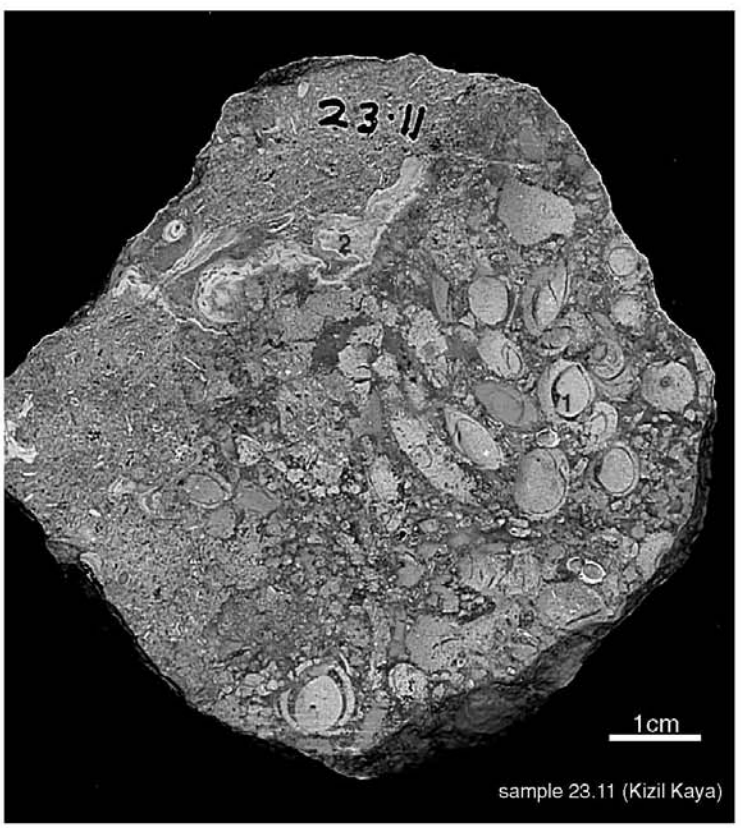

1. Lithophager borings
2. red-algal crusts

Figure 5.5 Coralgal framestones (facies 1 and 2)
Top photo shows a microfacies detail of encrusting organisms, the middle photo shows a *Porites* coral with plate morphology growing in a clay matrix, the bottom photo illustrates a highly bored and encrusted coral

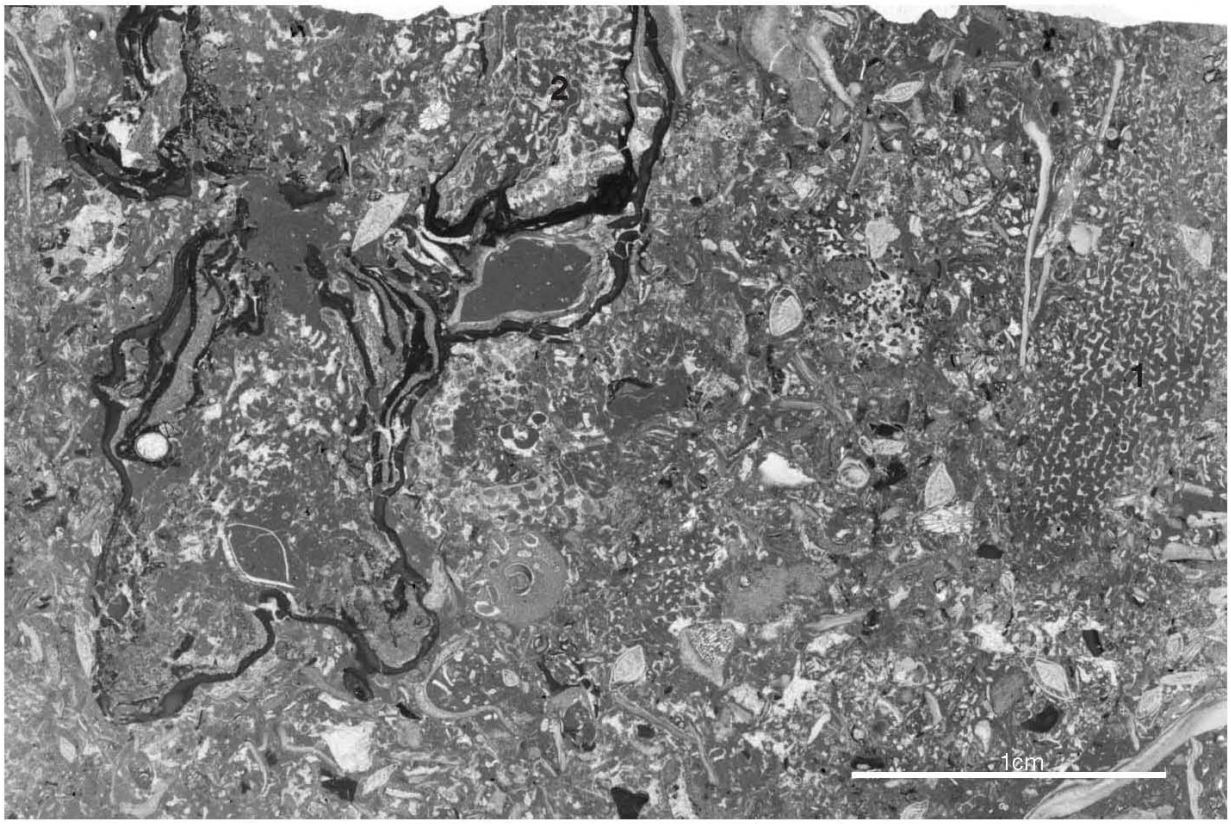

clean coralgal floatstones (facies 3) sample 29.8 (Kizil Kaya)

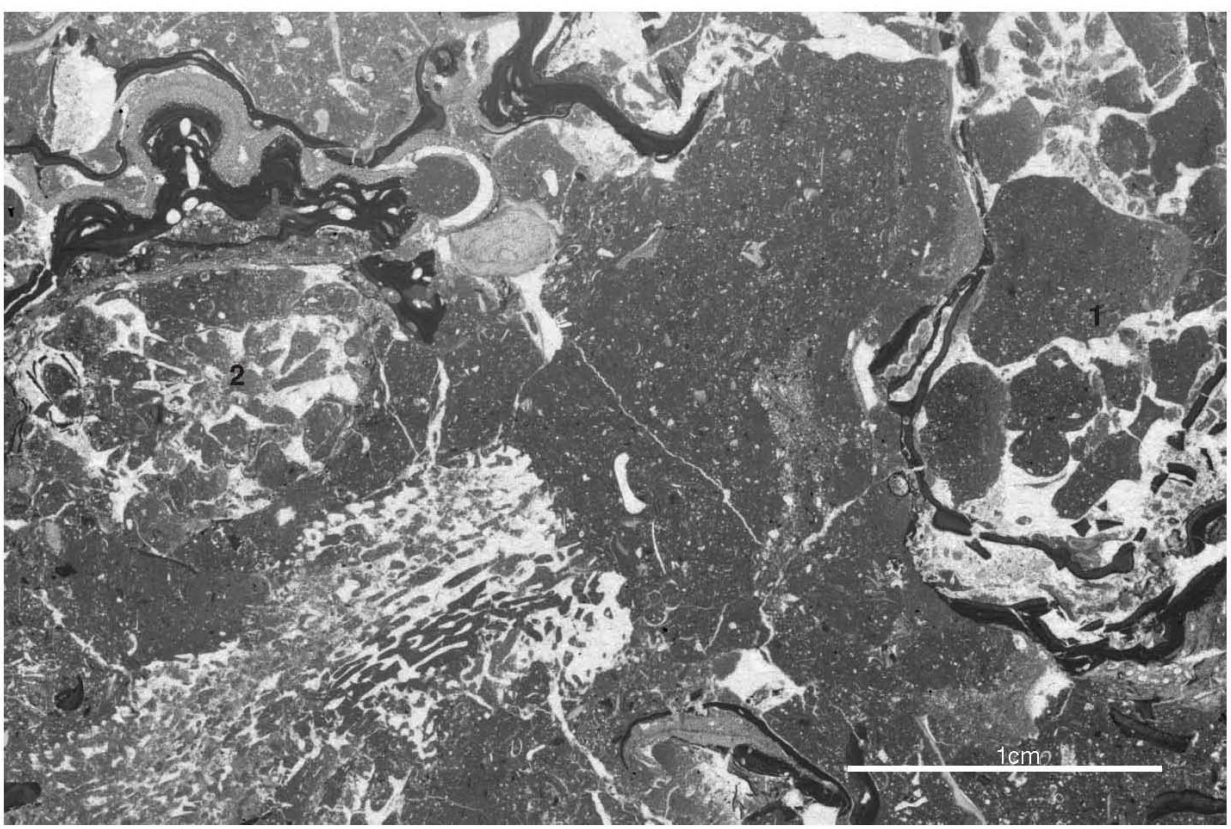

sample 28.19 (Kizil Kaya)

muddy coralgal floatstones (facies 4)

Figure 5.6 Facies 3 and 4
(the reference numbers on the photos are descibed in the text)

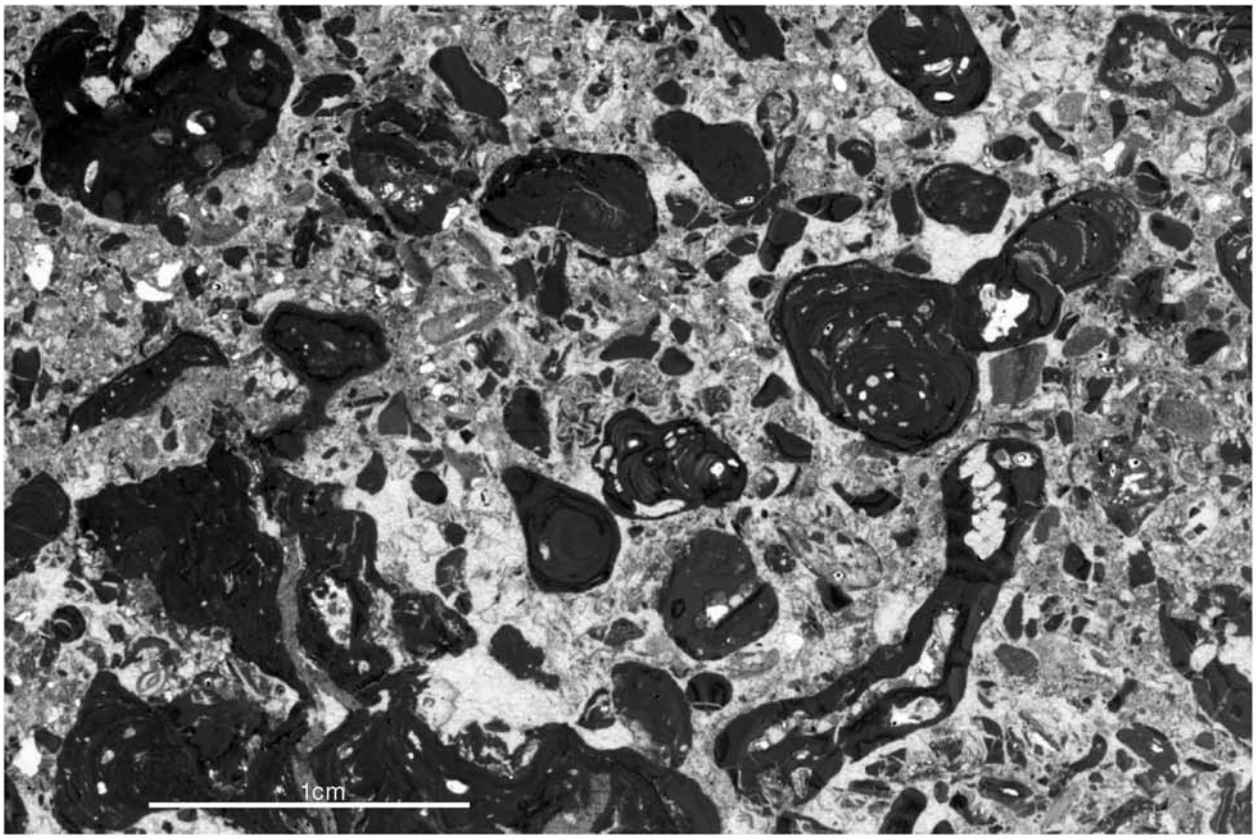

sample 40.21 (Zincir Kaya)

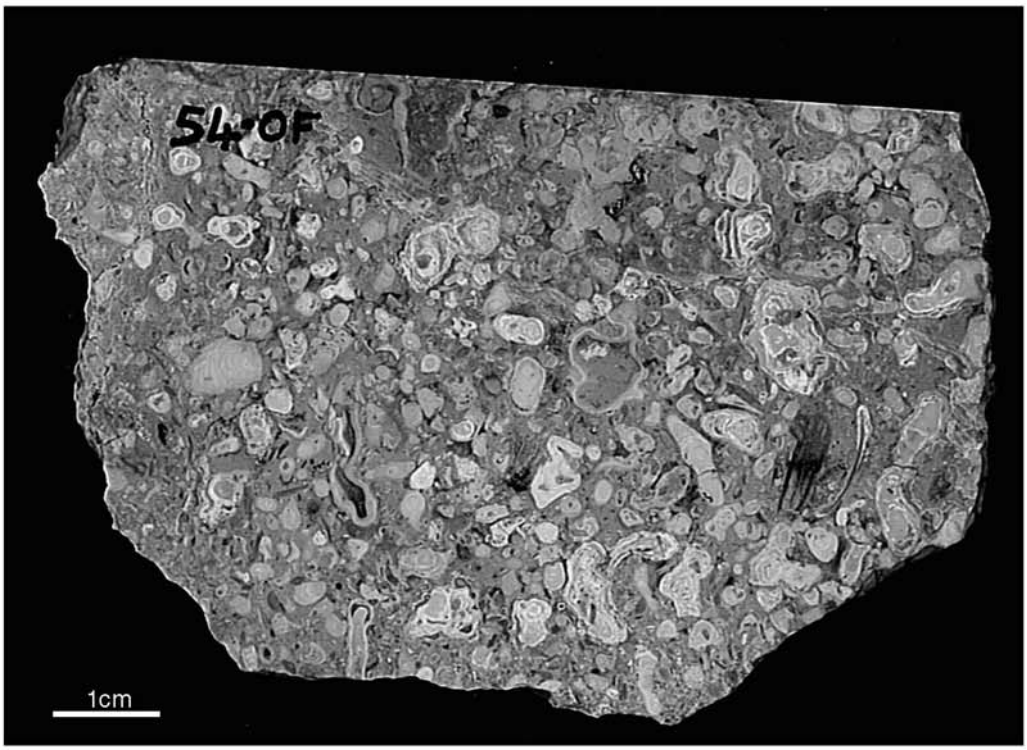

sample 54.0F (Kizil Kaya)

Figure 5.7 Clean rhodolithic float-boundstone (facies 5)
The top photo shows the microfacies texture of a well-washed rhodolite from the top of Zincir Kaya, while the bottom photo illustrates a similar hand-specimen texture from the top of Kizil Kaya

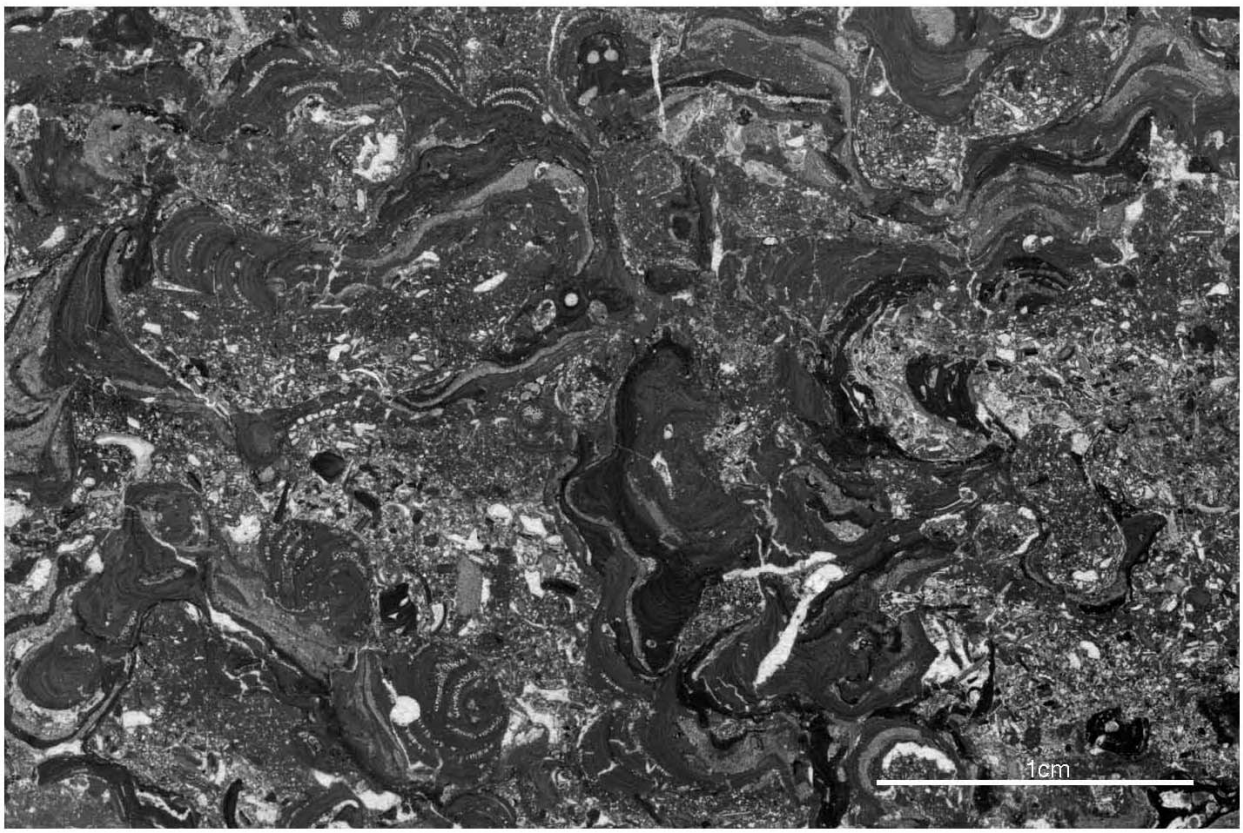

sample 28.7 (Kizil Kaya)

(Alahan section)

Figure 5.8 Muddy rhodolithic float-boundstone (Facies 6)
This illustrates the micro- (top) and macro- (bottom) textures of this facies

(top surface of Kizil Kaya outcrop)

log 40 (Zincir Kaya)

Figure 5.9 Microbial coralgal boundstones (facies 7)
This shows the outcrop texture and the bedding texture of facies 7 from Kizil and Zincir Kaya

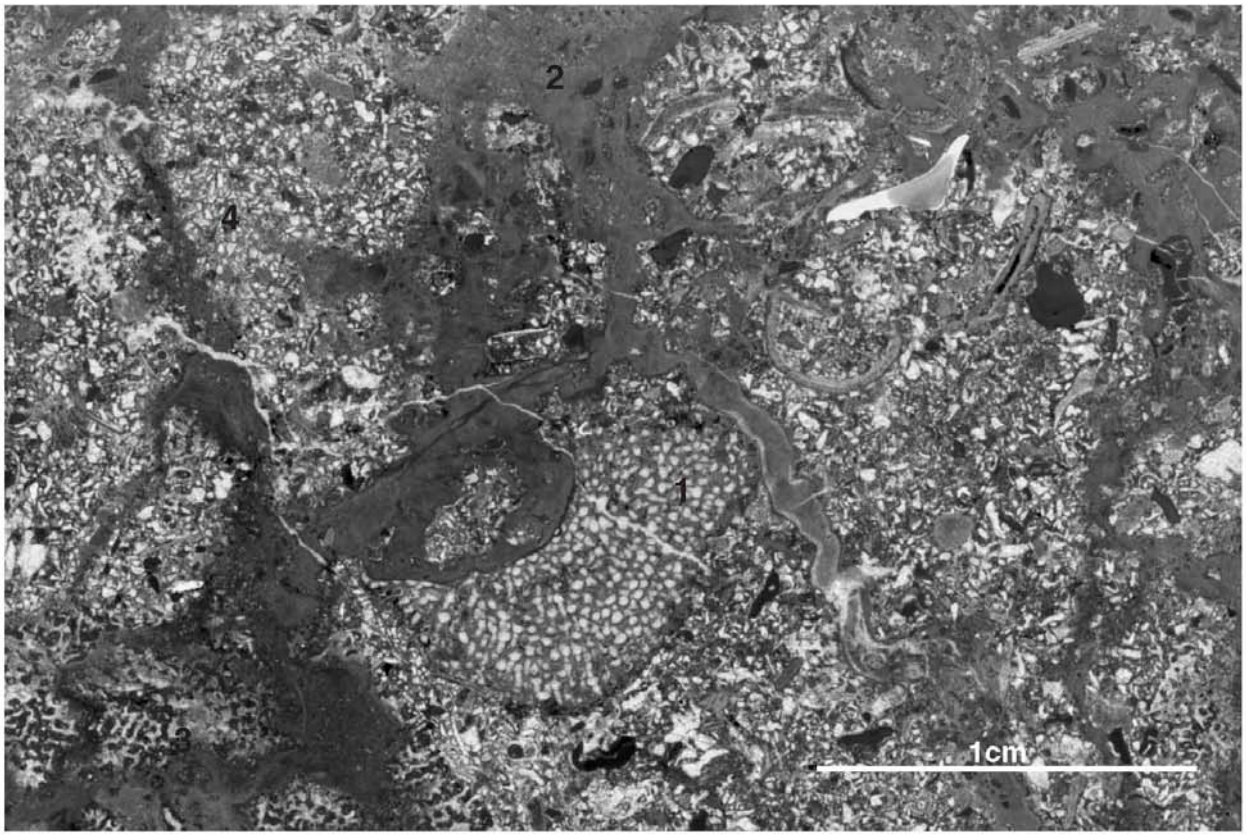

sample 40.16 (Kizil Kaya)

sample 40.16 (Zincir Kaya)

sample 54.0B (Kizil Kaya)

Figure 5.10 Microbial coralgal boundstone (facies 7)
This illustrates the microfacies (top) and hand specimen textures of this facies

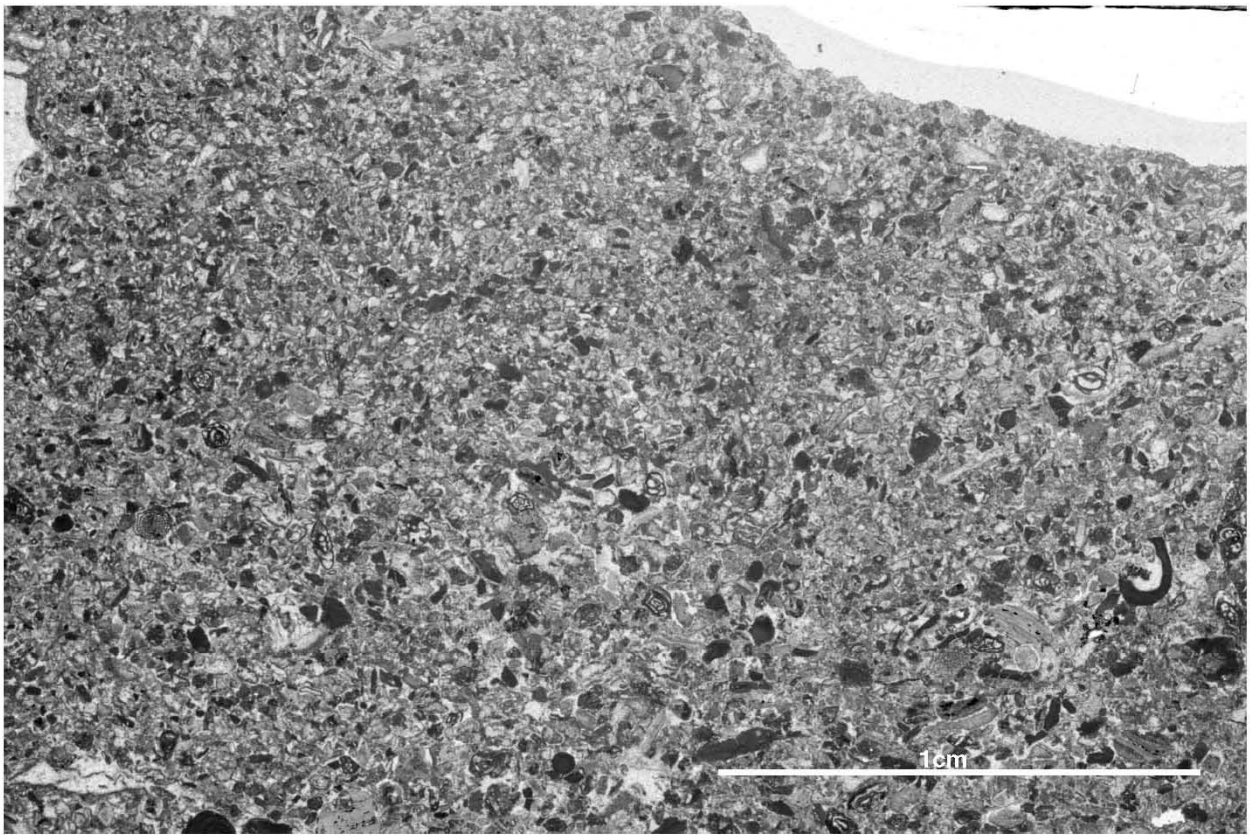

Facies 8 Miliolid grainstone (sample 28.5: Kizil Kaya)

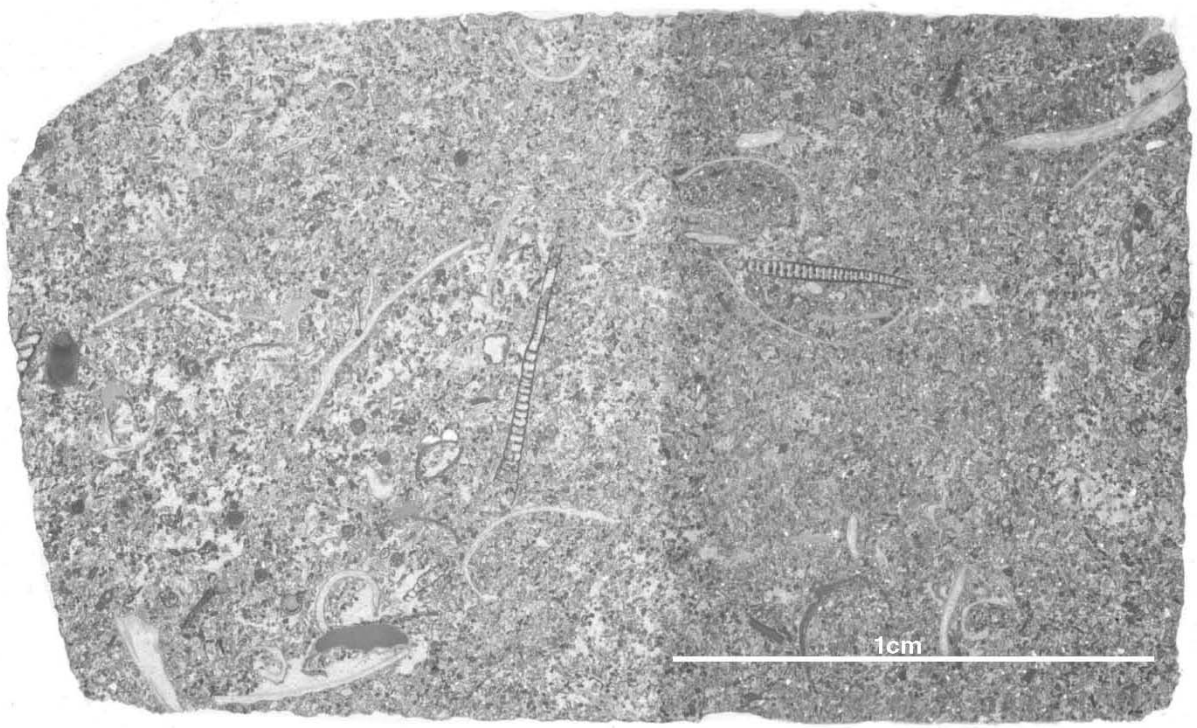

Facies 21: Soritid pack-wackestones, (sample 3.17 Dibekli)

Figure 5.11 Miliolid grainstone (facies 8) and Soritid packstones (facies 21)

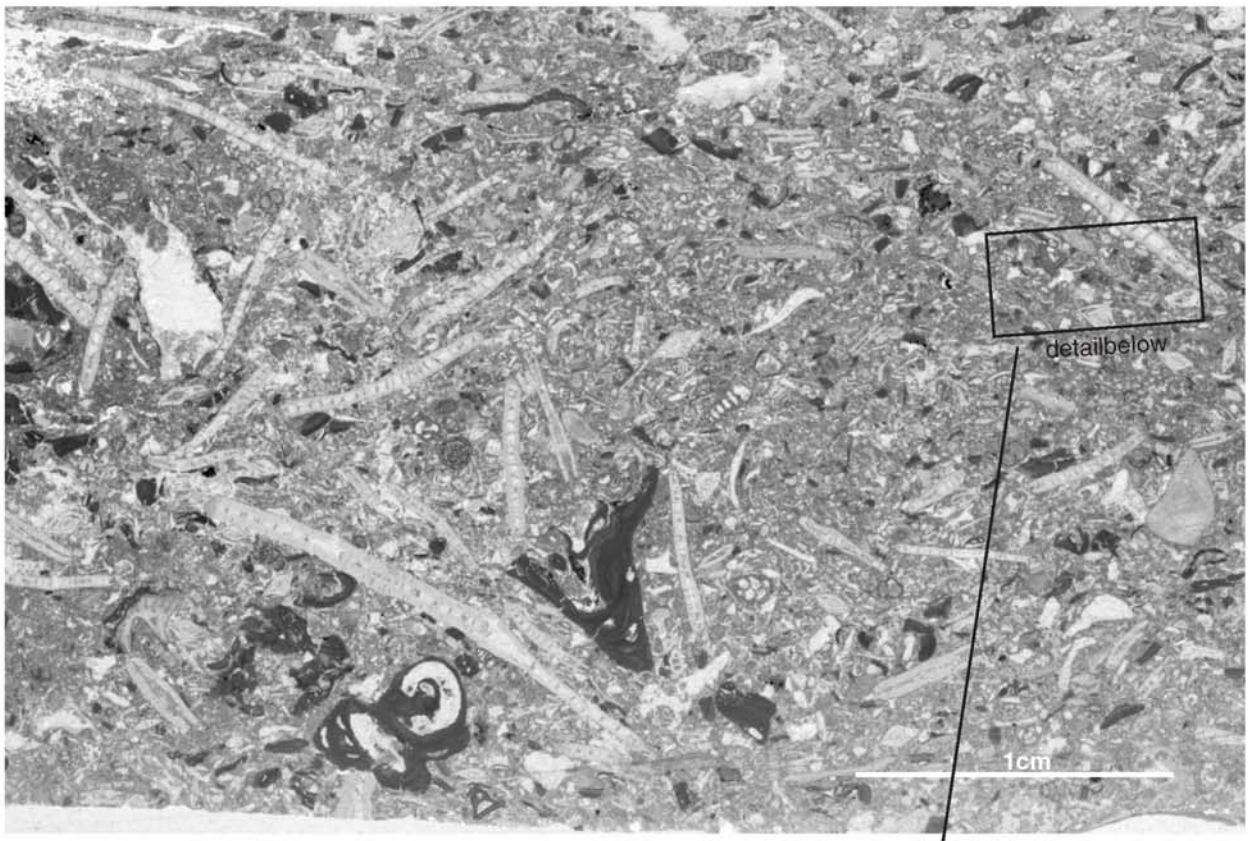

sample 35.4 (Kizil Kaya)

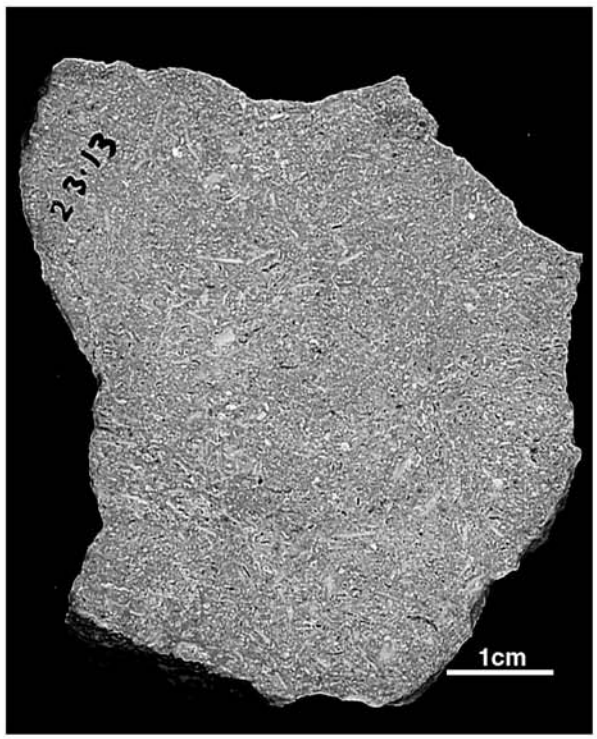

sample 23.13 (Pirinc Suyu)

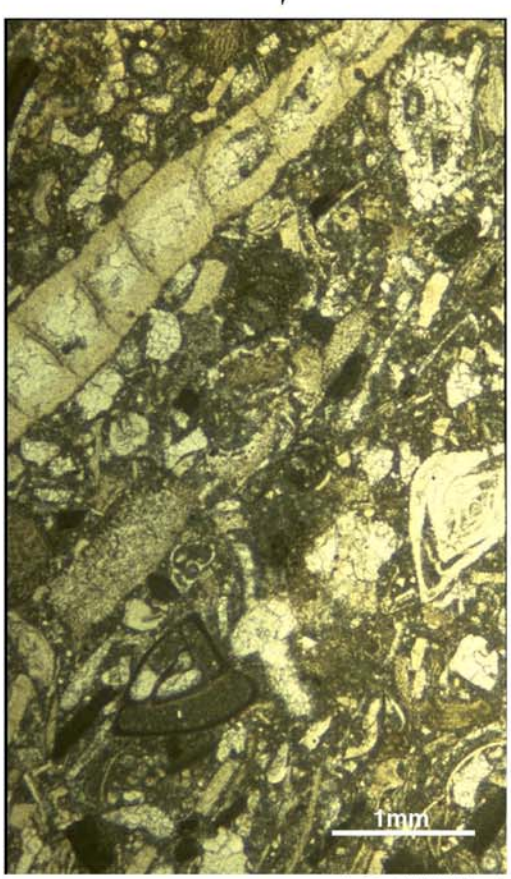

sample 35.4 (Kizil Kaya)

Figure 5.12 Nummulitid grain-packstone (facies 9)
This facies is here illustrated at three different scales.

Facies 10, marls: outcrop (log site 52, Silifke area)

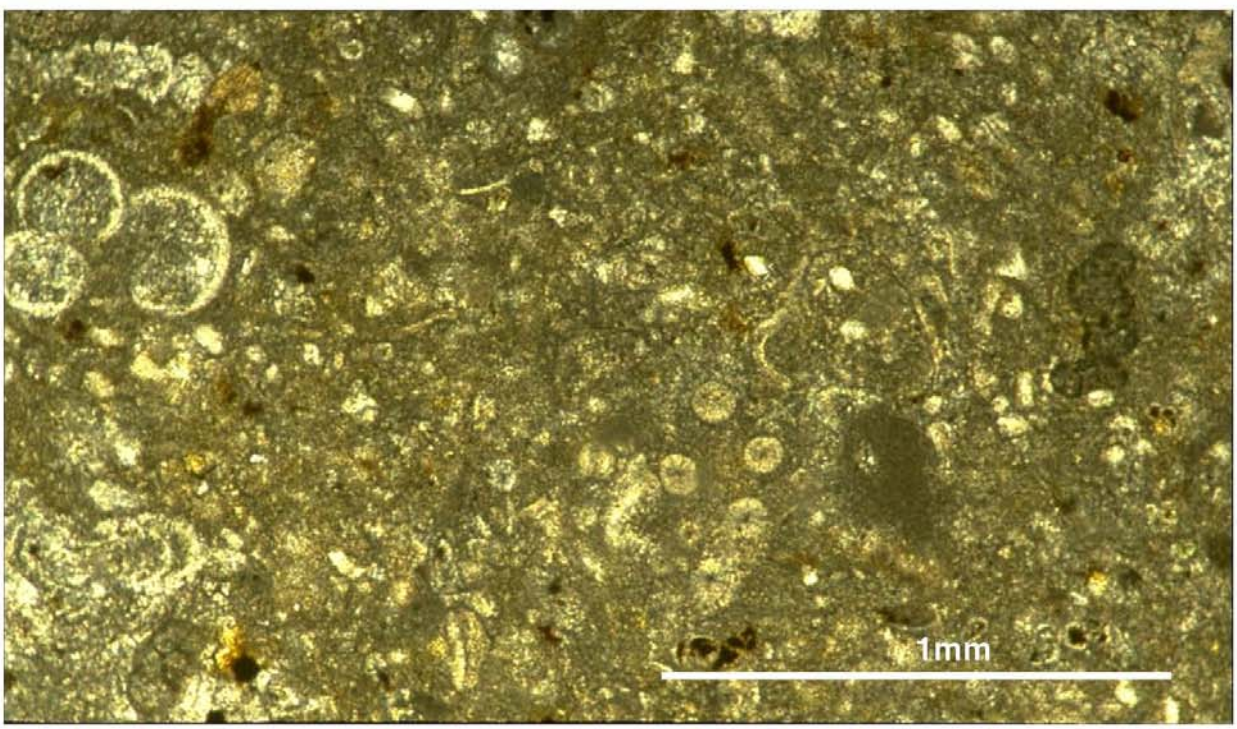

(sample 25.4, Kizil Kaya)

Facies 10, marls: microfacies texture

Figure 5.13 Marls (facies 10)

(Alahan section)

(detail from above-Alahan section)

Figure 5.14 Marine conglomerates (facies 14)

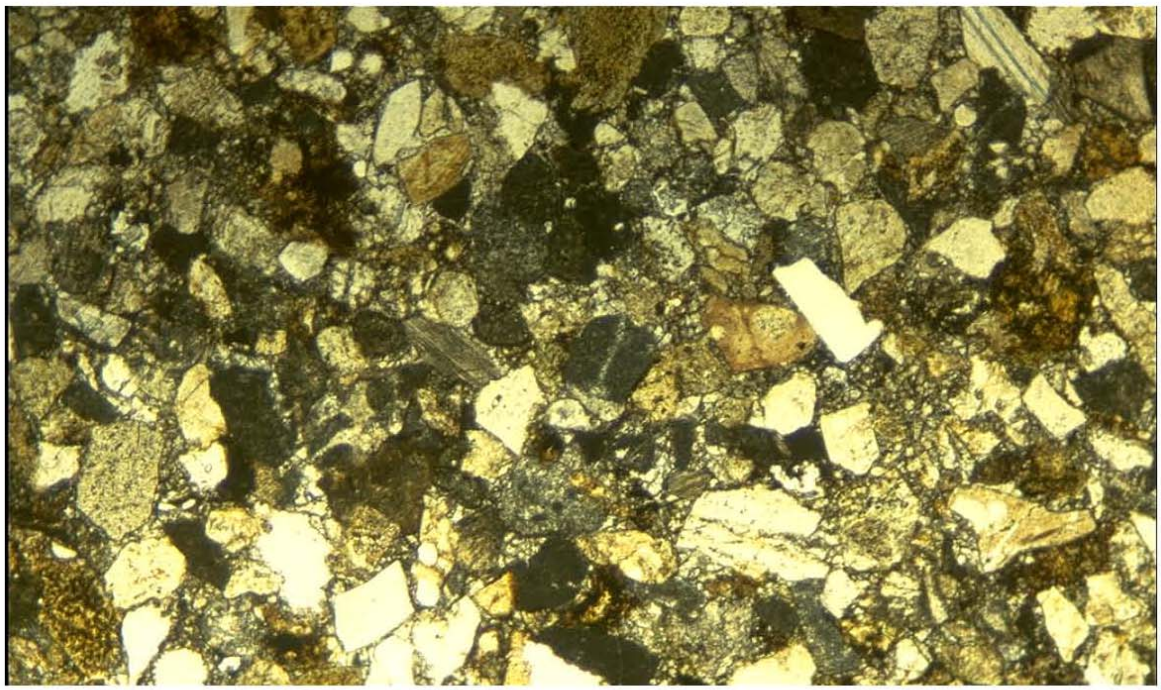

(sample 29.1 Kizil Kaya)

Facies 15: marine sands

(log 34 Kizil Kaya)

Facies 19: shallow marine silts/muds

Figure 5.15 Marine sands (facies 15) and Shallow-marine mudstones (facies 19)

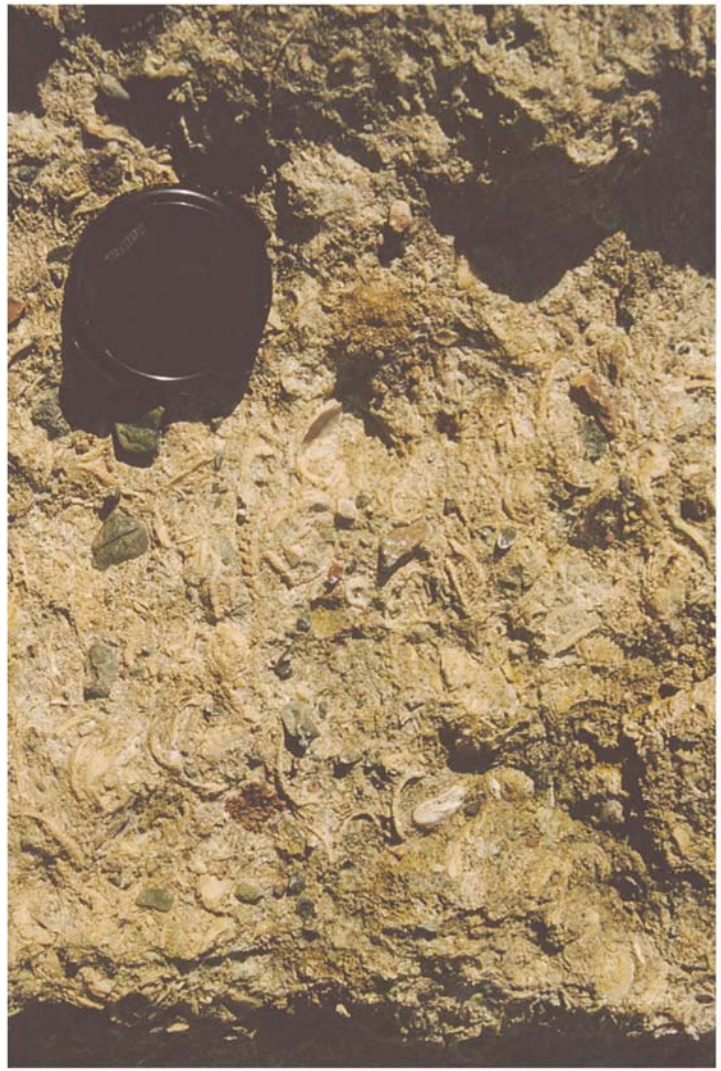

Facies 17: coquina rudstone

Facies 18: continental siliclastics
(Pirinc Suyu)

Figure 5.16 Facies 17 and 18

(near logsite 4, Slifke)

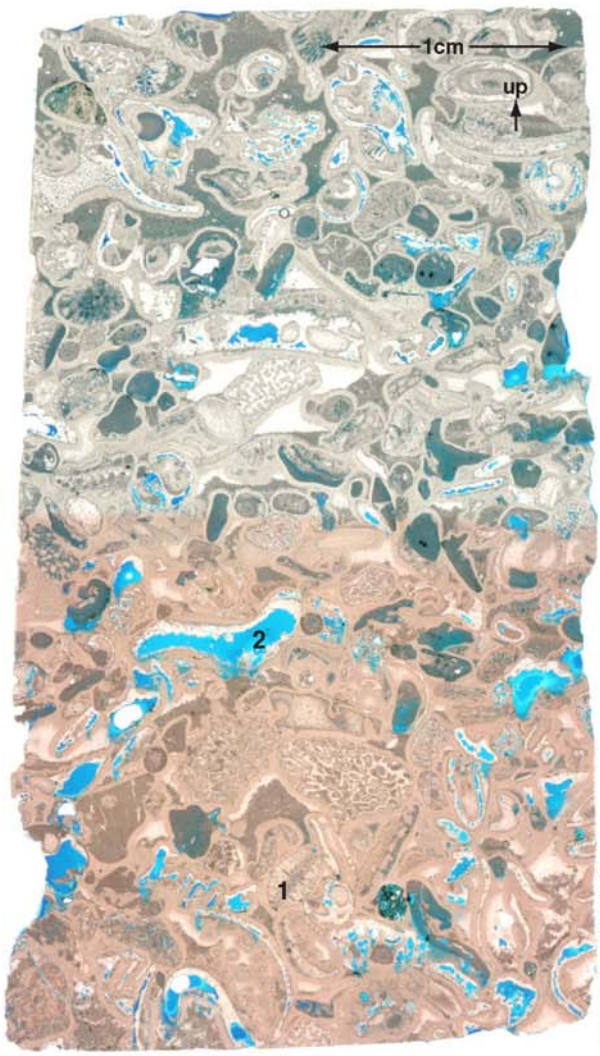

(sample 3.8, Dibekli, Slifke)

Figure 5.17 Bryozoan rudstones, facies 20
Above shows the typical bedding organisation of this facies (metre-scale cross-bedding), while below shows the microfacies texture, with the porosity highlighted by blue resin.

6 - PIRINÇ TRANSECT

6.1 INTRODUCTION

The Pirinç Suyu study site is 10km due north of Mut. It consists of a valley 1.4 km deep cutting into the northern escarpment of the Mut Basin, gouged out by the passage of the Pirinç River which decends from the Anatolian plateau to the north join the Goksu River further south. The valley is sufficiently deep to provide excellent exposure from the Mesozoic basement to the Miocene. The steep irregular valley sides are punctuated by vertical cliff faces. This geomorphology permits the observation of bedding patterns and the physical correlation of bedding surfaces from basement onlap to basinward lapout within the Miocene. The basement structural organisation is also clearly visible. Logs have been taken within the Miocene sediments in order to construct the stratigraphic crosss-section (see figure 6.1).

The Mesozoic basement is a grey, highly faulted Mesozoic limestone (Lower to Middle Triassic, Gokten et al. 1979; Cretaceous; Sezer, 1970), bound by a Palaeocene erosional unconformity, and overlain by Tertiary (probably Eocene?) dolomitised limestone, which has a highly karstified top surface. Normal faults, now with a strike of 110-120°, dropping down to the south, are activated during the basin opening phase in the Oligocene (see the Mut geological map, figure 4.7). The syn-extensional sediments are the continental clastics of the Derinçay Formation, and have been logged in this study (see appendix, figure 16.7). They pinch out as coarse conglomeratic alluvial fans against the pre-extension basement in the north and thicken to the south to fill the 110-120° trending graben structure with over 250m of fluvial and lacustrine sediment (see figure 4.6). The Miocene marine carbonates are first deposited during the Upper Burdigalian. They are considered as post extensional sediments, since they are almost undeformed by the basin faulting. However, some small faulting does occur that shares the same strike as the basin faults: a normal fault offsets the Miocene carbonates by 3m over the crest of a faulted basement block. It is sealed by the first slump unit in the Burdigalian study interval. This may be a small readjustment of the basement fault, or it may be the result of differential compaction of the underlying continental Derinçay Formation over the crest of the footwall block below.

6.2 VERTICAL FACIES EVOLUTION

In log 17 (figure 6.9) the vertical facies evolution is presented to illustrate how the sedimentary retrograding/prograding cycles are defined. The following discussion describes the vertical facies evolution observed in this log. Figures 6.14, 15 and 16 illustrate the microfacies described in the discussion. The bathymetric evolution determined from the facies (see facies chapter) is indicated on figure 6.9.

Sample 17.1 (facies 5) is a rhodolithic floatstone, with a green clay matrix. Encrusting Acervulinid foraminifera are found associated with the rhodoliths. This is interpreted as a shallow marine environment, with a soft muddy bottom. The mobile substrate prevented any encrusting fauna from establishing a community on the sediment surface itself, but red algae and Acervulinids were able to develop in this environment by creating their own micro-hardgrounds on which to grow, in the form of rhodolithic macroids. Their presence indicates some current action: this is required to both winnow the clays from the rhodolith surface, and to episodically overturned the rhodoliths, allowing growth on both sides.

Sample 17.2 (facies 8) is a poorly sorted packstone containing Soritid and Miliolid foraminera. The clay content is reduced, but still present. Extensive dissolution seems to have preferentially altered small centimetre-sized coral fragments. Now only ghost structures of these fragments remain: the form is defined by the undissolved envelope of encrusting fauna that coated the coral, and angular peloidal micritic pseudo-clasts, the original infill of the coral pores, is found floating in a microsparite cement. This implies that the original depositional texture is a rudstone or floatstone formed by the coral fragments, in a packstone matrix.

From sample 17.2 to sample 17.3 the sediment is organised into metre-scale coarsening-up packstone cycles, bound by flooding surfaces.

Sample 17.3 (facies 8) is also a Miliolid pack-grainstone, richer in Miliolids, and Soritids, than sample 17.2 and better sorted, also now containing Alveolinids.

At 10m there is a sudden facies change, with the deposition of 6.5m of coralgal framestones. The corals are mostly Porites plates and domes, with some rare short stick morphologies, mainly as debris. The beds are highly cemented and contain little clay. A clay rich interval defines the bedding.

Sample 17.4 illustrates the extensive dissolution of a Porites coral in this interval.

The top of the framestones is marked by a very irregular surface. Above this surface 2m of oyster rudstone and boundstone is deposited (facies 12): it consists almost solely of oyster debris. The oyster reef is covered by a 6m interval of irregularly bedded packstones containing Nummulitid foraminifera (facies 9). At the base of this interval, just overlying the oysters, these packstones contain abundant rhodoliths.

Sample 17.5 illustrates this facies: it is a fine argillaceous packstone/rhodolithic floatstone containing Miliolids, Alveolinids, Nummulitids and Amphisteginids, as well as some planktonic foraminifera. It also contains scaphopods, Serpulid worm tube debris and Textularinid foraminifera. The presence of both shallow platform foraminifera (the Miliolids) and planktonic foraminifera, as well as those typical of the slope environments, points to a high degree of mixing of shallow platform sediment into the lower slope environment. The presence of the scaphopods, worm tubes and encrusting textularinids indicates a muddy environment, while the rhodoliths indicate a mobile substrate, with episodic, if not periodic current action. The rhodoliths are relatively small and may be allochthonous, this environment being a base of slope repository for all the sediment that is washed out from the platform.

The sediment coarsens up over 6m to the 24m interval, where a surface develops encrusted with algae and small platey Porites corals.

Sample 17.6 (facies 9/1) is taken from just below this surface: the sediment is a fine wacke-packstone characterised by the presence of Nummulitids, Alveolinids, and planktonic foraminifera. The Miliolids are no longer present.

Sample 17.7 (facies 9) illustrates the sediment from just above this surface: it is compositionally very similar to that below, though much finer.

From sample 17.7 to 17.8 the sediment coarsens up.

Sample 17.8 (facies 8) is a pack-grainstone containing Miliolid foraminifera, as well as Nummulitids, while the planktonic foraminifera are absent.

The top half metre of these grainstones contains platey Porites corals and rhodolithic debris, before passing into 4m of coralgal framestone.

Sample 17.10 (facies 1) illustrates the coralgal framestones at 32-37m. The corals are highly bored, with Lithophaga bivalve shells preserved in place. The original coral is completely dissolved, and the angular micritic pore infills have in places collapsed before being re-cemented. Only very thin red-algal crusts develop on the surface of the corals.

From sample 17.10 to 17.11 the coralgal framestones are replaced by fine Nummulitid packstones, with a single renewed development of framestones at 38-39m.

Sample 17.11 (facies 9) is a very fine packstone containing Nummulitid, Amphisteginid and planktonic foraminifera, typical of the slope environment. Red-algal and coral debris is also common.

A distinct surface encrusted with small Porites corals occurs at 47m.

Sample 17.13 (facies 5) is a rhodolith packstone containing glauconite. This passes upwards into micropackstones and marls, dominated by planktonic foraminifera.

The base of the framestone interval starting at 76m has a sharp, possibly erosional contact with the marl sediments below.

Sample 17.14 (facies 1, though in microtexture facies 9) illustrates a mixture of Miliolids, Nummulitids, and planktonic foraminifera, as well as oyster fragments, coral fragments, bryozoans and encrusting Textularinids. Microfractures are infilled with fine blocky spar.

6.3 DEFINITION OF CYCLES

Different scales of retrograding/prograding sedimentary cycles have been distinguished in the Pirinç transect based on both the facies trends and the bedding patterns. 3 large-scale cycles and a total of 11 medium-scale cycles have been defined. The reasoning behind the definition of these cycle boundaries is given here.

Large-scale cycles

Cycle 1: two choices exist for cycle boundary 1. The first choice is defined by the facies as being near

the initial flooding of the continental environment. This interval is not well exposed in this area and has not been described in detail (see Kizil Kaya for a description of the continental to marine transition), so no precise surface can be defined. However, marine and continental sediments may be deposited contemporaneously, and the cycle boundary may be placed within the underlying continental sediments. The second choice is also defined by the facies: it lies approximately 50m below the marine flooding interval, where a thick packet of amalgamated channel deposits occurs in the fluvial sediments of the Derinçay Formation. The channel deposits may be filling the incisions created during the cycle boundary formation. This interval has been described in logs 14 and 15 (see appendix).

The maximum flooding surface of cycle 1 is defined from both the geometries and the facies. In the geometries it is marked by the most landward retreat of the large scale clinoforms observed at the northern end of the transect (see figure 6.1, 3 and 4). In the facies it is defined by an interval of marls (facies 10) covering the platform of the retrogradation, described in logs 17, 20a, 22 and 23 (see figures 6.9, 10, 12 and 13).

Cycle 2: cycle boundary 2 is defined from both the facies and the geometries. It has been described in logs 16, 17, 20 and 23. In the basin area it is defined by the facies evolution as the top surface of the lowest slump unit (see figure 6.1 and 3). A shallow marine platform develops in front of the slumps and onlaps against their top surface. this onlapping relationship implies a significant sea-level fall. Marls (facies 10) are found both above and below. These slumps and the associated platform represent a maximum of progradation (a major basinward shift of the facies belts) in the basin area. The cycle boundary is placed on the top of the slump unit and is an onlap surface for the platform deposits that develop above in the southern part of the transect. These slumps correspond to the falling-stage systems tract of Hunt and Tucker (1992, 1995). This cycle boundary is traced landwards in the bedding geometries. At the foot of the margin slope in log 23 this cycle boundary has been identified as a karstified surface at the top of a shallowing-up sediment trend. The top surface of these deposits is irregular, eroded, and has 50cm karst pipes infilled with massive calcitic spar. Thin sections show extensive dissolution of the corals. At the northern extremity of the transect on the large-scale margin top the cycle boundary has not been observed in detail since it was inaccessible in outcrop. From field and photograph observations of the geometries (following the beds up onto the platform) a conspicuous surface on the platform top has been proposed as the approximate position for the cycle boundary.

The maximum flooding interval has been identified as somewhere within the marls between the first and the second slump unit (see figure 6.1). Its exact position within the marls has not been defined.

Cycle 3: cycle boundary 3 is defined in the same manner as cycle boundary 2: in the basin it is the top of the second slump packet. This top surface is onlapped by a series of small basinally-positioned shallow-water carbonate platforms that develop at the base of the third cycle. This surface can be followed landwards up the slope of the large-scale platform margin. The position of this cycle boundary on the platform top is determined by identifying the highest bed truncated by the erosional scar on the platform front. This relationship is illustrated in figures 6.4 and 6.5. This top surface is innaccessible in the field, but some evidence for exposure has been preserved on the front of the slump scar: this consists of brecciated limestones in a ferruginous matrix, and ferruginous laminated sediment filling centimetre-sized cavities in the limestone (see figure 6.24).

Cycle 4: cycle boundary 4 is defined by applying the same logic as for cycle boundaries 2 and 3 to the third slump found in this area. The cycle boundary is positioned at the top of this slump unit. However, this slump is now the top of the outcrop, and no onlapping shallow-marine platform sediments have been observed, so it cannot be explicitly shown that this slump event is related to a major relative sea-level fall and cycle boundary formation. The slump scar is readily followed up the large-scale platform margin, steepening until it forms a sub-vertical wall in outcrop on the last truncated bed. The top of this bed is a distinct surface in the bedding geometries, and has been proposed as the cycle boundary. The surface itself is inaccessible in the field.

Medium-scale cycles

Five medium-scale cycles have been defined in large-scale cycle 1, two in large-scale cycle 2, and four in large-scale cycle 3. The description of the cycle definitions makes continual reference to figure 6.1 and 6.7. Note that certain of these cycles, especially cycles 2.2 and 3.4, may actually be including a number of medium-scale cycles. However, because the large-scale platform top at the northern end of the profile has not been logged, these extra cycles have not been resolved. This problem will be discussed later in the synthesis chapter.

Cycle 1.1: this cycle is defined only by its top cycle boundary, which is described below. the position of the lower cycle boundary has not been established for this cycle.

Cycle 1.2: cycle boundary 1.2 is defined principally from the geometries, where it is seen as a downlap surface of southward prograding clinoforms (see figure 6.2). A downlap surface could also be a maximum flooding, but the facies below the surface (in log 17) show a shallowing-up trend (progradation), and a deepening occurring across the surface. Placing a progradation (progradation above) over a

progradation (shallowing up below) creates a surface that contains the cycle boundary, the retrograding interval, and the maximum flooding. This can be compared to a parasequence geometry.

Cycle 1.3: cycle boundary 1.3 is defined from the geometries and the facies. Figure 6.2 and 6.3 illustrates this to be a downlapping surface. This downlaps the topsets of the last prograding cycle (1.2) and so is considered as a cycle boundary, including (as for CB1.2) the retrogradation and the maximum flooding in a parasequence geometry of stacked shallowing-up intervals. In the facies this surface is a sharp flooding in logs 23 and 22 over dominantly siliciclastic littoral to sub-littoral deposits. In log 17 (figure 6.9) oyster rudstones and rhodoliths initially re-colonise the sediment during the flooding, and rapidly deepen to Nummulitid packstones. Potential indicators of sub-aerial exposure along this cycle boundary have been found: in log 17 an irregular top surface, and micro-dissolution features in the framestones beneath CB1.3 occurs, and the facies changes very abruptly across the surface to pioneer communites of oysters and rhodoliths. In log 22 extensive dolomitisation below CB1.3 is observed in thin section. No evidence of an accommodation decrease is seen in the stratal geometries in this area.

cycle 1.4: cycle boundary 1.4 is well defined in the geometries as the toplap surface of the prograding clinoforms of cycle 1.3 in the northern part of the platform. Slight toplap also occurs on a landward prograding section of cycle 1.3, between logs 17 and 45. In the southern part of the transect it is seen as a downlap surface of the first isolated topography that develops on the site of the future isolated platform. In the facies this is seen as a sharp flooding, with rhodolithic coralgal framestones replacing the pack-grainstones of the underlying prograding clinoforms in log 17, and in log 22 it is a sharp deepening of the facies.

cycle 1.5: this cycle boundary is defined from the geometries as the topsets of prograding clinoforms in a number of positions across the profile at this time: progradation occurs in both a landward and seaward direction around the isolated platform, and from the landward platform margin in a seaward direction. In log 17 this cycle boundary is seen as a deepening shift from Nummulitid packstones (facies 9) to glauconitic rhodolithic packstones (facies 5). In logs 22 and 23 it is also seen as an abrupt flooding which is the start of a large-scale deepening trend. A maximum flooding interval has been identified for this cycle, and it corresponds to the maximum flooding of the large-scale cycle 1. There is some evidence for exposure along cycle boundary 1.5: dissolution features in the thin section samples in logs 22 and 23, as well as extensive dolomitisation of cycle 1.4 sediments beneath CB1.5 (log 23) point to emersion of the top of this cycle. This is supported by the stratal geometries: the erosive base of the prograding deposits, which places platform and slope sediments directly on basin sediments (facies 10), indicates a downward shift of relative sea-level.

cycle 2.1: the base of this cycle is the large-scale cycle boundary 2. No maximum flooding has been identified for this cycle.

cycle 2.2: cycle boundary 2.2 is placed at the top of the platform that develops in front of these first slumps. It is considered that the platform represents a prograding phase before the next retrogradation that floods this platform and the slump deposits. This cycle boundary has been described in logs 16 and 17 (top of log). In log 16 a symmetrical shallowing then deepening trend is seen, and the cycle boundary is placed at the turning point, being the turn-around from progradation to retrogradation.

cycle 3.1: the base of this cycle is the large-scale cycle boundary 3, as defined above.

cycle 3.2: cycle boundary 3.2 is placed at the top of the platform that develops during cycle 3.1. The abrupt change from a shallow platform environment to a basinal environment is the result of the retrogradation of cycle 3.2. This cycle boundary has been described in logs 18 and 19.

cycle 3.3: cycle boundary 3.3 is placed at the top of the platform that develops during cycle 3.2. The same logic is applied as for cycle boundary 3.1. This surface has been described in logs 20 and 21. Possible emersion of this surface is indicated by extensive dissolution features in logs 17, 22 and 23 below this surface, potentially associated with the development of a meteoric phreatic environment. Extensive dolomitisation occurs in log 23 below this surface, and may have the same causes. However, the stratal geometries do not give any evidence for a downward shift of relative sea-level.

cycle 3.4: this cycle boundary is placed at the top of the platform that develops during cycle 3.3, for the same reasons as cycle boundaries 3.2 and 3.3. This limit however, is more subtle: in the facies it is marked by a coralgal boundstone horizon 50cm thick, above which the sediments fine abruptly, and start a fining up trend. Additionally a geometric control is provided: the platform of cycle 3.3 below is seen to prograde slightly, and the cycle boundary 3.4 marks the end of this progradation. A maximum flooding is also defined for this cycle, which corresponds to the maximum flooding previously defined for the large-scale cycle 3 (see above).

6.4 PLATFORM EVOLUTION

Large scale cycles

Cycle 1: At the start of the first cycle, during lowstand times, relatively tabular strata gradually

onlap the gently sloping basement topography as accommodation space is created. A variety of facies are found, with coralgal boundstones building a gently sloping relief on the seaward extremity of the carbonate platform, with bioclastic sands in the internal areas of the platform, and some siliciclastic sediments, sourced locally (no major river system is found in this area), in the most proximal areas near the onlap with the basement. The medium-scale cycles in the proximal deposits are organised into prograding parasequences, and these are considered to form the shoreline area.

As the rate of creation of accommodation increases the stratal geometries change: sediment deposition becomes localised in two areas. Firstly in the most proximal setting, where large aggrading geometries are seen, and secondly on the rim of the seaward margin, where an isolated platform develops. This platform is considered to be roughly circular in plan view and is 500m in diameter. Sediment production on this platform finally gives up as the retrogradation accelerates, before the maximum flooding surface is reached. The isolated platform is then buried in marls, while the platform continues to aggrade in the more proximal setting. During the highstand this proximal platform margin starts to prograde. The maximum flooding surface and the steepening clinoforms of the progradation (highstand) are illustrated in figure 6.21. Then an abrupt sea level fall exposes the platform top. The steep platform margin collapses, sending slump deposits 2km out into the basin. The sea-level drop is estimated to be of the order of 100m, based on in-situ shallow-water platform carbonates being found in the basinal marls. This calculation is discussed in the synthesis chapter later on.

Cycle 2: the depositional locus shifts seawards, and shallow marine carbonate sediments are deposited in onlap against the top surfaces of the slumps. This onlap surface marks the end of this cycle, and the onlapping platform can be considered as the lowstand deposit of the second large-scale cycle. Relative sea-level rises rapidly, and platform sediments are deposited once again in the northern extremity of the study area, on the platform top. These sediments aggrade, then a second large-scale sea-level fall of the order of 100-150m provokes the collapse of the margin, sending slump deposits up to 2km out into the basin once again.

Cycle 3: shallow marine platform carbonates are deposited in onlap against the seaward-sloping top of these slump deposits. This onlap surface is the third large-scale cycle boundary. As relative sea-level rises a succession of small platforms are deposited against the slumps, and these represent the lowstand and retrograding deposits of this third cycle. Eventually sea-level refloods the platform top and approximately 60m of platform sediments are deposited here, before the third large-scale sea-level fall, that provokes the third slumping event. The first two sea-level falls have been demonstrated by the deposition of shallow marine deposits in front of the slump units, 100-150m below the platform top from where the slumping originated. However, this third slump unit has no onlapping sediment that outcrops, so the sea-level drop inferred here is by analogy with the first two slump events. Figure 6.17 illustrates an end on view of the slump deposits, showing the relationship between the three slump horizons.

Medium-scale cycles

These three large-scale cycles have been broken down into eleven medium scale cycles. The following description makes continual reference to figure 6.1, and to the stratal patterns photographed and drawn in figures 6.3-4.

Cycle 1.1 has a maximum thickness of 22m, thinning out distally, and proximally onlapping onto the underlying continental sediments. The stratal geometries are tabular. Only the top of the cycle has been logged, so the position of the base is unknown. The facies are described in log 17: the maximum flooding is marked by an argillaceous rhodolithic pack-floatstone (facies 5) bed. The prograding part consists of 9m of shallowing up bioclastic sands containing Miliolids (facies 8) organised into 5 metre-scale coarsening up cycles. These are interpreted as very shallow marine (<5m) para-autochthonous platform deposits. Coralgal framestones are proposed as the facies at the margin of the platform: this is consistent with observations made in similar settings in the detailed study areas of Kizil Kaya and Zincir Kaya, though no observations have been made in this area.

Cycle 1.2 is 20m thick at its thickest interval, and roughly isopachous. Internally oblique stratal patterns are observed in two areas: steep oblique parallel bedding 5m high progrades out distally from the 2500m to the 1400m mark on figure 6.1. Also shallower angle oblique-tangential bedding progrades out distally from 1300m to 750m. Both these progradations downlap directly onto the the underlying cycle boundary.The thickness change from 5-20m at 1300m is associated with variations in the rate of creation of accommodation space due to the differential compaction of the underlying continental sediment. The facies are described by logs 17, 22 and 23. In log 17 the entire cycle 1.2 consists of coralgal framestones, with bedding defined by an argillaceous horizon. In log 22, at the southern limit of the oblique-parallel bedding, gravelly siliciclastic basement sands containing some pebbles, and marine faunal debris are found, while further internally at log 23 a sorted, clast supported conglomerate is found: it consists of rounded basement clasts up to 30cm in diameter, often bored, with debris of red algae and molluscs in the matrix, and a calcitic cement. So in this cycle two general sediment styles are developed: at the margin of the platform the autochthonous coralgal

framestones trace the increasing accommodation by agrading, while in the internal platform seaward prograding packets of exported bioclastic and basement sands fill in the accommodation space once it has been created.

Cycle 1.3 is 12m thick and roughly isopachous. Oblique-parallel cross-stratification progrades seawards from the internal extremity of the section (2500m north), and a small break in slope is observed at 1050m. A slight depression starts to develop separating the margin deposits from the internal platform. It is at this time that the margin build-up first starts to possess topographic expression. The facies of cycle 3 have been described in logs 17, 45, 22 and 23. Facies in the margin build-up have not been observed, though by comparison with other build-ups studied in detail (Kizil Kaya and Zincir Kaya), and from observations made in log 16, a coralgal boundstone is inferred. Just behind the build-up on the landward side bioclastic sands containing Nummulitid foraminifera are found in log 17 (facies 9). These are typical slope deposits. Moving landwards, further into the depression, finer Nummulitid carbonate sands are found, the cycle then thickens again and the small break-in-slope at 1050m marks the transition from Nummulitid to Miliolid carbonate sands (facies 8), typical of the shallow platform top. Some coralgal boundstone textures have also been observed at the edge of this internal platform. Further landward, tabular beds of carbonate sands are found, as well as some coral bearing intervals, associated with the retrogradation and the maximum flooding in log 22. At the internal extremity of the section in log 23, 10m high oblique-parallel cross beds of Miliolid grainstones prograde seaward.

Cycle 1.4 has a very variable thickness: it is at this time that the isolated platform at the margin develops its distinct topography, separated from the internal platform by a trough from 700-1100m. On the margin the cycle has a total thickness of 22m, while in the trough it thins to 10m, thickening again to 20m on the internal platform. During the retrogradation a mounded topography develops on the margin edge: this builds first up, then out, partially filling the trough. On the internal platform only aggrading tabular bedding is observed during the retrogradation. The prograding deposits prograde out seaward from the platform, sitting out in front of the retrograding tabular beds, with some slight bevelling of the platform edge that formed during the retrogradation (Figure 6.21). Facies are controlled by logs 16, 17, 45, 22 and 23. The isolated platform slope front is built up by coral framestone carpets interbedded at high frequency with basinal marls (facies 10). During the final part of the the progradation 3m of Nummulitid packstones (facies 9) are deposited, which onlap the platform slope. On the landward slope of the isolated platform, in log 17, the retrogradation is characterised by coralgal framestone deposits (with rhodolith beds at the base), micropackstones-marls (facies 10) lie around the maximum flooding surface, and the progradation sees the arrival of Nummulitid packstones. In log 45, situated in the trough the final part of the progradation is found to be a 3m bed of coralgal rudstones (facies 13), with a very sharp, erosive downcutting base characterised by tool marks, and furrows. The bed itself has steep cross planar bedding surfaces: strong current action and channelling is inferred from this. On the internal platform the facies belts retrograde during the retrogradation, aggrade, and then shift basinwards with some erosion as described above. The facies are Nummulitid pack-grainstones (facies 9), distally changing into micropackstones (facies 10) and proximally becoming sandy Miliolid grainstones (see log 23). The facies shallow to the top of the cycle.

Cycle 1.5 varies from a thickness of 110m in the northern extreme of the study area to 28m above the isolated platform at the southern margin. During the retrogradation the isolated platform retrogrades symetrically, the shallow platform depocentre contracts and finally disappears leaving a drowning unconformity. To the north the internal platform retrogrades up to the maximum flooding, then progrades out, always with an aggradational component. During this time the drowned platform area is buried by a variable thickness of basinal marls (facies 10). These marls fill the irregular topography around the isolated platform on the southern margin. As the progradation progresses, the aggrading platform to the north is exposed and slumping occurs, sending large slump deposits out over the marls into the basin. It was not possible to log the internal platform, so the exact position of the cycle boundary on the platform top in the north is uncertain: a number of prominent surfaces were identified in the field. The cycle boundary was recognised in log 23, and this surface was then followed up visually onto the platform, and the most likely candidate chosen. The error in the positioning of this surface is estimated at +/-15m, by taking the extremes of the choices available. The slump deposits consist mainly of large rigid, or semi-rigid olistoliths. They are organised into a number of basinward sloping imbricated packets. Each packet is roughly tadpole shaped: the head is the largest block, and the tail consists of megabreccia and deformed bedding. The underlying bedding in front of the head is highly rucked, buckled and deformed, and can be reworked into flame structures caught between large blocks. Just beneath the slumps grain-flow beds are found, with sharp erosional bases, bioturbated tops, and an imbricated microstructure (see log 22, sample 22.14). The slump bodies found here are isolated deposits, and cannot be followed up onto the platform in this section: they may have arrived at an oblique angle to the section available. However, it is with some certainty that they are correlated to large-scale cycle boundary 2 as identified in log 23: the

slumps are sandwiched in marls, and the other available cycle boundaries above and below are traceable laterally. The other alternative is to correlate these slumps with the slump packet above, but then it is difficult to explain the 20m of basinal marl deposits that separate the two. Log 23 illustrates best the facies evolution of this cycle: the maximum flooding zone is readily identified as an echinoderm rich marl interval, though a single maximum flooding surface has not developed since the sedimentation rate was too high. A shallowing trend then occurs in the facies and is terminated by a 5m packet of coralgal bindstones, containing both Miliolids and planktonic foraminifera.

Cycle 2.1: this has a maximum thickness of 10m above the isolated platform. This cycle is comprised of shallow platform sediments deposited onlapping against the top surface of the slump deposits of cycle 1.5. These sediments are encased below and above in deeper water marls. Associated with the slump, they are important evidence supporting a dramatic sea-level fall as the cause of the slumping. They have been described in logs 16 and 17. In log 16 the distal limit is described, it consists of three 30cm beds of coralgal framestone, rich in rhodoliths with marls above and below. More proximally in log 17 10m of coralgal framestones are found. They have here been interpreted as being in-situ, since no deformed bedding is found within the outcrop, and they can be readily correlated with the sediments previously described in log 16. The stratal geometry is deformed by post-sedimentary sagging due to differential compaction of the marls beneath. These framestones have a characteristic well bedded appearance, with 20-50cm beds seperated by 1-10cm of marly packstones containing Nummulitids and planktonic foraminifera (facies 9). Diverse coral morphologies develop, including, small domes, plates and sticks, and coral rubble textures at times form rudstones, though the facies is generally described in figure 6.1 as coralgal framestone (facies 1).

Cycle 2.2: as relative sea-level once again rises most of the profile is covered with basinal marls, and the depositional locus migrates up the slope over the slump deposits to the northern extremity of the study area, where approximately 60m of shallow platform carbonates are deposited on the margin. Backfilling cross bedding progrades in a northward direction from the margin in the north, first creating, then filling a rimmed margin topography on the platform top. These have been observed in the cliff-face geometries, though the facies have not been observed. The slope facies are described in log 23 (note that CB2.2 is contained within CB2 in this log): Nummulitid packstones (facies 9) are dominant, with some intervals of coralgal framestones present. Rhodoliths are also common in this toe-of-slope environment. Some grain flow beds are also present, with Miliolids mixed with planktonic foraminifera (just below the next slumping event). Further distally, 20m of basinal marls are deposited.

The top of this cycle is marked by a dramatic relative sea-level fall estimated at 100-150m. This fall provokes karstification of the platform top in the north, evidence of which can be seen as ferruginous breccia fill and laminated micro-cavity fill on the slump front (see figure 6.24). Slope failure of the margin front also occurs at this time: the nature of the slump packets is varied: sitting against the upper slump scar rigid slices are rotated by listric fault sets that converge onto the main glide plane (figure 6.22). At the foot of the slope the slump deposits are dominantly olistolithic blocks up to 20m across (figure 6.23), while further distally the olistoliths become smaller, and plastically deformed bedding is intimately mixed with the mega-breccias. The deformed bedding includes both shallow marine carbonates and marls. Small extensional faults are common, with the void space created filled by the upward buckling of the marls below. Some of the deformed bedding shows very localised disruption, with only a few areas where slip is visible on the basal contact with the marls below, or rare extensional faulting and slip. In these cases some mechanical deformation has taken place, but it seems unlikely that the beds have moved very far. Here such beds have been interpreted as slumps, though with some uncertainty: this is the case for the most distal slumps in cycle 2.2 (at 500m and 1000m north). Marls are found above the slump packets in this cycle: these marls are characterised by the presence of coralgal and mollusc debris, as well as teeth and plant material with their long axis aligned perpendicular to the slope and fine lamina sometimes developed, as well as small erosional surfaces defining the base of a fining up sequence (see log 20b). These are interpreted to be the tail ends of gravity flows, and are indicated as small erosional surfaces in figure 6.1. Figure 6.23 illustrates the stratigraphic relationship of the slump in log 21, 50m to the north of the log site. Here we see fine to medium grainstones of the slump juxtaposed against a very steep erosional surface in the basinal marls, with marly gravity flow deposits overlying and sealing the slump. The interpretation of this grainstone body as a rigid or semi-rigid allochthonous unit delivered by gravitational processes into a distal environment is based on the lateral continuation of the body, where highly deformed and contorted bedding, as well as breccias are seen. However, an alternative explanation here is a sedimentary onlap of the "lowstand" deposits.

Cycle 3.1: consists of 8m of tabular platform sediments onlapping the top surface of the slump deposits of cycle 2.2. This platform is made of framestones possessing a characteristic, well bedded appearance. 20-50cm coral beds (facies 1) are separated by 1-10cm of marly packstones containing Nummulitids and planktonic foraminifera (facies 9).

Diverse coral morphologies develop, including, small domes, plates and sticks, and coral rubble textures at times form rudstones, though the facies is generally described as coralgal framestone (facies 1). It is this facies that is illustrated in the top photograph of figure 5.4. The top surface of this platform is a ferruginous hardground and a sharp flooding surface covered in basinal marls.

Cycle 3.2: this consists of tabular strata that onlap the top surface of the slumps in cycle 2.2. The platform is made of well bedded coralgal framestones (facies 1) similar in appearance to those of cycles 3.1 and 2.1. Figure 6.20 illustrates well bedded shallow marine carbonates of this cycle overlying the slumps and marly gravity flows of cycle 2.2. Additionally, small 3m wide coral patch reefs are preserved during this cycle on the front slope of the slump deposits below, and the remains of a manatee (sea-cow) were discovered (identified by W. Piller) at 0m on the horizontal scale in the marls overlying cycle 3.1. This sea-cow has been correlated with cycle 3.2, and may indicate the presence of sea-grass meadows at this time, in the area in front of the platform. A pair of small antithetic normal faults cuts these strata at 800m and the frontal limit of these beds has a slightly crumpled aspect suggesting some slip: this is associated with a slight creep of the platform due to the deformation of the marl sediment below: there is no evidence for a major displacement of this unit, and it is considered autochthonous. The top surface of this platform is a ferruginous hardground and a sharp flooding surface covered in basinal marls.

Cycle 3.3: this cycle onlaps onto the base of the northern margin slump scarp. It is approximately 20m thick and has first aggrading, then prograding stratal geometries. The initial flooding of the previously exposed top surface of the slump packets of cycle 2.2 is marked by rhodolithic rudstones containing planktonic foraminifera. This is the start-up phase of carbonate production, when space is created faster than sediment is produced, since the previously non-producing exposed surface must first be colonised. Then agrading and finally prograding sets of Miliolid and Nummulitid grainstones are deposited.

Cycle 3.4: in log 23 the Nummulitid packstones (facies 9) fine to a maximum flooding horizon, and coarsen up to the base of the slump. The sedimentary packet on the large-scale margin top is attributed to this cycle. Note, however, the likely existence within this packet of a number of extra medium-scale cycles, which have not been resolved, since they have not been logged.

6.5 EVIDENCE FROM THE OTHER SIDE

The east side of the Pirinç valley also provides excellent outcrops and geometries. A sketch interpretation is provided in figure 6.5. From the geometries and some knowledge of the facies evolution the two sides of the valley are readily correlated. These correlations are indicated on the figure. Certain aspects are better exposed, such as the rapid shallowing associated with the progradation of cycle 2: in figure 6.17 and 18, we see the grain flow deposits onlapped by cross-bedded grainstones (tidal deposits), and then being cut by the passage of slump deposits that slide as the progradation progresses. Here also the relationship with the underlying basement is more dramatic: cycles 2.1-4 onlap directly onto the eroded crest of a footwall basement block. This illustrates how the basement topography is very irregular, with bays and headlands forming on the northern flank of the basin, the result of the Eocene-Oligocene continental erosion of this once mountainous region.

6.6 SUMMARY

The following conclusions can be drawn from this detailed transect:

Structural organisation

Burdigalian syn-sedimentary deformation: only one small (3m throw) syn-sedimentary fault has been observed in this profile, and this has been related to the differential compaction of the underlying Derinçay Formation over the crest of a footwall block. No evidence has been seen to suggest that the major faults have been reactivated in this area since the Oligocene basin opening.

Some deformation of the original sedimentary geometries has occurred where the marl sediments have lateral thickness changes due to the infilling of an irregular topography. For example, the platform deposits of cycle 2.1 seem to sag over the underlying isolated platform topography.

Differential compaction of the underlying Derinçay Formation due to its highly variable thickness has an important influence on the Burdigalian bedding geometries, controlling the position of the development of the isolated platform.

Post-Burdigalian tectonic deformation: this transect has undergone major basinward sagging since the Burdigalian. By flattening on the toplap surface of most continuous sedimentary cycle (1.2) a basinward sag of 200-250m over a horizontal distance of 2km is estimated.

Stratigraphic organisation

Cycle hierarchy: the stratigraphy in this transect is readily broken down into two orders of retrograding-prograding sedimentary cycles. 3 large-scale cycles, and 11 medium-scale cycles have been described (distributed 5, 2 and 4 in the large-scale cycles).

The large-scale cycles are associated with 100-150m sea-level rises and falls. These large sea-level fluctuations rack the depocentre up and down the length of the depositional profile, juxtaposing shallow marine carbonates (deposited when sea-level is in a low position) with basinal marls (deposited when sea-level is in a high position).

Some evidence for platform top exposure occurs along some of the medium-scale cycle boundaries.

Cycle organisation: a series of different stratigraphic architectures is seen in this transect. They are:

a) low-relief tabular packets with internally prograding geometries,

b) isolated platform,

c) Large-scale (100m) clinoform margin geometries, sometimes with a rimmed margin and backfilling geometries,

d) slump deposits,

e) onlapping carbonate platform wedges with marls above and below.

The distribution of these different architectural objects is controlled by the position on the large-scale sea-level cycles, while the medium-scale cycles control the internal architectures and size of each object. In the following description each architectural element is allotted a position on the large-scale relative sea-level cycle. The low-relief tabular packets (a) are deposited when sea-level is in a low position and starting to rise. The isolated platform (b) develops as the sea-level rise accelerates. The large-scale clinoform geometries (c) develop in the middle and upper stages of sea-level rise, and as sea-level reaches its highest-point. The slump deposits (d) occur as sea-level falls, and the wedged platforms that onlap the slumps (e) are then deposited when sea-level is in a low position again. This cycle is repeated three times in total.

Facies evolution

No particular ecological evolution has been remarked in the sediments. The large-scale margin facies have not been logged, so their composition remains unknown, though their massive nature and the lack of internal bedding suggests that this margin is bioconstructed.

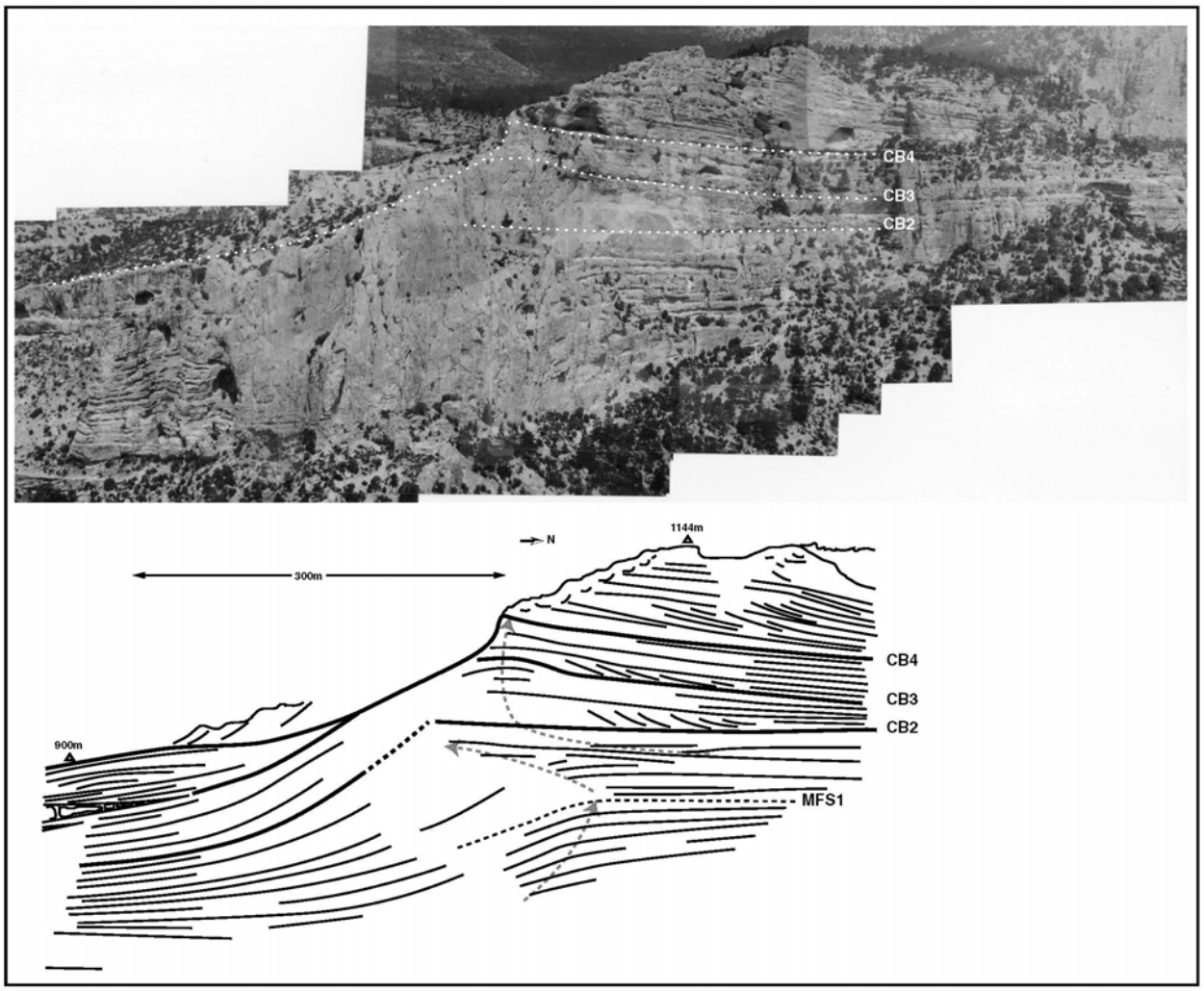

Figure 6.5 Detail of northern margin of Pirinç outcrop
Showing the proposed positions of the large-scale cycle boundaries on the platform top

FIGURE 6.5 SPLIT ON PAGES 78-79 IN THE ORIGINAL

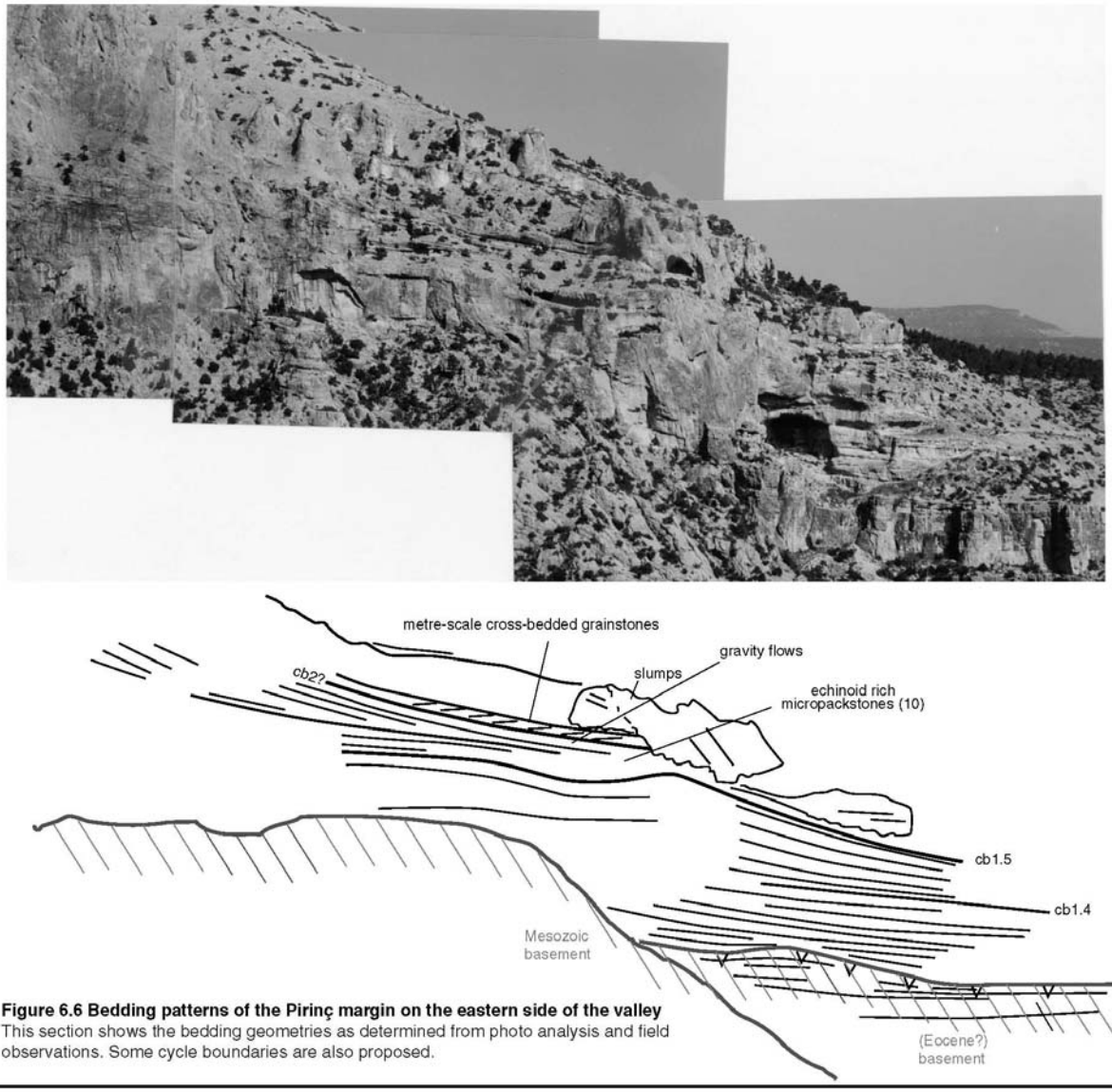

Figure 6.6 Bedding patterns of the Pirinç margin on the eastern side of the valley
This section shows the bedding geometries as determined from photo analysis and field observations. Some cycle boundaries are also proposed.

FIGURE 6.5 SPLIT ON PAGES 80-81 IN THE ORIGINAL

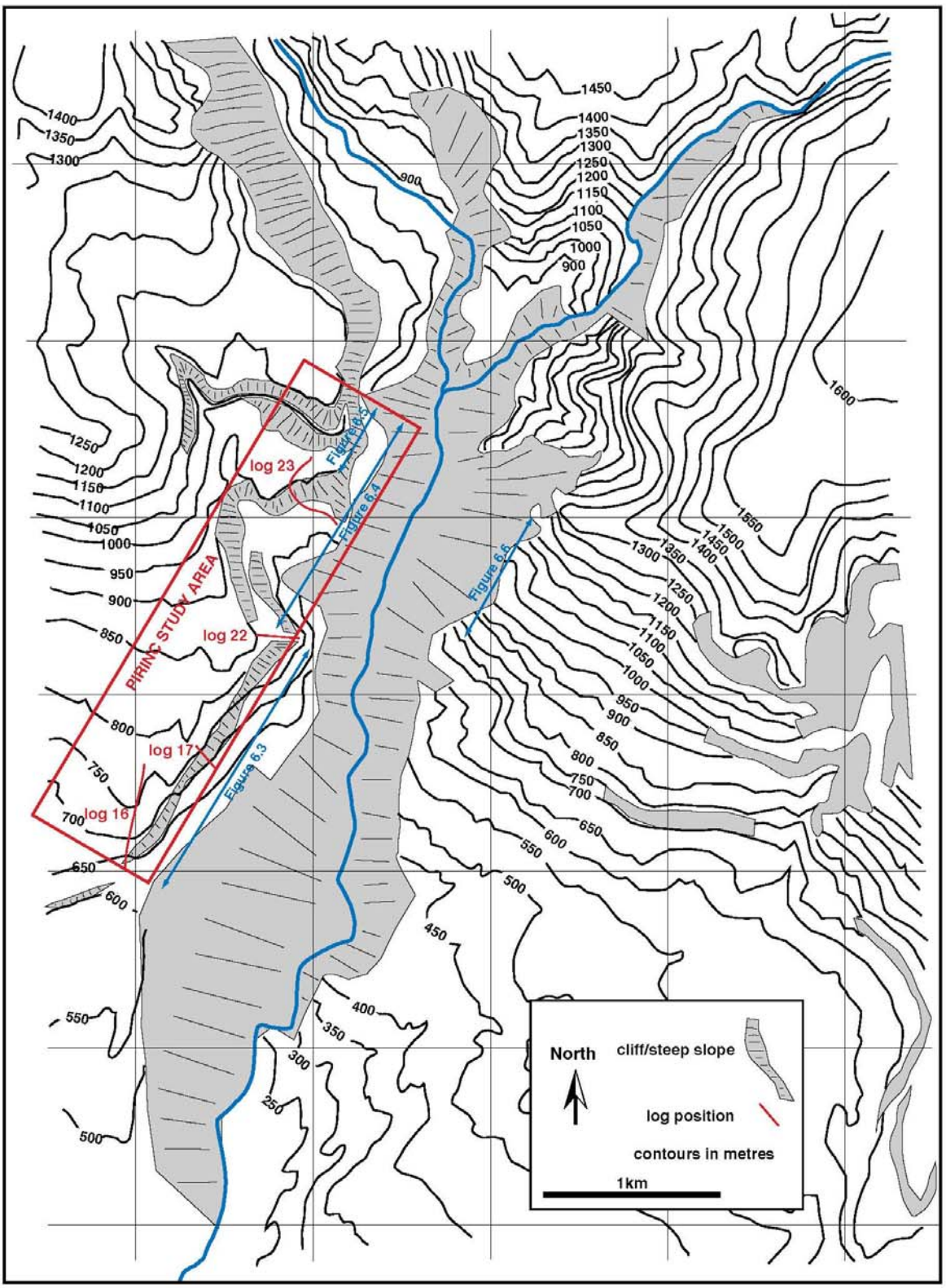

Figure 6.2 Pirinc location map

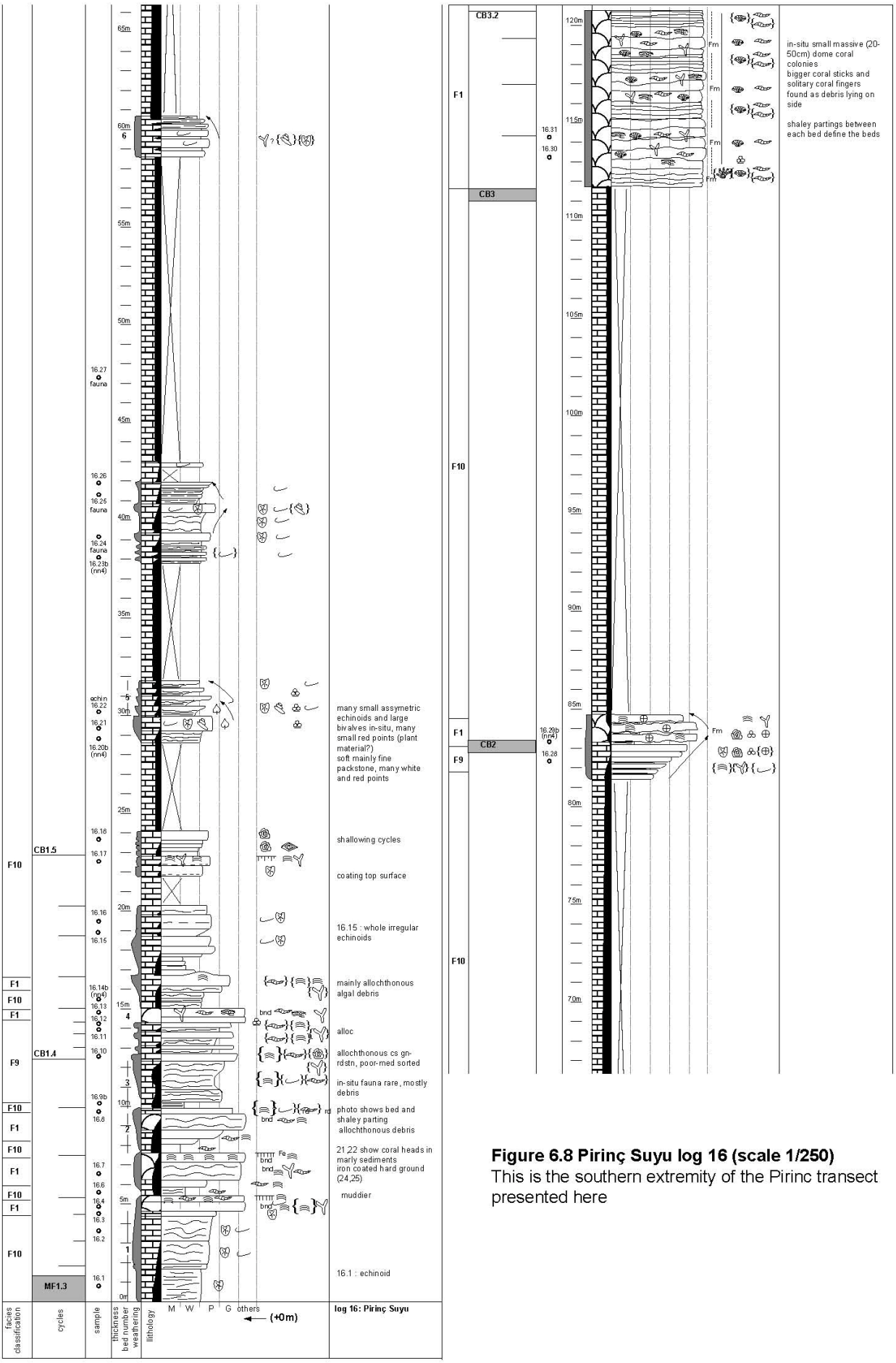

Figure 6.8 Pirinç Suyu log 16 (scale 1/250)
This is the southern extremity of the Pirinc transect presented here

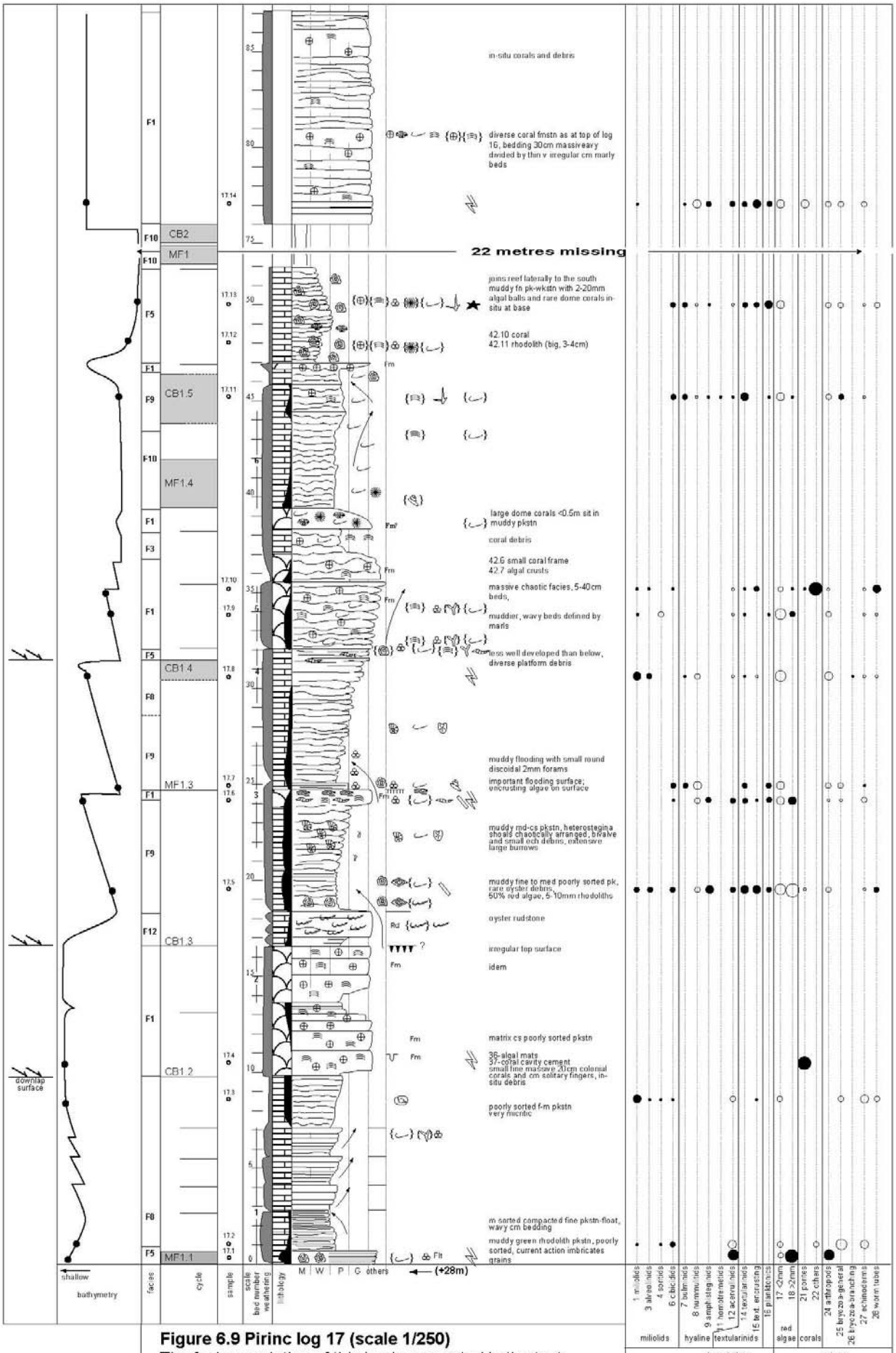

Figure 6.9 Pirinc log 17 (scale 1/250)
The facies evolution of this log is presented in the text

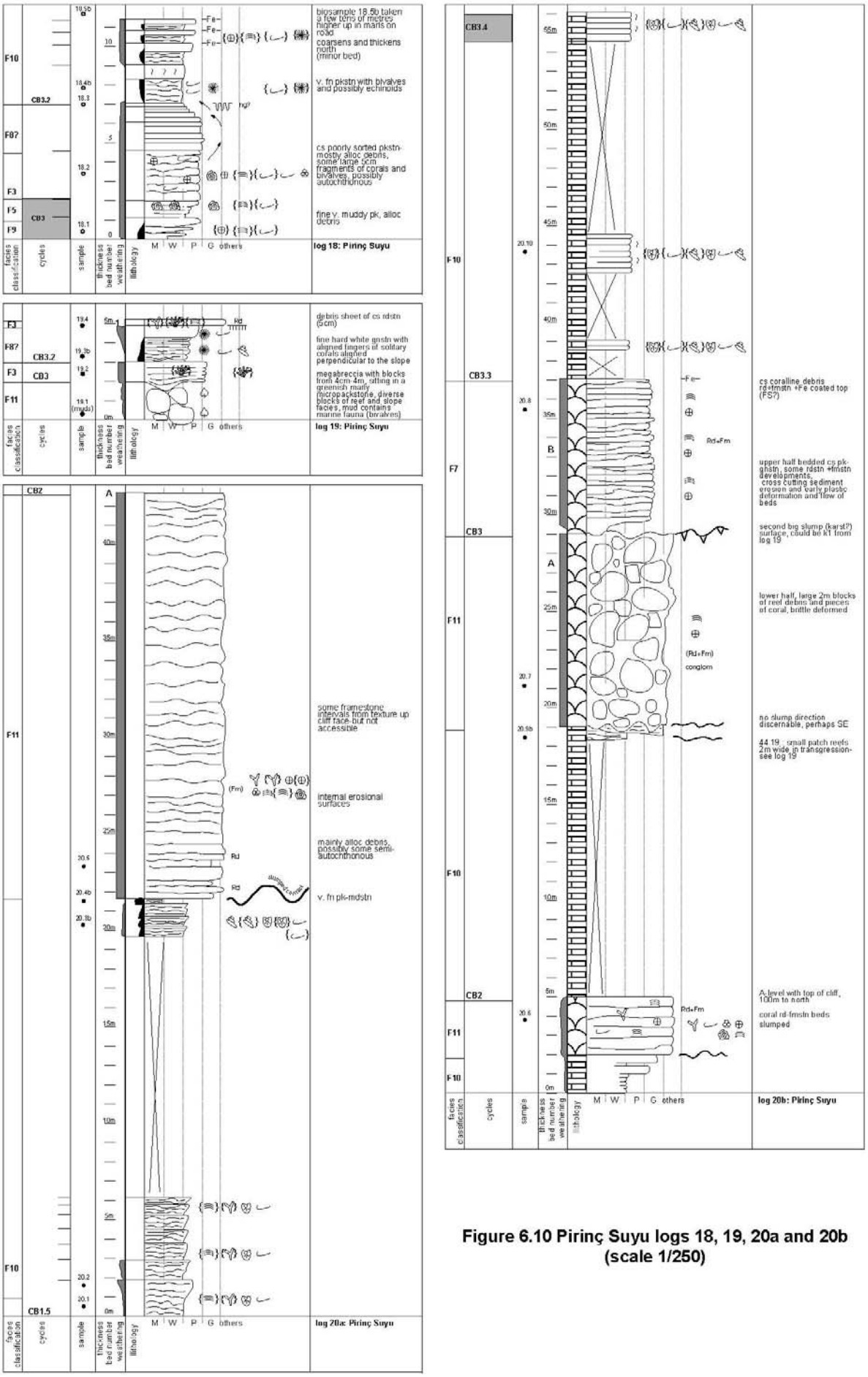

Figure 6.10 Pirinç Suyu logs 18, 19, 20a and 20b (scale 1/250)

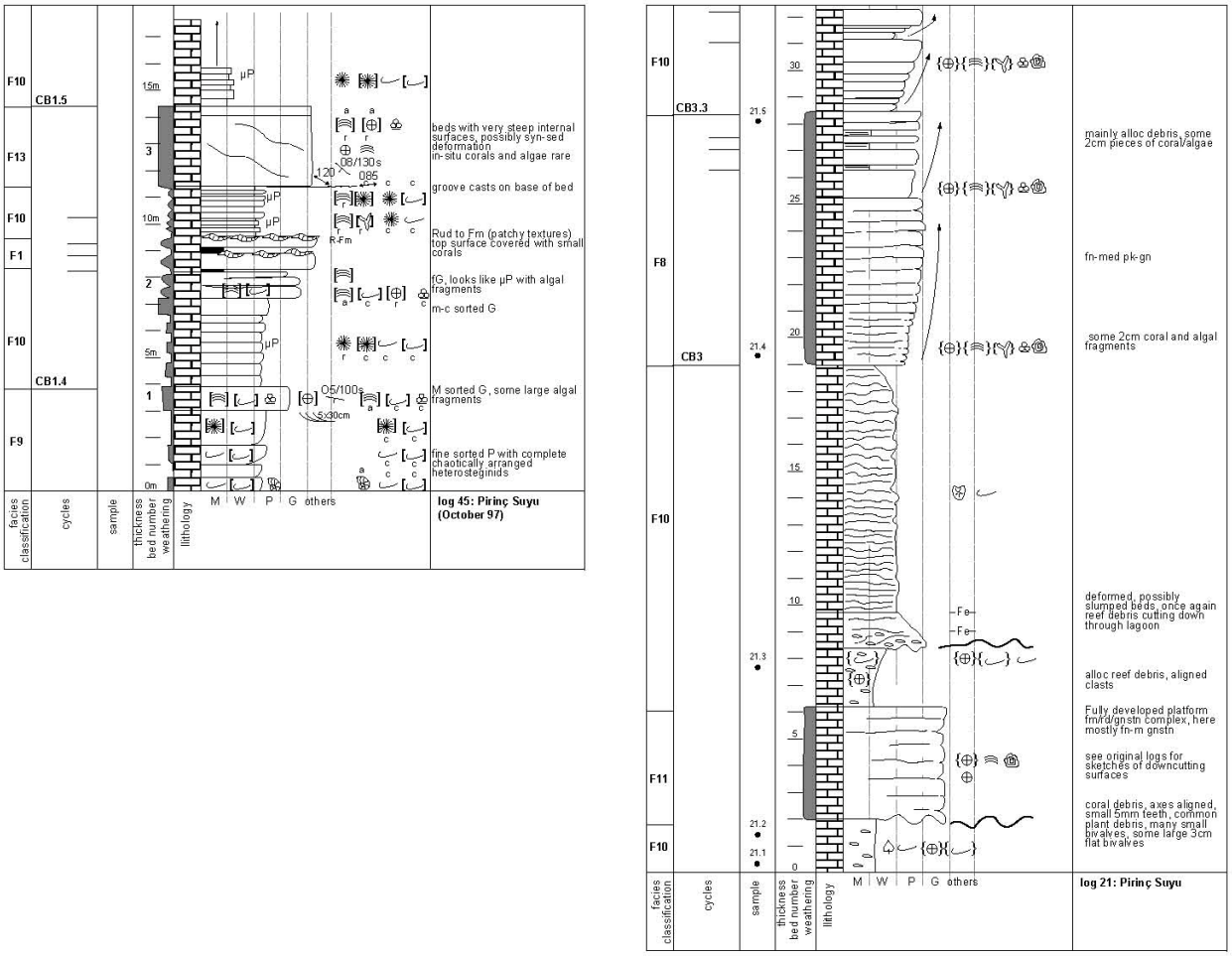

Figure 6.11 Pirinç Suyu logs 21 and 45 (scale 1/250)

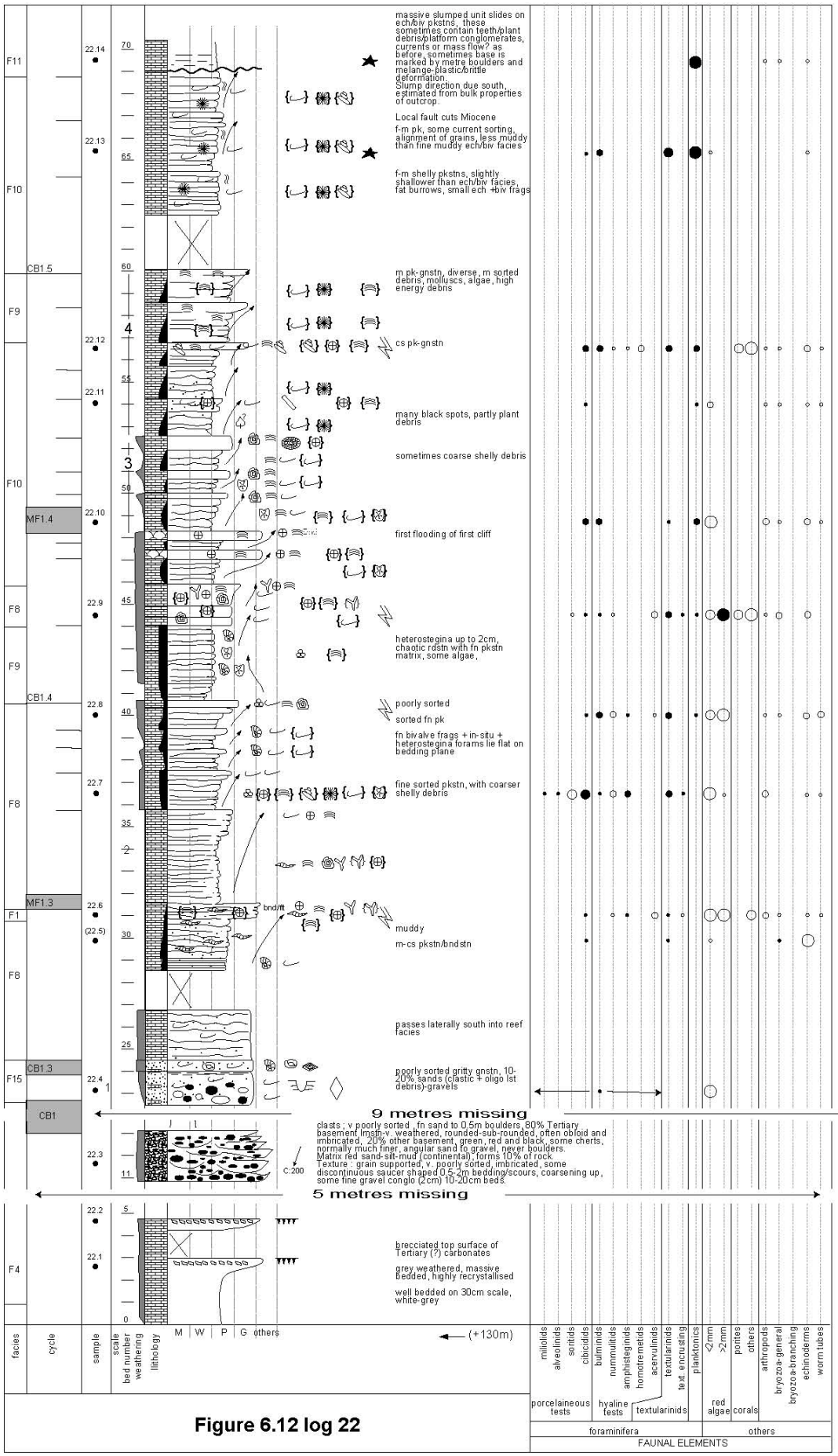

Figure 6.12 log 22

Figure 6.13 Pirinç Suyu: log 23

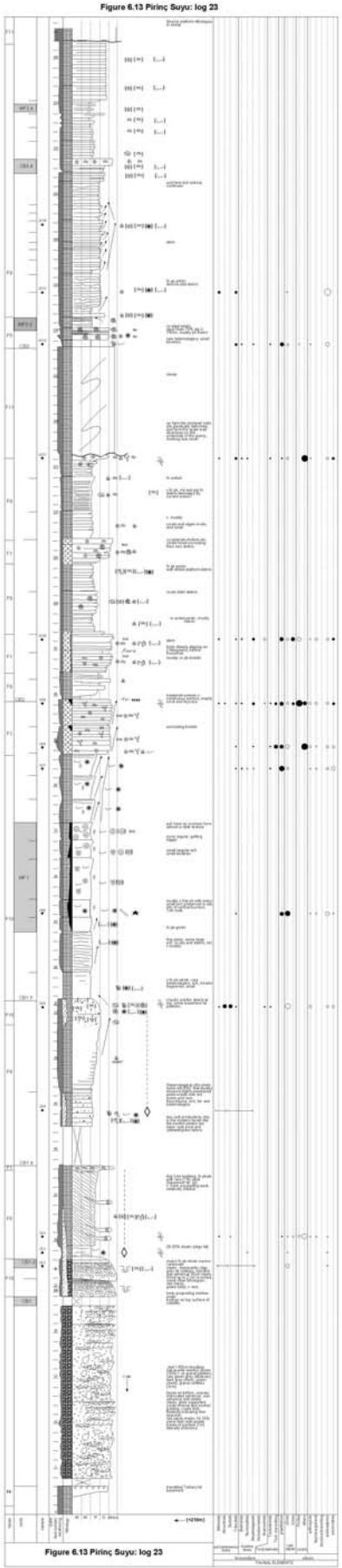

Figure 6.13 Pirinç Suyu: log 23

Figure 6.13 Pirinç Suyu: log 23

Figure 6.13 Pirinç Suyu: log 23

FIGURE 6.13 SPLIT ON PAGES 88-90 IN THE ORIGINAL

FIGURE 6.13 SPLIT ON PAGES 88-90 IN THE ORIGINAL

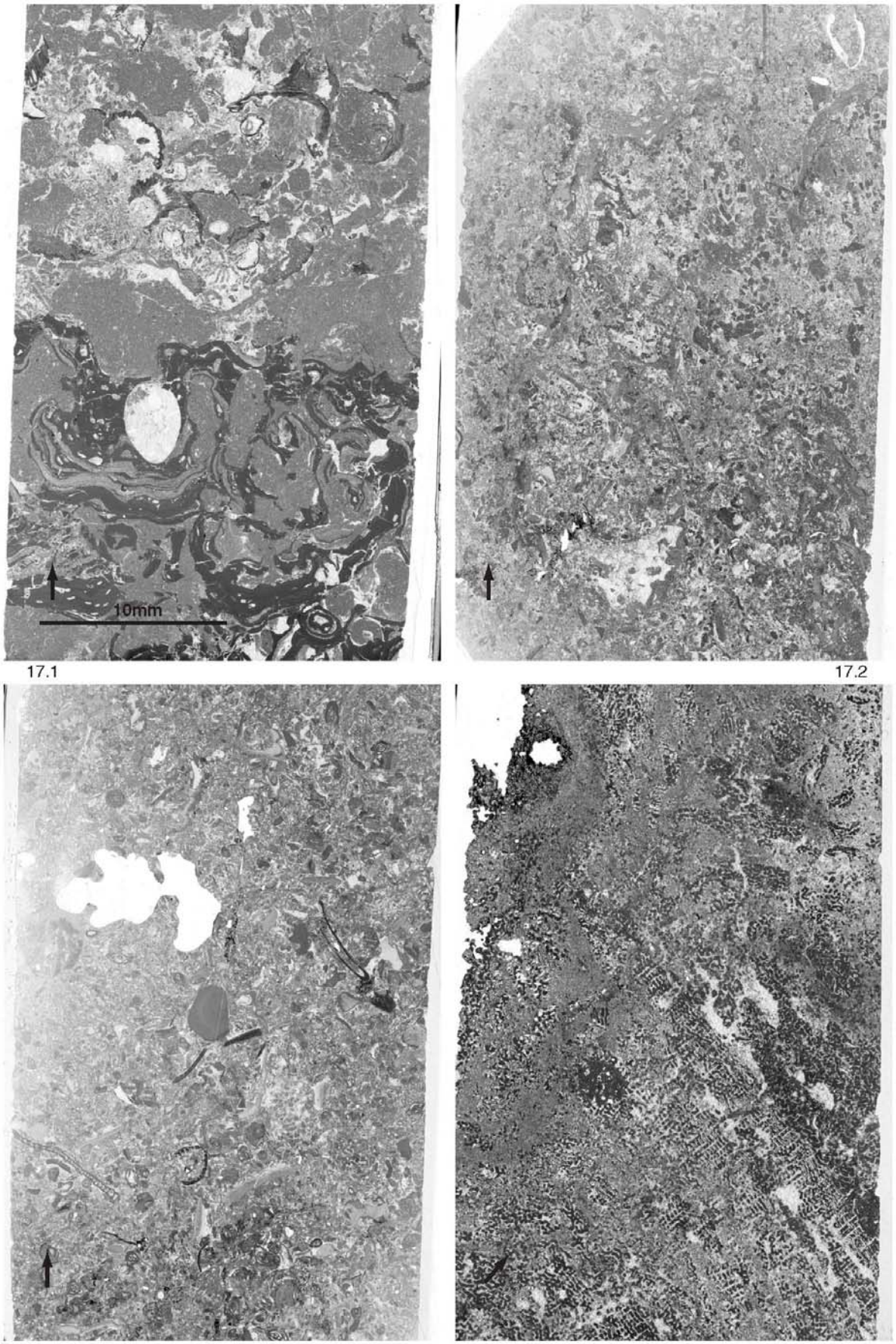

Figure 6.14 Vertical facies evolution of log 17 (Pirinç Suyu)
These facies are described in the text.

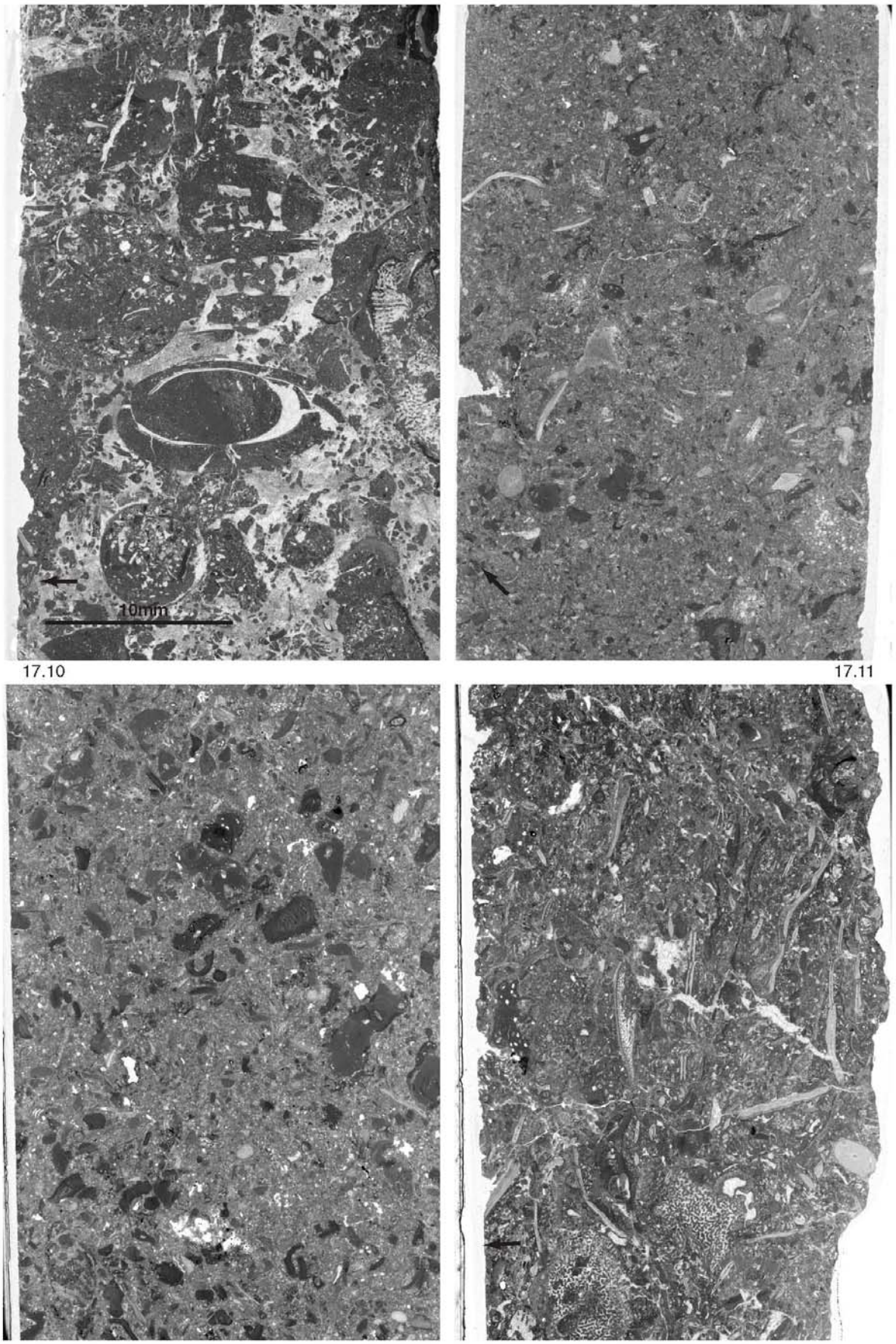

Figure 6.16 Vertical facies evolution of log 17
These facies are described in the text.

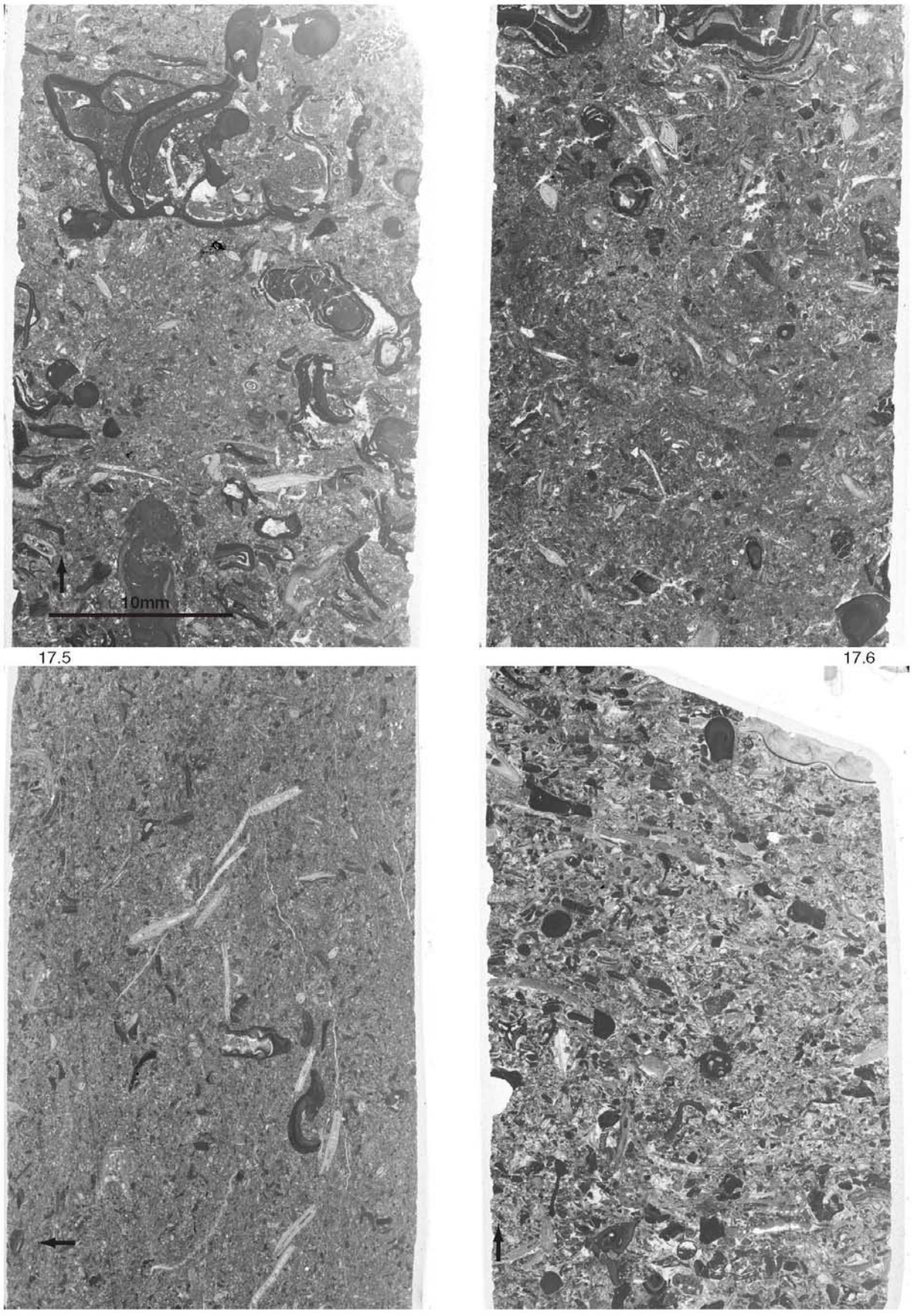

Figure 6.15 Vertical facies evolution of log 17
These facies are described in the text

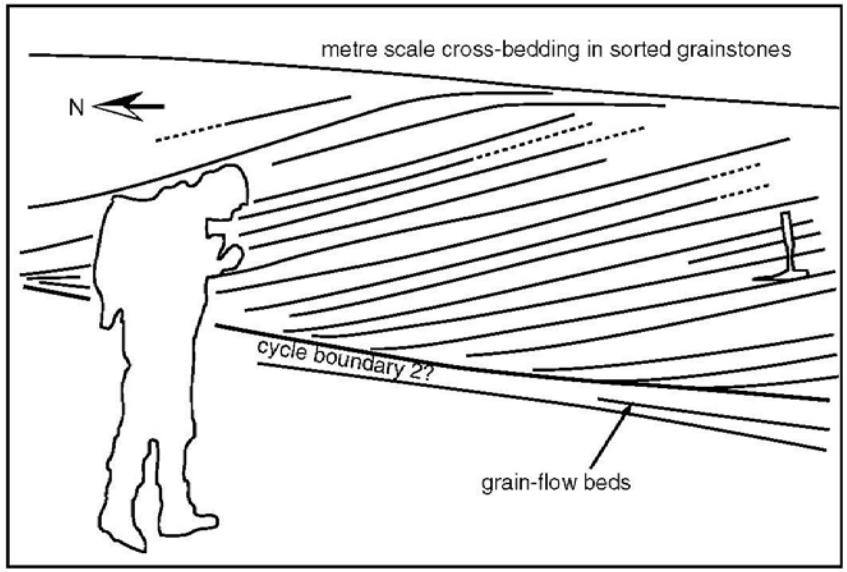

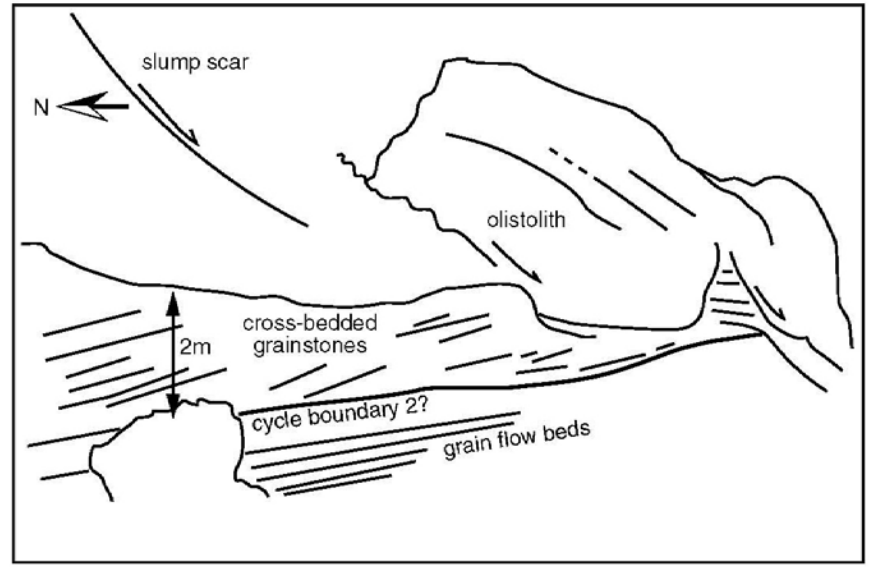

Figure 6.18 Outcrop photos 2
Illustrating coarse-grained cross-bedded deposits overlying debris-flow beds on the eastern side of the Pirinc valley

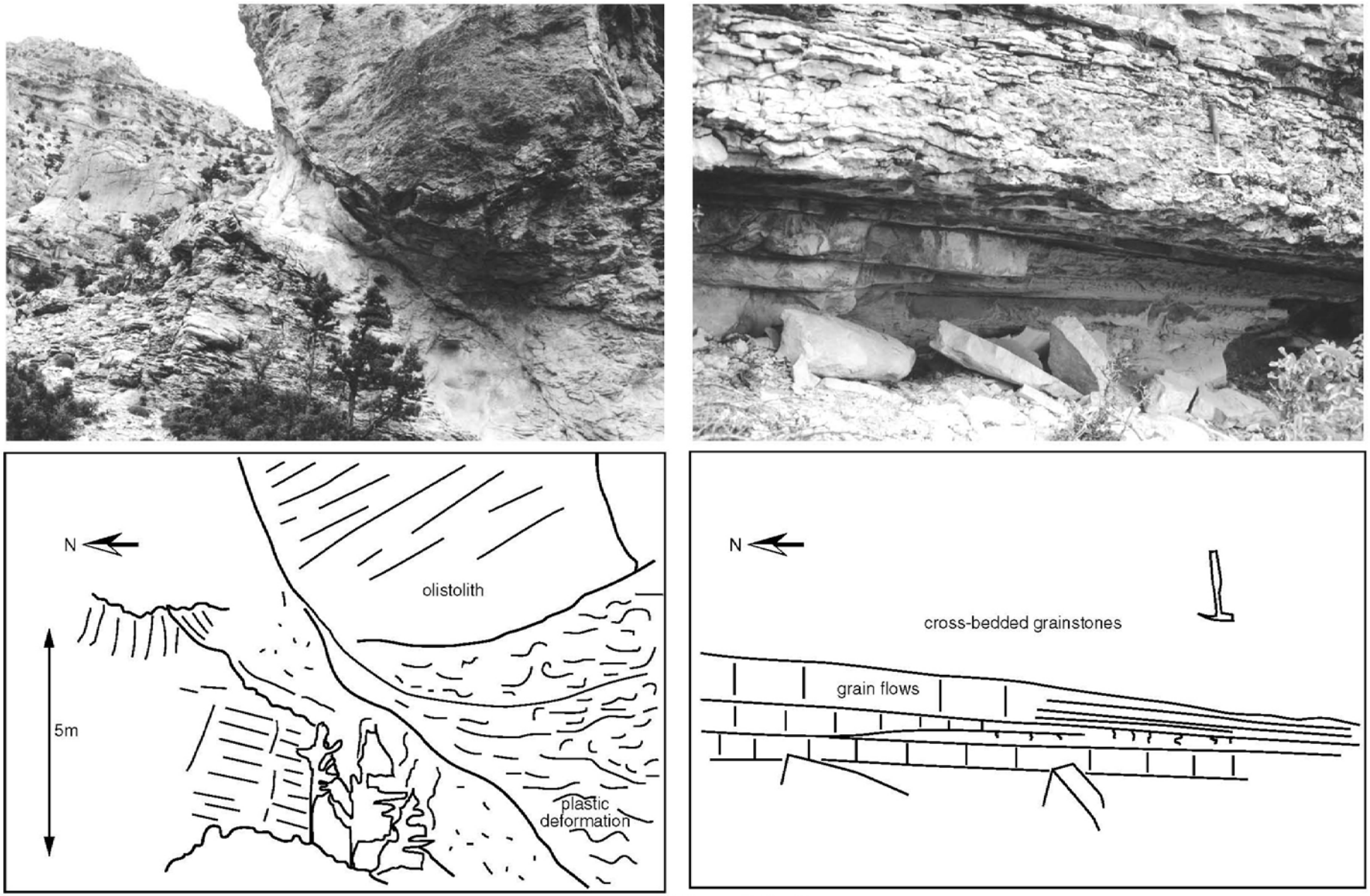

Figure 6.19 Outcrop photos 3
Illustrating the slumps and the grain-flow beds on the eastern side of the Pirinc valley.

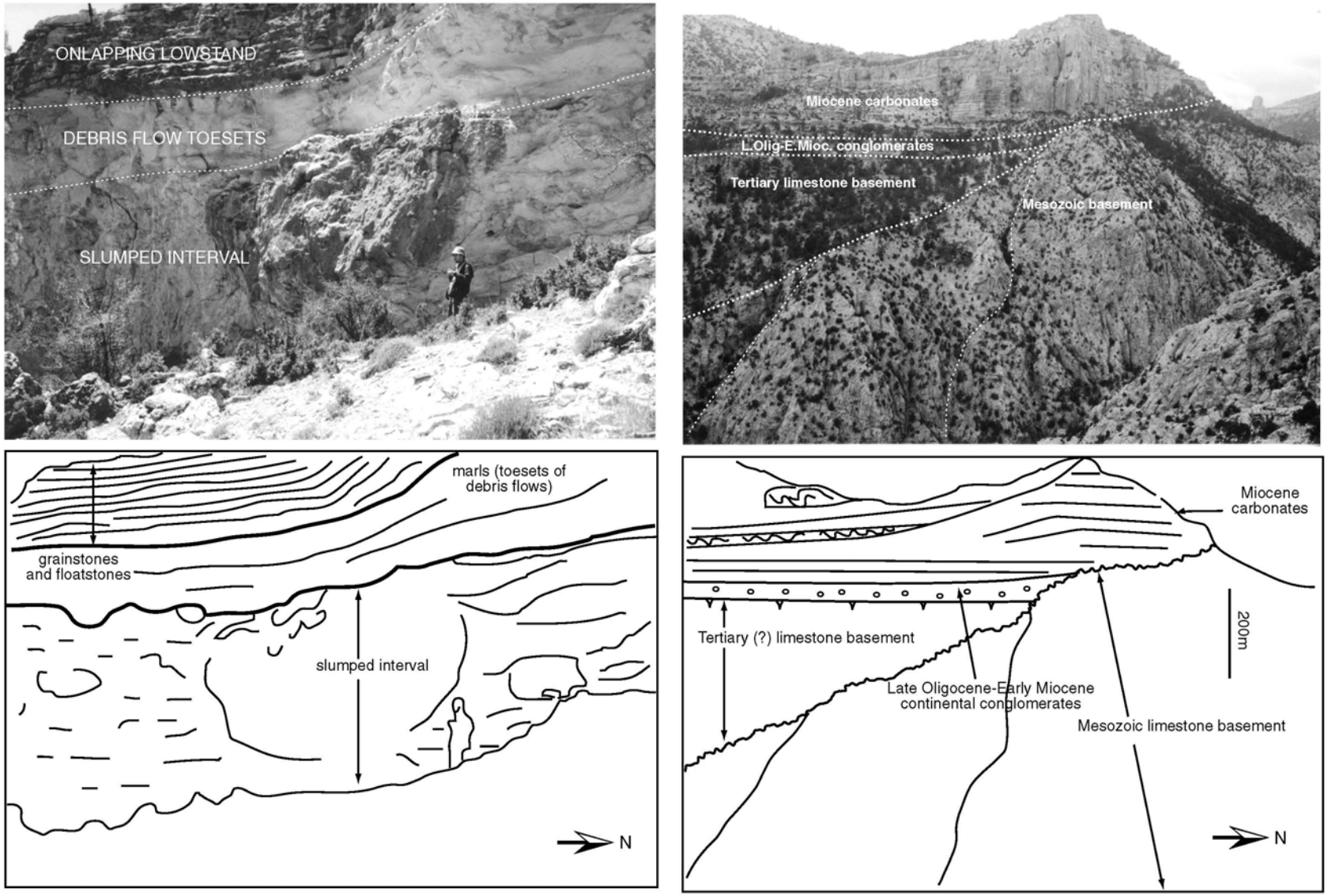

Figure 6.20 Pirinç outcrop photos 4
(Left) Illustrates the lowstand carbonate platform overlying the second slump deposits in the Pirinc transect.
(Right) Is an overview of the relationship of the Miocene with the Basement

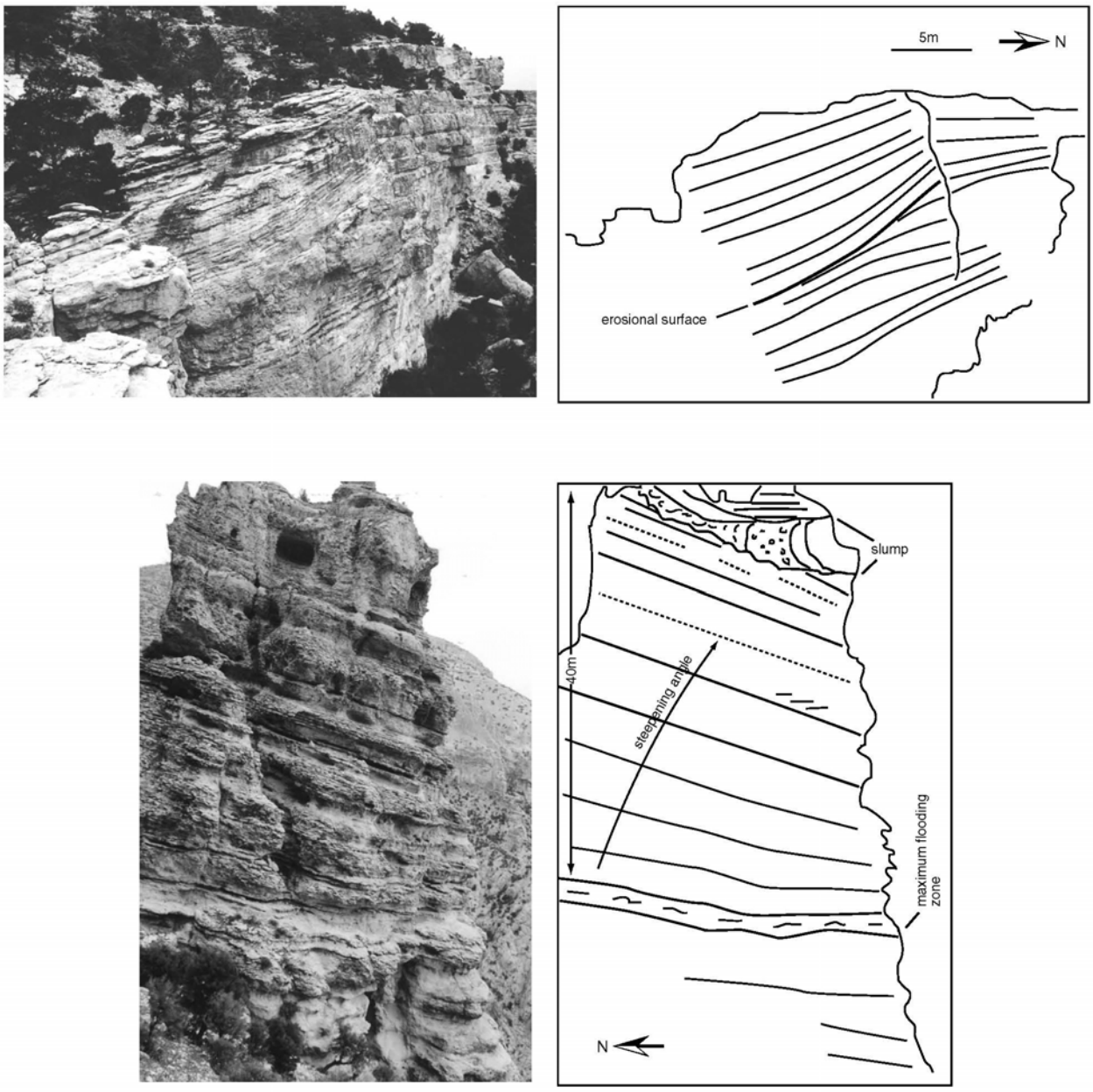

Figure 6.21 Pirinç outcrop photos 5
(Top) Shows erosional bevelling at the maximum flooding of cycle 1.4 in Pirinc.
(Bottom) Illustrates the steepening slope angle of the large-scale clinoforms of the margin as it progrades.

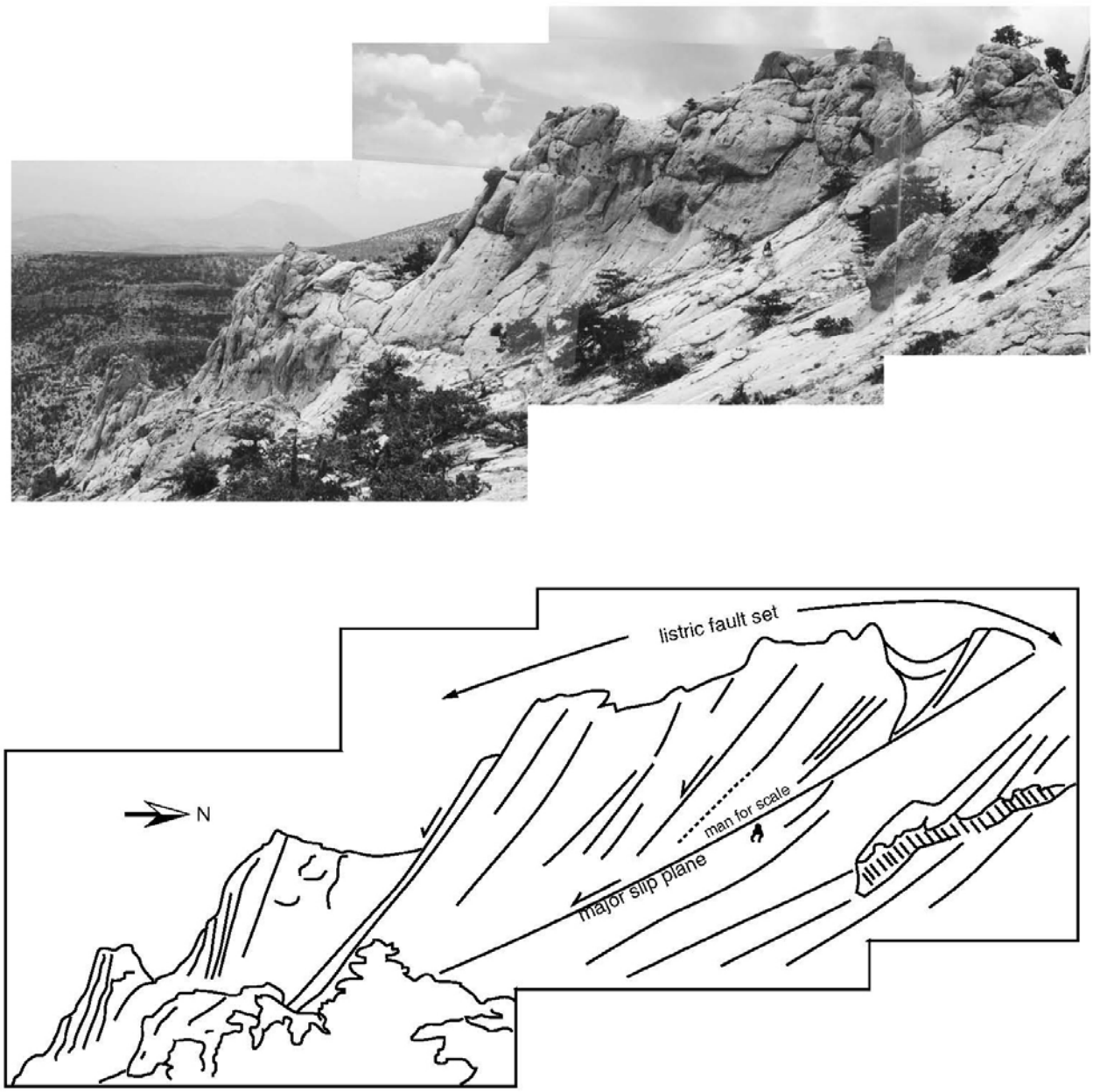

Figure 6.22 Pirinç outcrop photos 6
This shows a series of slid blocks on the eastern side of the Pirinc valley. The listric faulting for each block converges onto the major glide plane of the slump. These blocks are found on the upper part of the slump scar.

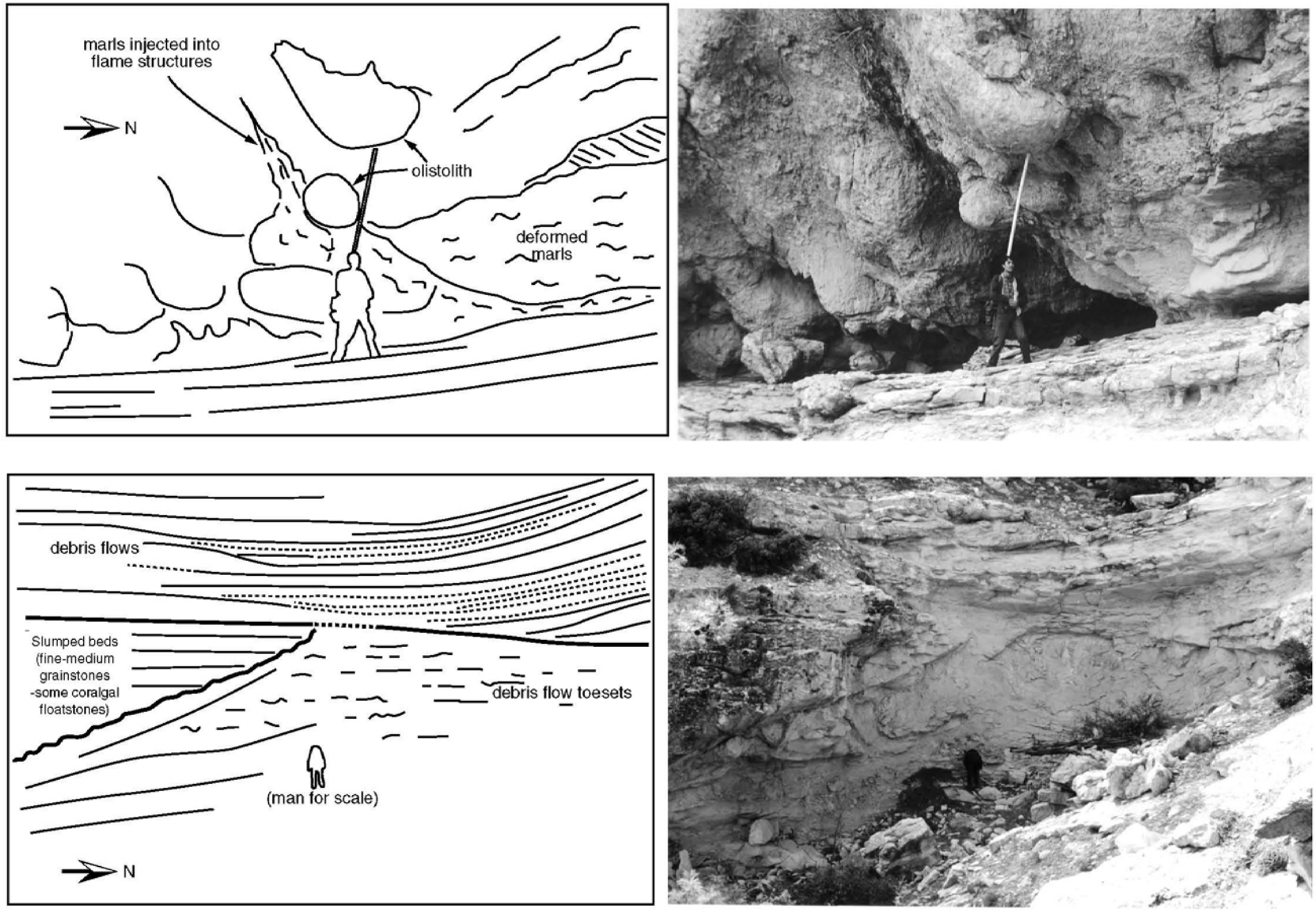

Figure 6.23 Pirinç outcrop photos 7
(Left) Shows the slump melange composed of olistoliths and deformed basement marls.
(Right) Illustrates the complexity of the slump contact with the surrounding sediment in the distal area of the slump.

Figure 6.24 Pirinç Suyu outcrop photos 8
(top) fault breccia infilled with ferruginous matrix
(bottom) L indicates laminated void infill

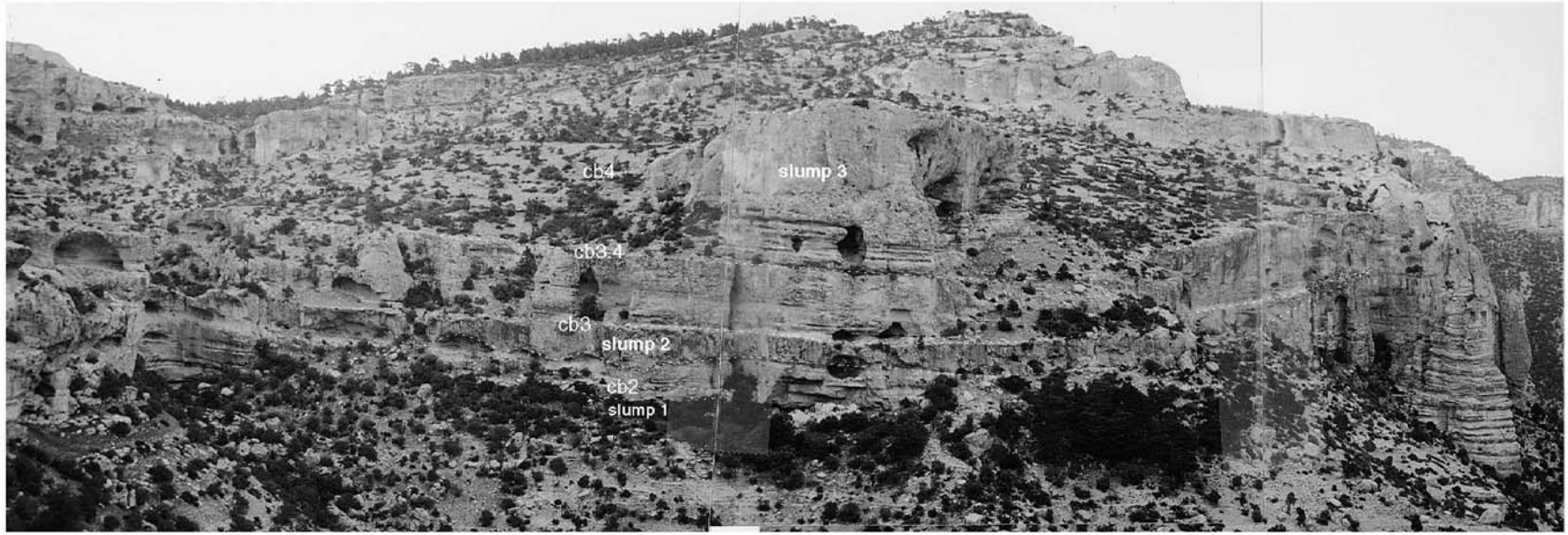

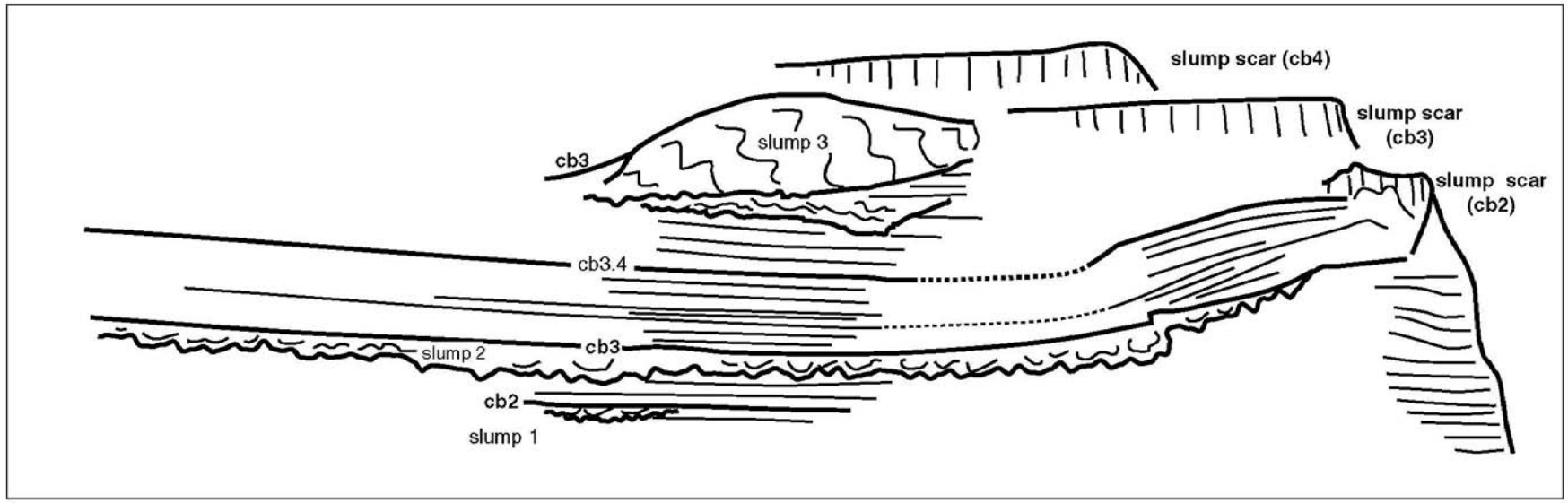

Figure 6.17 Pirinç outcrop photos 1
This is an up-dip view, looking north onto the Pirinc platform margin. Note the stacking of the three slump deposits and their relationship with the cycle boundaries.

7 - ALAHAN TRANSECT

7.1 INTRODUCTION

This chapter is organised into two parts. The first part describes the detailed study window of the Alahan area, and the second part describes the construction of a transect correlating the Alahan study to the Kizil Kaya study window. The Kizil Kaya transect per se will be described in chapter 10. The reason for this is that both the Alahan and the Kizil Kaya areas offer excellent outcrops ideally suited to detailed study, while few good outcrops occur between the two sites, and correlations between these areas are made by tying the available data into a coherent framework driven by our understanding of the sedimentary dynamics.

The Alahan study area is found 25km to the north-west of Mut town (figure 4.6 and figure 7.5), just beneath the main road leading from Mut to Karaman, after passing the Alahan village and the Alahan monastery access road, in the Karaman direction. The Alahan valley is notched out of the northern flank of the Mut Basin escarpment by a small stream, which flows down from the Anatolian Plateau to the north, to join the Derinçay, a tributary of the Goksu River, in the Mut Basin to the south. Outcrops are found on both sides of the valley from 900m to 1350m altitude. Hard limestones are interbedded with softer sands, silts and marls, and this forms a stepped relief of steep slopes separated by vertical cliff faces. The upper slopes of this valley are farmed, with abundant and diverse fruit plantations (apples, grapes, figs), and here the outcrop of the softer sediments is poor. An overview of this valley is provided in figure 7.4.

The Alahan transect is constructed from outcrop observations on both sides of the valley. Correlations between the two sides are easily made by physically following out the beds via the V of the valley. The field photographs of the eastern valley side are in a reverse orientation, when compared to the reconstruction in figure 7.1. This transect is constructed from (1) a sedimentary log that describes the complete interval (log 7, figures 7.11-14), (2) bedding pattern observations (figures 7.6-10) coupled with spot facies observations, and (3) detailed facies mapping (figure 7.7). Note that no microfacies analysis is presented here for this transect.

7.2 DEFINITION OF CYCLES

The definition of the cycle boundaries makes continual reference to the Alahan transect in figure 7.1, and to the logs in figures 7.11-14. Large, medium and small-scale cycles are distinguished in this area based on the following criteria:

1/ exposure surfaces

2/ erosional surfaces

3/ geometries

4/ It is observed that the siliciclastic sands are systematically organised into shallowing-up packets, while carbonate sediments directly overlay the shallowest siliciclastic bed found, and underlay the deepest siliciclastic bed of the next shallowing-up trend. Hence the carbonate deposition took place dominantly during transgession, and the siliciclastics accumulated dominantly during regression. Here the terms transgression and regression make reference to the siliciclastic shoreline.

Large-scale cycles

Cycle 1: only the top of this cycle has been seen in the Alahan area, and so the lower limit, cycle boundary 1, has not been defined here.

Cycle 2: cycle boundary 2 has been defined dominantly from the facies evolution. A shallowing-up trend in the shoreface sands (facies 15) of log 7.1 terminates in a major erosional surface, containing channels infilled with coarse gravels. In detail a number of amalgamated erosional surfaces occur to create a complex infill geometry. The channel-fill is rapidly overlain by carbonate grainstones of a thick platform development. The erosional surface represents the cycle boundary, with retrograding channel infilling, accompanied by a major lithological change to a carbonate system. The maximum flooding has not been defined for this cycle.

Cycle 3: cycle boundary 3 is defined by a major karst surface found at the top of platform carbonate deposits. The karst surface is autobrecciated, and infilled with siliciclastic sands and gravels. Shoreface sands directly overlie this surface. No maximum flooding has been defined for this interval.

Cycle 4: cycle boundary 4 is defined by an abrupt transition from a dominantly siliciclastic mixed-

system, to a thick carbonate platform interval. The style of this cycle boundary greatly ressembles that of CB2. An erosional surface underlying coarse-grained siliciclastic fan-delta deposits (facies 14) has been chosen to mark the exact position of the cycle boundary. The erosional surface has been interpreted to occur during a time of major platform top erosion, and represents an important temporal hiatus. The fan delta is deposited during the early part of cycle 4 in this area, and these deposits are rapidly overlain by a 46m thick carbonate platform. No maximum flooding has been determined for this cycle.

Cycle 5: the maximum of progradation is picked out by the arrival of a thin body of shallow marine siliciclastic sands (facies 15) in an otherwise dominantly carbonate environment. The cycle boundary 5 is therefore placed somewhere within these sands (a cycle boundary zone is in fact defined across the sands to express this uncertainty). No maximum flooding is defined here.

Cycle 6: as for cycle boundary 5, the maximum of progradation of this cycle is picked out by the arrival of siliciclastics in an otherwise carbonate environment, and this is used to define the cycle boundary here. No maximum flooding surface is defined for this cycle.

Medium-scale cycles

Cycle 2.1: cycle boundary 2 is the lower limit of this cycle.

Cycle 2.2: the maximum of progradation at CB 2.2 is indicated by the arrival of pebble-grade basement clasts, and a series of possible exposure surfaces marking the top of the prograding carbonate platform of cycle 2.1.

Cycle 2.3: cycle boundary 2.2 is the boundary between a shallowing-up siliciclastic unit below and carbonate platform deposits above.

Cycle 3.1: the base of this cycle corresponds to CB3 as defined above.

Cycle 3.2: cycle boundary 3.2 is defined as the erosional base of a fan-delta deposit. Beneath this surface a shallowing/coarsening-up siliciclastic trend is observed, while above the surface the fan-delta deposits represent the initial infill of the erosional relief associated with the cycle boundary formation, which is then covered by shallow platform carbonates. No maximum flooding surface has been defined for this cycle.

Cycle 3.3: this cycle boundary is defined in the same manner as for CB 3.2 above.

Cycles 4.1-4.5: the lower platform of cycle 4 is broken down into 5 medium-scale cycles principally from the geometries. Each cycle boundary represents a retrograding shift of the depocentres along a surface that marks the top of a progradational unit. No retrograding packets are preserved in this platform interval.

Small-scale cycles

Cycles 1.3.1-5: at the top of cycle 1 five small-scale cycles have been defined: from 35-72m on log 7.1 (figure 7.11) fine-medium sands and silts are periodically (5-8m scale) replaced by 3m packets of coarse sands. These sands have erosional bases, often with gravel and mud flakes (rip-up clasts) at the base and have shallow angle cross-bedding (figure 7.16, top). These are interpreted as being tidal channel fill sediments. The base of each channel packet is defined as a small-scale cycle boundary. The cycle boundary corresponds to a time of net erosion, while the channel fill sediments belong to the cycle above.

Cycles 3.1.1-7: within the cycle 3.1 seven 1-3m small-scale cycles are distinguished, as illustrated in figure 7.7. Silty muds bearing diverse molluscan debris coarsen up to poorly sorted gravelly medium-coarse sands. These are overlain by 0.5-1m of gravelly coquina beds (facies 17): poorly sorted gravelly sands containing 40-80% small bivalves. The bivalves are chaotically arranged and can be complete or fragmented: they are dominated by small equant thick shelled forms, and the diversity is often reduced, though no monospecificity has been observed. This evolution constitutes one small-scale cycle. Each coquina bed is then overlain by the silty muds of the next cycle. The cycle boundary is placed at the base of the coquina beds for each cycle, since the appearance of these beds is considered to mark the start of the retrogradation.

Cycles in 3.2: similar small-scale cycles to those found in cycle 3.1 are found here, though they have not been described in detail.

7.3 PLATFORM EVOLUTION

Large-scale cycles

Cycle 1: this cycle is Upper Burdigalian (NN4) in age; only the top 70m outcrop in this area and have been described. The facies evolution is shown in log 7.1 (figure 7.11), and this interval is illustrated in figure 7.6. Fine silts and muds, containing some shell debris, sand, and plant material, are found at the base of the log (figure 7.16, photo A). Packets of horizontally laminated, or unlaminated fine to medium sands of varying thickness (decimetric to metric scale) are found interbedded in these silty muds. Also distinct metre-scale sandy rudstone beds are found, containing diverse molluscan debris, coral debris and echinoderms. This is interpreted as being the offshore

environment, with the sand beds representing periodic grainflows. The facies succession shallows upwards, and towards the top small-scale cycles of tidal channelling develop in a shoreface environment, then the succession is capped by a large-scale cycle boundary, which is an important erosional surface here.

Cycle 2: this cycle is 70m thick, and is Upper Burdigalian (NN4 biozone) in age. The first 50m is a prograding carbonate platform, the facies are logged in figure 7.11 (log 7.1) from 70-120m, and in figure 7.12 (log 7.2) from 0-20m (the topmost section of the platform). The platform sediment is mostly red algae and corals. In the log (figure 7.11) sediments vary between autochthonous and para-autochthonous textures (bindstone, framestone and floatstone: here simplified together under the facies 1) and detrital carbonate (grainstones and packstones). Siliciclastic sand is abundant (up to 50% of sediment) in the first 8m of the carbonates, and is present throughout the platform, but in small quantities (<2%). It is mainly fine, well sorted heterolithic sands. The corals in the autochthonous textures are always small Porites (<10cm), with platey and knobby morphologies: the red algae have a fundamental role in stabilising the sediment, forming thin mats interbedded with small coral colonies. Judging from the fragmented nature of the corals and algae, transport followed by renewed growth seem to be common processes in this environment, hence the use of the term "para-autochthonous". In the detrital packstone and grainstone textures Nummulitid and Amphisteginid foraminifera are very common. These are typical of a slope environment. Miliolid foraminifera are only seen in the top few metres of this platform.

A depositional clinoform (see figure 7.1 and 7.4) was followed out in the field, and the facies examined: the topset consists of framestones with 10cm Porites corals in plate forms and abundant red algae; locally the red algae form bindstone textures. The top of the slope shows a variety of textures from framestones to grainstones, though the commonest was coralgal floatstone textures, with Nummulitid grainstones forming the bulk of the rock, and some red algae and corals also growing in place. The middle to lower slope is dominated by the Nummulitid grain-packstone textures. The total clinoform height corresponds to the height of the platform, approximately 50m. This facies distribution corresponds to a partially constructed platform slope, though with the arrival of detrital carbonate sands from the platform top being the most important process.

The bedding geometries of this platform are very distinct, and are illustrated in figures 7.4, 6 and 9b. Oblique tangential clinoforms are observed prograding in a south-easterly direction, with slopes of up to 20°. Some apparent toplap relationships are observed. The large-scale geometries show that the prograding packets are organised in lobes or tongues a few hundred metres across, and that they nest around each other as they prograde to fill up flush to the platform top surface, creating a grossly tabular platform geometry that is internally partitioned by the lobe boundaries. These geometries are interpreted as the result of a relative sea-level stillstand, and a shallow platform area several kilometres wide (see figure 7.9b) producing sufficient volumes of sediment to prograde.

A number of distinct features are observed just below the top of the platform: siliciclastic basement pebbles up to 5cm in size are found in the sediment (see the log in figure 7.12), as well as sharp surfaces with minor autobrecciation and ferruginous infill below. The arrival of pebble grade basement material indicates a maximum of progradation, while the autobrecciated surfaces are interpreted as exposure events. This hypothesis is supported by extensive dissolution of all clasts observed in thin section, including the red algae (normally the most resistant due to its mineralogy). The top of this platform, the CB2.2, is abrupt: it is a coral encrusted surface with overlying silty muds. These muds are poorly exposed (see log in figure 7.12), and coarsen up into fine sands over 10m, with some carbonate rich intervals (27-29m). This is interpreted as a shallowing up trend from lower shoreface (or offshore) silts to upper shoreface sands. In cycle 2.3 a carbonate platform then develops over these sands. This platform is illustrated in figure 7.7. The change from siliciclastics to carbonates occurs across cycle boundary 2.3. The coarsest siliciclastics (coarse sand, with some gravel, and 3cm pebbles) are overlain by coralgal framestones and bindstones. Some basement sand is reworked into the basal carbonate beds. In the logged section this platform is 9m thick: the coralgal framestones previously described form the base of the platform, while the top half is red-algal grainstones containing abundant Nummulitid foraminifera. the top surface of this platform is autobrecciated, and infilled with coarse siliciclastic sands. This top surface is illustrated in figure 7.17. The photo on the left shows a brecciated top surface with ferruginous infill, while the photo on the right shows well developed breccia with siliciclastic sand infill. This surface is interpreted as a karst. Figure 7.18 (left photo) shows the facies at the top of this platform: 20cm coral heads (Tarbellastrea or Montastrea?) growing surrounded by a pebbly matrix. Basement pebbles are found below, around and overlying the corals, and are considered contemporaneous to the coral growth. The exposure event is here a red-stained surface that tops the corals and the conglomerates. This facies does not feature in the log, being found laterally away from the log site.

When examining the bedding geometries of the platform in cycle 2.3 a number of features are of note: the thickness varies from 10m in the log, to 1m in the most proximal outcrop; prograding geometries are

observed (see figure 7.7); when the beds are followed laterally seaward in figure 7.7 (and 7.1), the single karstified surface on the top of the platform bifurcates into 2 karstified surfaces separated by siliciclastic sands. Gravelly sands and conglomerates then overlie this topmost karst.

Cycle 3: this cycle is 77m thick and is Upper Burdigalian (NN4 biozone) in age. This interval is illustrated in figures 7.7 and 8. The figure 7.7 shows an area where the facies have been mapped out in detail, and small scale cycles have been defined that do not appear in the log. The organisation of cycle 3 is best understood by examining the medium-scale evolution: three prograding siliciclastic cycles occur (3.1, 3.2 and 3.3). Fan-delta deposits overlie the cycle boundary, and carbonate platforms develop in cycles 3.2 and 3.3 during the retrogradation, while the siliciclastic depocentre is away in a more proximal position.

In cycle 3.1 fine sands to silty muds bearing diverse molluscan debris (facies 16) overlie the CB3, and this coarsens up over a 20m interval to coarse sands and gravels. Seven small-scale cycles of coarsening up siliciclastics topped by coquina beds occur within this interval, and these are illustrated in figure 7.7.

At the base of the next cycle 3.2 (at 60m on the log in figure 7.12) two 0.5-4m packet of coarse conglomerates are found. The conglomerate bed is illustrated in figure 7.18 (photo on the right): note the sharp basal and top contact. These are fan delta deposits (marine conglomerates of facies 14). They are overlain by a 12m thick carbonate platform. The transition from conglomerates to carbonate platform occurs rapidly across a sharp surface: coral framestones sit in direct contact on the conglomerates. Some pebbles, and sand grade siliciclastic material are reworked into the base of the carbonate beds, but this quickly diminishes to nothing. This 12m carbonate platform interval is illustrated in the figure 7.7: over the first 5m diverse types of dominantly dome corals give way to almost monospecific platey Porites morphotypes, then the framestones are replaced by Nummulitid pack-grainstones rich in red-algal debris. This change in coral morphology from domes (middle reef front; James, 1984) to plates (lower reef front) and final loss of corals seems to reflect an environmental deterioration for the growth of corals. Laterally the platform thickness varies rapidly: in the log in figure 7.12 only 2m of platform are found. The bedding geometries show that this platform progrades out to fill its own "back-reef" area (see figure 7.7). The platform is then covered by siliciclastics: silty muds to fine sands bearing diverse molluscan debris. These show a general coarsening up trend over a 21m interval to the base of the next conglomeratic fan delta at the base of cycle 3.3. Within this cycle 3.2, small scale cycles of coquina beds and variations in sand coarseness, similar to those found below in cycle 3.1, have been observed in the log, though the details of these cycles have not been resolved.

Cycle 3.3 has a very similar organisation to cycle 3.2: 6m of gravels and conglomerates of the fan delta at the base are then overlain by a 10m thick carbonate platform. The platform sediments consist mainly of sandy packstones and grainstones (facies 9), with no constructed facies observed. This platform is in turn overlain by 7m of siliciclastics which coarsen-up to cycle boundary 4.

Cycle 4: this cycle, with a total thickness of 46m, sits astride the NN4/NN5 biozone boundary. The bedding patterns for the carbonate platform that develops during this cycle are illustrated in figures 7.9. A conglomeratic fan delta forms the base of cycle 4. These beds are overlain by 5m of relatively tabular sandy shelly packstone and grainstone carbonate beds (facies 9). Then 40m of reefal carbonates are deposited. The reefal facies were examined in the field, and the back-reef deposits were logged (figure 7.13). A variety of coralgal boundstone textures form the platform, while fine Nummulitid packstones and wackestones form the back-reef deposits. The depositional geometries are illustrated in figure 7.8: initially production is localised in a seaward position, the beds aggrade then prograde out in a landward direction (backfilling). Four medium-scale cycles of aggradation and progradation are observed. The seaward margin geometries are not preserved in outcrop. A siliciclastic interval directly overlies this platform, and is composed of medium shelly sandstone containing some gravel. It also contains some rare nannoplankton, and this is the first NN5 date found in this section.

Cycle 5: this cycle is Langhian in age (NN5 biozone), and has a total thickness of 52m. The carbonate platform of cycle 5 sits directly on these sands. This platform is 38m thick and is illustrated in figure 7.10; the vertical facies evolution is described in figures 7.13 and 14. The platform core shows a variety of coralgal boundstone textures, with some Nummulitid grainstone intervals, and some thin beds of rhodolithic bindstones and rudstones (facies 5). Oyster boundstone levels are also common. The geometries (figure 7.10) show 10m thick cycles of localised aggradation then progradation in both seaward and landward directions. Four such medium-scale cycles have been defined. The top of this platform is marked by the arrival of sands (at 5m on figure 7.14). This basinward prograding sandwave is illustrated in figure 7.19 (top photo). A change in facies style then occurs from clean coralgal boundstone facies to a clay-rich 11m interval of rhodolithic and coralgal floatstones with localised small build-ups of clayey coralgal boundstones. 8m of medium sized sands, with some sorted conglomeratic textures, overlie these deposits, and it is these sands that define the cycle boundary zone 6.

Cycle 6: only the base of this cycle is described here. It is of Langhian age (NN5) and is greater than 27m thick. Above these sands lies 6m of coralgal boundstones, which prograde in a northerly, landward direction, then these boundstones are covered by a thick packet of rhodolithic marl deposits, interpreted as representing a flooding event. It is proposed that these marls have accumulated in a quiet-water environment such as a back-reef or lagoon, and that they represent a relative shallow marine environment.

7.4 ALAHAN-KIZIL KAYA CORRELATION

Here two hypotheses for the correlation between the Alahan and the Kizil Kaya study windows are presented. The key evidence is described, and the pros and cons of each hypothesis are discussed.

The detailed information described in the Kizil Kaya and the Alahan study areas, and the mapping work are used to correlate between the two areas. Additional information from between the two main study sites is also required to construct this correlation. This information is presented here below. The main problem encountered is that the intervening outcrop is poor to very poor, due to the nature of the rock (muds, silts and marls), and due to the tree cover (an intensive forest replantation programme was undertaken in the 1970's).

Miscellaneous logs: figure 7.15 shows logs 56 and 56b. Log 56b describes the most landward outcrop of the isolated platform complex mapped as Mi in the mapping study, as well as the sediments above and below. This outcrop is found at grid reference 260725 on the geological map of Mut (figure 4.7). The log describes the transition from the Derinçay continental clastics through a thin packet of shallow marine conglomerates (presence of red algae and barnacles) into a reduced platform thickness of 27m with both bioconstructed and detrital carbonate facies. The platform is then directly overlain by fine clastics: metric cycles of fine sands to muds, containing 36-40% carbonates.

Log 56 (grid reference 295685, Mut geological map, figure 4.7) was made by digging through poor soily outcrop in the 200m interval directly overlying Kizil Kaya. Here 180m of marls and mudstones are capped by medium to coarse siliciclastic sands. Within the marls (mainly 70-80% carbonate) there is a siliciclastic interval of note at 60-80m with only 33% carbonate content.

Calcimetry: other calcimetry measurements were made on relevent samples and this information added to the logs. Measurements of note here are those made at the base of the Alahan study area, in log 7, in the fine grained siliciclastic sediments, and those made in the log 34, at the north-western (landward) extremity of the Kizil Kaya study area. The Alahan measurements illustrate the carbonate content of the most proximal siliciclastic sediments, while the Kizil Kaya samples show the nature of the sediment that directly overlies the Kizil Kaya platform. Geographically intermediate values of the carbonate content of the sediment directly overlying the platform 1 are given by logs 56 and 56b as discussed above.

Slump outcrops: isolated outcrops of potentially slumped material have been described in two areas. Slump 1 (grid location 308689, 680m altitude, just above the top of Kizil Kaya) is a 20m thick outcrop of tilted shallow platform carbonate sediments. Neither the base nor the top contacts of the packet outcrop, but it seems that it is covered with in-situ marl deposits. Slump 2 (grid location 301699, 730-830m altitude) is a series of 10-30m thick rotated blocks, sealed by a few metres of conglomerates. The lithologies in the block include coarse to fine sandstones, some calcarenitic red-algal grainstones, and laminated mudstones rich in plant debris.

Hypothesis 1 (figure 7.2): this is the simpler of the two hypotheses. It is based on the following postulates:

1/ the major arrival of sand grade siliciclastic material into the basin as described at the top of log 56 is correlated with the cycle boundary 2 in the Alahan study area, and can be considered as the lowstand of cycle 3. This cycle boundary marks the top of the most important packet of siliclastics described in this site.

2/ slump 1 is the result of recent erosion, and has been wrongly interpreted. Else it is due to a minor phase of platform collapse that is poorly expressed or undescribed in the Alahan area. The slump is delivered laterally from carbonate platforms found out of the line of section.

3/ slump 2 is associated with cycle boundary 2.

4/ The clay rich interval at 60-80m in log 56 (figure 7.15) is of relative unimportance to this interpretation.

Hypothesis 2 (figure 7.3): this is based on the following postulates:

1/ the clay rich interval at 60-80m in log 56 is the distal equivalent of the cycle boundary 2 in the Alahan area, and can be considered as the lowstand of the cycle 3.

2/ the carbonate slump 1 correlates with the cycle boundary 3 in Alahan. This cycle boundary is a major karst surface, and so calcareous slump deposits from the collapse of this platform are not unexpected.

3/ the basinal sands at the top of log 56 correlate with the cycle boundary 4 in Alahan. Cycle 3 is a mixed siliciclastic/carbonate system, so in this case a siliciclastic lowstand is not unexpected.

Hypothesis 2 is preferred because it better fits the available data, and accounts for all the observations made, forming the most coherent interpretation of the two. None of the information is ignored or discounted. Also, the very isopachous geometry of the siliciclastic wedge that covers Kizil Kaya (cycle 1 in the Alahan area) in the first hypothesis seems unrealistic: it does not take into account the thickness variations to be expected along the clinoform of a depositional profile, nor the post-depositional compaction of the dominantly fine grained siliciclastics which would enhance the lateral thickness variations of such a sedimentary package. Secondly the volume of siliciclastics proposed in hypothesis 1 is remarkable and would need considerable explanation. Thirdly, in hypothesis 1 the fine grained siliciclastic input at 60-80m in log 56 and the carbonate slump 1 are ignored. For these reasons the hypothesis 2 is adopted in future discussions in this study.

7.5 SUMMARY

The following conclusions can be drawn from this study area:

Cycle hierarchy

A stratigraphic hierarchy exists with three distinct scales of sedimentary cycles observed (small, medium and large). Five large-scale cycles have been described.

A change in cycle organisation occurs at CB4, just below the NN4/NN5 boundary: the large-scale cycles below this limit have an average thickness of 80m and are divided into 20m-thick medium-scale cycles, while the large-scale cycles above this surface are 50m thick, sub-divided into 10m-thick medium-scale cycles. This scale-shift corresponds roughly to the Burdigalian/Langhian boundary.

Cycle organisation

A distinct cycle motif is observed, in which shallowing-up siliciclastics terminate with their coarsest and shallowest deposits (normally a fan delta), then the siliciclastics are abruptly replaced by platform carbonate sediments. There exists some evidence to show that the environmental conditions for healthy coral growth deteriorate up through the carbonate sequence, before the carbonates are replaced by the finest siliciclastic sediments at the base of the next siliciclastic shallowing-up packet. This can be conceptually understood if the siliciclastics are associated with the regression, and the carbonates grow during the transgression. Carbonate growth is prevented by the arrival of the siliciclastics during the regrssion, and so they opportunistically grow in a “carbonate window”, defined by the proximal shift of the siliciclastic depocentre.

This motif is observed at all three scales of cycles. However, the processes at each scale are not necessarily identical. At the medium and large scale the siliciclastics seem to inhibit the carbonate production, while at the small scale the same mechanism cannot be invoked, since the molluscan fauna that comprise the carbonate (coquina) beds at this scale are adapted to live in a siliciclastic environment (they are commonly found in siliciclastic environments throughout this area). Here there seems to be reworking processes occurring, and it is proposed that these coquina beds are reworked due to an increasing energy of the environment during small-scale transgressions.

The placing of the carbonate platforms within a transgressive context highlights the limits in the definition of retrograding/prograding cycles: these "transgressive" carbonates are deposited with prograding geometries. Their description as “retrograding” is concept-driven, and relies on the interaction between the carbonates and the siliciclastics (the term retrogradation in this sense is actually applied to the inferred siliciclastic response during this time).

Facies evolution

The vertical facies evolution of some of the carbonate intervals shows evidence for environmental change. For example, the carbonate platform in cycle 3.2 shows an evolution from a middle reef-front environment to a lower reef-front environment, before the coral community is replaced by bioclastic sands formed by Nummulitid foraminifera and red-algal debris. This shift is interpreted as a deterioration in the environmental conditions with respect to coral growth. A number of possible causes exist, and will be discussed later.

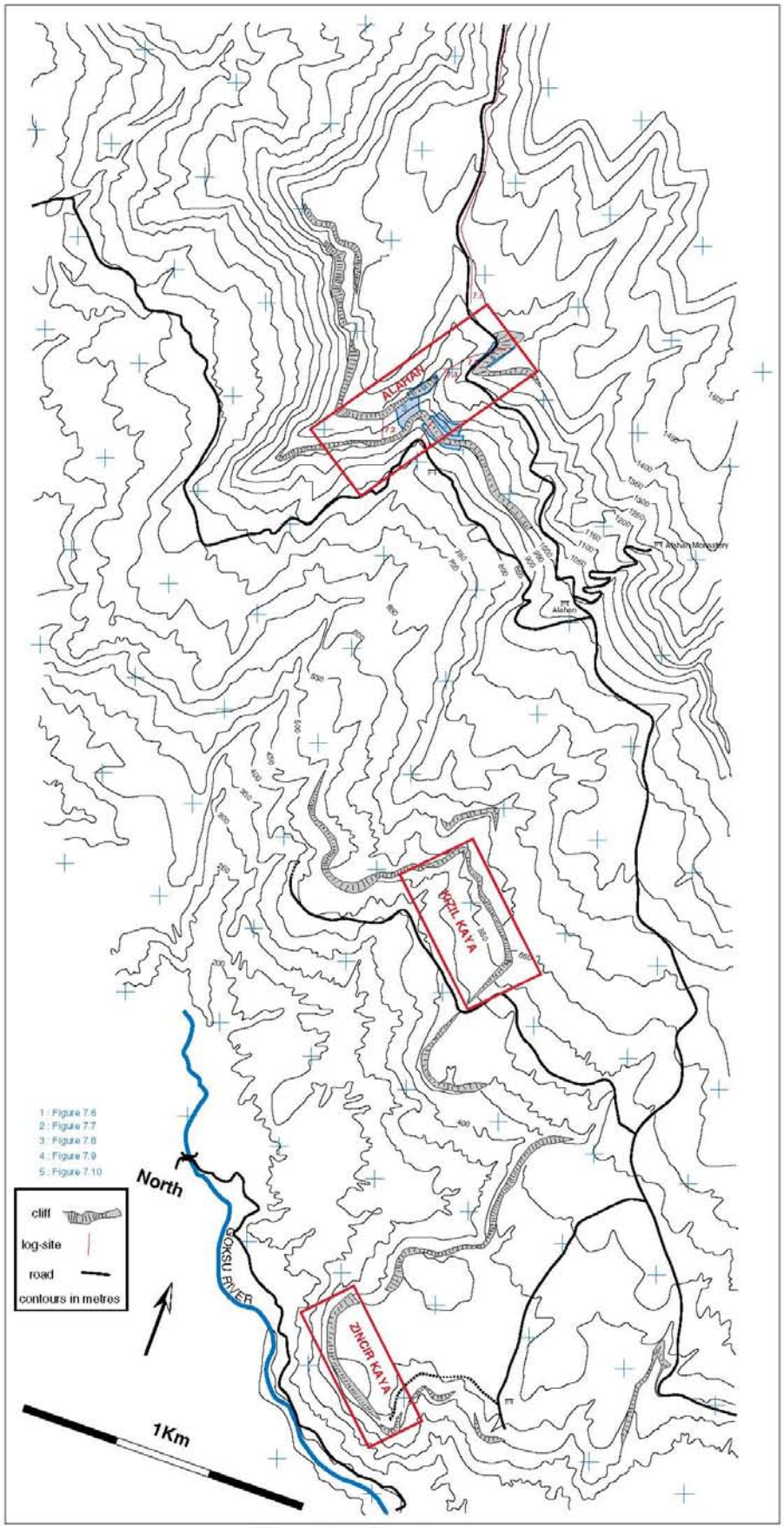

Figure 7.5 Alahan location map
(numbers indicate the figure locations for the Alahan site)

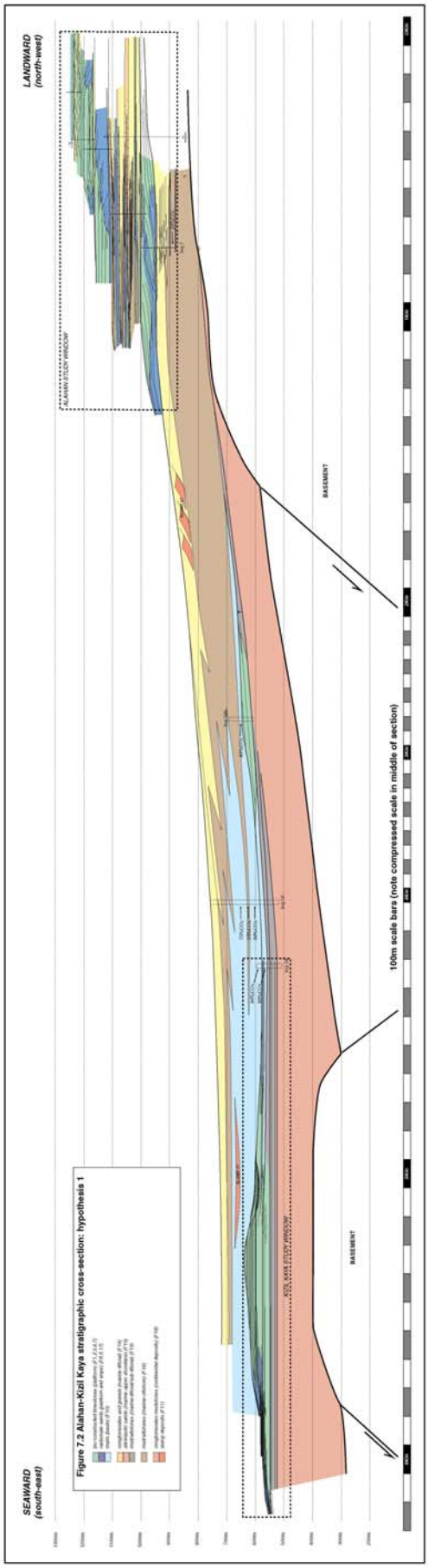
SEAWARD
(south-east)
LANDWARD
(north-west)
Figure 7.2 Alahan-Kizil Kaya stratigraphic cross-section: hypothesis 1
BASEMENT
BASEMENT
100m scale bars (note compressed scale in middle of section)

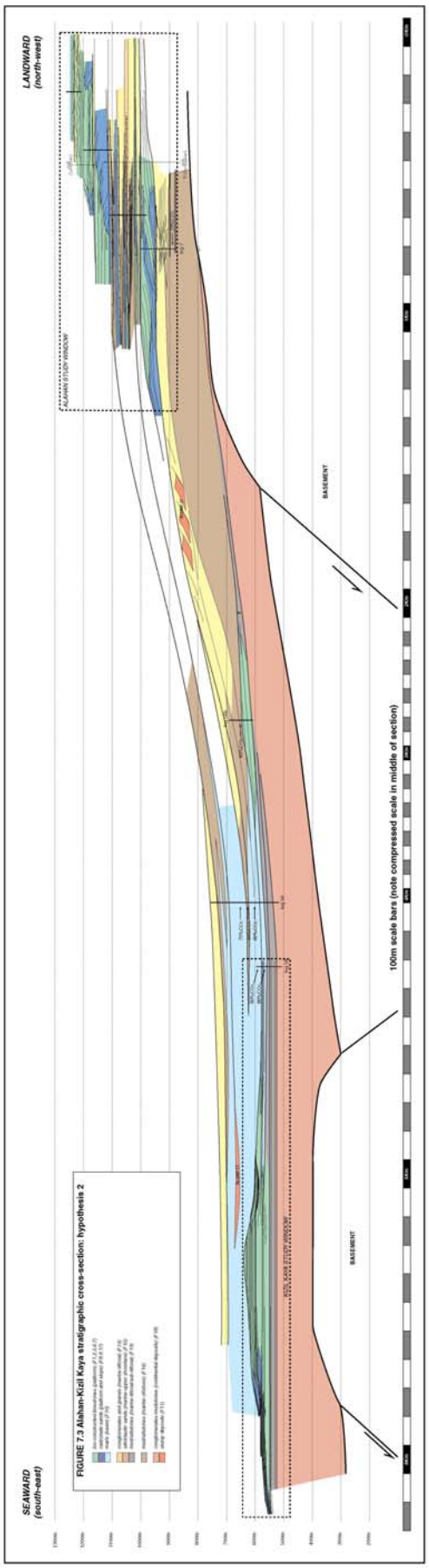
SEAWARD
(south-east)
LANDWARD
(north-west)
FIGURE 7.3 Alahan-Kizil Kaya stratigraphic cross-section: hypothesis 2
ALAHAN STUPA WINDOW
BASEMENT
BASEMENT
100m scale bars (note compressed scale in middle of section)

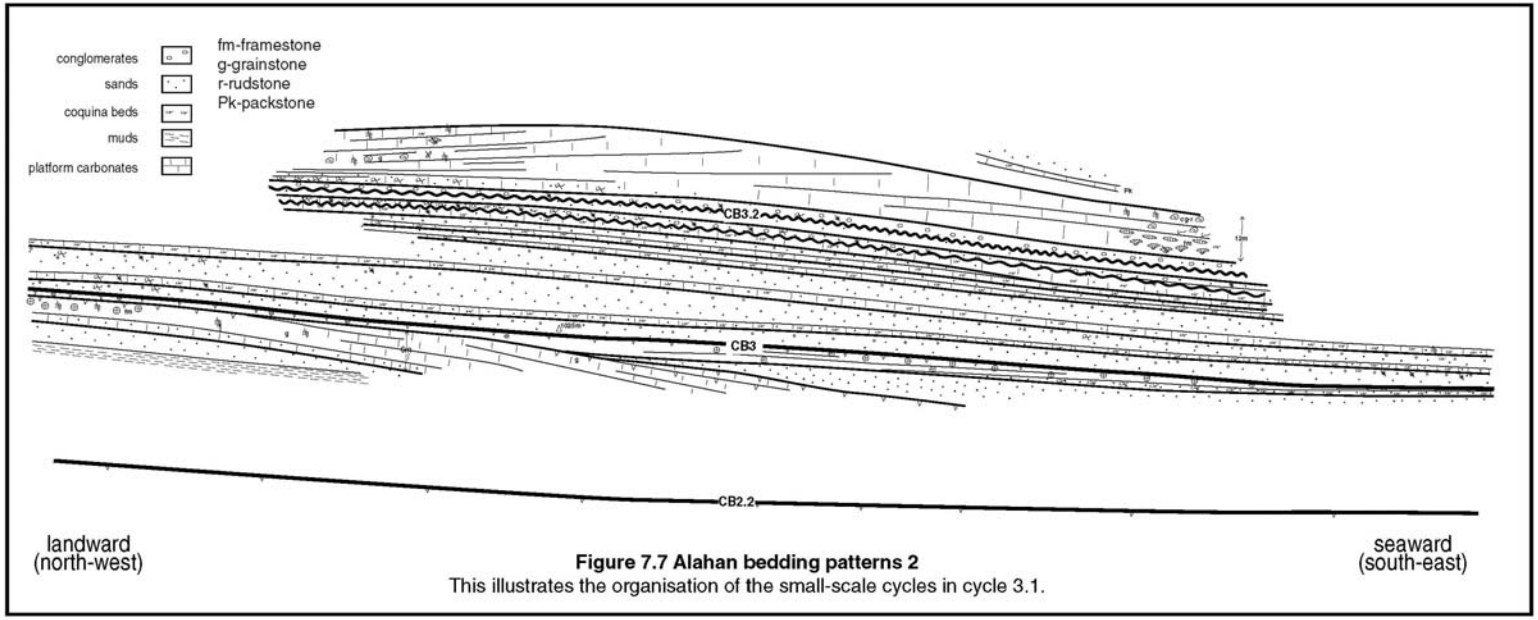

Figure 7.7 Alahan bedding patterns 2
This illustrates the organisation of the small-scale cycles in cycle 3.1.

FIGURE 7.7 SPLIT ON PAGES 112-113 IN THE ORIGINAL

Figure 7.4 Overview of the Alahan study site
This illustrates the northern side of the Alahan valley

Figure 7.6 Alahan bedding patterns 1
This shows a detail of the top of cycle 1 on the northern flank of the Alahan valley

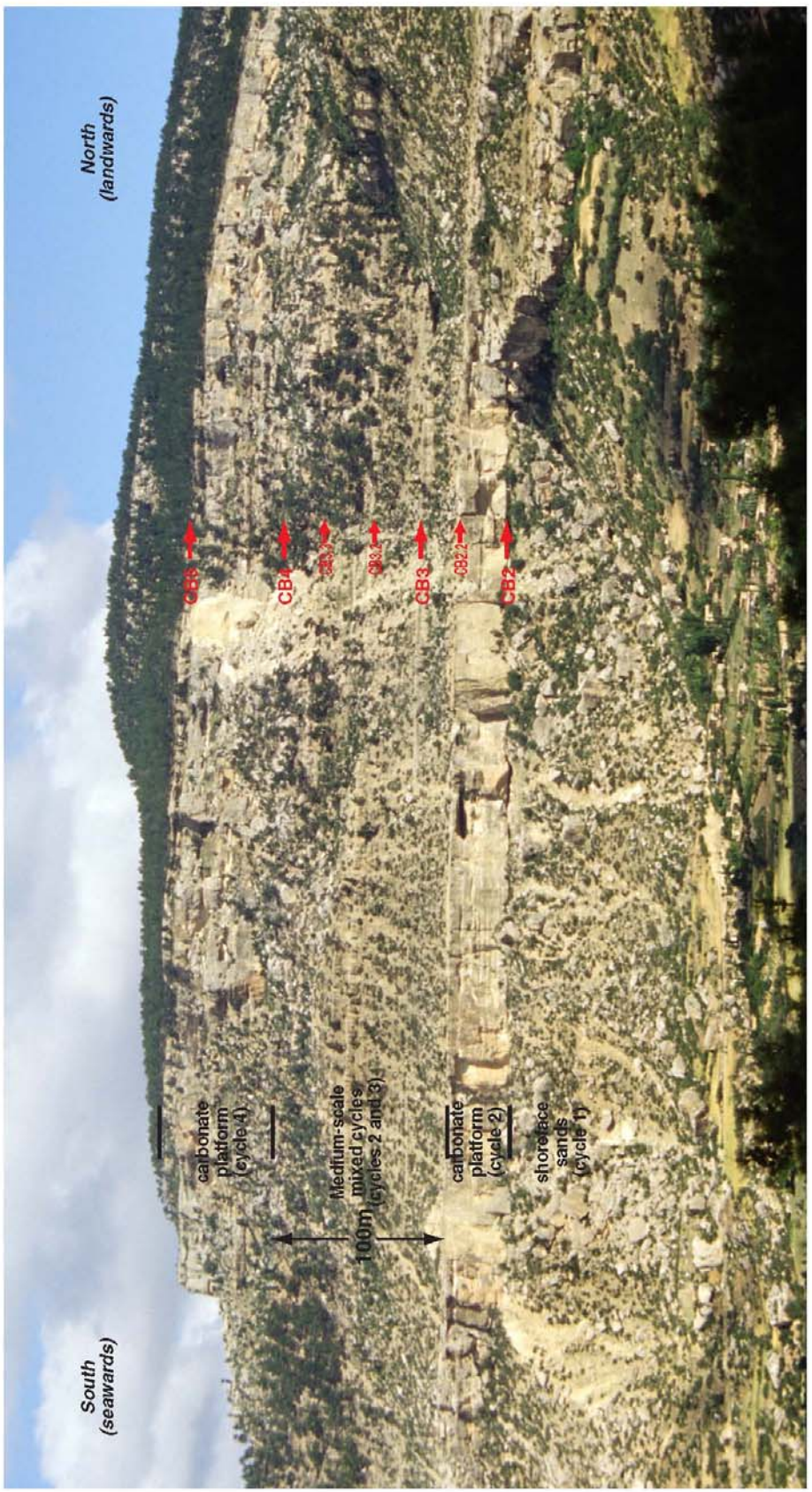

Figure 7.8 Alahan bedding patterns 3
This illustrates the organisation of the west side of the Alahan valley, showing the facies and cycle boundaries.

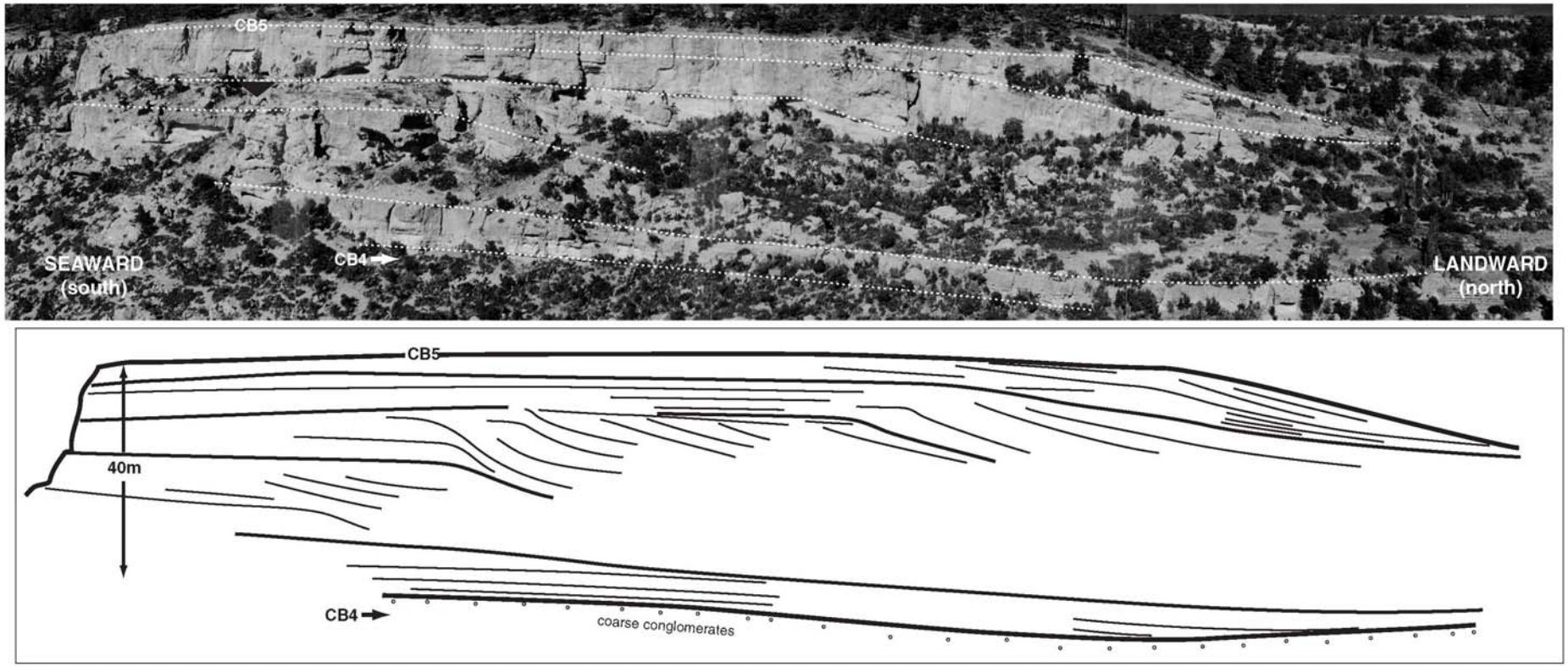

Figure 7.9a Alahan bedding patterns 4

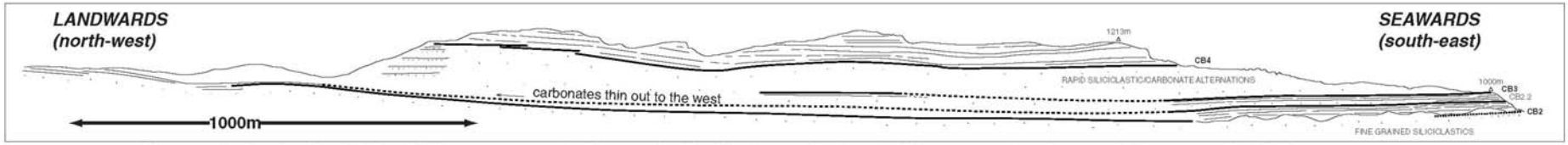

Figure 7.9b sketch of backside of Alahan outcrops showing proximally thinning and onlapping (?) contacts of carbonate platforms on siliciclastic sequence

FIGURES 7.9A AND 7.9B SPLIT ON PAGES 116-117 IN THE ORIGINAL

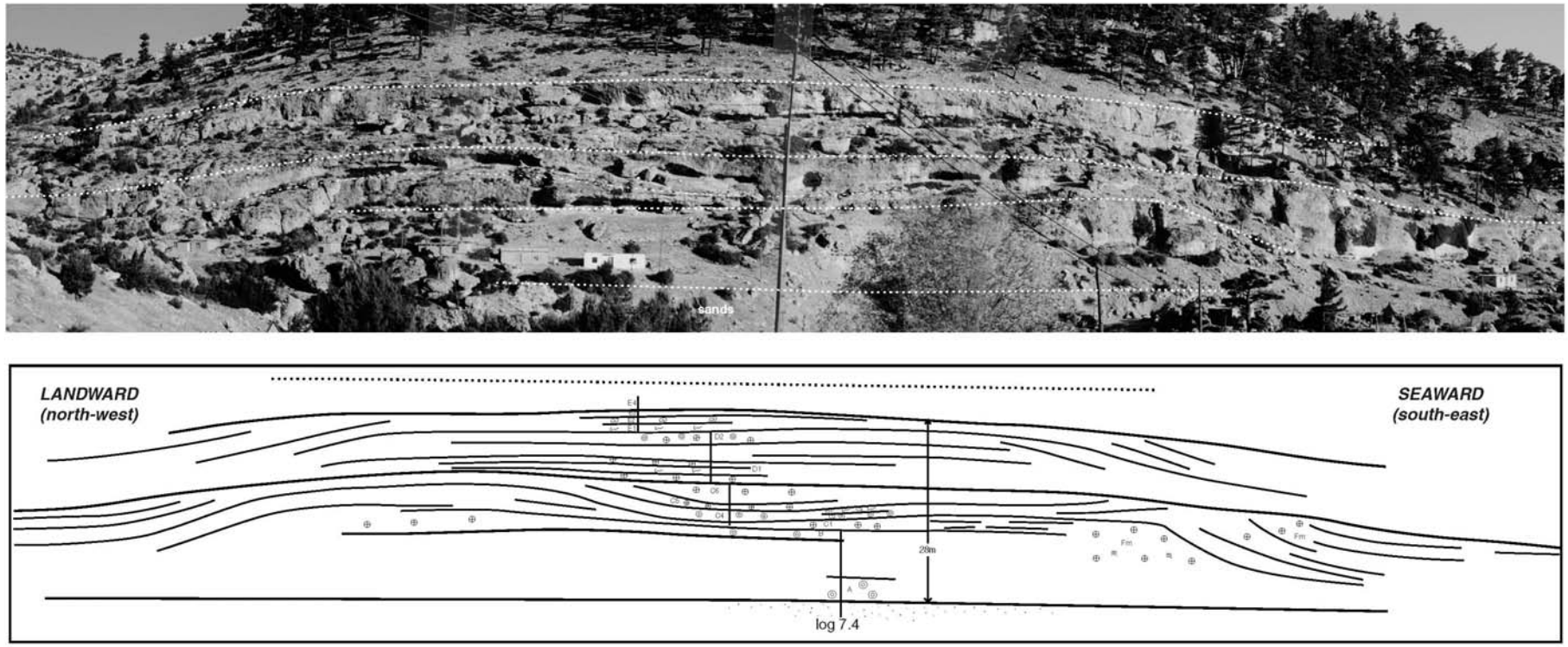

Figure 7.10 Alahan bedding patterns 5
This illustrates the Langhian age (NN5) isolated platform of cycle 5.

FIGURE 7.10 SPLIT ON PAGES 118-119 IN THE ORIGINAL

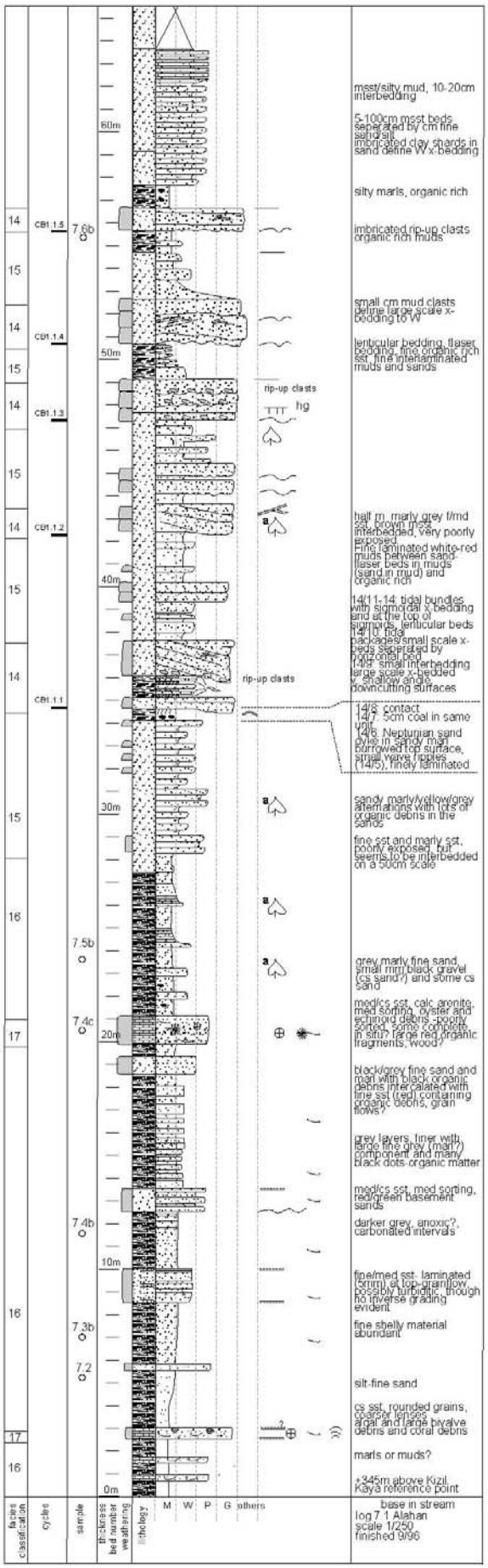

Figure 7.11 Alahan log 7.1

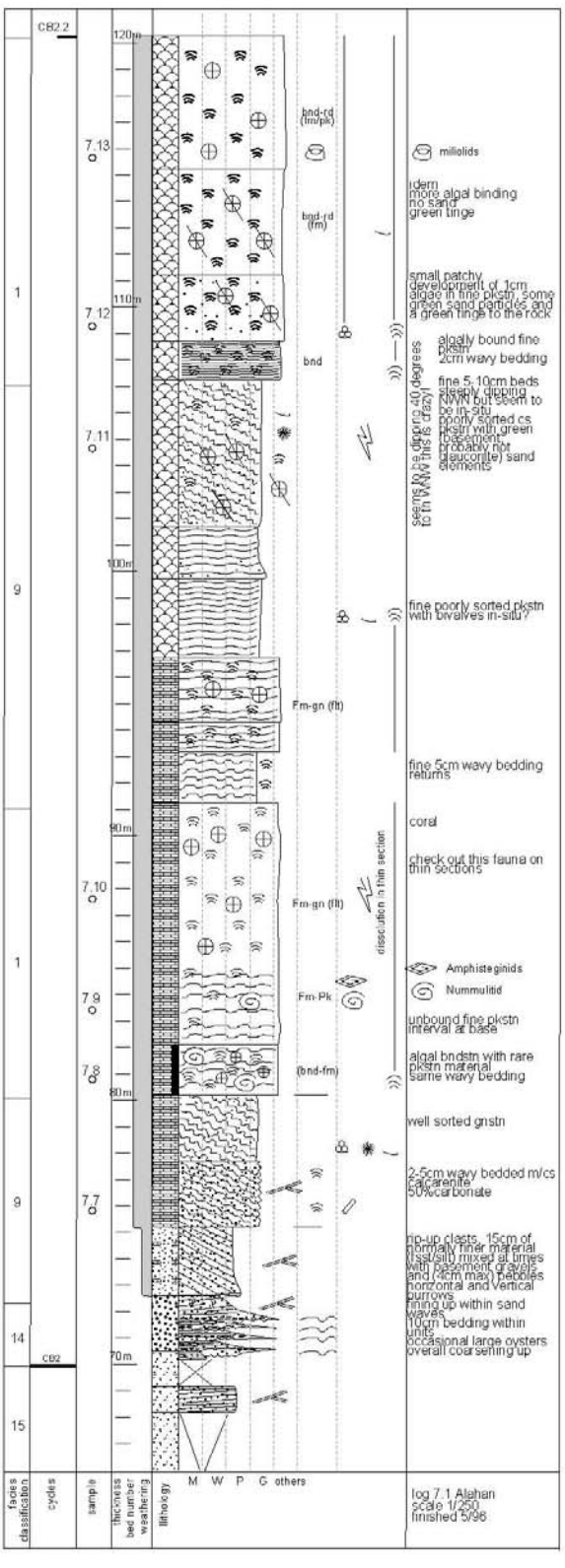

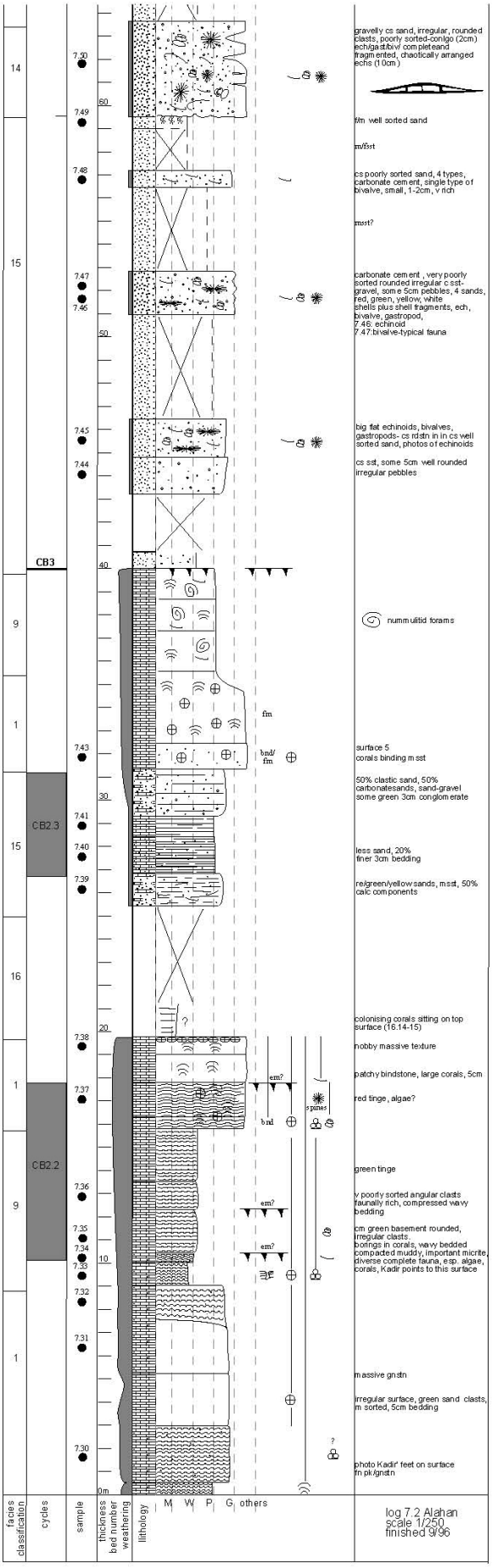

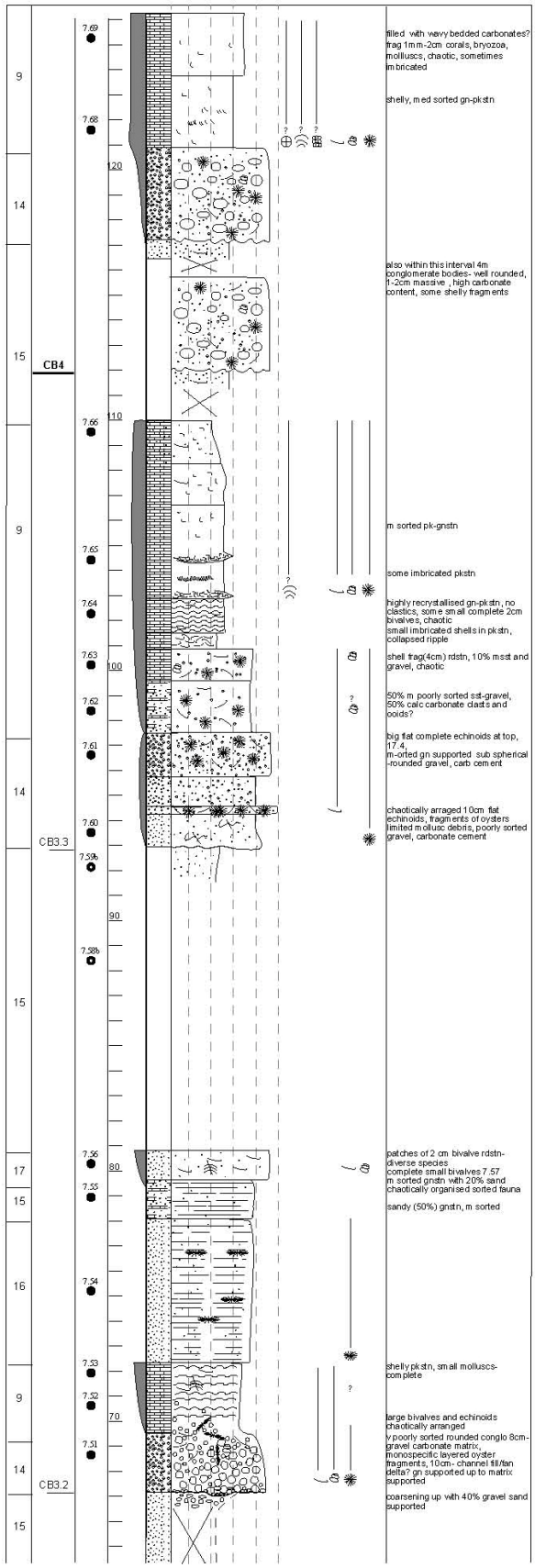

Figure 7.12 Alahan log 7.2

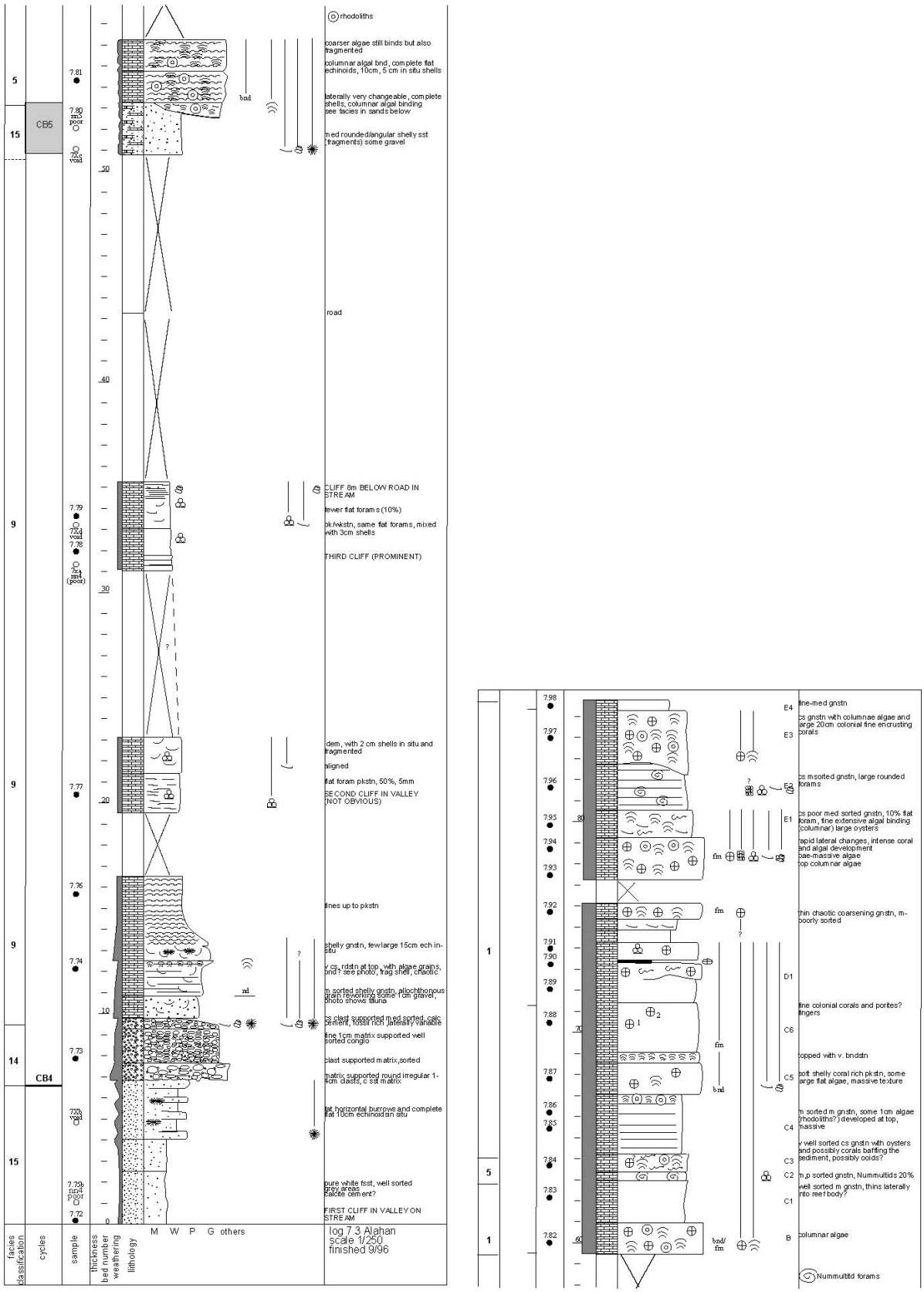

Figure 7.13 Alahan log 7.3

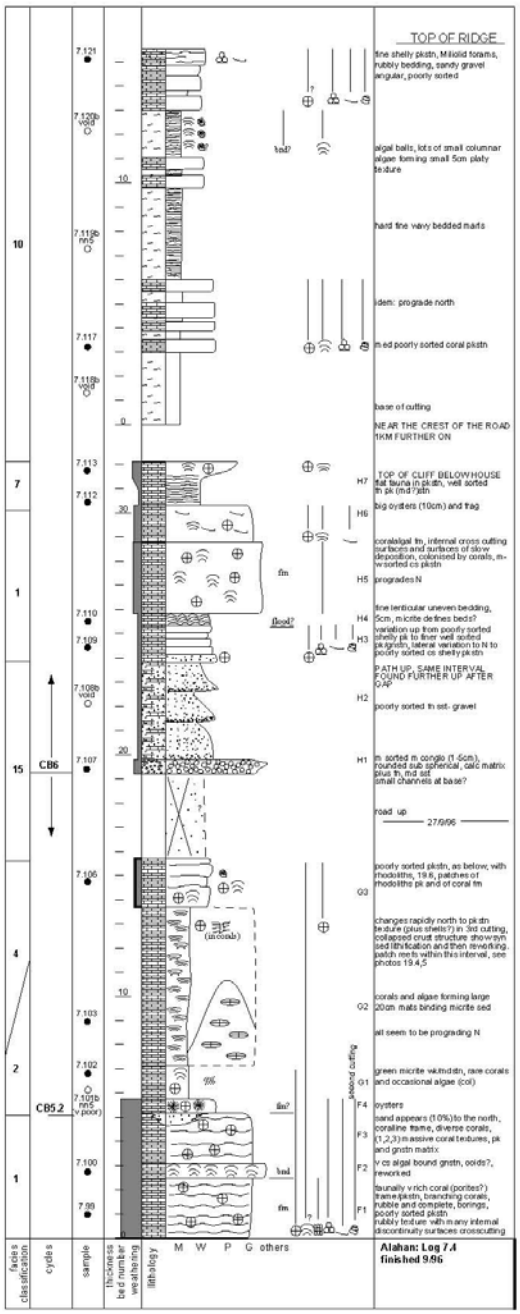

Figure 7.14 Alahan log 7.4

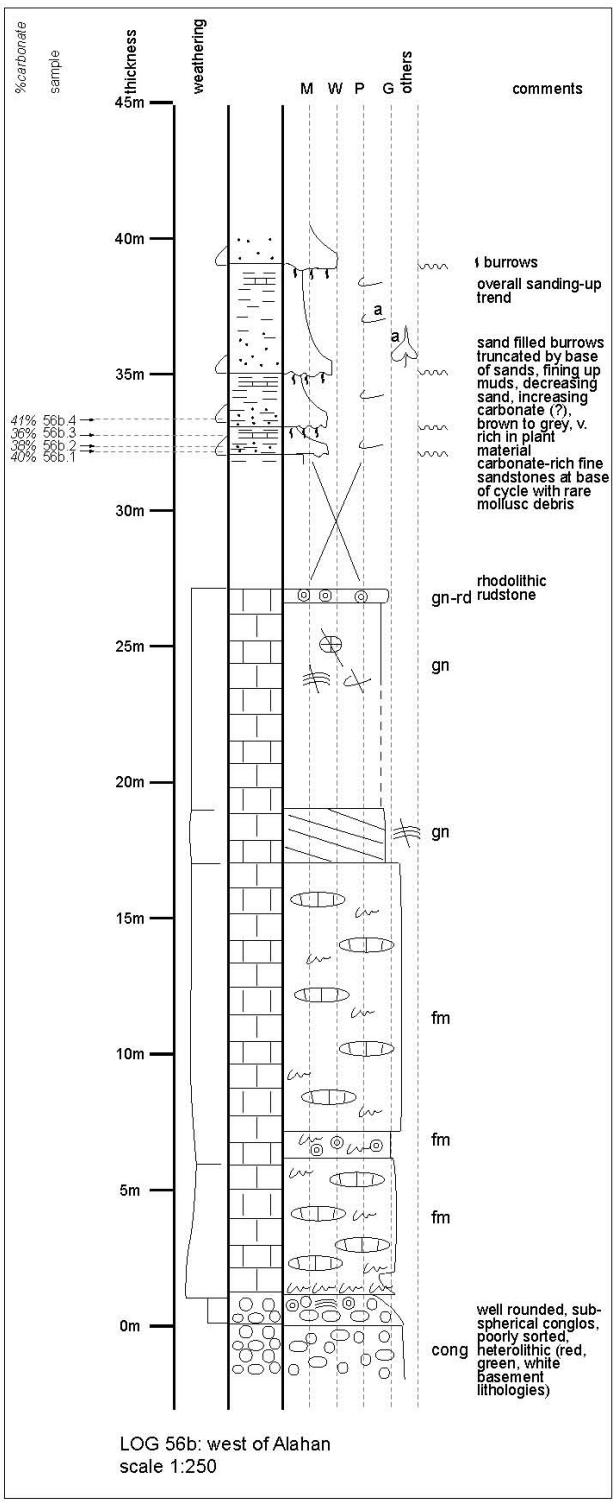

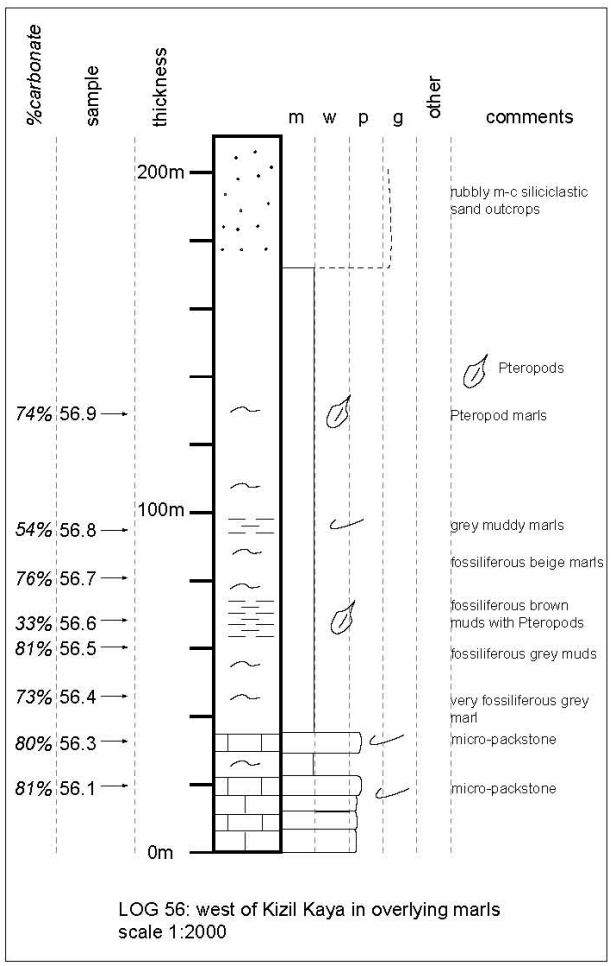

Figure 7.15 Alahan logs 56 and 56b

Log 56b describes the westernmost isolated platform of cycle 1, showing its contact with coarse marine conglomerates beneath, and fine-grained offshore silts and muds above. Log 56 is a sketch-log made by sampling the fine-grained sequence overlying Kizil Kaya: this includes calcimetry measurements to quantify the composition.

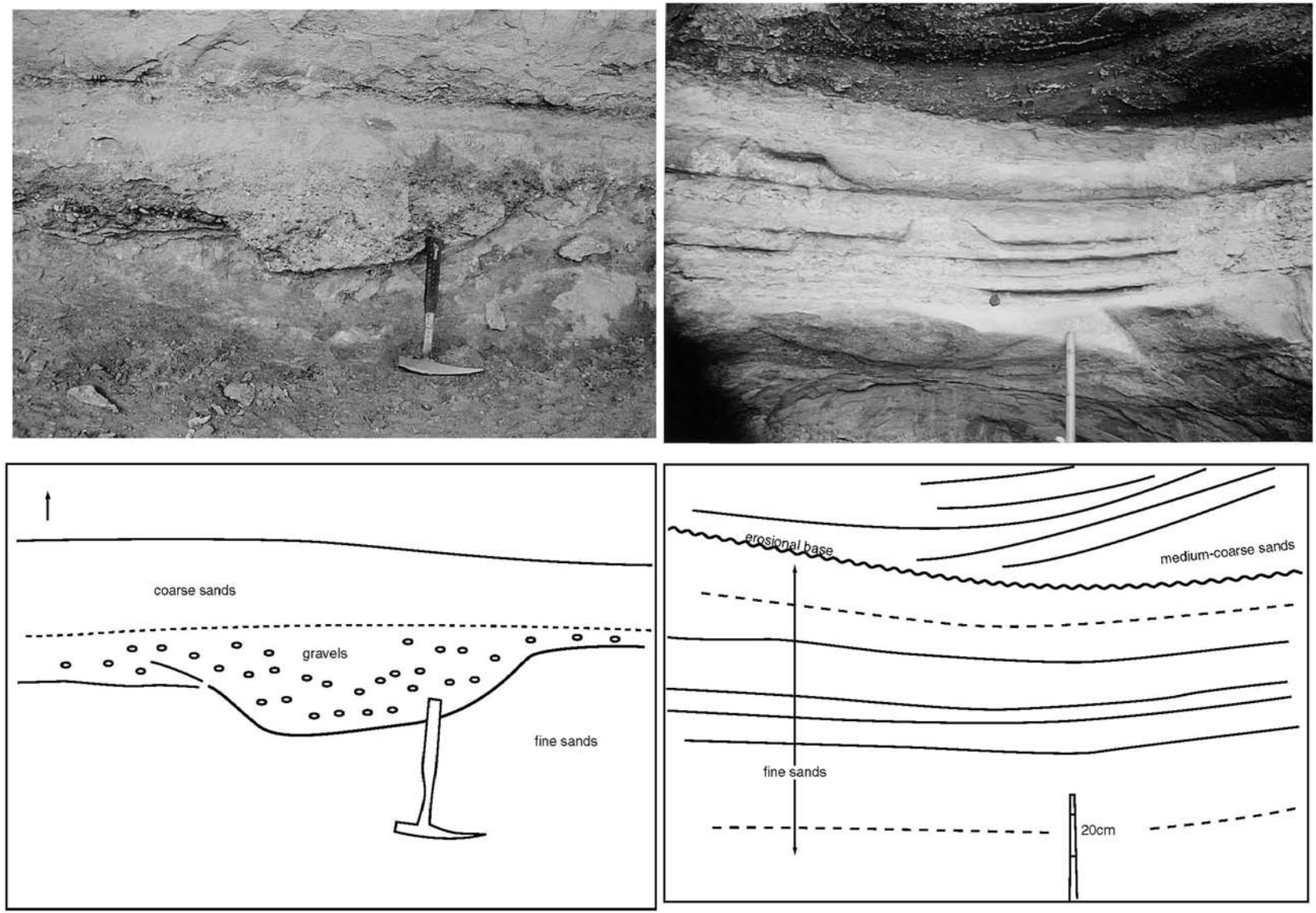

Figure 7.16 Alahan photos 1
Top photo illustrates the base of a tidal channel that forms one of the small-scale cycles in cycle 1.1.
Bottom photo illustrates cycle boundary 2: here a small gravel-filled gully.

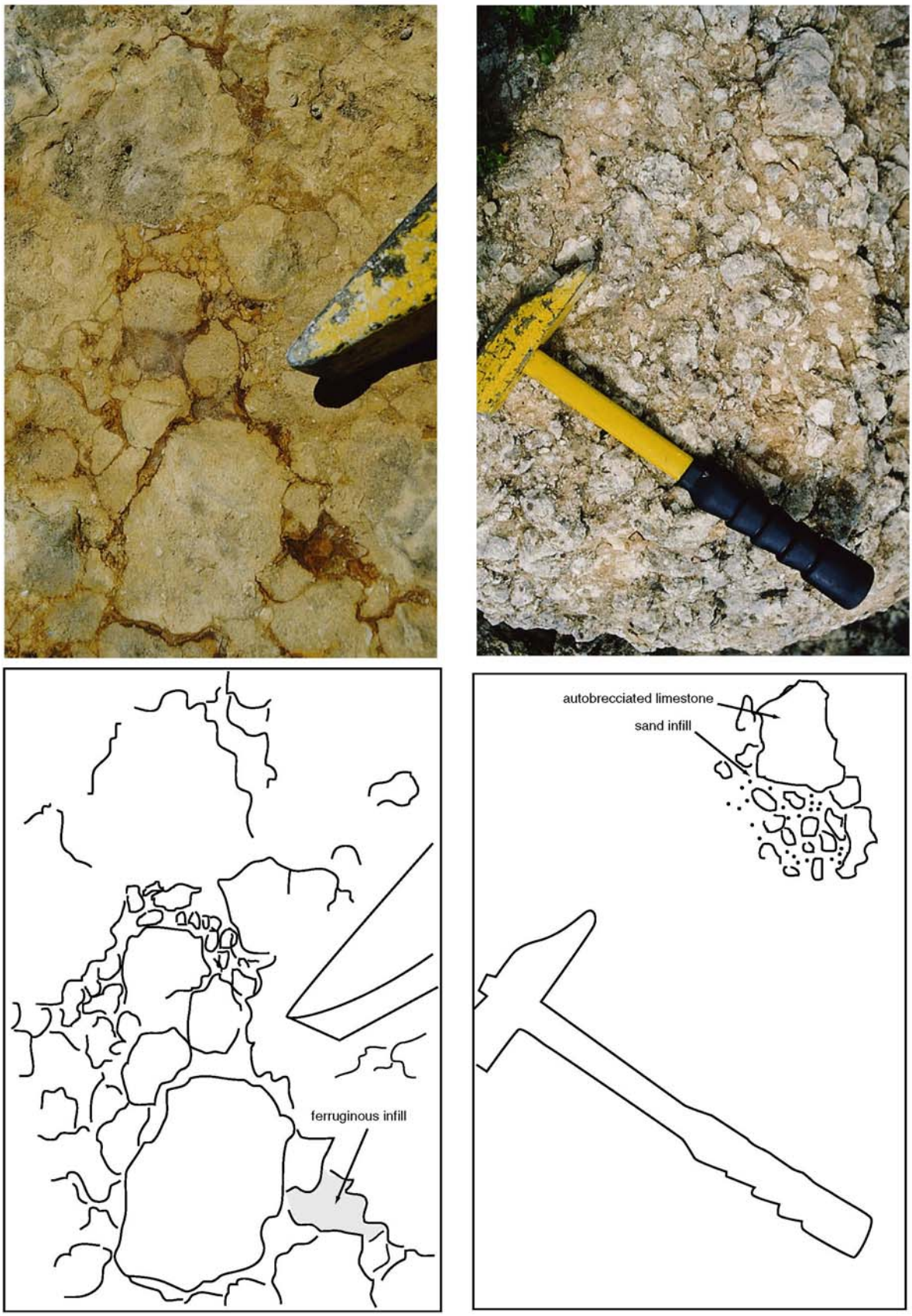

Figure 7.17 Alahan outcrop photos 2
Two examples of the karstified textures found at CB3:
(Left) An incipient brecciated surface with ferruginous infill, and
(right) an auto-breccia with allochthonous sand infill

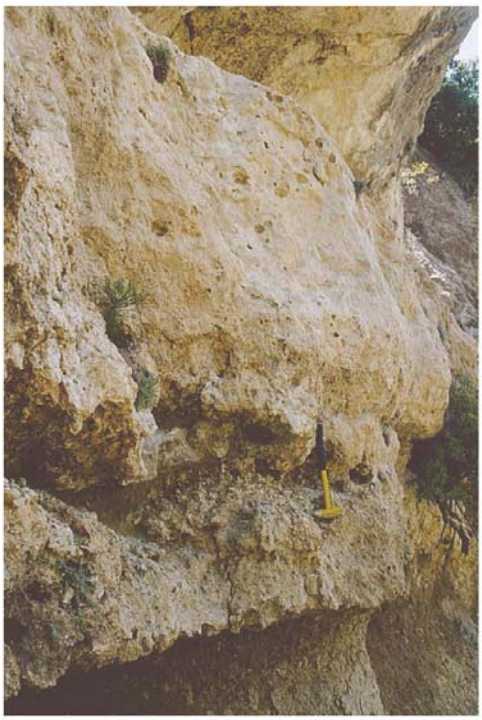

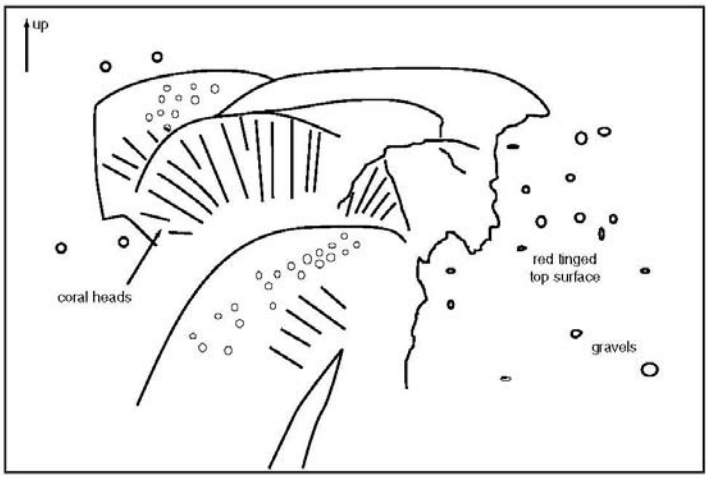

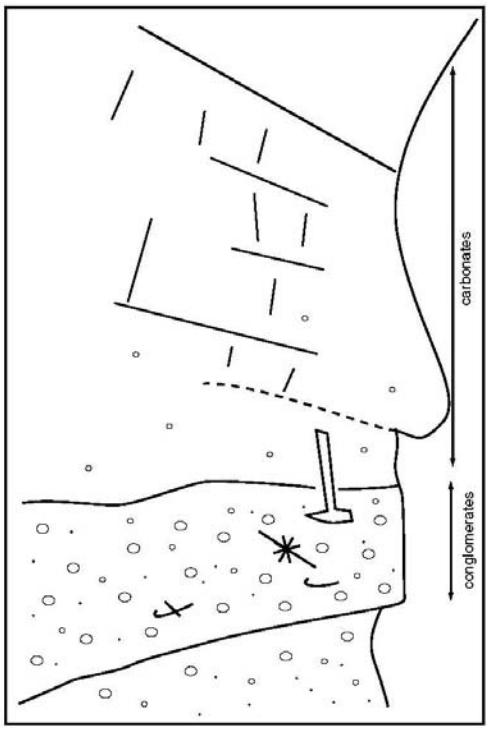

Figure 7.18 Alahan outcrop photos 3
(Left) Shows gravels surrounding corals on CB3, while (right) illustrates a typical fan delta contact with the overlying platform carbonates.

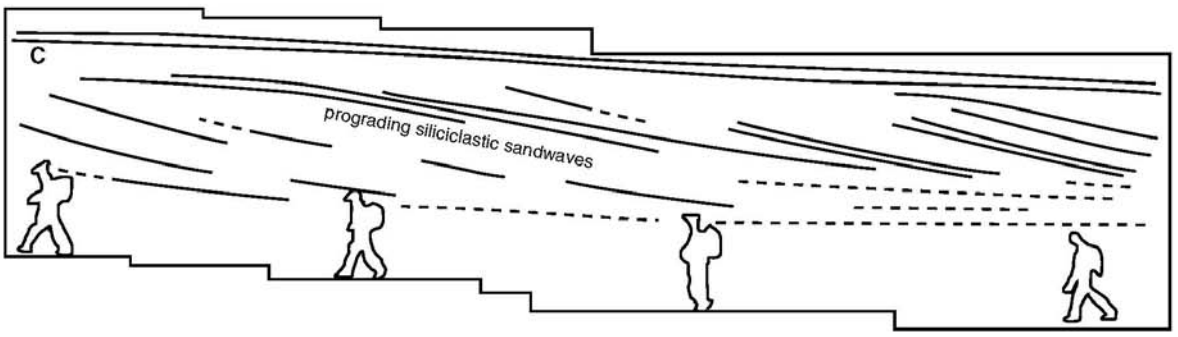

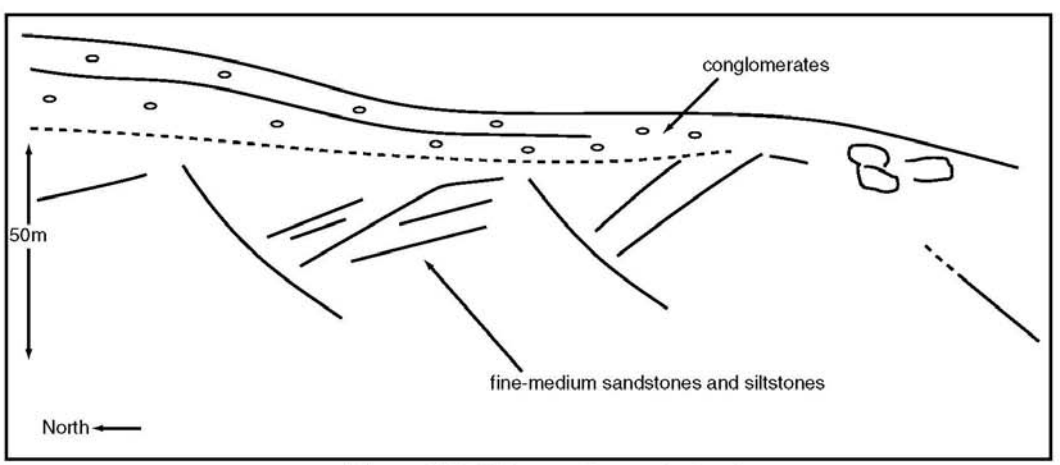

Figure 7.19 Alahan outcrop photos 4
The top photo illustrates a seaward prograding siliciclastic sandwave from the Langhian (NN5) at the top of the logged Alahan interval, while the lower photo shows the collapsed platform edge of the top of cycle 1, south-west of the Alahan area.

8 - DIBEKLI TRANSECT (SILIFKE)

8.1 INTRODUCTION

This chapter is divided into two parts. The first part describes the construction of the Dibekli transect, the only detailed study window in the Silifke area. The second part describes the construction of a general stratigraphic cross-section for the Silifke area, based on diverse field observations.

The Dibekli study area is situated in the Silifke region to the south of the Goksu river, at an altitude of 400-650m, around grid reference 660310 on the Silifke geological map (figure 4.8). The outcrop lies on the south-east facing shoulder of a ridge that rises up to the Gülnar plateau area to the south. A small road leads up to this area, branching off from the Silifke-Mut highway on the Silifke-side of the bridge that crosses the Goksu.

The Dibekli transect shown in figure 8.1 was constructed principally from the field log 3 and observations of the bedding patterns, calibrated by field measurements of distances and thicknesses. Thin-section analysis played a secondary role: the microfaunal content of 44 thin sections was examined, and this information was added to the field logs.

In this study interval a series of three carbonate platforms develop in apparent backstepping geometries against a steep basement topography (see figure 8.2 and 8.5). The depositional geometries are illustrated in figure 8.2. Log 3 which describes this interval is shown in figures 8.3 and 8.4. The resulting stratigraphic cross-section is shown in figure 8.1. Other features referred to in the discussion are illustrated in figures 8.5-9.

The basement poorly outcrops in this area, though the topography of the basement/Miocene contact is relatively easy to define: a step topography is seen, with two relatively steep intervals separating the flat areas. From the mapped relationships this relief has been associated with the presence of normal (oblique?) faults in the basement, and these have been marked as such in the Dibekli transect (figure 8.1).

8.2 DEFINITION OF CYCLES

Three large-scale retrograding/prograding cycles (cycles 1-3) and nine medium-scale cycles (cycles 1.1-3, 2.1-3 and 3.1-3) have been defined in this study.

Large-scale cycles

A distinct stratigraphic motif is observed to recur three times in this outcrop on the scale of 50-100m. It consists of 10-15m of basement conglomerates deposited in a marine environment (facies 14) at the base, overlain by 10-25m of platform carbonates, which are in turn covered by a thick packet (10-25m) of marls (facies 10). Surprisingly, few shallow or deepening facies evolutions, nor few prograding or retrograding geometries have been observed. The most dramatic facies changes take place abruptly across surfaces. When defining retrograding/prograding cycles a distal or proximal shift across a surface is the equivalent of a retrograding or a prograding sedimentary packet. In this transect the cycles are principally defined by these surfaces.

The large-scale cycle boundary is placed systematically at the base of the conglomerates which overlie the marl sediments. This (deep-water) marl to (shallow-marine) conglomerate change is a major shallowing shift (progradation), after which the transition from conglomerates to carbonate platform to marls represents a steady deepening (retrogradation). The cycle boundary is placed at the base of the conglomerates rather than in the middle or at the top because these beds are interpreted to be deposited during the initial retrogradation, with erosion of the underlying surface occurring during the progradation. This is consistent with the logic applied in the Alahan section, where similar conglomerates are found.

Cycles 1, 2 and 3: these cycle boundaries are placed at the base of the conglomeratic fan deltas, as discussed above. In cycle 1 these directly overlie the continental siliciclastics of the Derinçay Formation in this area. The maximum flooding interval is placed somewhere within the marls of each cycle.

Cycle 4: this cycle boundary is different from the others, in that a carbonate platform develops in the prograding part of cycle 3 (in the highstand). The cycle boundary develops as a karstified surface on the top of this platform, and this surface is directly overlain by marl sediments of the next cycle.

Medium-scale cycles

Cycle 1.1: the base of this cycle is the CB2.

Cycle 1.2: the base of the retrogradation of cycle 1.2 is indicated by the facies shift from fan-delta conglomerates to carbonate platform facies, and it is this that defines the cycle boundary 1.2. The exact position of the start of the retrograding trend is unclear, and may be found somewhere within the conglomerates just below the actual conglomerate/carbonate contact: this uncertainty is expressed by defining a cycle boundary zone.

Cycle 1.3: the transition from the shallow-marine carbonates of the platform in cycle 1.2, to deep water marls above is an abrupt deepening and retrogradation. Cycle boundary 1.3 is placed at the base of this retrograding trend, which is considered to be at (or near) the top surface of the platform unit. Additionally, some evidence exists for an exposure event near the platform top surface: in the microfacies in samples 3.5-8 (figure 8.3) large amounts of clast dissolution occurs, followed by the formation of pendant cements (meteoric vadose zone), which can be seen in the facies illustrations in figure 5.17. Such an event would constitute an ideal cycle boundary here.

Cycle 2.2: as for CB1.2, the cycle boundary 2.2 is placed at the base of the carbonate platform of cycle 2.2. The change from a fan-delta setting to a carbonate platform indicates the start of retrogradation of this cycle.

Cycle 2.3: as for CB 1.3, this cycle boundary is placed at the transition from shallow-marine platform carbonates to deep-water marls. Large dissolution cavities are found throughout the slumped part of this platform: their timing is undetermined, but if they are of Burdigalian age then this would indicate a time of sub-aerial exposure at the platform top surface. The slumping and cavities are illustrated in figure 8.7. If this interpretation is correct, then this supports the placing of the cycle boundary at the top of the platform deposits. Towards the top of the platform basement pebble-strewn surfaces are found, and these represent prograding maxima, supporting the placing of the cycle boundary at (or near) the top of the platform.

Cycle 3.2: as for CB 1.2, the cycle boundary 3.2 is placed at the transition from fan-delta deposits to platform carbonates.

Cycle 3.3: as for CB 1.3 and 2.3, this cycle boundary is placed at the transition from shallow-marine platform carbonates to deep-water marls. The top surface of the platform is strewn with centimetre-size rounded basement pebbles, and the limestone is brecciated (see figure 8.8). The arrival of the pebbles indicates a maximum of progradation on this surface, while the brecciation may be due to a period of sub-aerial exposure. Both these observations are further evidence for naming this a cycle boundary.

8.3 PLATFORM EVOLUTION

Cycle 1.1: 10m of this cycle have been described in figure 8.3, from 0-10m. The age is undetermined. The cycle here consists of three metric scale alternations of packstones to sandy packstones interbedded with basement conglomerates, each packstone/conglomerate pair being 3m thick. At the base of the log rounded, poorly sorted, grain supported basement conglomerates are found, with a matrix of basement siliciclastic sands. Marine fauna have not been observed and this conglomerate is considered as the top of the continental conglomerates (Derinçay Formation) in the area. A 2m packet of fine-medium well sorted siliciclastic sand overlies these conglomerates. It has a calcitic matrix and is yellow in colour. A 1.5m packet of conglomerates then overlies these sands. These conglomerates are illustrated in figure 8.6. The base and top of this bed consists of decimetric (5-20cm) rounded conglomerates, while the middle part of the bed consists of 40-50cm of rounded sorted fine cross-bedded conglomerates. These conglomerates are overlain by medium, sorted sandy bioclastic sands containing Miliolid foraminifera. Then 1.5m of basement conglomerates-breccias are deposited. These are sub-angular and poorly sorted, containing some metre-scale blocks. On top of this 2m of poorly sorted grainstones are deposited. These contain large amounts of oysters, and locally oyster floatstone-framestone textures develop. This bed is illustrated in figure 8.6. 2m of well rounded well sorted 10cm conglomerates are then deposited. These contain some oysters, both complete and as debris. These are then overlain by fine grainstones, consisting of red-algal debris, and containing some red algae growing in the sediment to form local bindstone textures. Rapid lateral facies variations occur to the north (seaward), with the conglomerates grading into sandy bioclastic sands over 100m.

Each conglomerate/calcarenite pair forms a small-scale cycle, with the conglomerate bed being the prograding part, and the bioclastic sands deposited over a sharp flooding surface during the retrogradation. Each consecutive small-scale cycle shows more marine characteristics: no marine fauna in the first sands, though the presence of calcitic cements and the colour may indicate a marine rather than continental depositional environment: Miliolids in the second calcarenite bed, indicating marine to restricted-marine conditions: oysters (marine to restricted-marine) and red algae (fully marine).

Cycle 1.2: this cycle has been described in figure 8.3 where 25m have been logged. The age is undetermined. It is organised into 6 massive packets of 5-6m thickness each, the packets being defined by a sharp bedding plane, or a finely bedded zone 1m thick. The lithologies are relatively homogenous: well sorted grainstones-rudstones (2-3mm size clasts)

consisting of red-algal, molluscan and bryozoan debris, and complete and fragmented foraminifera (this is facies 20). Amphisteginid

foraminifera are the most common, and Nummulitid debris is also found. Heterolithic basement sands and gravels (1-4mm) are also found in small quantities (1-2%) throughout the platform. 50m to the north of the logged area large scale cross-bedding develops within each massive 5-6m packet. The cycle also thickens in this direction. Marls directly overlie these sediments: the contact between the grainstones and the marls, though it is poorly exposed here, is abrupt.

Cycle 1.3: this cycle is 19m thick at logsite 3.1 (figure 8.3). It has been dated from one sample point (sample 3.11b) as belonging to the NN4 nannoplankton biozone (Late Burdigalian). It consists of 19m of poorly exposed marls capped by an erosional surface (the cycle boundary 2). No sediment is deposited during the progradation, and only erosion occurs.

Cycle 2.1: 100m to the south (landward) of log 3.2 (figure 8.1) a 10m packet of coarse very poorly sorted (1m-sand grade) rounded to sub-angular conglomerates is found. These conglomerates are internally interbedded with thin packstone beds of a few centimetres thickness, containing red-algal and diverse mollusc debris. The conglomerates themselves contain large echinoid (Clypeasters, among others) and oyster fragments. The top surface of these conglomerates is sharp, and slopes seawards (north). Overlying this top surface are the shallow marine carbonates of cycle 2.2. Following out these conglomeratic beds laterally, the facies changes rapidly (over 100m) to fine sorted basement sands, containing some centimetre size pebbles, as well as echinoid fragments, Nummulitid, Amphisteginid and rare planktonic foraminifera: this is found in log 3.2 (figure 8.3) in the first metre at the base of the log. These sands are interbedded with sandy marls.

These conglomerates are interpreted as a very locally sourced (from the coarseness of the components) fan delta that is deposited in the marine environment, and that progrades out directly over the marls. Local movement on the normal fault that defines the underlying basement topography may be responsible for this sudden generation of siliciclastic sediment. However, the deposition of very shallow marine siliciclastics (a few metres of water, maximum, due to the presence of Miliolids) over deep marine marls (minimum 50m water depth) also requires a dramatic sea-level fall between the deposition of the two sediment types.

Cycle 2.2: this cycle is 23m thick in the logged area (see figure 8.3, log 3.2), and belongs to the NN4 nannoplankton biozone (NN4 dates have been attained from samples above and below this cycle). In log 3.2 it consists of locally very variable shallow carbonate platform facies. The dominant facies are medium grainstones and packstones, made of red-algal sands, and characterised by the presence of Soritid foraminifera, as well as by Miliolids and Alveolinids. These are classified as facies 21. Locally bindstone textures develop, with red algae binding the sediment, and rhodolithic floatstones are also common. However, corals are rarely observed, and when they occur they appear as isolated small domal and knobby morphologies. Towards the top of the platform interval, centimetre-size well rounded basement pebbles appear concentrated along bedding planes. Following this platform out in a seaward direction slumping occurs. A series of listric faults converge onto a glide plane at the base of the platform interval and the dislocated platform blocks rotate and slide out seawards. a variety of deformation styles are observed. Simple plastic deformation forms miniature roll-over anticlines as the rotated blocks slide down the listric fault planes. This is illustrated in figure 8.7. The sediment below the slide plane is also deformed by a crumpling action as the keels of the rotated blocks furrow through the underlying strata. The complexity of this contact is illustrated in figure 8.5. Distally from the listric fault planes, detached platform units are shunted horizontally along the basal slip surface. These units are displaced laterally but undergo relatively little internal deformation. Locally some slid blocks undergo extensive internal plastic deformation, and this is illustrated in figure 8.7. Given the mixed plastic and rigid deformation features observed, a relatively early post-depositional timing is inferred. Extensive cavities are found throughout this platform interval. It is uncertain whether this is due to recent or Early Miocene dissolution and karstification processes.

In the transect in figure 8.1 an exposure surface is proposed at the top of cycle 2.2. This provides a mechanism for the slumping events seen, and interprets the cavity formation as Miocene karstic features.

Cycle 2.3: this cycle consists of 10-20m of marls (facies 10) of NN4 age (dates taken from above and below this interval). The top surface is defined by the base of the marine conglomerates above.

Cycle 3.1: it belongs to the NN4 nannoplankton biozone, since marls dated as NN4 are found both above and below this interval. It consists of marine conglomerates (facies 14). The top bed of these conglomerates is described in log 3.4 (figure 8.4): it is a poorly sorted conglomerate with angular to sub-rounded basement clasts 1-15cm in diameter, and with a grainstone matrix. These are interpreted as fan delta conglomerates deposited in a shallow marine environment. Shallow marine carbonates of the next cycle overlie these conglomerates.

Cycle 3.2: this cycle is described in log 3.4 (figure 8.4). It is 27m thick and is dated as belonging to the NN4 biozone by the NN4 samples found above and below this interval. The lower half of the logged

interval is composed of metre-scale bedded red-algal packstones to rhodolithic floatstones. They contain Amphisteginid and Nummulitid foraminifera (facies 9). The presence of Alveolinid foraminifera indicates some degree of sediment exportation from the more internal parts of the platform. The upper half of the logged interval consists of red-algal grainstones containing common Alveolinid and Miliolid foraminifera (facies 8), as well as some rare Soritids, indicating a platform top setting. Locally red-algal bindstone textures develop. This trend increases towards the top of the platform logged. The top surface at 27m is a sharp flooding surface, with an abrupt change from the massive bindstone textures to well-bedded grain-packstones which fine rapidly upwards to marls. This top surface is highly brecciated, and the breccia is completely autochthonous. This texture is illustrated in figure 8.8. Remark also the presence of fitted fabrics between the breccia clasts, indicating dissolution and compaction of the sediment. Extensive dissolution features, which also affect the red algae (normally the most resistant to dissolution) are observed in the thin section samples 3.33, 3.30 and 3.29 in the 15m below this surface. In the field a highly recrystallised aspect is observed. These features are interpreted as the result of a period of exposure along this top brecciated surface.

Cycle 3.3: this cycle is 34m thick, and is dated as belonging to the NN4 nannoplankton biozone by two samples (3.37b and 3.21b). The first 11m consists of marls. A 6m bedded interval of grainstones containing Miliolids and Alveolinids, is then deposited (facies 8). Laterally seaward this bed thickens downslope into a 15m packet of boundstones, containing diverse coral framestone and red-algal bindstone textures. Then 17m of massive algal bindstones are deposited (generalised to facies 1 in the stratigraphic cross-section of figure 8.1). These contain Miliolid and Soritid foraminifera, and this is interpreted as very shallow platform deposits. The top surface of this platform is highly brecciated, with extensive ferruginous infill to the breccia. Locally metric scale karstic cavities are found, infilled with thick concentric sparry cements, and intimately associated with the brecciated textures, and with the ferruginous infills. These textures are illustrated in figure 8.9. Some brecciated intervals are also found at 52m. In the microtextures extensive dissolution is observed in samples 3.38, 39, 40 and 41 (see figure 8.4). Microcodium is observed in sample 3.40. This evidence leads to the interpretation of the platform top surface as an important karst surface, with possibly multiple exposure sufaces occurring in the sediment below (though the outcrop is too poor to be certain). Following this surface in a seaward direction leads into a second slump complex, showing a variety of deformation mechanisms, as in the first slump complex. This slump interval has also been described in log 3.3 (see figure 8.4).

Cycle 4: The top surface of this platform is cycle boundary 4: it is overlain by fine grainstones that fine rapidly upwards into marls. Four samples have been dated from these marls, giving an NN5 age (Langhian). The study section ends here, though the outcrop continues further up the mountainside.

8.4 CROSS-BEDDED MEMBER (MX) ORGANISATION

The stratigraphic unit named the Cross-Bedded Member of the Mut Formation corresponds to the platform of cycle 1.2, as described in the Dibekli study area above. It can be traced in outcrop from east to west along the length of the Silifke area mapped (see the Silifke geological map). The mapping study shows that it is a roughly tabular packet of coarse grained cross-bedded carbonates over 25km in length in the east-west direction, and 4km wide in a north-south direction at the narrowest area, thickening to over 15km wide to the west of the mapped region. The platform is up to 100m thick in the middle, thinning to onlapping pinch-out to the north and to the south.

Figure 8.11 and 12 shows a photo and annotated line drawing of the Cross-Bedded Member near logsite 4 (grid reference 595325 on the Silifke geological map, figure 4.8). This is situated in the thickest part of this unit. The cliff-face photographed is estimated at 80m thick (partially measured, and its height controlled from the 1:25000 map, 10m contour intervals). It is separated into locally tabular packets by distinct surfaces labelled 0-8. Each package contains cross-bedding, and the nature of this cross-bedding changes vertically through the section. At the base, between surfaces 0-1, and 1-2, two intervals of 15m high cross-beds can be seen. From surfaces 2-6 an heterogenous mixture of metre-scale trough and planar cross-bedding can be seen. Most indicate a westward flow current direction, though a few cross-bed sets are visible that indicate an eastward flow direction. From surfaces 6-7 trough cross-bedding dominates, and the main flow direction seems to change slightly. Without being able to measure the directions on the cliff-face it is difficult to be more precise about the actual flow direction inferrable from the cross-bedding. Between surfaces 7-8 only shallow angle metre-scale bedsets are observed. Above surface 8 softer beds are picked out by the weathering, and these interbed with metre scale planar cross bedded packets. Surfaces 5, 6 and 7 are also picked out by the weathering of apparently softer sediment lying just above the surface, surface 7 being the most prominent.

The base of this cliff has been described in log 4 (see figure 8.16). This log was described 1km to the east of the cliff photographed in figure 8.11. The surfaces 0, 1 and 2 as defined in this figure have been reported onto log 4. The surface 0 is a metre interval of fine wackestone containing small red-algal debris

and bryozoa. The cross bedded intervals consist of coarse grainstones dominated by red-algal debris. Red-algae also seems to actively grow in the sediment, locally forming small areas of bindstone texture. Siliciclastic sands and gravels are common throughout the sediment, making up roughly 2-4%. Surfaces 1 and 2 are picked out by pebbly horizons containing up to 40% centimetre size rounded pebbles derived from the basement.

The facies evolution of the Cross-Bedded Member has been described more completely in log 52 (figure 8.16). This log is situated roughly 8km to the north-east of log 4 at grid reference 665350 on the Silifke geological map. Here the surfaces 0, 1, 7 and 8 as defined in figure 8.12 have been identified by visual correlation of the bedding patterns, by partially following the beds round in the field, and by correlation with log 4.

At the base of the log are found a metre of 10cm bedded medium grainstones which contain siliciclastic sand at their top surface. A sharp change in facies marks the change to 3m of marls interbedded on a 10cm scale with clay-rich rhodolithic floatstone beds, containing Nummulitid and Amphisteginid foraminifera. This marly interval is the surface 0 from the figure 8.16. The surface 1 is found in this log at 16m, and is characterised by the arrival of a small amount of siliciclastic basement sand. The 15m of sediment between surfaces 0 and 1 are metre-bedded Nummulitid packstones and grainstones (facies 9) containing some rare Miliolids in the first three metres at the base, and containing many rhodoliths and rhodolithic debris in the top 7m. Planar cross-bedding is developed from 9-13m with three packets of metre-high bedsets. Apart from this cross-bedding, the bed morphology of the packet between surfaces 0-1 is tabular.

Surface 2 overlies a thin interval of a few centimetres strewn with angular 5cm basement pebbles. The 10m interval between surfaces 1 and 2 is dominantly rhodolithic floatstones (facies 5) in a matrix of fine to medium grainstone. This develops into algal grainstones containing Nummulitid foraminifera (facies 9) and rare rhodoliths in the 5m below surface 2. These are cross-bedded with bedset heights of 3m. The toesets of the cross-bedding are made up of oyster frame-floatstones (facies12).

Surface 7 is readily traceable from logsite 4 and has been defined here. However, the intervening surfaces 3-6 have not been identified. Surface 7 is marked in the facies by a siliciclastic rich bed-top. It contains up to 10% heterolithic basement sands, and some centimetre basement pebbles. The interval between surfaces 2 and 7 is 20m thick. It consists of medium Nummulitid grainstones (facies 9) in the first 7m, with a metre-thick fine packstone bed near the base, and in the last 13m of sandy Miliolid grainstones (facies 8). Coral and oyster debris are found in the bed directly overlying the surface 2, and oyster debris is also found at the feet of a 4m bedset of trough cross-bedding from 29-33m. In the Miliolid grainstone interval from 33-46m the bedding is organised into 1m and 2m thick bedsets of planar cross bedding.

Above surface 7 two 4m intervals of cross-bedded fine Nummulitid grainstones (facies 8) are interbedded with fine Nummulitid packstones, before being overlain by micropackstone-marl interbeds (facies 10).

This is a shallow marine area, of no more than a few tens of metres of water depth, with the sea-floor sediment consisting of coarse sorted rounded biolastic sand (abundant foraminifera, bryozoa, mollusc debris, common red algae, lithoclasts, rare Porites coral debris) constantly worked by strong bi-directional tidal currents into sand-wave fields. Ebb and flow currents probably occupy different areas, and sometimes concentrate in channels (15m high clinoforms). No reefal production areas, and no bioconstructed topographies develop, probably because the energy conditions are too high for the constructing fauna available at this time. Rather encrusting epifauna (bryozoans, red algae, oysters) and infauna (foraminifera) develop in small patches on the lee-side of sand waves, on abandoned sand-wave tops, and in calmer littoral waters on the flanks.

8.5 SYNTHETIC CROSS SECTION

This sub-chapter presents the synthetic cross-section of the Silifke area shown in figure 8.10. The aim is to explain the spatial and temporal relationship between the diverse stratigraphic architectural elements observed: the basement topography; the Cross-Bedded Member, the backstepping platforms of cycles 2 and 3 in the Dibekli area, and the three slump units in the basin area around logsite 2 above the Goksu bridge. The line of section cuts south-west to north-east: this direction is chosen since it is approximately perpendicular to the structural strike (110 degrees) of the basement graben feature that controls the subsequent depositional evolution. Rather than take an awkward dogleg section across the relevent sites, it was chosen to report the salient observations along the line of structural strike onto the section: this is illustrated in the insert map in figure 8.10. In the cross-section the facies distribution has been simplified to distinguish between shallow water platform carbonates, basinal marls, slump deposits, basement and Derinçay Formation continental conglomerates. During the study interval of interest there is no major source of siliciclastic input in the area, so the small amounts of siliciclastics such as those found at Dibekli are not distinguished. In reconstructing this cross-section the vertical thicknesses are controlled by logs and by altitude data from altimeter measurements and from map contours. The relative vertical position of each outcrop has been

normalised to a datum-here the top of the Cross-Bedded Member. This removes to some degree the post-sedimentary deformation, and allows the comparison of thicknesses across the section.

Dibekli outcrop to logsite 2: the Dibekli outcrop section has been reproduced onto the cross-section directly from figure 8.1. No continuous outcrop exists between Dibekli and the next site on the section (log 2). However, the platform 1 is readily correlatable from Dibekli onto the north side of the modern Silifke (Goksu River) valley:

1) it is the lowest Miocene outcrop on both sides,

2) it has a comparable thickness on both sides,

3) the facies (9 and 20) is comparable, and distinct from all the other Miocene units,

4) the bedding organisation-extensive cross-bedding-is unique to these two cliffs on each side.

The outcrop on this northern side of the valley is illustrated by the figure 8.21. The Cross-Bedded Member has been identified, as well as the three basin slump horizons. Logsite 2 is found at the eastern extremity of the photograph going up through the three slumped intervals. Note how the platform 1 pinches out in onlap against the underlying basement to the east and in the centre of the photograph. In the western extremity the Cross-Bedded Member re-appears on the other side of the basement relief. This is also an onlap relationship against the basement, evident when seen from east. The Cross-Bedded Member slopes down to the east, dropping down by 150-200m over 2.5km from 715328 to 730300 at logsite 2 (grid references on the Silifke geological map). The platform deposits remain roughly isopachous, the internal bedding remains parallel to the top and the base of the platform, and neither onlap at the base, nor offlap at the top are observed. The slump bed 1 also shares the same slope. This slope is hence interpreted as being post-depositional tilting, and is corrected for when positioning logs 3 (Dibekli) and 2 relative to each other: the top of platform 1 is placed horizontally.

Logsite 2: the log is shown in figure 8.20: this log controls the thicknesses in order to construct the cross-section. The Cross-Bedded Member as well as slump units 1, 2, 3 are indicated. Figure 8.17 is an overview of the logsite 2 area seen from the east. The steep fault controlled basement topography is visible, as is the relationship between the Cross-Bedded Member and the underlying Derinçay Formation. The three slump units logged in log 2 are labelled, as is the Dibekli outcrop in the background. This photo shows how the Cross-Bedded Member in logsite 2 is very thin, the log being situated near to the pinchout contact against the climbing basement topography to the south. However, in placing logsite 2 on the synthetic section, it is positioned away from the basement high to the south. This discrepancy arises since the pinch-out contact of platform 1 against the basement to the south is irregular and only roughly follows the depositional strike. Figure 8.19 illustrates the relationship between the slumps and the Cross-Bedded Member looking north: note the lateral variability of the internal morphology of the slump deposits, varying from plastic deformation, to relatively well preserved horizontal strata. Figure 8.18 is a view looking east from logsite 2: it shows clearly the pinch-out of the Cross-Bedded Member against the basement relief to the south, and the position of slumps 1, 2 and 3. Note how the slumps cannot readily be followed up into the perched Miocene that is found on the basement high to the south.

Biostratigraphic dating of the slumps in the log 2 area: the slump unit 1 has been indentified in two surrounding locations as being the NN4/NN5 limit (approximately Upper Burdigalian/Langhian). This data is shown on the geological map of Silifke at locations 722322 and 765285. Dates are taken from marl samples between the top of the Cross-Bedded Member and the base of the slump 1 (NN4), and then from samples starting from directly above the slump unit 1 (NN5). Numerous samples showing an NN5 date (Langhian) are then found up to the base of slump unit 3, though all samples above this unit are barren.

Logsite 2 to logsite 50: logsite 50 is situated 5km to the east of logsite 2, though the distance down structural dip is only 2km, and this is the spacing used in figure 8.10. The Cross-Bedded Member, and slump unit 1 can be followed in outcrop between the two sites. The beds are tilted down to the east, and over the 5km distance the beds drop by another 200m. For the reasons discussed earlier this is considered to be post-depositional structural tilt, and is hence removed in the reconstruction in figure 8.10. Between these two sites the Cross-Bedded Member sits unconformably on an irregular topography of basement (Pre-Oligocene) with the hollows infilled by Derinçay conglomerates. Syn-sedimentary faulting is visible in this area and is illustrated in figure 8.15. It is a normal fault striking 110-120 degrees with a throw at the top of platform 1 of less than 20m. This faulting is coeval with the deposition of the Cross-Bedded Member and is sealed by the slump unit 1.

Log 50 is shown in figure 8.16: it is located at grid reference 785295 on the Silifke geological map. Figure 8.13 shows an outcrop photo of the logsite. The log describes the top of the Cross-Bedded Member and slump unit 1: 18m of metre-scale cross-bedding in coarse grainstones, containing 10% heterolithic basement sands. Within the metre scale cross-beds, a 10cm bedding is picked out by fine grainstones partitioning. A 1m interval of fine packstones separates a second 7m interval of coarse grainstones from the lowest 18m packet. This second packet coarsens up and contains two gravel strewn surfaces. A fine grainstone interval of 1m overlies

this, then the slump packet 1 is deposited: here it is 14m thick and contains a complex variety of deformation features: these are illustrated in figure 8.14. The top photo shows how the slump is internally heterogenous: at least two distinct packets of olistoliths and plastically deformed bedding are seperated by intervals of horizontally bedded sediment that drape and infill the slump packets. The middle photo shows a detail of the unsorted olistoliths and the sediment infilling above. The lower photo is taken in the same slump unit 1km to the west on the other side of the river, and shows a conglomeratic (debris-flow) bed contained within the slump packet. The figure 8.13 highlights the complexity of the the Cross-Bedded Member. The platform onlaps against the basement which outcrops to the left of the photo (see sketch). The facies near the onlap are oyster framestones and rudstones, and gravelly packstones. Further up, beds are seen to cross-cut down through the onlapping beds, bevelling off the edges of the underlying beds. The angular relationship indicating the erosion is seen only where the downcutting beds are sloping: elsewhere, on the platform top, and around around logsite 50 there is no angular uconformity. This downcutting bed is correlated with the second grainstone packet in log 50, at 20-27m. This relationship is shown in the synthetic cross-section in figure 8.10.

Seyhler cliff section: figure 8.22 and 8.23, show the Seyhler cliff outcrops. This outcrop is found at the northern side of the Goksu valley in the east of the study area (see the Silifke geological map). The photos show how the platform onlaps and backsteps against the rising northern side of the basement topography. This is represented in the figure 8.10. Two distinct surfaces are proposed as potential candidates to correlate with slump 1, and with the karstified top of platform 3 in the Dibekli area. No karstic features have been observed in either surface in the field. Surface 1 (with reference to figure 8.23) is considered since it represents a very distinct surface in the field, marking a change in bedding style. Surface 2 overlies a slightly downcutting bed, and is also a sharp flooding surface, being overlain by marls of NN5 age. Further up the outcrop slump deposits have been identified (see figure 8.23) and traced up into a distinct karstified surface (fairy pipes infilled with massive spar is the main feature associated with this surface). However, these slumps are underlain and overlain by marls of NN5 age, and from the field relationship and the dating, this slump is correlated with slump 2 in log 2.

8.6 SUMMARY

The following conclusions can be made from this study area:

Cycle hierarchy:

Three large-scale cycles have been described in the Dibekli area in the Burdigalian study interval. Each large-scale cycle is composed of three medium-scale cycles. Small-scale cycles have not been identified here.

Cycle organisation

Each large-scale cycle can be broken down into three phases, and each phase corresponds to a medium-scale cycle. The first phase sees the deposition of coarse-grained siliciclastic fan-delta deposits in a shallow-marine environment. This is the lowest part of the large-scale cycle preserved here. The second phase is the development of a 20m thick carbonate platform on top of the fan-delta deposits. There is some evidence for platform exposure at the top of this phase in each cycle. This development of carbonates over siliciclastics is the result of an accelerating sea-level rise. During the third phase basinal marls are deposited on top of the carbonate platform. In the third large-scale cycle these marls are topped by a prograding carbonate platform. The fan-delta conglomerates of the next large-scale cycle directly overlie the marls of the top of the cycle below at the cycle boundaries 2 and 3. Cycle boundary 4 is a very well developed karstified surface on the top of the carbonate platform, indicating a major exposure event.

Facies evolution:

The nature of the carbonate platforms deposited changes vertically. At the base of the series in cycle 1 the carbonates are deposited in a very high energy tidal environment, while in cycles 2 and 3 the carbonate platforms developed in medium to low energy settings. This change in hydrodynamic environment is linked to the deepening and widening of the strait passage: as flooding progresses the currents that develop in the strait due to the tidal resonance of the Mut Basin decrease because the channel is larger.

Carbonate platforms only develop in the highstand position of sea-level in the third large-scale cycle. This seems to be linked to the basement topography: in the first two cycles during the sea-level highstands the basement topography is steep and does not provide a shallow marine area on which a carbonate platform can develop, while in the third cycle a shallow-dipping shoulder of basement topography is finally flooded, allowing a carbonate platform to develop.

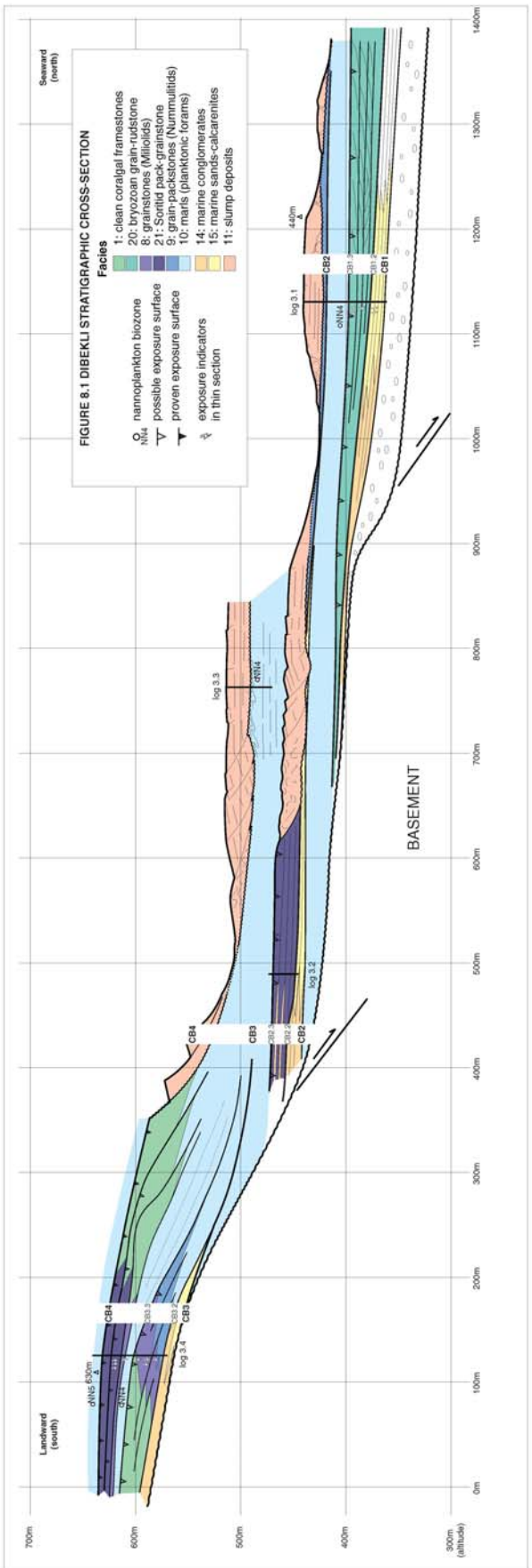
FIGURE 8.1 DIBEKLI STRATIGRAPHIC CROSS-SECTION
Facies
1: clean coralgal framestones
20: bryozoan grain-rudstone
8: grainstones (Miliolids)
21: Sorlid pack-grainstone
9: grain-packstones (Nummulitids)
10: marls (planktonic forams)
14: marine conglomerates
15: marine sands-calcarenites
11: slump deposits
nannoplankton biozone
possible exposure surface
proven exposure surface
exposure indicators in thin section
Seaward (north)
Landward (south)
BASEMENT
CB1
CB2
CB3
CB4
log 3.1
log 3.2
log 3.3
log 3.4
dNN4
dNN5
700m
600m
500m
400m
300m (altitude)
1400m
1300m
1200m
1100m
1000m
900m
800m
700m
600m
500m
400m
300m
200m
100m
0m

FIGURE 8.1 SPLIT ON PAGES 136-137 IN THE ORIGINAL

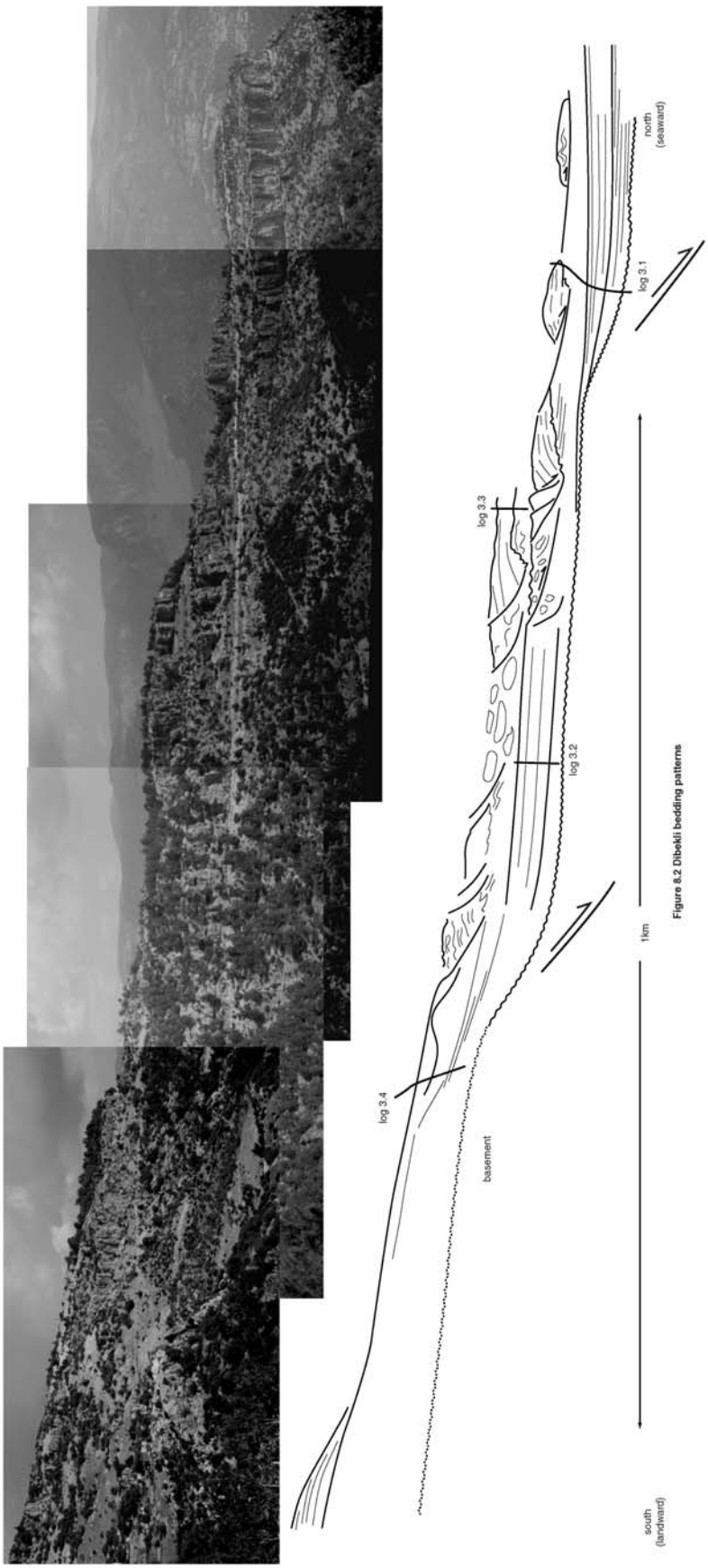

Figure 8.2 Dibekli bedding patterns

FIGURE 8.2 SPLIT ON PAGES 138-139 IN THE ORIGINAL

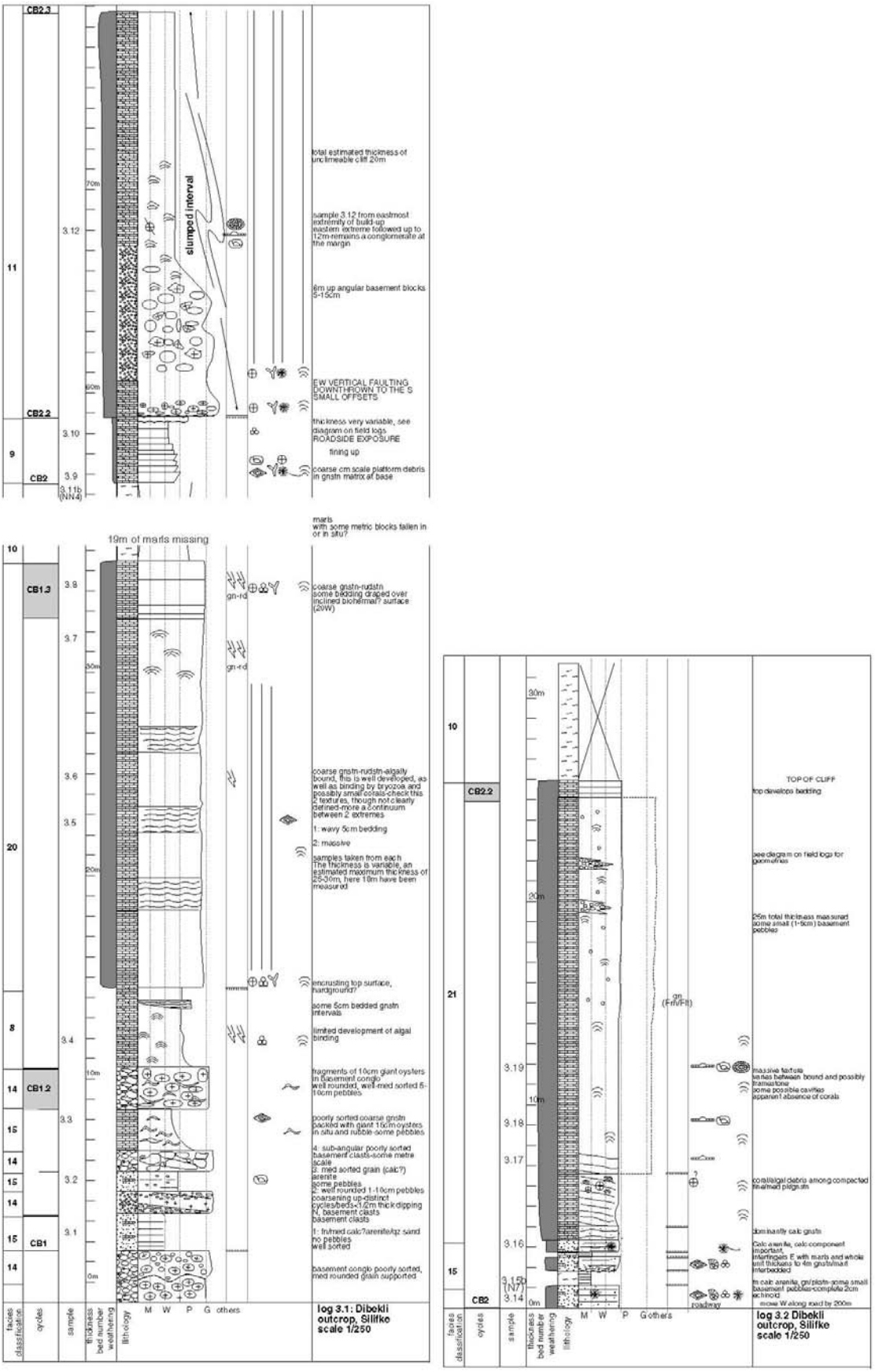

Figure 8.3 Logs 3.1 and 3.2

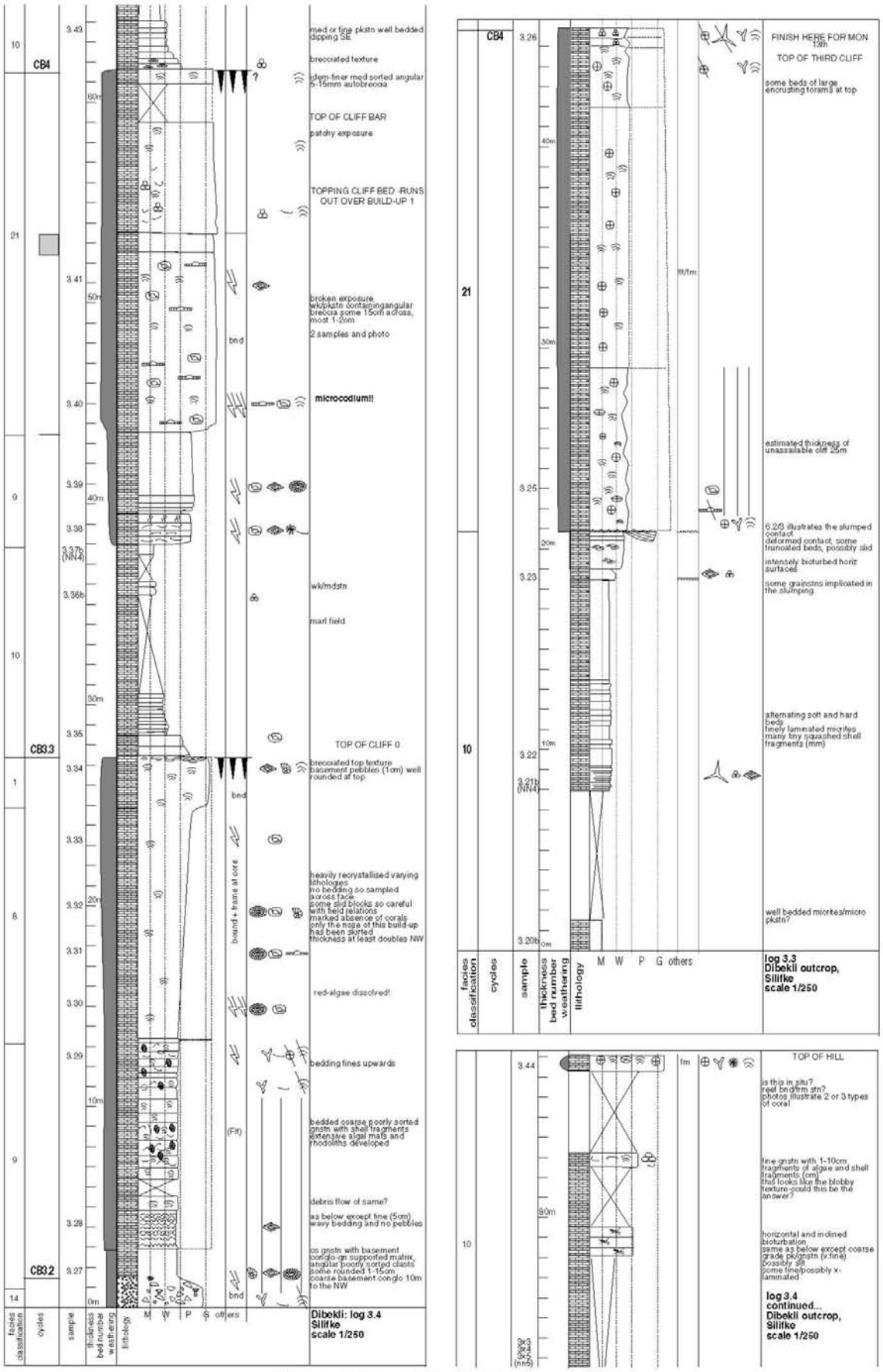

Figure 8.4 Logs 3.3 and 3.4

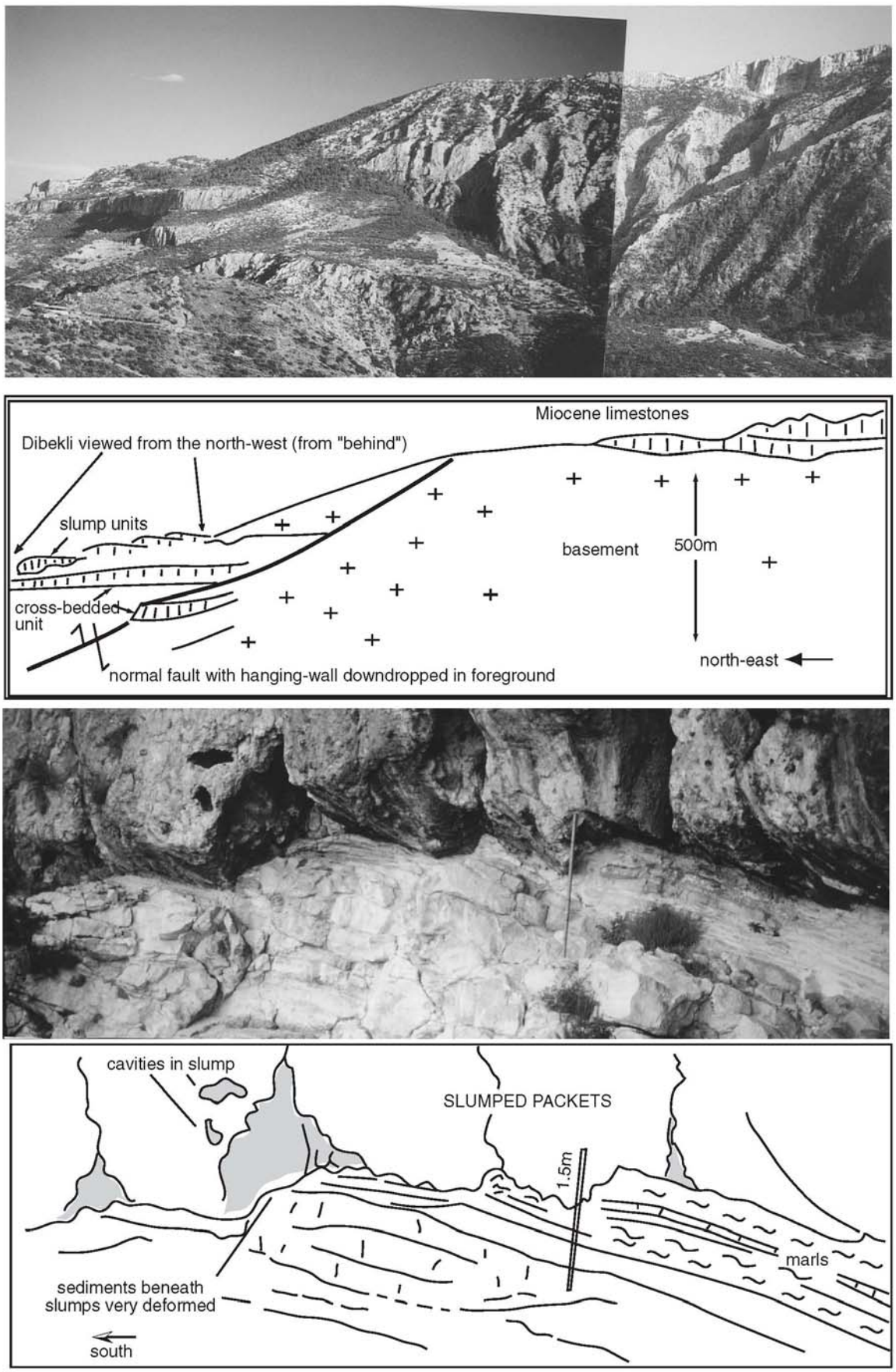

Figure 8.5 Dibekli outcrop photos 1

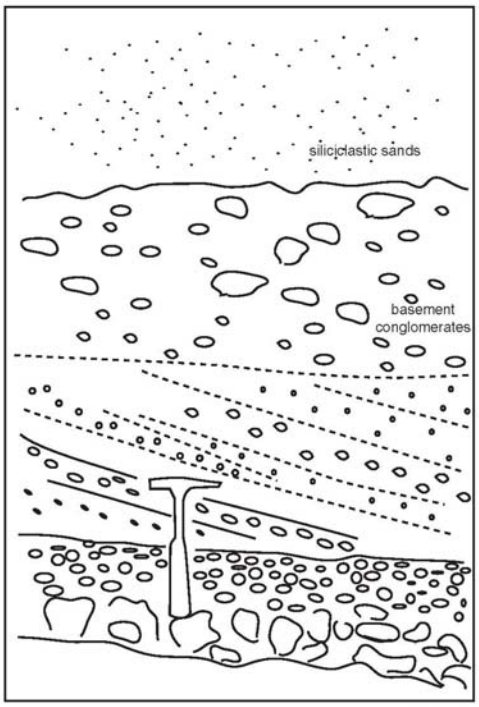

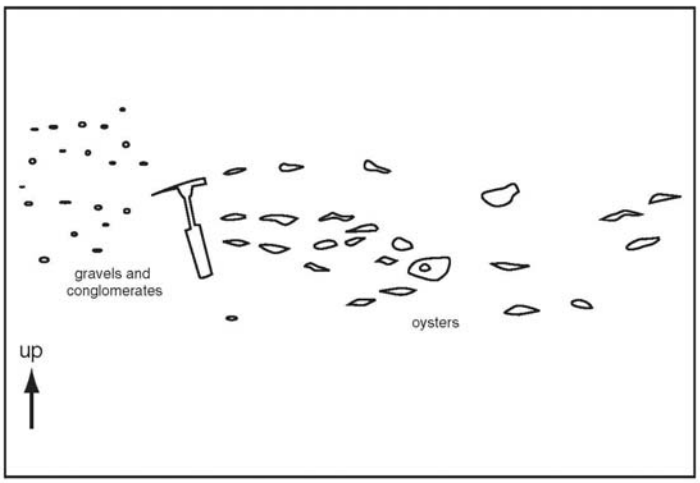

Figure 8.6 Dibekli outcrop photos 2
Illustrating the siliciclastic facies at the base of cycle 1

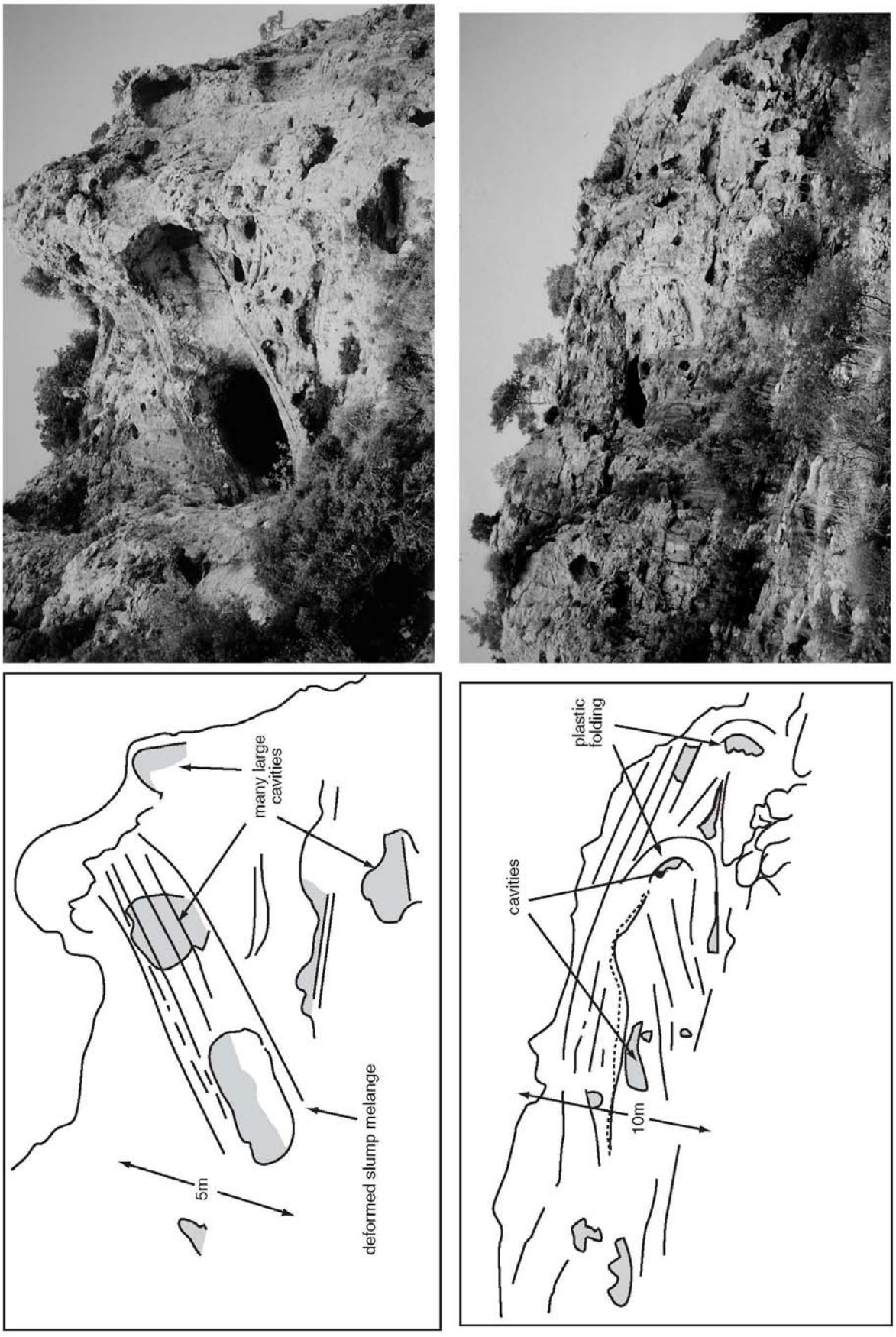

Figure 8.7 Dibekli outcrop photos 3
Illustrating the slumps and cavities in the carbonate platform of cycle 2

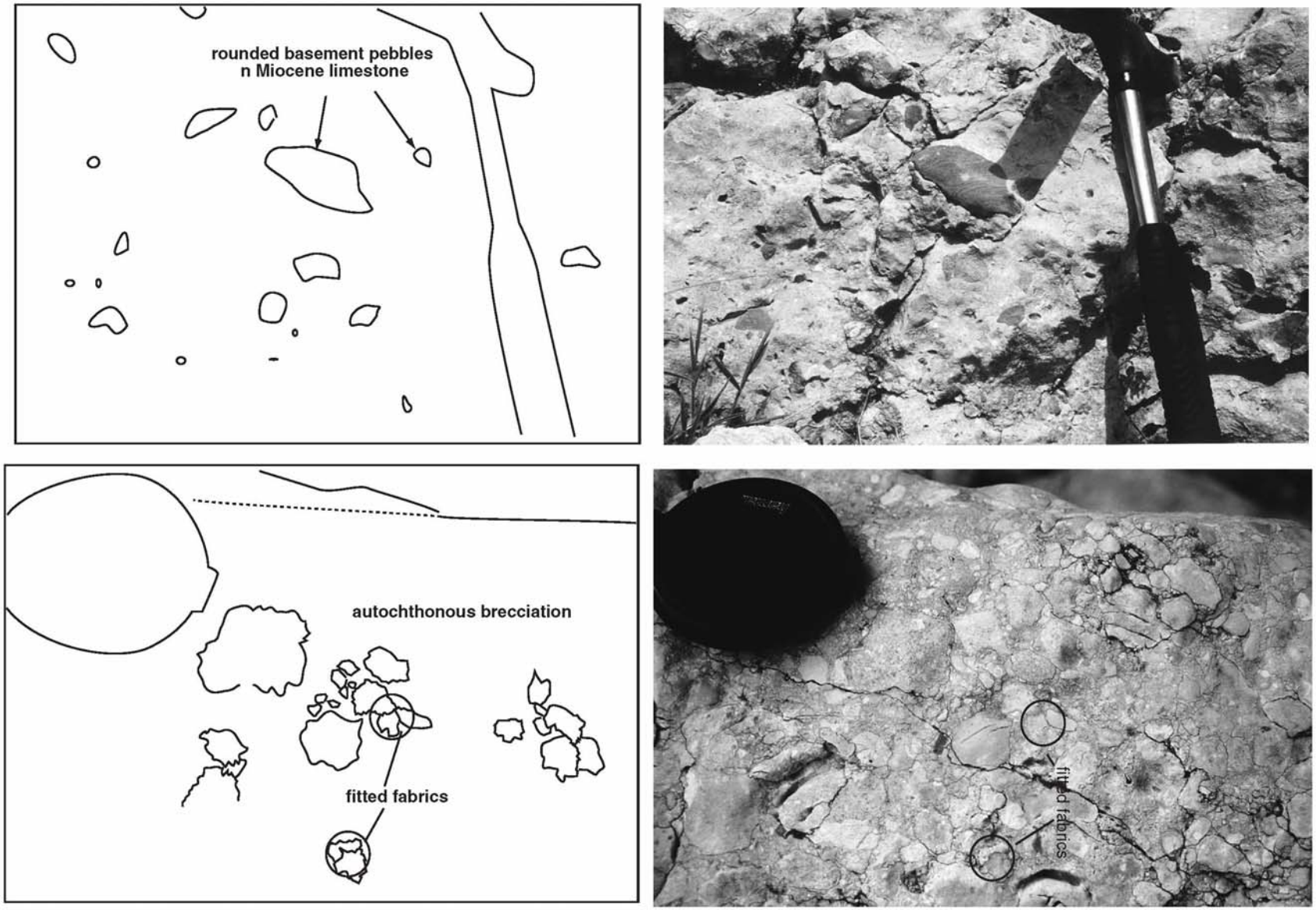

Figure 8.8 Dibekli outcrop photos 4
Illustrating the pebble basement content and the brecciated texture at the top of cycle 3.2.

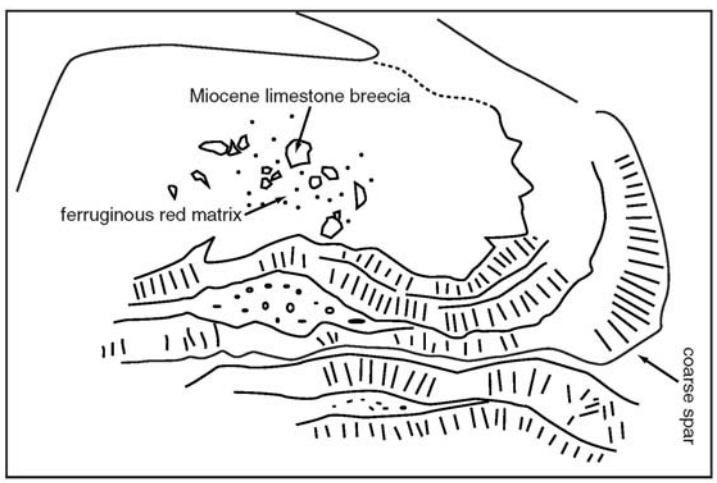

Figure 8.9 Dibekli outcrop photos 5
These photos illustrate the karstic features observed at cycle boundary 4.

Figure 8.14 textures of log 50 slump deposits
This (top and middle) illustrates the highly heterogeneous nature of the slumps in log 50, bottom photo illustrates conglomeratic debris contained within this slump body

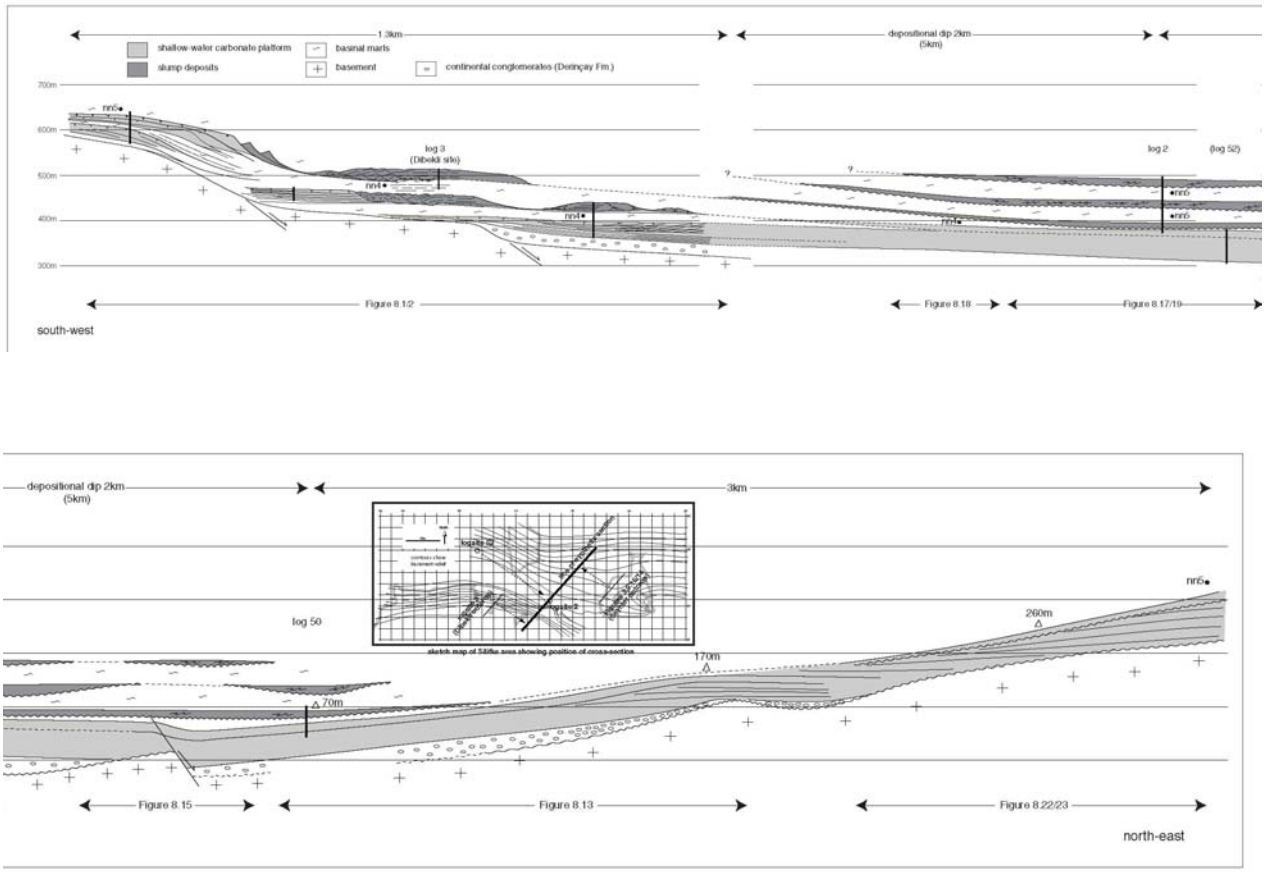

Figure 8.10 Silifke synthetic cross-section
This shows a cross-section of the Silifke graben area along structural dip reconstructed from field observations and the detailed Dibekli transect.

FIGURE 8.10 SPLIT ON PAGES 148-149 IN THE ORIGINAL

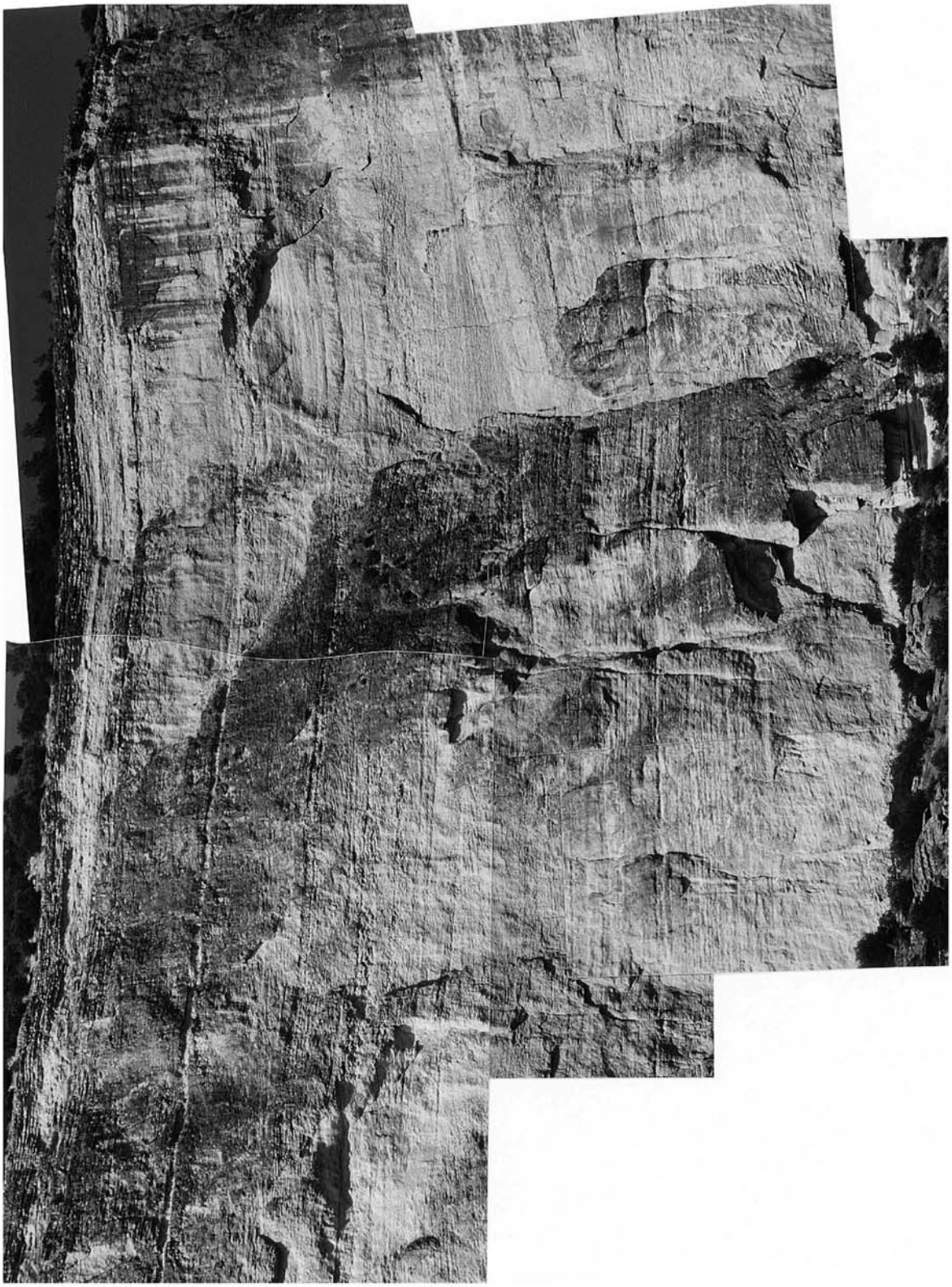

Figure 8.11 bedding organisation of the Cross-Bedded Member in Silifke

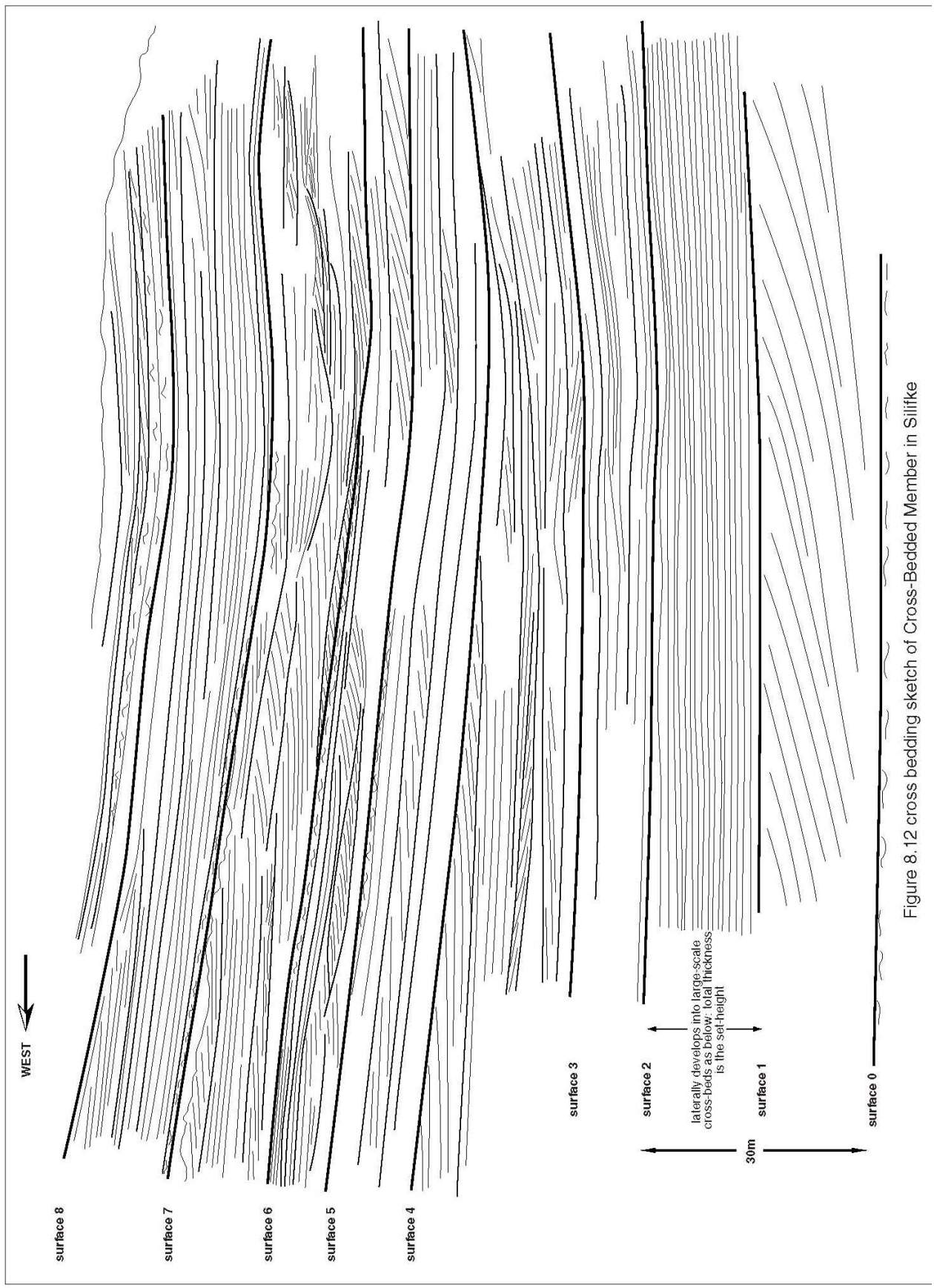

Figure 8.12 cross bedding sketch of Cross-Bedded Member in Silifke

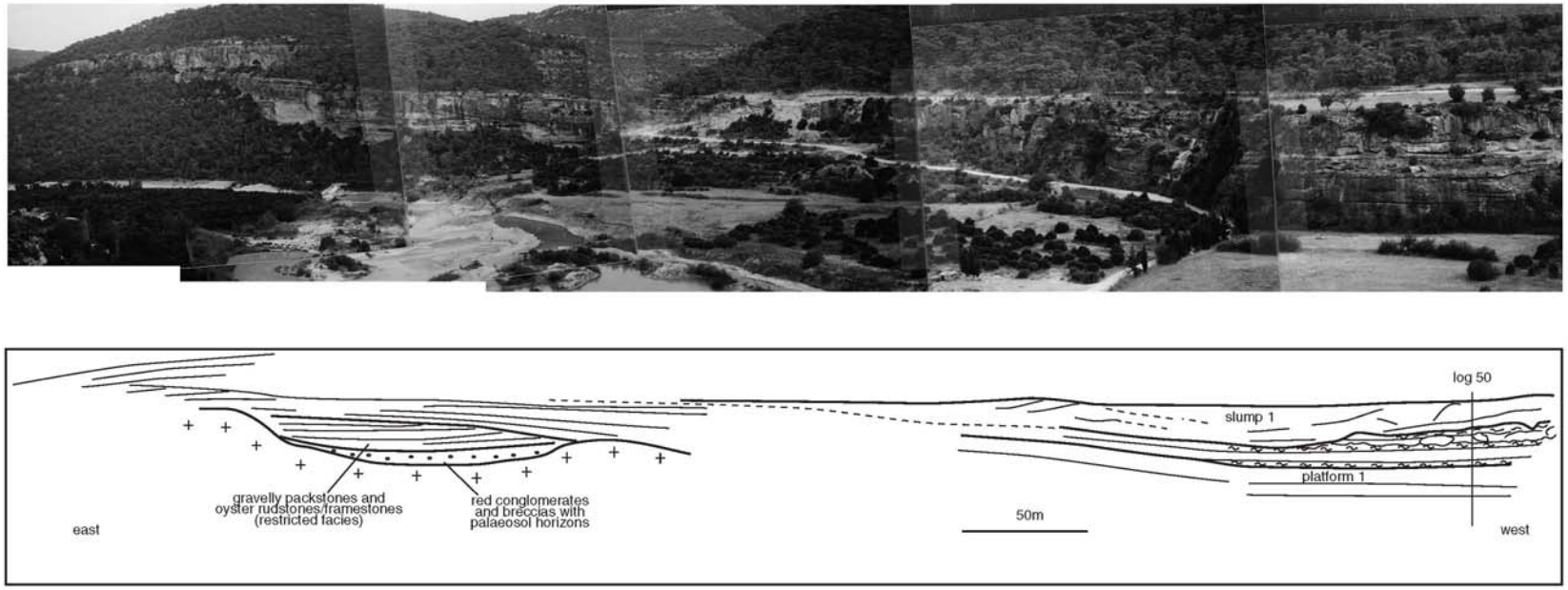

Figure 8.13 Bedding geometries near logsite 50
This area illustrated the downcutting geometries of the top of the Cross-bedded Member and the slumps at the east end of the Silifke valley.

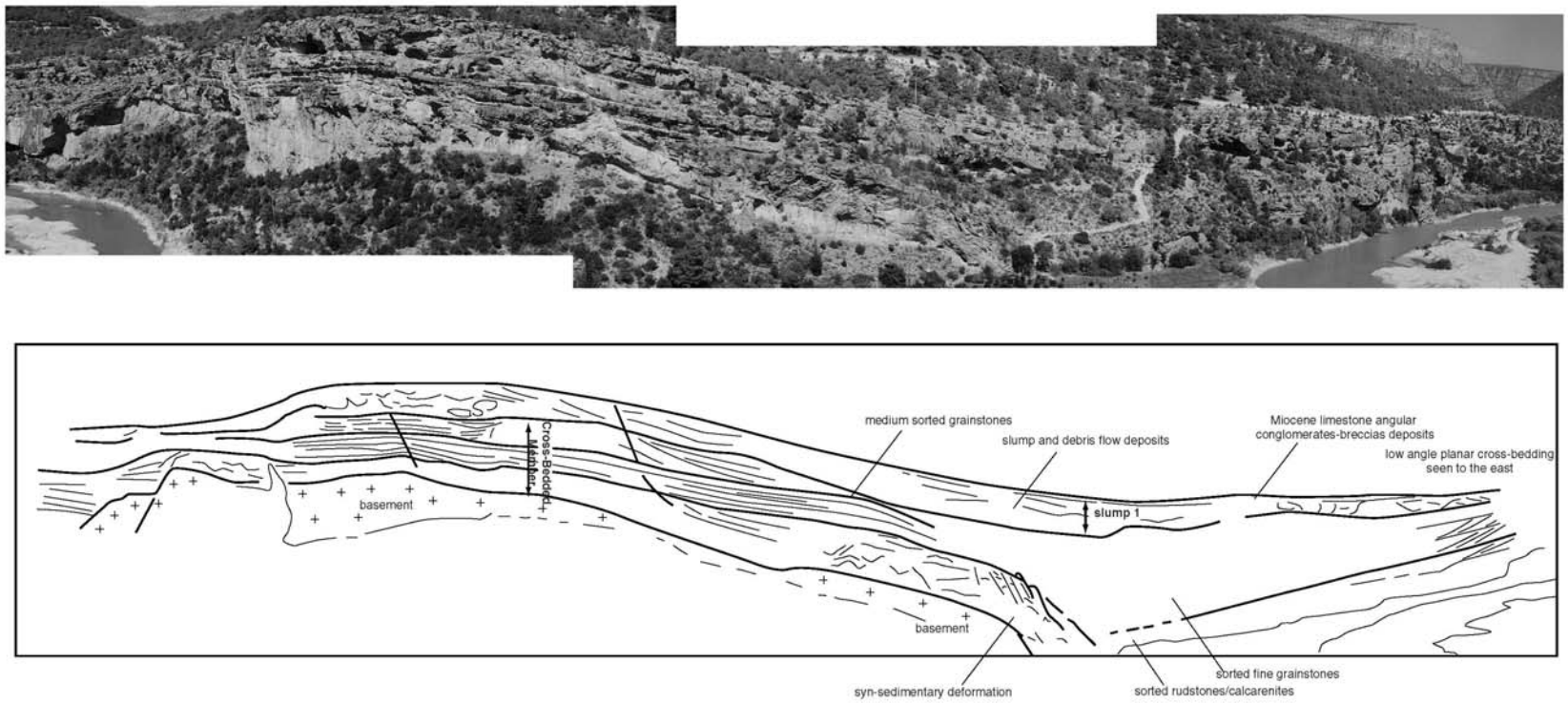

Figure 8.15 syn-sedimentary faulting in the Cross-Bedded unit
This figure illustrates minor (less than 20m throw) syn-sedimentary faulting on the north side of the Goksu valley, deforming the Cross-Bedded Member and being sealed by the first slump unit

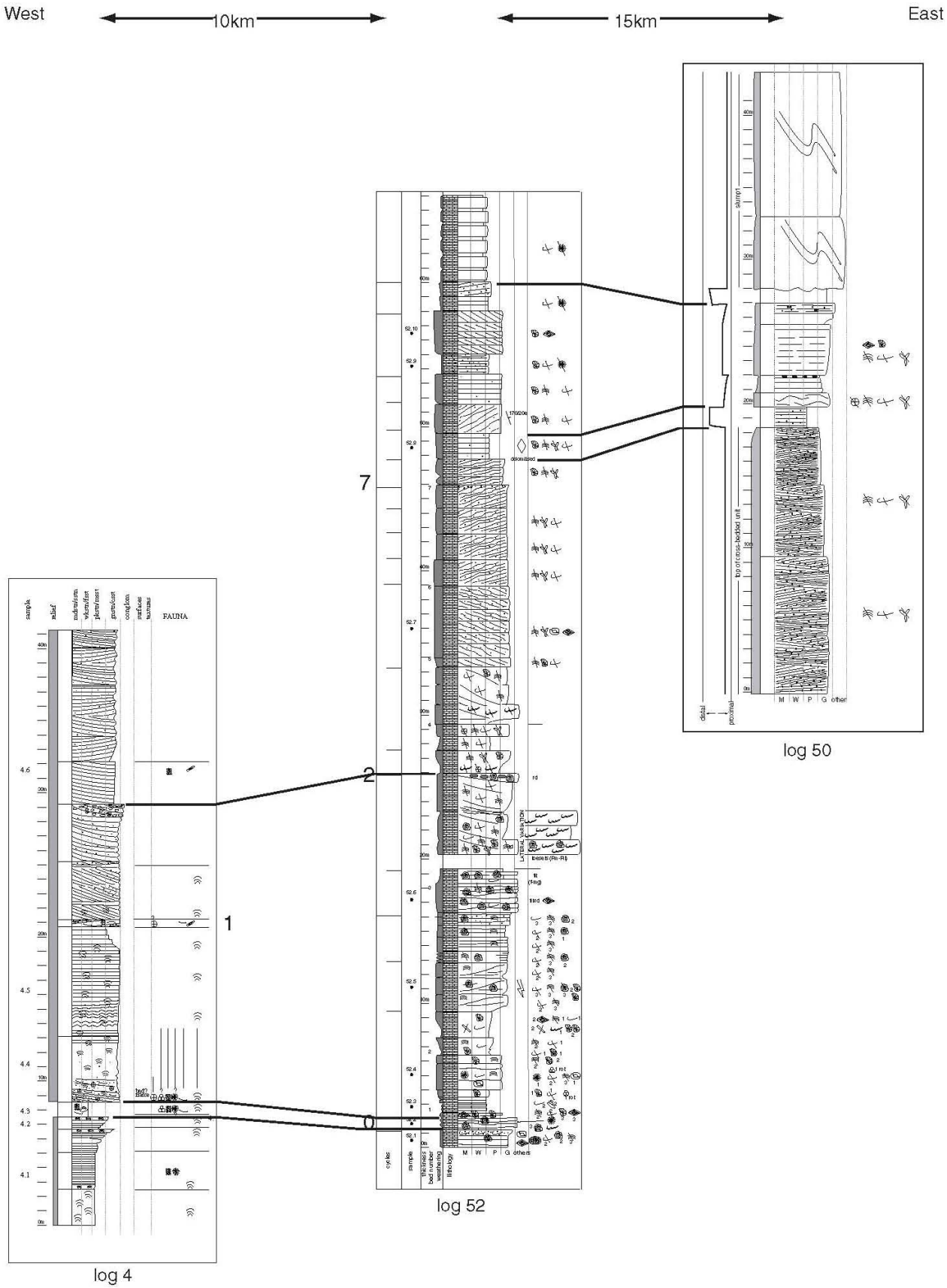

Figure 8.16 Correlation of logs 4, 52 and 50 (Silifke)
This figure illustrates the correlations within the Cross-Bedded Member along an east-west axis of the Silifke graben structure

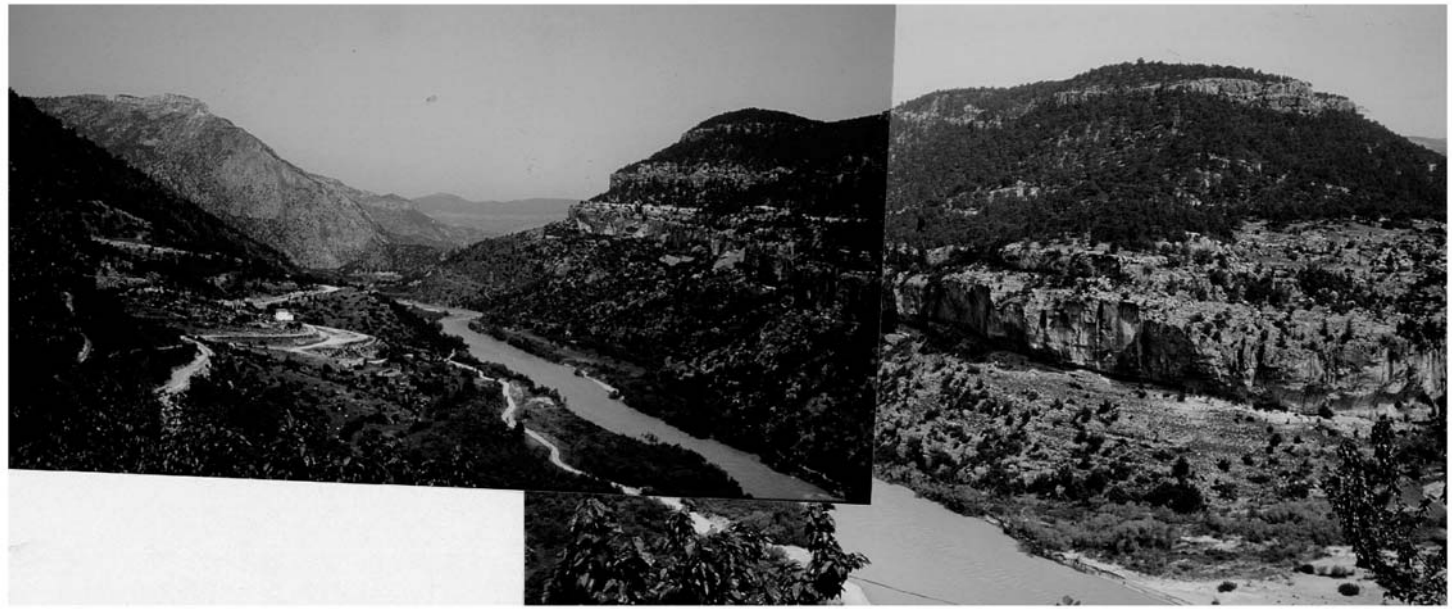

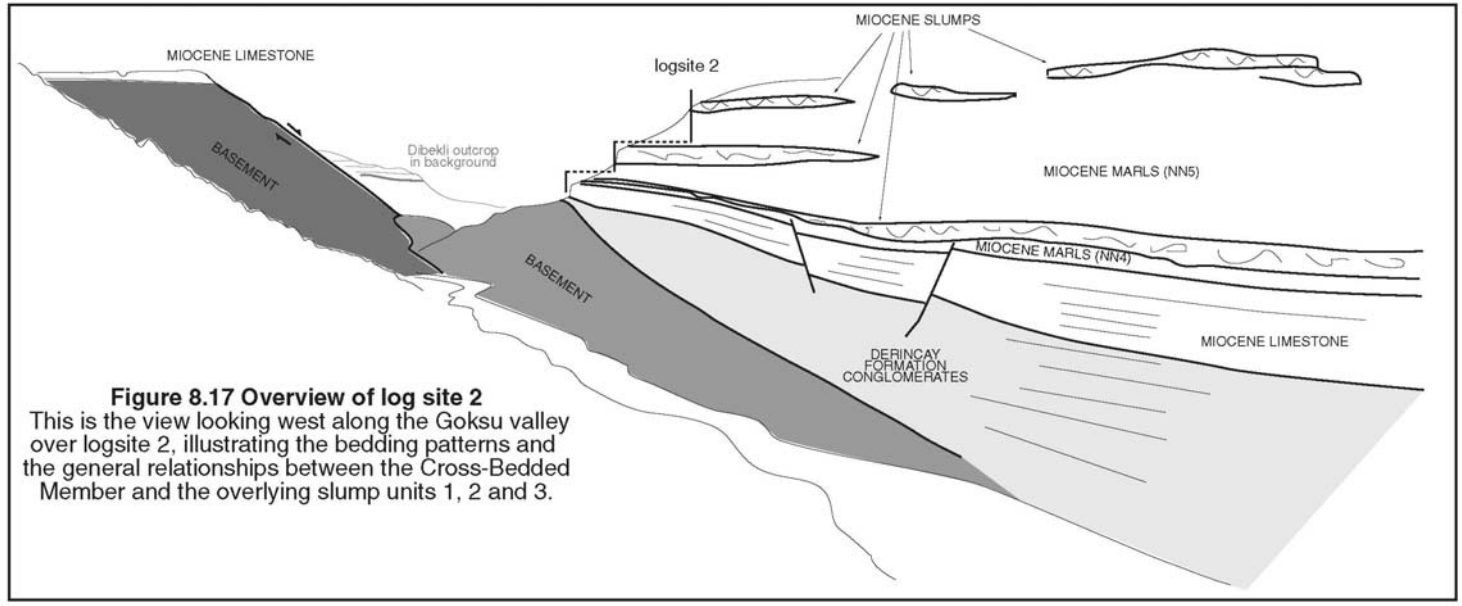

Figure 8.17 Overview of log site 2
This is the view looking west along the Goksu valley over logsite 2, illustrating the bedding patterns and the general relationships between the Cross-Bedded Member and the overlying slump units 1, 2 and 3.

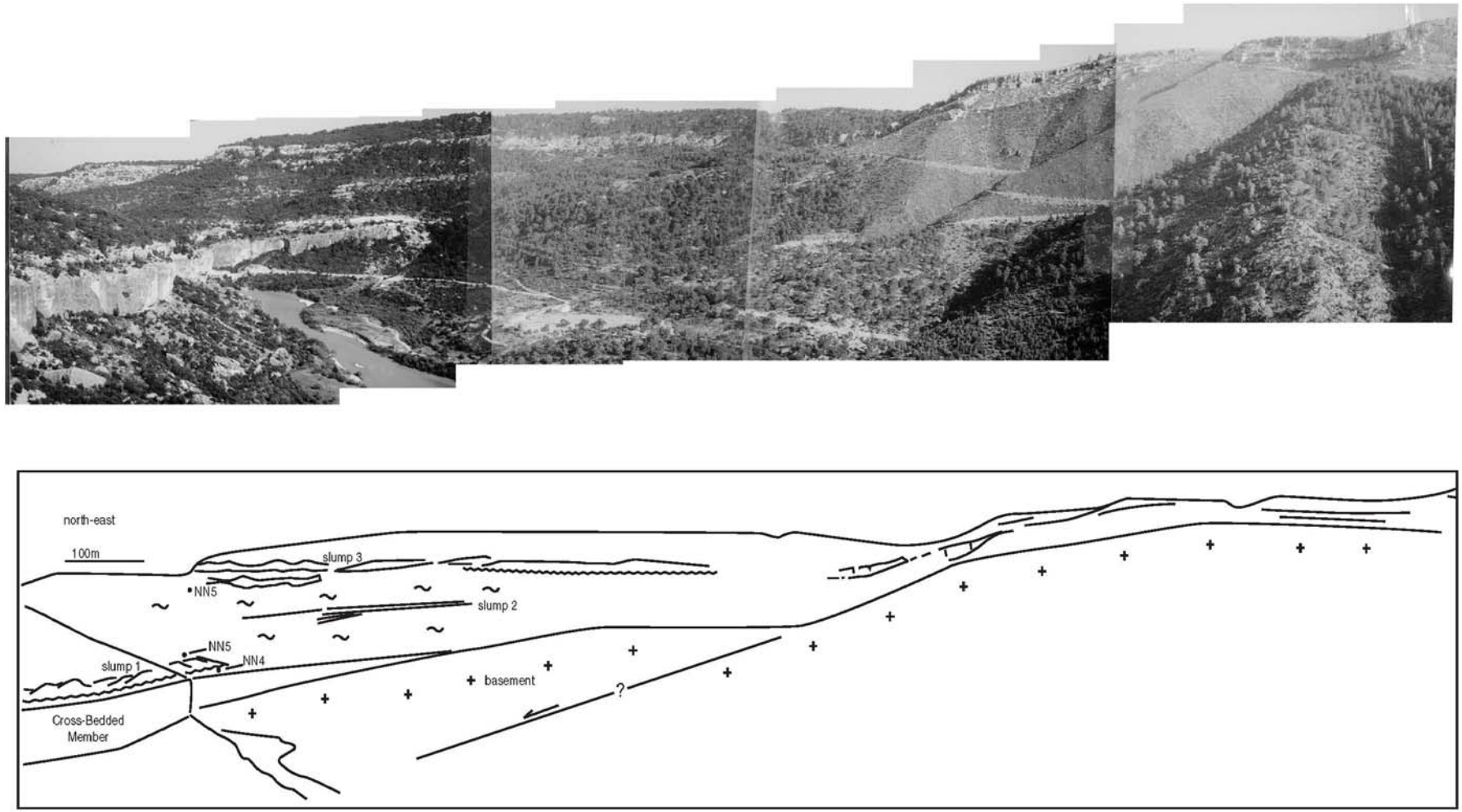

Figure 8.18 Overview of the southern margin geometries from log site 2
This view eastwards from the logsite 2 illustrates the relationship between the Miocene stratigraphy and the steep southern basement margin.

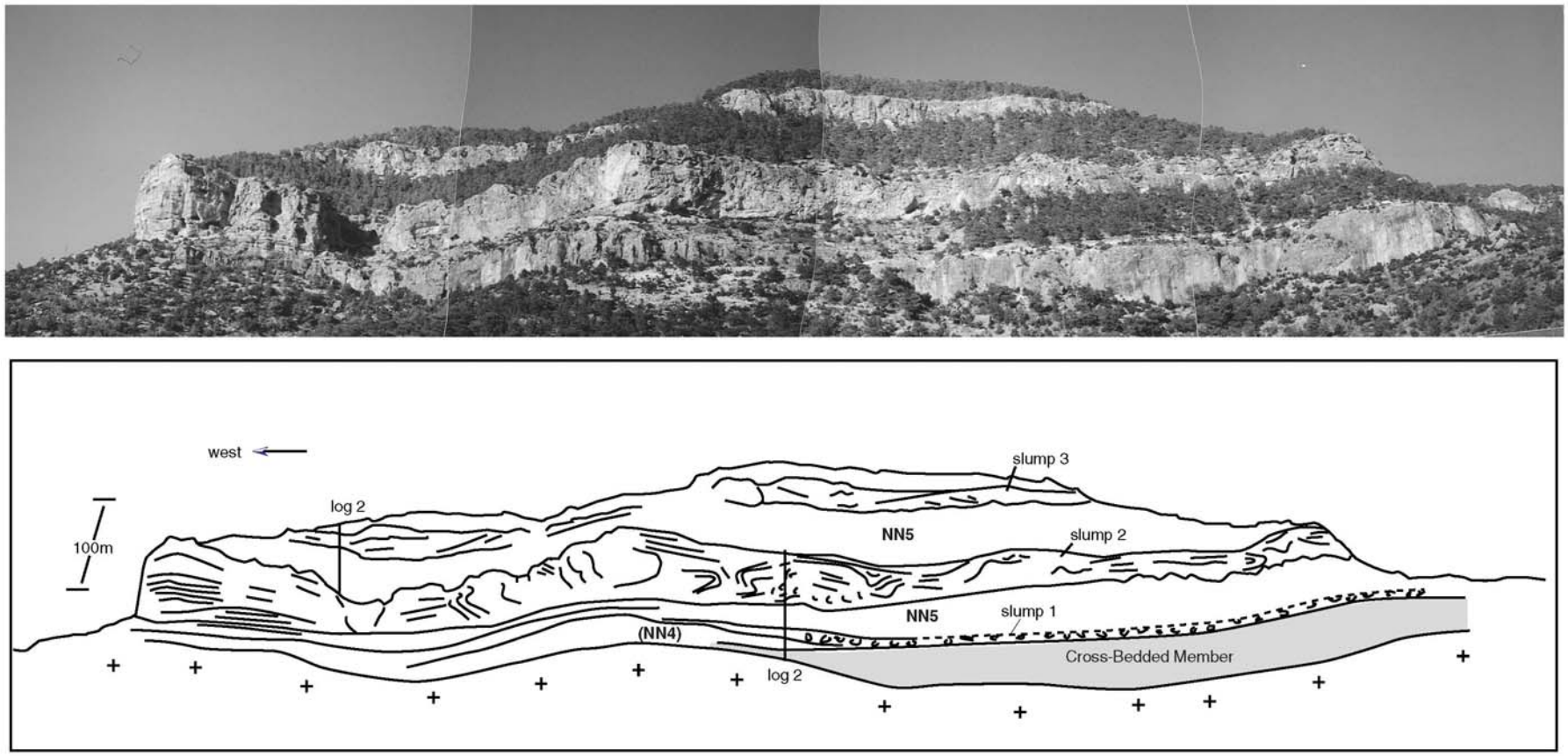

Figure 8.19 slumps 1, 2 and 3, in logsite 2
This northward (end-on) view of logsite 2 illustrates the complexity within the slumped horizons 1, 2 and 3

Figure 8.20 Log 2 (Silifke)
(Scale, 1:352)

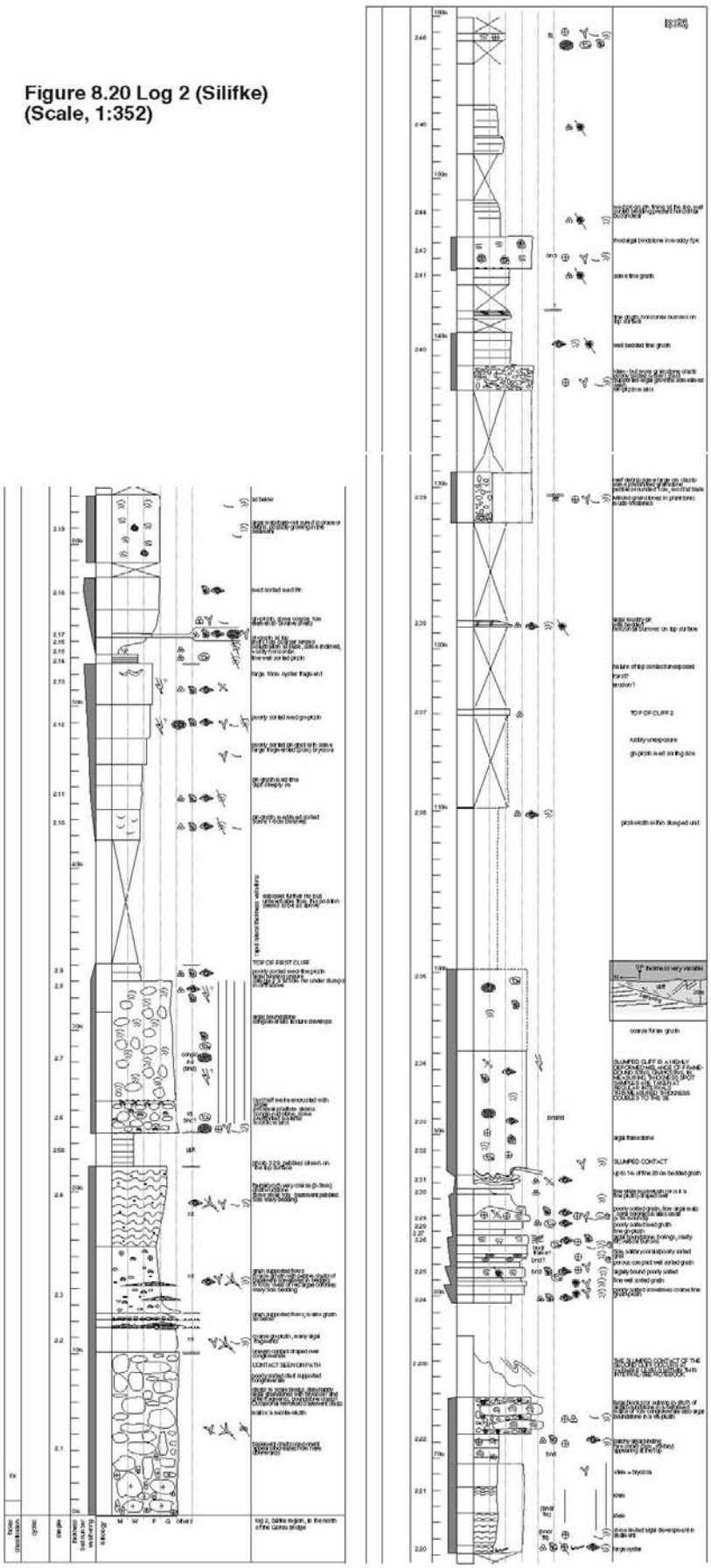

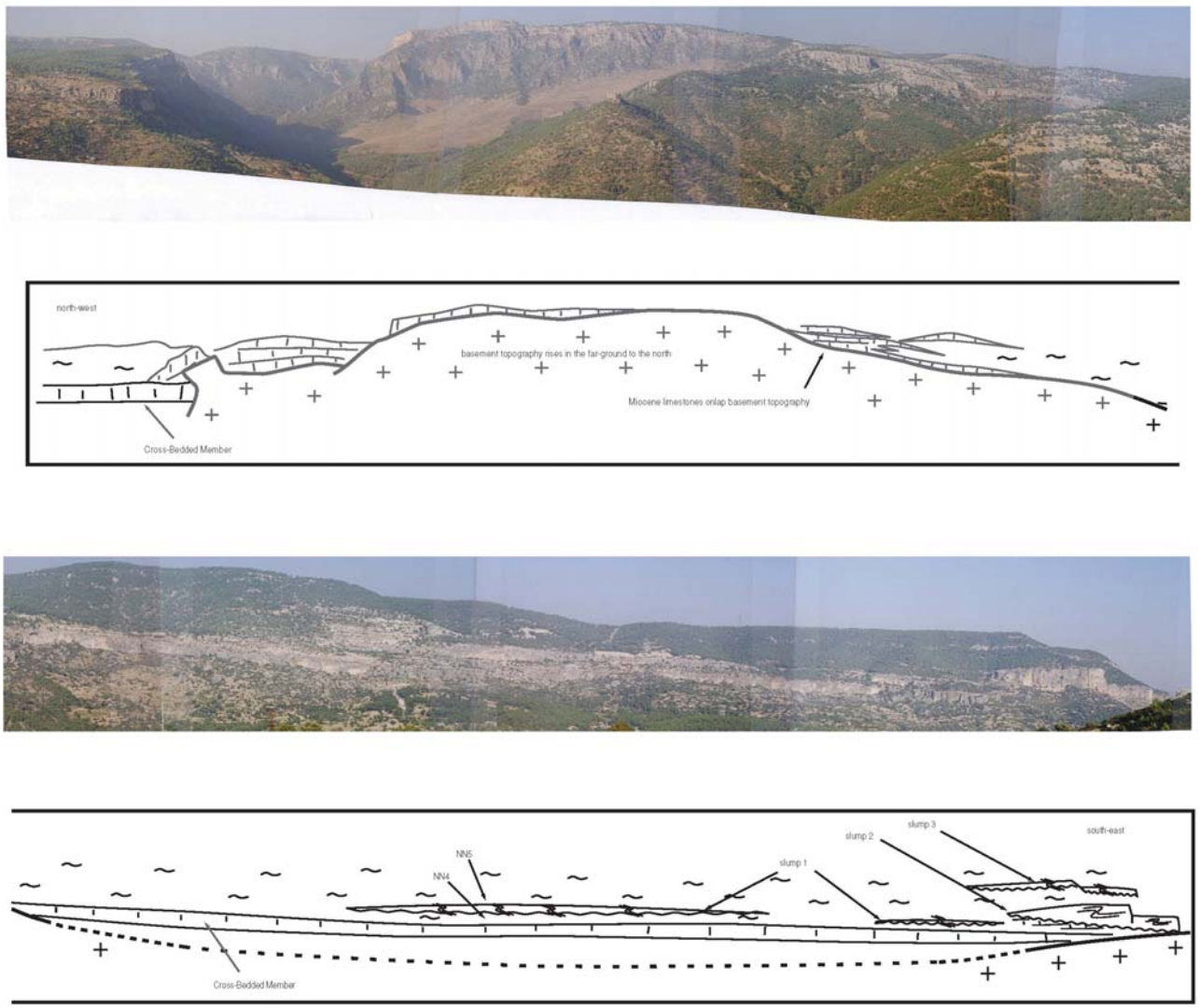

Figure 8.21 overview of the west end of the Silifke valley
This northward view over the western end of the Goksu valley region shows how the Miocene carbonates onlap against a rising basement topography, and also how all the Miocene beds are tilted eastwards.

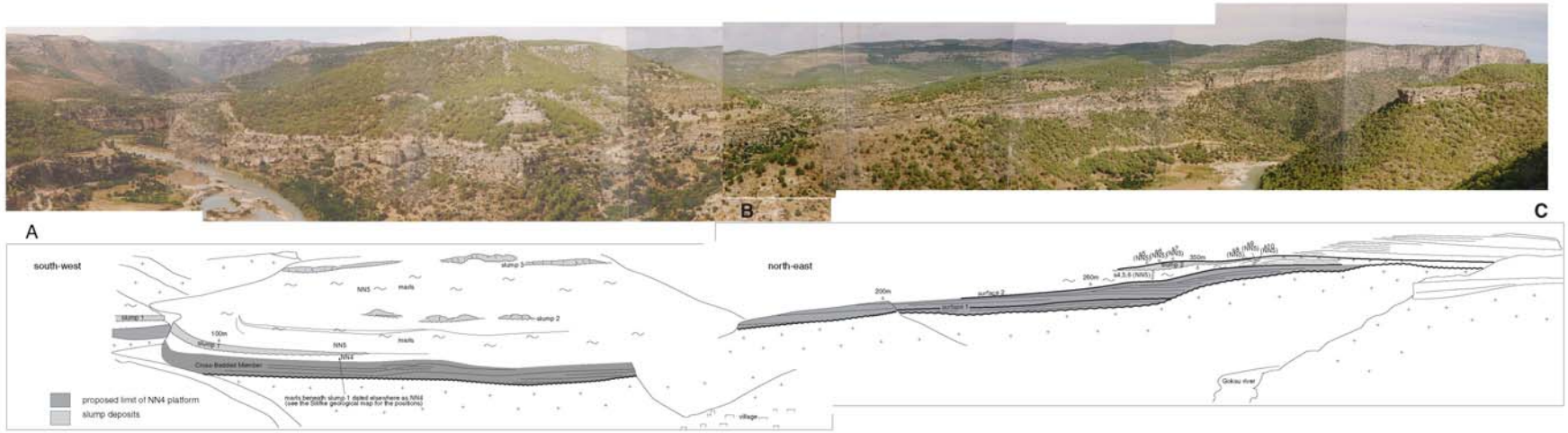

Figure 8.22 Seyhler cliff overview, southern end
This is the left-hand half of an overview of the Seyler area outcrop, where a thick succession of Early-Mid Miocene limestones (of the Mut Formation) are seen to backstep against the remenant basement topography. These limestones are dated as NN4 and NN5 (Late Burdigalian and Langhian). The right-hand half of this figure can be seen in figure 2.23.

Figure 8.23 Seyhler cliff overview, northern end
This is the right-hand half of an overview of the Seyler area outcrop, where a thick succession of Early-Mid Miocene limestones (of the Mut Formation) are seen to backstep against the remenant basement topography. These limestones are dated as NN4 and NN5 (Late Burdigalian and Langhian). The left-hand half of this figure can be seen in figure 2.22.

**FIGURES 8.22-8.23 SPLIT ON PAGES 160-161
IN THE ORIGINAL**

9 - ZINCIR KAYA (ISOLATED PLATFORM)

9.1 INTRODUCTION

This outcrop is located in the Mut area, at grid reference 315630 on the Mut geological map figure 4.6, with its summit at 480m, on the north slope of the Derinçay valley area. It is accessible by track, suitable for cars, from the north-east. It is an example of an isolated carbonate platform from the Mi unit in the Mut region (see map). The outcrop is a south-west facing cliff 100m in height and 1.2km in width. It was chosen for study since it presents a slice through an isolated platform clearly displaying the bedding pattern organisation, hence ideal for bedding pattern analysis. However, there is a playoff between visibility and accessibility of outcrop: only the edges and the base are accessible without rope. Logs were made (logs 39-44) and facies were mapped out in these places, and then sampling was performed by abseiling down the cliff face in the middle (log 55). Distances and angles were measured and placed on the bedding pattern sketch. The outcrop was photographed from a distance of 2km with a 200mm lens, thus reducing angular distortion of the image. From the measurements taken in the field the maximum distortion between the centre and the extremity of the image was evaluated at 10%. This error margin was considered acceptable for the subsequent reconstruction of bedding patterns, geometrical analysis of the outcrop, and facies distribution, and so these diagrams were reconstructed directly from the photograph.

Figures 9.1-9.3 present the outcrop photo, the bedding pattern sketch, the geometrical analysis and the facies distribution. Figures 9.5-7 show the logs, while figures 9.8-9 illustrate the microfacies evolution from log 41. Figure 9.4 is the correlation scheme, showing how the different surfaces and packets defined in the logs correlate. Figures 9.10-13 illustrate details of bedding patterns and geometrical relationships from the outcrop.

9.2 FACIES EVOLUTION

This discussion makes continual reference to log 41 on figure 9.7, and to the microfacies photographs on figures 9.8-9, corresponding to the samples taken from this log. The position of the log 41 can be seen in figure 9.1-2.

Beds 1-4 on log 41 contain diverse autochthonous and para-autochthonous debris of Porites corals, encrusting Acervulinid foraminifera, rare thin red-algal crusts, some Miliolids and Alveolinids, and diverse molluscs. The matrix is a green coloured clay-rich micritic mud. The corals grow with large (up to 40cm) platey morphologies and some small (20cm) dome forms. Macrotextures vary considerably within a bed: locally textures range from framestones and floatstones, to wackestones with occasional corals. These changes can occur laterally within a given bed over the space of a few metres. The microfacies illustrate this heterogeneous nature: sample 41.1 shows a floatstone texture of Porites coral fragments, partially encrusted by Acervulinid foraminifera, in a micritic matrix. Note the rare occurrences of red-algal debris as columnar debris, and the large amount of boring in the coral fragments. Sample 41.2 shows a bioclastic packstone containing Miliolids, Alveolinids and Soritid foraminifer debris. Thin crusts develop on the sediment, and the internal surfaces of borings are recolonised here by an Acervulinid encrusting foraminifer. Sample 41.3 shows successive thin plates of Porites corals encrusting in a micritic matrix. Boring of the corals is very common. Other organisms encrust the surface of the corals, most commonly Acervulinid foraminifera and bryozoans: red-algal crusts are thin and poorly developed. Bed 5 marks a distinct change in the facies. The macrofacies is a fine 20cm bedded bioturbated packstone containing mollusc and echinoid debris. In the microfacies Miliolids, Alveolinids and Soritids are common. Bed 6a marks another change in facies: the macrofacies show a rudstone texture of coral, molluscan and algal debris. This is the same as shown in the microfacies. Note the increased amounts of red-algal debris compared to the previous samples. Diverse encruster debris such as Acervulinids, Serpulids and bryozoa are very common, as is oyster debris. Bed 6b is composed of interbeds of platey Porites coral framestones in the form of 20-40cm "carpets" separated by 20-40cm beds of clayey wackestone. The sediment found between the corals is the same as in the wackestone intervals. The sample 41.7 illustrates the microfacies texture of this wackestone: Nummulitid, Amphisteginid and Textularinid foraminifera are common as well as planktonic foraminifera (note that this is their first appearance in this section). Bed 7 is composed of coral framestone

intervals separated by 3m of fine to medium sorted grainstone. The corals consist of platey and dome shaped Porites. Both the framestones and the grainstones are well bedded on a 15-30cm scale. Sample 41.8 is from the matrix surrounding the corals in the lower framestone bed. It shows a fine packstone containing Miliolids, Alveolinids, Nummulitids, Amphisteginids and planktonic foraminifera. Sample 41.9 is taken from the grainstone interval: it shows a fine-medium grainstone texture containing Miliolids, Alveolinids, Nummulitid debris, and Amphisteginids, but no planktonic foraminifera have been observed.

One cycle boundary zone (bed 5) and one maximum flooding zone (bed 6b) have been defined within this section. The cycle boundary (cycle boundary 2-see figure 9.4) is here distinguished by being the shallowest facies in the section. This is determined chiefly from the foraminifera (see facies chapter, figure 5.2): the presence of a Soritid, Miliolid, Alveolinid assemblage shows this interval to be in a restricted platform setting. The maximum flooding zone is determined likewise from the foraminifera: the deepest facies is picked out by the presence of planktonics, and the absence of Miliolids (to distinguish between beds 6b and 7 which both contain planktonics, but with bed 7 also containing Miliolids). The choice of surfaces as described so far has been determined solely from the facies. When the bedding patterns are examined (figure 9.1-2) the cycle boundary chosen is seen to mark the change from tabular bedding patterns to localised mounded aggradation, while the maximum flooding interval corresponds to the thin toesets of the mound. Hence the limits as defined by the facies and by the bedding patterns (geometries) are here comparable.

9.3 GEOMETRIES ANALYSIS

The bedding patterns were divided up into different architectural groups: wedged geometries, mounded geometries, shoal geometries, clinoform geometries and others. This was done purely from analysis of the bedding patterns, and no facies information was used. The results are shown in figure 9.1. Initially tabular beds prograde east. Then a 20m thick mounded geometry forms, localised in the centre of the outcrop photo. This has internally aggrading to slightly retrograding geometries, with some erosional bevelling on the eastern side of the mound (see also figure 9.13). Then prograding clinoforms fill out from the mound, and from the eastern break-in-slope of the platform topography, to fill up flush to a little over the top of the mound. Above this a thin interval of low-angle multi-directionally prograding beds is deposited: this is distinguished as shoal geometries. A second 15-20m thick mound then aggrades in the centre of the platform area, and the surrounding space is once again filled by beds that prograde out from the mound. These beds fill up flush to above the top of the mound. The eastern edge of these beds (the seaward side) shows erosional truncation. Then a wedge progrades out to the west of the platform. Toplap has been identified within this wedge, and the topsets are not preserved. A 15m thickness of aggrading beds are then deposited on the platform top. The eastern edge (seawards) is truncated by erosion, while the clinoform slope on the western (landward) end is preserved, and shows aggradation. 20m of prograding beds are then deposited on the platform top: the eastern edge is once again truncated by erosion, while the western end is preserved, and it is these slope sediments that show progradation, but with an important aggradational component. Over this on the western flank a small isolated wedge of sloping sediment is then deposited: it shows toplap, but it has no sediment cover, and it is uncertain whether this toplap is depositional or truncated, nor when it might have been truncated (ancient or modern?). The platform top is then capped with 10m of tabular beds, of which the slope sediments are not preserved due to erosional truncation on both flanks. On the eastern foot of the platform five isolated wedges are deposited. the lower three show thickening away from the platform, while the upper two show ponded geometries accumulated (at least in two dimensions) behind the third wedge, which has positive relief. It is this third wedge that can be followed physically up onto the platform (in the field, though not from the photo), and corresponds to the top surface of the prograding clinoforms above the second mound. The beds that are followed up also overlie and preserve the seaward erosional truncation of these prograding clinoforms.

9.4 DEFINITION OF CYCLES

Six medium-scale retrograding/prograding cycles have been defined in this outcrop from the geometries and the facies, four of which are completely preserved here, the uppermost and lowermost being incomplete. This discussion explains how each limit has been defined. Continual reference is made to the bedding pattern analysis in figure 9.1, to the logs, and to the correlation scheme (figure 9.4). These are defined as medium-scale cycles since they have a similar thickness to the medium-scale cycles defined in the previous chapters in the Alahan, Dibekli and Pirinç areas. No small or large-scale cycles are defined here.

Cycle boundary 2 is defined from the bedding patterns as being the limit between the prograding clinoform packet (a) (see figure 9.2) and the mounded retrograding to aggrading packet (b), since this is the turn around from progradation to retrogradation. In

the facies this limit has been identified in log 41 as the shallowest facies near the base of the log (see the discussion above). Log 43 shows a very similar facies evolution to that seen in log 41, and the same logic is used to define the cycle limit here. In log 39 this cycle boundary is more difficult to define. The choice is restricted by following out the beds from log 41. The most suitable candidate within these limits is then chosen from the facies evolution: floatstone bed between 2-3m with more constructed facies above and below. The maximum of progradation corresponds to the time of greatest sediment flux to the slope, and hence this bed is chosen.

The maximum flooding zone 2 is defined from the geometries as being somewhere in the mounded packet (b). This packet has dominantly aggrading geometries, with some slight retrogradation. It is clearly defined in the facies evolution of log 41 (see discussion above) as the deepest interval on the log. This same interval is re-found in log 43. In log 39 it is difficult to define the maximum flooding because the section is incomplete: no suitable maximum flooding candidate is available so it seems likely that this surface is lost somewhere in the covered interval (see figure 9.4).

Cycle boundary 3 is defined from the bedding geometries as the top of the prograding packet (c). This is the turn-around between prograding prograding geometries filling a restricted accommodation space (flush with the top of the mound), and renewed creation of space as indicated by the shoal of packet (d). No log crosses this limit on the platform. On the eastern flank of the platform this limit has been defined in log 40. Packet (l), as defined from the geometries, is a 3m packet of cross-bedded sorted grainstones with corals growing on the top surface. Marl sediments (facies 10) are found above and below, and the basal contact of the grainstone packet is erosional. The grainstones represent the maximum of progradation, and the cycle boundary is placed at the base of the bed.

Cycle boundary 4 is defined on the platform from the bedding patterns as the base of the second mounded package (e), the turn-around between the infilling of the shoal (d) beneath, and the renewed creation of accommodation space in the mound above. It has been identified in the facies only on the eastern (seaward) flank in log 44 where it is defined as a metre-thick bed of micro-packstone surrounded above and below by highly bioturbated clay-rich marls. The facies evolution is symmetrical in thickness, and no cycle boundary surface can be defined, so the whole bed is taken as the cycle boundary zone.

Cycle boundary 5 is defined on the platform by the geometries, and on both the western and the eastern flanks by the geometries and the facies. The topmost limit of the prograding clinoform packets (f) and (g) is chosen as the cycle boundary since it is the turn-around between progradation and aggradation/retrogradation: the overlying package (h) is aggrading.

In the facies on the western flank this cycle boundary has been identified from log 42. It is bed 2, a 2m bed of allochthonous grain-packstones overlying autochthonous and pseudo-autochthonous rhodolithic and coral boundstone beds. Metre-scale marl-grainstone cycles overlie this bed, and these are considered as being part of the next cycle. Here the maximum of progradation is indicated by the maximum of sediment transport from the platform, as indicated by this grainstone bed encased below in more constructed facies, and above by more distal facies.

On the eastern flank the cycle boundary is readily identified from the facies evolution in log 44: it is indicated by the deposition of a 10m packet of sorted medium cross-bedded grainstones (m). Metre scale cross-bedding at the base develops into decimetre-scale cross-bedding upwards through the section. The base of this packet is erosional, and the grainstones sit directly on highly bioturbated marls (facies 10). The cycle boundary is placed at the base of this packet. In log 39 this cross-bedded packet thins and sits on top of a metre-thick interval of slump deposits made up of plastically deformed bedding and 10-60cm rolled blocks (mostly coralgal boundstones). These are illustrated in figure 9.13, (middle). This grainstone bed and the one below it belonging to cycle 3 are interpreted as having similar origins: they are both deposited under the influence of relatively strong currents, capable of creating metre high cross-bedding at the base, and decimetre scale cross-bedding near the top of each packet (see figure 9.10). Each bed has a lenticular form, thinning laterally and at least 200m across. This is a bioclastic carbonate sand bar or shoal that forms at the foot of the platform relief during the low position of the sea-level cycle.

The maximum flooding of cycle 5 has been defined from the geometries as a downlap surface in packet (i) on the western flank. This maximum flooding has also been identified in the facies on the platform top in log 40, and on the western flank in log 42. On the platform it is a finely bedded coralgal boundstone interval (beds 2-8 on log 40), distinct from the surrounding beds due the presence of oysters and planktonic foraminifera. On the western flank in log 42 there are three possible candidates within one metre: they are bioturbated marls (facies 10) beds interbedded with coral rud-floatstone beds on a decimetric scale.

On the eastern flank in log 39 the maximum flooding has been recognised as the middle bed of marls in a series of marl-coral carpet (framestone) cycle.

Cycle boundary 6 is defined from the geometries as the top of the prograding and agggrading packet (i). This surface marks the maximum of progradation of the bedding preserved, and a sharp change in

depositional style. Additionally, if the sedimentary packet (j) is interpreted as showing depositional toplap, then the cycle boundary will continue over the top of this packet (j). In log 40 (and sample log 55) this cycle boundary as defined from the geometries corresponds to the first appearance of rhodolithic bindstones at the top of the platform (facies 5). However, this cycle boundary cannot be identified from the facies alone here and the geometrical information (or more facies or palaeoecological information?) is needed to define this limit. The platform top facies evolution preserves a signal expressed dominantly in the bedding patterns. This signal is at a higher frequency than the cycles identified from the geometries.

In the facies on the eastern flank of the platform the cycle boundary is not expressed as a discrete surface, but as a 3m thickness of Nummulitid packstones (facies 9) rich in rhodolithic debris. This sediment correponds to packet (n) in the geometrical analysis, and onlaps to the east against the raised topography of the cross-bedded grainstones of packet (m), and to the west against the steep slope of the platform.

Cycle boundary 7 is proposed at the top of the platform, since a slight shallowing trend is observed in the facies in log 40 below the drowning unconformity that marks the top of the platform (only basinal marls are found directly above).

9.5 PLATFORM EVOLUTION

Cycle 1: the base of this cycle has not been identified. The top 7m of the cycle have been described in log 41 from 0-7m, and the facies have been partially mapped out in the windows at the base of the outcrop as indicated in figure 9.1. The bedding is tabular, with rare development of weak relief. The facies are dominantly bioconstructed coral framestones in a green clay-rich micrite matrix. Lateral facies variations occur over a few metres. Framestone intervals grade laterally into coralgal floatstones, and into grainstones and packstones dominated by Miliolids or by Nummulitid foraminifera. This organisation is shown in the eastern window where facies have been mapped: here 5-10m wide and 5m thick framestone patches pass laterally into Miliolid grainstones (facies 8). There is no development of topography around the framestone areas. Three such constructed patches have been mapped out. Corals are highly bored and encrusted by diverse organisms. The amount of red algae is variable: the most clay rich framestone intervals are the poorest in red algae, while thin 50-80cm thick beds of rhodolite (facies 5 and 6) occur a number of times. The rhodoliths are normally small, no larger than 2cm, and often have small pieces of branching coral at the core. The top of the cycle is dominated by coralgal floatstones which prograde eastwards. Mililolid grainstones occur on the upper slope of these clinoforms.

Cycle 2: the retrograding part of cycle 2 is the mounded relief that forms in the centre of the platform area. It consists of muddy coralgal boundstone facies (facies 2), dominated by platey Porites coral framestones. This has been controlled with 6 samples from log 55. The areas at the foot of the mound are characterised by the deposition of carpets of coral framestones interbedded with marls containing Nummulitids and planktonic foraminifera, as seen in bed 6b in log 41. Figure 9.15 illustrates the internally horizontal bedding of the mound, and the erosional truncation of the seaward facing margin.

The topsets of the prograding part of the cycle are postulated also to be dominantly muddy coralgal boundstone textures (facies 2). However, these are relatively inaccessible, and observations have only been made from the sampling in log 55 (samples 5 and 6) and on the eastern slope in log 39. On this slope the coral framestones form 50cm beds interbedded with marls (facies 10), and these are named coral carpets, as distinct from more massive framestone textures such as those seen in the mound of the retrogradation. These coral carpets are illustrated in figure 9.13 (lower photo). From the facies mapping performed in the field the toesets of the seaward side of the mound in the prograding part of the cycle are made of marl, while the slope consists of Nummulitid packstones. On the landward side of the mound the toesets of the infilling clinoforms have been mapped as muddy coralgal floatstones (facies 4).

Cycle 3: the early retrogradation of this cycle is the cross bedded grainstone packet at the seaward foot of the platform in log 44 (facies 9). The platform facies of this cycle are controlled by samples 3 and 4 from log 55. These show muddy coralgal boundstone textures.

Cycle 4: the facies in the mounded topogaphy of the retrograding part of this cycle are controlled by two samples from the log 55, samples 1 and 2. Sample 2 is a rhodolithic bindstone, while sample 1 shows a muddy coralgal boundstone texture. The facies at the core of the mound are proposed as being the same muddy coralgal boundstones, by analogy with the facies information from the mound in cycle 2. The early retrogradation of cycle 4 is also identified on the seaward flank in log 44 as a metre thick packet of coarser marls-micropackstones surrounded by clay-rich bioturbated marls (see figure 9.2).

The facies of the prograding part of this cycle is controlled by three samples from log 55 (25,26 and 27), and also by the log 42 which describes the landward toesets of the prograding clinoforms. From the samples in log 55, the topsets of the clinoforms have been described as muddy coralgal boundstones

(facies 2), while the toesets are muddy coralgal floatstones. In log 42 at the western end the toesets consist of intervals of rubbly rhodolithic beds forming float- and rudstone textures, and coral framestone intervals with domes and plate morphologies. The rhodoliths in this interval can be up to 20cm in width and are rounded to slightly oblate. These beds are rich in clay, and are well bedded on a 20cm scale. These complex facies have here been simplified to muddy coralgal floatstones (facies 4). The seaward side of the prograding packet has been truncated by erosion, and this relationship is illustrated in figure 9.12.

Cycle 5: the early retrogradation of this cycle is the 10m thick packet of cross-bedded Nummulitid grainstones (facies 9) on the seaward foot of the platform as described in logs 44 and 39, lying unconformably (erosional hiatus) on the marls beneath. These are then covered by marl/coral carpet cycles (see log 39) as the retrogradation progresses and grainstone deposition stops. The retrogradation is preserved on the platform top and has been described in log 40. The platform top sediments of the retrogradation and the progradation of this cycle show similar facies: they are microbial boundstones (facies 7) containing small knobbly Porites corals no bigger than 10-15cm wide, and red-algal crusts and debris. Variations occur in the bedding patterns: the beds change from fine 10-30cm bedding to massive 2-3m beds on a 5-10m scale. On the landward slope of the platform in log 42 the slope deposits of this cycle have been described. The retrograding deposits are very thin constructed and debris beds and the maximmum flooding surface is picked out by two thin marl intervals. The prograding part is composed of 7 small scale cycles 1-2m thick each: these are of a hybrid composition, with a coarsening up fine packstone to medium grainstone trend capped by encrusting platey Porites and red algae. These encrusters are then covered by the fine packstones of the base of the next cycle.

Cycle 6: this cycle has been defined principally from the geometries. Sample 17 from log 55 however shows a thin rhodolithic bindstone (facies 5) bed sitting over the cycle boundary in the centre of the platform. This is a precursor to the thicker packet of rhodolithic bindstone (facies 5) that is deposited from 31-38m. The platform is then capped by a final metre thick bed of microbial boundstone (facies 7).

9.6 SUMMARY

Cycle hierarchy: six medium-scale cycles have been identified here. No other scale of cycle has been defined in this outcrop. There is some evidence for sub-aerial exposure along the cycle boundaries. The evidence comes from the bedding patterns (deposition of cross-bedded grainstone packets during the sea-level lowstand times, with no deposition occuring on the platform top), and from dissolution fabrics in the microtextures (see figure 5.10).

Cycle organisation: two distinct cycle architectures are of note in this outcrop. The first is seen in cycles 2 and 4, where cross-bedded grainstone shoals develop when sea-level is in a low position, localised mounded topographies develop during the retrogradation, and filling-out occurs around these mounds during the progradation. The second distinct architecture is seen in cycle 5, and is formed by tabular aggrading bedding.

Facies evolution: three phases of platform evolution are readily identifiable. These phases are characterised both by their geometries and by their facies. They are:

a) cycles 1-4: dominantly muddy coralgal framestones (facies 2). These form mounded topographies during the transgressions, with filling-out occuring during the progradation as the depocentre dilates. This is the start-up phase, where the isolated depocentre is first defined, and deposition occurs under the influence of a constant supply of fine-grained siliciclastics. Large plate and dome corals grow in abundance, though the morphotypes are limited.

b) cycle 5: microbial coralgal boundstones (facies 7), containing no siliciclastics typify this phase. They are deposited in aggrading horizontal tabular beds. This is a phase of environmental stress for the coral fauna, as indicated by the facies type. A number of potential causes exist for this stress, such as increasing nutrients, decrease or increase in water temperature, change in salinity or increasing turbidity: this will be discussed later. However, no deepening of the environment can be deduced from the facies, and the carbonate production seems to be able to keep up with sea-level rise.

c) cycle 6: these are dominantly clean rhodolithic floatstones and bindstones. They are deposited with horizontal tabular retrograding geometries. This is the incipient drowning phase, as indicated by the facies type, the retrograding bedding pattern, and the position of these beds as the final deposits on the top of the platform.

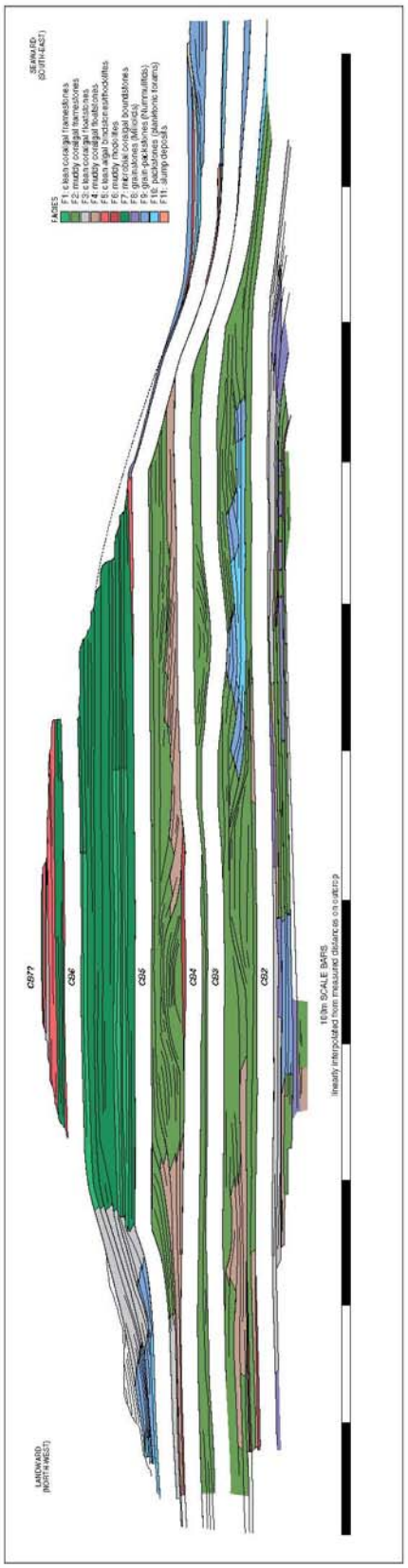

Figure 9.3 Zincir Kaya exploded cross-section showing cycle boundaries

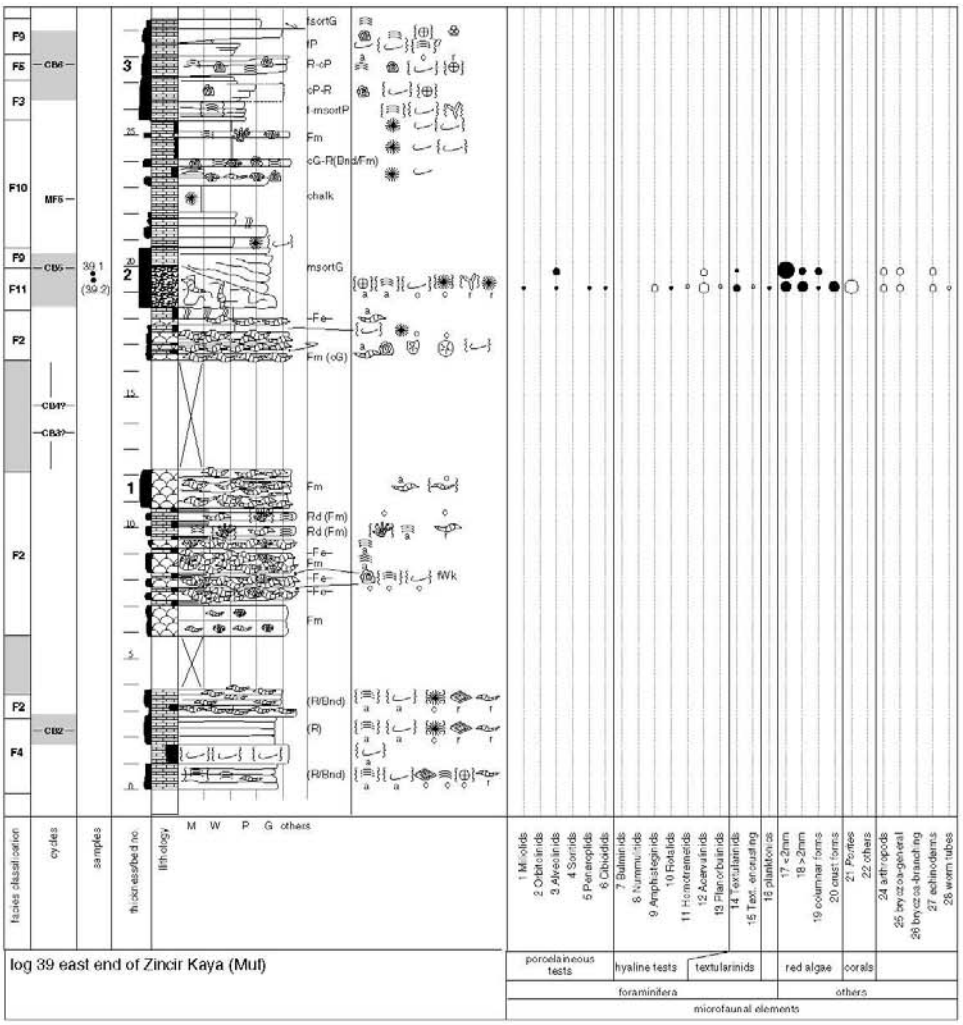

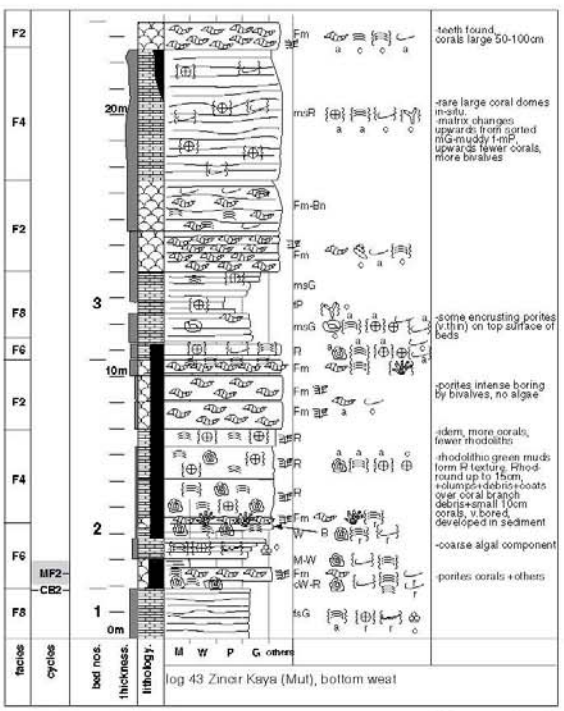

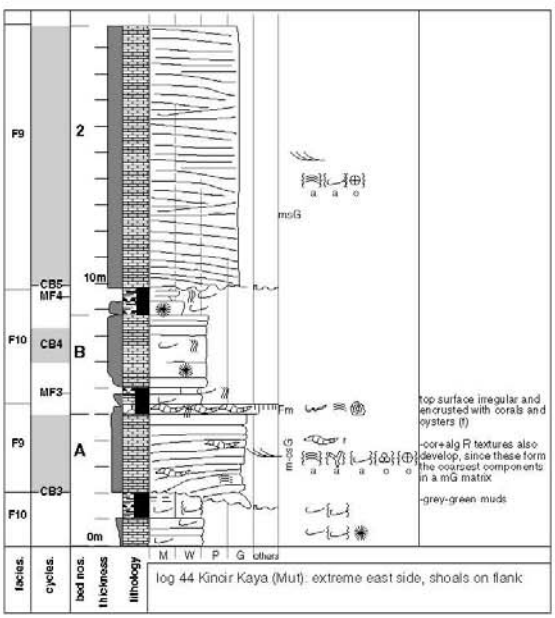

Figure 9.5 log 39/43/44

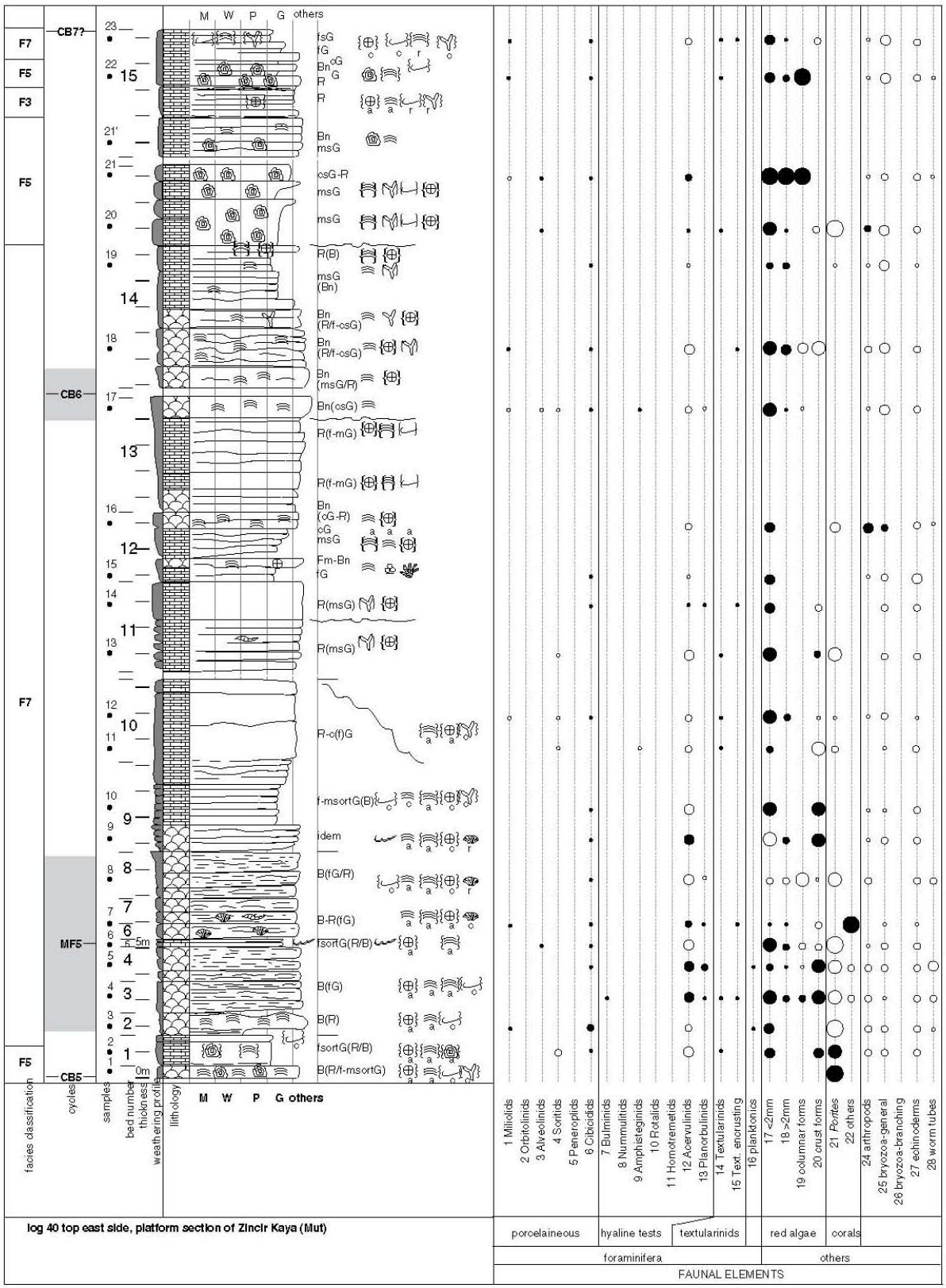

log 40 top east side, platform section of Zincir Kaya (Mut)

Figure 9.6 log 40 (Zincir Kaya)

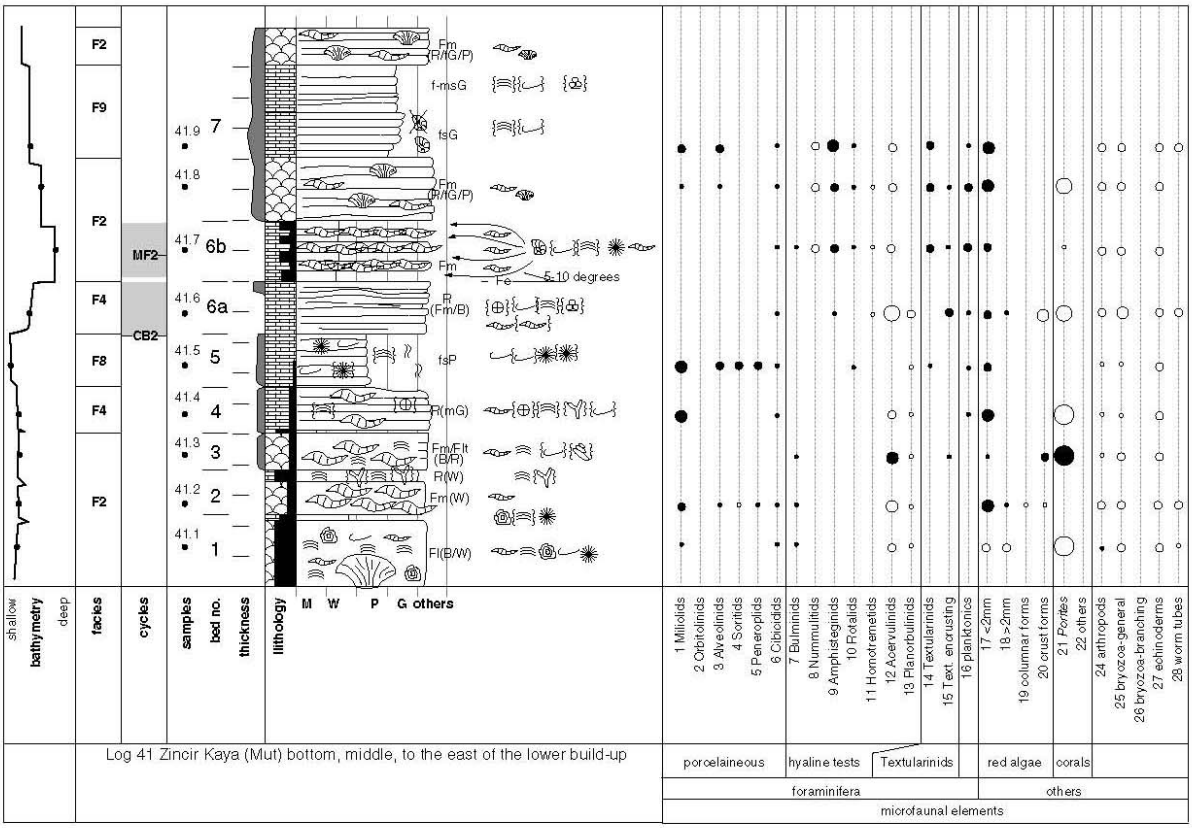

Log 41 Zincir Kaya (Mut) bottom, middle, to the east of the lower build-up

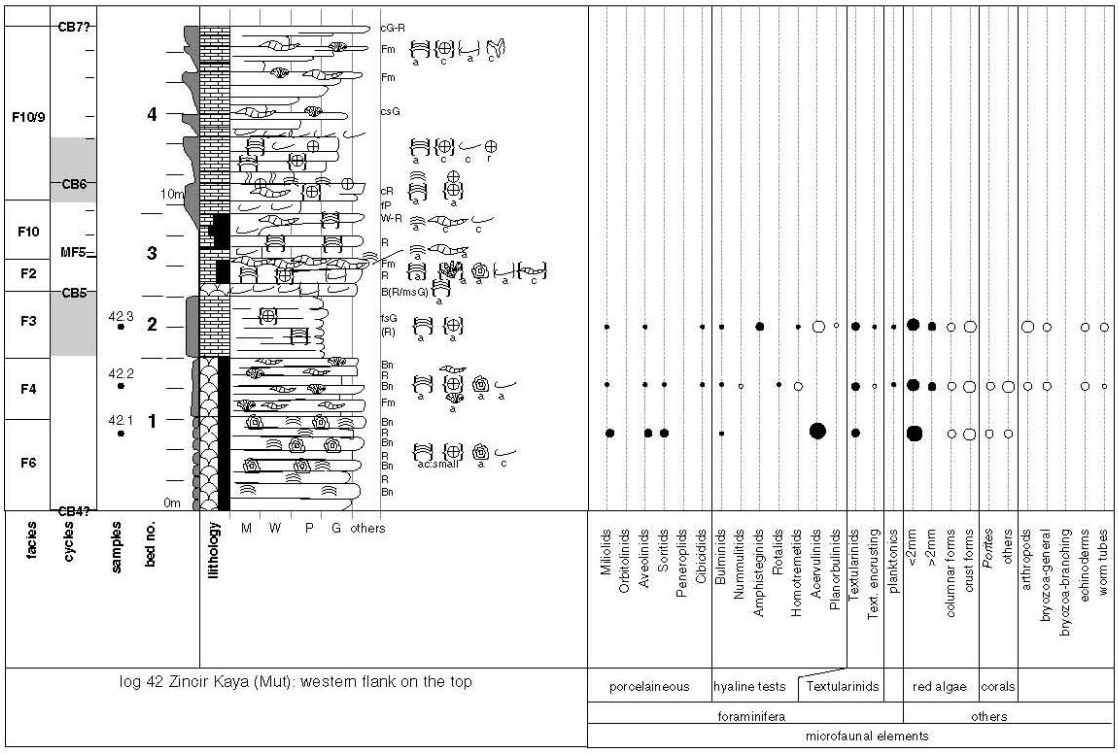

log 42 Zincir Kaya (Mut): western flank on the top

Figure 9.7 logs 41/42

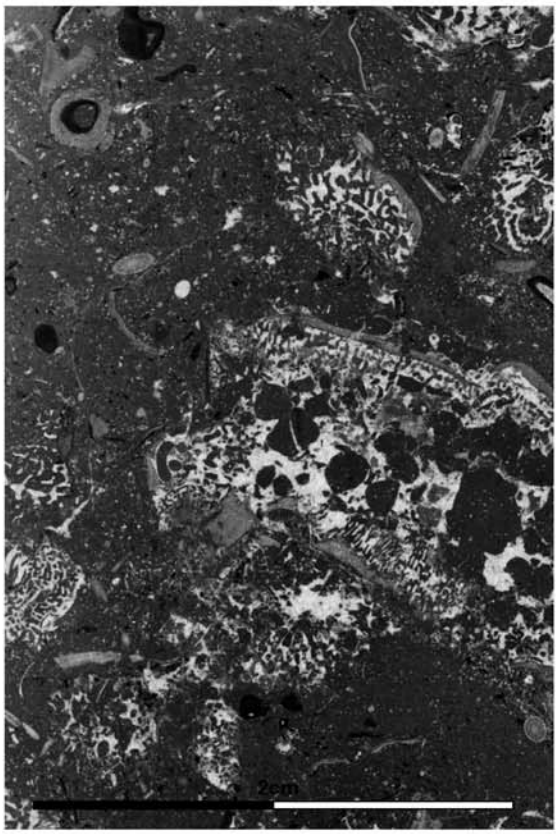

41.1

41.2

41.3

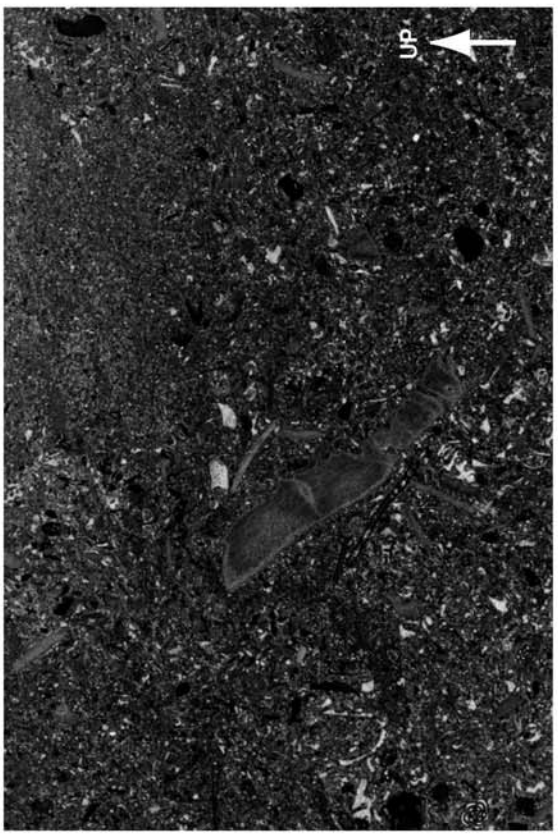

41.5

Figure 9.8 microfacies evolution of log 41 (Zincir Kaya)

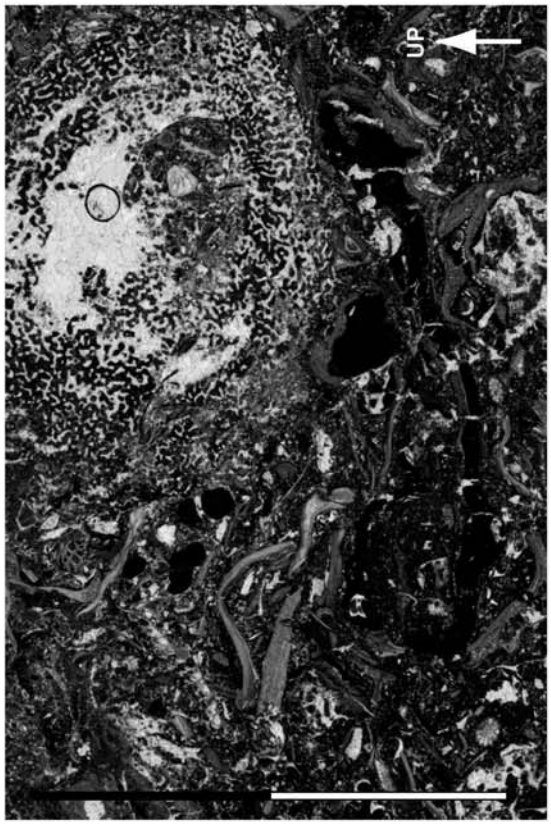

41.6

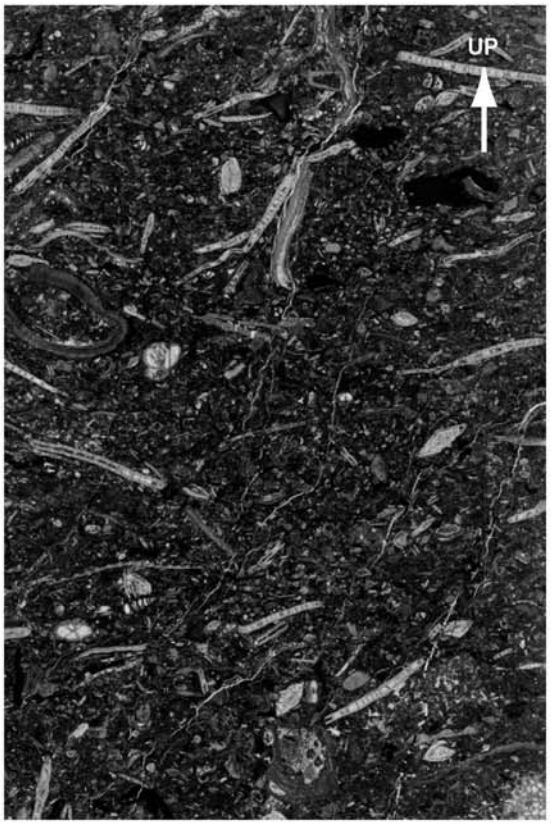

41.7

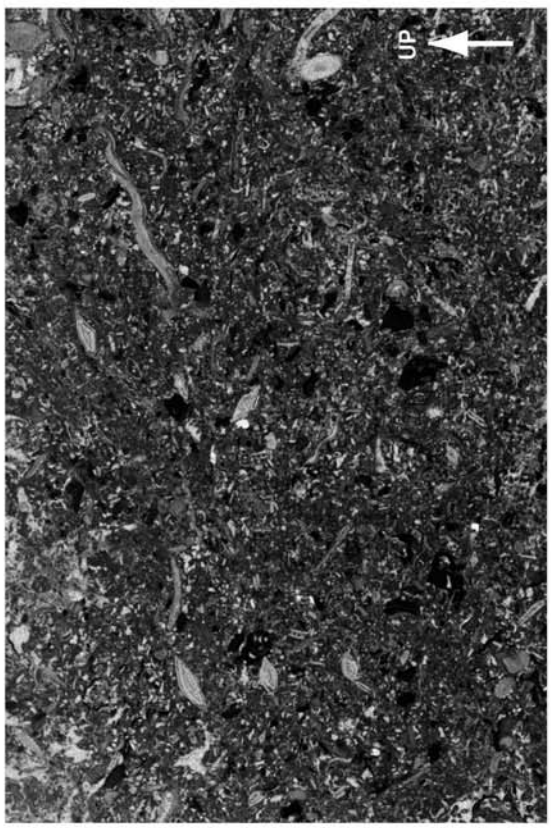

41.8

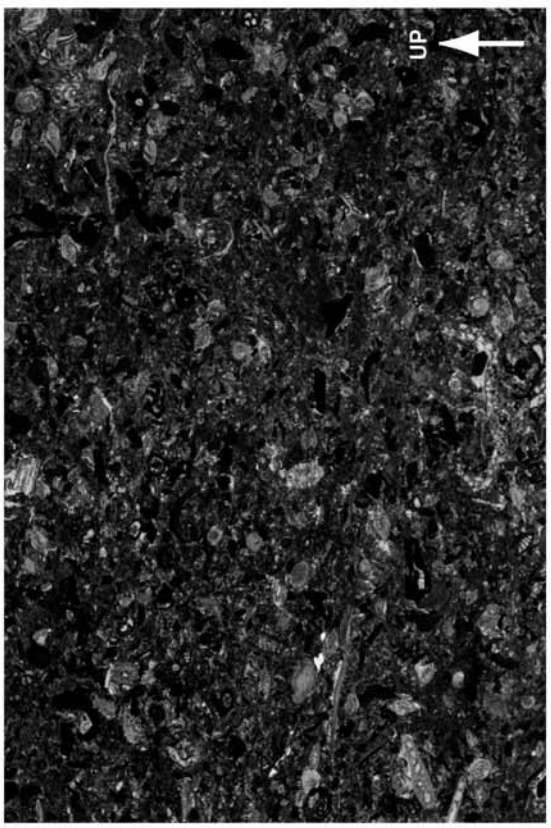

41.9

Figure 9.9 microfacies evolution of log 41 (Zincir Kaya), 2

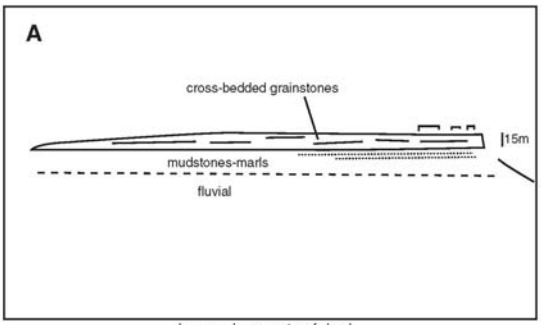

large-scale geometry of shoal

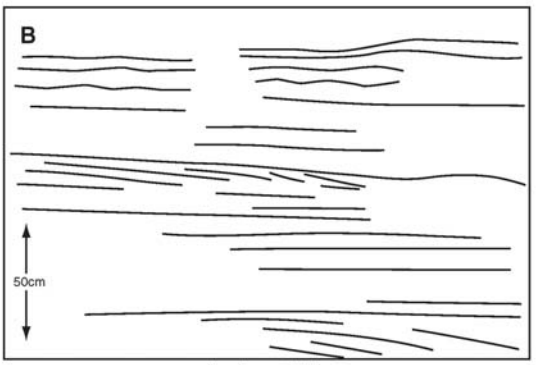

small-scale cross-bedding

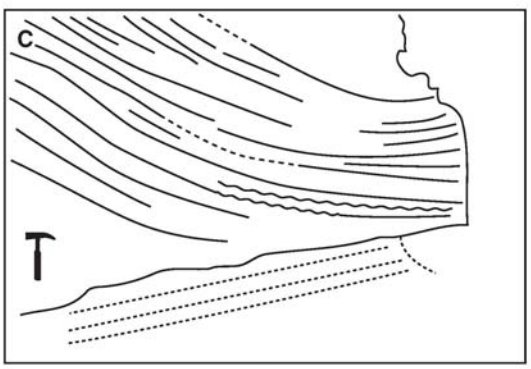

metre-scale trough cross-bedding

Figure 9.10+11 details of Zincir Kaya outcrop
This illustrates the grainstone shoal deposits on the eastern flank of the platform

FIGURES 9.10 AND 9.11 SPLIT ON PAGES 174-175 IN THE ORIGINAL

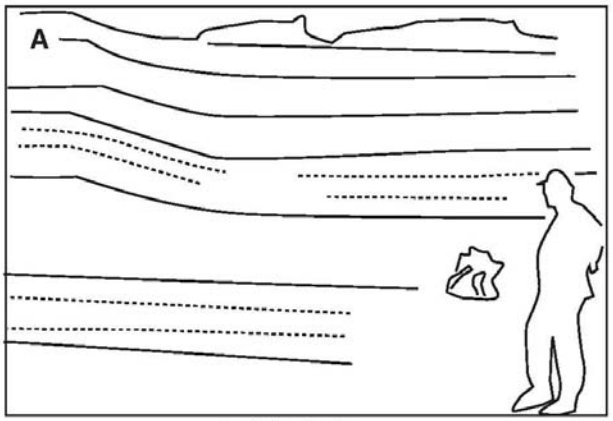

grain flow beds

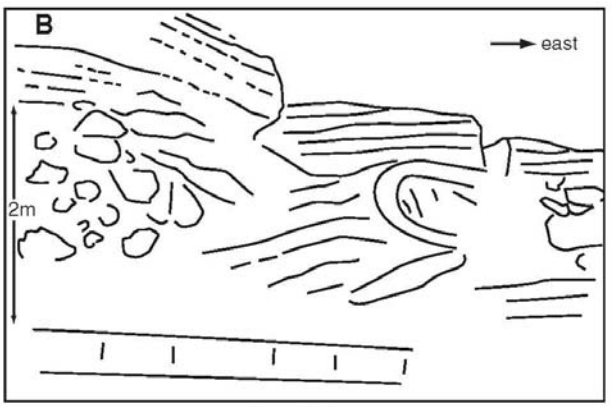

slump beds

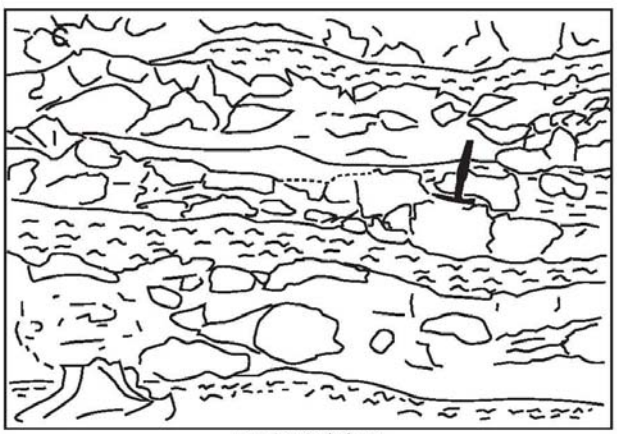

constructed slope

Figure 9.13+14 details of Zincir Kaya outcrop
This illustrates three different depositional mechanisms found in log 39 on the seaward flank of the platform: (top) shows grain flow beds, (middle) shows slumped beds, and (lower) shows a slope constructed of coral carpets

FIGURES 9.13-9.14 SPLIT ON PAGES 176-177
IN THE ORIGINAL

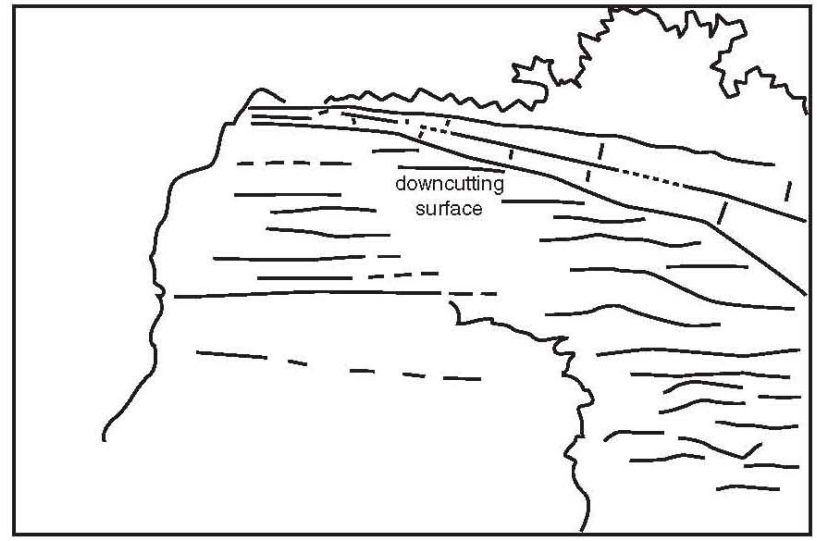

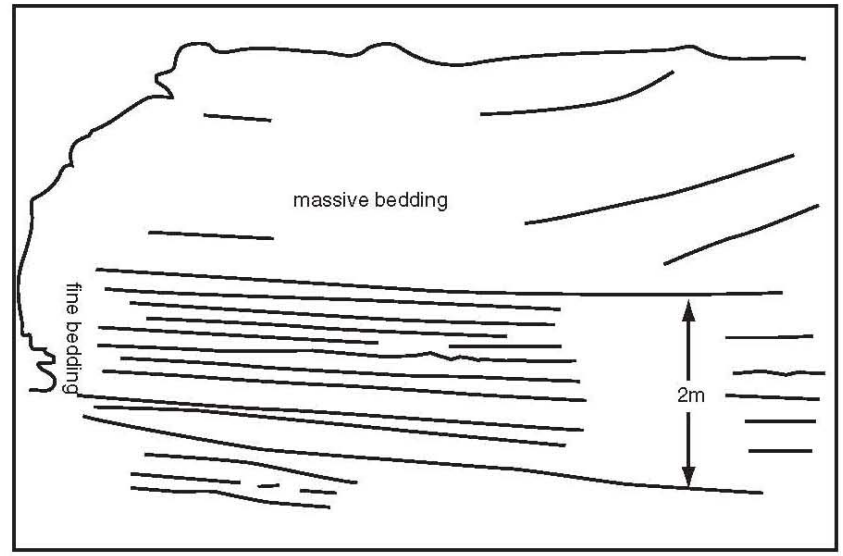

Figure 9.12 details of Zincir Kaya outcrop
This illustrates the erosional truncation on the seaward side of the platform (top), preserved by overlying beds, and (bottom) the bedding organisation of the microbial coralgal boundstones at the base of log 40 towards the top of the platform.

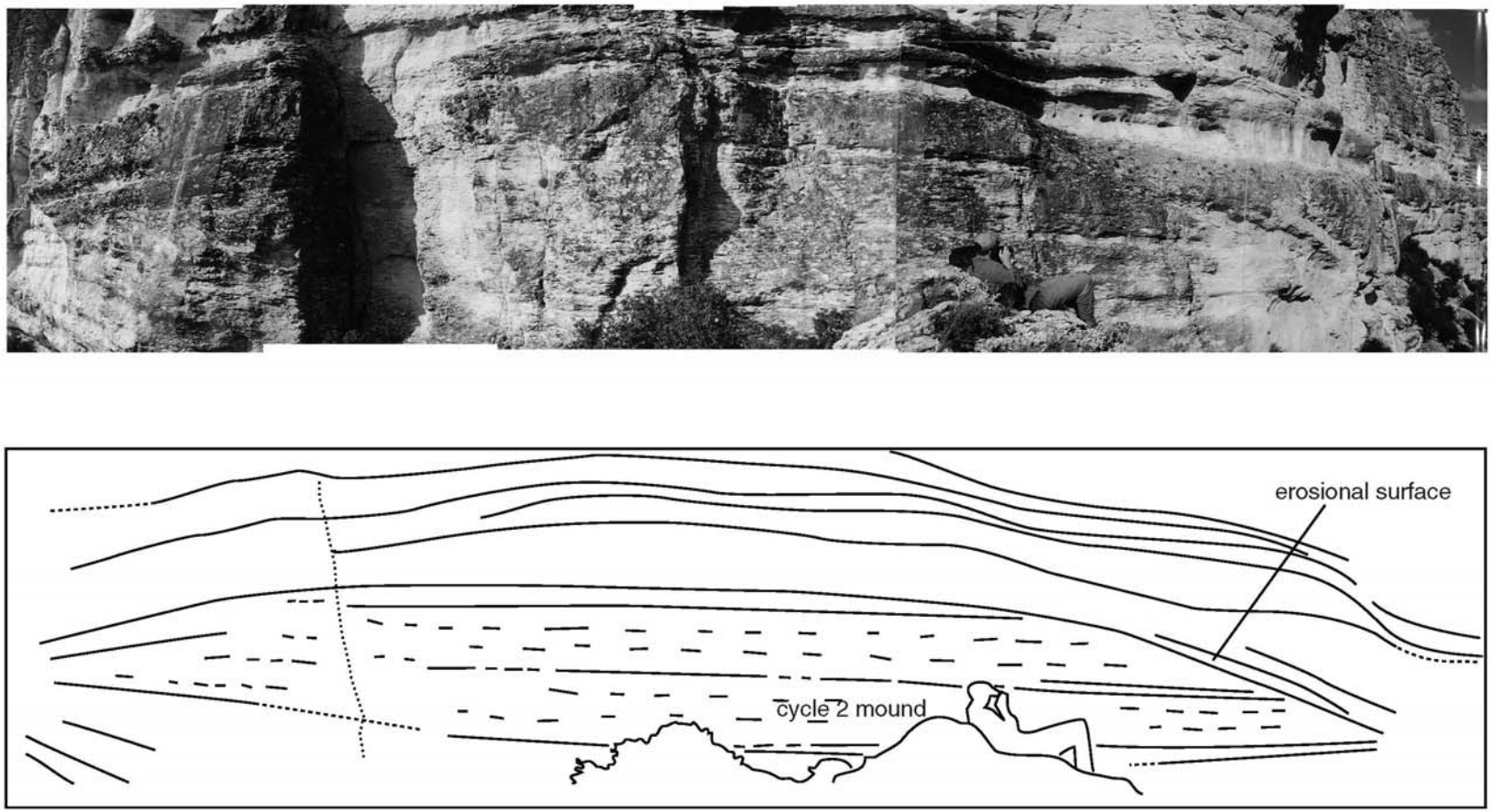

Figure 9.15 details of Zincir Kaya outcrop
This illustrates the mound that forms during the transgression of cycle 2: note the slight bevelling of the upper beds on the seaward (right) side of the mound.

10 - KIZIL KAYA (ISOLATED PLATFORM)

10.1 INTRODUCTION

Kizil Kaya is located in the Mut area at grid reference 315675 on the geological map of Mut (figure 4.6). The outcrop is formed by two cliffs at 100° angle. The eastern cliff, that runs approximately north-south and faces west, is 500m in length, while the northern cliff, running east-west, can be traced out over 1.5km. The two cliffs meet near the highest point, which is a little less than 100m high. This site was studied because it presents a 3-dimensional outcrop of one of the isolated platforms in the Mi Member of the Mut Formation in the Mut area. In contrast with the Zincir Kaya outcrop (chapter 9) this outcrop is more accessible, though the bedding patterns are not so well exposed. 14 sedimentary logs were made, and the cliff face was sampled by abseiling down the north face near the junction with the eastern face (log 54).

The outcrop is illustrated in figures 10.3-8. Figures 10.11-16 present the logs made in this area, including the microfaunal contents analysis. Figures 10.17-19 illustrate the microfacies evolution of log 28. The correlations between the logs are shown in figures 10.9-10, and the outcrop is reconstructed in figures 10.1-2. The former shows the geometrical analysis of the bedding patterns, the latter shows the facies distribution and defines the sedimentary cycles.

10.2 FACIES EVOLUTION

This discussion makes continual reference to log 28 on figure 10.13, and to the microfacies photographs on figures 10.17-19, corresponding to the samples taken from this log. The position of the log 28 can be seen in figures 10.3-8. The facies evolution of log 28 from 30-55m will be described.

From 30-34m coral framestones are seen in the macrofacies (facies 2). Large (10-30cm) plates of Porites coral sit in a greenish clay-rich micrite. Red-algae and is present but poorly developed as encrusters on the coral surfaces. The microfacies texture is illustrated in figure 10.17 by sample 28.17 (top) which shows a coral floatstone texture. Note the diversity of coral microtextures and the presence of Pelecypod mollusc debris. The sediment in this interval is autochthonous (framestones) or para-autochthonous (floatstones) constructed platform.

Just beneath the 34m mark, before the top of the bed, a second microfacies sample, 28.5, is illustrated in figure 10.17. This shows a sorted Miliolid grainstone texture (facies 8). The macrofacies indicates that this is the matrix surrounding the coral framestone, and has replaced the clay-rich micrites. At 34-34.5m a bed of rud-floatstone containing branching coral, platey corals, and their debris, is deposited. Then 5.5m more of muddy coral framestones (facies 2) are deposited. These are differentiated from the coral framestones below in that they contain domed rather than platey coral forms, and they also contain much more red algae, in the form of rhodoliths. The topmost bed is a rudstone containing coral debris and intraclasts. These are autochthonous to pseudo-autochthonous constructed platform sediments.

Directly overlying this bed is a fine wackestone bed bearing planktonic foraminifera and rhodoliths. Platey Porites corals also develop locally in the sediment, and this texture is illustrated in figure 10.18 in sample 28.9: here we see thin Porites crusts developed in a micritic matrix, with common columnar red-algal debris floating in the matrix, and very thin poorly developed crusts of red algae on the coral surfaces.Three 1-3m coarsening-up cycles occur to medium grainstones-rudstones up to 47.5m (facies 9). This texture is illustrated in figure 10.19 (bottom) where we see a rudstone composed of columnar red-algal debris, Nummulitid fragments, Amphisteginids, Pelecypod mollusc and bryozoan debris. A fourth such cycle occurs from 57.5-59m, and the top surface is encrusted with corals and red algae. Overlying this bed is a metre thickness of micro-packstones (facies 10) containing planktonic foraminifera and rare branching coral debris. Then three coarsening-up cycles of micro-packstone to medium grain-packstone are deposited. The micro-packstone texture and the grain-packstone texture are ilustrated in figure 10.19 (top and bottom respectively). These detrital carbonate sand beds (from 42-55m) are sloping to the south, and are interpreted as allochthonous slope sediments.

10.3 DEFINITION OF CYCLES

This discussion makes continual reference to the correlation scheme in figures 10.9 and 10.10, to the logs in figures 10.11-16, and to the bedding pattern photos in figures 10.3-10.8.

Cycle 1: cycle boundary 1 is defined from the facies in log 34: it is the surface that marks the first appearance of marine sediments on top of the continental muds and sands of the Derinçay Formation. This is the only log that goes down this far in the section. This section has been studied by a team of molluscan palaeontologists to determine the ecological environment from the molluscan assemblages (Schlaf et al. 1997). A summary of the results are shown in figure 10.11, marked on the log 24. The maximum flooding for cycle 1 is determined from the results of this study, the interval chosen being the most open enviroment (sub-littoral, stenohaline) surrounded above and below by more restricted environments (littoral to sub-littoral, euryhaline below, and intertidal above).

Cycle 2: cycle boundary 2 has been defined from the facies in logs 24, 34, 28 and 29 (figure 10.11, 13-14 and 15). In log 24 and 34 it is the inter-tidal interval as determined from the molluscan assemblage (Schlaf et al. 1997) and from the facies: a mixture of bioturbated gravels, coquina beds and siltstones. In log 28, in a more distal setting, this cycle boundary is defined from the most proximal facies: an interval of decimetric cycles of oyster beds colonised by branching corals, then covered with clay-rich micrites. The last bed in this interval is a 2m thickness of gravelly siliciclastic sands. The maximum flooding for this cycle has been defined in log 29 from both the facies and the geometries. In the facies a hardground surface is seen at 11m on log 29, encrusted with oysters and small Porites corals, and with a ferruginous crust. From the bedding patterns it is defined by a truncated surface bevelled away by the overlying prograding beds. This truncation only occurs where the contact is steep (see figure 10.4).

Cycle 3: cycle boundary 3 is defined principally from the geometries, and then is located in the facies. It has been described in logs 35, 31,32, 28, 38 and 37. In the geometries it is the top surface of a prograding packet of sediment seen on the eastern face of the outcrop, and refound on the northern face (see figure 10.4, and then follow the surface round into figures 10.5, 10.6, and 10.8). On the eastern flank at the southern extremity between logs 38 and 29 toplap is seen in the prograding packet (figure 10.4). In the facies in log 35 this cycle boundary is defined by a muddy rhodolithic bed (facies 6) overlying a coral framestone bed on the slope. On the platform top this limit is seen as a sharp flooding surface (log 28), and on the seaward slope in logs 38 and 29, as a change from allochthonous detrital carbonate sands to more constructed facies. In log 28 cycle boundary 3 is placed at 34m (figure 10.13): the shallowing trend observed from 30-34m is capped by a distal shift across a sharp surface. The change from framestone to rudstone-floatstone textures, the reduction of the clay content, and the appearance of branching coral morphologies all indicate an opening of the environment (a distal shift). The maximum flooding surface of cycle 3 has been defined from the geometries on the southern flank of the eastern cliff. It is shown in figure 10.4 to be a downcutting surface separating the eroded sediment packet below from the prograding sediment packet above, and it greatly resembles the maximum flooding surface of cycle 2 below.

Cycle 4: the CB4 is defined in a very similar way to the CB3: it is the top surface of a prograding packet of sediment. This is illustrated in figure 10.4. This is a distinct surface in outcrop and can be followed physically round to the western side of the northern cliff-face (see figures 10.7 and 10.8). It has been identified in most of the logs at this site. On the eastern edge in logs 29 and 37 this is the topmost limit of the outcrop. On the platform top in logs 28 and 35 it is represented by a major flooding surface. In log 28 CB4 is placed at 40m: it is defined here using the same logic as for CB3. The maximum flooding interval (MF4) at 41m is defined by being the most distal facies as indicated by the presence of planktonic foraminifera (see figure 5.2). On the western extremity of the outcrop on the landward side of the platform it is also a major flooding surface. In this area in logs 24 and 34 it marks the deepening (Schlaf et al. 1997) transition from siliciclastic muds and silts to micro-packstones (facies 10). The maximum flooding has been defined on the platform in log 28 by the facies evolution (see discussion above). It here lies directly on the cycle boundary, and corresponds to a downlap surface in the geometries (see figure 10.6).

Cycle 5: the cycle boundary 5 is defined principally from the bedding geometries. On the eastern cliff it is seen as the top surface of a prograding wedge, that is then overlain by a retrograding packet (figures 10.5, and 10.6). This surface is followed down into log 28, where it is found to be a flooding surface that defines the limit of a coarsening up packstone-grainstone cycle on the slope of the platform. The top of each coarsening-up cycle from 41-49m is a flooding surface and a maximum of progradation, hence a good potential candidate for a cycle boundary determined solely from the facies. However, when the geometries are examined (figure 10.5-6) the turn around from progradation to retrogradation occurs at 47.5m, and so the cycle boundary 5 is placed here. The tops of the other coarsening up cycles are relegated to smaller scale cycle boundaries. Each of the finest end members of the coarsening-up cycles, the micro-packstones, is a potential candidate for a maximum flooding surface. In the same way as for the cycle boundary, the most important maximum flooding is chosen by examining the geometries: the turn around from retrogradation to progradation as seen in the

geometries is found at 49m (see figure 10.5-6), and this corresponds to MF5.

On the northern cliff, on the landward side of the platform, this surface is also defined principally by the geometries. It is defined by the top surface of an isolated wedge that onlaps against the landward slope of the platform, and fills up flush to the same height as the cycle boundary 5 as defined on the platform (see figure 10.4). When examining the facies, this wedge is constructed by clean coralgal framestone (facies 1), and the top surface is a flooding surface, with marls overlying the framestones (see log 25). The maximum flooding of this cycle is defined on the seaward margin as a downlap surface with associated bevelling of the edge of the retrograding sedimentary packet beneath (see figure 10.5 and 6).

Cycle 6: This surface is principally defined from the geometries as the top surface of the next prograding sedimentary packet on both the seaward side (figure 10.6) and the landward side of the platform (figure 10.7). This surface has no clear expression within the platform, and is difficult to follow round from the landward to the seaward flank. In the facies on both the seaward (log 28) and the landward side (log 36) this is the top limit of the outcrop. Marls (facies 10) containing pteropods overlay the top of the outcrop, though in the localities logged these have been weathered away.

Cycle 7: the topmost beds of the platform truncate the beds just beneath on the slope, in the same manner as for the prograding packets in cycles 2, 3, 5 and 6. For this reason it is proposed that the topmost surface of the platform may be a cycle boundary. The facies at the top are principally coralgal framestones, with rhodalgal grainstones, rudstones and bindstones deposited on the flanks. There is no clear evidence from the facies for this cycle boundary.

10.4 PLATFORM EVOLUTION

Cycle 1: a maximum flooding interval has been defined for this cycle, so the retrogradation and the progradation are distinguished across the profile. The bedding geometries have been reconstructed by correlating only the topmost beds of this cycle across the profile, and placing them sub-horizontally. The geometries of both the retrograding and the prograding phase have been reconstructed as tabular: being the simplest solution considering the lack of outcrop control.

The facies in the retrograding phase consist of littoral to sub-littoral muds and siltstones (facies 19), with some intervals of cross-bedded siliciclastic sands (facies 15) and coquina beds (facies 17). The maximum flooding surface has been identified as an interval of reefal facies development, the most open marine interval in this cycle. The prograding phase is composed of intertidal gravelly highly bioturbated muds and sands, containing oysters.

Cycle 2: a maximum flooding surface has been defined along most of the profile, so the retrogradation and progradation can be distinguished. It is only on the landward side of the platform, in logs 24 and 34, that the maximum flooding has not been identified. From the reconstruction the retrograding phase creates a 20m thick mounded topography 1000m wide with the flanks gently dipping at 5-8°. The oblique-angled nature of the outcrop allows an estimation of the shape of this mound in plan view: it is approximately round or ellipsoid in form. The prograding phase fills out the flanks of the mound on the seaward and the landward sides, with deposits on the top of the mound being thin to absent. On the seaward side toplap is observed in the prograding prograding wedge.

Only the tops and the lateral extremities of this cycle are visible in outcrop. On the seaward side (log 29) the retrogradation starts with Miliolid grainstones (facies 8) containing some corals. On the landward side (log 24) sub-littoral mudstones and siltstones (facies 19) are found. The facies of the mounded area at the top of the trangression are muddy coralgal framestones and floatstones (facies 2 and 4 respectively). The progradation on the landward side is composed of muddy coralgal floatstones, while on the seaward side it is dominantly Miliolid grainstones (facies 8), grading distally into Nummulitid grain-packstones (facies 9).

Cycle 3: a maximum flooding surface has been defined along parts of this profile, so the retrogradation and progradation can be distinguished. The retrograding phase deposits an aggrading packet 7m thick on the underlying mounded topography created by the second cycle. This packet is relatively isopachous across the profile, except on the seaward margin, where it is thinned by erosional truncation of the top surface. The prograding phase is deposited as wedges on the landward and seaward flanks of the mounded relief. It is thin to absent on the top of the platform.

The retrogradation consists dominantly of muddy coralgal framestones on the platform, while on the landward side sub-littoral mud-siltstones (facies 19) are deposited. The prograding phase consists of a wedge of Miliolid grainstones (facies 8) deposited on the seaward side, grading distally into Nummulitid grain-packstones (facies 9). On the landward side Nummulitid packstones deposited on the flanks grade laterally landwards into silty sandstones (facies 15) deposited at the feet of the platform.

Cycle 4: a maximum flooding surface has been defined on the flanks of the platform, permitting the distinction of the retrograding and the prograding parts of the cycle in these areas. During the retrogradation a mounded relief aggrades on the platform. It is 20m thick and roughly 500m across, being approximately circular to elipsoid in plan view.

The progradation is deposited on the seaward flank as a prograding wedge, and on the landward flank as a distinct isolated relief, filling up flush to the same level as the top of the cycle on the main platform. On the platform itself the progradation is thin to absent.

The retrogradation is composed dominantly of muddy coralgal framestones (facies 2) on the platform. Off the seaward side of the platform the retrograding deposits are of negligible thickness. On the landward side 10m of well-bedded micro-packstones (facies 10) are deposited. The base of this cycle marks a sudden reduction in the siliciclastic contents of the facies in this area. The progradation on the seaward side consists of prograding clinoforms, with Nummulitid packstones (facies 9) forming the toesets. On the landward side the progradation is formed by a build-up of clean coralgal framestones (facies 1) that prograde out away from the platform in a landward direction over the micropackstones of the retrogradation.

Cycle 5: a maximum flooding surface has been defined for this cycle on the landward and seaward flanks of the platform. This allows the distinction of the retrograding from the prograding phase. During the retrogradation the bedding forms aggrading geometries on the platform. This creates a mounded relief 400m wide and 20m high, roughly round to ellipsoid in plan view. During the progradation deposits are thin to absent on the top of the platform, while prograding wedges are deposited on the landward and seaward flanks. Erosional bevelling of the underlying retrogradation occurs at the base of these prograding deposits on the edges of the topography. On the seaward side toplap has been identified in the bedding.

The facies of the retrograding phase on the platform are dominantly microbial coralgal boundstones (facies 7). On the flanks Nummulitid grain-packstones (facies 9) are preserved. The facies distribution during the progradation is identical. Note that deposition away from the platform topography is negligible.

Cycle 6: a maximum flooding surface has been defined on the landward and seaward flanks of the platform. This allows the distinction of the retrograding from the prograding phase. During the retrogradation a 20m thickness of aggrading to retrograding beds are deposited only on the top of the platform topography. The progradation caps the platform, and deposition also occurs on the flanks. Erosional bevelling of the underlying retrograding sediments occurs on the edges of the platform topography. The prograding sediments are volumetrically unimportant compared to the previous regressions.

The retrograding facies are dominated by rhodolithic sediments (facies 5), and the platform is capped by clean coralgal framestones (facies 1) deposited during the progradation. The corals in these framestones are 1-3cm knobbly Porites crusts and stubby vertical fingers, with the surfaces lightly encrusted by red algae, and surrounded by red-algal and bioclastic grainstone debris. The rock is highly cemented.

10.5 SUMMARY

Cycle organisation and thickness in this outcrop are virtually identical to Zincir Kaya, and the two outcrops can be correlated cycle-for-cycle (cycle 1 in Zincir Kaya is considered the same as cycle 1 in Kizil Kaya).

Cycle hierarchy: as in Zincir Kaya, six medium-scale cycles have been identified here and no other scale of cycle has been defined.

Cycle organisation: one of the major differences compared to Zincir Kaya is that a spreading out of the depocentre occurs during cycle 4, with the development of a secondary reefal body on the landward side of the outcrop. This occurs at the same time as a decrease in siliciclastic input in the area starting from the base of cycle 4 (see the abrupt switch from a mud-dominated environment to a carbonate environment at cycle boundary 4 in log 24 at the western end of the outcrop).

Facies evolution: the three phases of platform evolution identified in Zincir Kaya are also identified here. A major difference between the two outcrops is observed at the base in cycle 1. In Zincir Kaya this cycle is a carbonate environment, with some clay input, whereas in Kizil Kaya this cycle consists of littoral muds and silts. This is due to the more proximal position of this site.

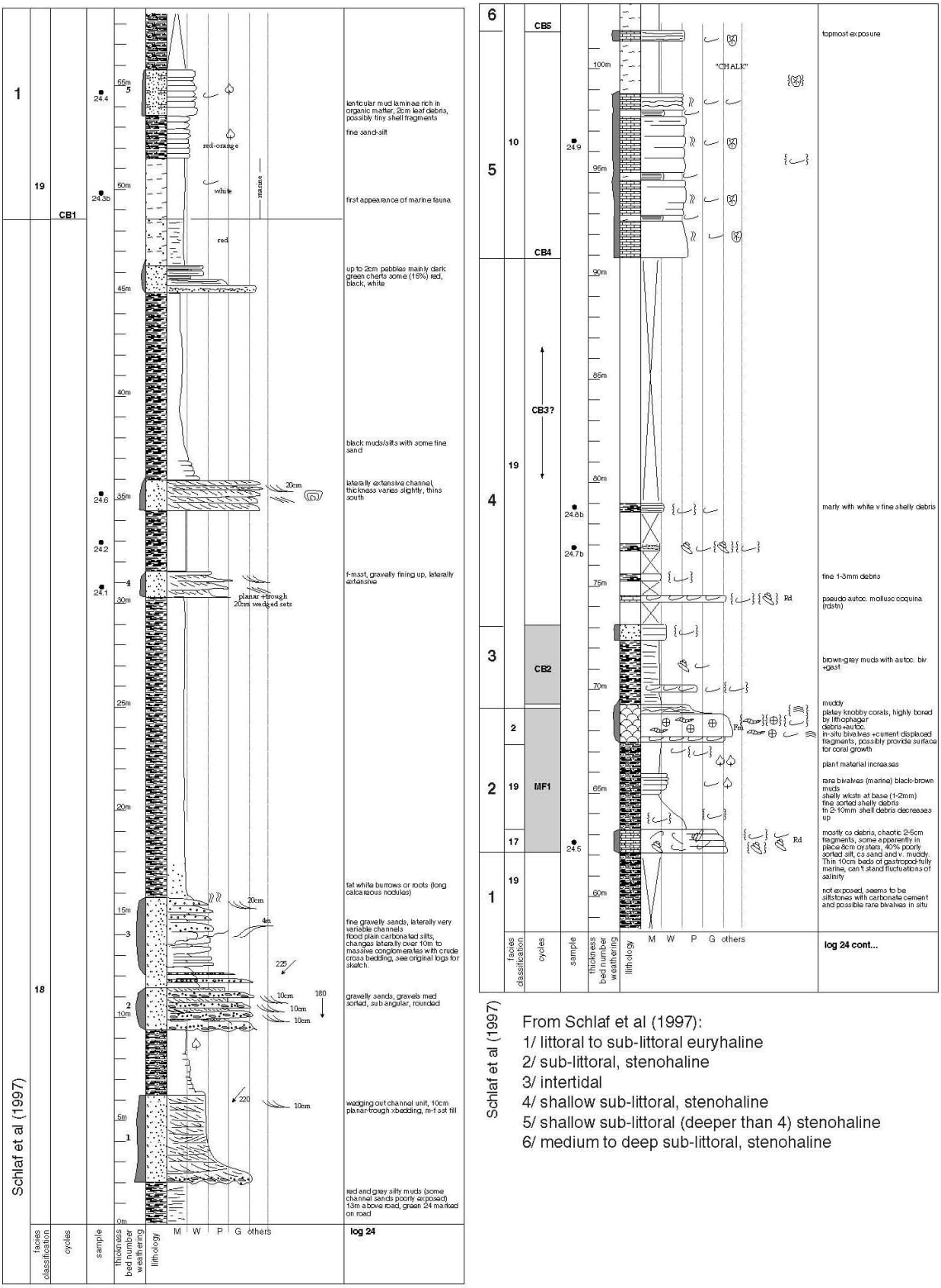

Schlaf et al (1997)

From Schlaf et al (1997):
1/ littoral to sub-littoral euryhaline
2/ sub-littoral, stenohaline
3/ intertidal
4/ shallow sub-littoral, stenohaline
5/ shallow sub-littoral (deeper than 4) stenohaline
6/ medium to deep sub-littoral, stenohaline

Figure 10.11 log 24 (Kizil Kaya)

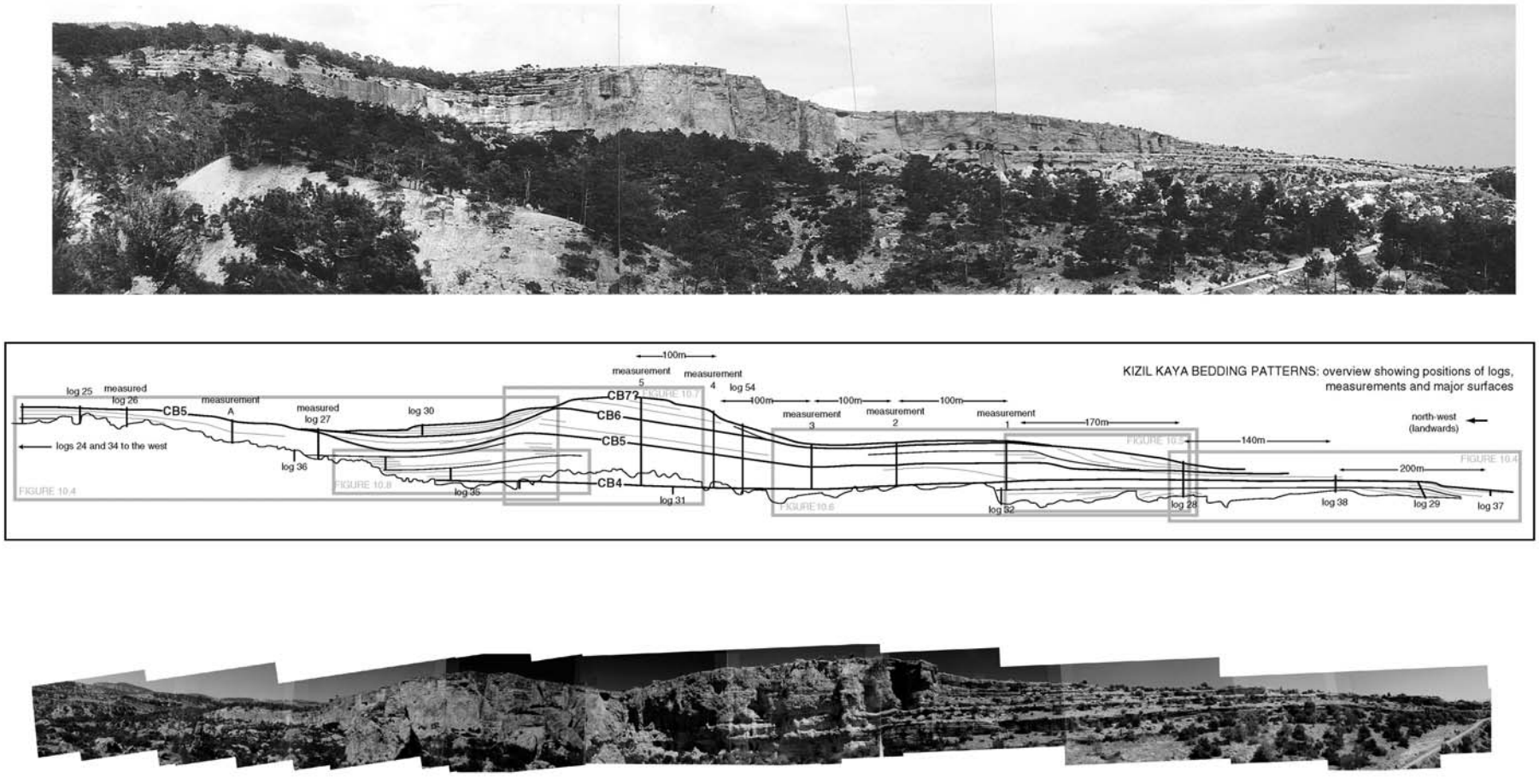

Figure 10.3 photos of Kizil Kaya bedding patterns (1)

FIGURE 10.3 SPLIT ON PAGES 186-187 IN THE ORIGINAL

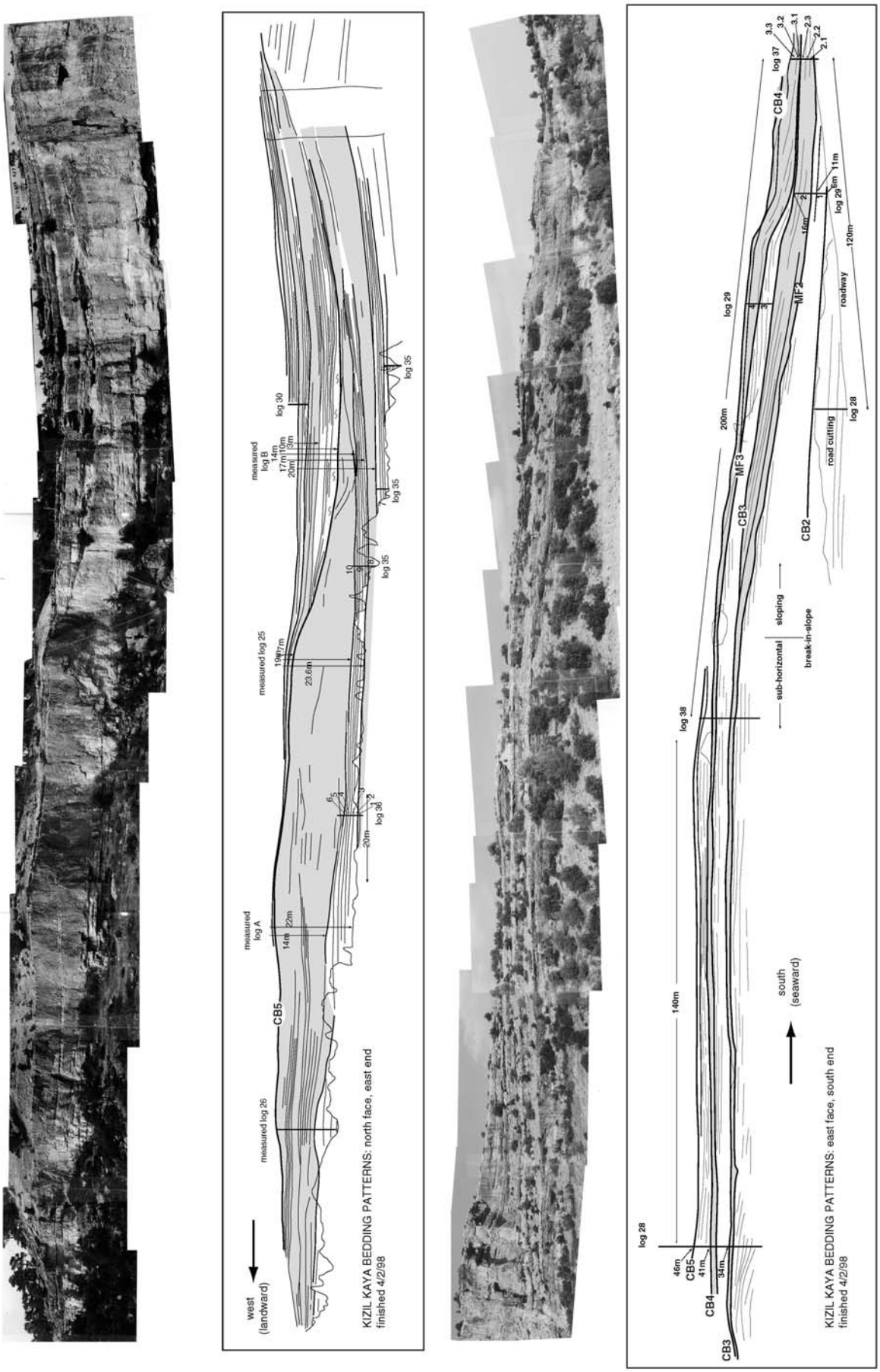

Figure 10.4 Kizil Kaya outcrop photos (2)

FIGURE 10.4 SPLIT ON PAGES 188-189 IN THE ORIGINAL

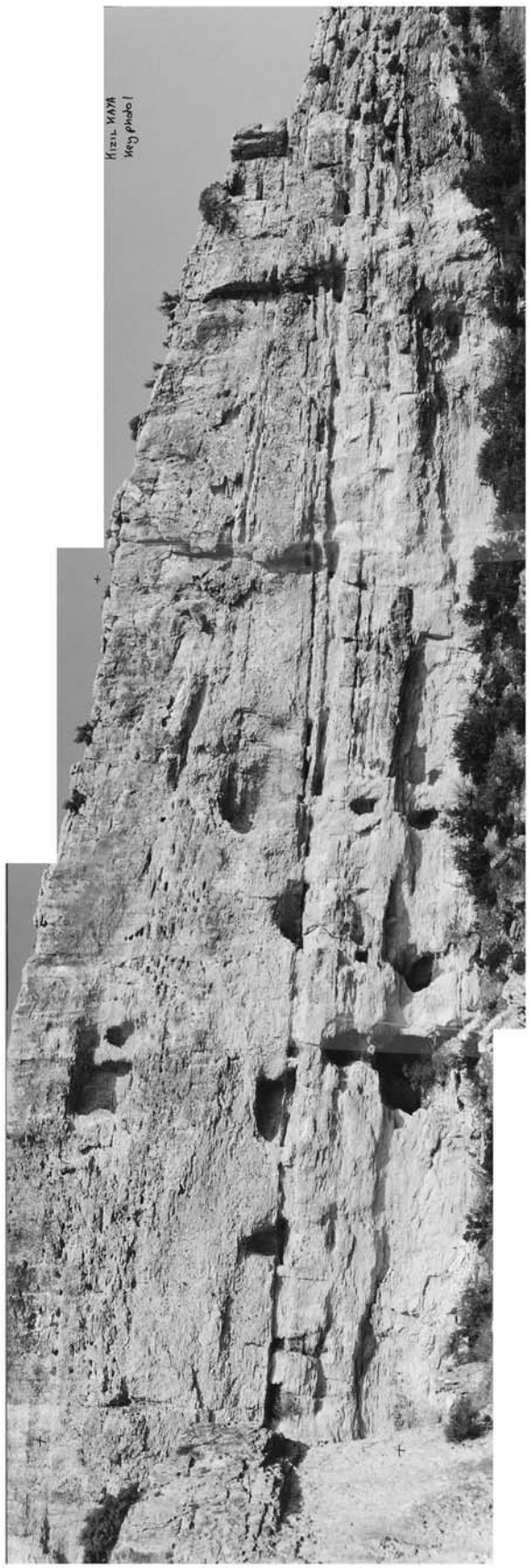

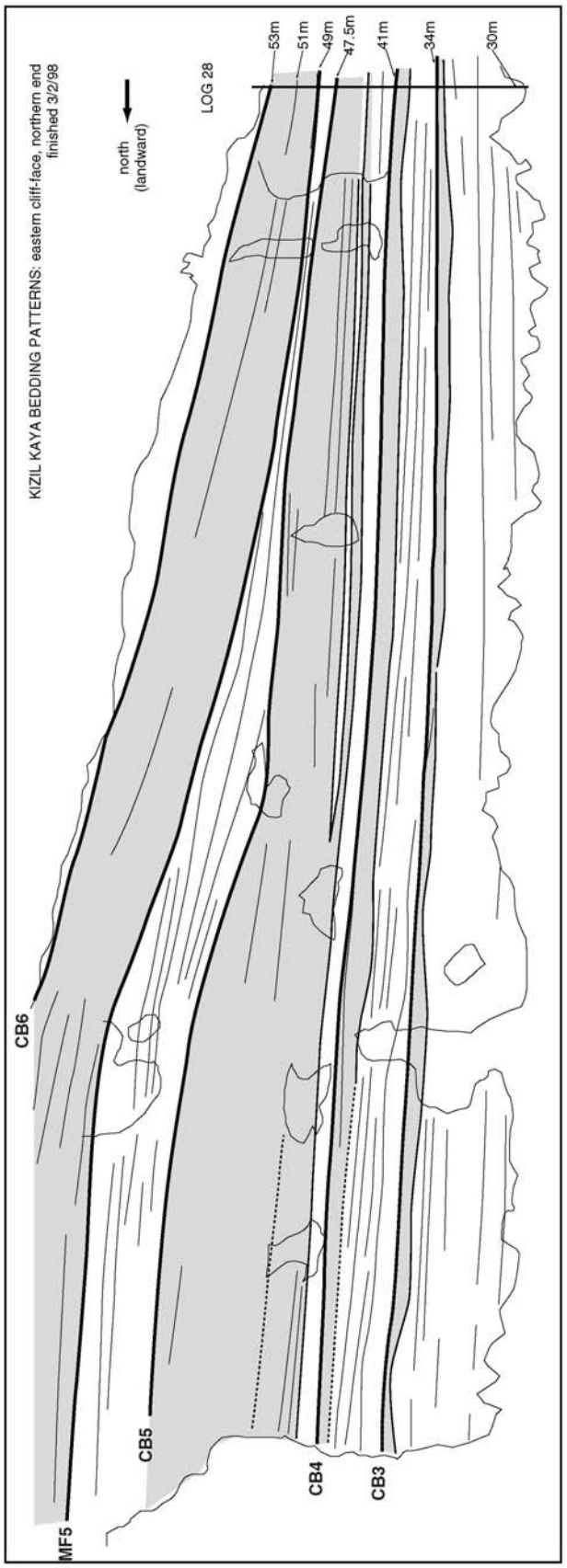

Figure 10.5 Kizil Kaya bedding pattern photos (5)

FIGURE 10.5 SPLIT ON PAGES 190-191 IN THE ORIGINAL

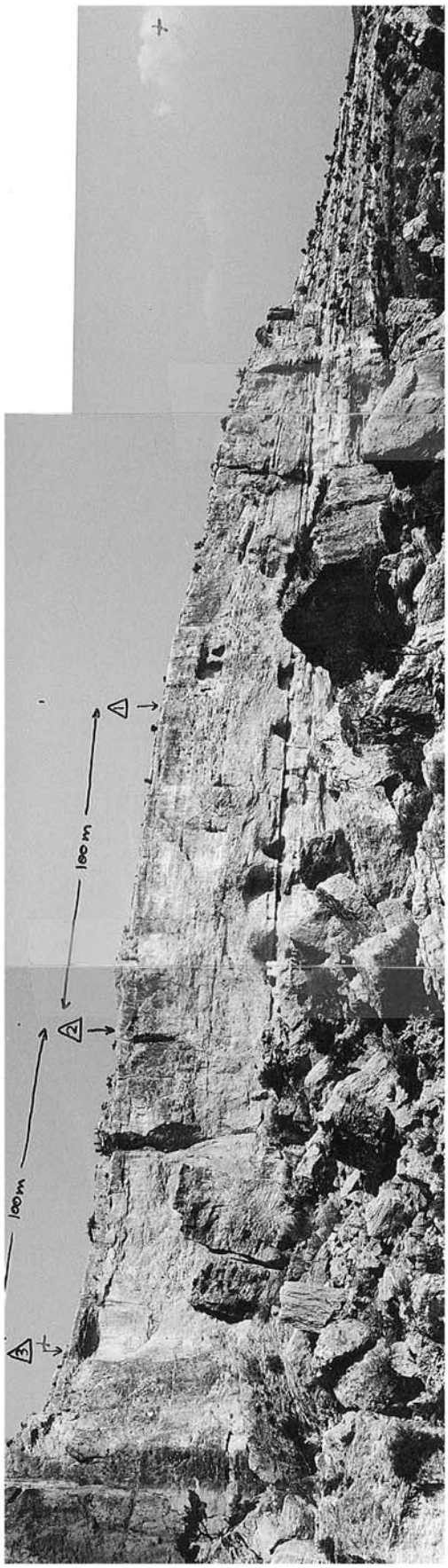

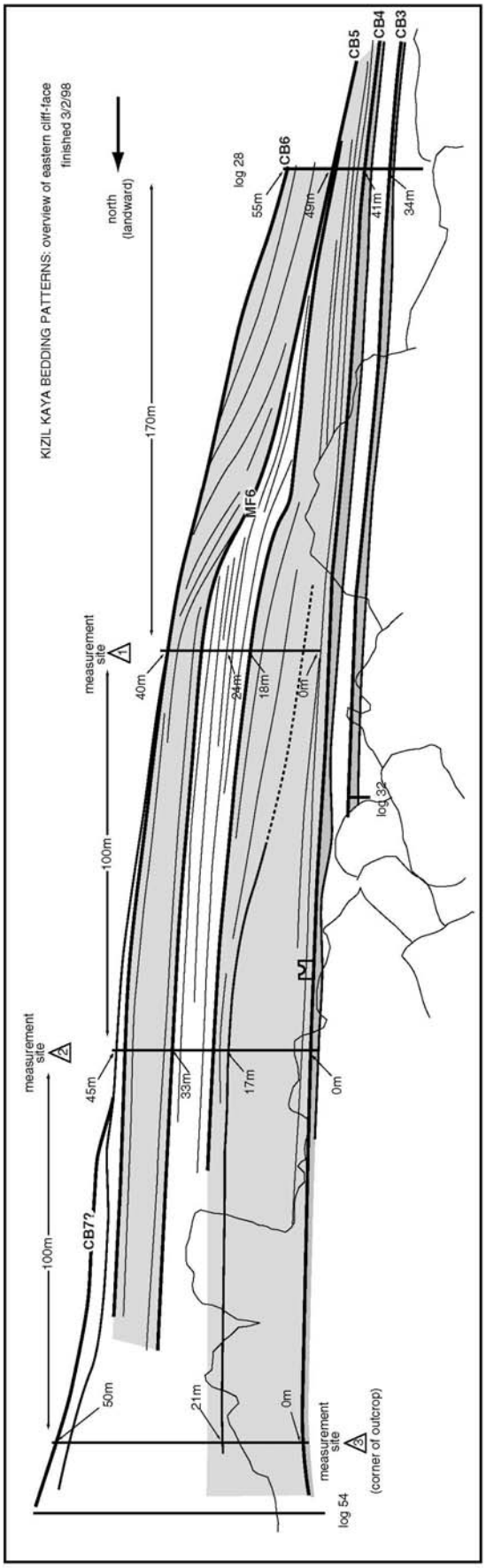

Figure 10.6 Kizil Kaya bedding patterns (4)

FIGURE 10.6 SPLIT ON PAGES 192-193 IN THE ORIGINAL

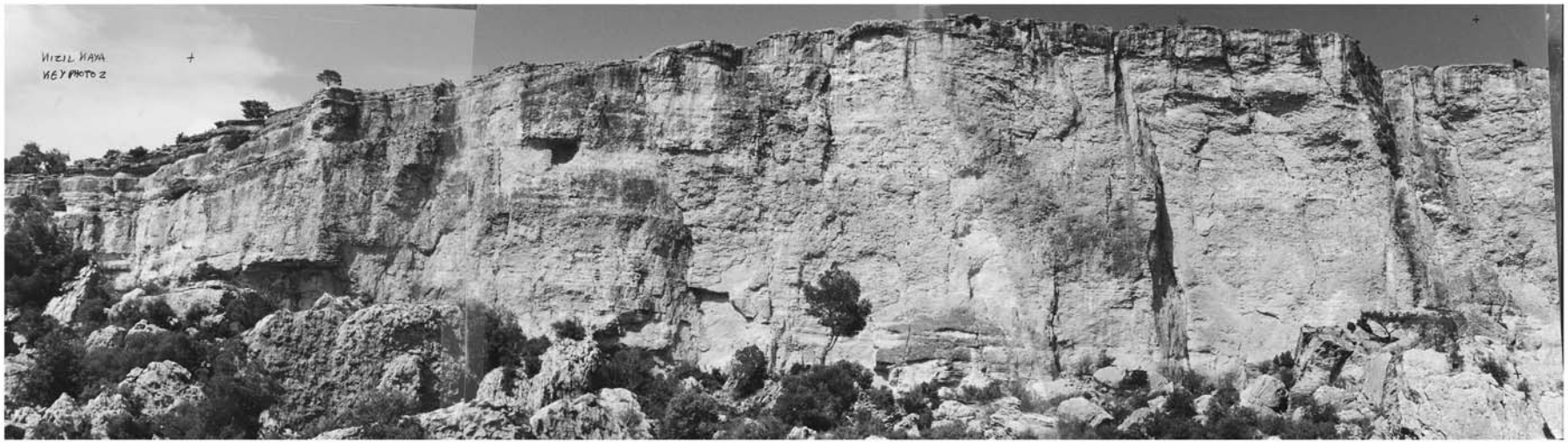

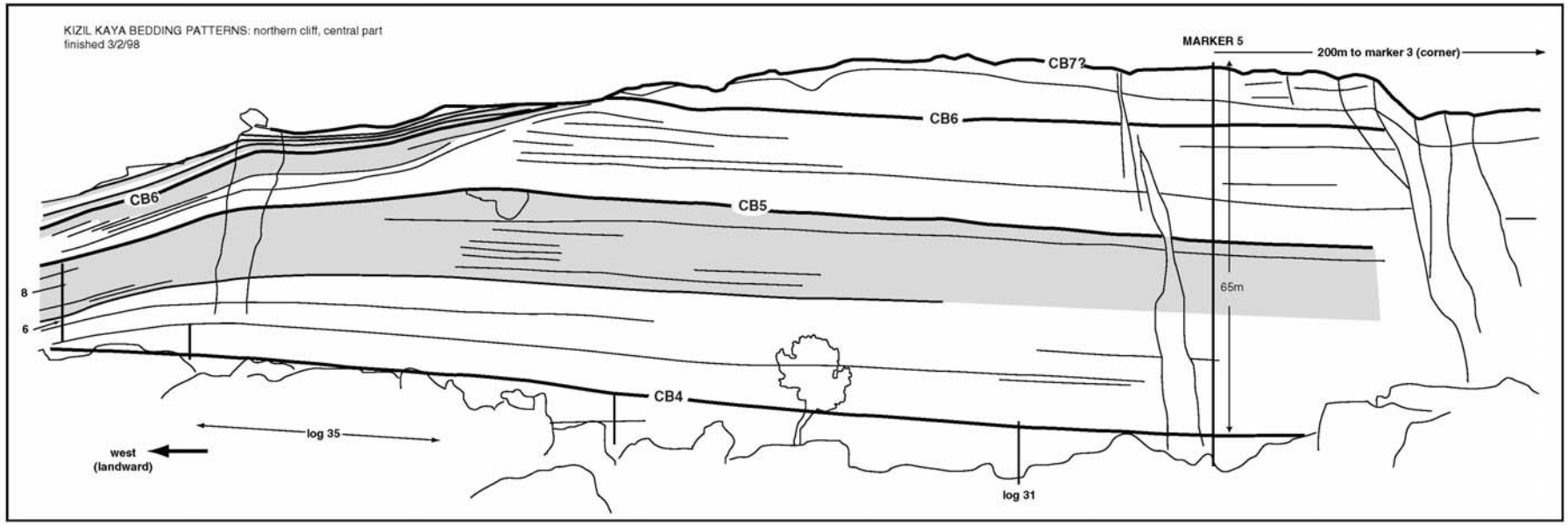

Figure 10.7 Kizil Kaya bedding patterns (4)

FIGURE 10.7 SPLIT ON PAGES 194-195 IN THE ORIGINAL

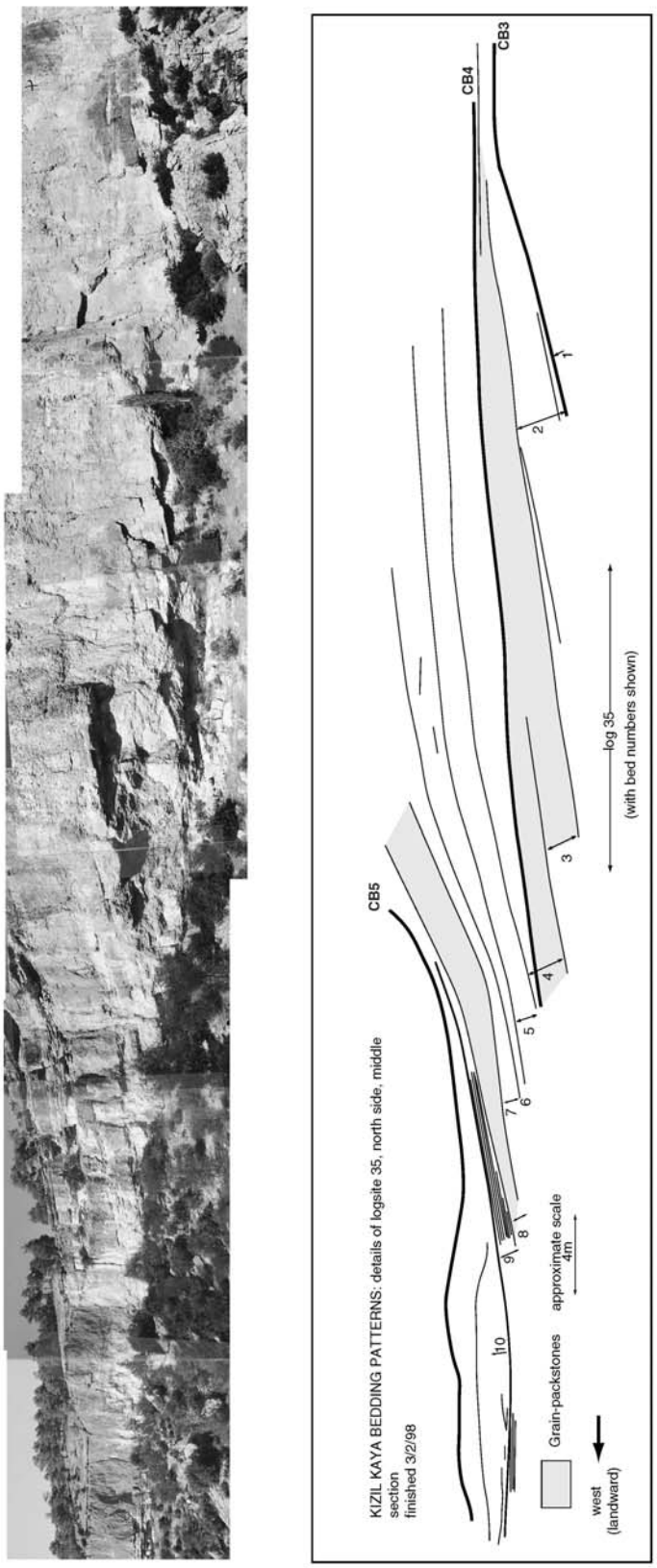

Figure 10.8 bedding pattern photos (6)

FIGURE 10.8 SPLIT ON PAGES 196-197 IN THE ORIGINAL

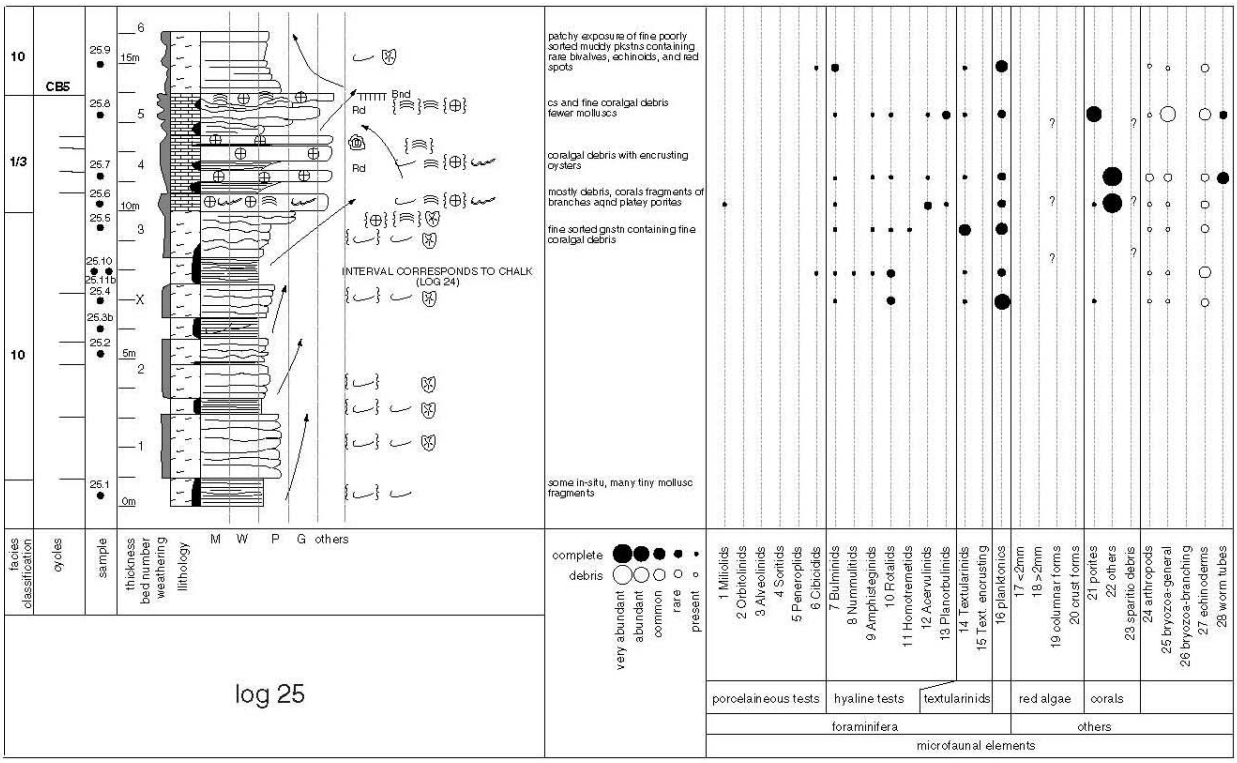

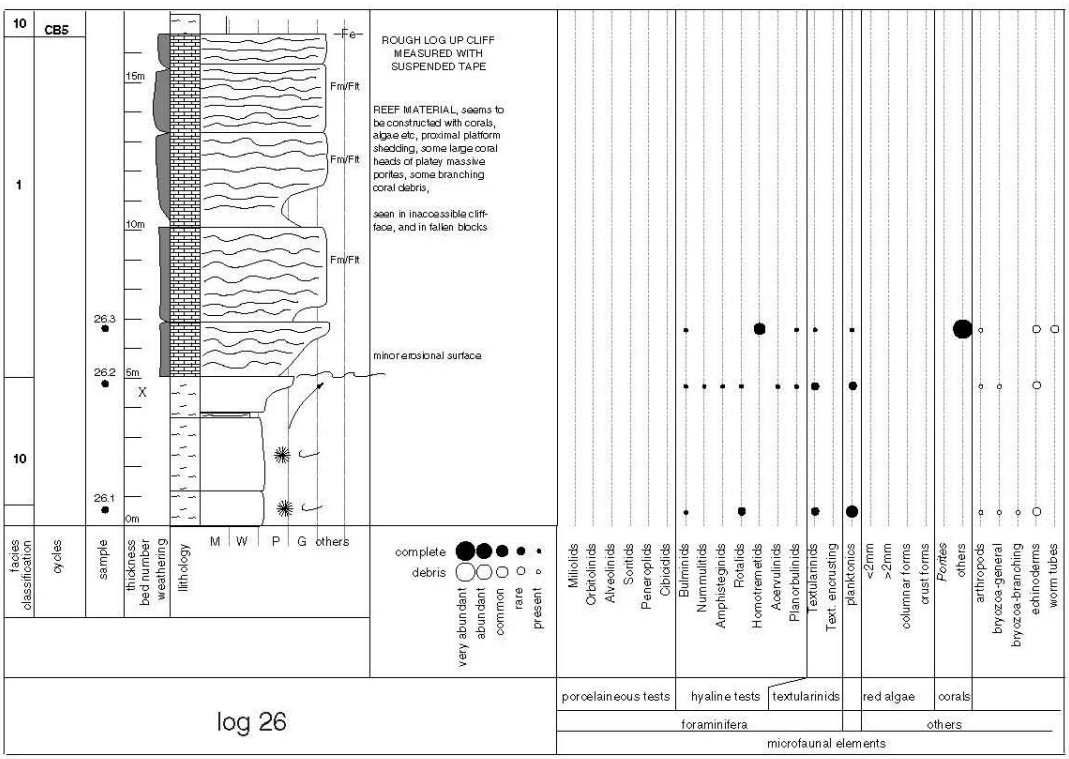

Figure 10.12 logs 25 and 26 (Kizil Kaya)

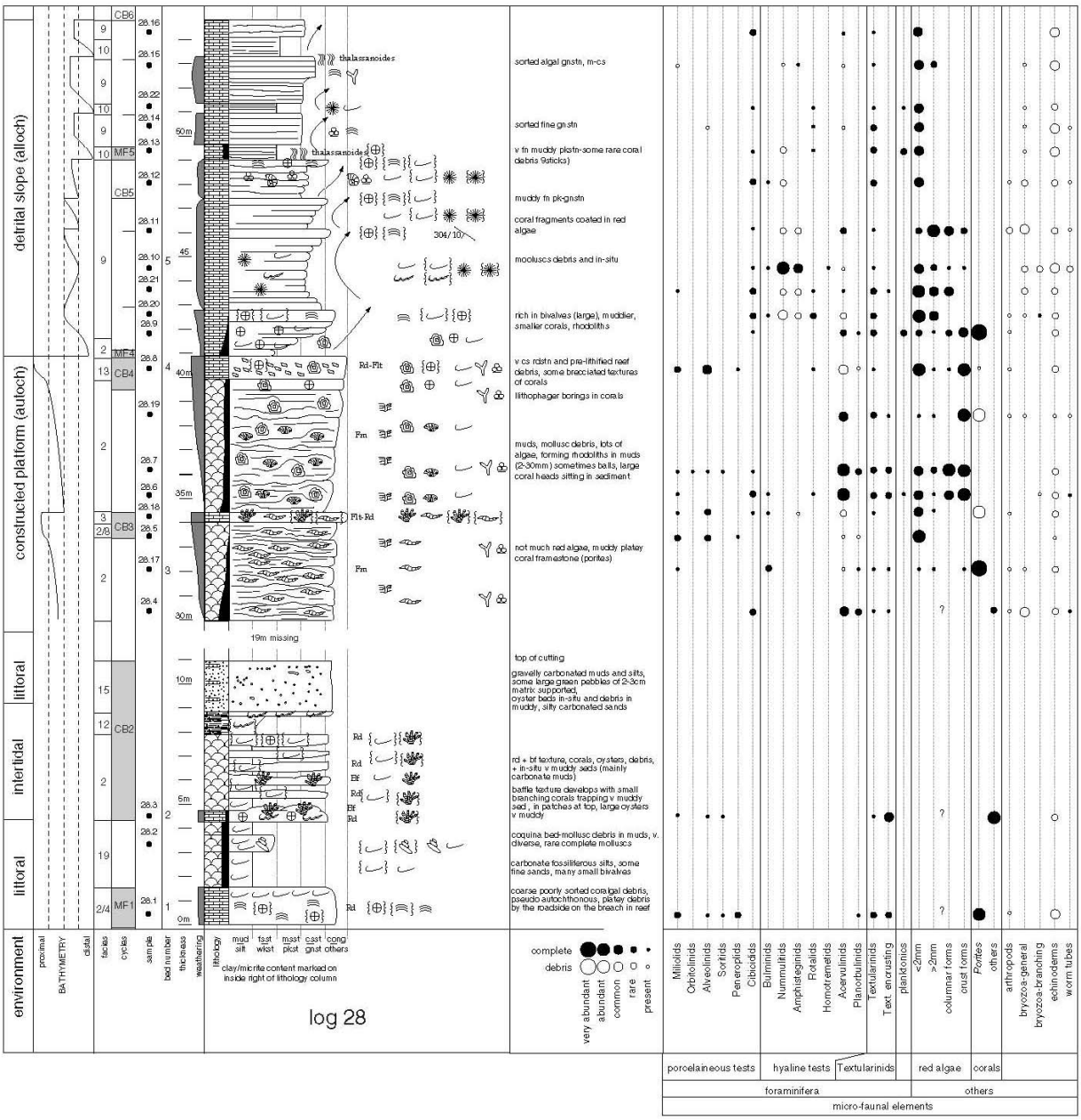

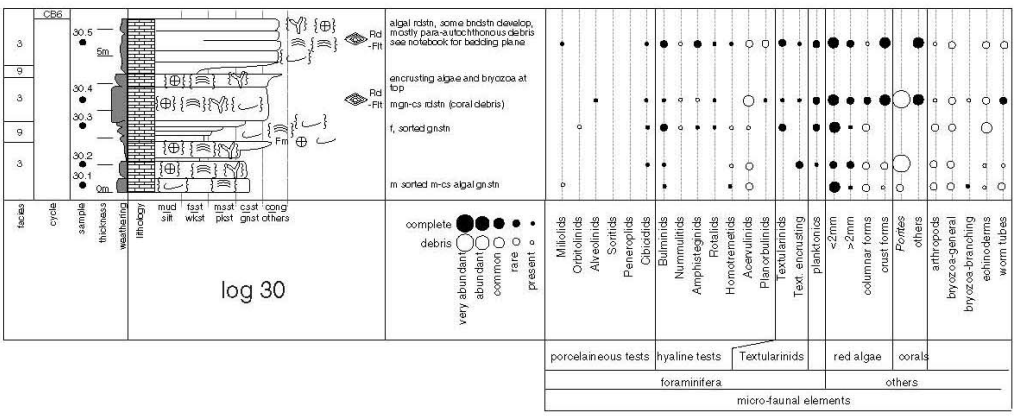

Figure 10.13 logs 28 and 30 (Kizil Kaya)

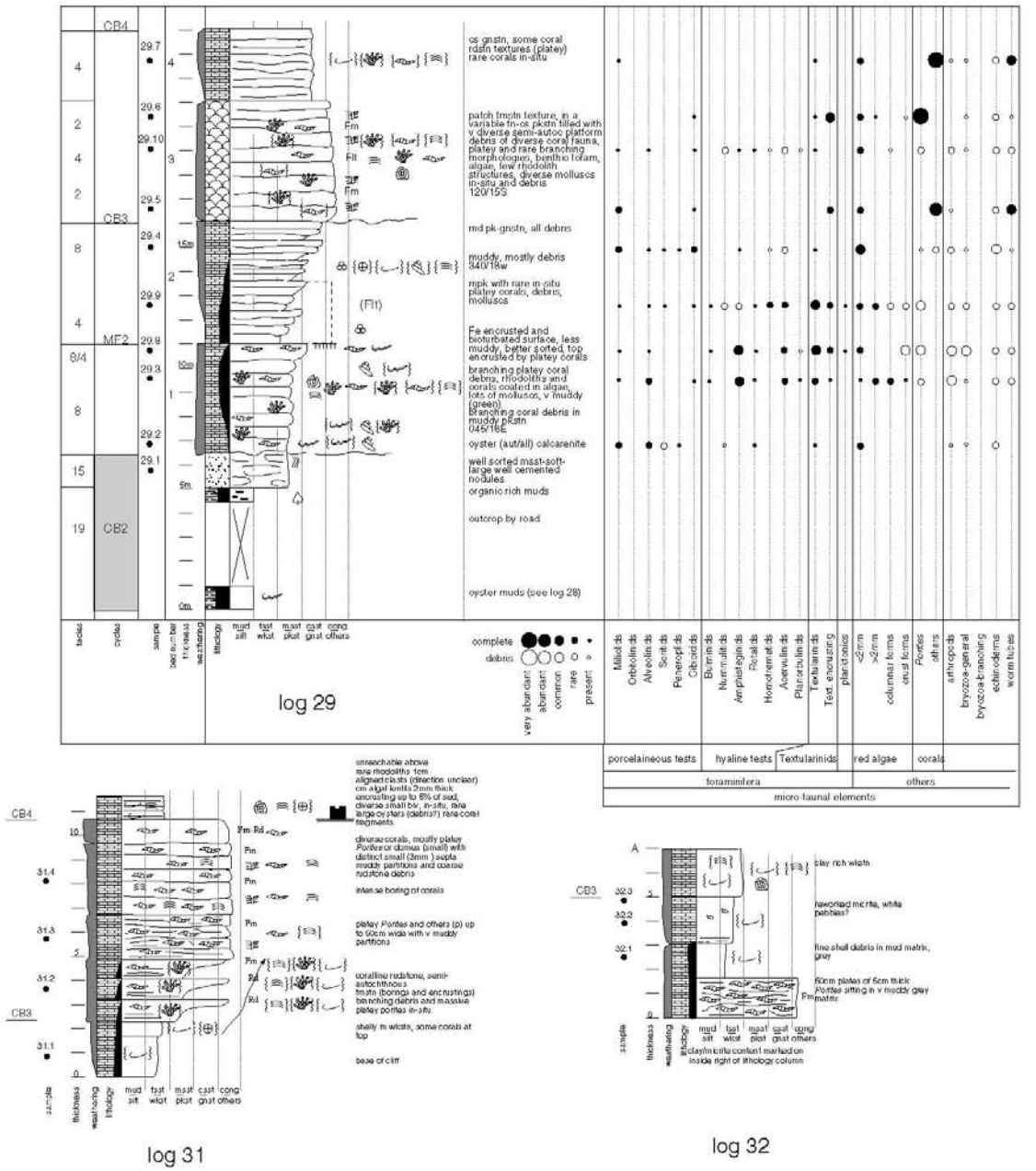

Figure 10.14 logs 29, 31, 32 and 36 (Kizil Kaya)

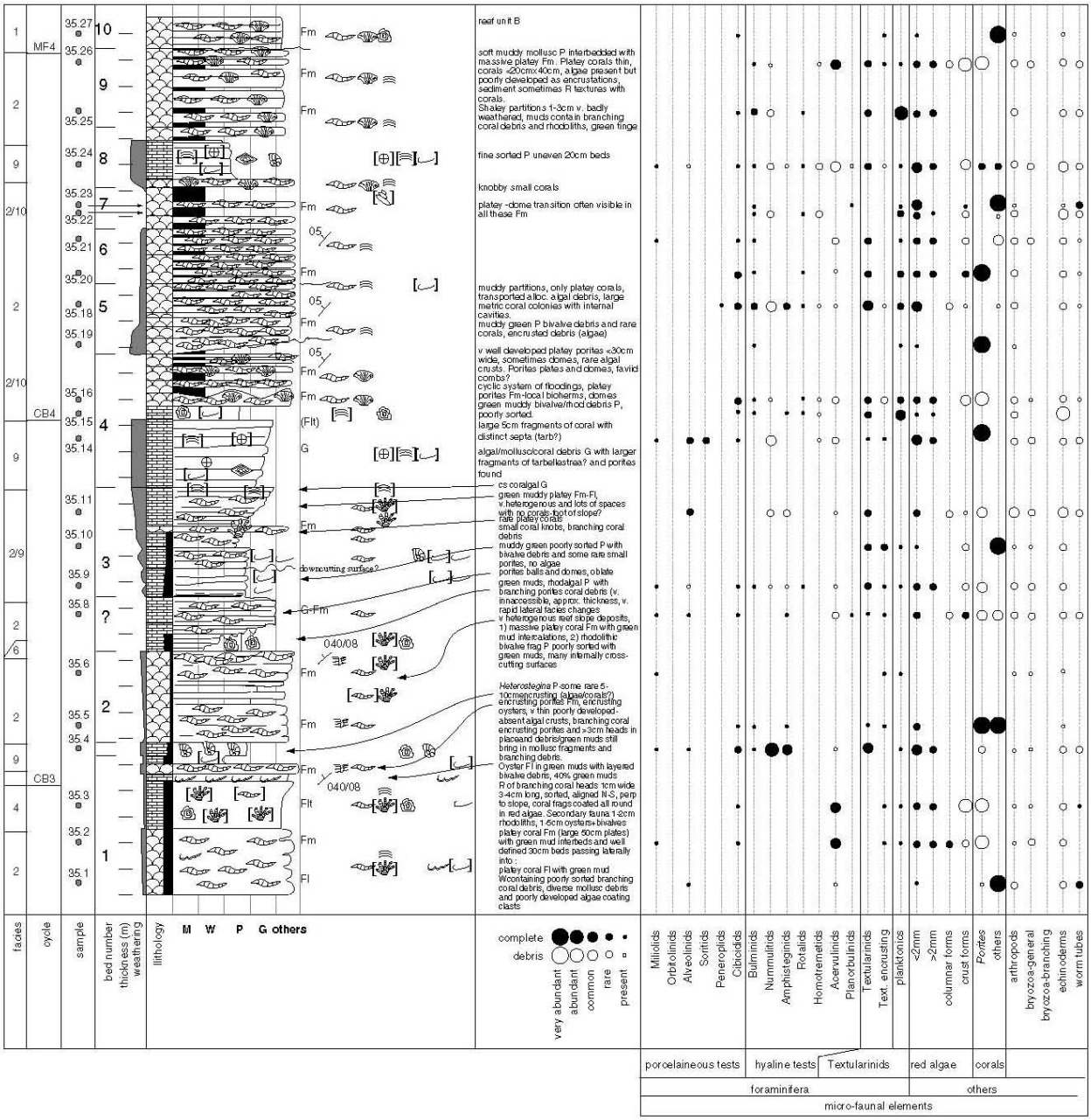

Figure 10.16 log 35 (Kizil Kaya)

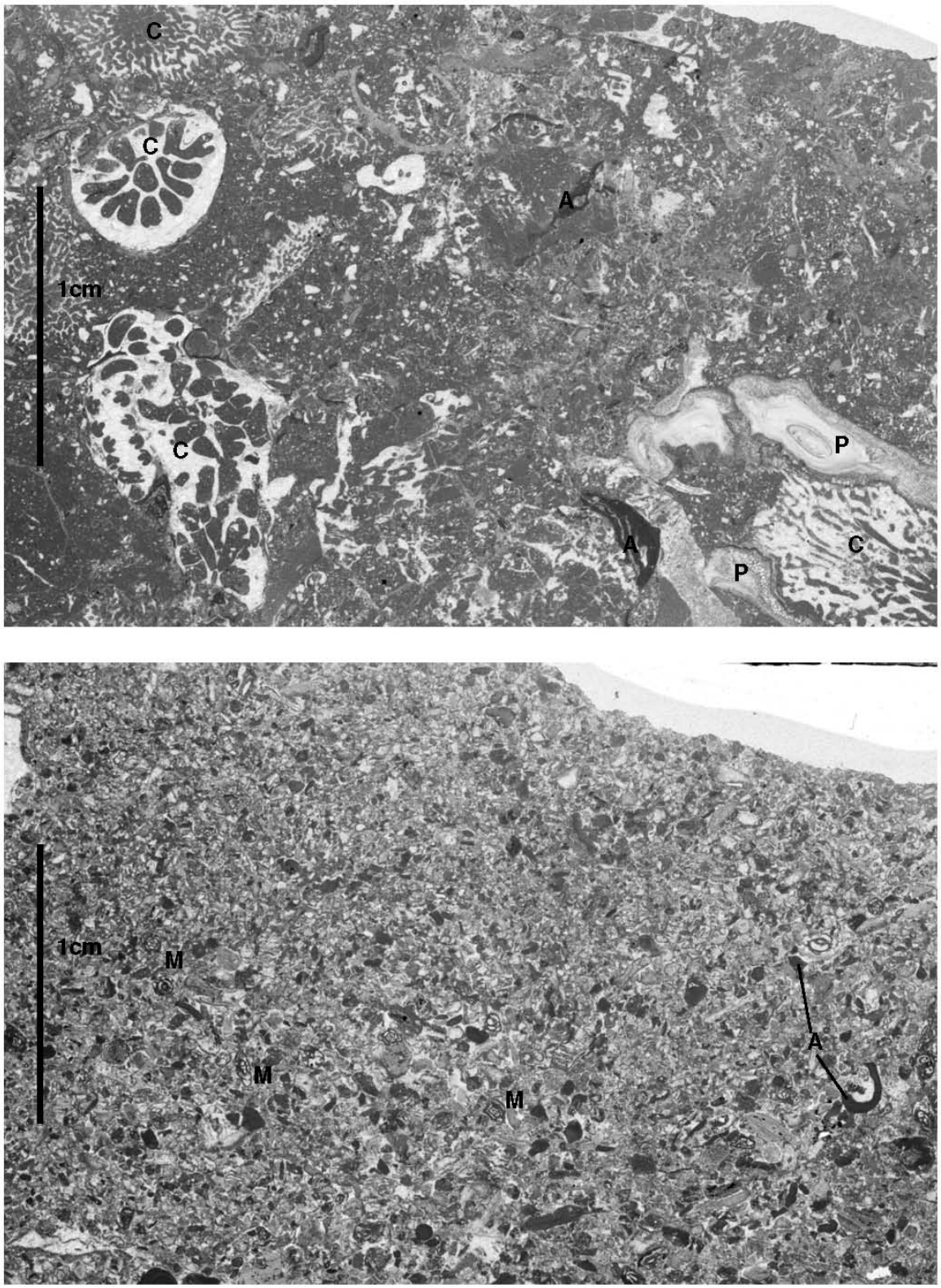

Figure 10.17 log 28 textures, plate 1: Thin section scale photos of the sedimentary textures for cycle 2 as seen on log 28 in Kizil Kaya. The first section (sample 28.17, above) shows a muddy coralgal floatstone typical of the transgressive phase of this cycle in this log. P indicates Pelecypod fragments, C coral fragments of diverse kind, and A indicates rare fragments of coralline red-algae. The second section (sample 28.5, below), shows a medium, sorted grainstone belonging to the regressive part of cycle 2 on log 28. Diverse Miliolid forams are common (M), and coralline red algae is an abundant constituent of the sediment (A).

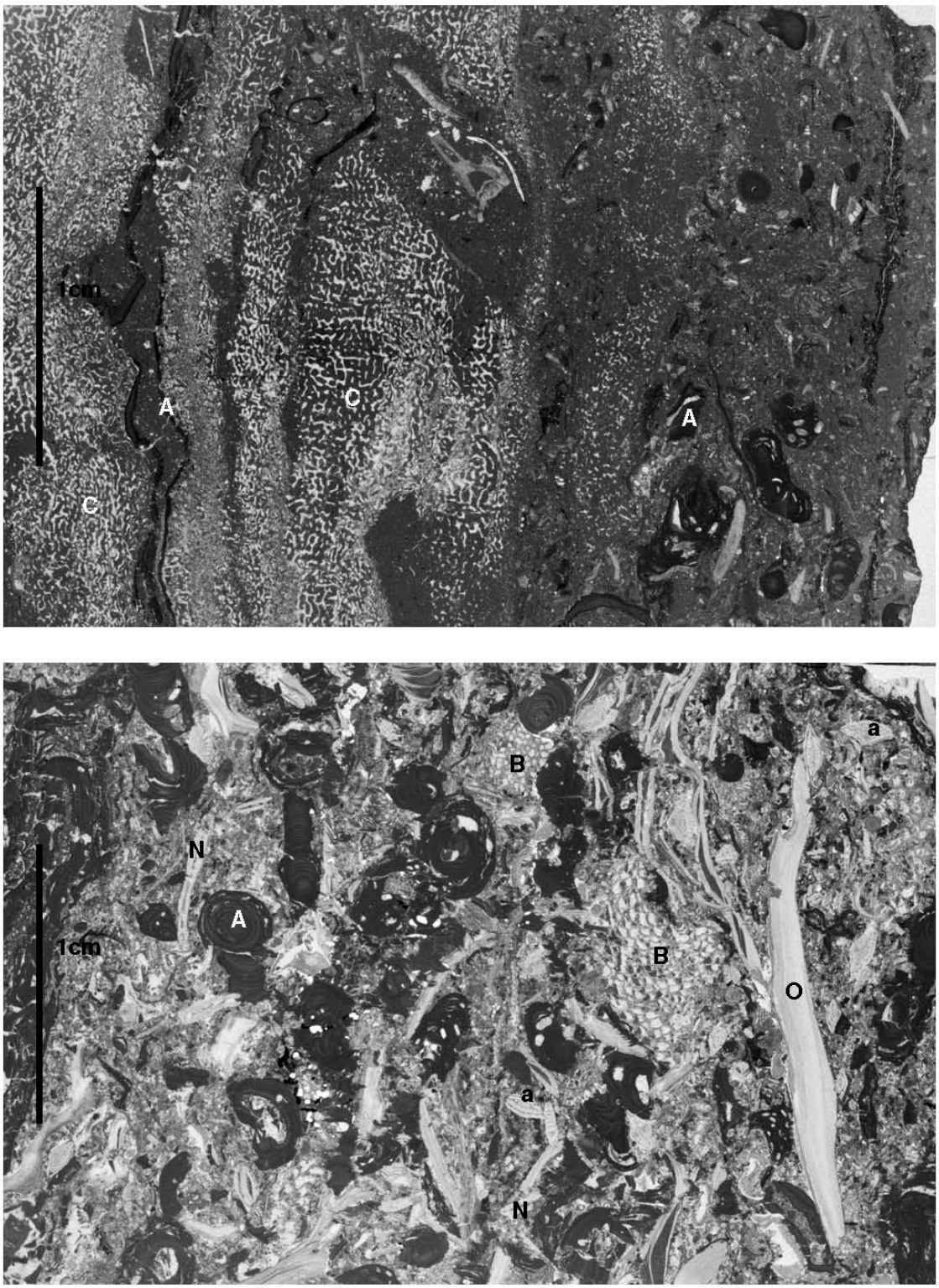

Figure 10.18 log 28 textures, plate 2: Thin section scale photos of sedimentary textures for cycle 4 as seen on log 28 in Kizil Kaya. The first section (sample 28.9, above) shows a *Porites* coral (C) with some encrusting coralline red algae (A), and dark muddy sediment containing columnar fragments of red-algae, this represents toeset deposits during the transgressive part of cycle 3. The second section (sample 28.11, below) shows toeset rudstone deposits belonging to the regressive part of cycle 3: columnar fragments of coralline red-algae (A), bryozoan debris (B), and diverse bivalve debris, mainly oyster fragments (O), are abundant. Nummulitid (N) and Amphisteginid (a) foraminifera, typical of the slope environment, are also very common here (up is to the left in both photographs).

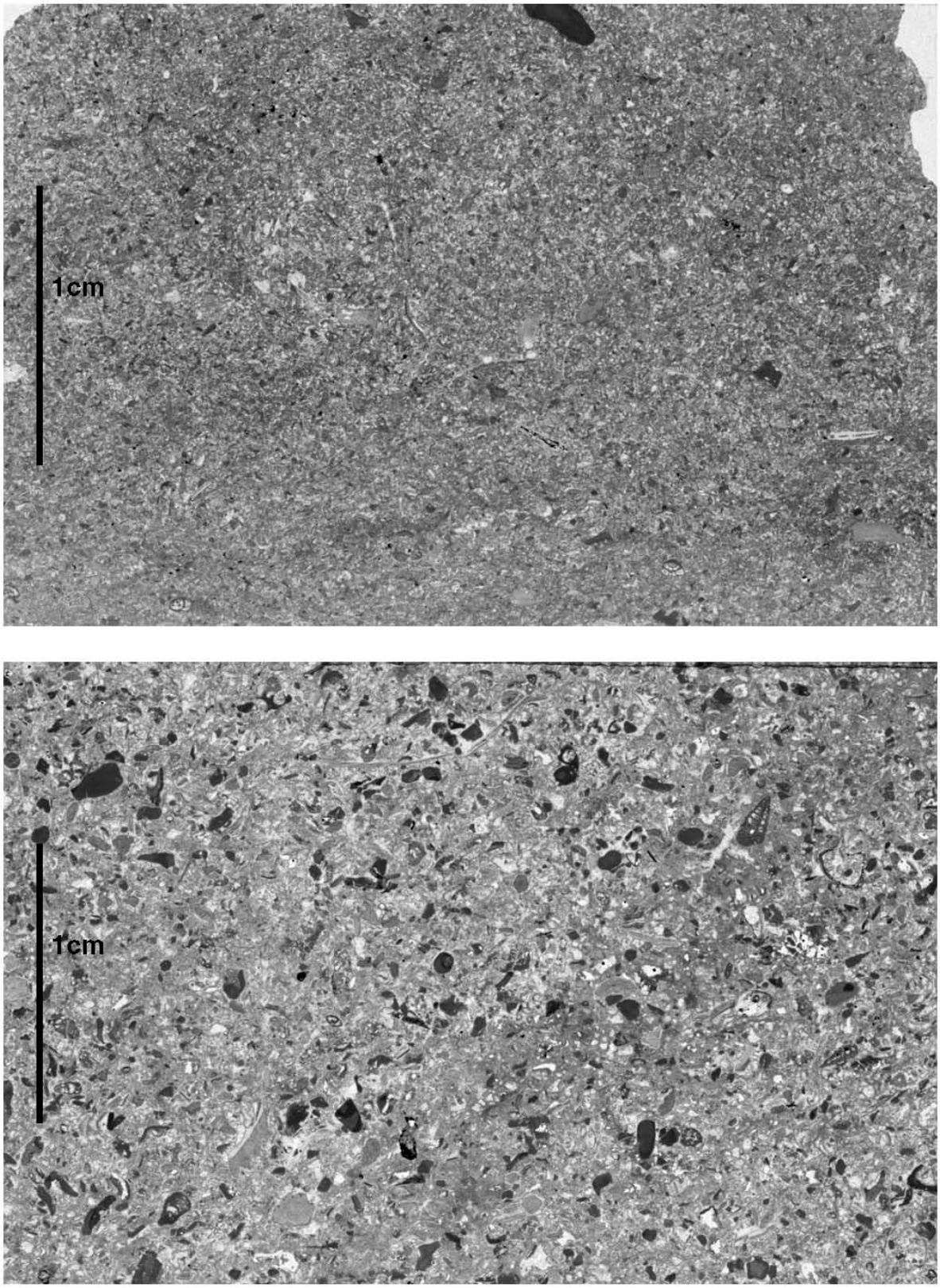

Figure 10.19 Thin section scale photos of the sedimentary textures for cycle 5 as shown on log 28 in Kizil Kaya. The first section (sample 28.13, above) shows a micropackstone facies 10), the finest end-member of the coarsening up beds, while the second section (28.14, below) shows the coarsest end-member of these same beds.

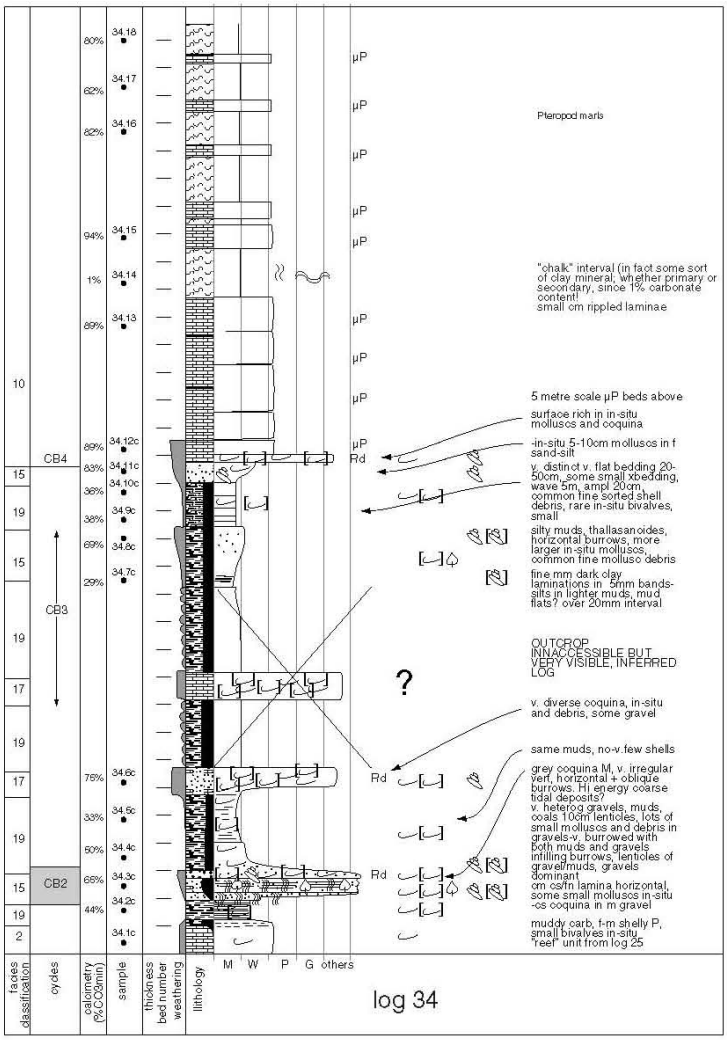

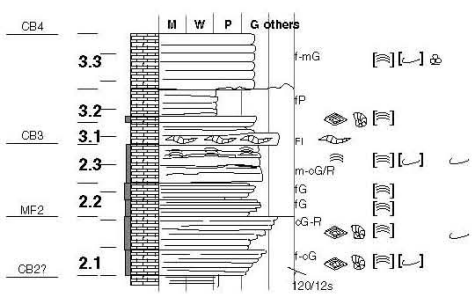

log 37

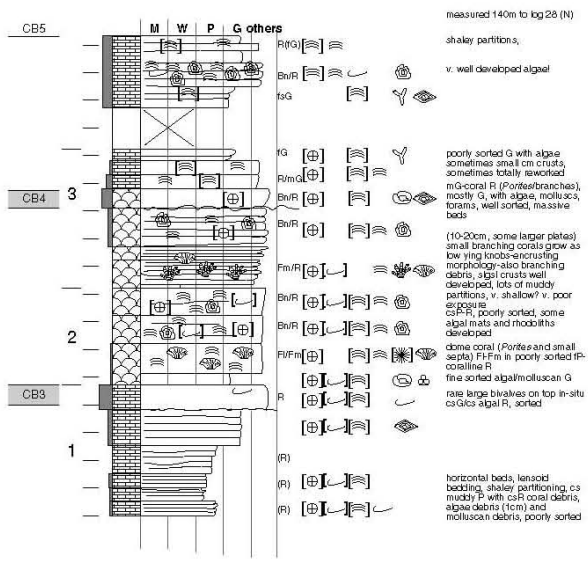

log 38

Figure 10.15 logs 34, 37 and 38 (Kizil Kaya)

11 - SYNTHESIS

This chapter synthesizes the observations from the Mut region and from the Silifke region into a stratigraphic evolution story, based on correlations made locally, and then between the two regions. The method by which the correlations are made is explained here. The implications of these correlations will be analysed in the discussion chapter that follows, not in this chapter.

The nature of the study areas is highly varied: each occupies a different position on a platform to basin profile, and contains different lithologies and organisations. The Alahan section is situated in a shallow platform-top setting, and is a mixed carbonate-siliciclastic system. Only sediments deposited during the relative sea-level high stands are preserved here, while the sediment deposited during times of sea-level low stand are represented by omission surfaces. The Pirinç section describes a platform to basin profile of a carbonate system, with most of the description situated in the basinal area. Sediments deposited during the sea-level lowstands and transgressions are extensively described, while the highstand sediments have only been observed from a distance in the cliff-face. The Dibekli site describes a dominantly carbonate system with the episodic arrival of small amounts of siliciclastics, deposited against a steep basement topography. Sediments deposited during sea-level low stands and transgressions are most frequently preserved here.

So at first sight it seems problematic to want to draw any convincing correlations between them. However, by accepting that any eustatic signal that may exist will be experienced throughout the basin, and that the tectonic setting of each area is not dramatically different, the construction and comparison of a relative sea-level curve (eustasy and tectonics combined) allows correlations to be proposed.

11.1 CONSTRUCTION OF THE RELATIVE SEA-LEVEL CURVES

Figures 11.1-4 reconstruct the undecompacted relative sea-level (eustasy and subsidence) evolution for four of the study areas (Dibekli in the Silifke area, Alahan, Pirinç and Zincir Kaya in the Mut area). On the right-hand side an undecompacted synthetic stratigraphic column is displayed: this is generated from the stratigraphic cross-section for each area. The synthetic log is simplified and does not represent the complex internal facies variations, however, care is taken to mark on all the surfaces that have been identified as cycle boundaries. The vertical scale is in metres (indicated in metres above sea-level, ie. modern altitude), while the horizontal scale is in arbitrary time units. Decompaction is not performed because the absolute values of the relative sea-level variations are not of primary importance to the analysis that follows, and because the development of a decompaction procedure is beyond the scope of this study. It is the hierarchical organisation, and the relative position on the sea-level curves that are of interest here, and these do not require decompaction to be resolved.

To construct the relative sea-level curve a tie-point method used is similar to that of Goldstein and Franseen (1995). Key horizons are chosen from the synthetic log that are considered to represent extreme values of the relative sea-level variations (minima and maxima): upper and lower limits of facies packets are chosen, as well as important surfaces within a facies packet, including any horizon that has been interpreted as a cycle boundary. For a given horizon the bathymetry of the sediment is estimated. This bathymetry is added to the vertical position of the horizon, and is plotted as a point, an arbitrary distance to the right of the last point plotted (in chronological order). Intermediate values between chosen horizons are considered to lie on the continuum of values between the extremes corresponding to the horizons chosen above and below. This continuum is plotted as linear in time.

A surface representing an abrupt facies change will generate two data points: one estimated from the sediment below the surface and the other from the sediment above.

Where there is evidence for exposure on a surface, with deposition of sediment laterally below the surface (a "lowstand"), it may generate three data points: from the sediment above, below, and from the estimation of the sea-level drop or missing sediment. Quantifying the sea-level drop may be problematic, and a gap is often left to represent this missing sediment/time. Such estimates are made from the stratigraphic reconstructions of each area: shallow marine onlap of sediments often gives the best quantitative control.

Small cycle boundaries where an actual relative sea-level fall is uncertain are nevertheless indicated by a small knee, or drop, in the curve. The actual value of this drop is negligible (<4m), and the error bar indicates the uncertainty in this representation.

This methodology is illustrated for the Dibekli study area (figure 11.1):

Value 0 is the initial flooding of the basement topography in this area. The small drop between 0 and 1 is added to represent the small-scale cycle boundary that defines the top of the siliciclastic unit and the transition to carbonates. Value 1 is calculated from the top of platform 1.1. The top surface is added to the estimated bathymetry of the sediment at this top surface, and the error margin is estimated. The topmost facies is estimated to be deposited in a shallow platform environment, from 0-20m water depth. Value 2 is the estimate of the relative sea-level drop at this surface. This is problematic to estimate. The drop could be as little as a short period in the intertidal regime, or could be a major sea-level drop of several tens of metres: hence the error bar ranges from 0 to -40m, and the actual value used is dotted in to highlight the uncertainty. Value 3 uses the top of the marls of cycle 1 as the reference point. The bathymetry of deposition of these marls has been estimated at greater than 40m. This top surface is erosional, so the estimated values are minimum values. Value 4 uses the base of the fan delta in cycle 2 as the reference surface. This is the same surface as that used for value 3. There is an abrupt facies change across the surface, but when the estimated bathymetries are taken into account above and below the surface the relative sea-level calculated is different. The bathymetry of deposition of the fan delta is estimated at 0-5m (very shallow marine). However, before the fan delta is deposited erosion occurs, and this is expressed as a hiatus. A small drop is added to represent the small-scale cycle boundary that defines the top of the siliciclastic unit. Value 5 takes the top of platform 2 and adds 0-10m estimated bathymetry. Value 6 is an estimate of the sea-level drop at the top of this platform, as implied from the slumping and from the macro-dissolution features in outcrop on this platform. The magnitude of the sea-level fall is difficult to estimate, the error margin is large, and the actual value is expressed as a hiatus. Value 7 takes the top of the marls in cycle 2 as the reference. The bathymetry of deposition of these marls has been estimated at greater than 40m. This top surface is erosional, so the estimated values are minimum values. Value 8 uses the base of the fan delta in cycle 3 as the reference, with an estimated bathymetry of 0-5m. However, before the fan delta is deposited erosion occurs, and this is expressed as a hiatus. Between values 8 and 9 a small drop is added to represent the small-scale cycle boundary that defines the top of the fan-delta deposits. Value 9 takes as reference the top of the platform 3.1 and adds 0-10m bathymetry. Value 10 estimates the sea-level drop implied from this surface, taking into account the lateral extent of the karst features. Once again, the error margin associated with this value is large, so the drop is represented as a hiatus (an expression of the gross uncertainty of the value of the fall). Value 11 uses the top of the platform 3.2 as the reference horizon, with 0-10m added as the estimated bathymetry. Value 12 is the estimated sea-level drop associated with the top surface of platform 3.2. The error margin is large, and the drop is once again represented by a hiatus. Value 13 is taken from the marls overlying this surface: the bathymetry of such sediment is estimated as being deposited in greater than 40m of water.

11.2 CORRELATIONS BETWEEN THE RELATIVE SEA-LEVEL CURVES

Figure 11.5 superimposes the relative sea-level curves for each site so their magnitudes and organisation can be compared. Figure 11.6 presents the correlations made between these curves, and shows the relationship between times of cycle boundary formation (grey vertical lines) in the different areas. Figure 11.7 illustrates the correlations made between the synthetic logs for each area by reconstructing a south-east to north-west schematic transect across the Mut Basin joining the different study sites. Figures 11.8 and 9 re-label the detailed study sites with the new homogenised and correlated cycle names. Note that these do not correspond to the cycle names used in the results chapters when presenting the individual outcrops. The correlated large-scale cycles are re-named using A-F to highlight this change and avoid confusion.

The correlation process starts at the large scale and works down, getting finer with each step. The biostratigraphy defines the largest scale correlations. Then relative sea-level cycles are correlated. Large-scale cycles allow broad packets to be correlated beyond the resolution of the biostratigraphy. Peaks of relative sea-level are correlated with peaks, and troughs with troughs. Then within each large-scale cycle the medium-scale cycles can be compared and correlated, and then eventually the small scale cycles. The time axis is plastic, as the original time

distribution for each curve is arbitrary. When correlations are made between these curves this time axis can be stretched or compressed as need be, with no loss of information. Once the correlations have been constructed a hypothesis is be made about the distribution of time at the resolution of the finest cycles defined, and the cycles can then be plotted out against time.

Qualities of sameness and difference are examined between the four relative sea-level curves, and between the stratigraphic architectures associated with these curves. A relative sea-level motif (amplitude and hierarchical organisation) may be repeated in different areas to produce very different stratigraphic architectures, though the fundamental motif (the driving factor) is relatively unchanged. In different settings this relative sea-level motif may be more or less easy to determine, or may be completely masked, whether due to absence (omission surfaces) or stratigraphic noise or damping.

Relationship between relative sea-level cycles and retrograding-prograding cycles

Each relative sea-level cycle contains a corresponding retrograding/prograding cycle boundary, or cycle boundary zone. However, the cycle boundary is found on the downward limb of the relative sea-level cycle, offset from the peak. This is because the position of the cycle boundary is controlled by the ratio between the rate of change of relative sea-level and the sediment deposition rate, and is not a function only of relative sea-level.

The cycle boundary positions at different scales are marked on the correlated relative sea-level curves in figure 11.6.

Biostratigraphic correlations

The biostratigraphic framework defines the major correlations made. In each area the nannoplankton NN4/NN5 boundary has been identified. The interval between the last NN4 sample and the first NN5 sample is marked on the relative sea-level curves in figure 11.6. The stratigraphic interval between the initial marine flooding of the continental Derinçay deposits, and this boundary is all NN4 (Late Burdigalian) in age.

Large-scale cycle correlations

Within the NN4 interval three large scale cycles of similar amplitudes of relative sea-level fluctuation have been defined in each of the study areas (Alahan and Pirinç in Mut, and Dibeki in Silifke). These cycles are correlated one to another (see figure 11.6). The logic controlling the positions of the cycle boundaries has been developed in the previous chapters describing each site (Chapters 6-10). These large-scale cycles have been renamed A-F.

Medium-scale cycle correlations

Cycle A (age: NN4): within the first large-scale cycle six medium scale cycles have been defined (named A.1, A.2...). Cycles A.1-A.5 have been correlated between the Pirinç area (Mut) and the Zincir Kaya and Kizil Kaya isolated platforms (Mut). Cycles A.1-A.4 belong to the isolated platform interval and possess a relative sea-level motif that is expressed in the stratigraphic architecture by very distinct stratal geometries: in cycles A.2 and A.3 20-25m retrograding isolated mounded build-ups dilate during the progradation to create isolated platforms. This happens twice, and is separated by a distinct cycle boundary (A.3) which has been doubled up by the superposition of small-scale cycles (A.3.1 and A.3.2). This organisation can be identified in Zincir Kaya, Pirinç Suyu and Kizil Kaya (see figures 11.8), and acts as the tie point from which to correlate the cycles found above and below this distinct interval (cycles A.1, A.5 and A.6?). The correlations with the Silifke region (Dibekli study site) are less straightforward. By superimposing the relative sea-level curves for Pirinç (Mut) and Dibekli (Silifke) with the relative sea-level maximum of the top of cycle one as a datum, it is clear that the isolated platform unit (Mut) and the bioclastic tidal deposits (Silifke) are coeval. However, the exact correlation of the medium-scale cycles between the two areas is uncertain, within an error of plus or minus one cycle. It is proposed that the shut-down in carbonate production between the two areas is approximately synchronous. This supposition implies the correlation of the last cycle boundary (A.6) in the shallow-water carbonates.

Cycle B (age: NN4): within this large-scale cycle, five medium-scale cycles have been identified. Cycle boundaries B.1. B.2 and B.3 defined in the Dibekli area and in the Pirinç area (not B.2), correspond to the large-scale cycle boundary B in the Alahan area: during the deposition of cycle B.1-2 in Dibekli, the Alahan area remains sub-aerially exposed. This conclusion is reached by superimposing the relative sea-level curves (see figure 11.5) and observing that cycles B.1 and B.2 fit most readily into the gap provided by the exposured interval in Alahan. Also, the Alahan relative sea-level curve offers no suitable candidates for correlation. Cycles B.4 and B.5 have been recognised only in the Alahan area, since they occur towards the top of the relative sea-level cycle, and lie in too proximal a position to have been observed in either the Dibekli or Pirinç study areas.

Cycle C (age: NN4): six medium-scale cycles have been identified in this large-scale cycle. The lower four of these cycle boundaries (C.1-C.4) have been identified in the Pirinç study area. When the relative sea-level cycles are superimposed (see figure 11.5) using the maximum peak of large scale cycles B or C as a datum, it is seen that cycle boundaries C.1-C.4

correspond to the hiatus contained in cycle boundary C in the Alahan area. The upper three cycles (C.4-C.6) have been found in both Alahan and Dibekli areas. By aligning the relative sea-level curves to the maximum peak of cycle C it is observed that the Dibekli and Alahan cycles C.4-C.6 have a very close fit.

Cycles D and E (age: NN5): cycles D, E and F of Langhian age have been defined in this correlation scheme, though they are beyond the scope of this study. They have only been identified in the Alahan area, and hence are not correlated. Cycle D has been sub-divided into five medium-scale cycles, and cycle E into three (or possibly 4?).

Small-scale cycle correlations

Small scale cycles have been distinguished in two situations, both in the Alahan area. In cycle A they have been defined at the top of the cycle in a shallowing-up siliciclastic sequence. In cycle C they have been defined in cycles C.4 and C.5 in a mixed carbonate-siliciclastic environment. They have not been correlated between areas, since they have not been observed elsewhere.

11.3 PALAEOGEOGRAPHIC RECONSTRUCTIONS

This part describes the evolution of the Silifke and Mut regions with the help of the palaeogeographic maps reconstructed from the field data (figures 11.10-20). The map numbers are indicated on the correlation diagram in figure 11.6, allowing comparison of contemporaneous environments. The reconstructions are discussed here in chronological order, and switch between the Silifke and Mut regions. The terms sea-level lowstand, transgression and highstand are applied here to describe the approximate sea-level position in the large scale cycles. Note that no systems tracts have been defined in the sediments.

Basin opening phase (Late Oligocene-Early Miocene)

Silifke 1 (figure 11.10): a narrow graben structure opens during the Late Oligocene to Early Miocene (Aquitanian) controlled by normal faulting which is now orientated at 100-110°. The graben extends over 20km in an east-west direction, being a connecting passage between the Mediterranean Basin (to the south-east) and the Mut Basin (to the north-west). At its narrowest point it reaches 4km in breadth between the bounding faults. The graben is now assymmetrical, with gradual downstepping into the graben on the northern flank by a series of normal faults, and a single bounding fault with a large offset on the southern side.

The graben is partially filled by coarse alluvial conglomerates with the depocentre at the narrowest point of the graben structure, where over 300m of deposits are found. This estimate is calculated by interpolation during the construction of the isopach and isobath maps for the interval, see figure 4.8. The morphology of the depositional locus indicates that the major source direction is perpendicular from the crests of the rising footwall blocks. This is indicated by arrows on the diagram.

Mut 1 (figure 11.14): the normal faulting that defines the basin (now striking 100-120°) is active during the Late Oligocene to Early Miocene (Aquitanian). The flank of the basin rises rapidly to the north. 900m of vertical offset over a horizontal distance of 6km are now preserved, but an important proportion of this (over 300m) is considered to be post-depositional (Late Miocene to recent) tilting and basin subsidence. The modern mountain Mahras Dagi is a horst structure, plunging to the south-east, and rising up to the same altitude as the basin flanks to the north. The graben structure defined by this faulting is partially infilled by syn-extensional continental clastics of a diverse nature, thickening to over 250m at the depocentre in the middle of the graben (from the isopach reconstruction in figure 4.6). Coarse grained alluvial fan deposits are found against the northern flanks of the basin, while the axis of the graben contains fluvial channel and flood-plain sediments with a very high mud to channel-sand ratio. Lacustrine deposits are found to the south against the northern bounding faults of the Mahras Dagi horst structure. The major source axis, at least for the fluvial system, is considered to be (from the depositional locus, and from the flow directions within the fluvial system) along the graben axis from the north-west end. A palaeo-Goksu River, sharing a similar drainage pattern as the modern Goksu, is defined. The limits of the floodplain are approximately defined by metre scale shallow marine oyster-bearing mud intervals interbedded with the floodplain muds, found to the south and to the south-east of the study area. This limit is shown on the diagram. The exact time relationship between the different continental clastic units is uncertain.

Cycle A sea-level lowstand-transgression (age NN4)

Silifke 2 (figure 11.10): cycle A.1-5: these cycles are deposited in a low but rising sea-level position. During this time up to 80m of cross-bedded bioclastic sands (grainstones and rudstones) are deposited under the action of bi-directional currents generated by tidal processes in the strait topography formed by the graben. Current directions are indicated in the diagram from measurements of cross-bedding azimuths.

During this time minor syn-sedimentary faulting has been observed (the fault is marked on the diagram, see figure 8.15), though the throw is small (20m) and these deposits are considered as post-extensional. This unit is internally divided into a number of cycles, with cycle boundaries picked out by the arrival of siliciclastic basement pebbles across a bedding plane surface. The cross-bedding bedset heights shows a decreasing trend upwards, starting with bedforms 12-15m high, decreasing to 1m high bedsets.

Mut 2-5 (figures 11.14-16): cycles A.1-6: this interval has been broken down into four phases, due to the detailed study of the isolated platform outcrops at Kizil Kaya and ZIncir Kaya. These phases correspond to cycles A.1, A.2-3, A.4-5, and A.6 respectively. These phases are illustrated in figures 11.14, 11.15, and 11.16. No syn-sedimentary structural activity has been observed for this interval.

In the first phase, cycle A.1, a low-relief carbonate platform 15-20m develops, with relatively tabular, biostromal geometries. Slope, external platform (carbonate dominated), and internal platform (clay dominated) environments have been observed. The Kizil Kaya outcrop is situated in the internal part of this platform, where littoral to sub-littoral muds dominate, with thin intervals of coquina beds, oyster beds, thin muddy reefal carpets, and cross-bedded siliciclastic sands (see figure 11.8). The Zincir Kaya outcrop is situated on the external platform, where constructed carbonate facies dominate. Patches of muddy coralgal framestones 5-10m across develop, separated laterally by grain and packstones containing Miliolids and Nummulitids. The platform slope can be seen on the south-east side of Zincir Kaya: it forms a relief 20m high, ie. the height of the platform cycle. During the retrogradation the slope is dominantly a constructed reefal framework (coral carpets) while during the progradation the arrival of Miliolid grainstones and coralgal floatstones dominates, with no constructed slope developing.

The second phase corresponds to cycles A.2 and 3. A muddy internal platform to the north-west, as well as a carbonate dominated external platform, and slope have been distinguished. Within this cycle the retrogradation and the progradation represent two distinct phases of platform architecture. During the retrogradation littoral to sub-littoral muds are deposited in the internal platform. These are observed on the landward side of Kizil Kaya. While on the external (carbonate dominated) platform isolated build-ups develop. These can be observed in Zincir Kaya, and inferred in Kızıl Kaya. They are made of muddy coralgal framestone, 20m high, and 100m or more across. The position of the slope developed in the previous cycle (A.1) does not change (seaward side of Zincir Kaya), and during the retrogradation these slope deposits are constructed coralgal framestones, forming coral carpets separated by thin marl beds. During the progradation littoral to sub-littoral muds continue to be deposited in the internal platform, while on the external platform the space around the isolated build-ups is partially filled by muddy coralgal autochthonous and pseudo-autochthonous facies, prograding out from the isolated build-ups developed during the retrogradation. These incompletely fill out the platform area, creating a patchwork of coalescing to isolated build-ups. The edges of these build-ups on the platform are erosionally bevelled, and this may be associated with the development of currents in restricted passages between the build-ups. Also, a relative sea-level fall might have occurred during the late progradation of this cycle, creating an island topography. During the progradation the slope of the external platform undergoes extensive erosion, while during the early transgression of the next cycle cross-bedded shoals of Nummulitid grainstones are deposited at the foot of the slope. This indicates a change in hydrodynamic regime with an increase in energy, and possibly a relative sea-level drop, since no deposition occurs on the platform top. Cycle A.3 is structured in a very similar way to cycle A.2: during the retrogradation isolated mounded build-ups of muddy coralgal framestones 20-25m thick and over 100m wide grow, which then spread out laterally during the progradation. However, this spreading-out phase is less complete than in cycle A.2, and truely isolated platforms with a 25m topography form. The progradation sees the formation of up to 10m thick shoals of cross-bedded Nummulitid grainstones on the seaward flank of Zincir Kaya, preserving erosional truncation of the front of the isolated platform, and depositing nothing on the platform top. This shoal formation may be associated with a relative sea-level drop, the exposure of the platform top, and the heterogenisation of the local current flow field around the platform. This would be responsible for locally generating currents capable of creating shoals.

The third phase corresponds to cycle A.4-5, the top of the isolated platforms. During these cycles the isolated platforms continue to grow vertically, and to contract in area. Cycle limits become more difficult to distinguish, and prograding times are associated with increased deposition of bioclastic sands and rudstones on the slopes, exported from the platform top under the action of gravity processes. Deposition on the relict shelf area surrounding the isolated platforms is limited to thin beds of marls and micro-packstones (facies 10). To the north-west limit of the shelf area towards the coastal contact with the basement hinterland shallow water carbonate platform sediments are deposited. These consist mainly of bioclastic sands with no constructed facies found, and can be seen in the Pirinç area. To the north-west limit of the shelf area fine siliciclastics continue to be deposited, and the most north-westerly isolated platform (grid location 295680) is directly overlain by offshore muds and silts.

The fourth phase is the maximum flooding of cycle A (A.6 base). Deposition of shallow platform

carbonates is restricted to the north-east margin against the coastal onlap with the basement topography. Large 50m high clinoforms in the Pirinç study site are seen to retrograde up to the maximum flooding, before prograding out during the highstand described later. To the north-west siliciclastics continue to be delivered by the Palaeo-Goksu River, and offshore muds (seen at the base of log 7 in the Alahan area) are deposited in the area described.

Cycle A sea-level highstand position: (age NN4)

Silifke 3 (figure 11.10): cycle A.6: shallow platform carbonates develop against the northern flank of the graben in Silifke across a relatively wide area. These can be seen in the Seyhler outcrops in the east of the region, though the precise cycle limits cannot readily be defined. The cycle boundary 2 as defined in Dibekli is an erosional surface directly overlying marls, and no highstand carbonate platform has been observed against the southern flank of the graben. This seems to be because the basement flank is too steep, and a sufficient shallow-marine area is not available across which a platform may develop. The marls deposited during the retrogradation provide neither a firm substrate, nor a sufficiently shallow environment.

Mut 6 (figure 11.16): cycle A.6-top: the carbonate platform area against the northern margin of the basement progrades out to the south. This can be seen as 50-100m high clinoforms in the Pirinç outcrop. To the north-west, near the mouth of the Palaeo-Goksu a siliciclastic tide dominated shoreline can be seen to shallow-up to cycle boundary 2. This is determined from the facies evolution, though no geometries are visible. High frequency, small-scale cycles of tidal channels embedded in shoreface sands can be seen to develop within this siliciclastic complex.

Cycle B sea-level lowstand-transgression (age NN4)

Silifke 4 (figure 11.11): cycle B.1: relative sea-level falls exposing the platform deposits to the north of the graben, and eroding the marls deposited to the south. Marine waters once again fill a more restricted strait topography, similar to the early transgression of cycle A. This leads to the deposition of a packet of cross-bedded bioclastic sands under the action of strong tidal currents, directly overlying the tidal deposits of the transgression of cycle A. This stacking of the lowstands-transgressions of cycles A and B, and the bevelling of the edge of the platform developed in cycle 1 due to the sea-level fall can best be observed in figure 8.13 and log 50 in figure 8.16. During this time small amounts of siliciclastics produced by (local) erosion of the basement are fed into the marine environment. This is shown schematically on the palaeogeographic reconstruction as two fan deltas. The fan delta to the south is observed in Dibekli, and directly overlies the marls of the top of cycle A. It is likely that it post-dates the deposition of the tidal deposits, being deposited as the transgression of cycle B refloods the erosional surface formed during the sea-level fall.

Silifke 5 (figure 11.11): cycle B.2: a 2-4km wide carbonate platform develops on the northern flank of the Silifke graben during the transgression. The position of the margin of this platform is in constant backstepping during this time. These geometries can be seen in the Seyhler cliff interval in the east of the graben area. On the southern flank of the graben a 20m thick shallow carbonate platform develops on the top of the clastic fan-delta deposits during cycle 2.2. The coarse clastics below may have provided a local hardground permitting the development of shallow-platform carbonate fauna such as red algae and corals. This carbonate platform extends out beyond the limits of the fan delta, and directly overlays the marls below (see figure 11.9). Slumping collapse occurs in this carbonate platform. This is considered as a local effect and cannot be correlated with the slumps found in the basin area in log 2. These slumps in log 2 lie at or above the NN4/NN5 boundary, while the slump described here in cycle 2.2 is surrounded below and above in NN4 age marls. The cause of the slumping here is considered to be the loading of the weak, compactable marl sediments by a more rigid, and heavy, carbonate platform. A cycle boundary occurs towards the top of the platform, as indicated by a basement-pebble strewn interval, and exposure due to a relative sea-level drop may also have taken place, as indicated by the metre-scale dissolution cavities in the platform. If exposure did indeed occur then this would also be, in part, responsible for the slumping collapse of this platform. This platform is then covered by a few tens of metres of marls of NN4 age, also deposited during the retrogradation.

Mut 7 (figure 11.17): cycle B.1-2: a relative sea-level drop estimated at roughly 100m (see the relative sea-level curve for the Pirinç study site, figure 11.3) exposes the platform top to the north and the north-east of the area. The exact position of this emergent surface has been proposed in the Pirinç cross-section in figure 6.1 by following the strata up the slope and picking the most suitable horizon from field observations of the cliff-face, though it is inaccessible in outcrop. In the Alahan area this interval corresponds to a major erosional surface. During the sea-level drop collapse of the platform front occurs on the northern flank, sending slump deposits 2-3km out into the basinal marls. When sea-level is at its lowest position a narrow 10m thick carbonate platform develops in onlap against the front of the slump deposits. This can be seen in the Pirinç cross section (figure 11.8) and is labelled as cycle B.1. The

siliciclastic lowstand in the Alahan-Kizil kaya region is poorly outcropping, but has been identified as a siliciclastic peak recognised by calcimetry measurements in the fine-grained distal marl-siltstone series above the Kizil Kaya outcrop.

Cycle B sea-level highstand (age NN4)

Silifke 6: cycle B.3 (figure 11.11): this interval greatly resembles the highstand of cycle A in this area. On the northern flank of the graben a 3-4km wide shallow-water carbonate platform is deposited, while to the south no carbonate platform is seen to develop, apparently because the graben flank to the south is too steep.

Mut 8: cycle B.3-5 (figure 11.17): a shallow-water carbonate platform is seen to develop throughout the study area against the basement topography. In the Pirinç area the distance between the platform margin and the onlapping contact with the basement topography is estimated to be approximately 2-3km. In the north-west corner, in the Alahan area, a carbonate platform is also observed with a strongly prograding character, and slopes which are partially constructed, and partially consisting of exported shallow-platform debris. A thin siliciclastic interval is deposited, marking the top of this platform in the Alahan area. A medium scale cycle boundary and the subsequent retrogradation then reverts the area to a carbonate domain, and this last small carbonate platform is then exposed, with the exposure of a major karstified horizon, marking cycle boundary C.

Cycle C sea-level lowstand-transgression (age NN4)

Silifke 7: cycle C.1-4 (figure 11.12): the organisation of this interval on the northern flank of the Silifke graben is poorly controlled, though a reconstruction can still be proposed, based on the observations of the Seyhler cliff geometries and by extension from the Dibekli site on the southern flank. A basinward shift of the depocentre of the carbonate platform is inferred, with continued deposition of shallow-water platform carbonates. This implies development of an exposure surface on the platform, as the cycle boundary 3. Surface 1 in the Seyhler outcrop (see figure 8.23) is the most likely candidated for this surface.

On the southern flank in the Dibekli outcrop a relative sea-level drop of at least 50m (the Pirinç area gives a better estimate of this -see below) has been inferred, eroding the marls deposited during cycle B, and bringing out a small fan delta system over the marls and the underlying erosional surface.

Mut 9: cycle C.1 (figure 11.18): the Pirinç site provides good control on the amount of sea-level fall that occurred, and here it can be estimated at 120m. This exposes the platform top and provokes slumping collapse of the platform margin, sending slump deposits out 2-3km into the basinal marls. During the relative sea-level lowstand position a narrow 10m thick carbonate platform develops in onlap against the top of the slumps. These slump deposits have also been observed in the Alahan area, outcropping 1km to the north-west of Kizil Kaya. During this lowstand a karstified surface develops in Alahan (cycle boundary C). A similar surface is inferred in the Pirinç area, though this has not been observed because the surface is inaccessible. Exposure features can be seen on the margin front at this level, associated with the slump surfaces.

Mut 10: cycle C.2-3 (figure 11.18): two carbonate platforms (C.2 and C.3) are observed to progressively backstep against the relict top of the slump in onlap in the Pirinç area. No outcrop of this interval is seen in the Alahan area, and during the deposition of cycles C.2-3 the Alahan site described is considered to remain sub-aerially exposed.

Cycle C sea-level transgression-highstand (age NN4)

Silifke 8: cycle C.5 (figure 11.12): on the northern flank of the Silifke graben area a 2-3km wide carbonate platform develops. On the southern flank of the graben a narrow carbonate platform belonging to cycle C.5 develops. From the reconstruction in Dibekli (figure 11.9) it is shown that a shallowly sloping area of the basement topography is flooded, producing a wider platform area than found against steeper topography. This carbonate platform is topped by a medium scale cycle boundary, with evidence for exposure. This cycle boundary shuts down production in this area, so that give-up of the platform productivity occurs during the flooding of cycle C.6 and marls are deposited up to the large-scale maximum flooding of cycle C.

Silifke 9: cycle C.6 (figure 11.12): a wide carbonate platform develops during this period on the northern flank of the Silifke graben. On the southern flank a carbonate platform progrades out basinwards. A small-scale cyclicity superimposed on the highstand here creates at least two exposure surfaces, converging to the most important, which is the cycle boundary D, marking the top of the platform.

Mut 11: cycle C.4-6 (figure 11.19): in Pirinç the bedding geometries have been observed, though the facies have only been accessed on the eroded margin-front: no siliciclastic deposits have been observed in this interval here. The geometries show a rimmed carbonate platform with the back-reef area being repeatedly filled out by sediment backfilling from the margin. In the Alahan area the facies of this interval have been logged. This highstand is organised into 3 medium-scale cycles, C.4-6, each approximately 20m thick. These are shallowing-up siliciclastic cycles (or

"parasequences") which range from offshore/lower shoreface muds and silts, to uppershoreface/foreshore conglomerates, interpreted as fan-deltas. During each medium-scale retrogradation, the siliciclastic input is sufficiently diminished to allow the development of small isolated carbonate platforms. The carbonate production ceases as the siliciclastics prograde out over them.

Cycle D sea-level lowstand (age NN4/5)

Silifke 10: cycle boundary D (figure 11.13): a major relative sea-level fall of many tens of metres is inferred from the Dibekli site, both from the deeply karstified cycle boundary 4, and from the extent of the slumping collapse of the carbonate platform margin from the flanks of the graben, which can be correlated out to the basin section in log 2 by the biostratigraphy. The platform top is exposed throughout the area during this time, and slumping of the platform margin occurs where the margin was steepest (dominantly to the south). Such slumping has mainly been observed at the eastern end of the graben, where the passage is most restricted.

Mut 12: cycle boundary D (figure 11.19): a major relative sea-level fall is proposed in this area. In the Pirinç study site major slumping collapse of the platform margin is observed, corrsponding to large olistolith blocks in the basin. In the Alahan area a thick packet (more than 20m) of shoreface sands are deposited near the Kizil Kaya area, overlying offshore muds, silts and marls. On the platform top an erosional surface (the base of the last fan delta) cuts down into the siliciclastic deposits, and this is interpreted as sub-aerial exposure.

Cycle D sea-level transgression-highstand

Silifke 11: cycle D (figure 11.13): during this transgression, shallow marine carbonate platforms are deposited on the northern and southern flanks of the Silifke graben. The southern platform is reconstructed as being 1-2km wide: the increased width compared to previous south flank platform developments, is due to the flooding of a gently sloping shoulder of basement topography, creating a larger shallow marine area to that generated by previous transgressions, where relatively steep topography was flooded. The Dibekli site is covered with marls of NN5 (Langhian) age during this transgression, since the position of the platform margin has backstepped further to the south.

Mut 13: cycle D (figure 11.19): in the Pirinç area bedding geometries are observed that show the construction of a rimmed platform margin, with a number of back-filling progradation events occurring. No siliciclastic sediments have been observed in this interval at the platform margin front in the Pirinç area. In the Alahan area two 40-50m thick isolated platforms are constructed, possessing distinct back-reef, or lagoonal environments.

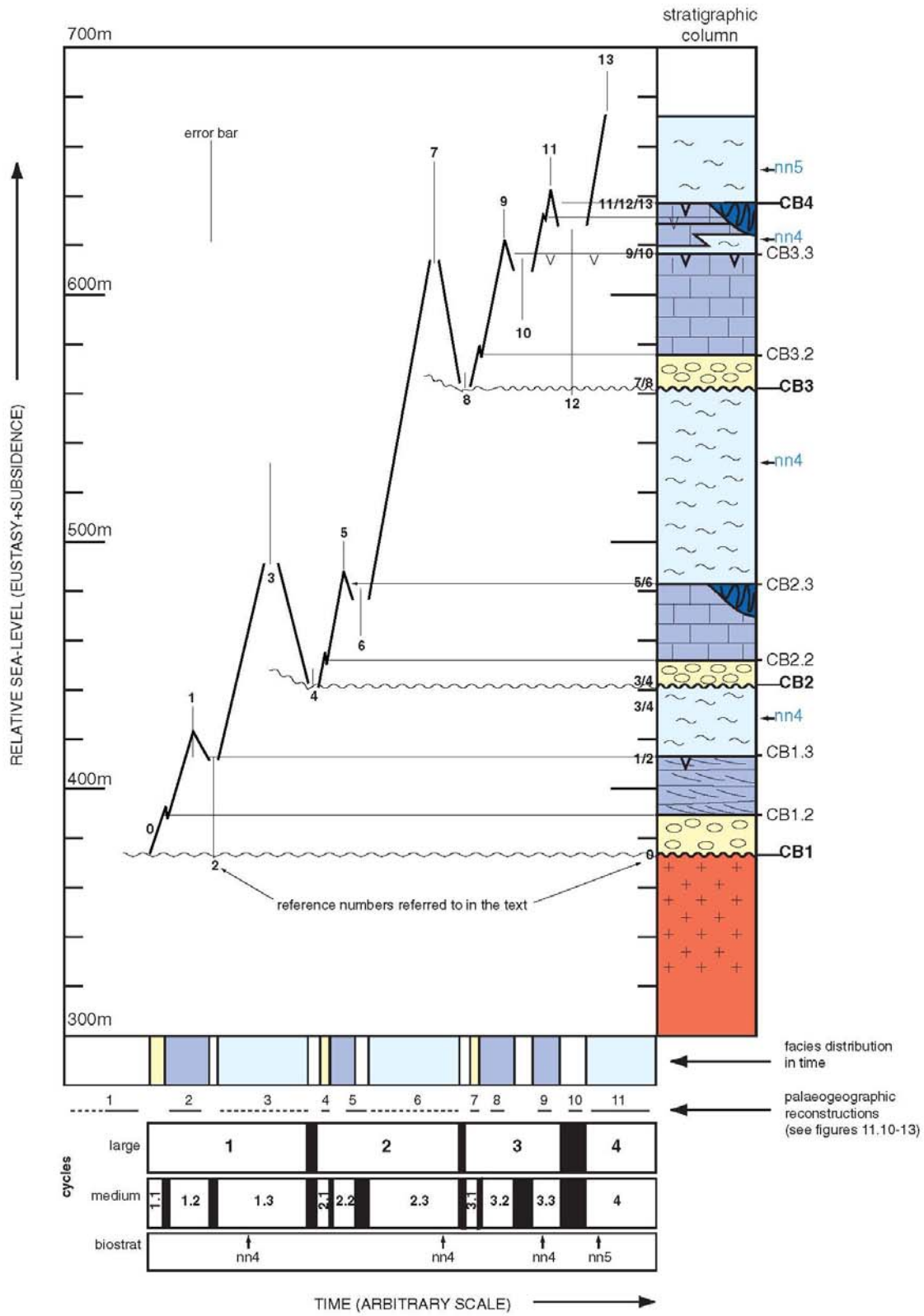

Figure 11.1 Dibekli relative sea-level curve

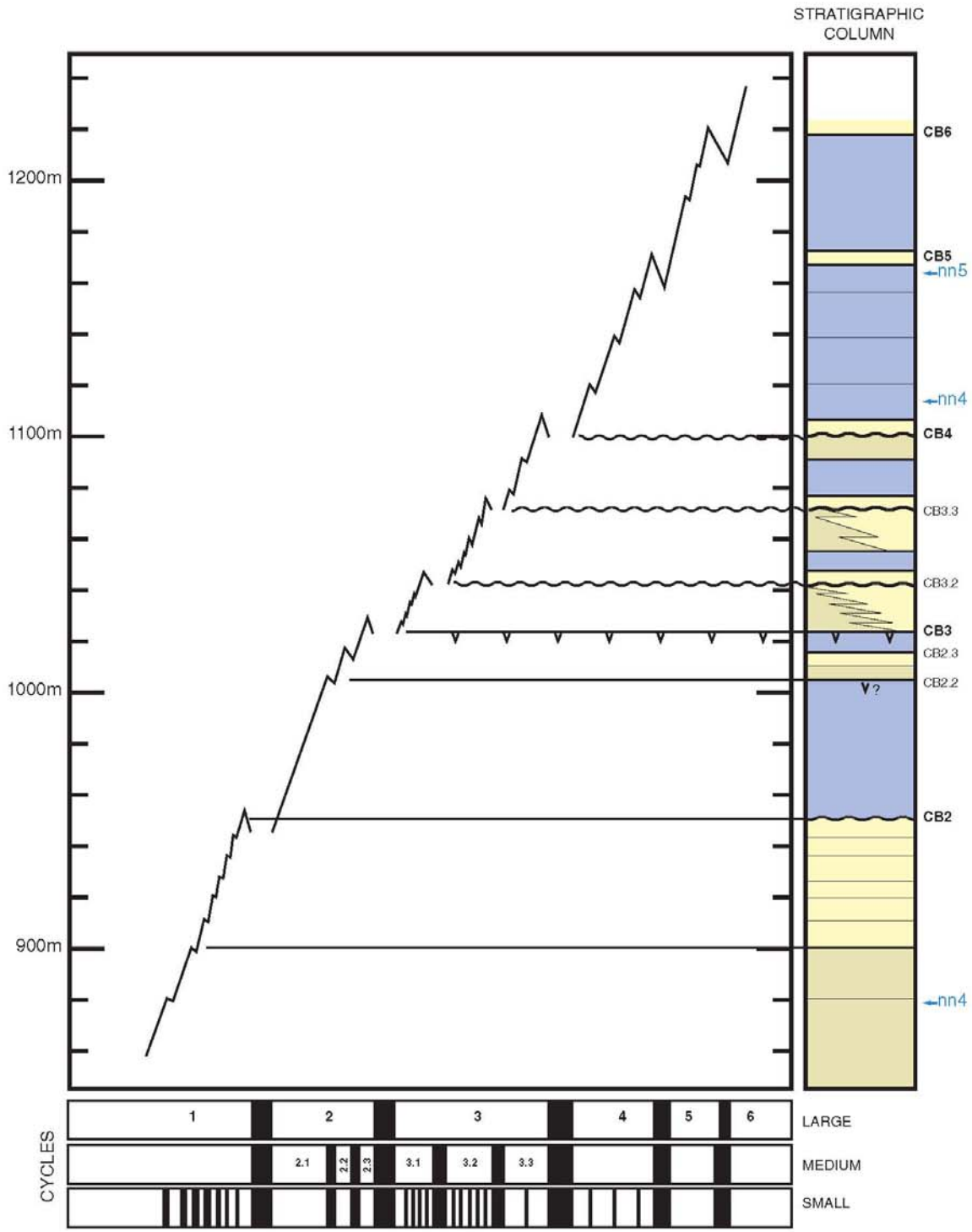

Figure 11.2 Alahan relative sea-level curve

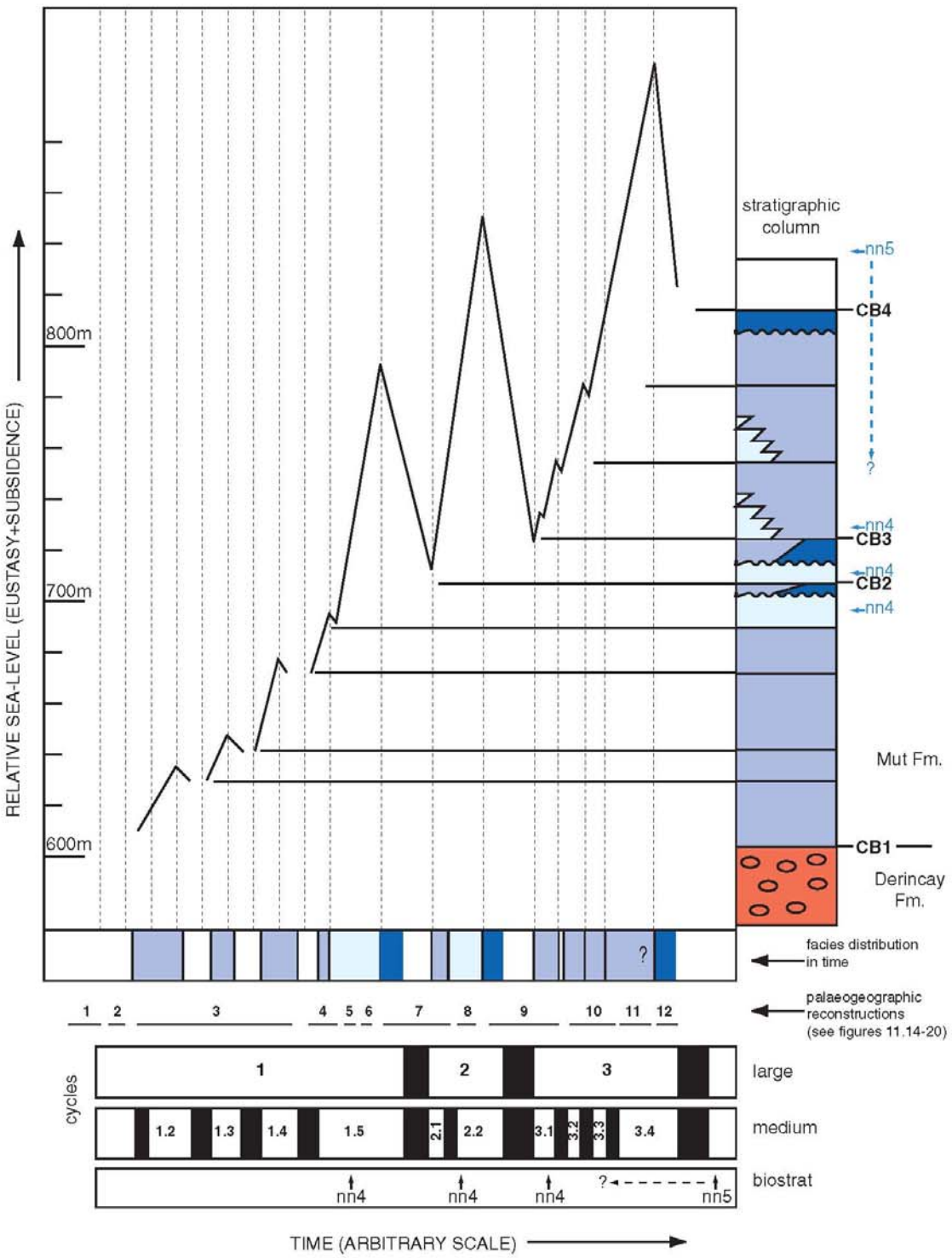

Figure 11.3 Pirinç relative sea-level curve

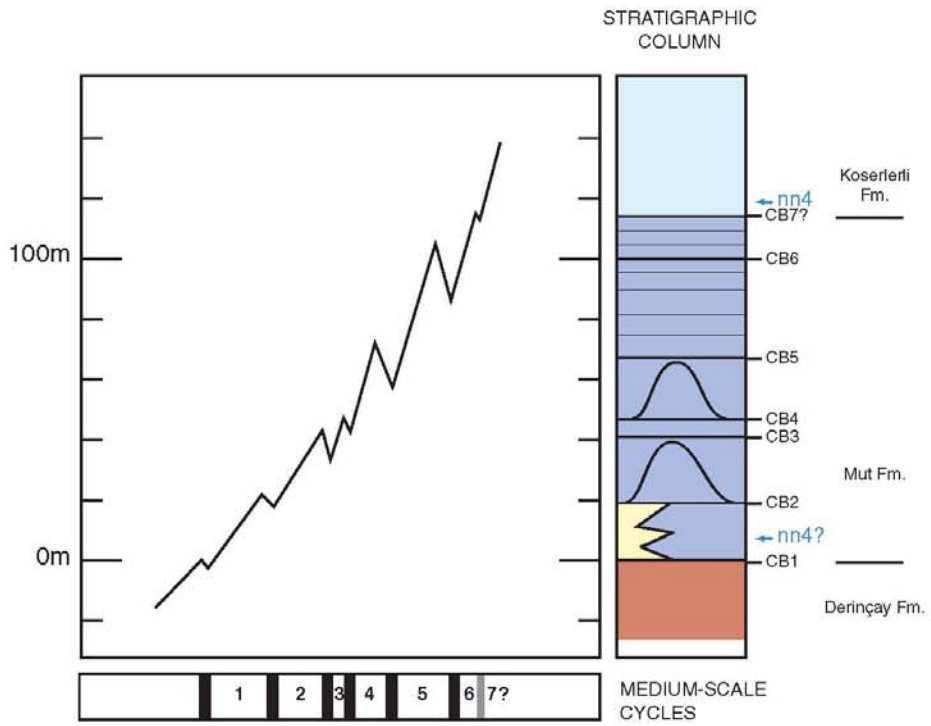

Figure 11.4 Zincir Kaya relative sea-level curve

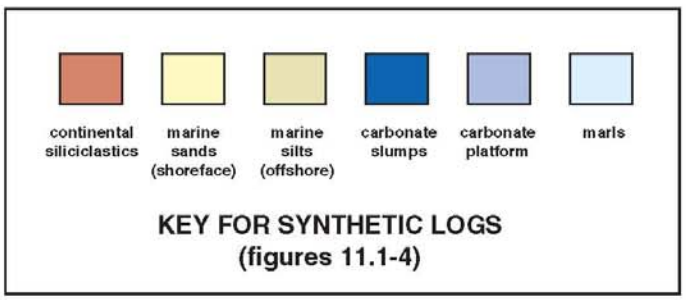

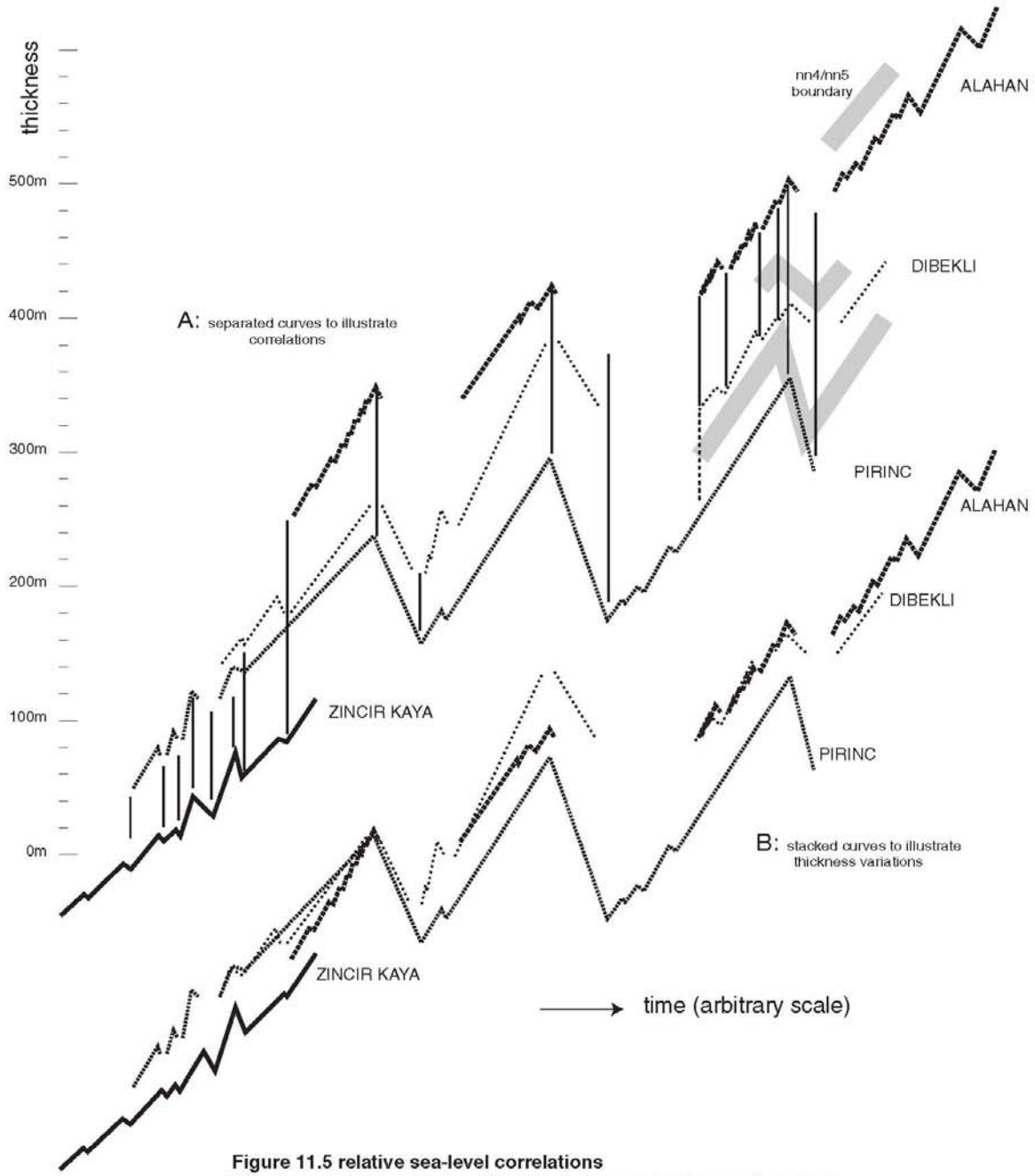

Figure 11.5 relative sea-level correlations
This diagram juxtaposes the different relative sea-level curves in order to illustrate how they have been correlated. Note that the overall accommodation rise is similar in all the areas, and that the three large-scale relative sea-level cycles are readily correlatable within the framework provided by the biostratigraphy.

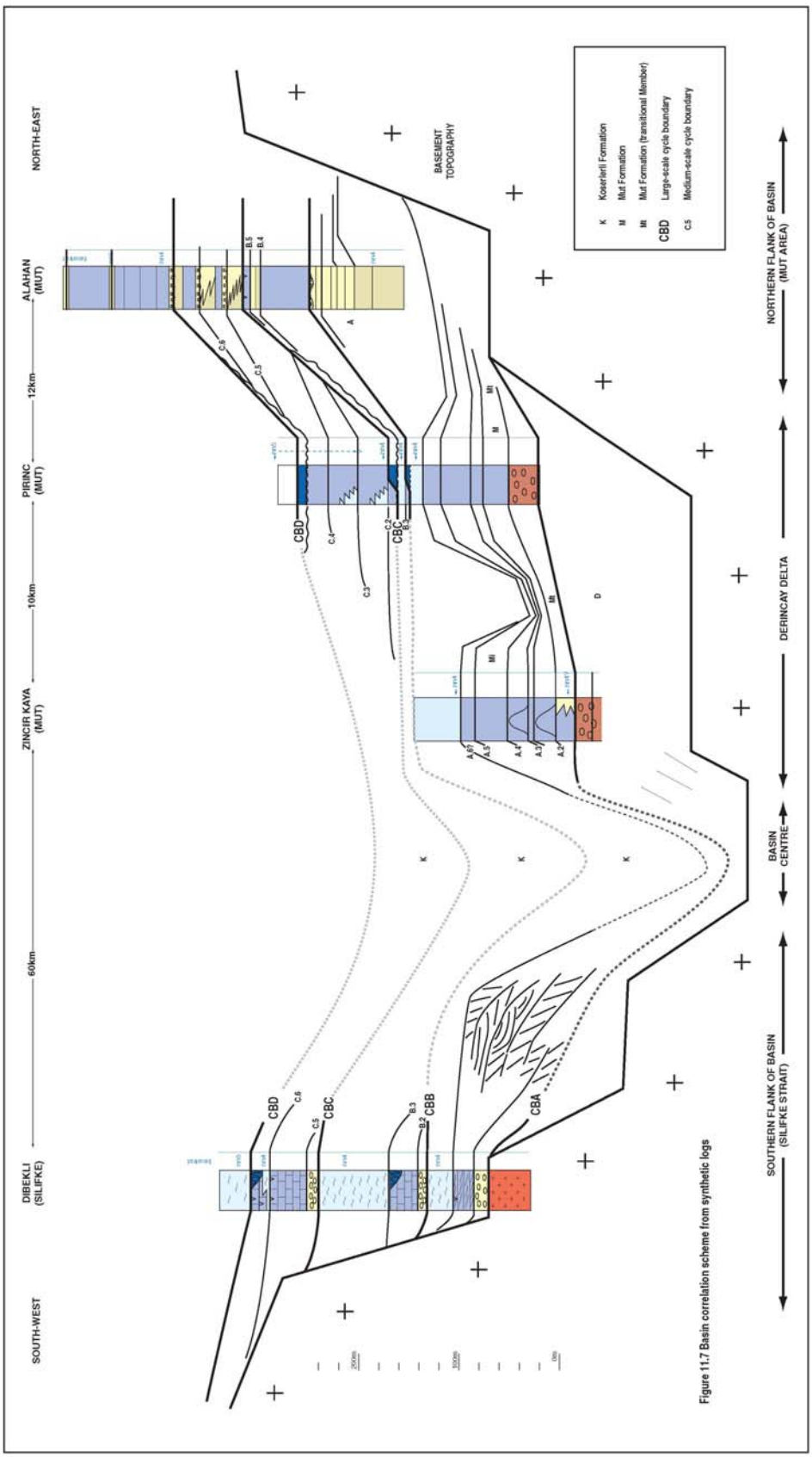

Figure 11.7 Basin correlation scheme from synthetic logs

FIGURE 11.7 SPLIT ON PAGES 220-221 IN THE ORIGINAL

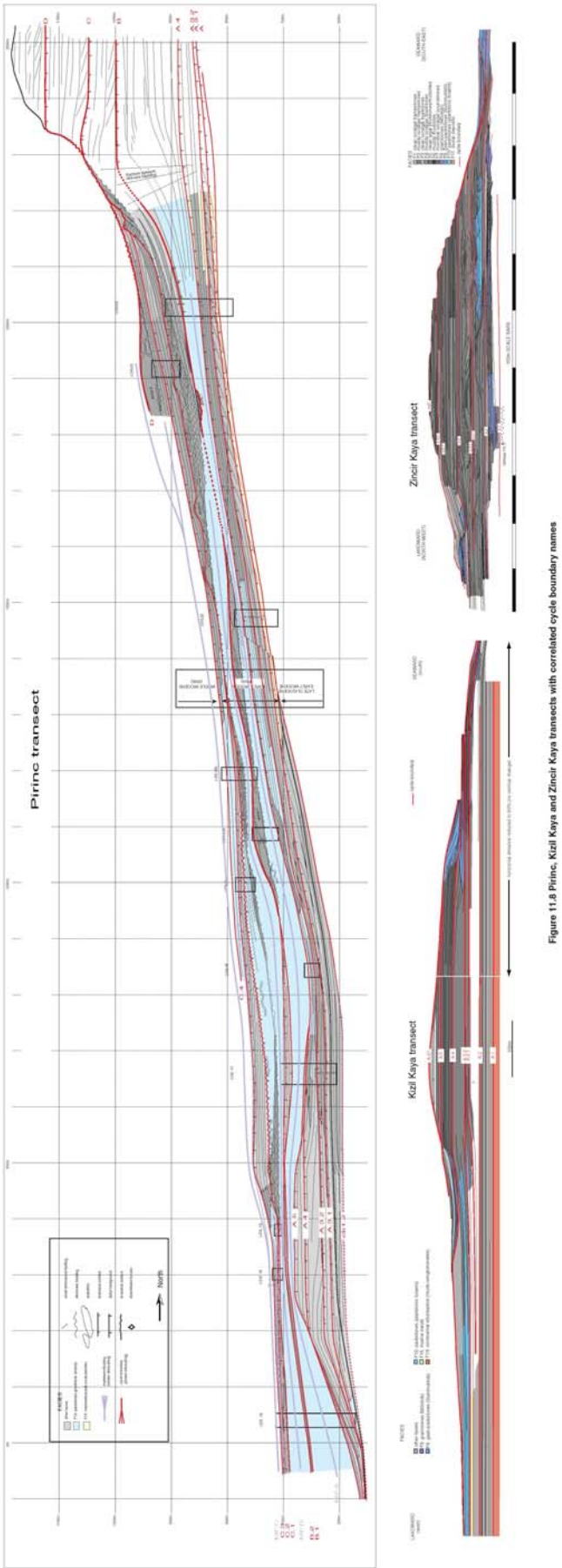

Figure 11.8 Pirinc, Kizil Kaya and Zincir Kaya transects with correlated cycle boundary names

FIGURE 11.8 SPLIT ON PAGES 222-223 IN THE ORIGINAL

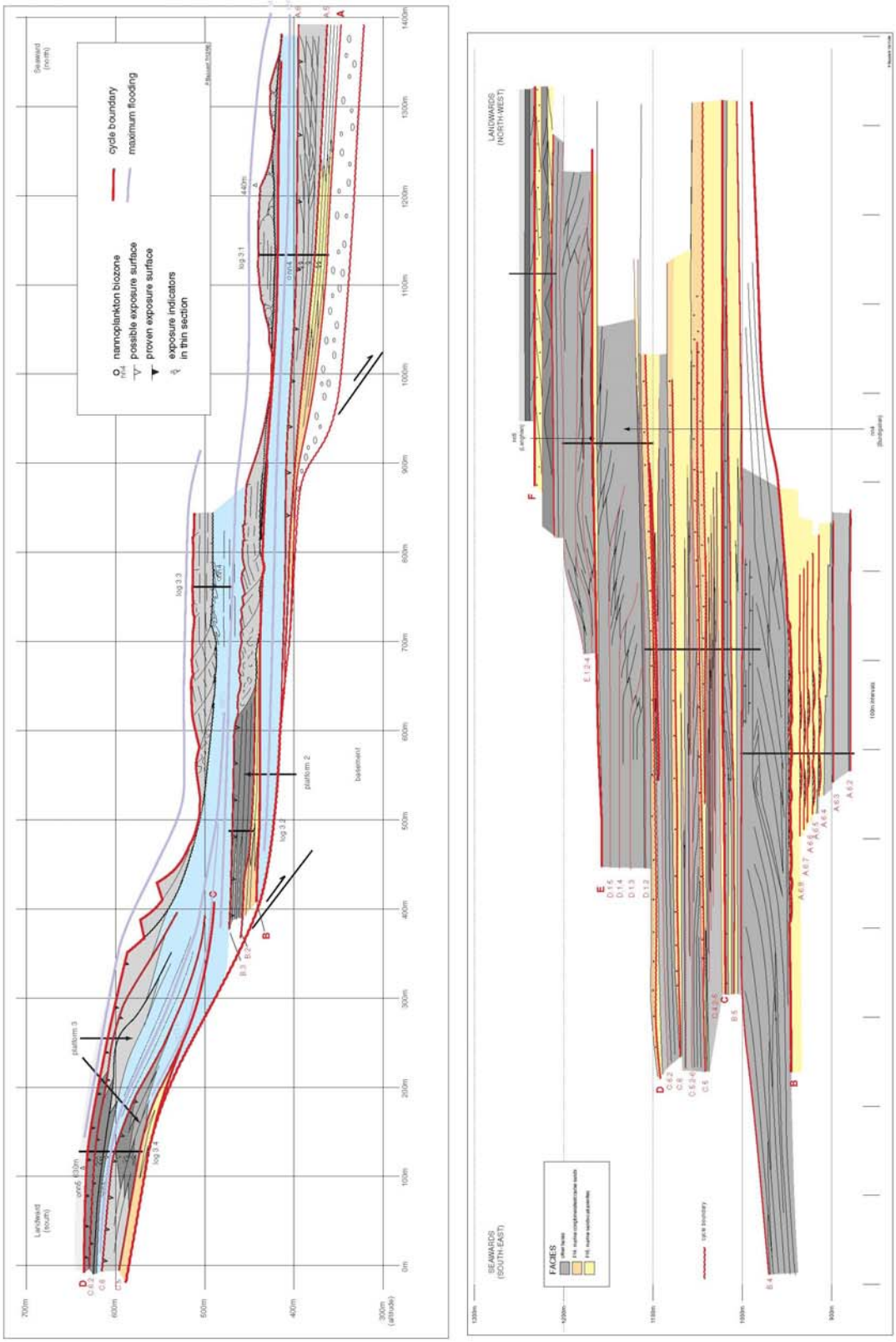

Figure 11.9 Alahan and Dibekli transect correlated cycle boundary numbering

FIGURE 11.9 SPLIT ON PAGES 224-225 IN THE ORIGINAL

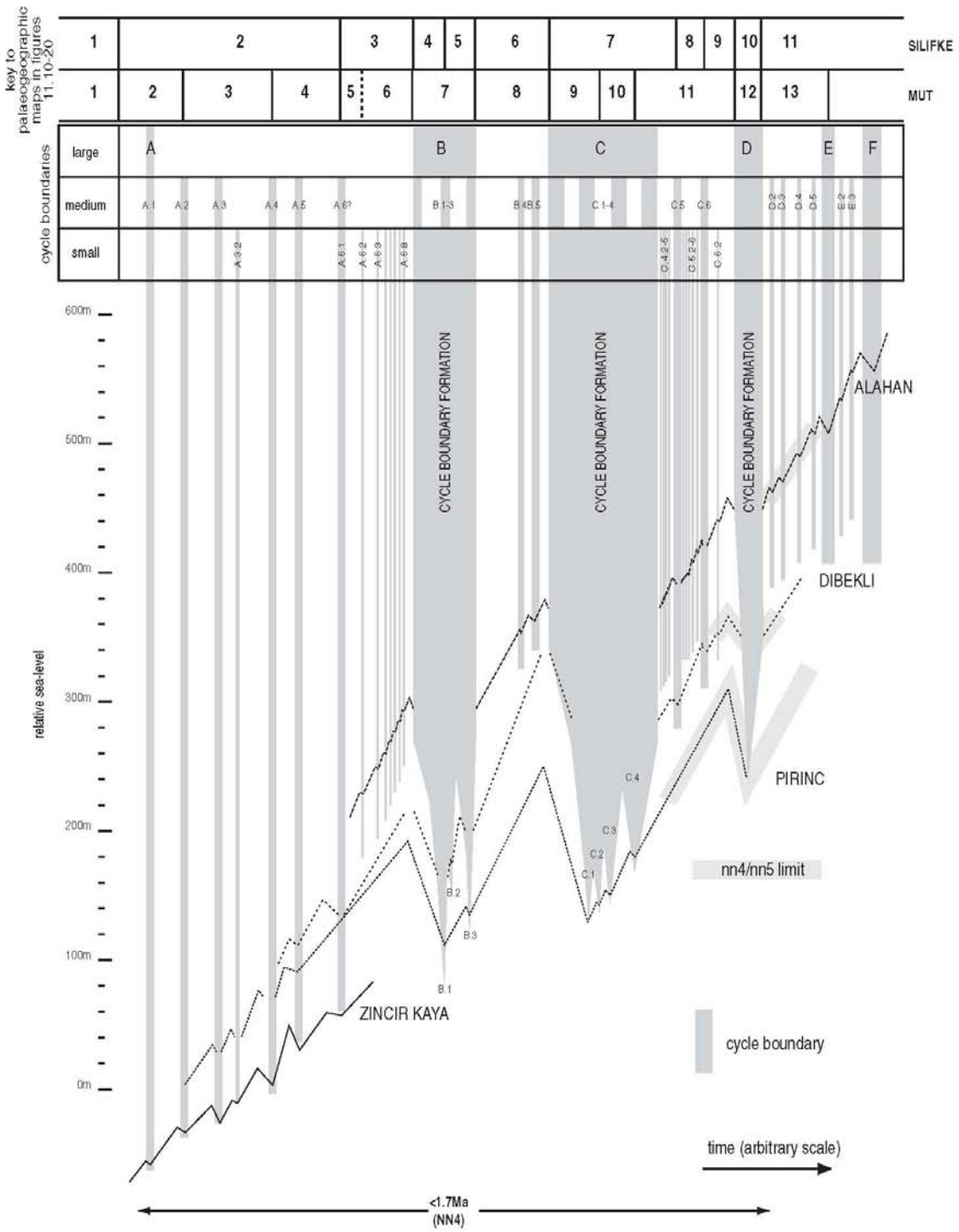

Figure 11.6 Relative sea-level correlations with cycle boundaries indicated

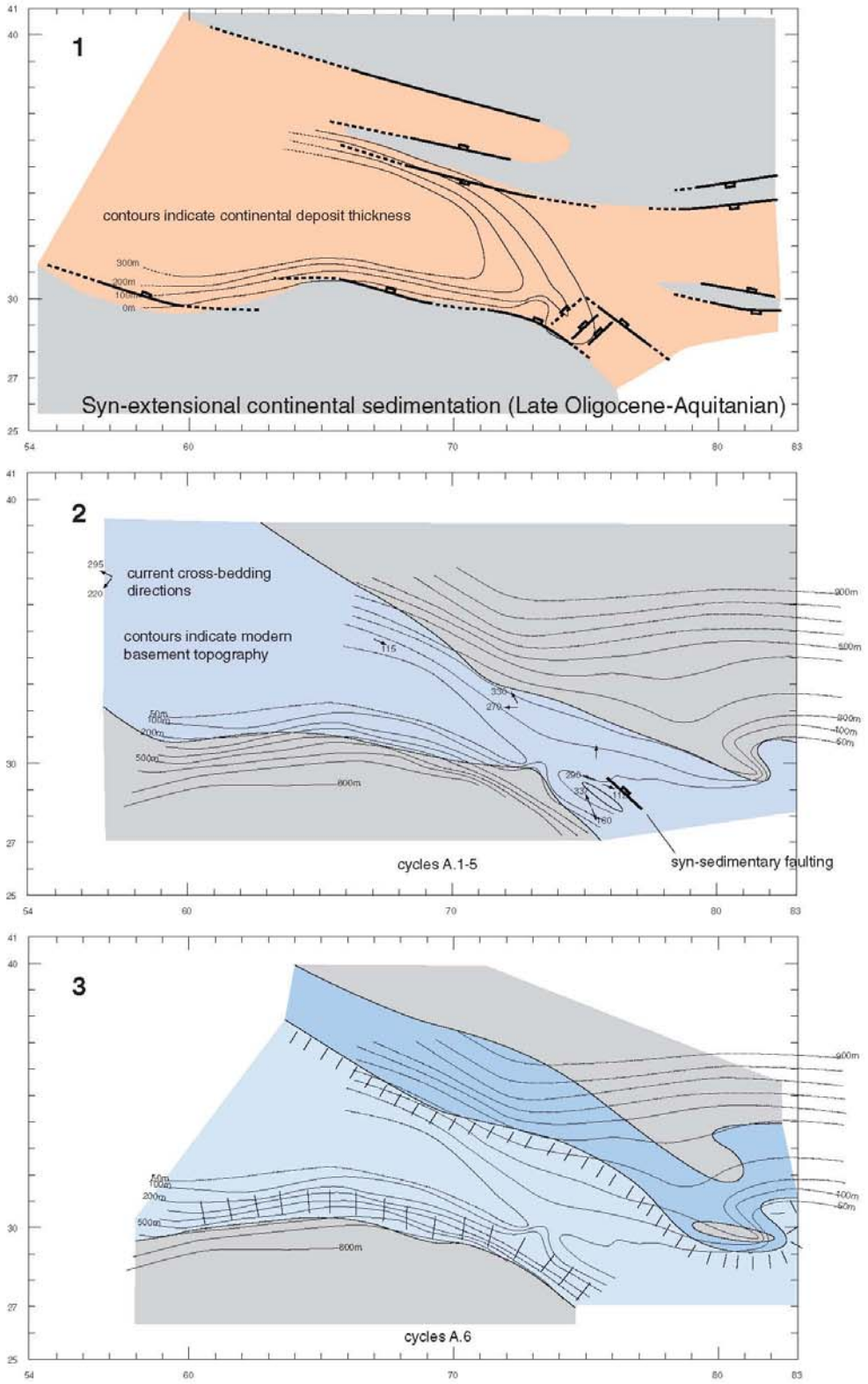

Figure 11.10 Silifke palaeogeographic reconstruction 1

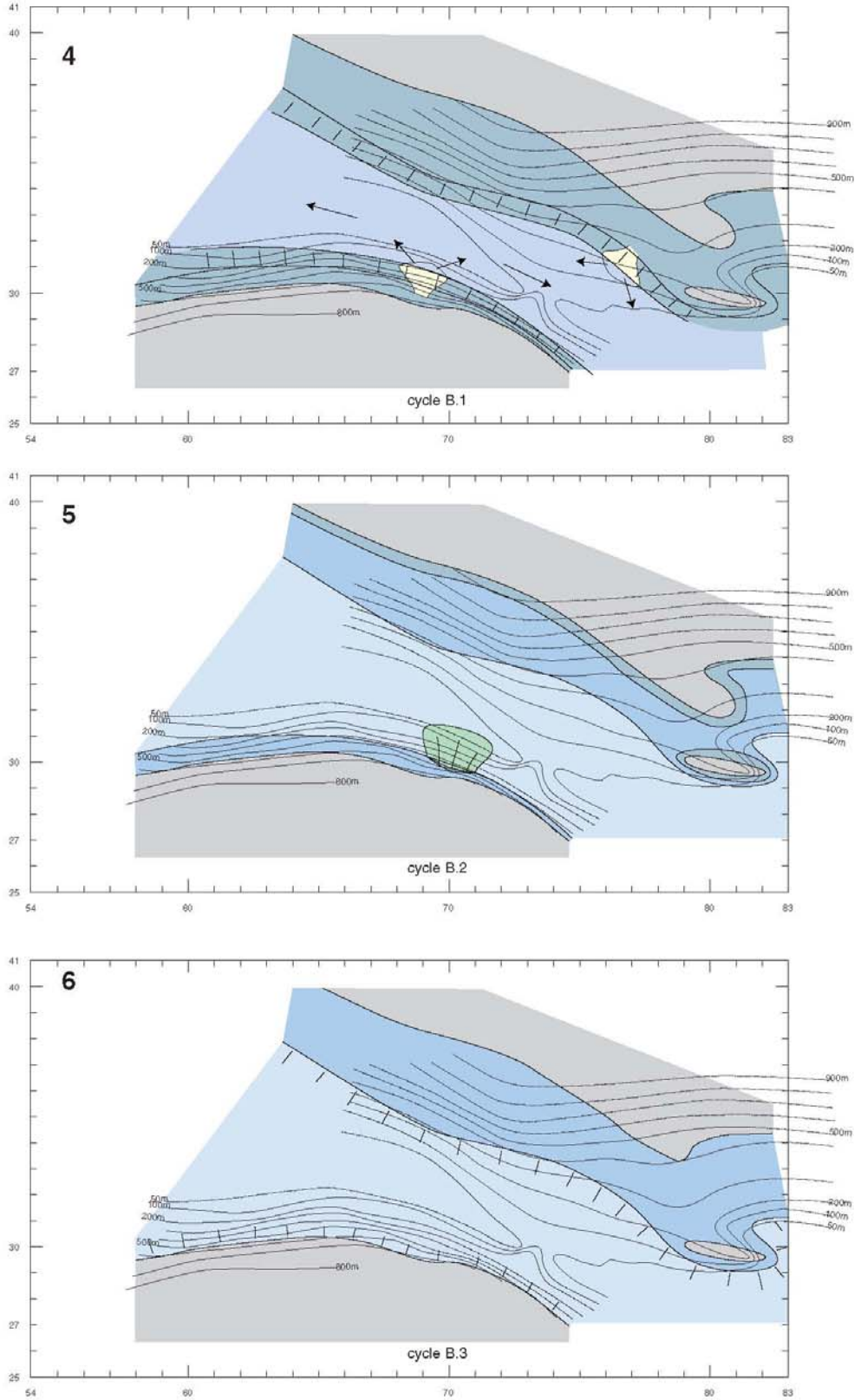

Figure 11.11 Silifke palaeogeographic reconstruction 2

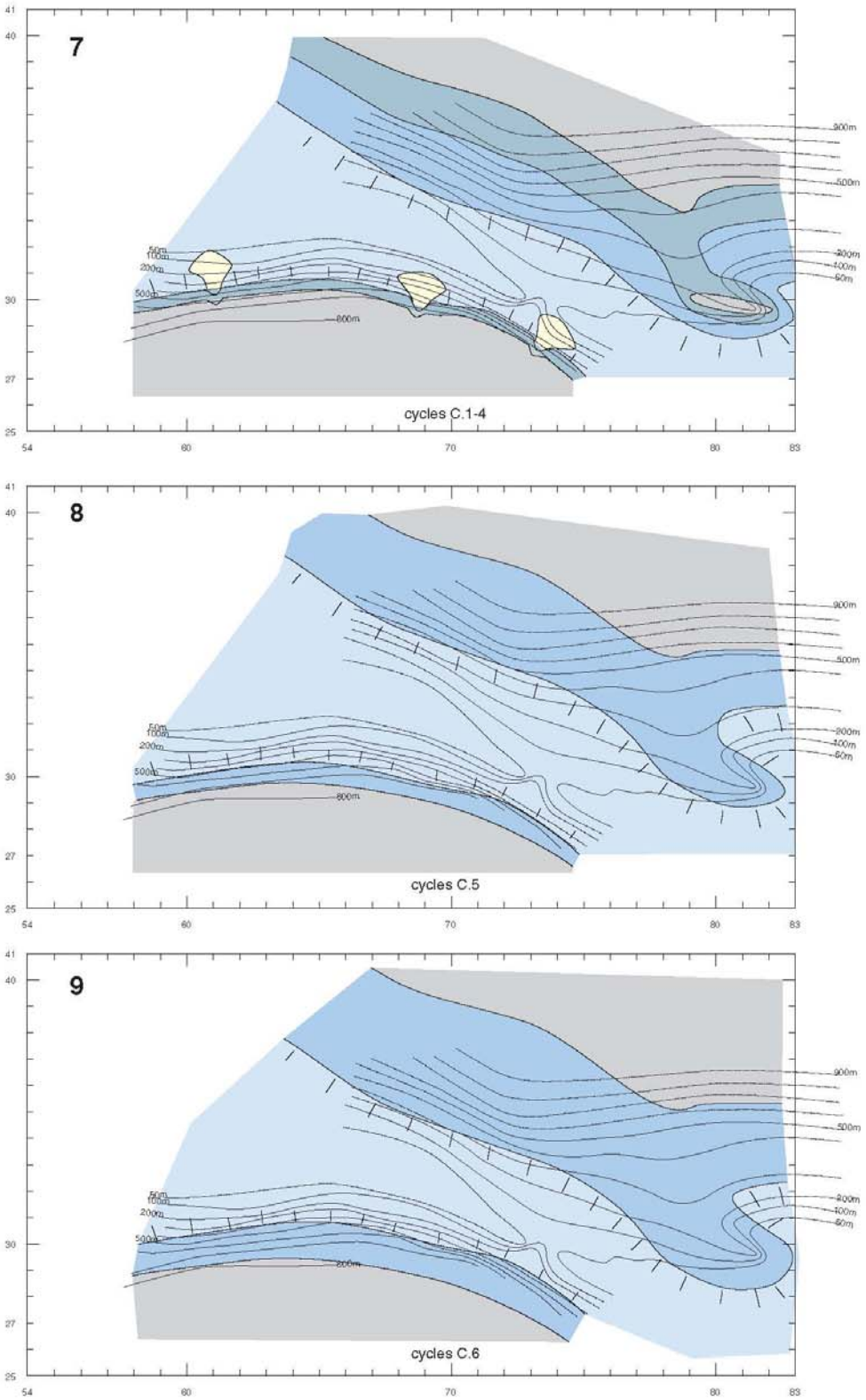

Figure 11.12 Silifke palaeogeographic reconstruction 3

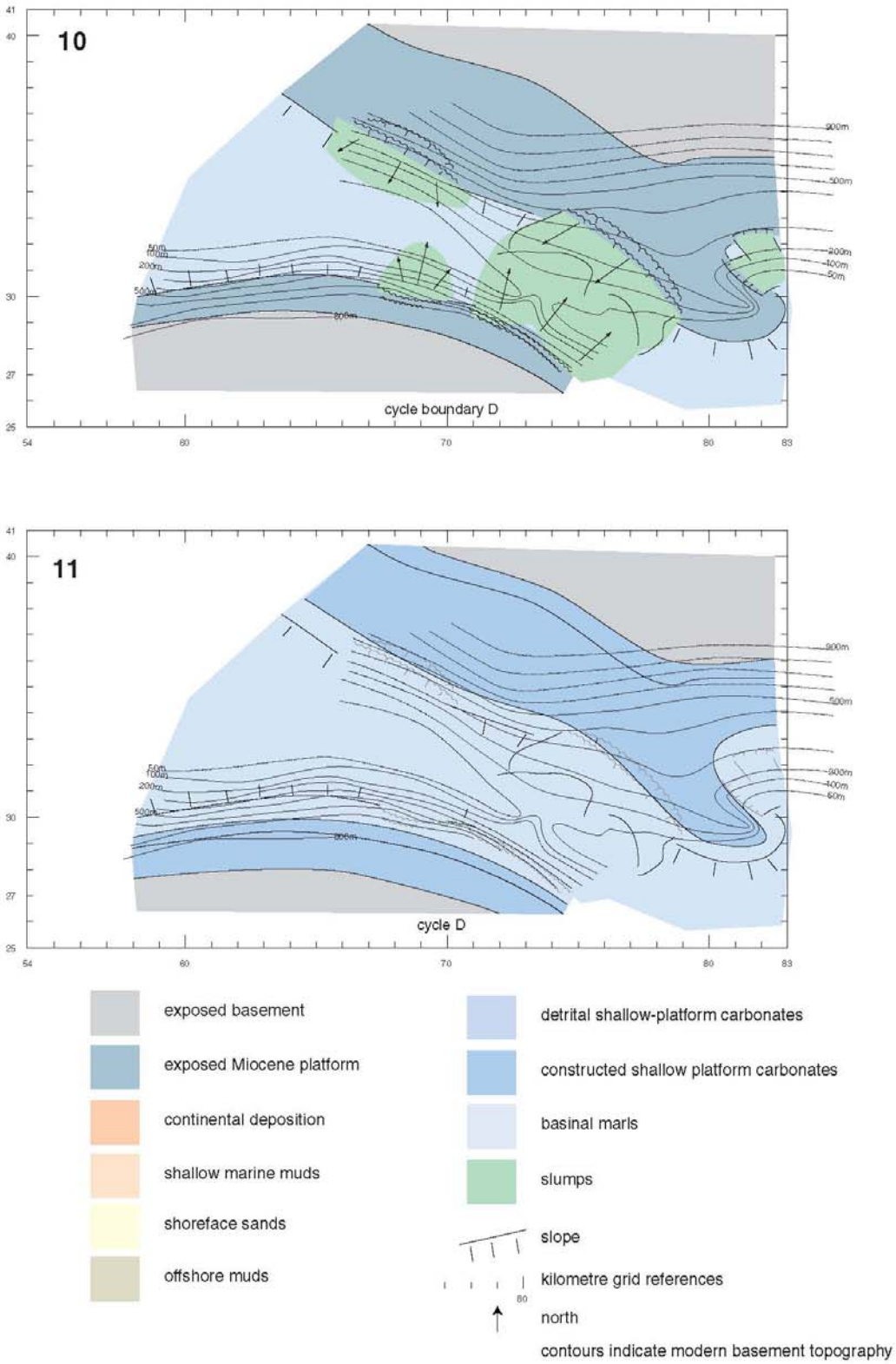

Figure 11.13 Silifke palaeogeographic reconstruction 4

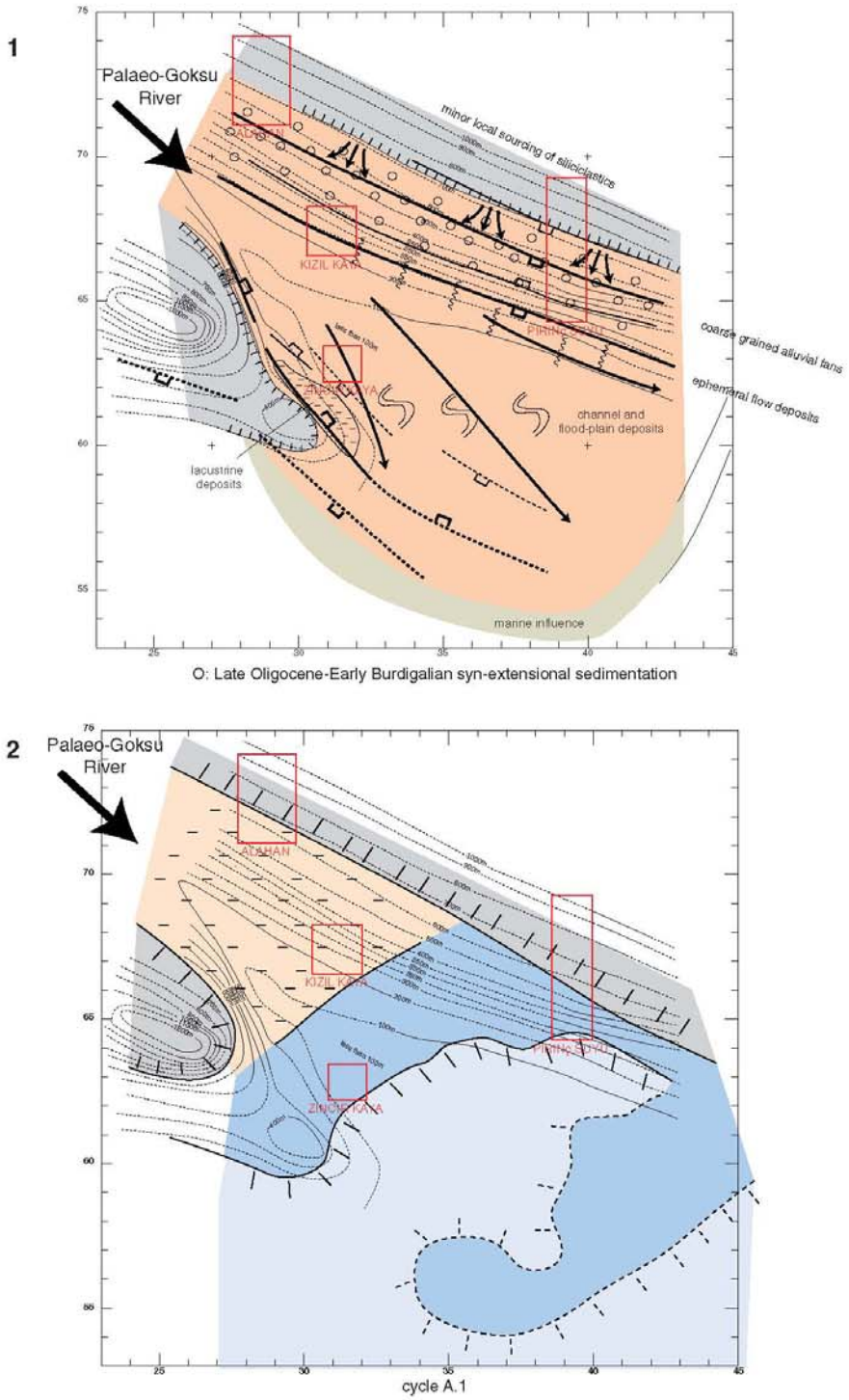

Figure 11.14 Mut palaeogeographic reconstruction 1

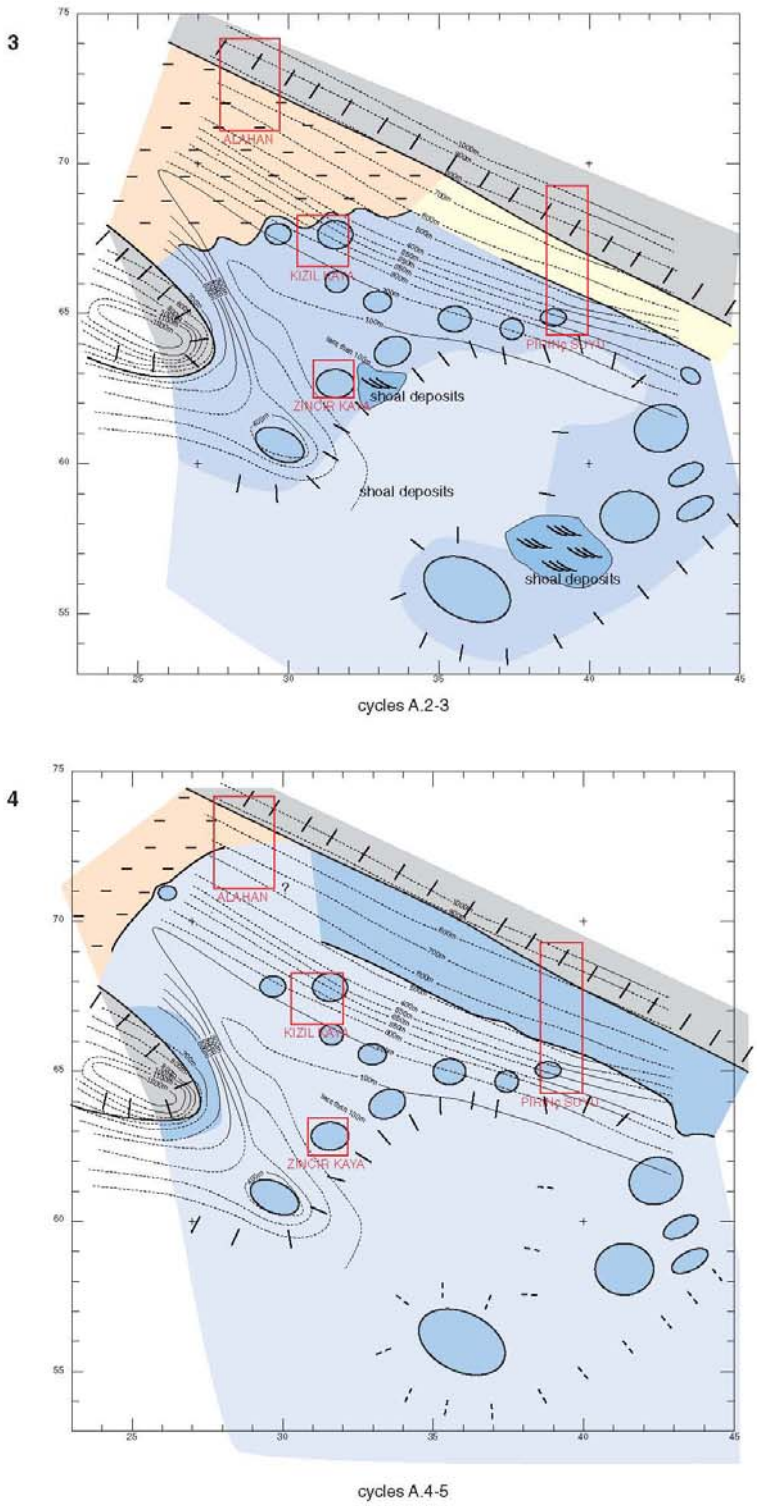

Figure 11.15 Mut palaeogeographic reconstruction 2

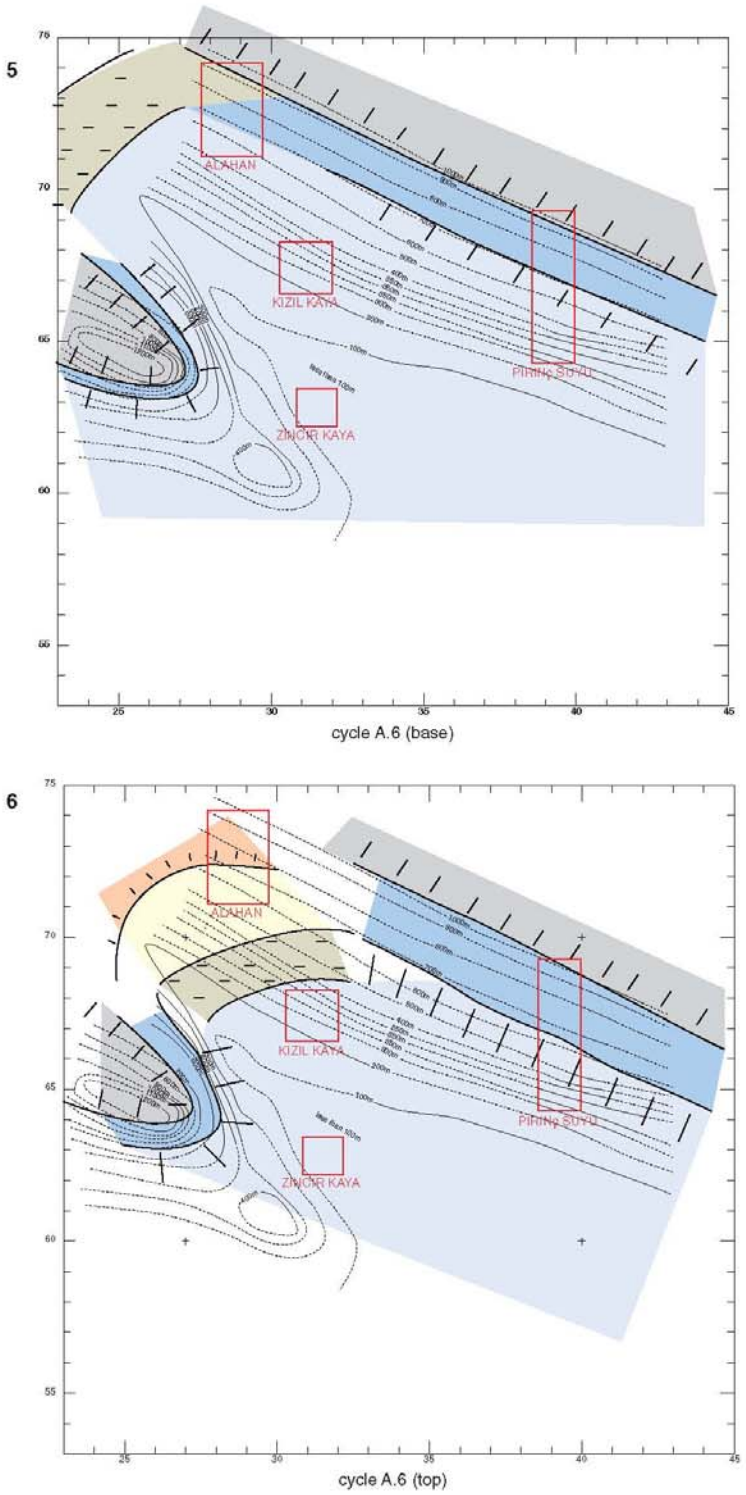

Figure 11.16 Mut palaeogeographic reconstruction 3

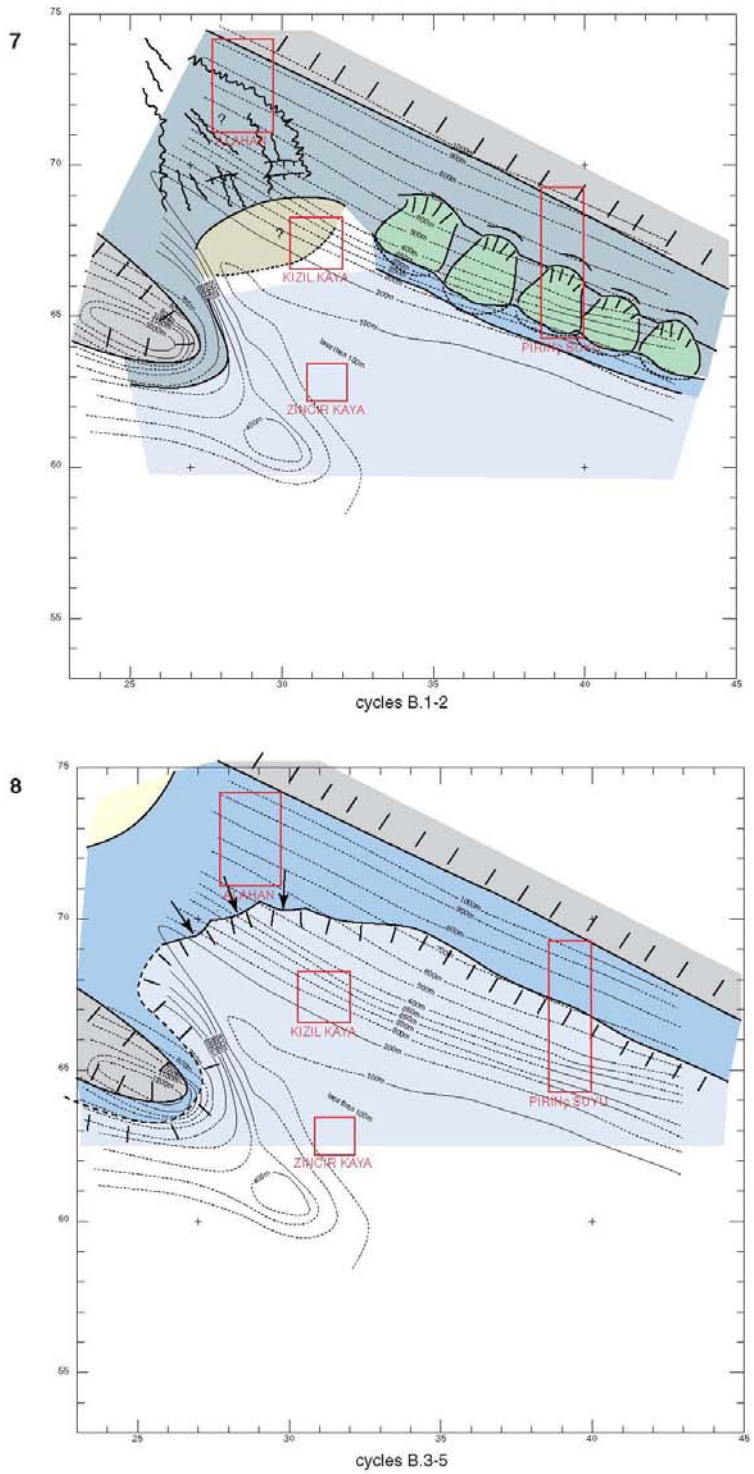

Figure 11.17 Mut palaeogeographic reconstruction 4

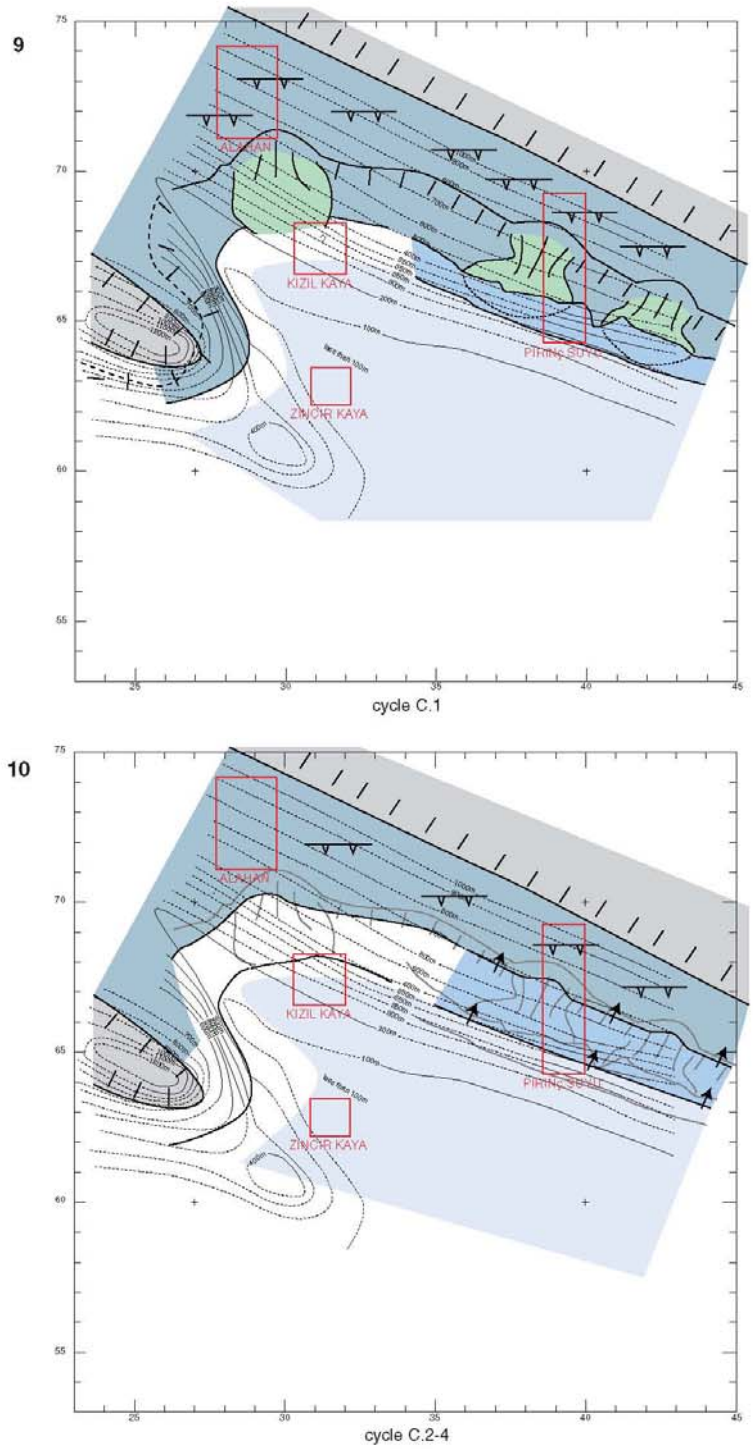

Figure 11.18 Mut palaeogeographic reconstruction 5

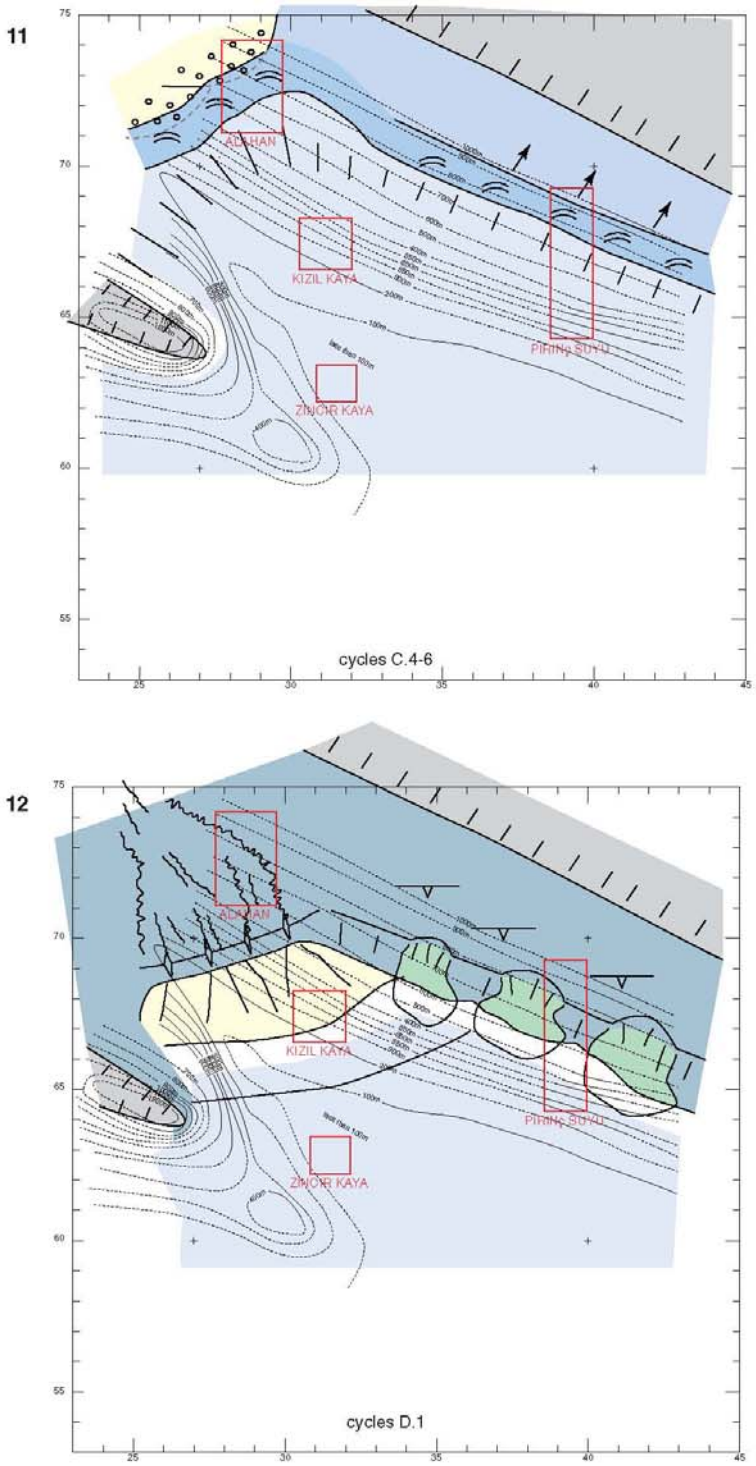

Figure 11.19 Mut palaeogeographic reconstruction 6

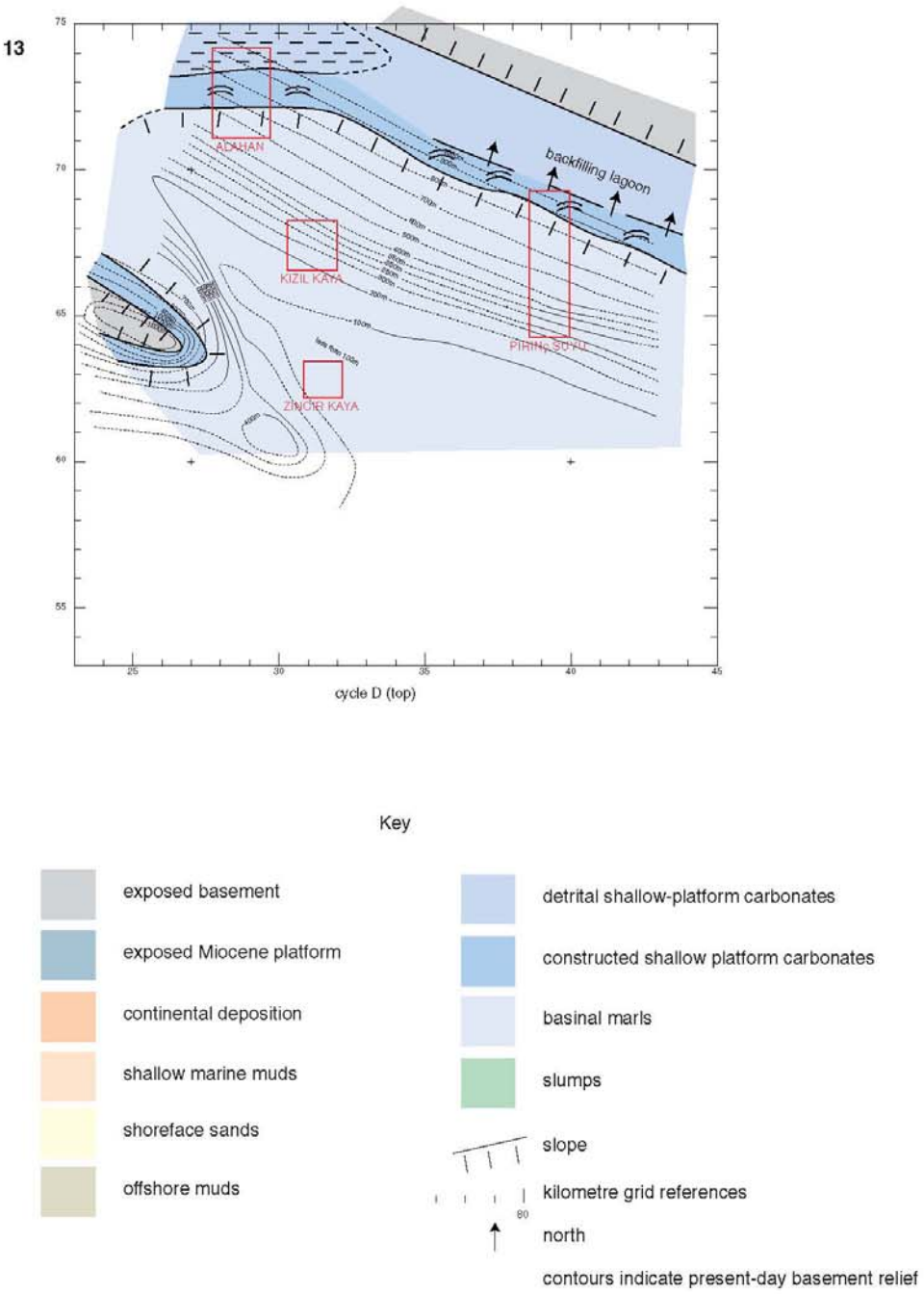

Figure 11.20 Mut palaeogeographic reconstruction 7

12 – DISCUSSION

A discussion of the factors that control the different scales of sedimentary cycles observed (section 12.1) is followed by a focus on specific problems posed by elements of the stratigraphy (section 12.2), and a comparative discussion of the stratigraphic development (section 12.3). This chapter ends with a discussion of the limitations of the methodology (section 12.4).

12.1 CYCLIC DEPOSITS AND PROCESSES

Three scales of retrograding-prograding cycles (small, medium and large) have been identified and used as building blocks in this study (see figure 11.6). A fourth scale exists, and can be considered as a very large-scale cycle. In the studied interval it is represented by a monotonous "background" creation of accommodation space. This decomposition of the stratigraphic record into its constituent signals, as defined by their relative scales, can be considered as a kind of qualitative Fourier analysis. Each component signal is considered to occupy a characteristic bandwidth in the frequency domain (here expressed as a period) and a characteristic amplitude (of cycle thickness or relative sea-level change). This assumption is justified by the uniformity with which these signals are expressed in the stratigraphy through time (in a given position) and through space (for a given horizon). Additionally, each order of cycle may have controlling factors specific to that scale (Van Buchem et al. 1994).

Potential causes for sedimentary cycles

1/ Tectonics: tectonic uplift or subsidence of an area directly controls a', and may indirectly control s' by providing a siliciclastic source due to syn-tectonic erosion of uplifted areas. Field observations of the structural geology of the area give information about the tectonic mechanisms that were active during the deposition of the study interval. The tectonic processes can be expressed either as local faulting (intra-plate stress) or regional uplift/subsidence (epeirogenesis) (Allen and Allen, 1990). The mapping studies of the Silifke and Mut areas in chapter 4 have demonstrated that the Burdigalian of the Mut Basin is a post-extensional sedimentary infill deposited during a time of relative tectonic quiescence within the basin, though intra-basinal post-extensional thermal subsidence or regional epeirogenetic processes may have occurred during this time.

2/ Eustasy: eustatic change is driven by different processes. Tectono-eustatic processes are dominantly low-frequency, acting on a time scale of millions of years and producing first to third order relative sea-level cycles (see figure 3.4). For instance, changes in sea-floor ridge volume (Hallam, 1963) can account for sea-level changes of 300m, but over a time-scale of 50-100Ma, with rates of 0.002-0.01m/Ka (Miall, 1997), while changes in ocean basin volume due to variations in plate geometries during super-continental cycles (Dockal and Worsley, 1991) can account for eustatic variations of 100m over 100Ma (Miall, 1997).

Eustatic sea-level at the time-scale examined in this study, that of third, fourth, fifth order cycles and greater (see figure 3.4) is mostly controlled by glacio-eustatic processes: variations in ice-volume stored in polar ice-caps and in glaciers. This can produce rapid high-amplitude eustatic sea-level fluctuations of over 100m in 10-100Ka. The presence of polar ice-caps is required to produce significant amplitudes of eustatic sea-level variation due to this process. It has been shown that ice-caps existed at this time (Lower Miocene) in Antarctica, with the East Antarctica ice-sheet already well installed, and the West Antarctica ice-sheet under development (Abreu and Anderson 1998). High frequency glacio-eustatic cycles have been shown to be driven by insolation variations principally controlled by astronomical cycles, namely in the Milankovitch wavebands (Hays et al. 1976; Imbrie, 1985; de Boer and Smith, 1994). These glacio-eustatic variations due to orbital forcing have been calculated back to the Miocene by Mathews (1995).

3/ Climate: climate includes changes in the environment such as temperature, salinity, turbidity, terrestrial sediment and nutrient input, energy conditions, seasonality and storminess. Climatic changes will principly affect s'. Carbonate productivity is directly affected by temperature and salinity, and siliciclastic input is directly affected by the rate of rainfall in the hinterland.

Low-frequency global climate changes on the scale of 1st-3rd order sequences are dominantly driven by tectonic cycles (eg. the onset of monsoons due to the uplift of the Himalayas, or the closure of the eastern end of the Mediterranean at the end of the Miocene, a precursor to the Messinian salinity crisis in the Mediterranean). Such general climatic trends for this study interval have been described from the literature in chapter 2.

High-frequency global climate changes, on the scale of 4th-5th order cycles, can be related to changes in global insolation patterns due to astronomical forcing by orbital cycles (de Boer and Smith, 1994). The climatic response to astronomical forcing is complex, since it is controlled by the shifting of the atmospheric circulation cells (the Hadley, Ferrel and Polar cells). Areas of atmospheric upwelling and downwelling shift latitudinally, changing local climate conditions (Miall, 1997; Perlmutter and Mathews, 1990). De Boer and Smith (1994) summarise the effects on mid-lattitudes (20-40°)...

"...the orbital variations affect the relative length of the seasons and the contrast between summer and winter, and hence of monsoon intensity."

High frequency climatic variations and glacio-eustasy are intimately interlinked, since they share the same driving mechanism: insolation cycles due to orbital forcing. The situation is further complicated, since there is a feedback relationship between climate and relative sea-level changes (Smith, 1994), both on a regional and a global scale. This must be taken into account when discussing the cause and effect of climatic variations and relative sea-level cycles observed.

5/ Autocyclicity: these are self organised cyclic to pseudo-cyclic processes spontaneously set up in the sedimentary system, with no external forcing. Examples are delta-lobe switching, or peritidal carbonate cycles (Strasser, 1991; Pratt et al. 1992). They can be distinguished from allocycles by the process of formation, and by the lateral continuity: if they can readily be correlated with other settings then they are more likely to be allocyclic.

Causes of very large-scale cycle (period >3.4Ma, amplitude >200m)

This corresponds to the monotonous creation of space (rising relative sea-level). In the study interval 200m of relative sea-level rise occurs due to this signal in under 1.7Ma (the duration of the NN4 biozone). If the signal is cyclic, then only the rising limb of the cycle is observed, and the period must be at least twice this time interval (>3.4Ma). The rate of sea-level change is 0.12m/Ka. Tectonic subsidence may explain this creation of accommodation space. This can be attributed to either post-extensional thermal subsidence on the basin scale, or to a more regional subsidence of the whole area. Post-extensional thermal subsidence is attributed with a speed of 0.03-0.07m/Ka (Miall, 1997) which can only partly explain the rate of change observed. A eustatic sea-level signal may also be contained in this component. Indeed, the eustatic curve of Haq et al. (1987) indicates a gradual sea-level rise throughout the Burdigalian, though totalling no more than 100m. This gives a rate of roughly 0.02m/Ka. A low frequency mechanism is required: sea-level ridge volume changes can account for only 0.002-0.01m/Ka (Miall, 1997). Glacio-eustatic effects are the most rapid, and could readily account for the rate of sea-level change observed. However, a sufficient ice volume is required to melt to create over 200m of eustatic sea-level rise. Also a glacio-eustatic rise would occur too quickly to produce the gradual rise observed. The preferred solution to explain this signal is a combination of basinwide post-extensional subsidence, accounting for around 100m of subsidence, and a eustatic signal accounting for another 100m of sea-level rise.

Large-scale cycles (average period of <570Ka, amplitude 100-150m)

Three large-scale cycles with an average thickness of 60-90m each, are deposited in the study interval. These cycles are produced by relative sea-level cycles (changes in a'): this has been demonstrated by the juxtaposition of in-situ shallow marine carbonates over basinal marls in the Pirinç area. During each cycle the relative sea-level rises and falls by 100-150m. These values were determined from the Pirinç study site. The error margin is intentionally large since a number of approximations needed to be made: decompaction was not performed, and the post-depositional basinward sagging deformation in the Pirinç transect had to be taken into account. A sagging of 200-250m between the northern and southern extremity of the transect was calculated by horizontalising on the clinoform topsets of cycle boundary A.3. The time period was calculated by

dividing the maximum total time for the interval (1.7Ma for the NN4 biozone, accepting that this is a maximum value, since the base of this biozone may be beneath the study interval) by the number of cycles observed, 3, arriving at a maximum time-span of 570Ka. This is an average, based on the hypothesis that time is evenly distributed among the cycles.

One rise and fall of relative sea-level at this scale corresponds to the deposition of one large-scale cycle, with a large-scale cycle boundary forming when the base-level drops beneath the sediment surface in a given position. Hence the large-scale cycles observed are considered to be the direct result of relative sea-level variations.

This relative sea-level signal is most readily explained by glacio-eustatic effects: the waxing and waning of the Antarctic ice-cap with a <570Ka period. A tectonic mechanism has not been found that will satisfactorily account for such a rapid rise and fall of relative sea-level in a post-extensional tectonic setting. This cycle period could potentially correspond to the 400Ka Milankovitch eccentricity cycles.

Medium scale cycles (average period of <100ka, relative sea-level amplitudes of 18-30m)

These retrograding/prograding sedimentary cycles average 18-25m thick. Their average period has been estimated by dividing the maximum time alloted to the study interval (the duration of the NN4 biozone, 1.7Ma: a maximum value since the base of the biozone may be below the study interval) by the total number of cycles of this scale observed in this interval (17) as shown in figure 11.6. The accuracy of this value relies on the completeness of the reconstructed stratigraphic record and the equal partitioning of time between the cycles of the same order. Construction of the stratigraphy from the three different study sites of Alahan, Pirinç and Dibekli has allowed the "missing beats" from any transect to be observed in elsewhere, and so missing time is accounted for.

Some of these cycles are the direct result of relative sea-level changes (variations in a'), while others have a more ambiguous origin. In the Zincir Kaya outcrop cycles A.2, A.3 and A.4 (figure 11.8) have been shown to contain a fall in relative sea-level at the end of each cycle, and hence are associated with accommodation cycles. The same is true for cycles A.2, B.2, C.5 and C.6 in the Dibekli outcrop (figure 11.9).

By comparison, in the cycles C.1, C.2 and C.3 in the Pirinç area no observations implying exposure were made, and the cycles could potentially be caused by either a variation in s' or in a'. These are three platforms that backstep against an underlying sloping surface. Each platform is deposited in aggradation, or aggrading progradation. The top of each platform is a hardground surface covered with deep water marl sediments. Each platform top is a cycle boundary, since it represents the start of the retrogradation that floods the platform, and the end of the progradation that builds the platform. This clearly demonstrates that the platforms have been drowned, followed by a proximal shift of the depocentre, but the question remains as to why. If we consider a monotonous increase in accommodation space (a'>0) and we vary either a' or s' then two end member solutions exist:

1/ Variation in s': keeping a' constant, s' simply decreases such that s'<a'. This implies a time of ecological stress during a constant gradual sea-level rise. Proof of this stress should be visible in the faunal contents of the rock record.

2/ Variation in a': keeping s' constant, a' suddenly increases such that a'>s'. This implies that a deepening trend should be observed in the fauna at the top of the platform. Note that a simple deepening trend may be difficult to distinguish from an ecological catastrophe.

These two possibilities are simply end-members of the pay-off between a' and s'. A continuum of possibilites exists between the two that could potentially explain the stratigraphy observed. To make matters more complicated, an ecological crisis (decrease in s') could be the result of a change in relative sea-level (a' suddenly increases or decrease): in this case a' and s' are coupled, and the driving force becomes more difficult to distinguish.

If we allow a' to have negative values then a third solution exists:

3/ Exposure of platform and production shutdown: relative sea-level drops to below the level of the platform top, emerging the platform. In this case production shuts down completely (s'=0, or s'<0 in the case of erosion). When the platform is re-flooded a'>s' for one of two reasons: either s' is initially small, because production must "start up" (Neumann and Macintyre, 1985) again ; or a' is high, since by the time the platform is initially flooded the accommodation curve is already well advanced, and on the steepest part (high a'). Once again these are end-member reasons, and both would potentially play some part. Proof of exposure of the platform top would verify this hypothesis.

Insufficient information is available from the observations made to distinguish between these three possibilities. However, with more detailed examination the solution should be discernible. The author prefers the third solution, where a small proximal hiatus (with or without platform exposure) causes the temporary shut-down of production before a rapid flooding and drowning occurs: this is most coherent with the general organisation of these medium-scale cycles seen in other places, where some evidence for a relative sea-level fall and possible sub-aerial exposure is often observed.

Where a mixed system occurs, with marine siliciclastics interacting with shallow marine carbonates, the reasons for the formation of retrograding-prograding cycles become more complex. This is the case for cycles C.4, C.5 and C.6 in the Alahan area. The retrograding-prograding terminology becomes more difficult to apply in these settings because there are effectively two sedimentary systems active at the same time, and they are out of phase: while the siliciclastic component is in retrogradation the carbonate component is actively producing and prograding. It is proposed that the variation in siliciclastic input controls the carbonate production: the absence of siliciclastics creates a window in which carbonates are able to develop until the siliciclastic depocentre returns and shuts off the carbonate production. The tops of some of the carbonate units show faunal evidence for environmental degradation (with respect to ideal coral-growing conditions). An example of this is seen in the vertical facies evolution of the transgressive carbonate unit of cycle C5 in the Alahan area (see figure 11.9). This is interpreted as being due to the influence of the approaching siliciclastic depocentre, or its associated nutrient cloud, which encroaches on the carbonate environment. This interpretation is supported by the sequential evolution of the facies with the arrival of siliciclastic sediments observed just above the onset of the environmental crisis in the carbonates. The siliciclastics themselves are organised into shallowing up packets akin to parasequences. The top of each cycle is marked by an erosional surface, over which lies a fan delta deposit. This erosional surface is interpreted as indicating a relative sea-level fall. This interpretation implies that these cycles are controlled by the variations in a'. If there were no proof of sea-level fall, or if the proof is rejected, then these siliciclastic "parasequences" could also be explained by a variation in s': the amount of siliciclastic input varies cyclically, whether due to hinterland tectonic cycles, or climatic cycles affecting the rate of hinterland weathering and fluvial activity.

The medium-scale cycles thus have potentially diverse origins: most can be shown to be directly due to relative sea-level cycles, while others remain of uncertain origin (possibly a', or s'). The cause of the relative sea-level changes is considered to be eustatic rather than tectonic: sea-level rises and falls to form sedimentary cycles of regular thickness and it is difficult to envisage a tectonic mechanism that can behave in such away. On the other hand, glacio-eustatic fluctuations provide an ideal candidate to explain the rises and falls of relative sea-level at this frequency. The amplitude of such sea-level cycles is approximately equivalent to the thickness of the retrograding-prograding cycles generated, since the platform carbonates trace the sea-level to within a few metres. The period calculated for these cycles could potentially correspond to the 100Ka Milankovitch eccentricity cycles.

Small scale cycles (average period of 13-20ka, 1/ autocyclic, and 2/ relative sea-level amplitudes of 3-6m?)

These cycles have an average thickness of 3-6m. The period of these cycles has been calculated by dividing the period for the medium-scale cycle by the number of small-scale cycles observed (which varies between 5 and 8). They have been observed only in the Alahan area, at the top of cycle A and in cycles C.4 and C.5. The cycles at the top of cycle A consist of tidal channel fills cutting into shoreface sands and silts. No relative sea-level change can be discerned associated with these cycles, since the tidal channel deposits and the surrounding sediment are considered as bathymetrically equivalent. It is possible that they are contemporaneous facies. This, and the nature of the environment suggest that autocyclic processes are responsible for these cycles. Tidal channels develop and shift laterally in a stable shallow marine environment, and delta lobe switching in a more proximal position may also be driving these cycles.

The small-scale cycles in C.4 and C.5 (see figure 11.6 and 11.9) consist of coarsening up siliciclastic cycles topped by gravelly coquina beds. These coquina beds are in turn overlain by the finest member of the next coarsening-up siliciclastic cycle. The coarsening-up siliciclastics form a prograding parasequence, while the coquina beds represent the initial retrogradation and reworking of the benthic fauna. Changes in the rate of siliciclastic input are required to explain these facies variations seen, with the lowest input rate giving rise to the deposition of the coquina beds, and the highest input rate during the deposition of the coarsest siliciclastics.

Three possible mechanisms are discussed here that could account for these cycles:

1/ these variations can be explained by small rises and falls of relative sea-level (whether due to eustatic or tectonic causes), driving the landward and seaward migration of the siliciclastic depocentre. The

amplitude of these sea-level variations is estimated at approximately 3-6m, from the bathymetric contrasts of the facies. The most likely driving force behind the relative sea-level cycles is considered to be glacio-eustasy rather than tectonic activity because of the rhythmic, even nature of the cycles, and the lack of a suitable tectonic mechanism to create such cyclicity. Local faulting effects which could potentially explain such high frequency pulses are unlikely, since the siliciclastics, though poorly sorted, are well-rounded and heterolithic: local faulting would produce angular clasts from the faulted lithologies.

2/ alternatively, these may be the result of lateral shifts of the siliciclastic depocentre. This is an autocyclic mechanism. Small deltas develop along the shoreline, and episodically processes such as channel shifting change the position of these deltas. The carbonate environments develop between the deltas. More lateral control would be required, to demonstrate the contemporaneous nature of the carbonate and siliciclastic environments, if this were the case.

3/ the third possibility is that the rate of siliciclastic sediment input fluctuates as a result of processes in the hinterland. Changes in pluviality would be the most likely cause of such fluctuations. Clay mineral analysis may be of use here in examining these processes.

Climatic variations in the study interval

Environmental changes have been observed in the study interval at the large and the medium scale. These variations have been associated with local effects of changing hydrodynamic regime, and shifting siliciclastic depocentres, and can be explained as a response to relative sea-level variations rather than any regional or global climatic change.

At the large-scale in the Dibekli area a decreasing trend in the energy of the environment is observed between the carbonate platforms that develop in cycle A.2 (high-energy tidal regime) and the carbonate platforms of subsequent cycles in B.2 and C.2, which are deposited in much lower energy conditions. This change has been related to the deceleration of tidal currents due to the increasing cross-sectional area of the strait waters during sea-level rise, and is apparently not due to any regional changes in climate.

Within large-scale cycle A, the isolated platforms in the Mut area have a facies evolution that indicates a deterioration in (local) environmental conditions with respect to coral growth: this has been associated with the influence of prograding siliciclastics and nutrients, and is discussed in detail below.

A similar environmental deterioration is observed at the medium-scale in cycles C.5 and C.6 in Alahan in the retrograding carbonates of each cycle: facies evolve vertically over 12m (see figure 7.7) from a middle reef-front environment with diverse coral fauna, through a lower reef-front environment before the coral fauna is replaced by bioclastic sands, finally to be covered by fine siliciclastics. This environmental deterioration has also been associated with the influence of the prograding siliciclastics, and is discussed later.

Both of these examples of environmental change seem to be driven by the relative sea-level cycles, and not by any regional climatic change. The carbonates seem to develop during rapid sea-level rise when the siliciclastic depocentre shifts landwards, and the carbonate demise seems to be due to the return of the siliciclastics during the progradation.

12.2 OBJECT ORIENTATED DISCUSSION

The following discussions are organised thematically around aspects of the stratigraphy described.

isolated platforms - why isolated, why drowned?

Cycle A in the Mut area sees the development of isolated platforms across a shallow flooded marine shelf area. These platforms are approximately round in plan view, with a diameter varying from 500m (Pirinç area) to 4km (west of Mut town), and a thickness of 80-100m. At the top of these platforms shallow marine carbonate production stops, and they are finally drowned and covered with deeper water sediment (marls) deposited beyond the photic zone. The term drowned, is used in the sense of the drowning unconformity, as defined by Schlager (1989). Two main questions concerning these platforms are addressed here: firstly, why are they "isolated"; secondly, why are they "drowned"? The first question is important, since a continuous, or rimmed platform morphology might also have been developed. The factors that impose the construction of isolated platforms, rather than a rimmed margin or a ramp topography (for example) need to be examined. The second question (why drowned?) has been the subject of much discussion in the literature, and is also

of economic importance, since the drowning of carbonate platforms creates potentially excellent petroleum reservoirs with good seals (Greenlee and Lehmann (1993): the Baturaja limestone of the Jene field in South Sumatra Basin, and; Rudolph and Lehmann (1989), the Natuna platform, offshore Indonesia). The question stems from the observation by Schlager (1981) that shallow platform productivity should potentially far outstrip even the fastest relative sea-level rise (s' should always be potentially greater than a'). Schlager (1992) and Emery and Myers (1996) give a clear summary of this problem.

Reasoning in terms of a' and s', this means that we should look for a decrease in s' to explain the give-up evolution (Neumann and Macintyre, 1985), rather than trying to explain it by an increase in a', which should never be greater than s' for a healthy carbonate platform. A number of possible reasons for an ecological crisis leading to a decrease in s' have been described in the literature. The arrival of siliciclastics can smoother reefal fauna and increase the water turbidity. The arrival of nutrients -often a precursor to the approaching siliciclastic depocentre- can provoke the smothering of oligotrophic-adapted calcareous bioconstructors, by mesotrophic-adapted soft-bodied fauna and flora (green-algae, soft-bodied corals, sponges, and diverse micro-encrusters). An increase or decrease in water salinity can provoke the demise of healthy reefal fauna. Predation by organisms, or an epidemic can decrease the growth potential of reefs (Emery and Myers; 1996). Erlich et al (1993) attribute the drowning of the Miocene Wilmington Platform to the arrival of siliciclastics and nutrients. Epting (1989) illustrates how isolated platforms of the Miocene of Luconia Province, offshore Sarawak, are progressively shut-down by the advancing siliciclastic deltaic sediments. Stoakes and Wendte (1988) and Scaturo et al (1989), describe platform margin retreat under the influence of incoming siliciclastics, in the Devonian build-ups of Western Canada. Zempolich (1993) explains drowning of a Jurassic carbonate platform in Italy due to excessive nutrients and oxygen deficiency during a time of rapid eustatic sea-level rise. Bice and Stewart (1990) describe drowning in a Jurassic platform in the Appenines due to a variety of tectonic and ecological factors, including lack of reef builders, lack of fringing rims, small size of seamounts, incursion of colder, less saline waters into the basin and crustal subsidence and sea-level changes. Roberts and Phipps (1988) describe the growth of coral competitors in the East Java Sea, Indonesia, due to nutrient influx from upwelling. Neumann and Macintyre (1985) describe how salinity variations can kill off a healthy reefal system, and Schlager and Philip (1990) propose a causal link between lack of oxygen (Cretaceous anoxic seas) and platform demise. Schlager (1981) proposes a volumetric argument to explain platform drowning. He illustrates how the amount of sediment required to be exported onto the platform slopes to buttress up an aggrading platform increases with platform height. This implies that for a given sediment exportation rate, an isolated platform will naturally diminish its surface area and eventually be drowned.

Reason for isolated development: to answer this question we must examine the stepwise development of the isolated platform bodies at Kizil Kaya and Zincir Kaya (figure 11.8). In the discussion that follows, "shelf' denotes the large-scale shallow marine area on which the isolated platforms develop. Medium-scale cycle A.1 is the first major marine flooding in both areas. In the more proximal setting (Kizil Kaya) only littoral and sub-littoral muds and silts are deposited, while in the more distal setting (Zincir Kaya) a carbonate shelf margin develops with a low angle slope and a relief of just a few metres. On the shelf margin a heterogenous mixture of constructed patches 5-20m wide is surrounded by shallow grainstone deposits. No relief is created on the shelf and this cycle is tabular. In cycle A.2 the shelf margin aggrades to a 30m relief and small platforms develop during the retrogradation (see Zincir Kaya): these serve as nucleii for the outward growth and partial coalescence of the platforms during progradation. In the internal shelf area to the north-west of Kizil Kaya fine grained siliciclastics continue to be deposited in a littoral marine environment. The corals (the main framebuilders at this time) are of very low diversity, being almost monospecific Porites, and show only platey and dome morphologies, surrounded by clay sediment and some red-algal encrustation. It is clear that the presence of fine siliciclastics, though not preventing coral growth, severely limits its production potential. This would explain why during the retrogradation of cycle A.2 sediment only accumulates in localised build-ups. The sediment in these build-ups is autochthonous or pseudo-autochthonous, and no sediment exportation occurs. The limited growth potential also explains why the progradation of cycle A.2 only partially fills out from the nucleation points (the mounds). The creation of relief may also be an implicit strategy adopted by the carbonate system that permits partitioning of the carbonate growth area (platform tops) from the siliciclastic deposition area (inter-platform areas). Local deformation of the energy field (from waves, tides and currents) by the creation of topography further enhances the separation effect produced by gravity, by continually winnowing the platform tops of fine siliciclastics. Coarse siliciclastics cannot be deposited on the platform tops since they are too heavy to be carried in suspension. The production potential of this whole system remains poor due to the constant arrival of siliciclastics, and so successive cycles simply amplify the isolated platform topography initiated in cycle A.2.

Reason for drowning: the isolated platforms of Zincir Kaya and Kizil Kaya are organised into a number of medium-scale cycles with exposure

probably occurring at the cycle boundaries (most probable at cycle boundaries A.3, A.4 and A.5). The cycle architectures are similar to those of Salleret al. (1993), or Handford and Loucks (1993) for isolated platforms. These exposure events show that we cannot talk of drowning or incipient drowning until the very last cycle at the top of the platform is reached: the surface area of the platform diminishes progressively but the bathymetry of the facies shows no overall deepening trend until the very top of the platform.

The sediment near the top of the platform is a well washed rhodolithic bound-rudstone, similar to that described by Erlich et al (1990), which he explains by being too deep an environment for prolific coral growth: corals being suited to euphotic conditions, while the red-algae being able to thrive in the mesophotic environment. This can be considered as the final drowning sequence. This facies appear near the top of both Kizil and Zincir Kaya, though the topmost facies is always a coralgal boundstone with microbial encrusters, and stunted monospecific (Porites knobs) coral and algal growth.

An ecological crisis is apparent from the facies in cycle A.4 in both Zincir Kaya and Kizil Kaya: the coralgal boundstones with microbial encrusters indicate an environment far from ideal for rapid platform sediment production. Stunted coral growth and the presence of micro-encrusting organisms suited to mesotrophic environments indicates that this may be due to excess nutrients. Other reasons for environmental stress are also possible, such as a decrease (or increase) in water temperature so that corals can no longer grow and compete successfully with other organisms, or a change in water salinity, though the facies observations alone made in this study do not allow us to say more about the role of these factors. Whatever the reasons, this shift seems to result in a decrease in productivity potential (s').

It has been shown that the prograding part of large-scale cycle A consists of an advancing siliciclastic shoreline, that progrades from the north-west out over the Mut isolated platforms that developed during the cycle-A retrogradation (see figure 7.3). Although Kizil Kaya, Zincir Kaya and the isolated platform in the Pirinç study area are directly overlain by marl sediments the most north-westerly isolated platform at logsite 56b (grid reference 260725 on the Mut geological map) is directly overlain by siltstones belonging to the offshore environment. This indicates that although siliciclastics were not being deposited directly over most of the isolated platforms, they were being deposited a few kilometres to the north-west at the same time as platform growth. This may have provided the source of nutrients, to the detriment of the sediment producers' growth potential on the platforms. The more distally positioned isolated platforms found in the south-east of the mapped area (to the east and west of Mut town) are of a comparable height to Kizil and Zincir Kaya, though they are up to four times larger in diameter. The higher rates of platform production that this size difference implies may well be due to the reduced influence of the nutrients incoming from the north-west. This is a hypothesis that can be tested by examining these distal platforms in the same manner as for Kizil Kaya and Zincir Kaya. Platform shut-down also occurs in these reefs, but it remains to be seen (by correlation) if it is simultaneous or younger than the shut-down in the reefs already studied. If it occurs later due to a progressively advancing nutrient front (a precursor to the siliciclastics) this situation would be very comparable to that of the Luconia Province in offshore Sarawak as described by Epting (1989).

Another possible cause of environmental stress is the shut-down of platform production due to sub-aerial exposure along the cycle boundaries. This cannot be the only reason for platform drowning, since the platform recovers and grows a number of times after successive exposure at cycle boundaries A.3 and A.4. Also there is no evidence that explicitly indicates an exposure surface at the very top of the platform. However, if exposure occurs during a time of environmental stress, time spent in the start-up phase may just be sufficient to push the platform production far enough below the rate of relative sea-level rise that it cannot recover, and facies characteristic of incipient drowning are deposited. The progradation at the top of the cycle that starts the drowning of the platform may deposit a frosting of slightly shallower fauna over the incipient drowning facies (here rhodoliths), but this may not last long enough to fully correct the sediment deficit, before the next retrogradation starts, finally drowning the platform. This would, indeed be expected if the medium scale cycles continued to be of approximately the same amplitude (18-30m), and this prograding "frosting" in an otherwise drowning trend is indeed observed in Zincir Kaya.

The platform drowning event is situated around the maximum flooding of large-scale cycle A (the exact position of the maximum flooding relative to the platform top is uncertain). This means that the rate of relative sea-level rise at the large scale is potentially at its highest at this time.

It is proposed that a decreased production potential (s') is principally responsible for the inability of the platform to keep pace with rising sea-level. The facies changes observed within the platform suggest that this decrease in production rate is related to an environmental change of some kind. The nature of the facies seems to indicate an increase in nutrients as the main environmental change. This is also consistent

with the proximity of the prograding siliciclastic delta system, that eventually progrades out over the carbonate shelf area, bringing with it terrestrially derived nutrients. Other environmental variations (eg. temperature and salinity) may also be responsable for the facies change observed, but for the moment these cannot be demonstrated. A detailed palaeoecological analysis of the facies changes may provide more precise answers to the exact nature of this environmental shift. Another source of environmental stress that may depress the productivity of the platform are the frequent exposure events that occur on at least some of the cycle boundaries within the platform (the first drowning facies are seen soon above cycle boundary A.5), though these alone are not sufficient to explain the drowning. The need for a proportional increase of exported sediment with platform height to buttress up the platform flanks (Schlager 1981) imposes an additional burden on the sediment budget, reducing the effective s' (the rate of sediment deposition on the platform top) as the platform grows.

So during a period of decreased s', the limiting value of a' (beyond which the platform drowns) is finally surpassed during a medium scale retrogradation (cycle A.5 in Zincir Kaya and Kizil Kaya), enhanced by its position around the maximum flooding of the large-scale cycle, and we push the platform over the threshold long enough for production to shut down completely, and drowning and burial in marls to occur.

Cross-bedded bioclastic sands (Silifke, base of cycle A)

The tidal regime that dominates during the deposition of these sediments is depends on two factors. Firstly the Mut Basin must resonate to the diurnal signal to generate tidal variations within the basin. Secondly the tidal passage must be restricted enough to generate strong currents. As the passage widens and deepens the flow per unit cross-sectional area diminishes and the current weakens. This would explain why during the retrogradation of cycle A the tidal system eventually shuts down, flooding by deeper water marls occurs, and shallow platform carbonates are deposited in a lower energy setting as fringing platforms against the northern flank of the graben. The exact time of tidal system shut-down is determined by the a'/s' ratio: as soon as a'>s' shut-down starts. If a'>s' for only a short time before a' once again drops to below s', then the system will go through a deepening trend, before once again shallowing, and drowning will not occur.

There is some evidence of exposure near the top of the tidal deposits before the drowning occurs (pendant and meniscus cements in Dibekli). If this is truely contemporaneous exposure, productivity would temporarily be shut-down. Then when the area is once again flooded the system is initially in a start-up phase, with a depressed productivity potential.

The producing ecology contains many bryozoa, red algae and molluscs. Coral debris is rare. This faunal assemblage is typical of sub-tropical environments. The contemporaneous abundance of corals (though of limited variety) in the Mut area indicates that this difference may be a local effect rather than due to the regional climate. Possible causes for the lack of corals are 1) the high energy conditions unsuitable for growth of the limited coral fauna available, 2) the influence of open marine colder waters from the Mediterranean, or 3) depth of the channel: corals being more suited to shallower environments. Note that this third factor is a counter-argument against the interpretation of these sediments as being shallow sub-tidal deposits.

Similar tidal deposits filling narrow topographies occur elsewhere at about this time during the Early Miocene flooding in New Zealand (the Otorohanga Limestone of the Te Kuiti Group, Anastas et al. 1998) in a temperate setting, and in the western limb of the closing Paratethys from the Molasse Basin in Switzerland (siliciclastic setting), through the Venasque area in Southern France (bioclastic tidal deposits) down to the southern tip of Corsica in the cliffs of Bonifacio, where thick bioclastic tidal deposits are seen. It seems that the flooding of relatively young orogenic terrains often creates strait basin geometries in which tidal currents are likely to be generated.

Slumps

Slumping has been observed in both the Silifke and the Mut areas. The causes evoked to explain this slumping in each area are different. The slumping in Pirinç has been shown to occur during a time of rapid sea-level fall. Progradation and steepening of the platform slope also occur at this time. The slope steepening created potentially unstable slope deposits, though it is proposed that the slumping was initiated by the sea-level fall due to the coastal and sub-aerial erosional processes that took place at this time. Rigid block rotation is observed at the top of the slump, indicating that the topmost beds were already cemented before deformation occurred. The basinal slump deposits are a mixture of rigid olistolith blocks that have slid from the shallow platform setting, and plastically deformed slope sediments mixed with deep marl sediments (see Pirinç chapter). This indicates that not all the sediment was lithified before slumping

occurred. Some of the slump beds are underlain by grain-flow deposits (mostly micro-packstones). This is explained by the steepening slope angle and associated sediment gravity flow processes prior to the sea-level fall.

In the Dibekli transect slumping is observed in two places: firstly at the base of cycle B, then at the top of cycle C. The principle cause of the first slump is considered to be due to the deformation of the underlying sediment: a 20m thick carbonate platform develops initially on the firm substrate of a coarse-grained fan-delta (cycle B.1), then builds out over the more distally positioned marls. Differential compaction occurs in these underlying marls, probably due to loading by the platform. The overlying partially lithified platform undergoes listric faulting to compensate for the deformation: rotation, plastic deformation, and shunting of un-deformed blocks occurs along a glide plane situated at the base of the platform. A possible sub-aerial exposure surface has been proposed for the top surface of the platform (as indicated by extensive cavity formation that may be a fossil karst), and this may also have played a role in the slumping/creep, though it is not essential to the explanation. Note that this mechanism is very different to the catastrophic collapse/exposure mechanism to which the Pirinç slumps are attributed. The second slump deposits in the Dibekli area (top cycle C) are explained by a similar mechanism to the Pirinç slumps: a prograding platform constructs out over a steep slope, so that collapse is provoked by a prolonged period of sub-aerial exposure of the platform top. Additionally, the platform progrades out over softer, more compactable marls in a similar way to the first Dibekli slump: the post-depositional differential compaction and flexure of the (partially) lithified platform sediments.

Carbonate-siliciclastic cycles

Carbonate/siliciclastic cycles have been observed at the large, medium and small-cycle scale in the Alahan transect. In all three scales it has been interpreted that one carbonate-siliciclastic couplet constitutes a retrogradational-progradational cycle, and that the carbonates develop during the retrogradation while the siliciclastics arrive during the progradation (this labelling causes some conceptual problems, since the retrogradational carbonates often in fact have progradational geometries: this is discussed later).

Although the repetition of a lithological motif at different scales has been demonstrated, the causes are not necessarily identical, and each scale needs to be examined separately.

During large-scale cycle A the isolated platforms form in the Mut region, and "drown", possibly because of the influence of siliciclastic-associated nutrients on their production potential. During the progradation of this cycle a siliciclastic shoreline advances seawards, and the top cycle boundary defines the top of these prograding siliciclastics overlain by the retrograding carbonates of cycle B. This cycle B sees the arrival and mixing of centimetre-size basement pebbles at the top of the retrograding carbonate platform (cycle boundary B.4), indicating an increasing siliciclastic input just prior to platform-production shut-down. This is consistent with the hypothesis of siliciclastic influence causing the platform shut-down here.

The medium-scale cycles C.5 and C.6 show some evidence for the detrimental effect of siliciclastics on carbonate production. Figure 7.7 illustrates how the retrograding carbonates of cycle C.5 contain diverse coral fauna typical of the middle reef-front environment at the base, developing into lower reef-front facies, and finally into Nummulitid grainstones with no corals at the top. The disappearance of the corals is associated with the deterioration of environmental conditions: a pre-cursor to the deposition of the fine-grained siliciclastics found above.

The idea that the arrival of siliciclastics is always detrimental to carbonate production does not systematically hold true: many field examples exist in modern-day carbonate environments, such as the Belize platform (A. Strasser, pers com.) where corals actively grow under the influence of incoming siliciclastics. This leads us to an alternative mechanism that may explain the carbonate-siliciclastic cycles. Carbonates and siliciclastics may be contemporaneous and occupy equivalent positions on the platform, with lateral accretion of the siliciclastic depocentre occuring due to auto-cyclic processes, and creating the carbonate-siliciclastic cycles. This would produce much less abrupt lithological switching, with siliciclastics being abundant within the carbonate lithologies, and carbonate producers being found commonly within the siliciclastic beds. This is not observed at the medium and large scales, though it is seen in the small scale cycles. Another consequence would be that carbonate and siliciclastic complexes would be found laterally within close proximity, but this not been observed (the field of observation in Alahan is roughly 2km wide). Hence lack of evidence means that autocyclicity seems unlikely as the cause of the medium and large-scale cycles.

Autocyclicity may, however, explain the small-scale cycles. Take for example the small-scale cycles of cycle C.5: the molluscan debris that constitutes the retrograding carbonates is intimately mixed with poorly sorted siliciclastics, from gravels to silts. These molluscs are also found throughout the siliciclastic horizons, though more dispersed than in the coquina beds. Hence the deposition of siliciclastics cannot be considered to inhibit the growth of these molluscan fauna. The positioning here of carbonates in the retrogradation and siliciclastics in the progradation is

rather due to a shifting hydrodynamic regime, resulting in reworking of shell debris during the retrogradation.

In summary, at the large- and medium-cycle scales there is evidence to suggest that carbonate productivity is severely stunted by the arrival of siliciclastics and associated nutrient-rich waters. So a carbonate production "window" is created when retrogradation of the siliciclastics occurs and the siliciclastic depocentre migrates in a proximal direction, and it is at this time that carbonate edifices are constructed. The retrogradation and progradation of the siliciclastic depocentre may be driven either by relative sea-level variations (a'), or by fluctuations on the siliciclastic sediment input rate (s') due to hinterland processes. Some medium-scale cycles in other areas are shown to be the result of relative sea-level cycles, making it likely that this mechanism also applies here. However, this is far from being a proof. More analysis would be required to adequately demonstrate fluctuations in siliciclastic sediment supply rate: clay mineral analysis may give information about the pluviality, and erosion rates in the hinterland, while oxygen isotope analysis may provide tighter control on the time framework, and hence on absolute sedimentation rates.

Distribution of time in the sediment

The correlations show us that the formation of surfaces in some settings corresponds to the deposition of important thicknesses of sediment accumulation in other places. We take the example of the correlated large-scale sequence boundary C (see figure 11.6): in the Alahan transect (figure 11.9) this corresponds to a single discrete surface. In the Pirinç transect (figure 11.8) the same surface has been identified in the updip position, while following it downdip, it is shown to diverge into four medium-scale cycle boundaries, bounding three medium-scale cycles C1-C3. So the cycle boundary C in Alahan is time-equivalent to cycles C1-C3 in Pirinç.

The identification of the missing sedimentary packet that corresponds elsewhere to a hiatus surface gives us some relative control on the amount of time concentrated in the surface. Again taking the example of cycle C in the Alahan area, we see that only three of the six medium-scale cycles belonging to large-scale cycle C are preserved here. The other three cycles, observed in the Pirinç transect, were deposited during a time of platform exposure in Alahan. By assuming that cycles of a given scale have approximately the same duration, we can estimate that half of the duration of cycle C is contained within the cycle boundary C during a time of sub-aerial exposure. Stretching this further by working with our hypothesis that the large-scale cycles correspond to the 400-Ka Milankovitch periodicities, we can allot approximately 200-Ka as the exposure time in this cycle boundary. The same relationship can also be demonstrated for cycle B in the Alahan area (see figure 11.6), where a similar proportion of the time for the deposition of cycle B can be allocated to the cycle boundary B.

A similar distribution of time also seems to apply to smaller-scale cycles. Take the example of Zincir Kaya as presented in figure 9.4 (using the pre-correlation nomenclature): cycle boundaries 3, 4, 5 and possibly 6 are discrete surfaces (probable exposure surfaces) on the platform top. Their lateral time-equivalents are packets of sediment found on the south-eastern flank of the platform. The relative amount of time contained within the hiatus surfaces on the platform top cannot be readily estimated: no finer cycle subdivision has been made here which could act as a proxy for time.

So it seems that different scales of temporal hiatuses are distributed throughout the sedimentary record, and the scale of hiatus observed depends on the scale at which we look. This is very similar to the stratigraphic temporal hiatus distribution described by Plotnick (1986), and Sadler and Strauss (1990).

The recognition that the downslope time-equivalent of a sequence boundary is a packet of sediment, and not a single distinct surface may go some way to explaining why the definition of a sequence boundary in distal settings is so problematic, and has often been the subject of dogmatic argument. Sequence boundaries have a clear chronostratigraphic significance in the proximal position where they exist as discrete surfaces representing temporal hiatuses, but in the distal position they correspond to packets of sediment and may only be definable as intervals or zones. If there is no temporal hiatus they have no chronostratigraphic significance, and their definition may be meaningless. The definition of maximum flooding surfaces follows a similar logic, with their definition being most meaningful in the distal position where they correspond to temporal hiatuses.

12.3 COMPARATIVE STRATIGRAPHY DISCUSSION

The results and synthesis chapters have described the stratigraphy across the Mut Basin and proposed correlations to define contemporaneous environments. This chapter has so far discussed the possible causes of the various features seen, as well as the driving forces behind the different scales of cycles observed. The correlations constructed between the Silifke and Mut areas permit the comparison of contemporaneous environments. The differences between coeval deposits can now be discussed.

Isolated platforms and tidal deposits

The contemporaneous nature of the isolated platforms at the base of cycle A in the Mut area and the tidal deposits in the Silifke area, has been demonstrated with some certainty. These are very different stratigraphic architectures which would normally be difficult to compare and correlate. The fundamental reason for such different styles can be attributed to the difference in hydrodynamic regime: the Silifke graben area experiences very strong bi-directional tidal currents, while the Mut shelf is a relatively low to moderate-energy environment, though the tidal range must have been similar to that of the Silifke area. Some evidence for strong current activity does exist on the Mut shelf area, but this is limited to times of medium-scale lowstand, when the weak tidal currents (ubiquitous across the basin) are deformed and concentrated around the shoreline topography created at the base of the emergent isolated platforms. During these times carbonate sand shoals with metre-scale cross-bedding are preserved. These deposits are localised in space and time, and are atypical of the general inferred low-medium energy shelfal environment that dominates.

This difference in hydrodynamic energy is a result of the fault-controlled basin geometry. The basin dimensions generate tidal resonance, and the Silifke graben (possibly the only connection between the Mut and the Mediterranean Basins) funnels the tidal ebb and flow into strong currents. The Mut shelf area is at the closed end of the basin which explains the lower energy conditions found there.

This difference in hydrodynamic conditions affects both the nature of the producing ecologies, and the sedimentary processes of erosion, transportation and deposition. The bioconstructors available at this time (mainly Porites corals) are unsuited to the high-energy conditions found in the Silifke graben area, so they produce little sediment, and cannot construct edifices. Bryozoans, molluscs, foraminifera and red algae are better adapted to these environments. They produce large amounts of bioclastic sands which are transported and re-deposited as migrating sand waves in a complex tidal setting. Production potential is very high and internally cross-stratified tabular bedsets are produced that completely fill the strait area.

A difference in bathymetry may also explain the variation in producing fauna between Mut and Silifke. The isolated platforms in Mut seem to closely trace sea-level, so water depth is never greater than a few metres, while the bioclastic tidal deposits in the Silifke area are potentially deposited in greater water depth, though still within the mesophotic zone (due to in-situ crusts of red-algae on the tops of sandwaves). Working with the idea that the corals are best suited to the euphotic zone, this may explain their virtual absence from the Silifke area.

Another reason why isolated platforms develop in the Mut area may be that this is an adaptive strategy/response to cope with the simultaneous influx of siliciclastics, by partitioning the siliciclastic from the carbonate depocentres. It is possible that without the influence of these siliciclastics the Mut carbonate shelf of cycle A may have developed a more continuous fringing platform morphology, possibly with a rimmed margin, similar to that observed from the top of cycle A to cycle C in the Pirinç transect.

The large scale correlations demonstrate that production shut-down (drowning) of both the Silifke tidal deposits and the Mut isolated platforms of cycle A was roughly contemporaneous. At the medium-scale cycle resolution it is difficult to be certain of the cycle-for-cycle correlation, and the error is estimated at plus or minus one cycle. Shut-down of production leading to the drowning of the Mut isolated platforms has been attributed to a depressed productivity potential during a time of rapid relative sea-level rise (across the maximum flooding of large-scale cycle A). This depressed production potential has been explained by the influence of fine-grained siliciclastics and associated nutrients prograding from the palaeo-Goksu delta to the north-west. This reason is less valid as a cause for production shut-down in the Silifke area, since this is 40km from the delta: clouds of nutrients and turbid water may be carried across the basin, but this seems relatively implausible here, considering the local extent of the influence of this delta system. The shut-down of platform production in the Silifke area is more gradual than the abrupt drowning of the isolated platforms (figure 8.16, log 52 demonstrates this gradual deepening of the Silifke tidal deposits), and may simply be explained by the inability of production to keep pace during a time of rapid relative sea-level rise.

Contemporaneous siliciclastic and carbonate depositional systems

In the mixed system described on the northern flank of the Mut Basin in the Alahan and Pirinç transects siliciclastics and carbonates are inferred to have been deposited simultaneously in settings around only ten kilometres apart (the approximate distance between the Pirinç and Alahan transects). Unfortunately the Alahan transect only preserves the sediments deposited during highstands of sea-level, with the sea-level lowstands represented by erosional surfaces. The positions of the lowstand deposits have been inferred distally from Alahan in marl-silt units by calcimetry, though no detailed study was carried out because of the poor exposure (see figures 7.2-3).

Further west along the flank of the basin at the Pirinç transect the sea-level lowstand carbonate platforms have been identified. These are thin coralgal framestone units (up to 20m thick) with a distinct 20-40cm bedding, separated by softer marly sediments. Each unit pinches-out rapidly up-dip against the underlying slump-top or marl, where the near-shore water becomes too shallow. Basinward, these units seem to thin rapidly, though present-day erosion has masked the exact position of any distal pinch-out that may have occurred (except for cycle C2 in figure 11.8). They form what can be considered as fringing platforms, and these were never much more than a kilometre wide. Their lateral extent is difficult to estimate since the outcrop is poor, though occasional glimpses allow some of these platforms to be partially followed in the field. The transition from carbonate fringing platforms to the siliciclastic lowstand does not outcrop.

Fortunately both siliciclastic and carbonate units deposited during the large-scale sea-level highstands outcrop, permitting a comparison. This is best illustrated by looking at the highstand of cycle A in the Pirinç and Alahan transects (see figures 11.8 and 11.9). Both show large-scale shallowing-up trends, sub-divided into small-scale cycles (see logs in figures 6.13 and 7.11). Very different settings have been described in these logs: Alahan shows an offshore to upper shoreface transition, while the carbonates observed in the Pirinç area for this interval are from the slope area. The contemporaneous development of a high-relief carbonate platform margin fringing the basement hinterland and a siliciclastic delta within 10km of each other illustrates how these two environments are not mutually exclusive. The lack of siliciclastics within the Pirinç transect (above the cycle A maximum flooding) would suggest that the terrigenous material brought by the Palaeo-Goksu is flushed out into the basin or maybe transported south and west along the shoreline, with no eastward transportation to influence the carbonate production at Pirinç.

Highstand platforms of cycle A in Mut and Silifke

In the Dibekli (Silifke) transect area no carbonate platform develops during the highstand of cycle A, while on the northern flank of the Silifke graben continuous platform deposition is seen, and on the Pirinç transect a wide highstand platform develops and progrades. In the Alahan area the cycle A highstand is a prograding siliciclastic shoreline. The lack of platform in the Dibekli area is principally explained by the steepness of the underlying basement topography: producing-fauna need a firm substrate on which to grow, and a platform needs a relatively wide shallow area on which to generate sufficient quantities of sediment, neither of which are provided by the steep Dibekli basement topography during the cycle A highstand. The Silifke graben structure is assymetrical, with the flanks steeply dipping in the south, and gently dipping in the north. This explains why a platform can develop on the northern flank. The southern flank is in places steep, but is also highly irregular: the cycle C highstand in Dibekli develops a carbonate platform since a wide shallow area is flooded at this time.

12.4 DISCUSSION OF METHODOLOGY

The methodology as defined in chapter 3 was found to be satisfactory in reaching the objectives set out in this study. Some comments useful to its future application are made here, and some refinements to the conceptual framework are proposed.

Relative roles of geometries and facies in defining cycles

It was found that the relative importance of the different dataforms (facies and geometries) in defining sedimentary cycles was highly dependant upon the scale of the cycles being defined: medium-scale cycles were readily defined from the bedding geometries since the size of these cycles was such that the lateral and vertical bedding variations involved could readily be observed within an "outcrop-sized" field of view. Small-scale cycles were best resolved from the facies evolution within the logs, since the lateral variations of bedding patterns at this scale are undramatic and were not readily observed in an outcrop view. The large-scale cycles were defined principally during the construction of the stratigraphic cross-sections: these cross-sections gave an overall view that was not physically available in the field, allowing the most important surfaces to be determined. The bedding geometries and facies observations played an equally important role here.

Divergence from simplified conceptual base of prograding/retrograding packets

The use of the terms progradation and retrogradation to describe the sedimentary cycles into which we divide the stratigraphic record is not always appropriate, as has been demonstrated by a number of cases in this study:

Case 1: abrupt facies changes define the cycles, though no progradation or retrogradation is observed in the bedding geometries, and no gradual facies trends are seen: this is illustrated by cycles C1-4 in the Pirinç transect (see figure 11.8), where discrete facies changes from shallow platform carbonates to deep

marine marls mark the cycle boundaries, though with no accompanying progradations/retrogradations. At the large scale the stacking-pattern of medium-scale cycles C1-4 constitutes a deepening-up and retrograding trend. Within each cycle deposition rates are relatively homogenous along the depositional profile observed, so the creation of relief necessary for the formation of progradation/retrogradation within the field of observation does not occur. If the sediment is simply aggrading, with no progradation at the unseen margins of each of these cycles, this implies that a'/s'=1 during the deposition of each cycle, separated by periods when a'/s'>1, during which time the the facies belts retreat landward. This infers that cyclic variations in the a'/s' ratio may form sedimentary cycles, whether or not they fluctuate around 1. Secondly it must be noted that bathymetric trends of deepening or shallowing, and geometric trends of progradation and retrogradation may be replaced by equivalent but abrupt changes or shifts.

Case 2: geometries define cycles, though no clear deepening or shallowing trends are observed: cycle A4 in Zincir Kaya illustrates this, with the cycle being defined principally by the progradation visible off the western side of the platform, though when the corresponding sedimentary packet is examined on the platform in log 40 it is difficult to see a distinct shallowing-up trend in the "prograding" packet of the sediment above the maximum flooding (see figure 9.6). The depocentre is dilating since a'/s'<1, so progradation occurs, but the platform top traces sea-level, with no observed bathymetric change (at least to within the resolution of our observations). Note that the net a'/s'<1 and the local platform-top a'/s'<1 for the logsite 40, however, since the platform top seems to have already filled up to base level, excess sediment production cannot be stored here, but is transported to the flanks. This has important implications: when a'/s'<1 a shallowing-up trend will be observed only until base-level is reached, then the excess will be transported away.

Clearly cycles of "progradation and retrogradation" may not always be observed during a'/s' cycles. The a'/s' cycle is the key stratigraphic building block, and it is this that has been systematically used here. Shallowing and deepening of the platform-top may occur as a'/s' fluctuates below and above 1 with no observed progradation/retrogradation. Equally, progradation and retrogradation of the platform edge may occur in response to a'/s' cycles, with little or no discernible bathymetry change of the platform top facies (eg. Zincir Kaya). Cycles of a'/s' are thus best defined from the sum of the observations made, and not from only one type of information. They represent the net response of the sedimentary system within the field of observation. Note also the the value of a'/s' need not cross 1 as it rises and falls, in order to produce sedimentary cycles: if it stays above or below 1 cycles will still be preserved in the rock record, though these will have net distal or proximal-stepping trends respectively.

So to define the a'/s' cycles as cycles of progradation and retrogradation is unsatifactory, since these geometries may not have been observed (though they may be taking place outside of the field of observation). An alternative nomenclature is required, though nothing entirely appropriate has been found. The terms transgression and regression came the closest: they are traditionally defined as the flooding of the land by the sea, and the exposure of the land by the withdrawl of the sea. This advance and retreat of the shoreline is a response to the net balance between relative sea-level (a', eustasy and subsidence) and sedimentation rates (s') in the littoral region, as Reading (1986) illustrates:

"Two situations may be envisaged.

(1) Transgressive: when subsidence and rise of sea level are more important than the supply of terrigenous sediment, the environment is starved of sediment. This results in reworking, erosion and diagenesis of deposits, transgression and deepening of the environment...

(2) Regressive: when subsidence and rise of sea-level are less important than terrigenous sediment supply, progradation and an increase in the proportion of continental facies result."

So transgression is a time when a'/s'>1 in the littoral region, and regression when a'/s'<1 in the littoral region. However, since they apply specifically to the littoral region, and not to any given sedimentary system observed, these terms cannot be used universally to define a'/s' cycles. The problem is illustrated by considering the common case of a carbonate platform that progrades (depocentre dilates) during a time of relative sea-level rise, contemporaneous with a landward movement of the shoreline (eg. Pirinç transect, progradation of large-scale cycle A, although we have no information about the position of the shoreline, accommodation space is continually being created throughout this time, and the coastline could feasibly be migrating landwards).

Some nomenclature needs to be developed and I tentatively propose that an a'/s' cycle that fluctuates above and below 1 be broke into "distal" and "proximal" trending packets, with "proximal trending" indicating that a'/s'<1. (Note that the terms landward and seaward stepping often cause confusion when referring to isolated platforms, or rimmed margins).

Mixed system complexities

An interesting problem is highlighted by the definition of cycles in the mixed system in the Alahan transect: carbonate production, as already discussed, is out of phase with the siliciclastic deposition. During the siliciclastic retrogradation the carbonates develop and produce prograding geometries while the facies bathymetry traces sea-level. Then when the siliciclastics prograde out the carbonate production shuts down. So the retrograding/prograding cycles defined in the carbonate deposits are different to the cycles defined in the siliciclastics. This appears contradictory, until we realise that the terms retrogradation and progradation are not characteristic of a time interval, but describe the response of a specific sedimentary body to changes through time. Also that different sedimentary systems in the same time interval will have different responses to the same signal (of accommodation change and climatic variation etc.), and that these systems may be coupled, as is the case here. The retrograding/prograding cycles as defined here in the siliciclastics tell us about the accommodation variations (and possibly about the siliciclastic sediment supply variations), while the retrograding/prograding cycles in the carbonates tell us principly about the changing nature of the environment. We are here dealing with two sedimentary systems.

13 – CONCLUSIONS

In this study the relative sea-level variations (eustasy and subsidence combined) for each site were constructed by taking into account the total cumulative thickness and the estimated bathymetry. The resultant curves were compared, and found to be very similar: indeed, so similar that they can be considered to share a single common relative sea-level evolution. This implies that the subsidence rate in each of the study sites was identical.

This common relative sea-level signal has a hierarchical organisation, and has been broken down into four distinct component signals. Each component has a well-defined amplitude of sea-level variation, which produces equivalent sedimentary cycles in the observed stratigraphy. Approximate cycle periods have been calculated by dividing the total time interval by the number of cycles for each cycle-scale. From knowledge of the cycle amplitudes, cycle periods, the global climatic context (presence of ice-caps), and the regional structural setting (a post-extensional setting), mechanisms for each scale of cycle have been proposed. These are summarised here:

CYCLE SCALE	AMPLITUDE	PERIOD	CAUSES	ORDER
very large	>200m	>3.4Ma (non-periodic?)	basin subsidence + eustasy (probably tectono-eustatic)	(2nd)
large	100-150m	<570Ka	glacio-eustasy possibly driven by 400Ka eccentricity cycles	(3rd)
medium	18-30m	<100Ka	glacio-eustasy possibly driven by 100Ka eccentricity cycles	(4th)
small	3-6m (when relative sea-level change demonstrated)	13-20Ka	most auto-cyclic/some glacio-eustatic (?) possibly driven by 20Ka precession cycles	(5th)

The very large-scale monotonous relative sea-level rise cannot be adequately explained by any single mechanism, because of its relatively high rate, so a combination of basin subsidence and tectono-eustatic sea-level rise is proposed. By comparison of the rates and amplitudes of the relative-sea level changes observed with those of possible contemporaneous processes, large and medium-scale cycles are attributed to glacio-eustatic mechanisms. Tectonic mechanisms, although well-able to match the rates of eustatic rise and fall observed, were unable to explain the cyclic nature (both rising and falling) of these changes. The calculated frequencies of these glacio-eustatic cycles are similar to Milankovitch-frequencies, and so it is proposed that these cycles were driven by astronomical forcing. Changes in global insolation patterns drive the melting and forming of the Antarctic ice-cap, generating the eustatic variations described. Most of the small-scale cycles observed are simple lateral facies shifts, with no distinct bathymetric changes, so they are considered autocyclic. However, a few show some bathymetric variation, and may be due to relative sea-level cycles.

Matching the relative sea-level curves permitted high-resolution correlations to be made between the different study areas, well beyond the resolution of the biostratigraphy. Each study area is markedly different, so a simple comparison of the facies evolution could not generate viable correlations. Contemporaneous depositional environments were identified across the basin, and within this time-framework contrasting environments were compared. The most prominent variations within the basin are:

1/ in large-scale cycle A, high energy tidal-strait deposits of allochthonous sediment in the Silifke area developed contemporaneously with isolated platforms constructed from autochthonous or para-autochthonous deposits in the Mut area. This was a direct result of intra-basinal variation in hydrodynamic regime: the Straits of Silifke formed a narrow connecting passage between the Mediterranean and the Mut Basins, in which strong tidal currents were generated as the Mut Basin resonated to the diurnal

signal. These currents did not develop in the Mut area, being the closed northern end of the basin. The hydrodynamic variations were themselves a result of the basin geometry as defined by the bounding basement faults and the resultant basement topography.

2/ the highstand carbonate platform deposits of large-scale cycles A and B are undeveloped in the Dibekli transect, though they are present on the north side of the Silifke Graben and in the Mut (Pirinç) area. This is explained by the form of the underlying basement topography in the Dibekli area: during these times the shallow-marine substrate (basement) is steeply inclined and narrow. Little sediment is produced (small production area), and down-slope processes dominate (steep-slope), so sediment accumulation in the shallow-marine environment is very low, and a carbonate platform cannot develop. During the highstand of cycle C a wide, flat basement shelf area is flooded in Dibekli, and a carbonate platform accumulates. The basement topography in the Mut area is not so steep as in Dibekli, and carbonate platforms can develop during highstand times.

3/ the presence of the palaeo-Goksu river system feeding into the north-west corner of the basin strongly influences the sedimentary environment in the Alahan study area. Here a mixed system develops, and small-scale cycles not observed in the other sites are preserved. The two-component sedimentary system generates distinct carbonate-siliciclastic cycles, with carbonates developing during the transgression of the deltaic system, and siliciclastics deposited during the regression. No such deposits are observed in the Pirinç section, even though this is only 15km from Alahan, so the influence of the terrigenous input is highly localised.

This demonstrates how, given a common relative sea-level history, but very different local conditions (here principally hydrodynamic regime, basement topography, and siliciclastic input) very diverse stratigraphic organisations are generated. It also shows how these factors can vary rapidly over the space of a few kilometres within a basin: strong tidal currents develop in the southern connecting sea-way (Silifke), while siliciclastics pour into the basin from the north-west corner (Alahan), and a carbonate platform develops a short distance away against the northern flank of the basin (Pirinç).

The detailed time-stratigraphic correlations developed in this work have shown how packets of sediment can correlate to hiatus surfaces in other areas (eg. cycles C1-3 in the Pirinç area correlate with cycle boundary C in the Alahan area, see figure 11.6). This allows the relative distribution of time in the sediment and in the hiatus surfaces to be estimated. Large-scale cycle boundaries B and C in the Alahan area have been demonstrated to contain approximately half the total amount of time allotted to each cycle (only half the number of medium-scale cycles allotted to this large-scale cycles are found in the Alahan transect). A similar organisation is true for the maximum flooding surfaces, which correspond to packets preserved in a more proximal position. This relationship has been demonstrated at the large and medium-scale of cycle, with a similar proportion of time concentrated in the hiatus surfaces for a given scale of observation.

This has direct implications for the way in which we sub-divide the sedimentary system: the chronostratigraphic importance of the sequence boundary diminishes in a distal direction, until it corresponds to a thickness of sediment containing no major temporal hiatus. In this position it may be more appropriate to define a sequence boundary zone, or even to leave the sequence boundary undefined. Similarly, the chronostratigraphic significance of a maximum flooding surface decreases in an up-dip direction. This model is at odds with the concept that the sedimentary record is sub-divided into discrete packages bound by well-defined surfaces running its entire length. Rather, emphasis should be placed on the distribution, relative importance, and lateral variability of chronostratigraphically significant surfaces.

14 - FUTURE WORK

It is difficult to escape the feeling that this study is just the beginning, since more questions now exist than when this work began three years ago. The large-scale synthetic nature of this study has left many stones unturned. The first stone to turn is the diagenetic aspect: I have described many cycle boundary surfaces that have some inconclusive indicators of sub-aerial exposure, and it would be of great interest to study the cements in thin section, and the surfaces in the field to resolve this question.

Secondly, in order to provide a more complete picture of the platform to basin transition, it would be necessary to log the internal platform sediments in the northern extremity of the Pirinç outcrop. This would help to tie down the exact position of the cycle boundaries B, C and D on the platform.

Detailed time-control would add much value to this work, by testing the correlations made, and quantifying the distribution of time within the sediment. This may be achievable by generating an oxygen isotope curve for the study interval, and correlating it to other published curves that contain fine time-control.

The relative sea-level changes observed were dramatic compared to other stratigraphic intervals (eg. The Mesozoic) simply due to the presence of the glacio-eustatic mechanism, and the size of the amplitudes that were generated, and so this aspect was emphasised here. Detailed observations of climatic variations remained relatively undeveloped. Clay mineral analysis within the siliciclastic units may give important information about climatic variations, and it would be interesting to see if these correspond in any way to the relative sea-level variations observed.

The palaeoecology of the isolated platforms of cycle A in the Mut area would provide a wonderful study, since the time control now exists with which to compare coeval environments down to a sub-metric scale along almost continuous and rapidly varying depositional profiles. Such a study could be done in many of the outcrops in this area.

The Mut Basin provides such a plethora of excellent outcrops, that the list of potential field studies is endless. On a larger scale, the Mut Basin is a tectonically quiet setting during the study interval examined: but to the east the Adana Basin is undergoing active extension and normal (oblique?) block-faulting at this time, and in the west the Antalya Basins may be undergoing active compression. It would be fascinating to see what kind of signal is preserved in these two very different tectonic settings in the same time interval.

15 - ACKNOWLEDGEMENTS

First and foremost I would like to thank my supervisor and friend Frans Van Buchem for all his help and encouragement during these last three years, without whose support and enthusiasm in the face of adversity (and bureaucracy) this project would never have existed.

Many thanks to Andre Strasser, for his time, his discussions and for always pointing out the good things first (and also for teaching me the real meaning of the numbers 4 and 5).

Naci Görür from the Istanbul Technical University provided invaluable aid for working in Turkey, and shipping samples, and without who's help this work would not have been possible.

Many thanks to Carla Muller, who dated my nannoplankton samples, and to Roland Wernli of Geneva, who dated my forams.

Big thanks to my field assistants who put up with the field work and me during long hard weeks in the field, in a little town called Mut...Kadir Eris (the Organiser) who's incredible organisational abilities never ceased to astound me. Gursel Sinan whom I'm afraid got rather bored (sorry!), but was a great help, and Christophe Prince, who risked life and limb dangling off big cliffs to get some rocks.

This project was sponsored by TOTAL, Elf and the IFP by the joint ARTEP project. Many thanks to them for making it all possible. But their contribution did not stop there, so I would like to say thanks to Robert Boichard (TOTAL) for the time and interest that he dedicated to this project, and Peter Homewood and Herbert Eichenseer of Elf, for their excellent scientific advice, especially in orientating the project in the first year.

To Oleg, Mathius and Jurgen from the Palaeontology Institute in Vienna, thanks for a great time in the field and lots of cold beers on Mut castle; and to Werner Piller for his time and help with the microfauna, and for telling us all about Mut in the first place!

And to Gilbert Kelling for his advice in the beginning, and for showing me round the Derinçay Formation. Thanks also to Gilbert Camoin for his comments on my microbial coralgal framestones. Many thanks to an unknown student at Fribourg University who hand picked my forams for dating, and to the Swiss National Research Fund who paid for his time. I am also indebted to the Swiss National Science Foundation for financial help in a field trip to Bermuda to look at modern carbonate systems in sub-tropical settings (No. 20-46625.96).

Et, bien sur, mille remerciements a ma chère Carine....pour tout.

16 – APPENDIX

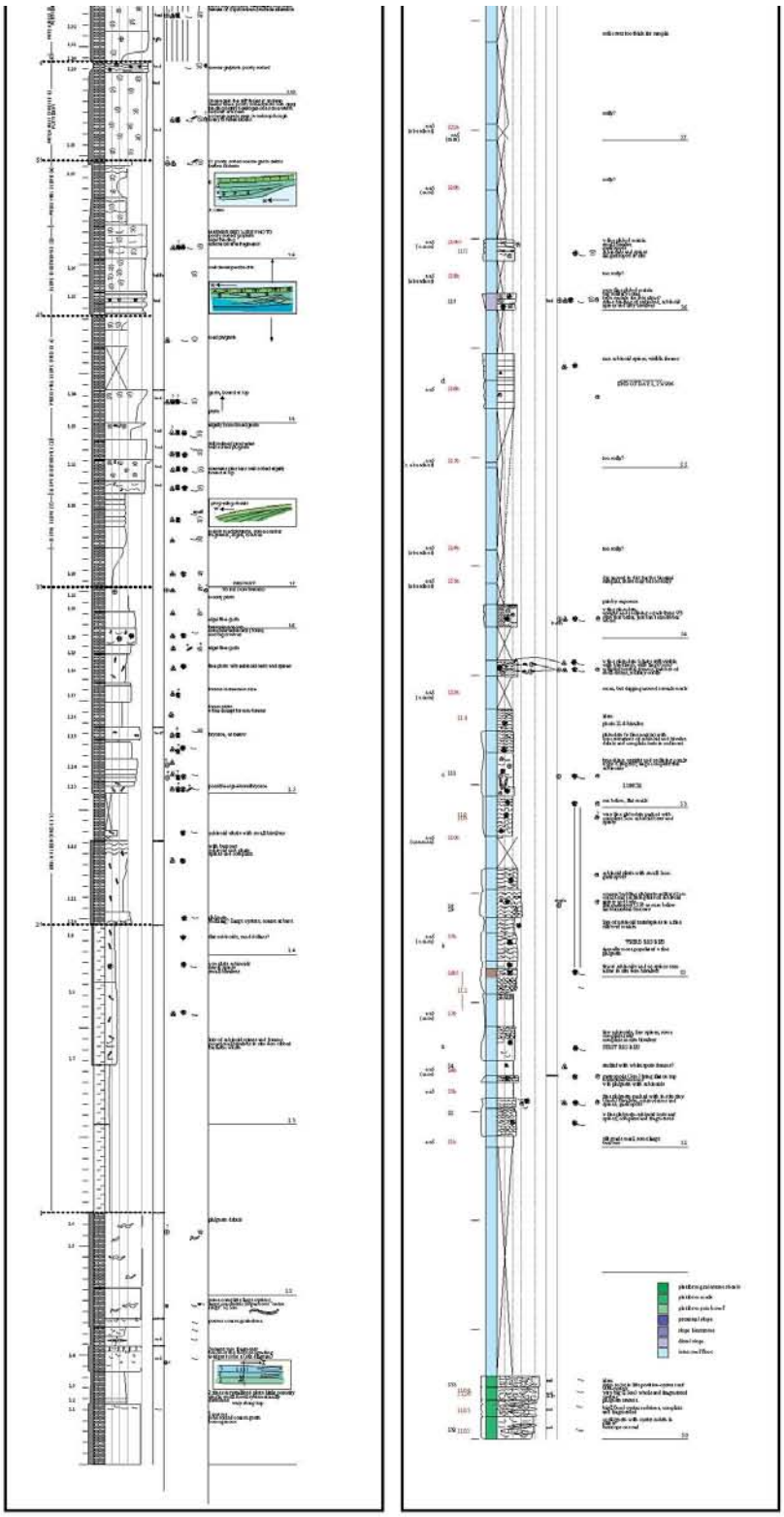

Appendix figure 16.1-2: Ermenek Region: logs 1 (left) and 5 (right)
(Valley area 16km north of Ermenek)

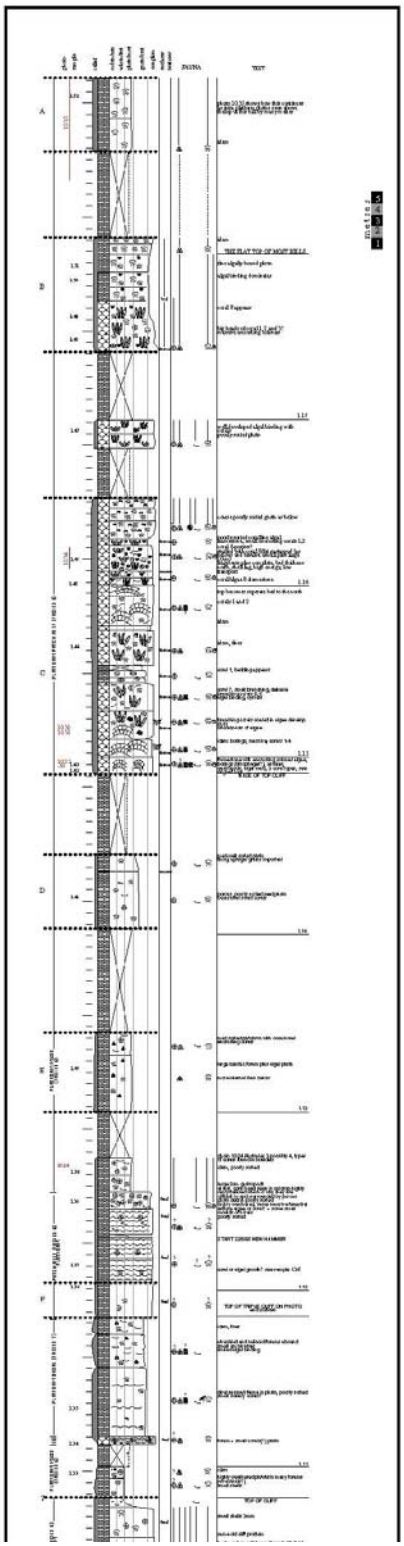

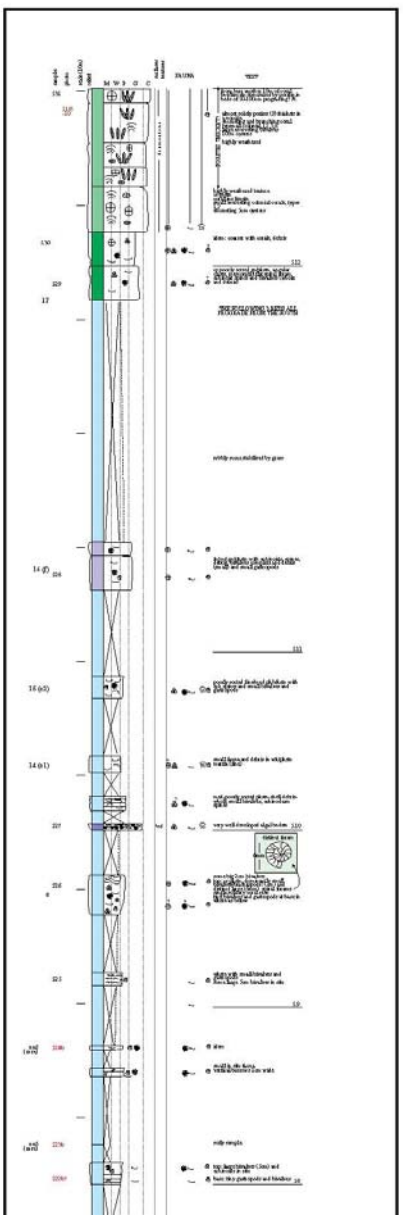

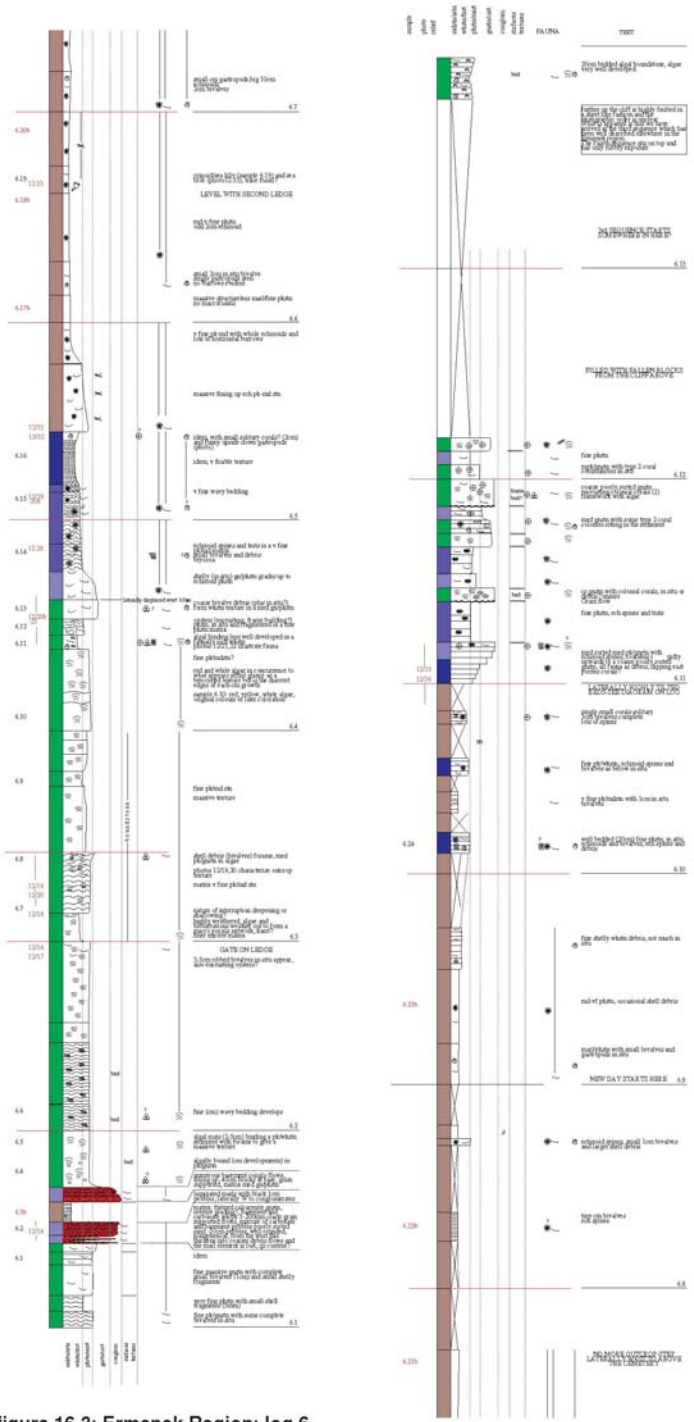

Appendix figure 16.3: Ermenek Region: log 6 (above Ermenek town to the east)

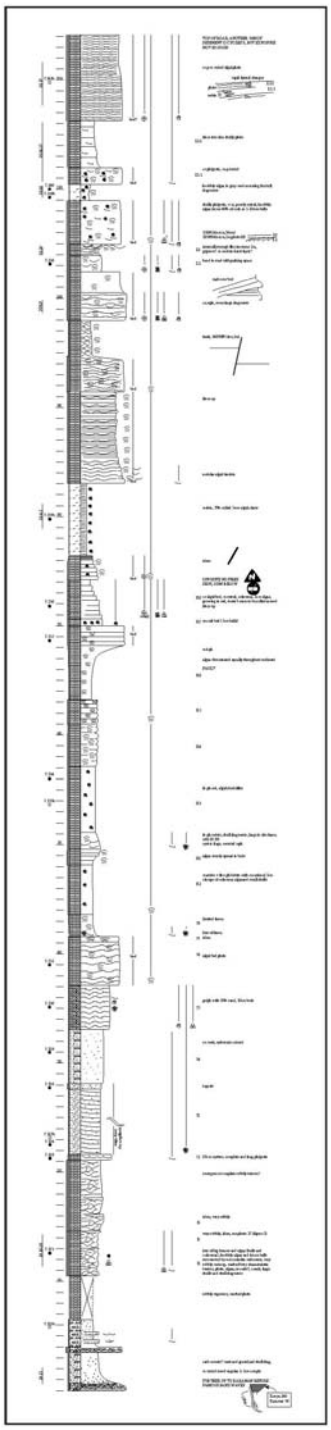

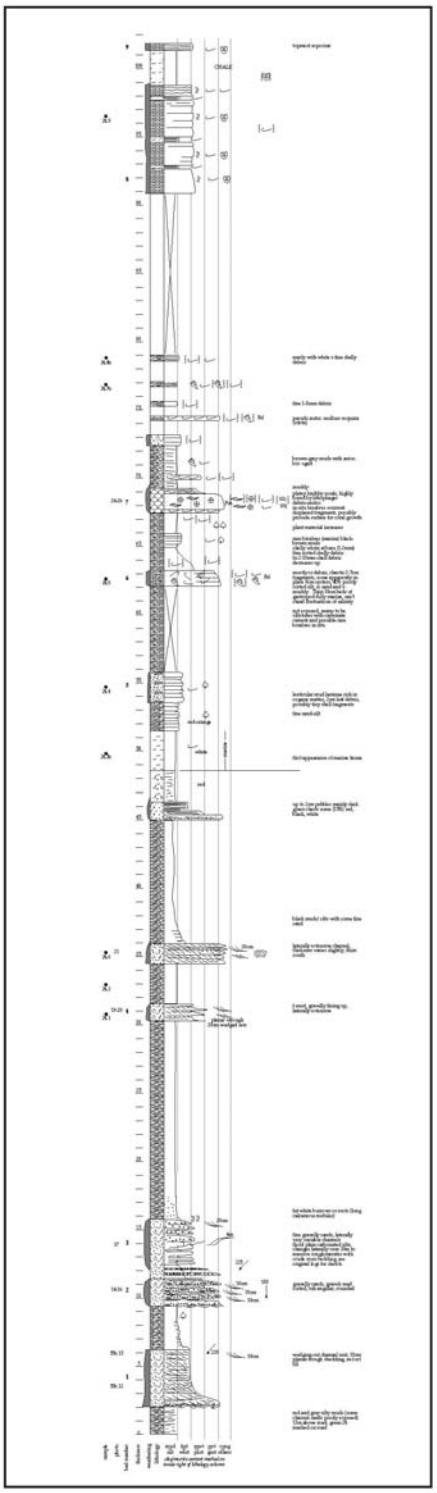

Appendix figure 16.4: Mut, top of Alahan: log 7.5 (left) Kizil Kaya log 24 (right)

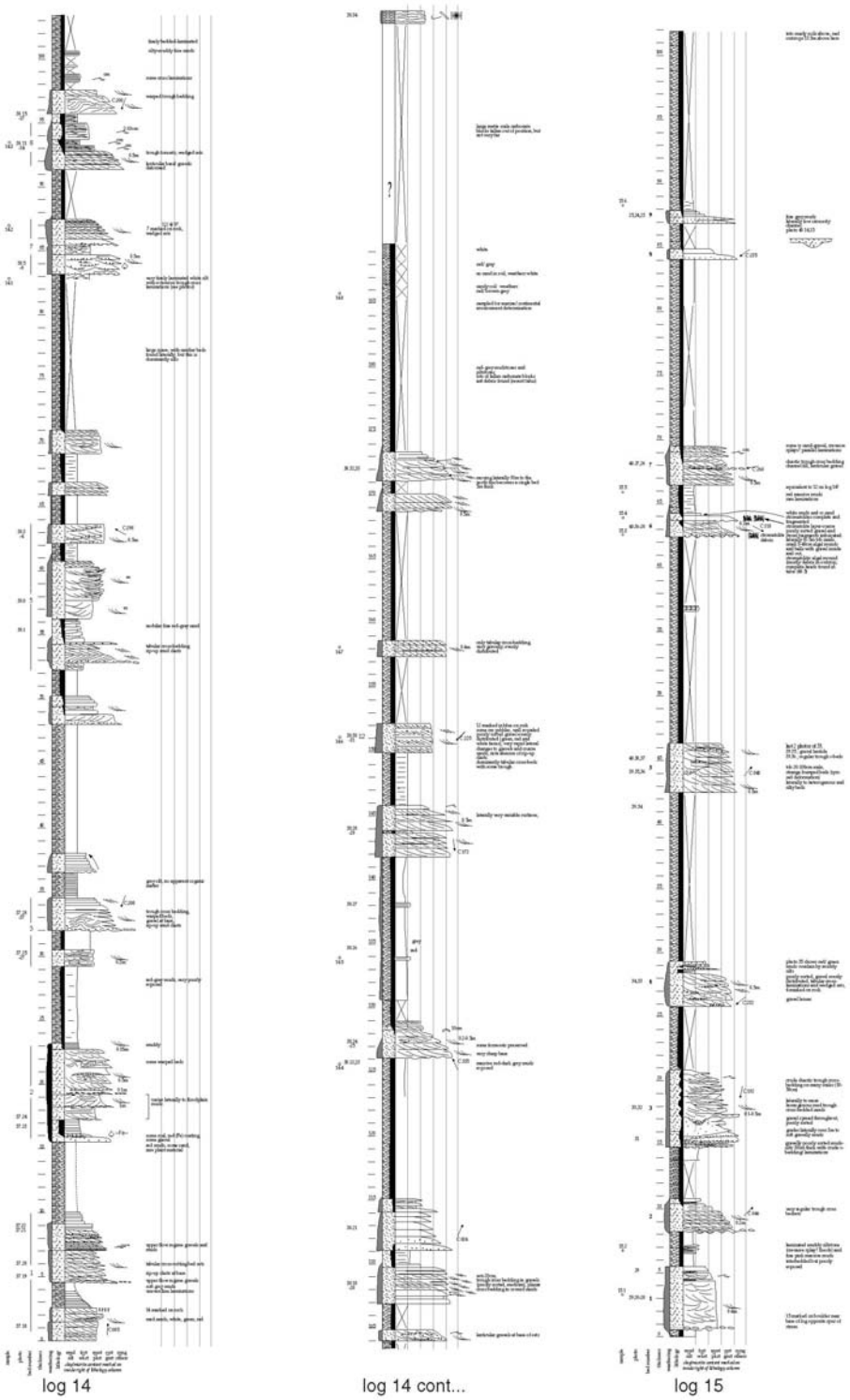

log 14 log 14 cont... log 15

Appendix figure 16.7: Mut, Pirinc area to the south in the Derincay Fm.: log 14 (left) and log 15 (right)

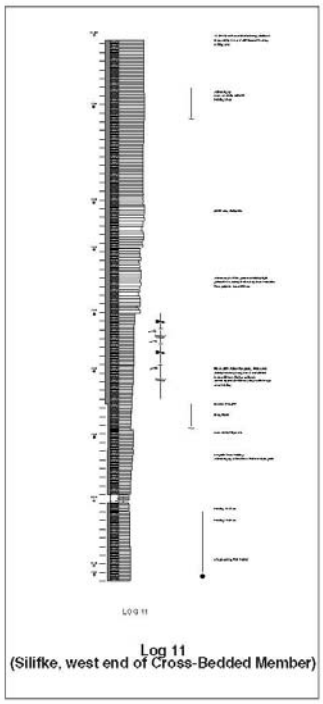

Log 11
(Silifke, west end of Cross-Bedded Member)

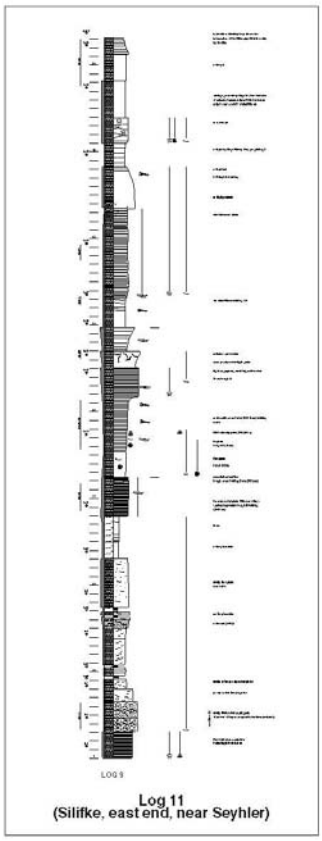

Log 11
(Silifke, east end, near Seyhler)

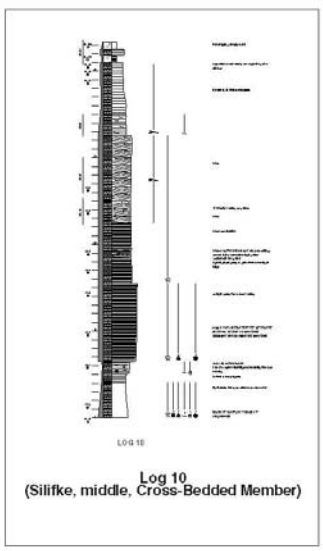

Log 10
(Silifke, middle, Cross-Bedded Member)

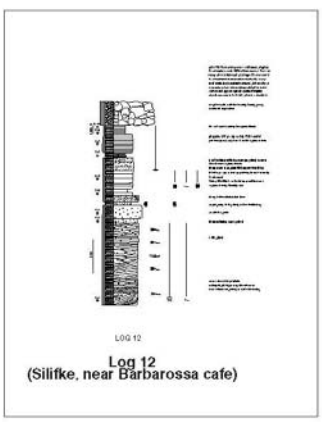

Log 12
(Silifke, near Barbarossa cafe)

Appendix figure 16.6: logs 9, 10, 11 and 12 (Silifke region)

FIGURE LIST

The complete set of documents indicated as oversized (14 in total) can be found on the cd-rom (both PC and Mac versions available). However, for practical reasons those marked [1] are here reproduced at a reduced scale, and those marked [2] have been left out.

REFERENCES CITED

Abreu, V.S. and Anderson, J.B. (1998) Glacial Eustasy during the Cenozoic: sequence stratigraphic implications. *AAPG Bull.*, **82**, 1385-1400.

Akarsu, I. (1963) Mut bölgesinin jeolojisi, MTA Dergisi, **54**, 36-45.

Akay, E., Uysal, S., Poisson, A., Cravatte, J. and Müller, C. (1985) Stratigraphy of the Antalya Neogene Basin. *Bull. Geol. Soc. Turkey*, **28,** 105-119.

Algeo, T.J. and Wilkinson, B.H. (1988) Periodicity of mesoscale Phanerozoic sedimentary cycles and the role of Milankovitch orbital modulation. *J. Geol*., **96**, 313-322.

Allen, P.A. and Allen, J.R. (1990) Basin analysis: principles and applications. Blackwell, Oxford, 451pp.

Anastas, A.S., James, N.P., Nelson, C.S. and Dalrymple, W. (1998) Deposition and textural evolution of cool-water limestones: outcrop analog for reservoir potential in cross-bedded calcitic reservoirs. *AAPG Bull.*, **82**, 160-180.

Barron, J.A. and Keller, G. (1982) Widespread deep-sea Miocene hiatuses: Coincidence with periods of global cooling. *Geology*, **10,** 577-581.

Berger, A. (1988) Milankovitch theory and climate. *Rev. Geophys*., **26**, 624-657.

Bice, M.D. and Stewart, K.G. (1990) The formation and drowning of isolated carbonate seamounts: tectonic and ecological controls in the northern Apennines. In: *Carbonate Platforms: Facies, Sequences and Evolution* (ed. by M.E. Tucker, J.L. Wilson, P.D. Crevello, J.R. Sarg and J.F. Read) IAS Spec. Pub., **9**, 145-168.

Bingöl, E. (1989) Geological map of Turkey (1/2000000). MTA, Ankara.

Bizon, G., Biju-Duval, B., Letouzey, J., Monod, O., Poisson, A., Özer, B. and Öztümer, E. (1974) Nouvelles précisions stratigraphiques concernant les bassins Tertiares du Sud de la Turquie (Antalya, Mut, Adana). Revue de l'Institut Français du Pétrole, **29**, no.3, 305-325.

Blumenthal, M., M. (1963) 1/500.000 lik Turkiye'nin jeolojik haritalari. MTA, Ankara.

Bolli, H.M., Saunders, J.B. and Perch-Nielsen, K. (1985) Plankton Stratigraphy. Cambridge University Press, 327pp.

Bosence, D.W.J. (1983) Description and Classification of Rhodoliths (Rhodoids, Rhodolites). In: *Coated Grains* (ed. by T.M.Peryt). Springer-Verlag.

Bosence, D.W.J. (1991) Coralline Algae: Mineralization, Taxonomy, and Palaeoecology. In: *Calcareous Algae and Stromatolites* (ed. by R.Riding) . Springer, Heidelberg, 98-113.

Bradley, W.B. (1929) The varves and climate of the Green River epoch. *US Geol. Surv. Prof. Pap*., **158**, 87-110.

Braga, J.C. and Martin J.M. (1988) Neogene coralline-algae growth forms and their palaeoenvironments in the Almanzora River Valley (Almeira, S.E.Spain). *Palaeogeography, Palaeoclimatology, Palaeoecology*, **67,** 285-303.

Braga, J.C., Aguirre J. (1995) Taxonomy of fossil coralline algal species: Neogene Lithophylloidea (Rhodophyta, Corallinaceae) from Southern Spain. *Review of Palaeobotany and Palynology*, **86,** 265-285.

Braga, J.C., Bosence, D.W.J. and Steneck, R.S. (1993) New Anatomical Characters in Fossil Coralline Algae and their Taxanomical Implications. *Palaeontology*, **36,** 535-547.

Brasier, M.D. (1980) Microfossils. George Allen and Unwin.

Cavelier, C., Butterlin, J., Clermonte, J., Colchen, M., Guennoc, P., Guiraud, R., Lorenz, C. and Ricou, L.-C. (1993) Late Burdigalian (18-16.5 Ma); In: Dercourt, J., Ricou, L.P. and Vrielynck, B. (eds) *Atlas Tethys Palaeoenvironmental Maps*, Beicip-Franlab.

de Boer, P.L. and Smith, D.G. (1994) Orbital forcing and cyclic sequences. *International Association of Sedimentologists, Spec. Publs.* **19**, 1-14.

Demirel, I.H. and Koksoy, M. (1992) The lithostratigraphy and geological evolution of Ermenek region. 9th Petroleum congress of Turkey, 198-206.

Dercourt, J., Ricou, L.P. and Vrielynck, B. (eds) (1993) *Atlas Tethys Palaeoenvironmental Maps*, Beicip-Franlab.

Dercourt, J., Ricou, L.P., Kazmin, V. G., Le Pichon, X., Knipper, A.L., Grandjacquet, C., Sbortshhikov, I.M., Geyssant, J., Lepvrier, C., Perchersky, D.H., Boulin, J., Sibuet, J.-C., Savostin, L.A., Sorokhtin, O., Westphal, M., Bazhrnov, M.L., Lauer, J.-P. and Biju-Duval, B. (1986) Geological evolution of the Tethys belt from the Atlantic to the Pamirs since the Lias. *Tectonophysics*, **123,** 241-315.

Dewey, J.F., Hempton, M.R., Kidd, W.S.F., Saroglu, F. and Sengor, A.M.C. (1986) Shortening of continental lithosphere: the neotectonics of Eastern Anatolia-a young collision zone. In: *Collision Tectonics* (Ed. by Coward, M.P. and Ries, M.C.), Geological Society, London, Special Publication, **19,** 3-36.

Dockal, J.A. and Worsley, T.R. (1991) Modeling sea-level changes as the Atlantic replaces the Pacific: submergent versus emergent observers. J. Geophys. Res., **96B**, 6805-6810.

Dunham, R.J. (1962) Classification of carbonate rocks according to depositional texture. In: *Classification of Carbonate Rocks* (ed. by W.E. Ham), AAPG Mem., **1**, 108-121.

Eaton, S. and Robertson, A.H.F. (1993) The Miocene Pakhna Formation, southern Cyprus and its relation to the Neogene tectonic evolution of the Eastern Mediterranean. *Sedimentary Geology*, **86,** 273-296.

Einsele , G., Rickens, W. and Seilacher, A. (1991) Cycles and Events in Stratigraphy. Springer-Verlag, 955pp.

Embry, A.F. and Klovan, J.E. (1971) A Late Devonian reef tract on northeastern Banks Island,Northwest Territories. *Bull. Can.Petrol. Geol.*, **19**, 730-781.

Emery, D. and Myers, K.J. (eds.) (1996) Sequence Stratigraphy. Blackwell Science, 297pp.

Epting, M. (1989) Miocene carbonate build-ups of Central Luconia, offshore Sarawak. In *Atlas of Seismic Stratigraphy Vol.3* (ed. by A.W. Bally), AAPG, Tulsa, Studies in Geology, **27**, 168-173.

Erlich, R.N, Barrett, S.F. and Guo, B.J. (1990): Seismic and geological characteristics of drowning events on carbonate platforms: AAPG Bull., **74**, 1523-1537.

Erlich, R.N., Longo, Jr., A.P. and Hyare, S. (1993) Response of carbonate platform margins to drowning: evidence of environmental collapse. In: *Carbonate Sequence Stratigraphy* (ed. by R.G.Loucks and J.F.Sarg). Memoir of the American Association of Petroleum Geologists, Tulsa, **57**, 241-266.

Eschard, R. and Doligez, B. (1992) Subsurface Reservoir Characterization from Outcrop Observations. Éditions Technip, Paris, 189pp.

Esteban, M. (1996) An overview of Miocene reefs from Mediterranean areas: general trends and facies models. In: *Models for Carbonate Stratigraphy from Miocene Reef Complexes of Mediterranean Regions* (Ed. by Franseen E.K., Esteban, M. and Rouchy, J.-M.), SEPM, Concepts in Sedimentology and Palaeontology, **5,** 3-53.

Fischer, A.G. (1964) The Lofer cyclothems of the Alpine Triassic. *Kans. Geol. Survey Bull.*, **169**, 107-149.

Flecker, R. (1995) Miocene Basin Evolution of the Isparta Angle, Southern Turkey. *PhD Thesis*, University of Edinburgh.

Flecker, R., Robertson, A.H.F., Poisson, A. and Müller, C. (1995) Facies and tectonic significance of two contrasting Miocene basins in south coastal Turkey. *Terra Nova*, **7,** 221-232.

Flügel, E. (1982) Microfacies Analysis of Limestones. Springer-Verlag, Berlin, 633pp.

Follows, E.J. (1992) Patterns of reef sedimentation and diagenesis in the Miocene of Cyprus. *Sedimentary Geology*, **79,** 225-253.

Follows, E.J., Robertson, A.H.F. and Scoffin, T.P. (1996) Tectonic controls on Miocene reefs and related carbonate facies in Cyprus. In: *Models for Carbonate Stratigraphy from Miocene Reef Complexes of Mediterranean Regions* (Ed. by Franseen E.K., Esteban, M. and Rouchy, J.-M.), SEPM, Concepts in Sedimentology and Palaeontology, **5,** 295-315.

Frakes, L.A. (1979) Climates Throughout Geological Time. Elsevier.

Fulthorpe, C.S. and Schlanger, S.O. (1989) Paleo-Oceanographic and Tectonic Settings of Early Miocene Reefs and Associated Carbonates of Offshore Southeast Asia. *AAPG Bull.* **73,** no.3, 729-756.

Gedik, A., Birgili, S., Yilmaz, H. and Yoldas, R. (1979) Geology of the Mut-Ermenek-Silifke (Konya, Mersin) area and petroleum possibilities. *Bull. Geol. Soc. Turkey*, **22,** 7-26.

Gilbert, G.K (1895) Sedimentary measurement of geological time. *J. Geol.*, **3**, 121-127.

Gökten, E. (1976) Basement rock units and the Miocene stratigraphy of Silifke region. *Bull. Geol. Soc. Turkey*, **19**, 117-126.

Goldhammer, R.K., Dunn, P.A. and Hardie, L.A. (1990) Depositional cycles, composite sea-level changes, cycle stacking patterns, and the hierarchy of stratigraphic forcing: examples from platform carbonates of the Alpine Triassic. *Geol. Soc. Am. Bull.*, **102**, 535-562.

Goldstein, R.H. and Franseen, E.K. (1995) Pinning points: a method providing quantitative constraints on relative sea-level history. *Sedimentary Geology*, **95**, 1-10.

Görür, N. (1992) A tectonically controlled alluvial fan which developed into a marine fan-delta at a complex triple junction: Miocene Gildirli Formation of the Adana Basin, Turkey. *Sedimentary Geology*, ***81***, 245-252.

Görür, N. (1994) Tectonic control in the development of a Lower Miocene reef at a complex triple junction: depositional history of the Karaisali Formation of the Adana Basin, Turkey. *Géologie Méditerranéenne*, **XXI**, 49-67.

Görür, N., Okay, F.Y., Seymen, I. and Sengör, C. (1984) Palaeotectonic evolution of the Tuzgolu basin complex: sedimentary record of a Neotethyan closure. In: *The Geological Evolution of the Eastern Mediterranean* (Ed. by Dixon, J.E. and Robertson, A.H.F.), Geological Society, London, Special Publications, **17,** 467-482.

Görür, N., Sakinç, M., Barka, A., Akkök, R. and Ersoy, S. (1995) Miocene to Pliocene palaeogeographic evolution of Turkey and its surroundings. *Journal of Human Evolution, **28***, 309-324.

Greenlee, S.M. and Lehmann, P.J. (1993) Stratigraphic framework of productive carbonate build-ups In: *Carbonate Sequence Stratigraphy* (ed. by R.G.Loucks and J.F.Sarg). AAPG Mem., **57**, 43-62.

Gürbüz, K. and Kelling, G. (1993) Provenance of Miocene submarine fans in the northern Adana Basin, southern Turkey: a test of discriminant function analysis. *Geological Journal*, **28,** 277-293.

Gürbüz, K. and Uçar, L. (1995) Book view Miocene biohermal reef bodies in the Mut Basin, Southern Turkey (*abstract*). In: *Second International Turkish Geology Workshop 1995, Abstracts Volume*, Cumhuriyet University, Sivas, Turkey.

Hallam, A. (1963) Major epeirogenic and eustatic changes since the Cretaceous and their possible relationship to crustal structure. Am. J. Sci., **261**, 397-423.

Hallock, P. and Glenn, E.C. (1986) Larger Foraminifera: A Tool for Paleoenvironmental Analysis of Cenozoic Carbonate Depositional Facies. *Palaios*, **1,** 55-64.

Handford, C.R. and Loucks, R.G. (1993) Carbonate Depositional Sequences and Systems Tracts-Responses of Carbonate Platforms to Relative Sea-Level Changes. In: *Carbonate Sequence Stratigraphy* (ed. by R.G.Loucks and J.F.Sarg). AAPG Mem., **57**, 3-41.

Haq, B.U., Hardenbol, J. and Vail, P.R. (1987) Chronology of fluctuating sea-levels since the Triassic. *Science*, **235**, 1156-1167.

Hays, J.D., Imbrie, J. and Shackleton, N.J. (1976) Variations in the earth's orbit: pacemaker of the ice-ages. *Science*, **194**, 1121-1132.

Hillgärtner, H. (1998) The evolution of the French Jura platform durig the Late Berriasian to Early Valanginian: controlling factors and timing. Unpubl. PhD Thesis, Fribourg (in press).

Homewood, P.W., Guillocheau, F., Eschard, R. and Cross,T. (1992) Corrélations haute résolution et stratigraphie génétique: une démarche intégrée. *Bull. Rech. Explor.-Prod. Elf Aquitaine*, **16,** 357-381.

Hottinger, L. (1977) Distribution of larger Peneroplidae, *Borelis*, and Nummulitidae in the Gulf of Elat, Red Sea. *Utrecht Micropal. Bull.* **15**, 35-110.

Hottinger, L. (1983) Neritic Macroid Genesis, an Ecological Approach. In: *Coated Grains* (ed. by T.M.Peryt), Springer-Verlag.

House, M.R. and Gale, A.S. (1995) Orbital Forcing Timescales and Cyclostratigraphy. Geological Society Special Publication, **85.**

Hsü, K.J., Cita, M.B. and Ryan, W.B.F. (1973) The origin of the Mediterranean evaporites. *International Report Deep Sea DrillingProject 13*, Washington D.C., United States Government Printing Office, 1203-1231.

Hunt, D. and Tucker, M.E. (1992) Stranded parasequences and the forced regressive wedge systems tract: deposition during base-level fall-reply. *Sed. Geol.* **81**, 1-9.

Hunt, D. and Tucker, M.E. (1995) Stranded parasequences and the forced regressive wedge systems tract: deposition during base-level fall-reply. *Sed. Geol.* **95**, 147-160.

Imbrie, J. (1985) A theoretical framework for the Pleistocene ice-ages. J. Geol. Soc.London, **142**, 417-432.

Imbrie, J., Hays, J.D. *et al.* (1984) The orbital theory of Pleistocene climate; support from a revised chronology of the marine O-18 record. In *Milankovitch and Climate Pt. 1* (ed. by A. Berger, J. Imbrie, J. Hays, G. Kukla and B. Saltmann), Reidel, Dordrecht, **11.5.2**, 269-305.

James, N.P. (1984) Reefs. In: *Facies Models* (Ed. by R.G.Walker). Geoscience Canada, 229-244.

Kelling, G., Gökcen, N.S. and Safak, U. (1995a) Factors influencing genesis and evolution of Neogene Basins, Southern Turkey (*abstract*). In: *Second International Symposium on the Geology of the Eastern Mediterranean Region, 1995, Program and Abstracts.* Jerusalem, Israel.

Kelling, G., Safak, U. and Gokcen, N.S. (1995b) Mid-Cenozoic evolution of the Mut Basin, South Turkey, and its regional significance (*abstract*). In: *International Earth Sciences Colloquium on the Aegean Region 1995, Program and Astracts*, Izmir, Turkey.

Korkmaz, S. and Gedik, A. (1990) Study of source rock facies and petroleum occurrence in Mut-Ermenek-Silifke (Konya-Mersin) basin, through geochemical methods. *Bull. Geol. Soc. Turkey*, **33**, 29-38.

Lafont, F. (1994) Influences relatives de la subsidence et de l'eustatisme sur le localisation et la géométrie des réservoirs d'un système deltaique. *Thèse, Geosciences Univ. de Rennes, Mem.*, **54**.

Lauer, J.P. (1984) Geodynamic evolution of Turkey and Cyprus based on paleomagnetic data. In: *The Geological Evolution of the Eastern Mediterranean* (ed. by J.E. Dixon and A.H.F. Robertson), Geological Society, London, Special Publications, **17**. 483-492.

Lees, A. (1975) Possible influences of salinity and temperature on modern shelf carbonate sedimentation. *Marine Geology*, **19**, 159-198.

Martini, E. and Müller, C. (1986) Current Tertiary and Quaternary calcareous nannoplankton stratigraphy and correlations. Newsl. Stratigr., **16**, 99-112.

Mathews, R.K. (1995) RKMn: Neogene sea-level files: a manual to accompanying files. R.K. Mathews and Associates, Barrington, R102806, USA, 10pp.

Miall, A.D. (1997) The Geology of Stratigraphic Sequences. Springer-Verlag, 433pp.

Milankovitch, M. (1941) Kanon der Erdbestrahlung und seine Anwendung auf das Eiszeitenproblem. Königl. Serb. Akad. Belgrad: 633pp.

Murray, J.W. (1991) Ecology and Palaeontology of Benthic Foraminifera. Longmann.

Nelson, C.S., Hyden, F.M., Keane, S.L., Leask, W.L. and Gordon, P.D. (1988) Application of bryozoan zoarial growth-form studies in facies analysis of non-tropical carbonate deposits in New Zealand. *Sedimentary Geology*, **60,** 301-322.

Neumann, A.C. and Macintyre, I. (1985) Reef response to sea-level rise: keep-up, catch-up or give-up. *Proceedings Fifth International Coral Reef Congress, Tahiti*, **3**, 105-110.

Perlmutter, M.A. and Matthews, M.D. (1990) Global stratigraphy- A model. *In:* Cross, T.A. (ed.) Quantitative Dynamic Stratigraphy. Prentice Hall, Englewood Cliffs, 233-260.

Perrin, C., Bosence, D.W.J. and Rosen, B. (1995) Quantitative approaches to palaeozonation and palaeobathymetry of corals and coralline algae in Cenozoic reefs. In: *Marine Palaeoenvironmental Analysis from Fossils*, Geological Society Special Publication, **83,** 181-229.

Piller, W.E. and Pervesler, P. (1989) The northern Bay of Safaga (Red Sea, Egypt): an actuopalaeontological approach. I topography and bottom facies. *Beitr. Palaont. Osterr.*, **15**, 103-147.

Piller, W.E. and Rasser, M. (1996) Rhodolith formation induced by reef erosion in the Red Sea, Egypt.. *Coral Reefs*, **15,** 191-198.

Pittet, B. (1996) Controles climatiques, eustatiques et tectoniques sur des systèmes mixtes carbonates-siliciclastiques de plate-forme: exemples de l'Oxfordien (Jura suisse, Normandie, Espagne). Unpubl. PhD Thesis, Fribourg, 258pp.

Plotnick, R.E. (1986) A fractal model for the distribution of stratigraphic hiatuses. *Journal of Geology*, **94**, 885-890.

Pomar, L. Fornos, J.J. and Rodriguez-Perea, A. (1985) Reef and shallow carbonate facies of the Upper Miocene of Mallorca. Excursion 11. In: *6th IAS European Regional Meeting. Lleida, Excursion Guidebook* (Ed. by M.D. Mila and J. Rosell), Institut d'Estudis Ilerdencs, Lleida. 493-518.

Posamentier, H.W. and James, D.P. (1993) An overview of sequence stratigraphic concepts: uses and abuses. In: *Sequence Stratigraphy and Facies Associations* (ed. by H.W. Posamentier, C.P Summerhayes, B.U. Haq and G.P. Allen). Special Publication, International Association of Sedimentologists, **18,** 3-18.

Posamentier, H.W. and Vail, P.R. (1988) Eustatic controls on clastic deposition II-sequence and systems tract models. In: *Sea-Level Changes: An Integrated Approach* (ed. by C.K. Wilgus, B.S. Hastings, C.G.St C. Kendall, H.W. Posamentier, C.A. Ross and J.C. Van Wagoner). Special

Publication, Society of Economic Paleontologists and Mineralogists, Tulsa, **42,** 39-45.

Posamentier, H.W., Jervey M.T. and Vail, P.R. (1988) Eustatic controls on clastic deposition I-conceptual framework. In: *Sea-Level Changes: An Integrated Approach* (ed. by C.K. Wilgus, B.S. Hastings, C.G.St C. Kendall, H.W. Posamentier, C.A. Ross and J.C. Van Wagoner). Special Publication, Society of Economic Paleontologists and Mineralogists, Tulsa, **42,** 39-45.

Pratt, B.R., James, N.P. and Cowan, C.A. (1992) Peritidal carbonates. In: *Facies Models: Response to Sea-Level Change.* Geological Association of Canada, St. John's, Newfoundland, 303-322pp.

Rasser, M. and Piller, W.E. (1997) Depth distribution of calcareous encrusting associations in the Northern Red Sea (Safaga, Egypt) and their geological implications. *Proc. 8th Int. Coral Reef Sym.* **1,** 743-748.

Reading, H.G. (1986) Sedimentary environments and facies. 2nd edition, *Blackwell Publications, Oxford,* 615pp.

Reiss, Z. and Hottinger, L. (1984) The Gulf of Aqaba. Ecological Micropaleontology. VIII, Springer (Berlin), 354pp.

Riegl, B. and Piller, W.E. (1997) Distribution and environmental control of coral assemblages in Northern Safaga Bay (Red Sea, Egypt). *Facies,* **36**, 141-162.

Roberts, H.H. and Phipps, C.V. (1988) Proposed oceanographic controls on modern Indonesian Reefs: a turn-off/turn-on mechanism in a monsoonal setting. Proceedings Sixth International Coral Reef Symposium, Townsville, **3**, 529-534.

Robertson, A.H.F. (1998) Mesozoic-Tertiary tectonic evolution of the easternmost Mediterranean area: integration of marine and land evidence. In: *Proceedings of the Ocean Drilling Program, Scientific Results* (Ed. by A.H.F.Robertson, K.-C.Emeis, C.Richter and A.Camerlenghi), **160**, 723-782.

Robertson, A.H.F. and Dixon, J.E. (1984) Introduction: aspects of the geological evolution of the Eastern Mediterranean. In: *The Geological Evolution of the Eastern Mediterranean* (Ed. by Dixon, J.E. and Robertson, A.H.F.), Geological Society, London, Special Publications, **17,** 1-74.

Robertson, A.H.F. and Grasso, M. (1995) Overview of the Late Tertiary-Recent tectonic and palaeo-environmental development of the Mediterranean region. *Terra Nova,* **7,** 114-127.

Robertson, A.H.F., Dixon, J.E., Brown, S., Collins, S., Pickett, E., Sharp, I. and Ustaömer, T. (1996) Alternative tectonic models for the Late Palaeozoic-Early Tertiary development of Tethys in the Eastern Mediterranean region. In: *Palaeomagnetism and Tectonics of the Mediterranean Region* (Ed. by A.Morris and D.H.Tarling), Geological Society, London, Special Publications, **105,** 239-263.

Rudolph, K.W. and Lehmann, P.J. (1989) Platform evolution and sequence stratigraphy of the Natune Platform, South China Sea. In *Controls on Carbonate Platforms and Basin Development* (ed. by P.D. Crevello, J.L. Wilson, J.F. Sarg and J.F. Read), SEPM Spec. Pub., **44**, 353-361.

Sadler, P.S. and Strauss, D.J. (1990) Estimation of completeness of stratigraphic sections using empirical data and theoretical models. *Journal of the Geological Society, London,* **147**, 471-485.

Saller, A., Armin, R., Ichram, L.O. and Glenn-Sullivan, C. (1993) In: *Carbonate Sequence Stratigraphy* (ed. by R.G.Loucks and J.F.Sarg). AAPG Mem., **57**, 267-290.

Sarg, J.F. (1988) Carbonate sequence Stratigraphy. In: *Sea-Level Changes: An Integrated Approach* (ed. by C.K. Wilgus, B.S. Hastings, C.G.St C. Kendall, H.W. Posamentier, C.A. Ross and J.C. Van Wagoner). Special Publication, Society of Economic Paleontologists and Mineralogists, Tulsa, **42,** 39-45.

Savin, S.M., Douglas, R.G. and Stehli, F.G. (1975) Tertiary marine paleotemperatures. *GSA Bulletin,* **86,** 1499-1510.

Savostin, L.A., Sibuet, J.-C., Zonenshain, L.P., Le Pichon, X. and Roulet, M.-J. (1986) Kinematic evolution of the Tethys belt from the Atlantic Ocean to the Pamirs since the Triassic. *Tectonophysics,* **123,** 1-35.

Scaturo, D.M., Strobel, J.S., Kendall, C.St.G., Wendte, J.C., Biswas, G., Bezdek, J. and Cannon, R. (1989) Judy Creek: a case study for a twodimensional sediment deposition simulation. In *Controls on Carbonate Platforms and Basin Development* (ed. by P.D. Crevello, J.L. Wilson, J.F. Sarg and J.F. Read), SEPM Spec. Pub., **44**, 3-76.

Schlaf J., Mandic O., Piller W., Harzhauser M., and Bassant, P. (1997) Palaeoecology in the Lower Miocene of the Mut Basin (S. Turkey): *European Palaeontological Society Meeting, Vienna,* abstract.

Schlager, W. (1981) The paradox of drowned reefs and carbonate platforms. GSA Bull., **92**, 197-211.

Schlager, W. (1989) Drowning unconformities on carbonate platforms. In *Controls on Carbonate Platforms and Basin Development* (ed. by P.D.

Crevello, J.L. Wilson, J.F. Sarg and J.F. Read), SEPM Spec. Pub., **44**, 15-25.

Schlager, W. (1992) Sedimentology and Sequence Stratigraphy of Reefs and Carbonate Platforms. American Association of Petroleum Geologists, Continuing Education Course Notes Series, **34,** 71pp.

Schlager, W. (1993) Accommodation and supply-a dual control on stratigraphic sequences. *Sedimentary Geology*, **86**, 111-136.

Schlager, W. and Philip, J. (1990) Cretaceous carbonate platforms. In *Cretaceous resources, events and rhythms* (ed. by R.N. Ginsburg, B. Beaudoin), NATO ASI Series, C, **304**, 173-195.

Schlanger, S.O. (1981) Shallow-water limestones in oceanic basins as tectonic and paleoceaonographic indicators. In: *The Deep Sea Drilling Project, a Decade of Progress* (Ed. by J.E.Warme, R.G.Douglas and E.L.Winterer), SEPM, Spec. Pub., **32**, 209-226.

Schmidt, G.C. (1961) Stratigraphic nomenclature for the Adana region petroleum district VII. *Petroleum Administration Bulletin*, **6,** 47-63.

Sengör, A.M.C, Yilmaz, Y. and Süngürlu, O. (1984) Tectonics of the Mediterranean Cimmerides: nature and evolution of the western termination of Palaeo-Tethys. In: *The Geological Evolution of the Eastern Mediterranean* (Ed. by Dixon, J.E. and Robertson, A.H.F.), Geological Society, London, Special Publications, **17**, 77-112.

Sengör, A.M.C. and Yilmaz, Y. (1981) Tethyan evolution of Turkey, a plate tectonic approach. *Tectonophysics*, **75,** 181-241.

Sengör, A.M.C., Görür, N. and Saroglu, F. (1985) Strike-slip faulting and basin related formation in zones of tectonic escape. SEPM, Special Publications, **37,** 227-440.

Sezer, S. (1970) The Miocene Stratigraphy of the Mut Region. *PhD thesis, Birbeck College, London University*, 155pp.

Smith, D.G. (1994) Cyclicity or chaos? Orbital forcing versus non-linear dynamics. *International Association of Sedimentologists, Spec. Publs.* **19**, 531-544.

Sonnenfeld, M.D. and Cross, T.A. (1993) Volumetric partitioning and facies differentiation within the Permian Upper San Andres Formation of Last Chance Canyon, Guadalupe Mountains, New Mexico. In: *Carbonate Sequence Stratigraphy* (ed. by R.G.Loucks and J.F.Sarg). AAPG Mem., **57**, 435-474.

Steininger, F.F. and Rögl, F. (1984) Paleogeography and palinspastic reconstruction of the Neogene of the Mediterranean and Paratethys. In: *The Geological Evolution of the Eastern Mediterranean* (Ed. by Dixon, J.E. and Robertson, A.H.F.), Geological Society, London, Special Publications, **17,** 659-668.

Stoakes F.A and Wendte J.C. (1988) The Woodbend Group. In *Devonian Lithofacies and Reservoir Styles in Alberta* (ed. by F.F. Krause and O.G. Burrows), Canadian Society of Petroleum Geology 13th Core Conference, Calgary, 153-170.

Strasser, A. (1991) Lagoonal-peritidal sequences in carbonate environments: autocyclic and allocyclic processes. In: *Cycles and Events in Stratigraphy* (ed. by G. Einsele, W. Ricken and A. Seilacher). Springer-Verlag, Berlin, 709-721pp.

Strasser, A., Pittet, B., Hillgärtner, H. and Pasquier, J-B (in press) Depositional sequences in shallow carbonate-dominated sedimentary systems: concepts and definitions.

Tanar, U. and Gökçen, N. (1990) Mut-Ermenek Tersiyer istifinin stratigrafisi ve mikropaleontolojisi. *MTA Dergisi*, **110,** 175-180.

Tucker, M.E. and Wright, V. (1990) Carbonate Sedimentology. Blackwell Scientific Publications, Oxford, 496pp.

Vail, P.R., Mitchum, R.M., Jr., Todd, R.G., Widmier, J.M., Thompson, S. III, Sangree, J.B., Bubb, J.N. and Hatleid, W.G. (1977) Seismic stratigraphy and global changes in sea level. In: *Seismic Stratigraphy -Applications to Hydrocarbon Exploration* (ed. by C.E.Payton). Memoir of the American Association of Petroleum Geologists, Tulsa, **26,** 49-62.

Van Andel, T.H., Heath, G.R. and Moore, T.C.,Jr. (1975) Cenozoic history and paleoceanography of the central equatorial Pacific Ocean: *Geological Society of America Memoir*, **143,** 134pp.

Van Buchem, F.S.P. and McCave, I.N. (1989) Cyclic sedimentation patterns in Lower Lias mudstones of Yorkshire (GB). *Terra Nova*, **1**, 461-467.

Van Buchem, F.S.P. McCave, I.N. and Weedon, G.P. (1994) Orbital induced small-scale cyclicity in a siliciclastic epicontinental setting (Cleveland Basin, Lower Lias, Yorkshire, UK). *In:* deBoer, P.L. and Smith, D.G. (eds.) Orbital Forcing and Cyclic Sedimentary Sequences, *IAS Special Publication*, **19**, 345-366.

Van Wagoner, J.C., Mitchum, R.M., Jr., Campion, K.M. and Rahmanian, V.D. (1990) Siliciclastic Sequence Stratigraphy in Well Logs, Cores and Outcrops: Concepts for High Resolution Correlation of Time and Facies. *American Association of Petroleum Geologists Methods in Exploration Series, Tulsa*, **7,** 55pp.

Van Wagoner, J.C., Posamentier, H.W., Mitchum, R.M., Vail, P.R., Sarg, J.F., Loutit, T.S. and Hardenbol, J. (1988) An overview of the fundamentals of sequence stratigraphy and key definitions. In: *Sea-Level Changes: An Integrated Approach* (ed. by C.K. Wilgus, B.S. Hastings, C.G.St C. Kendall, H.W. Posamentier, C.A. Ross and J.C. Van Wagoner). Special Publication, Society of Economic Paleontologists and Mineralogists, Tulsa, **42,** 39-45.

Wagner, C.W. (1964) Manual of Larger Foraminifera: Generic Determination and Stratigraphic Value. Bataafse Internatronale Petroleum Maatschappij N.V., The Hague, Exploration and Production, 310pp.

Walther, J. (1894) Einleitung in die Geologie als Historische Wissenschaft. Lithogenesis de Gegenwart, **3**, Fischer Verlag, Jena, 535-1055.

Westphal, M., Bazenhenow, M.L., Lauer, J.P., Pechersky, M.D. and Sibuet, J.C. (1986) Paleomagnetic implications on the evolution of the Tethys Belt from the Atlantic Ocean to the Pamirs since the Triassic. *Tectonophysics*, **123**, 37-86.

Williams, G.D., Ünlügenç, U.,C., Kelling, G. and Demirkol, C. (1995) Tectonic controls on the stratigraphic evolution of the Adana Basin, Turkey. *Journal of the Geological Society of London*, **152**, 873-882.

Wilson, J.L. (1975) Carbonate Facies in Geological History. Springer-Verlag, Berlin, 471pp.

Yetis, C. (1988) Reorganisation of the Tertiary Stratigraphy in the Adana Basin, Southern Turkey. *Newsletters Stratigraphy,* **20,** 43-58.

Yetis, C., Kelling, G., Gökçen, S.L. and Baroz, F. (1995) A revised stratigraphic framework for Late Cenozoic sequences in the northeastern mediterranean region. *Geol Rundsch,* **84,** 794-812.

Yilmaz, C. and Ozer, E. (1994) Temperate skeletal carbonate deposits in the Northeasternmost part of the Taurus Belt during Miocene (Turkey). *Géologie Méditerranéenne*, **XXI**, 1-2, 147-155.

Zempolich W.G. (1993) The drowning succession in Jurassic carbonates of the Venetian Alps, Italy: a record of supercontinent break-up, gradual eustatic rise, and eutrophication of shallow-water environments. In: *Carbonate Sequence Stratigraphy* (ed. by R.G.Loucks and J.F.Sarg). AAPG Mem., **57**, 63-106.

CURRICULUM VITAE

I, Philip Bassant, was born in King's Lynn, England, on the 25th of April 1972, to Keith and Georgette Bassant (née Vallotton). I attended secondary school at Brighton College in the South of England. After leaving Brighton, Hove and Sussex Sixth Form College (BHASVIC) in 1990 I took a year off, in which I worked as a laboratory assistant for three months in Lausanne (Switzerland) before travelling round Europe. For the remainder of the year I worked at BP Research (Sunbury-on-Thames) in the rock mechanics laboratory. In 1991 I went up to Cambridge University (St. John's College) to study natural sciences. During part 1 of the tripos I focused on physics, and studied geology for part 2, achieving an Upper Second Bachelor's degree (Hons.).

On leaving Cambridge University in 1994, I went to the Ecole Nationale Supérieure du Pétrole et des Moteurs (ENSPM) in Paris to study for a Diplôme d'Ingénieur in Petroleum Exploration (geology option). The summer thesis project involved a sedimentological field study of the Cenomanian platform of Cassis, near Marseille, in the South of France. This project was financed by Elf Aquitaine, and organised by Frans Van Buchem from the Institut Français du Pétrole (IFP, Paris). After finishing this degree in 1996, I began working on my doctoral thesis in carbonate sedimentology at the University of Fribourg (Switzerland). The field study area was the Mut Basin of southern Turkey. This project was directed by André Strasser (University of Fribourg) and Frans Van Buchem (Institut Français du Pétrole), and was financed by Elf Aquitaine, Total, and the IFP.

On successfully completing and defending my thesis in 1999, I was hired by Chevron Overseas Petroleum Inc., and sent to the Middle East to explore for ou. I married Carme Dauger in the same year, and we are now living in Bahrain.

ISSN 1424 - 1463